$SU(2)$ Quantum Link Models and Doubled Lattice Chern-Simons Theories

Inauguraldissertation
der Philosophisch-naturwissenschaftlichen Fakultät
der Universität Bern

vorgelegt von

Therkel Andreas Zøllner Olesen

von Dänemark

Leiter der Arbeit:
Prof. Dr. U.-J. Wiese
Albert Einstein Center for Fundamental Physics
Institut für Theoretische Physik, Universität Bern

$SU(2)$ Quantum Link Models and Doubled Lattice Chern-Simons Theories

Inauguraldissertation
der Philosophisch-naturwissenschaftlichen Fakultät
der Universität Bern

vorgelegt von

Therkel Andreas Zøllner Olesen

von Dänemark

Leiter der Arbeit:
Prof. Dr. U.-J. Wiese
Albert Einstein Center for Fundamental Physics
Institut für Theoretische Physik, Universität Bern

Von der Philosophisch-naturwissenschaftlichen Fakultät angenommen.

Bern, 22. September 2017

Der Dekan:
Prof. Dr. G. Colangelo

Abstract

In this thesis, we consider two aspects of lattice quantum field theory. In the first part of the thesis, we investigate an $SU(2)$ quantum gauge theory in the quantum link model (QLM) formulation, on a 2-dimensional lattice. QLMs provide an unconventional formulation of lattice gauge theories, where the field variables are non-commuting quantum link operators, and the local link Hilbert space is finite-dimensional. The dimension of the Hilbert space depends on the chosen representation of an embedding algebra. We consider such models on both the square and the honeycomb lattice, for the two lowest representations of the embedding algebra. We construct the most general $SU(2)$ gauge-invariant elementary plaquette ring-exchange Hamiltonian, that respects the lattice symmetries. On the honeycomb lattice, the lowest representation yields a model that is equivalent to the quantum dimer model on the Kagomé lattice. On the square lattice, we perform exact diagonalizations of the Hamiltonian, for lattice sizes up to 4×4. For the honeycomb lattice, we construct a Monte Carlo cluster algorithm, and we show the model has crystalline confined phases with spontaneously-broken translational symmetries. External half-integer non-Abelian charges are introduced, and found to be confined by a $\mathbb{Z}(2)$ flux string. This flux string fractionalizes in one of the crystalline phases.

Motivated by the subject of topological computation, in the second part we consider lattice Chern-Simons theories lattice with anyons. We construct doubled square lattice Chern-Simons-Yang-Mills theories on the torus, for non-compact and compact continuous gauge groups, and for four discrete gauge groups, $\mathbb{Z}(k) \subset U(1)$, $S_3 \subset O(2)$, $\bar{D}_2 \subset SU(2)$, and $\Delta(27) \subset SU(3)$. For continuous gauge groups we show that the model contains Abelian anyons. For the compact $U(1)$ gauge group, we find two self-adjoint extension parameters, that break the manifest gauge symmetry down to $\mathbb{Z}(k)$. In the pure Chern-Simons limit of infinite "photon" mass, this leads to a $\mathbb{Z}(k)$-symmetric extended variant of Kitaev's toric code. For each of the discrete gauge groups we determine the spectrum, and we investigate the nature of the lowest-lying states, with a special focus on the role of the center symmetry in relation to the confinement of charges. The statistical properties of the charges in the discrete gauge groups are not addressed here, but await future investigation.

Acknowledgements

First and foremost, I would like to thank my supervisor U.-J. Wiese, for giving me the opportunity to write my Ph.D. thesis at the University of Bern, and for being a great help during the project. For the first part of the thesis, I thank D. Banerjee, F.J. Jiang, P. Orland and U.-J. Wiese, with whom I have been collaborating on this part of the project. They have all been a great help in both discussions and work related to the theory of the quantum link models. Without their help, this project could not have been completed in its present form. The second part of the thesis is a result of close collaboration with S. Caspar, D. Mesterházy, N.D. Vlasii, and U.-J. Wiese, who I am grateful to.

In addition, I would like to thank all the new friends and acquaintances I have made during my time in Bern. They have all contributed to making the time in Bern a much more treasured time.

Last but certainly not least, I like to give a great thank you to my dear wife Rosana Martínez Turtos, who has been a great support throughout the whole process. Especially in helping with the final writing process.

The research leading to these results has received funding from the Schweizerischer Nationalfonds and from the European Research Council under the European Union's Seventh Framework Programme (FP7/2007-2013)/ ERC grant agreement 339220.

Contents

1 Introduction **1**

2 Introduction to Group Theory **5**

2.1 Group Definitions 5

2.1.1 Abelian Groups and Centers 6

2.1.2 Group Abelianization 6

2.1.3 Conjugacy Classes 7

2.1.4 Group Representations and Characters 7

2.1.5 Group Generators 10

2.1.6 Lie Groups 10

2.2 Group-Morphisms and 1-Cocycle 11

2.2.1 Homomorphisms of Groups 11

2.2.2 Group Action 12

2.2.3 One-Cocycle 12

2.3 Specific Groups and Subgroups 13

2.3.1 Group $U(n)$ 13

2.3.2 Continuous Group $O(n)$ 14

2.3.3 Group $SU(n)$ 16

I Quantum Link Model

(QLM) **23**

3 SU (2) Quantum Link Models **25**

3.1 Quantization of Classical Spin Models 25

3.2 SU (2) QLM 27

3.3 Rishon Representation of SU (2)-QLM 33

3.4 $\mathbb{Z}$(2) Center Symmetry 36

3.5 Site-Based QLM Gauge Covariant Basis 37

3.5.1 Square Lattice 37

3.5.2 Honeycomb Lattice 45

3.6 Exact Diagonalization on the Square Lattice 50

3.6.1 Lattice Setup 50

3.6.2 Results 51

4 Height Variable Monte Carlo on the Honeycomb Lattice **55**

4.1 Height Variables 55

4.1.1 Reduced Hamiltonian Parameter Space 63

4.1.2 Inclusion of Charges and Dirac-Strings 64

4.1.3 Height Variables on a Torus 65

4.1.4 Symmetries of the Hamiltonian in Terms of Height Variables 66

4.2 Different Confined Phases 68

4.2.1 Mean Field Calculations in the Reduced Parameter Space 68

4.2.2 The Pinwheel Phase 70

4.2.3 The Anti-Pinwheel Phase 76

4.3 Monte Carlo Simulations 77

4.3.1 Cluster Algorithm 78

4.4 Quantum Link Model Monte Carlo Results 80

4.4.1 Pinwheel Phases 81

4.4.2 Anti-Pinwheel Phase 92

II Doubled Lattice Chern-Simons Models **95**

5 Doubled Lattice Chern-Simons-Maxwell Theory **97**

5.1 Chern-Simons-Maxwell Theory in the Continuum 97

5.1.1 Single Abelian Gauge Field Lagrangian 97

5.1.2 Doubled Abelian Gauge Field Lagrangian 100

5.2 Non-Compact Doubled Chern-Simons-Maxwell Theory on Doubled Lattice Geometry 103

5.2.1 Anyonic Statistics of the Direct and Dual Charges 110

5.3 Compact Doubled Chern-Simons-Maxwell Theory on the Lattice 112

5.3.1 Compact Fields and Relations 112

5.3.2 Behaviour on a Single Lattice Cross 114

5.3.3 $\mathbb{Z}(k)$ Gauge Symmetry and Gauss' Law 124

5.3.4 Pure Chern-Simons Limit 125

5.3.5 Relation to the Toric Code 128

5.3.6 Rotating θ and $\widetilde{\theta}$ into the Hamiltonian 129

6 Doubled Lattice Chern-Simons-Yang-Mills Theories with Discrete Gauge Group **133**

6.1 Hamiltonian Formulation of Standard Lattice Gauge Theories with Discrete Gauge Group 134

6.1.1 Link-Based Operator Algebra 134

6.1.2 Gauge Symmetry and Gauss' Law 136

6.1.3 Hamiltonian Formulation 137

6.1.4 Standard $\mathbb{Z}(k)$ Lattice Gauge Theory 140

6.1.5 Standard S_3 Lattice Gauge Theory 141

6.1.6 Standard $\bar{D}_2$ Lattice Gauge Theory 143

6.1.7 Standard $\Delta(27)$ Lattice Gauge Theory 144

6.2 Hamiltonian Formulation of Doubled Lattice Gauge Theories with Discrete Gauge Group 146

6.2.1 Cross-Based Operator Algebra 146

6.2.2 One-Cocycles and Non-Commuting Operator Algebra 149
6.2.3 Gauge Transformations and Gauss' Law 151
6.2.4 Hamiltonian Formulation 151
6.3 Explicit Calculations for the Specific Discrete Gauge Groups Examples 156
6.3.1 Doubled $\mathbb{Z}(k)$ Lattice Gauge Theory 156
6.3.2 Doubled S_3 Lattice Gauge Theory 158
6.3.3 One-Cocycles and W Factors 158
6.3.4 Doubled $\bar{D}_2$ Lattice Gauge Theory 163
6.3.5 One-Cocycles and W Factors 163
6.3.6 Doubled $\Delta(27)$ Lattice Gauge Theory 166
6.3.7 One-Cocycles and W Factors 166
6.3.8 Center Symmetry and Confinement 168

7 Conclusion **173**

A States with 0, 1, or 2 Rishons per Link **177**
A.1 Fermionic Rishons 177
A.1.1 0 Rishons $\{1\}_1$-Representation 177
A.1.2 1 Rishon $\{4\}$-Representation 177
A.1.3 2 Rishons $\{5\}$-Representation 178
A.2 Bosonic Rishons 180
A.2.1 2 Rishons Singlet $\{1\}_2$-Representation 180
A.2.2 2 Rishons Triplet $\{10\}$-Representation 180

B Site-Based States **183**
B.1 Square Lattice 183
B.2 Honeycomb Lattice 185

C Square Plaquette Hamiltonian **187**
C.1 Overall Sign 187

C.2 Symmetric Basis 188

D Map Between the $SU(2)$ QLM on the Honeycomb Lattice with the $\{4\}$-Representation and the Quantum Dimer Model on the Kagomé Lattice **189**

E QLM Additional Plots **193**

E.1 Magnetic Order Parameters for the Pinwheel Phase Transition 193

F Explicit Energy Eigenstates for Specific Doubled CSYM Theories **201**

F.1 $\mathbb{Z}(k)$ Energy-Eigenstates 201

F.1.1 $\mathbb{Z}(2)$ with a Trivial Cocycle: ω_1 201

F.1.2 $\mathbb{Z}(2)$ with a Non-Trivial Cocycle: ω_2 202

F.1.3 $\mathbb{Z}(3)$ with a Trivial Cocycle: ω_1 203

F.1.4 $\mathbb{Z}(3)$ with a Non-Trivial Cocycle: ω_2 203

F.2 S_3 with a Non-Trivial Cocycle: ω_2 204

F.3 $\bar{D}_2$ Energy Eigenstates 216

F.3.1 $\bar{D}_2$ with a Non-Trivial Cocycle: ω_2 216

F.3.2 $\bar{D}_2$ with a Non-Trivial Cocycle: ω_{11} 221

F.4 $\Delta(27)$ Energy-Eigenstates 222

F.4.1 $\Delta(27)$ with a Non-Trivial Cocycle: ω_2 222

F.4.2 $\Delta(27)$ with a Non-Trivial Cocycle: ω_4 223

List of Figures **227**

List of Tables **231**

Bibliography **233**

Chapter 1

Introduction

This thesis is split into two main parts. In each part we study a different aspect of lattice quantum field theories (QFT).

In the first part we construct an $SU(2)$ lattice gauge theory, called quantum link model (QLM). The standard method to put quantum gauge field theories on the lattice is to use Wilson's formulation [1]. In Wilson's lattice gauge theory the gauge field variables are represented by classical parallel transporters. These are continuous variables residing on the lattice links. Here, in contrast to Wilson's formulation, the gauge fields are represented by intrinsically quantum mechanical objects, the so-called quantum link operators. These are non-commuting quantum operators, which reside on the lattice links.

A classical spin model is quantized by replacing the classical spin variables with spin operators. In a similar manner, a QLM is obtained from Wilson's formulation by replacing the classical parallel transporters with quantum link operators. The dimension of the local Hilbert space is finite. The dimension of the link Hilbert space is determined by the choice of representation of an embedding algebra. The finite-dimensional Hilbert space of QLMs is interesting from both theoretical and experimental viewpoints. From the experimental viewpoint, a finite Hilbert space makes QLMs suitable for quantum simulations of dynamical gauge theories, with ultra-cold atoms. The finite Hilbert space can be realized with the discrete quantum states of atoms, coupled together in an optical lattice [2, 3, 4, 5, 6, 7, 8, 9, 10, 11, 12, 13]. The $(2+1)$-dimensional $U(1)$ QLM, has already been simulated with an efficient cluster algorithm [14, 15]. There are two distinct crystalline confinement phases, separated by a weak first-order transition. Both phases were found to spontaneously break the translation invariance by a singe lattice spacing. One of these crystalline phases was also found to spontaneously break the charge conjugation symmetry. In both phases static external charge-anticharge pairs are confined by a flux string connecting the charges. This flux fractionalizes into four distinct strands, where each individual strand carries $1/2$ unit of electric flux. Each of these flux strands plays the role of an interface, separating different realizations of the given crystalline confinement phase. The interior of the strands themselves consists of the phase found in the bulk on the opposite side of the phase transition [14, 15]. The goal of the first part of the thesis is to continue this work, and to investigate a QLM with the non-Abelian gauge group SU (2). This can be viewed as both a step towards simulating QCD, in the form of an $SU(3)$ QLM, and as the introduction of a new model, which has interesting properties in its own right.

Here we will present preliminary data obtained for an $SU(2)$ QLM simulation. We find that several of the features found in the $U(1)$ QLM are also present in the $SU(2)$ QLM.

The idea of representing gauge fields in terms of quantum link operators is not a new idea. The idea was first presented by Horn in 1981 [16] under the name of "Finite Matrix Models". In this paper, Horn described the basic idea behind QLMs, and developed both an SU (2) and an U (1) gauge-invariant QLM model. Horn emphasized that the construction, could not be generalized to an arbitrary SU (N) model, without introducing a slight change to the model. In 1990 the model was rediscovered, under the name of "Gauge Magnets", by Orland and Rohrlich [17]. Here the model was expanded, and a variety of local SU (2) invariant QLM Hamiltonians was constructed. It was shown, among other things, how the operators of an SU (2) QLM can be realized by the generators of an $so(5)$ Lie algebra. In this thesis we follow a similar approach, and embed the SU (2) QLM operators in the $so(5)$ Lie algebra. Later, in 1997 the model was rediscovered for a second time, and once again the model was extended; this time by Chandrasekharan and Wiese, who named it a "quantum link model" [18]. In their paper, Chandrasekharan and Wiese redeveloped both the U (1), and the SU (2) lattice gauge theories in the QLM formulation. There the relation to Wilson's formulation was shown to be analogous to the relation between a quantum and a classical spin model. Here it was shown that universality arguments suggest that QLM formulated in 5 dimensions, can be dimensionally reduced to 4 dimensions. This renders QLMs useful for particle physics, since they are also reformulations of ordinary quantum field theories. Chandrasekharan and Wiese further speculated how the discrete nature of QLMs could advance numerically simulating lattice gauge models, if a Monte Carlo cluster algorithm could be constructed. In Chapter 4, we examine this idea and construct a cluster algorithm for a reduced set of local SU (2) invariant QLM Hamiltonians. Two years later, this was developed further in an additional paper, this time by Brower, Chandrasekharan, and Wiese [19]. Here the QLM was expanded to describe any SU (N) gauge-invariant model, and quarks were furthermore introduced. In addition, a new method of representing QLMs was introduced, the so-called "rishon" representation.[1] Rishons are mathematical objects reminiscent of particles residing on lattice links of QLMs, and for a general $SU(N)$ QLM all the operators of the model can be represented in terms of rishons. This provides an intuitive picture of the models. In writing this thesis, the rishon representation has proven to be a tool of great importance. This has been true for both analysing QLMs in terms of a more general Hamiltonian, and for constructing highly-efficient numerical simulations of QLMs.

This first part of the thesis is organized as follows: In Chapter 3, we introduce the $SU(2)$ QLM. We emphasize the construction of a manifestly gauge-invariant rishon site basis, and how a general set of elementary plaquette ring-exchange Hamiltonians can be constructed in this basis. For the square lattice, we use this basis to perform exact diagonalization studies of the general set of Hamiltonians for lattice sizes up to 4×4. In Chapter 4 we introduce height variables to describe the model on the honeycomb lattice. This makes it possible to construct a Monte Carlo cluster algorithm that is also introduced in this chapter, together with the results obtained from these Monte Carlo simulations.

The second part of the thesis, motivated by the idea of topological quantum computation using anyons, is concerned with so-called Chern-Simons (CS) theories. Exchanging two particles twice brings the particles back to their initial positions; this is topologically the same as moving

[1] The rishon formulation was previously introduced by Orland in an unpublished paper in 1990. The paper was only available online as a scanned document until 2012, but can now be found in [20].

one particle in a closed loop, around the other. In 3 or more spatial dimensions, the loop can be topologically deformed into a point. Hence, only particles with a statistical phase of $+1$ (bosons) or -1 (fermions) under exchange are allowed. In 2 spatial dimensions no such deformation of the loop is possible, thereby allowing for anyons with any statistical phase [21, 22]. This part of the thesis is in large part built on work carried out in collaboration with S. Caspar[2], D. Mesterházy[2], N.D. Vlasiia[2,3] and U.-J. Wiese[2], which has previously been published in [23] and [24].

A large effort has been devoted to the promise of a universal quantum computer [25]. Recently, experimental progress has been made in the design and control of macroscopic quantum many-body systems [26, 27], This has led to the study of many-body phenomena that were previously hard to study in either solid-state materials or in classical computer models. A fundamental challenge to be overcome in building a quantum computer is the correction of inevitable errors. Those errors due to decoherence are of special interest. A promising proposal is the use of so-called topological quantum computing [28]. Quantum information is protected from decoherence by encoding quantum information throughout the entire system [29, 30, 31]. The actual quantum processing is done through the braiding of non-Abelian anyonic quasi-particles [32, 33, 34, 35, 36, 37, 38], from which unitary quantum gates can be constructed [28, 39, 40]. It is important that the anyons show non-Abelian braid statistic; other statistics are not rich enough to construct those quantum gates needed for achieving universal quantum computation (see e.g. [41]).

An example of a topological quantum memory [42] is Kitaev's toric code [28]. Since the toric code corresponds to a $\mathbb{Z}(2)$ Ising gauge theory, the model is Abelian, and therefore not suitable for universal quantum computing. If we are to achieve universal quantum computing, Kitaev's toric code must be generalized to non-Abelian theories [43, 44]. The actual realization of a quantum computer is still beyond reach. The study of non-Abelian Chern-Simons theories have, however, added to our understanding of how Jones polynomials can be used in quantum algorithms [45, 46, 47]. On the experimental side, no conclusive evidence exists, thus far, that non-Abelian anyonic quasi-particles can be found in nature. Some evidence has been presented for this in the $\nu = 5/2$ fractional quantum Hall state [48, 49, 50], but is not yet conclusive.

Motivated by the papers [51, 52, 53, 54, 55, 56], this part of the thesis concerns the possibility of directly constructing lattice gauge theories [57] in the Hamiltonian formulation [58, 59, 60], featuring topological phases with the desired quasi-particle excitations. The models that we consider are Chern-Simons type theories [61] in 2 spatial dimensions. These are models with an additional Chern-Simons term added to the Lagrangian. In the Hamiltonian formulation, this term is absent from the Hamiltonian, but modifies the commutation relations [61, 62, 63, 64, 65].

The Chern-Simons term is only possible in an even number of spatial dimensions. Both parity and time-reversal symmetry are explicitly broken by this term. It gives mass to the gauge field, and endows charged particles with fractional anyonic statistics [32, 34, 35, 66]. The braiding of these particles leads to a non-Abelian Berry phase, which maybe used to encode quantum information [67, 68], and therefore be useful in topological quantum computation [28, 42, 69, 70, 40, 71]. In pure Chern-Simons gauge theory, the Hamiltonian vanishes and the states are solely determined by the topological properties of the manifold on which the gauge field resides [72, 73]. We will

[2]Albert Einstein Center for Fundamental Physics, Institute for Theoretical Physics, University of Bern, Sidlerstrasse 5, 3012, Bern, Switzerland

[3]Bogolyubov Institute for Theoretical Physics, National Academy of Sciences of Ukraine, 14-b Metrologichna Str., Kyiv, 03680, Ukraine

instead, add a Chern-Simons term to a Maxwell action in Chapter 5; to construct a Chern-Simons-Maxwell (CSM) theory, and to a more general Yang-Mills (YM) action in Chapter 6; to construct a Chern-Simons-Yang-Mills (CSYM) theory. This creates massive gauge fields [74, 75, 62, 76] for the two models. Even though Chern-Simons gauge theories with Abelian fields do not allow for universal quantum computation, they are still interesting theories in their own right, in relation to 2-dimensional conformal field theories [77, 72], to the toric code, and in their relation to bosonization or Fermi-Bose transmutation in $(2+1)$ dimensions [78, 79, 80, 81]. They also play a fundamental role in the context of the fractional quantum Hall effect [82, 83, 84] and other condensed matter systems [85, 86, 87, 88, 89, 90, 91].

Topologically massive gauge fields suffer from a lattice doubling problem, similar to that of fermion fields. A natural lattice geometry for the Chern-Simons theories is a doubled lattice [92, 93, 81, 80, 94]. An additional dual lattice is introduced, containing a second doubled dual gauge field. In this unconventional lattice formulation, the fundamental gauge degrees of freedom are not associated with the links themselves, but rather with "lattice crosses". These are intersections between a direct and a dual link. Here two gauge fields residing on the same lattice cross are coupled together through the Chern-Simons term. In the Hamiltonian formulation the one-cocycles of the gauge group fully characterize the lattice cross algebra. It should be noted that a similar lattice geometry was used in [92, 94]. This geometry is the fundament on which we explore these models. This is in contrast to ordinary lattice gauge theories [57, 58, 95, 60], where the field algebra is link-based, and has been the basis of most studies of Chern-Simons lattice gauge theories [79, 96, 97, 98, 99].

The second part is organized as follows: In Chapter 5, we introduce both the Chern-Simons theory and the doubled lattice geometry. Another purpose of Chapter 5 is to perform a detailed mathematical derivation of an extended version of the $\mathbb{Z}(k)$-variant of the toric code, as a limit of a doubled $U(1)$ Chern-Simons-Maxwell lattice gauge theory. In this context, we put particular emphasis on the role played by the self-adjoint extension parameters of the cross-based Hamiltonian. This embeds the toric code in a wider theoretical framework, and provides a broader perspective on quantum information processing. In Chapter 6 a more general setting is introduced, and the results from the previous chapter are generalized to this setting. Chern-Simons theories are introduced with finite Abelian and non-Abelian gauge groups [100, 101, 102]. We introduce a general lattice cross algebra, based on the one-cocycles of the groups. A detailed description of the energy spectra will be given for four specific gauge groups, with a special focus on the confinement properties of each gauge group.

Since group theory plays a fundamental role throughout the thesis, we begin in Chapter 2 with a brief introduction to basic concepts of group theory, before moving to the two main parts of the thesis. Chapter 2 also introduce several groups that are important for both parts of the thesis. Finally, Chapter 7 contains our conclusions and outlook for the entire the thesis.

Chapter 2

Introduction to Group Theory

The present chapter is not intended as a comprehensive review of group theory, but is merely meant as an introduction to those concepts important to this thesis. For a more thorough discussion of group theory, the reader is referred to introductory textbooks on the subject, e.g. [103, 104], and online resources such as [105] and references therein.

This chapter is organized as follows: In Section 2.1 we introduce some general group properties. In Section 2.2 we introduce group morphisms with the goal of introducing one-cocycles, which will play a fundamental role in the later formulation of Chern-Simons theories. Finally, in Section 2.3 we introduce several groups and derive several of their group properties.

2.1 Group Definitions

A group $\mathcal{G}$ is an algebraic structure containing a set of elements $\mathcal{G} = \{\Omega_1, \Omega_2, \Omega_3, \ldots\}$. The set can either be a finite discrete set or an infinite (often continuous) set of elements. These are called a finite discrete group or an infinite (continuous) group, respectively. The total number of elements in a group is called the order of the group, denoted by $\mathrm{Ord}(\mathcal{G})$. A group is equipped with a multiplication rule for combining two elements $\Omega_1\Omega_2 = \Omega_3$. The elements in the group must obey four conditions under the multiplication rule:

I The closure property. The product of any two elements belonging to the group, must give an element which also belongs to the group:

$$\Omega_i\Omega_j = \Omega_k \in \mathcal{G}, \quad \forall \quad \Omega_i, \Omega_j \in \mathcal{G}. \tag{2.1}$$

II The associative law. The multiplication of three group elements is independent of the order in which the multiplication is carried out, as long as the sequence of elements is not changed:

$$\Omega_i \left(\Omega_j\Omega_k\right) = \left(\Omega_i\Omega_j\right)\Omega_k, \quad \forall \quad \Omega_i, \Omega_j, \Omega_k \in \mathcal{G}. \tag{2.2}$$

III The set must contain a unique identity element $\mathbb{1}$:

$$\mathbb{1}\Omega_i = \Omega_i\mathbb{1} = \Omega_i, \quad \forall \quad \Omega_i \in \mathcal{G}. \tag{2.3}$$

IV For every group element Ω_i, there exists a unique element in the group $\Omega_i^{-1} \in \mathcal{G}$, under which the multiplication by Ω_i gives the identity:

$$\Omega_i \Omega_i^{-1} = \Omega_i^{-1} \Omega_i = \mathbb{1}, \quad \forall \quad \Omega_i \in \mathcal{G}. \tag{2.4}$$

The simplest way to define a finite group of small order, is with a multiplication table, also known as a Cayley table. A Cayley table specifies the product of all possible pairs of elements. Examples of Cayley tables for discrete groups are given in Table 2.1, Table 2.5 and Table 2.9 below.

A subgroup $\mathcal{G}_{\text{sub}} \subseteq \mathcal{G}$ is a subset of group elements in $\mathcal{G}$, which themselves constitute a subgroup under the multiplication rule of $\mathcal{G}$. If $\mathcal{G}_{\text{sub}} \neq \mathcal{G}$, then $\mathcal{G}_{\text{sub}}$ is called a prober subgroup of $\mathcal{G}$.

2.1.1 Abelian Groups and Centers

A group is said to be Abelian if all elements of the group commute under the given multiplication rule:

$$\Omega_i \Omega_j = \Omega_j \Omega_i, \quad \forall \quad \Omega_i, \Omega_j \in \mathcal{G}. \tag{2.5}$$

If this is not the case, the group is said to be non-Abelian.

For any group $\mathcal{G}$, there exists a subgroup, called the center $Z(\mathcal{G})$, which consists of those group elements that commute with all elements of the group:

$$Z(\mathcal{G}) = \{ z \in \mathcal{G} \mid \forall\, g \in \mathcal{G},\ zg = gz \}. \tag{2.6}$$

For an Abelian group, the center is identical to the group itself $Z(\mathcal{G}) = \mathcal{G}$. If the center only contains the identity element, then the group is said to have a trivial center.

2.1.2 Group Abelianization

For any (non-Abelian) group $\mathcal{G}$ we can define an Abelian subgroup $\mathcal{A}_\mathcal{G} \subseteq \mathcal{G}$ by a process called Abelianization. To do this, we first define the commutator-normal-subgroup of $\mathcal{G}$.[1] This is the group consisting of all elements which can be obtained through commutation

$$[\mathcal{G}, \mathcal{G}] = \left\{ g_i g_j g_i^{-1} g_j^{-1} \mid \forall\, g_i, g_j \in \mathcal{G} \right\}. \tag{2.7}$$

For an Abelian group, the commutator subgroup is just the identity element. Taking the quotient of $\mathcal{G}$ by the commutator subgroup gives the Abelian subgroup

$$\mathcal{A}_\mathcal{G} = \mathcal{G} / [\mathcal{G}, \mathcal{G}]. \tag{2.8}$$

[1] This is also known as the derived subgroup of $\mathcal{G}$.

2.1.3 Conjugacy Classes

For a given group $\mathcal{G}$, we assign to every group element Ω a conjugacy class $\Omega \in C_i$. Two group elements Ω_i and Ω_j belong to the same conjugacy class if and only if there exists an element $\Omega' \in \mathcal{G}$ such that $\Omega_i = \Omega' \Omega_j \Omega'^{-1}$. By definition, center group elements $z \in Z(\mathcal{G})$ commute with all the elements in the group. Each center element therefore forms its own conjugacy class

$$\Omega' z \Omega'^{-1} = \Omega' \Omega'^{-1} z = z, \quad \forall \quad z \in Z(\mathcal{G}), \quad \Omega' \in \mathcal{G}. \tag{2.9}$$

Consequently, every element of an Abelian group constitutes its own conjugacy class. On the other hand, a non-Abelian group has at least one conjugacy class containing more than one group element.

Group elements belonging to the same conjugacy class share important properties. In particular, one can often consider the behaviour of a conjugacy class, rather than having to consider the individual group elements. When it is clear from the context that we are just considering a single group element, in contrast to the whole conjugacy class, we will use C as shorthand notation for any group element belonging to that conjugacy class.

2.1.4 Group Representations and Characters

A group is nothing more than an abstract mathematical collection of elements. To make the group useful in terms of QFT calculations, we need *representations*. This can be done with unitary matrices, where each group element Ω_i is represented by a single unitary matrix $\Gamma\left(\Omega_i\right)$. Here Γ is called a unitary representation of the group. For Γ to be a representation of the group it must preserve the group structure

$$\Gamma\left(\Omega_i\right)\Gamma\left(\Omega_j\right) = \Gamma\left(\Omega_i \Omega_j\right), \quad \forall \quad \Omega_i, \Omega_j \in \mathcal{G}. \tag{2.10}$$

The dimension d_Γ of the unitary matrices is called the dimension of the representation. The choice of representation Γ for a group $\mathcal{G}$ is not unique. Two different group-representations Γ_i and Γ_j are said to be unitarily equivalent, if there exists a single unitary matrix V, such that

$$\Gamma_i(\Omega) = V \Gamma_j(\Omega) V^\dagger, \quad \forall \quad \Omega \in \mathcal{G}. \tag{2.11}$$

The conjugate representation $\overline{\Gamma}$ is obtained by taking the complex conjugate of the matrices in Γ:

$$\overline{\Gamma}(\Omega) = \Gamma(\Omega)^*, \quad \forall \quad \Omega \in \mathcal{G}. \tag{2.12}$$

A representation Γ is said to be real if the conjugate representation is equal to the representation itself:

$$\overline{\Gamma}(\Omega) = \Gamma(\Omega), \quad \forall \quad \Omega \in \mathcal{G}. \tag{2.13}$$

If the conjugate representation is unitarily equivalent to the representation itself:

$$\overline{\Gamma}(\Omega) = V \Gamma(\Omega) V^\dagger, \quad \forall \quad \Omega \in \mathcal{G}, \tag{2.14}$$

then the representation is said to be pseudo-real. If a representation is neither real nor pseudo-real, then the representation is said to be complex.

An important set of unitary representations are the irreducible representations. We denote the set of all irreducible representations of a group by $\{\Gamma^{Irr}\}$. A d_Γ-dimensional representation is said to be reducible if it is unitarily equivalent to a representation where all the matrices are block diagonal in blocks of dimensions smaller than d_Γ. Otherwise, the representation is said to be irreducible. Any representation Γ of a finite group (or semi-simple Lie group) can be expanded into a direct sum over irreducible representations. The irreducible representations can be used as a basis from which other representations can be constructed. They therefore have a special importance in group theory.

A central result in the theory of finite groups is the orthogonality theorem

$$\sum_{\Omega\in\mathcal{G}} \Gamma\left(\Omega\right)^*_{ij} \Gamma'\left(\Omega\right)_{kl} = \frac{\mathrm{Ord}\left(\mathcal{G}\right)}{d_\Gamma} \delta_{ik}\delta_{jl}\delta_{\Gamma\Gamma'}, \tag{2.15}$$

where Γ and Γ' are any representations of the group $\mathcal{G}$. From this it follows that the order of the group equals the sum over the squares of the dimensions of all irreducible representations

$$\sum_{\Gamma_i\in\{\Gamma^{Irr}\}} d^2_{\Gamma_i} = \mathrm{Ord}\left(\mathcal{G}\right). \tag{2.16}$$

An individual conjugacy class $\mathcal{C}$ is characterized by the trace of a unitary representation. This is called the character $\chi(\Omega)$, $\Omega \in \mathcal{C}$, of the group element Ω. Explicitly,

$$\chi_\Gamma\left(\Omega\right) = \mathrm{Tr}\left(\Gamma\left(\Omega\right)\right). \tag{2.17}$$

The cyclic property of the trace implies that the character is constant over elements in a conjugacy class:

$$\begin{aligned} \chi_\Gamma\left(\Omega_i\right) &= \chi_\Gamma\left(\Omega'\Omega_j\Omega'^{-1}\right) \quad \forall \quad \Omega_i, \Omega_j \in \mathcal{C} \\ &= \mathrm{Tr}\left(\Gamma\left(\Omega'\right)\Gamma\left(\Omega_j\right)\Gamma\left(\Omega'^{-1}\right)\right) \\ &= \chi_\Gamma\left(\Omega_j\right). \end{aligned} \tag{2.18}$$

The character depends on the choice of representation, but is unchanged for a unitarily equivalent representation. This follows directly from the cyclic properties of the trace.

From the orthogonality theorem it follows that the characters of two irreducible representations Γ^{Irr}_i and Γ^{Irr}_j are orthogonal:

$$\sum_{\Omega\in\mathcal{G}} \chi_{\Gamma^{Irr}_i}\left(\Omega\right)^* \chi_{\Gamma^{Irr}_j}\left(\Omega\right) = \mathrm{Ord}\left(\mathcal{G}\right)\delta_{ij}. \tag{2.19}$$

In the special case of $\Gamma^{Irr}_i = \Gamma^{Irr}_j$, eq. (2.19) states that the sum of the squares of the characters equals the order of the group:

$$\sum_\mu N\left(\mathcal{C}_\mu\right)\left|\chi_{\Gamma^{Irr}_i}\left(\mathcal{C}_\mu\right)\right|^2 = \mathrm{Ord}\left(\mathcal{G}\right). \tag{2.20}$$

Here the sum is over conjugacy classes and $N\left(C_\mu\right)$ is the number of elements in C_μ. The characters have their own orthogonality theorem over the irreducible representations

$$\sum_{\Gamma_k^{Irr}\in\{\Gamma^{Irr}\}} \chi_{\Gamma_k^{Irr}}\left(C_i\right)^* \chi_{\Gamma_k^{Irr}}\left(C_j\right) = \frac{\mathrm{Ord}\left(\mathcal{G}\right)}{d_{C_i}}\delta_{ij}. \tag{2.21}$$

Next we prove that the number of irreducible representations equals the number of conjugacy classes. First we write an arbitrary representation as a linear combination of irreducible representations:

$$\Gamma\left(\Omega\right) = \bigoplus_{i=1}^{N\left(\{\Gamma^{Irr}\}\right)} m_i \Gamma_i^{Irr}\left(\Omega\right). \tag{2.22}$$

Here $N\left(\{\Gamma^{Irr}\}\right)$ denotes the number of irreducible representations for the group. By taking the trace, we find in terms of the characters

$$\chi\left(\Omega\right) = \sum_{i=1}^{N\left(\{\Gamma^{Irr}\}\right)} m_i \chi_{\Gamma_i^{Irr}}\left(\Omega\right), \tag{2.23}$$

where

$$m_i = \frac{1}{\mathrm{Ord}\left(\mathcal{G}\right)} \sum_{\mu=1}^{N(C)} N\left(C_\mu\right) \chi_{\Gamma_i^{Irr}}\left(C_\mu\right)^* \chi\left(C_\mu\right). \tag{2.24}$$

Here $N\left(C\right)$ denotes the number of conjugacy classes of the group. Therefore, the number of irreducible representations equals the number of conjugacy classes.[2]

$$N\left(\{\Gamma^{Irr}\}\right) = N\left(C\right). \tag{2.25}$$

In the special case where the representation Γ is the direct product of two irreducible representations Γ_i^{Irr} and Γ_j^{Irr}. Then the character of the product equals to the product of the characters

$$\chi_{\left(\Gamma_i^{Irr}\otimes\Gamma_j^{Irr}\right)}\left(\Omega\right) = \chi_{\Gamma_i^{Irr}}\left(\Omega\right)\chi_{\Gamma_j^{Irr}}\left(\Omega\right), \quad \forall \quad \Omega\in\mathcal{G}. \tag{2.26}$$

In this case the two equations of eq. (2.22) and (2.23) are reduced to

$$\Gamma_i^{Irr}\otimes\Gamma_j^{Irr} = \bigoplus_{\mu=1}^{N\left(\{\Gamma^{Irr}\}\right)} m_\mu \Gamma_\mu^{Irr}, \tag{2.27}$$

$$\chi_{\Gamma_i^{Irr}}\left(\Omega\right)\chi_{\Gamma_j^{Irr}}\left(\Omega\right) = \sum_{\mu=1}^{N\left(\{\Gamma^{Irr}\}\right)} m_\mu \chi_{\Gamma_\mu^{Irr}}\left(\Omega\right). \tag{2.28}$$

Below we use these equations to construct character tables for irreducible representations, constructing the representations explicitly. To do so, two additional facts are needed. First, the

[2]For the coefficients m_i to be uniquely given, there must be as many independent equations, as there are coefficients. The total number of coefficients is the number of irreducible representations, and the number of independent equations is the number of conjugacy classes.

trivial irreducible representation always exists. In other words, for every group there exists a 1-dimensional representation for which all characters equal 1. Second, the representations are given in terms of unitary matrices. Any character must be a sum over d_Γ numbers of $\mathrm{Ord}(\mathcal{G})$-roots of unity. If needed, characters for higher representations can be obtained directly from eqs. (2.27)-(2.28) by combinations of irreducible representations. The character of the unit element, which is also the dimension of the representation, is called the degree of the representation.

2.1.5 Group Generators

A subset of a group $\mathcal{T} \subset \mathcal{G}$ is called a generating set of the group, if every element in the group can be expressed as a product of elements in $\mathcal{T}$. The elements of the generating set $T_i \in \mathcal{T}$ are called the generators of the group. This is not a unique set.[3] Only the minimum generating set, that is the generating set with the minimal number of generators will be used here. The size of a minimum generating set is called the rank of the group $\mathrm{Rank}(G)$.

Given a minimal generating set $\left\{T_1, T_2, \ldots, T_{\mathrm{Rank}(G)}\right\}$, we can express any group element g in terms of a set of parameters $\theta_{i\in\{1,2,\ldots,\mathrm{Rank}(\mathcal{G})\}}$:

$$g = T_1^{\theta_1} T_2^{\theta_2} \cdots T_{\mathrm{Rank}(G)}^{\theta_{\mathrm{Rank}(G)}}. \tag{2.29}$$

Since any element can be constructed from the minimal set of generators, it is clear that the set of parameters $\theta_{i\in\{1,2,\ldots,\mathrm{Rank}(\mathcal{G})\}}$ is not unique.

2.1.6 Lie Groups

Lie groups, which play a special role in physics, are groups for which the elements form a smooth analytic manifold. We can construct a generating set, for all elements connected to the identity, for which the generators are infinitesimally close to the identity

$$dT_i = \lim_{\epsilon\to\infty} \left(\mathbb{1} + \epsilon T_i\right), \tag{2.30}$$

such that

$$g = \lim_{l\to\infty} \left(\mathbb{1} + i\frac{\theta_i}{l} T_i\right)^l = exp\left(i\theta_i T_i\right). \tag{2.31}$$

T_i are called the infinitesimal generators. Note that dT, not T, are the actual generators, in the sense above. Here we have rewritten the generators in terms of a parameter l, which is sent to infinity.

Lie Algebra

The global properties of a group are sometimes of little interest. The local behaviour of a Lie group is given by the vector space tangential to the smooth manifold, spanned by the infinitesimal

[3] As a trivial case one could simply choose the generating set to be the whole group $\mathcal{T} = \mathcal{G}$, which obviously constitutes a generating set of the group $\mathcal{G}$. This set is clearly not the smallest possible set – e.g. the identity element can trivially be removed, which shows that the generating set is not unique.

generators of the Lie group, and the Lie algebra is defined as the commutator algebra between the infinitesimal group generators T_i

$$\left[T_i, T_j\right] = i f_{ijk} T_k. \tag{2.32}$$

Here f_{ijk} are the structure constants of the Lie algebra. We denote the Lie algebra by lower case letters.[4]

2.2 Group-Morphisms and 1-Cocycle

2.2.1 Homomorphisms of Groups

A homomorphism ϕ, maps the elements from a group $\mathcal{G}$ to the elements of a group $\mathcal{H}$. To be a homomorphism ϕ must preserve the group structure of the domain group $\mathcal{G}$. I.e. $\phi : \mathcal{G} \to \mathcal{H}$ is a homomorphism if[5]

I $\phi\left(gg'\right) = \phi(g)\,\phi\left(g'\right), \quad \forall \quad g, g' \in \mathcal{G},$

II $\phi(\mathbb{1}) = \mathbb{1},$

III $\phi\left(g^{-1}\right) = (\phi(g))^{-1}.$

Isomorphism

A homomorphism is said to be an isomorphism, if the map is bijective, and the inverse map is a group homomorphism. In other words, in addition to the above conditions, there exist an inverse map $\phi^{-1} : \mathcal{H} \to \mathcal{G}$ that is a homomorphism. In terms of Cayley tables, a map $\phi : \mathcal{G} \to \mathcal{H}$ is an isomorphism, if ϕ can be expressed as a relabelling rule of the elements in $\mathcal{G}$, such that one obtains the Cayley table of $\mathcal{H}$. Since an isomorphism is a relabelling of the group elements, because it preserves the group properties. If two groups $\mathcal{G}$ and $\mathcal{H}$ related by an isomorphism, we say that they are isomorphic and we write $\mathcal{G} \cong \mathcal{H}$.

Automorphism

An isomorphism that maps the group to itself $\phi : \mathcal{G} \to \mathcal{G}$ is called an automorphism. For any group $\mathcal{G}$ we define the automorphism group $\mathrm{Aut}(\mathcal{G})$, that is the group of all automorphisms $\phi_i : \mathcal{G} \to \mathcal{G}$ of the group. The multiplication rule of $\phi_i(\cdot)$ and $\phi_j(\cdot)$ is the composition of the two maps, $\phi_i\left(\phi_j(\cdot)\right) : \mathcal{G} \to \mathcal{G}$. In addition to the automorphism group, we define the symmetric group $\mathrm{Sym}(\mathcal{S})$, which the automorphism group is a subgroup of: $\mathrm{Aut}(\mathcal{G}) \subset \mathrm{Sym}(\mathcal{G})$. This is the group of all permutations of the elements. A symmetric group is defined for any set (even if the set is not a group).

[4] In addition, it should be noted that a Lie algebra must satisfy the Jacobi identity. This will, however, not be of any special importance here.

[5] We emphasize that condition I implies both condition II and III.

2.2.2 Group Action

The map $\alpha : \mathcal{G} \times S \to S$ is a group action[6] of the group $\mathcal{G}$ on the set S, if α obeys,[7]

I $\alpha\left(gg', s\right) = \alpha\left(g, \alpha\left(g', s\right)\right), \quad \forall \quad g, g' \in \mathcal{G} \quad \wedge \quad \forall \quad s \in S,$

II $\alpha\left(\mathbb{1}, s\right) = s, \quad \forall \quad s \in S.$

We can restate this in terms of homomorphisms. Then α is an action of a group $\mathcal{G}$ on a set S, if α is a homomorphism from $\mathcal{G}$ to the symmetric group of S:

$$\alpha : \mathcal{G} \to \mathrm{Sym}\left(S\right). \tag{2.33}$$

2.2.3 One-Cocycle

Having defined homomorphisms and actions of groups, we are ready to define one-cocycles.[8] A one-cocycle ω of a group $\mathcal{G}$ is a function from the $\mathcal{G}$ to an associated Abelian group $\mathcal{A}$:

$$\omega : \mathcal{G} \to \mathcal{A}. \tag{2.34}$$

The one-cocycle is defined through a group action α of the group $\mathcal{G}$ onto the Abelian group $\mathcal{A}$. In other words, α is a homomorphism from the original group $\mathcal{G}$ to the automorphism group of the Abelian group $\mathcal{A}$:

$$\alpha : \mathcal{G} \to \mathrm{Aut}\left(\mathcal{A}\right). \tag{2.35}$$

For ω to be a one-cocycle, it must satisfy the one-cocycle condition

$$\omega\left(gg'\right) = \omega\left(g\right) \cdot \left(\alpha\left(g, \omega\left(g'\right)\right)\right). \tag{2.36}$$

One-cocycles are closely related to the Abelianization of a group. For a trivial action on the set, that is $\alpha\left(g, s\right) \equiv s$, all elements of $[\mathcal{G}, \mathcal{G}]$ have a trivial cocycle of 1.[9] In this case the one-cocycle condition reduces to $\omega\left(gg'\right) = \omega\left(g\right)\omega\left(g'\right)$, and the one-cocycle is effectively a homomorphism from the Abelianization of $\mathcal{G}$ to the Abelian group $\mathcal{A}$, $\omega : \mathcal{G}/\left[\mathcal{G}, \mathcal{G}\right] \to \mathcal{A}$.

[6] This is also known as the "group action on the left", since the group element g is acting from the left. An analogous definition exists for the "group action on the right".

[7] Condition I implies II.

[8] As the name suggests, one-cocycles are special cases of a larger class of n-cocycles. These will not be playing a role in this thesis, and are not discussed here. The interested reader is referred to e.g. [105].

[9] To see this, consider the one-cocycle of a group element obtained as a commutator between two other group elements, $U_{[U_1,U_2]} = U_1U_2U_1^{-1}U_2^{-1}$. This gives a one-cocycle $\omega\left(U_{[U_1,U_2]}\right) = \omega\left(U_1U_2U_1^{-1}U_2^{-1}\right) = \omega\left(U_1\right)\omega\left(U_2\right)\omega\left(U_1^{-1}\right)\omega\left(U_2^{-1}\right) = 1$.

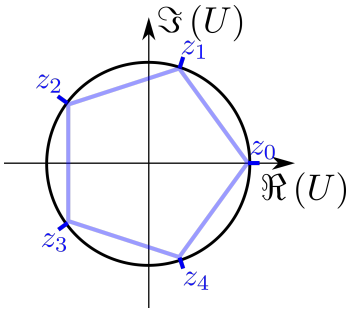

Figure 2.1: *Visualization of the group* $U(1)$ *(unit circle), and the discrete subgroup* $Z\,(k=5) \subset U\,(1)$ *(pentagon).*

2.3 Specific Groups and Subgroups

2.3.1 Group $U\,(n)$

$U\,(n)$ is the group of all $n \times n$ unitary complex matrices

$$UU^{\dagger} = U^{\dagger}U = \mathbb{1}_{n\times n}, \qquad \Rightarrow \qquad |\det(U)| = 1. \tag{2.37}$$

It is closed under multiplication:

$$\left(U_i U_j\right)^{\dagger}\left(U_i U_j\right) = U_j U_i^{\dagger} U_i U_j = \mathbb{1}, \quad \forall \quad U_i, U_j \in U\,(n)\,, \tag{2.38}$$

and contains the identity element as the $n \times n$ unit matrix, $\mathbb{1}_{n\times n}$. The associative law follows from matrix multiplication. The existence of the inverse element follows from the definition of a unitary matrix.

The special case of $U\,(1)$ is the set of all complex numbers with magnitude 1. This is a continuous Lie group, with a single Lie algebra generator. The group elements can be parametrized by a single parameter θ:

$$U\,(\theta) = e^{i\theta} \in U\,(1)\,, \quad \theta \in [0; 2\pi[\,. \tag{2.39}$$

We illustrate this in Figure 2.1. Here the group elements of $U\,(1)$ are illustrated by a unit circle in the complex plane. With a single generator, the Lie algebra is trivial, and the group is Abelian.

The Discrete Cyclic Subgroup $\mathbb{Z}\,(k) \subset U\,(1)$

The cyclic group $\mathbb{Z}\,(k)$ is a discrete finite subgroup of $U\,(1)$, and consists of the kth roots of unity:

$$\mathbb{Z}\,(k) \equiv \left\{ z_n = \exp\left(\frac{2\pi n}{k} i\right), n \in \{0, 1, \ldots, k-1\} \right\}. \tag{2.40}$$

We illustrate this, for the case of $\mathbb{Z}\,(k=5)$, in Figure 2.1. The elements of $\mathbb{Z}(5)$ are represented by the corners of the blue pentagon. Working with $\mathbb{Z}(k)$, it is convenient to define the short-hand notation

$$[n]_k \equiv n \mod k. \tag{2.41}$$

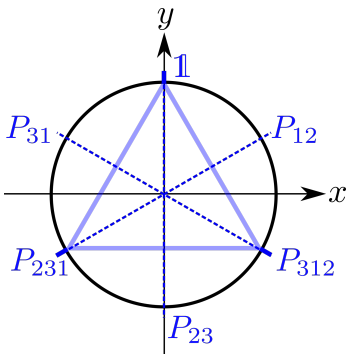

Figure 2.2: *Visualization of the group $O(2)$ and the discrete subgroup S_3. The continuous rotations of $O(2)$ are marked as a black circle, and the $O(2)$ reflections are omitted. The three discrete rotations of S_3 are marked by the edges of the blue triangle, and the three reflections are marked by dashed blue lines.*

Since $\mathbb{Z}(k)$ is closed under multiplication,

$$z_n z_m = z_{[n+m]_k} \in \mathbb{Z}(k), \tag{2.42}$$

it follows trivially from the group properties of $U(1)$, that $\mathbb{Z}(k)$ constitutes a sub-group. $\mathbb{Z}(k)$ is Abelian and therefore contains k conjugacy classes, which implies that there are k 1-dimensional irreducible representations,

$$\Gamma_p(z_n) = (z_n)^{p-1} = \exp\left(\frac{2\pi(p-1)n}{k} i\right) = z_{[(p-1)n]_k}. \tag{2.43}$$

2.3.2 Continuous Group $O(n)$

$O(n)$ is the continuous subgroup of $U(n)$, that contains all real $n \times n$ orthogonal matrices O,

$$O^T O = O O^T = \mathbb{1}_{n\times n}, \quad \forall \quad O \in O(n) \qquad \Rightarrow \qquad \det(O) = \pm 1. \tag{2.44}$$

These matrices describe all distance preserving transformations in an n-dimensional Euclidean space. For the special case of $O(2)$ these are rotations around the origin, and reflections along an axis through the origin. This is illustrated in Figure 2.2. Here rotations in two Euclidean dimensions are illustrated by a circle The reflections along an arbitrary axis through the origin are omitted in the figure.

$SO(n)$ is the continuous subgroup of $O(n)$ that excludes reflections. It can be shown that the groups $SO(2N)$, and $SO(2N+1)$ are of ranks $2N^2-N$, and $2N^2+N$, respectively. Since $O(N)$ and $SO(N)$ are only distinguished by the exclusion of the "large" improper transformations, with $\det(O) = -1$, the two groups are locally identical, and share the same Lie algebra.

The group $SO(3)$ has three infinitesimal generators of rotations around the x-, y-, and z-axis,

	$\mathbb{1}$	P_{12}	P_{23}	P_{31}	P_{231}	P_{312}
$\mathbb{1}$	$\mathbb{1}$	P_{12}	P_{23}	P_{31}	P_{231}	P_{312}
P_{12}	P_{12}	$\mathbb{1}$	P_{312}	P_{231}	P_{31}	P_{23}
P_{23}	P_{23}	P_{231}	$\mathbb{1}$	P_{312}	P_{12}	P_{31}
P_{31}	P_{31}	P_{312}	P_{231}	$\mathbb{1}$	P_{23}	P_{12}
P_{231}	P_{231}	P_{23}	P_{31}	P_{12}	P_{312}	$\mathbb{1}$
P_{312}	P_{312}	P_{31}	P_{12}	P_{23}	$\mathbb{1}$	P_{231}

Table 2.1: *Cayley table of* S_3.

respectively

$$T_1 = \begin{pmatrix} 0 & 0 & 0 \\ 0 & 0 & 1 \\ 0 & -1 & 0 \end{pmatrix}, \qquad T_2 = \begin{pmatrix} 0 & 0 & -1 \\ 0 & 0 & 0 \\ 1 & 0 & 0 \end{pmatrix}, \qquad T_3 = \begin{pmatrix} 0 & 1 & 0 \\ -1 & 0 & 0 \\ 0 & 0 & 0 \end{pmatrix}. \tag{2.45}$$

From these generators, we obtain the $so(3)$ Lie algebra

$$\left[T_i, T_j\right] = -\epsilon_{ijk} T_k. \tag{2.46}$$

The center of $SO(3)$ is trivial: $Z(SO(3)) = \left\{\mathbb{1}\right\}$.

The discrete subgroup $S_3 \subset O(2)$

S_3 is the group of all permutations of three objects. It is a discrete subgroup of $O(2)$. The elements of S_3 are rotations through angles which are multiples of $2\pi/3$ and reflections through the corresponding directions. We illustrate this in Figure 2.2. The three rotations are illustrated by the edges of the blue triangle, and the three axes of reflection are illustrated by dashed blue lines. The three rotations correspond to the identity $\mathbb{1}$, and the two cyclic permutations P_{231}. and P_{312}. The three reflections correspond to the three pair permutation elements P_{12}, P_{23}, and P_{31}. The Cayley table of S_3 is shown in Table 2.1. S_3 is a non-Abelian group with three conjugacy classes,

$$\mathcal{C}_1 = \{\mathbb{1}\}, \qquad \mathcal{C}_2 = \left\{P_{12}, P_{23}, P_{31}\right\}, \qquad \mathcal{C}_3 = \left\{P_{231}, P_{312}\right\}, \tag{2.47}$$

and a trivial center $Z\left(S_3\right) = \mathbb{1}$.

We identify the commutator subgroup as $\left[S_3, S_3\right] = \left\{\mathbb{1}, P_{231}, P_{312}\right\} = \mathcal{C}_1 \cup \mathcal{C}_3 \equiv \mathcal{C}_{13}$, which is isomorphic to $\mathbb{Z}(3)$. By identifying elements of S_3 that are related by multiplication with an element in $\mathcal{C}_{13}$, we obtain the multiplications table for the Abelianization of S_3. This is shown in Table 2.2. Here $\mathcal{C}_{13}$ and $\mathcal{C}_2$ each plays the role of a single element in $S_3/\left[S_3, S_3\right]$. Thus we we identify $S_3/\left[S_3, S_3\right] \cong \mathbb{Z}(2)$.

S_3 contains three conjugacy classes, and hence three irreducible representations. From equation (2.16) two of these must be 1-dimensional irreducible representations. These are the fully symmetric, and the fully antisymmetric representations, denoted by Γ_1 and Γ_2, respectively. The last representation is the 2-dimensional mixed representation Γ_3. The character table for the three irreducible representations is presented in Table 2.3. The product rules for the irreducible representations are presented in Table 2.4.

	$\mathcal{C}_{13}$	$\mathcal{C}_2$
$\mathcal{C}_{13}$	$\mathcal{C}_{13}$	$\mathcal{C}_2$
$\mathcal{C}_2$	$\mathcal{C}_2$	$\mathcal{C}_{13}$

Table 2.2: *Cayley table of $S_3/[S_3, S_3]$. $\mathcal{C}_{13}$, and $\mathcal{C}_2$ each plays the role of a single group element.*

	$\mathcal{C}_1$	$\mathcal{C}_2$	$\mathcal{C}_3$
χ_{Γ_1}	1	1	1
χ_{Γ_2}	1	-1	1
χ_{Γ_3}	2	0	-1

Table 2.3: *Character table for the three irreducible representations of S_3.*

2.3.3 Group $SU(n)$

The special unitary group $SU(n)$ is the continuous sub-group of $U(n)$ excluding improper transformations. That is, the group of unitary $N \times N$ matrices U for which $\det(U) = 1$. The groups $SU(2)$ and $SU(3)$ play a special role in QFT. Both groups are non-Abelian Lie groups. $SU(2)$ has rank 3, and the three infinitesimal generators can be chosen as $T_i = \frac{1}{2}\sigma_i$. Here σ_i are the Pauli matrices

$$\sigma_1 = \begin{pmatrix} 0 & 1 \\ 1 & 0 \end{pmatrix}, \qquad \sigma_2 = \begin{pmatrix} 0 & -i \\ i & 0 \end{pmatrix}, \qquad \sigma_3 = \begin{pmatrix} 1 & 0 \\ 0 & -1 \end{pmatrix}. \tag{2.48}$$

This gives an $su(2)$ Lie algebra

$$\left[T_i, T_j\right] = i\epsilon_{ijk}T_k, \tag{2.49}$$

isomorphic to the $so(3)$ Lie algebra of eq. (2.46). The two groups are closely related, and are locally, but not globally, identical. In contrast to $SO(3)$, $SU(2)$ has the non-trivial center of $Z(SU(2)) = \left\{-\mathbb{1}, \mathbb{1}\right\}$. In fact, it turns out that the two groups are related by a map from $SU(2)$ to $SO(3)$. Elements of $SU(2)$, that are related by transformations in the center, are mapped to the same $SO(3)$ element. In other words, $SO(3)$ is insensitive to the center of $SU(2)$. All representations of $SU(2)$ are real or pseudo-real. For later convenience we emphasize that elements of $SU(2)$ can be parametrized in terms of four parameters U^μ, that are restrained to lie on the unit sphere S^3:

$$U = U^0\mathbb{1}_{2\times 2} + iU^i\sigma_i, \quad U^0U^0 + U^iU^i = 1. \tag{2.50}$$

	Γ_1	Γ_2	Γ_3
Γ_1	Γ_1	Γ_2	Γ_3
Γ_2	Γ_2	Γ_1	Γ_3
Γ_3	Γ_3	Γ_3	$\Gamma_{3\otimes 3}$

Table 2.4: *Product rules for the irreducible representations of S_3. $\Gamma_{3\otimes 3}$ is given by $\Gamma_1 \oplus \Gamma_2 \oplus \Gamma_3$.*

	$\mathbb{1}$	$-\mathbb{1}$	$i\sigma_1$	$-i\sigma_1$	$i\sigma_2$	$-i\sigma_2$	$i\sigma_3$	$-i\sigma_3$
$\mathbb{1}$	$\mathbb{1}$	$-\mathbb{1}$	$i\sigma_1$	$-i\sigma_1$	$i\sigma_2$	$-i\sigma_2$	$i\sigma_3$	$-i\sigma_3$
$-\mathbb{1}$	$-\mathbb{1}$	$\mathbb{1}$	$-i\sigma_1$	$i\sigma_1$	$-i\sigma_2$	$i\sigma_2$	$-i\sigma_3$	$i\sigma_3$
$i\sigma_1$	$i\sigma_1$	$-i\sigma_1$	$-\mathbb{1}$	$\mathbb{1}$	$-i\sigma_3$	$i\sigma_3$	$i\sigma_2$	$-i\sigma_2$
$-i\sigma_1$	$-i\sigma_1$	$i\sigma_1$	$\mathbb{1}$	$-\mathbb{1}$	$i\sigma_3$	$-i\sigma_3$	$-i\sigma_2$	$i\sigma_2$
$i\sigma_2$	$i\sigma_2$	$-i\sigma_2$	$i\sigma_3$	$-i\sigma_3$	$-\mathbb{1}$	$\mathbb{1}$	$-i\sigma_1$	$i\sigma_1$
$-i\sigma_2$	$-i\sigma_2$	$i\sigma_2$	$-i\sigma_3$	$i\sigma_3$	$\mathbb{1}$	$-\mathbb{1}$	$i\sigma_1$	$-i\sigma_1$
$i\sigma_3$	$i\sigma_3$	$-i\sigma_3$	$-i\sigma_2$	$i\sigma_2$	$i\sigma_1$	$-i\sigma_1$	$-\mathbb{1}$	$\mathbb{1}$
$-i\sigma_3$	$-i\sigma_3$	$i\sigma_3$	$i\sigma_2$	$-i\sigma_2$	$-i\sigma_1$	$i\sigma_1$	$\mathbb{1}$	$-\mathbb{1}$

Table 2.5: *Cayley table of* $\bar{D}_2$.

$SU(3)$ is of rank 8, and the eight infinitesimal generators can be chosen as $T_a = \frac{1}{2}\lambda_a$. Here λ_a are the Gell-Mann matrices,

$$\lambda_1 = \begin{pmatrix} 0 & 1 & 0 \\ 1 & 0 & 0 \\ 0 & 0 & 0 \end{pmatrix}, \qquad \lambda_2 = \begin{pmatrix} 0 & -i & 0 \\ i & 0 & 0 \\ 0 & 0 & 0 \end{pmatrix}, \qquad \lambda_3 = \begin{pmatrix} 1 & 0 & 0 \\ 0 & -1 & 0 \\ 0 & 0 & 0 \end{pmatrix}, \tag{2.51}$$

$$\lambda_4 = \begin{pmatrix} 0 & 0 & 1 \\ 0 & 0 & 0 \\ 1 & 0 & 0 \end{pmatrix}, \qquad \lambda_5 = \begin{pmatrix} 0 & 0 & -i \\ 0 & 0 & 0 \\ i & 0 & 0 \end{pmatrix}, \qquad \lambda_6 = \begin{pmatrix} 0 & 0 & 0 \\ 0 & 0 & 1 \\ 0 & 1 & 0 \end{pmatrix},$$

$$\lambda_7 = \begin{pmatrix} 0 & 0 & 0 \\ 0 & 0 & -i \\ 0 & i & 0 \end{pmatrix}, \qquad \lambda_8 = \frac{1}{\sqrt{3}} \begin{pmatrix} 1 & 0 & 0 \\ 0 & 1 & 0 \\ 0 & 0 & -2 \end{pmatrix}.$$

This gives the $su(3)$ Lie algebra of

$$\left[T_a, T_b\right] = i f_{abc} T_c, \quad f_{abc} = -\frac{i}{4} \mathrm{Tr}\left(\left[\lambda_a, \lambda_b\right] \lambda_c\right). \tag{2.52}$$

The center of $SU(3)$ is $Z(SU(3)) = \left\{\mathbb{1}_{3\times3}, z\mathbb{1}_{3\times3}, z^*\mathbb{1}_{3\times3}\right\} = \mathbb{Z}(3)$ where $z \equiv e^{\frac{2\pi}{3}i}$. In contrast to $SU(2)$, some representations of $SU(3)$ are complex.

The Binary Dihedral Discrete Subgroup $\bar{D}_2 \subset SU(2)$

The binary dihedral group $\bar{D}_2$ is an eight element discrete finite subgroup of $SU(2)$, and shares several of its properties. Both groups are non-Abelian, both have the same center, and both groups have a 2-dimensional pseudo real irreducible representation. We define, and represent, $\bar{D}_2$ in terms of the three Pauli matrices σ_i, and the 2×2 unit matrix $\mathbb{1}$:

$$\bar{D}_2 = \left\{\mathbb{1}, -\mathbb{1}, i\sigma_1, -i\sigma_1, i\sigma_2, -i\sigma_2, i\sigma_3, -i\sigma_3\right\}. \tag{2.53}$$

The Cayley table of $\bar{D}_2$ is shown in Table 2.5. From this table, we identify the center as $Z(\bar{D}_2) = \left\{\mathbb{1}, -\mathbb{1}\right\} = \mathbb{Z}(2)$. We see that $\bar{D}_2$ has five conjugacy classes,

$$C_1 = \left\{\mathbb{1}\right\}, \quad C_2 = \left\{-\mathbb{1}\right\}, \quad C_3 = \left\{i\sigma_1, -i\sigma_1\right\}, \quad C_4 = \left\{i\sigma_2, -i\sigma_2\right\}, \quad C_5 = \left\{i\sigma_3, -i\sigma_3\right\}. \tag{2.54}$$

	$\mathcal{C}_{12}$	$\mathcal{C}_3$	$\mathcal{C}_4$	$\mathcal{C}_5$
$\mathcal{C}_{12}$	$\mathcal{C}_{12}$	$\mathcal{C}_3$	$\mathcal{C}_4$	$\mathcal{C}_5$
$\mathcal{C}_3$	$\mathcal{C}_3$	$\mathcal{C}_{12}$	$\mathcal{C}_5$	$\mathcal{C}_4$
$\mathcal{C}_4$	$\mathcal{C}_4$	$\mathcal{C}_5$	$\mathcal{C}_{12}$	$\mathcal{C}_3$
$\mathcal{C}_5$	$\mathcal{C}_5$	$\mathcal{C}_4$	$\mathcal{C}_3$	$\mathcal{C}_{12}$

Table 2.6: *Cayley table of* $\bar{D}_2/\left[\bar{D}_2, \bar{D}_2\right]$. *Each of the conjugacy classes* $\mathcal{C}_3$ *to* $\mathcal{C}_5$*, and the commutator subgroup* $\mathcal{C}_{12}$*, plays the role of a single group element.*

	$\mathcal{C}_1$	$\mathcal{C}_2$	$\mathcal{C}_3$	$\mathcal{C}_4$	$\mathcal{C}_5$
χ_{Γ_1}	1	1	1	1	1
χ_{Γ_2}	1	1	1	−1	−1
χ_{Γ_3}	1	1	−1	1	−1
χ_{Γ_4}	1	1	−1	−1	1
χ_{Γ_5}	2	−2	0	0	0

Table 2.7: *Character table of* $\bar{D}_2$.

The commutator subgroup of $\bar{D}_2$ is $\left[\bar{D}_2, \bar{D}_2\right] = \left\{\mathbb{1}, -\mathbb{1}\right\} = \mathcal{C}_1 \cup \mathcal{C}_2 \equiv \mathcal{C}_{12}$, which is isomorphic to $\mathbb{Z}(2)$. By identifying elements in $\bar{D}_2$ that are related by multiplication of elements in the commutator subgroup, we obtain the Cayley table for the Abelianization of $\bar{D}_2$. This is presented in Table 2.6. Here $\mathcal{C}_{12}$, $\mathcal{C}_3$, $\mathcal{C}_4$ and $\mathcal{C}_5$ each plays the role of a single element. From this we find that $\bar{D}_2/\left[\bar{D}_2, \bar{D}_2\right] \cong \mathbb{Z}(2) \times \mathbb{Z}(2)$. $\bar{D}_2$ has five irreducible representations. These are four 1-dimensional representations Γ_1 to Γ_4, and a single 2-dimensional representation Γ_5. In the 2-dimensional representation the elements are represented by the matrices in eq. (2.53). The 1-dimensional representations are all real, and the 2-dimensional representation is pseudo-real. This is analogue to the entire group $SU(2)$ where all representations are real or pseudo-real. The character table of $\bar{D}_2$ is presented in Table 2.7. The 1-dimensional representations all have trivial centers with a trivial duality. The 2-dimensional representation has a non-trivial duality, with a negative sign for the character of $\Gamma_5\left(\mathcal{C}_2\right)$. Applying eq. (2.27) and (2.28), we obtain the rules for products of irreducible representations. These are presented in Table 2.8.

	Γ_1	Γ_2	Γ_3	Γ_4	Γ_5
Γ_1	Γ_1	Γ_2	Γ_3	Γ_4	Γ_5
Γ_2	Γ_2	Γ_1	Γ_4	Γ_3	Γ_5
Γ_3	Γ_3	Γ_4	Γ_1	Γ_2	Γ_5
Γ_4	Γ_4	Γ_3	Γ_2	Γ_1	Γ_5
Γ_5	Γ_5	Γ_5	Γ_5	Γ_5	$\Gamma_{5\otimes5}$

Table 2.8: *Product rules for the irreducible representations of* $\bar{D}_2$*, where* $\Gamma_{5\otimes5} = \Gamma_1 \oplus \Gamma_2 \oplus \Gamma_3 \oplus \Gamma_4$.

	$D(c,d)$	$U(c,d)$	$L(c,d)$
$D(a,b)$	$D(ac,bd)$	$U(ac,bd)$	$L(bc,a^*b^*d)$
$U(a,b)$	$U(ad,bc^*d^*)$	$L(bc^*d^*,a^*b^*c)$	$D(ac,bd)$
$L(a,b)$	$L(ac,bd)$	$D(a^*b^*c^*d^*,ac)$	$U(a^*b^*d,ac^*d^*)$

Table 2.9: *Cayley table of* $\Delta(27)$. *Here a, b, c and d each take any value in* $\{1, z, z^*\}$.

The Discrete Subgroup $\Delta(27) \subset SU(3)$

$\Delta(27)$ is a 27-element discrete finite subgroup of $SU(3)$, that shares several of its properties. Both groups are non-Abelian, both have the same center, and both have two complex 3-dimensional irreducible representations. We define, and represent, the 27 elements of $\Delta(27)$ in terms of three sets of 3×3 matrices

$$D(a,b) = \begin{pmatrix} a & 0 & 0 \\ 0 & b & 0 \\ 0 & 0 & a^*b^* \end{pmatrix}, \quad U(a,b) = \begin{pmatrix} 0 & a & 0 \\ 0 & 0 & b \\ a^*b^* & 0 & 0 \end{pmatrix}, \quad L(a,b) = \begin{pmatrix} 0 & 0 & a^*b^* \\ a & 0 & 0 \\ 0 & 0 & b \end{pmatrix}, \tag{2.55}$$

where a and b each take values in $\{1, z, z^*\}$, with $z \equiv e^{\frac{2\pi}{3}i}$.

$$\Delta(27) = \left\{ D(a,b), U(a,b), L(a,b) \mid a,b \in \left\{1, z, z^*\right\} \right\}. \tag{2.56}$$

The Cayley table for $\Delta(27)$ is summarized in terms of D, U, and L, in Table 2.9 From here we identify the center,

$$Z(\Delta(27)) = \left\{ D(1,1), D(z,z), D\left(z^*,z^*\right) \right\} = \left\{ \mathbb{1}_{3\times3}, z\mathbb{1}_{3\times3}, z^*\mathbb{1}_{3\times3} \right\} = \mathbb{Z}(3), \tag{2.57}$$

which is identical to the center of $SU(3)$. We find 11 conjugacy classes

$$\begin{aligned}
C_1 &= \left\{\mathbb{1}_{3\times3}\right\} = \overline{C}_1, \\
C_2 &= \left\{z\mathbb{1}_{3\times3}\right\} = \overline{C}_3, \\
C_3 &= \left\{z^*\mathbb{1}_{3\times3}\right\} = \overline{C}_2, \\
C_4 &= \left\{D(1,z), D\left(z,z^*\right), D\left(z^*,1\right)\right\} = \overline{C}_5, \\
C_5 &= \left\{D\left(1,z^*\right), D\left(z^*,z\right), D(z,1)\right\} = \overline{C}_4, \\
C_6 &= \left\{U(1,1), U(z,z), U\left(z^*,z^*\right)\right\} = \overline{C}_6, \\
C_7 &= \left\{U(1,z), U\left(z,z^*\right), U\left(z^*,1\right)\right\} = \overline{C}_8, \\
C_8 &= \left\{U\left(1,z^*\right), U\left(z^*,z\right), U(z,1)\right\} = \overline{C}_7, \\
C_9 &= \left\{L(1,1), L(z,z), L\left(z^*,z^*\right)\right\} = \overline{C}_9, \\
C_{10} &= \left\{L(1,z), L\left(z,z^*\right), L\left(z^*,1\right)\right\} = \overline{C}_{11}, \\
C_{11} &= \left\{L\left(1,z^*\right), L\left(z^*,z\right), L(z,1)\right\} = \overline{C}_{10}.
\end{aligned} \tag{2.58}$$

The conjugacy classes are matched in pairs by complex conjugation. The commutator subgroup is given by $[\Delta(27), \Delta(27)] = \left\{\mathbb{1}, z\mathbb{1}, z^*\mathbb{1}\right\} = C_1 \cup C_2 \cup C_3 \equiv C_{123}$ which is isomorphic to $\mathbb{Z}(3)$. By

	$\mathcal{C}_{123}$	$\mathcal{C}_4$	$\mathcal{C}_5$	$\mathcal{C}_6$	$\mathcal{C}_7$	$\mathcal{C}_8$	$\mathcal{C}_9$	$\mathcal{C}_{10}$	$\mathcal{C}_{11}$
$\mathcal{C}_{123}$	$\mathcal{C}_{123}$	$\mathcal{C}_4$	$\mathcal{C}_5$	$\mathcal{C}_6$	$\mathcal{C}_7$	$\mathcal{C}_8$	$\mathcal{C}_9$	$\mathcal{C}_{10}$	$\mathcal{C}_{11}$
$\mathcal{C}_4$	$\mathcal{C}_4$	$\mathcal{C}_5$	$\mathcal{C}_{123}$	$\mathcal{C}_7$	$\mathcal{C}_8$	$\mathcal{C}_6$	$\mathcal{C}_{10}$	$\mathcal{C}_{11}$	$\mathcal{C}_9$
$\mathcal{C}_5$	$\mathcal{C}_5$	$\mathcal{C}_{123}$	$\mathcal{C}_4$	$\mathcal{C}_8$	$\mathcal{C}_6$	$\mathcal{C}_7$	$\mathcal{C}_{11}$	$\mathcal{C}_9$	$\mathcal{C}_{10}$
$\mathcal{C}_6$	$\mathcal{C}_6$	$\mathcal{C}_7$	$\mathcal{C}_8$	$\mathcal{C}_9$	$\mathcal{C}_{10}$	$\mathcal{C}_{11}$	$\mathcal{C}_{123}$	$\mathcal{C}_4$	$\mathcal{C}_5$
$\mathcal{C}_7$	$\mathcal{C}_7$	$\mathcal{C}_8$	$\mathcal{C}_6$	$\mathcal{C}_{10}$	$\mathcal{C}_{11}$	$\mathcal{C}_9$	$\mathcal{C}_4$	$\mathcal{C}_5$	$\mathcal{C}_{123}$
$\mathcal{C}_8$	$\mathcal{C}_8$	$\mathcal{C}_6$	$\mathcal{C}_7$	$\mathcal{C}_{11}$	$\mathcal{C}_9$	$\mathcal{C}_{10}$	$\mathcal{C}_5$	$\mathcal{C}_{123}$	$\mathcal{C}_4$
$\mathcal{C}_9$	$\mathcal{C}_9$	$\mathcal{C}_{10}$	$\mathcal{C}_{11}$	$\mathcal{C}_{123}$	$\mathcal{C}_4$	$\mathcal{C}_5$	$\mathcal{C}_6$	$\mathcal{C}_7$	$\mathcal{C}_8$
$\mathcal{C}_{10}$	$\mathcal{C}_{10}$	$\mathcal{C}_{11}$	$\mathcal{C}_9$	$\mathcal{C}_4$	$\mathcal{C}_5$	$\mathcal{C}_{123}$	$\mathcal{C}_7$	$\mathcal{C}_8$	$\mathcal{C}_6$
$\mathcal{C}_{11}$	$\mathcal{C}_{11}$	$\mathcal{C}_9$	$\mathcal{C}_{10}$	$\mathcal{C}_5$	$\mathcal{C}_{123}$	$\mathcal{C}_4$	$\mathcal{C}_8$	$\mathcal{C}_6$	$\mathcal{C}_7$

Table 2.10: *Multiplication table of* $\Delta(27) \,/\, [\Delta(27), \Delta(27)]$. *Each of the conjugacy classes* $\mathcal{C}_4$ *to* $\mathcal{C}_{11}$ *together with the commutator subgroup* $\mathcal{C}_{123}$ *plays the role of a single element.*

	$\mathcal{C}_1$	$\mathcal{C}_2$	$\mathcal{C}_3$	$\mathcal{C}_4$	$\mathcal{C}_5$	$\mathcal{C}_6$	$\mathcal{C}_7$	$\mathcal{C}_8$	$\mathcal{C}_9$	$\mathcal{C}_{10}$	$\mathcal{C}_{11}$
$\chi_{\Gamma_1} = \chi^*_{\Gamma_1}$	1	1	1	1	1	1	1	1	1	1	1
$\chi_{\Gamma_2} = \chi^*_{\Gamma_3}$	1	1	1	1	1	z	z	z	z^*	z^*	z^*
$\chi_{\Gamma_3} = \chi^*_{\Gamma_2}$	1	1	1	1	1	z^*	z^*	z^*	z	z	z
$\chi_{\Gamma_4} = \chi^*_{\Gamma_7}$	1	1	1	z	z^*	1	z	z^*	1	z	z^*
$\chi_{\Gamma_5} = \chi^*_{\Gamma_9}$	1	1	1	z	z^*	z	z^*	1	z^*	1	z
$\chi_{\Gamma_6} = \chi^*_{\Gamma_8}$	1	1	1	z	z^*	z^*	1	z	z	z^*	1
$\chi_{\Gamma_7} = \chi^*_{\Gamma_4}$	1	1	1	z^*	z	1	z^*	z	1	z^*	z
$\chi_{\Gamma_8} = \chi^*_{\Gamma_6}$	1	1	1	z^*	z	z	1	z^*	z^*	z	1
$\chi_{\Gamma_9} = \chi^*_{\Gamma_5}$	1	1	1	z^*	z	z^*	z	1	z	1	z^*
$\chi_{\Gamma_{10}} = \chi^*_{\Gamma_{11}}$	3	$3z$	$3z^*$	0	0	0	0	0	0	0	0
$\chi_{\Gamma_{11}} = \chi^*_{\Gamma_{10}}$	3	$3z^*$	$3z$	0	0	0	0	0	0	0	0

Table 2.11: *Character table for* $\Delta(27)$.

identifying elements related through elements in $\mathcal{C}_{123}$, we obtain the Cayley table for the Abelianization of $\Delta(27)$. This is presented in Table 2.10. Each of the conjugacy classes $\mathcal{C}_4$ through $\mathcal{C}_{11}$, and the set $\mathcal{C}_{123}$ play the role of a single group element. There exists 11 irreducible representations of $\Delta(27)$. These are nine 1-dimensional representations Γ_1 to Γ_9, and two 3-dimensional representations Γ_{10} and Γ_{11}. Except for the trivial representation Γ_1, the 1-dimensional representations are all complex. They are matched in pairs by complex conjugation. The 3-dimensional representations are also complex, and are matched to each other by complex conjugation. Γ_{10} is given by the matrices in eq. (2.56), and Γ_{11} is given by the conjugation of the same matrices. The character table of $\Delta(27)$ is given in Table 2.11. Applying eq. (2.27) and (2.28) we obtain the rules for products of irreducible representations. These are presented in Table 2.12.

	Γ_1	Γ_2	Γ_3	Γ_4	Γ_5	Γ_6	Γ_7	Γ_8	Γ_9	Γ_{10}	Γ_{11}
Γ_1	Γ_1	Γ_2	Γ_3	Γ_4	Γ_5	Γ_6	Γ_7	Γ_8	Γ_9	Γ_{10}	Γ_{11}
Γ_2	Γ_2	Γ_3	Γ_1	Γ_5	Γ_6	Γ_4	Γ_8	Γ_9	Γ_7	Γ_{10}	Γ_{11}
Γ_3	Γ_3	Γ_1	Γ_2	Γ_6	Γ_4	Γ_5	Γ_9	Γ_7	Γ_8	Γ_{10}	Γ_{11}
Γ_4	Γ_4	Γ_5	Γ_6	Γ_7	Γ_8	Γ_9	Γ_1	Γ_2	Γ_3	Γ_{10}	Γ_{11}
Γ_5	Γ_5	Γ_6	Γ_4	Γ_8	Γ_9	Γ_7	Γ_2	Γ_3	Γ_1	Γ_{10}	Γ_{11}
Γ_6	Γ_6	Γ_4	Γ_5	Γ_9	Γ_7	Γ_8	Γ_3	Γ_1	Γ_2	Γ_{10}	Γ_{11}
Γ_7	Γ_7	Γ_8	Γ_9	Γ_1	Γ_2	Γ_3	Γ_4	Γ_5	Γ_6	Γ_{10}	Γ_{11}
Γ_8	Γ_8	Γ_9	Γ_7	Γ_2	Γ_3	Γ_1	Γ_5	Γ_6	Γ_4	Γ_{10}	Γ_{11}
Γ_9	Γ_9	Γ_7	Γ_8	Γ_3	Γ_1	Γ_2	Γ_6	Γ_4	Γ_5	Γ_{10}	Γ_{11}
Γ_{10}	Γ_{10}	Γ_{10}	Γ_{10}	Γ_{10}	Γ_{10}	Γ_{10}	Γ_{10}	Γ_{10}	Γ_{10}	$3\Gamma_{11}$	$\Gamma_{10\otimes 11}$
Γ_{11}	Γ_{11}	Γ_{11}	Γ_{11}	Γ_{11}	Γ_{11}	Γ_{11}	Γ_{11}	Γ_{11}	Γ_{11}	$\Gamma_{10\otimes 11}$	$3\Gamma_{10}$

Table 2.12: *Product table for the irreducible representations of* Δ (27). *The product of* Γ_{10} *and* Γ_{11} *is given by* $\Gamma_{10\otimes 11} = \Gamma_1 \oplus \Gamma_2 \oplus \Gamma_3 \oplus \Gamma_4 \oplus \Gamma_5 \oplus \Gamma_6 \oplus \Gamma_7 \oplus \Gamma_8 \oplus \Gamma_9$.

Part I

Quantum Link Model (QLM)

Chapter 3

$SU(2)$ Quantum Link Models

This chapter is organized as follows: In Section 3.1 we briefly review how a classical spin model can be quantized. This is used to construct an $SU(2)$-QLM in Section 3.2, by quantizing the corresponding Wilson-type lattice gauge theory in a similar manner. In Section 3.3 we introduce a rishon representation, in terms of fermionic degrees of freedom, which we use to construct a gauge-invariant site-based basis in Section 3.5. In this chapter we use the gauge-invariant site basis to construct the most general ring-exchange $SU(2)$ QLM Hamiltonian, which respects the lattice symmetries.

3.1 Quantization of Classical Spin Models

Let us consider the quantization of a classical $O(3)$ spin model, on a 2-dimensional square lattice Λ.[1] A classical 3-component spin-vector, namely a real-valued 3-component unit-vector $\vec{s}_x$, is placed at every lattice site $x \in \Lambda$. We illustrate this in Figure 3.1. The spin-vectors are represented by red arrows, lying on the S^2 unit-sphere, shown in black. A simple example of a concrete model, has a classical Hamilton function of the form

$$\mathcal{H}[\mathbf{s}] = J \sum_{x \in \Lambda} \sum_{i} \vec{s}_x \cdot \vec{s}_{x+\hat{\imath}}. \tag{3.1}$$

Here $\hat{\imath}$ denotes a lattice vector of length a (where a is the lattice spacing) in the direction i, and $\mathbf{s}$ denotes the spin configuration of the entire lattice. Neighbouring spins at $\vec{s}_x$ and $\vec{s}_{x+\hat{\imath}}$ are coupled, with a coupling constant J. For $J < 0$ neighbouring spins are energetically favoured to align, yielding ferromagnetism. For $J > 0$ neighbouring spins are energetically favoured to anti-align, yielding antiferromagnetism. Since the above Hamiltonian depends only on the relative spin between neighbouring lattice sites, the model has a global $O(3)$ symmetry. We are interested in the partition function

$$Z = \int \mathcal{D}\mathbf{s} \exp\left(-\beta \mathcal{H}[\mathbf{s}]\right). \tag{3.2}$$

[1] This model is also known as the classical Heisenberg model in 2-dimensions.

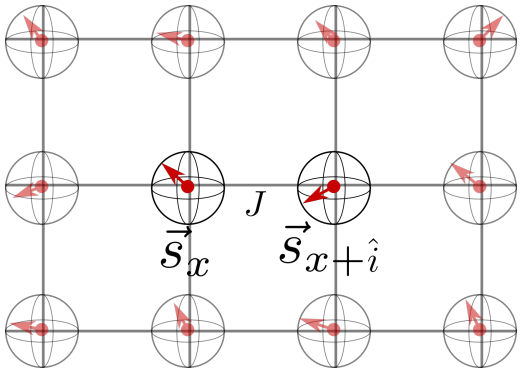

Figure 3.1: *Classical O* (3) *spin model on a 2-dimensional square lattice. Every lattice site* $x \in \Lambda$ *has an associated classical spin-vector* $\vec{s}_x$ *(red arrow), in the form of a 3-component vector restricted to the unit-sphere* S^2 *(black sphere).*

Here $\beta = T^{-1}$ is the inverse temperature of the system. To quantize the model, we promote the individual elements of the classical spin vector $\vec{s}_x$ from real-valued variables to quantum spin operators, that take their values in the Lie algebra of the symmetry group. We distinguish quantum operators from their classical counterparts by denoting them with upper case letters $\vec{S}_x$. For the classical O (3) model, we construct a corresponding quantum model by promoting the 3-component unit-vectors $\vec{s}_x$ to vectors of quantum operators, taking their values in the su (2) Lie algebra[2] [106],

$$\left[S_x^a, S_y^b\right] = \delta_{xy} i\epsilon^{abc} S_x^c. \tag{3.3}$$

The classical Hamilton function is similarly promoted to a quantum Hamiltonian operator, by replacing the classical spin $\vec{s}_x$ in eq. (3.1) by the quantum spin operators $\vec{S}_x$

$$\mathcal{H} = J \sum_{x\in\Lambda} \sum_i \vec{S}_x \cdot \vec{S}_{x+\hat{i}}. \tag{3.4}$$

From the commutation relations of eq. (3.3), it follows that the total spin

$$\vec{S} = \sum_{x\in\Lambda} \vec{S}_x, \tag{3.5}$$

is conserved

$$\left[\vec{S}, \mathcal{H}\right] = 0. \tag{3.6}$$

We obtain the quantum partition function by promoting the classical Hamilton function in eq. (3.2) to the corresponding quantum Hamilton operator of eq. (3.4). There is, however, a subtlety. Since the Hamiltonian is now a quantum operator, in contrast to a classical function, the integration over [**s**] is replaced by a trace over the Hilbert space

$$Z = \mathrm{Tr}\left(e^{-\beta\mathcal{H}}\right). \tag{3.7}$$

This Hilbert space is the direct product of the individual spin Hilbert spaces associated with lattice sites. Unlike the spin-vectors of the classical model, the quantum operators of the quantized model

[2] As was noted in Chapter 2 the Lie algebra of su (2) is isomorphic to the Lie algebra of both so (3) and o (3).

are non-commuting abstract objects, defined through the commutation relations in eq. (3.3). To evaluate the partition function, we first choose a representation for the quantum spin operators corresponding to $S = \frac{1}{2}, 1, \frac{3}{2}, \ldots$. The local Hilbert space on a single lattice site, and by extension the entire Hilbert space of the entire lattice, depends on the choice of representation. It is important to note that, for any choice of representation, the local Hilbert space is finite-dimensional.[3] We emphasize that, this is in contrast to the classical spin model, where each spin-vector is represented by continuous commuting variables. The quantum spin model can be realized with any choice of spin representation, satisfying the commutation relations of eq. (3.3). The simplest non-trivial representation of the quantum spin operators is the fundamental spin $1/2$ representation. Here the spin operators are represented in terms of Pauli matrices σ_a,

$$S^a = \frac{1}{2}\sigma_a, \tag{3.8}$$

and every lattice site has a 2-dimensional local Hilbert space. By coupling two fundamental representations to a triplet, we obtain the spin 1 representation (also known as the vector-representation). This representation has a 3-dimensional local Hilbert space at each lattice site and the quantum spin operators are given by

$$S_1^1 = \frac{1}{\sqrt{2}}\begin{pmatrix} 0 & 1 & 0 \\ 1 & 0 & 1 \\ 0 & 1 & 0 \end{pmatrix}, \qquad S_1^2 = \frac{1}{\sqrt{2}}\begin{pmatrix} 0 & -i & 0 \\ i & 0 & -i \\ 0 & i & 0 \end{pmatrix}, \qquad S_1^3 = \begin{pmatrix} 1 & 0 & 0 \\ 0 & 0 & 0 \\ 0 & 0 & -1 \end{pmatrix}. \tag{3.9}$$

Since the two models differ in the choice of representation, they have different physical properties [107, 108].

3.2 SU (2) QLM

Let us first review Wilson's formulation of SU (2) gauge theories. For concreteness let us consider the model on a square lattice Λ in 2 spatial dimensions. The theory can easily be generalized to other lattice geometries. We endow every link (x, i) with a link variable $u_{x,i} \in SU(2)$, that takes its value in the gauge group. Here (x, i) is the link connecting lattice site $x \in \Lambda$ with $x + \hat{i} \in \Lambda$. The $SU(2)$ link variables can be expanded in terms of Pauli-matrices τ_a as

$$u_{x,i} = u^0_{x,i} + iu^a_{x,i}\tau_a, \qquad\qquad u^0_{x,i}u^0_{x,i} + u^a_{x,i}u^a_{x,i} = 1 \quad \wedge \quad u^\rho_{x,i} \in \mathbb{R}. \tag{3.10}$$

Here we have introduced a second set of Pauli matrices τ_a. These are distinguished from σ_a by operating in a different space, $\left[\tau_a, \sigma_b\right] = 0$, but they are otherwise identical. In particular, τ_a is numerically identical to σ_a, as presented in eq. 2.48. In addition to the link variable, we introduce two sets of generators $\vec{L}_{x,i}$ and $\vec{R}_{x,i}$ to each link. These generators produce an $SU(2)_L \otimes SU(2)_R$ algebra on the link,

$$\left[L^a_{x,i}, L^b_{y,j}\right] = i\delta_{xy}\delta_{ij}\epsilon_{abc}L^c_{x,i}, \qquad \left[R^a_{x,i}, R^b_{y,j}\right] = i\delta_{xy}\delta_{ij}\epsilon_{abc}R^c_{x,i}, \qquad \left[L^a_{x,i}, R^b_{y,j}\right] = 0. \tag{3.11}$$

We refer to these as the left and right operators. This is illustrated in Figure 3.2 for a single link (x, i). The left and right operators transform the link variable u by

[3] It is still possible to choose a representation which gives rise to an arbitrarily large local Hilbert space.

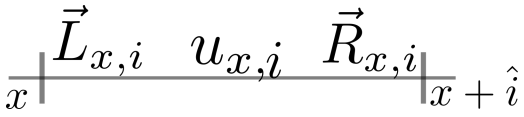

Figure 3.2: *Single link in the in the standard Wilson formulation of an SU (2) lattice gauge theory. Each link has a link variable $u_{x,i} \in SU$ (2) together with two sets of generators $\vec{L}_{x,i}$, and $\vec{R}_{x,i}$ that realize an $SU(2)_L \otimes SU(2)_R$ algebra on the link.*

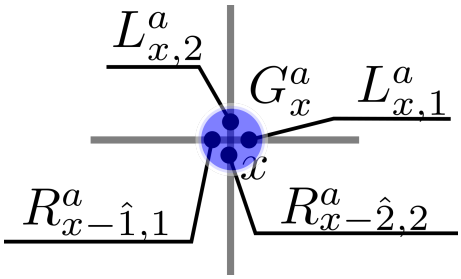

Figure 3.3: *Gauss' law on a site x is constructed from the left and right operators residing near the site.*

$$\left[L^a_{x,i}, u_{y,j}\right] = -\delta_{xy}\delta_{ij}\frac{\tau^a}{2}u_{y,j}, \qquad \left[R^a_{x,i}, u_{y,j}\right] = \delta_{xy}\delta_{ij}u_{y,j}\frac{\tau^a}{2}, \tag{3.12}$$
$$\left[L^a_{x,i}, u^\dagger_{y,j}\right] = \delta_{xy}\delta_{ij}u^\dagger_{y,j}\frac{\tau^a}{2}, \qquad \left[R^a_{x,i}, u^\dagger_{y,j}\right] = -\delta_{xy}\delta_{ij}\frac{\tau^a}{2}u^\dagger_{y,j}.$$

On a lattice site x, Gauss' law is constructed from the left and right operators residing near the site,

$$G^a_x \equiv \sum_i \left(L^a_{x,i} + R^a_{x-\hat{i},i}\right). \tag{3.13}$$

This is illustrated in Figure 3.3. For a state $\left|\Psi\right\rangle$ to be physical, it must satisfy Gauss' law at every lattice site,

$$G^a_x\left|\Psi\right\rangle = 0, \quad \forall \quad x \in \Lambda. \tag{3.14}$$

Eqs. (3.11) and (3.12) implies that

$$\left[G_x, \mathrm{Tr}\left(u_{\square_{x,i,j}}\right)\right] = 0, \qquad \left[G_x, \vec{L}^2_{x,i}\right] = 0, \qquad \left[G_x, \vec{R}^2_{x,i}\right] = 0. \tag{3.15}$$

Here we have defined the elementary plaquette variable $u_{\square_{x,i,j}}$ on the square lattice as the loop around four links (see Figure 3.4).

$$u_{\square_{x,i,j}} \equiv u_{x,i}u_{x+\hat{i},j}u^\dagger_{x+\hat{j},i}u^\dagger_{x,j}. \tag{3.16}$$

We can thereby construct the gauge-invariant Hamiltonian

$$\mathcal{H} = J^{-1}\sum_{x,i}\mathcal{H}_{E_{x,i}} + J\sum_{\square_{x,i,j}}\mathcal{H}_{\square_{x,i,j}}, \tag{3.17}$$
$$\mathcal{H}_{E_{x,i}} \equiv \left(\vec{L}^2_{x,i} + \vec{R}^2_{x,i}\right),$$
$$\mathcal{H}_{\square_{x,i,j}} \equiv \mathrm{Tr}\left(u_{\square_{x,i,j}} + u^\dagger_{\square_{x,i,j}}\right).$$

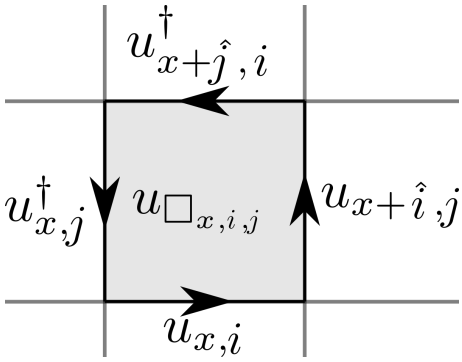

Figure 3.4: *Elementary lattice plaquette $u_{\square_{x,i,j}}$ in the standard Wilson formulation of an SU (2) lattice gauge theory on a 2-dimensional square lattice.*

Here we have introduced the electric Hamiltonian on a single link $\mathcal{H}_{E,i}$ and the magnetic Hamiltonian[4] on a plaquette $\mathcal{H}_{\square_{x,i,j}}$ together with a parameter J controlling the relative strength between the two contributions. These are summed over all links and all plaquettes, respectively, to make the full Hamiltonian invariant under translation and rotations on the lattice. In the Wilson formulation the link variables $u_{x,i}$ are matrices in SU (2) with c-number entries. We obtain the link algebra of eqs. (3.11) and (3.12) by parametrizing the link variable in terms of three variables α, θ, and ϕ, thereby removing the additional constraint of eq. (3.10),

$$u = \begin{pmatrix} \cos\alpha + i\sin\alpha\cos\theta & \sin\alpha\sin\theta\sin\phi + i\sin\alpha\sin\theta\cos\phi \\ -\sin\alpha\sin\theta\sin\phi + i\sin\alpha\sin\theta\cos\phi & \cos\alpha - i\sin\alpha\cos\theta \end{pmatrix}. \tag{3.18}$$

The left and right operators are then given in the form of (see e.g. [109]),

$$\vec{L} = \frac{1}{2}\begin{pmatrix} i\cos\phi\sin\theta\partial_\alpha + i\left(\sin\phi + \cos\phi\cot\alpha\cos\theta\right)\partial_\theta + i\left(\cot\theta\cos\phi - \sin\phi\frac{\cot\alpha}{\sin\theta}\right)\partial_\phi \\ i\sin\phi\sin\theta\partial_\alpha + i\left(\sin\phi\cot\alpha\cos\theta - \cos\phi\right)\partial_\theta + i\left(\sin\phi\cot\theta + \cos\phi\frac{\cot\alpha}{\sin\theta}\right)\partial_\phi \\ i\cos\theta\partial_\alpha - i\cot\alpha\sin\theta\partial_\theta - i\partial_\phi \end{pmatrix}, \tag{3.19}$$

$$\vec{R} = \frac{1}{2}\begin{pmatrix} -i\cos\phi\sin\theta\partial_\alpha + i\left(\sin\phi - \cos\phi\cot\alpha\cos\theta\right)\partial_\theta + i\left(\cot\theta\cos\phi + \sin\phi\frac{\cot\alpha}{\sin\theta}\right)\partial_\phi \\ -i\sin\phi\sin\theta\partial_\alpha - i\left(\cos\phi + \sin\phi\cot\alpha\cos\theta\right)\partial_\theta + i\left(\sin\phi\cot\theta - \cos\phi\frac{\cot\alpha}{\sin\theta}\right)\partial_\phi \\ -i\cos\theta\partial_\alpha + i\cot\alpha\sin\theta\partial_\theta - i\partial_\phi \end{pmatrix}.$$

Since the individual entries in the link variable matrix $u^{\rho}_{x,i}$ are c-numbered continuous variables, the single-link local Hilbert space is infinite-dimensional, and the individual elements of the link variables are commuting objects

$$\left[u^{\rho}_{x,i}, u^{\sigma}_{y,j}\right] = 0. \tag{3.20}$$

[4]The sums are conventionally taken over both the plaquette-variable $u_{\square_{x,i,j}}$ and the Hermitian conjugated plaquette-variable $u^{\dagger}_{\square_{x,i,j}}$. Since this is an $SU(2)$ gauge theory, this is of no importance here, but we have chosen to include both terms.

These are therefore intrinsically classical variables,[5] which are reminiscent of the classical spin-vectors discussed above.

In the QLM formulation, we realize the link algebra of eqs. (3.11) and (3.12) with a simpler finite local Hilbert space, by giving up the commutativity between individual link variable elements (eq. (3.20)). To do this, we promote the link variables $u^{\rho}_{x,i}$ to Hermitian quantum link operators $U^{\rho}_{x,i}$:

$$U_{x,i} = U^0_{x,i}\mathbb{1} + iU^a_{x,i}\tau^a, \qquad U^{\dagger}_{x,i} = U^0_{x,i}\mathbb{1} - iU^a_{x,i}\tau^a. \tag{3.21}$$

These operators must satisfy the same link algebra as above,

$$\left[L^a_{x,i}, U_{y,j}\right] = -\delta_{xy}\delta_{ij}\frac{\tau^a}{2}U_{y,j}, \qquad \left[R^a_{x,i}, U_{y,j}\right] = \delta_{xy}\delta_{ij}U_{y,j}\frac{\tau^a}{2}, \tag{3.22}$$

$$\left[L^a_{x,i}, U^{\dagger}_{y,j}\right] = \delta_{xy}\delta_{ij}U^{\dagger}_{y,j}\frac{\tau^a}{2}, \qquad \left[R^a_{x,i}, U^{\dagger}_{y,j}\right] = -\delta_{xy}\delta_{ij}\frac{\tau^a}{2}U^{\dagger}_{y,j}. \tag{3.23}$$

but are no longer required to commute among themselves. The QLM Hamiltonian is obtained by promoting the Wilson link variables $u_{x,i}$ in eq. 3.17 to the new quantum link operators $U_{x,i}$:

$$\begin{aligned}
\mathcal{H} &= J^{-1}\sum_{x,i}\mathcal{H}_{E_{x,i}} + J\sum_{\square_{x,i,j}}\mathcal{H}_{\square_{x,i,j}}, \\
\mathcal{H}_{E_{x,i}} &\equiv \left(\vec{L}^2_{x,i} + \vec{R}^2_{x,i}\right), \\
\mathcal{H}_{\square_{x,i,j}} &\equiv \mathrm{Tr}\left(U_{\square_{x,i,j}} + U^{\dagger}_{\square_{x,i,j}}\right).
\end{aligned} \tag{3.24}$$

The QLM plaquette operators are defined analogously to Wilson plaquettes. On the square lattice they are given by

$$U_{\square_{x,i,j}} = U_{x,i}U_{x+\hat{i},j}U^{\dagger}_{x+\hat{j},i}U^{\dagger}_{x,j}. \tag{3.25}$$

This construction of the $SU(2)$ QLM results in a link algebra with 10 generators. This algebra is isomorphic to $so(5)$. Like the quantization of the spin model above, the quantum operators of the SU (2) QLM are still rather abstract objects. To fully specify the model, we must choose a representation for these operators. The simplest, non-trivial, realization of the $so(5)$ algebra is the spinor representation. This is the 4-dimensional fundamental representation, analogous to the spin $1/2$ representation in the quantum spin model considered above. Henceforth we refer to this as the $\{4\}$-representation. The left and right colour operators commute with each other. We choose a basis in terms of their eigenstates[6]

$$R^a_{x,i} = \begin{pmatrix} \frac{1}{2}\sigma^a & 0 \\ 0 & 0 \end{pmatrix}_{x,i} \qquad L^a_{x,i} = \begin{pmatrix} 0 & 0 \\ 0 & \frac{1}{2}\sigma^a \end{pmatrix}_{x,i} \tag{3.26}$$

$$U^0_{x,i} = \begin{pmatrix} 0 & \frac{1}{2}\mathbb{1}_{2\times 2} \\ \frac{1}{2}\mathbb{1}_{2\times 2} & 0 \end{pmatrix}_{x,i} \qquad U^a_{x,i} = \begin{pmatrix} 0 & -\frac{i}{2}\sigma^a \\ \frac{i}{2}\sigma^a & 0 \end{pmatrix}_{x,i}. \tag{3.27}$$

[5] The full $u_{x,i}$ is still an element of SU (2).

[6] The interested reader can confirm, by direct calculations, that these operators indeed satisfy the necessary link algebra of eqs. (3.11) and (3.22).

Unlike the standard formulation, the individual elements of the quantum link matrix $U^{\rho}_{x,i}$ are non-commuting:

$$\begin{aligned}
\left[U^0_{x,i}, U^0_{y,j}\right] &= 0, \\
\left[U^0_{x,i}, U^a_{y,j}\right] &= i\delta_{xy}\delta_{ij}\left(R^a_{x,i} - L^a_{x,i}\right), \\
\left[U^a_{x,i}, U^b_{y,j}\right] &= i\delta_{xy}\delta_{ij}\epsilon_{abc}\left(R^c_{x,i} + L^c_{x,i}\right).
\end{aligned} \tag{3.28}$$

There is a strong analogy with the quantization of the classical spin model above, see eq. (3.3).

The link algebra can be realized by any representation of the $so(5)$ embedding algebra. We discuss the two lowest representations. In addition to the $\{4\}$-representation, this includes the 5-dimensional vector $\{5\}$-representation:[7]

$$L^1_{x,i} = \begin{pmatrix} 0 & \frac{1}{2} & 0 & 0 & 0 \\ \frac{1}{2} & 0 & 0 & 0 & 0 \\ 0 & 0 & 0 & \frac{1}{2} & 0 \\ 0 & 0 & \frac{1}{2} & 0 & 0 \\ 0 & 0 & 0 & 0 & 0 \end{pmatrix}_{x,i}, \qquad R^1_{x,i} = \begin{pmatrix} 0 & 0 & \frac{1}{2} & 0 & 0 \\ 0 & 0 & 0 & \frac{1}{2} & 0 \\ \frac{1}{2} & 0 & 0 & 0 & 0 \\ 0 & \frac{1}{2} & 0 & 0 & 0 \\ 0 & 0 & 0 & 0 & 0 \end{pmatrix}_{x,i}, \tag{3.29}$$

$$L^2_{x,i} = \begin{pmatrix} 0 & -\frac{i}{2} & 0 & 0 & 0 \\ \frac{i}{2} & 0 & 0 & 0 & 0 \\ 0 & 0 & 0 & -\frac{i}{2} & 0 \\ 0 & 0 & \frac{i}{2} & 0 & 0 \\ 0 & 0 & 0 & 0 & 0 \end{pmatrix}_{x,i}, \qquad R^2_{x,i} = \begin{pmatrix} 0 & 0 & -\frac{i}{2} & 0 & 0 \\ 0 & 0 & 0 & -\frac{i}{2} & 0 \\ \frac{i}{2} & 0 & 0 & 0 & 0 \\ 0 & \frac{i}{2} & 0 & 0 & 0 \\ 0 & 0 & 0 & 0 & 0 \end{pmatrix}_{x,i},$$

$$L^3_{x,i} = \begin{pmatrix} \frac{1}{2} & 0 & 0 & 0 & 0 \\ 0 & -\frac{1}{2} & 0 & 0 & 0 \\ 0 & 0 & \frac{1}{2} & 0 & 0 \\ 0 & 0 & 0 & -\frac{1}{2} & 0 \\ 0 & 0 & 0 & 0 & 0 \end{pmatrix}_{x,i}, \qquad R^3_{x,i} = \begin{pmatrix} \frac{1}{2} & 0 & 0 & 0 & 0 \\ 0 & \frac{1}{2} & 0 & 0 & 0 \\ 0 & 0 & -\frac{1}{2} & 0 & 0 \\ 0 & 0 & 0 & -\frac{1}{2} & 0 \\ 0 & 0 & 0 & 0 & 0 \end{pmatrix}_{x,i},$$

$$U^0_{x,i} = \frac{1}{\sqrt{2}}\begin{pmatrix} 0 & 0 & 0 & 0 & 0 \\ 0 & 0 & 0 & 0 & -1 \\ 0 & 0 & 0 & 0 & 1 \\ 0 & 0 & 0 & 0 & 0 \\ 0 & -1 & 1 & 0 & 0 \end{pmatrix}_{x,i}, \qquad U^1_{x,i} = \frac{1}{\sqrt{2}}\begin{pmatrix} 0 & 0 & 0 & 0 & -i \\ 0 & 0 & 0 & 0 & 0 \\ 0 & 0 & 0 & 0 & 0 \\ 0 & 0 & 0 & 0 & i \\ i & 0 & 0 & -i & 0 \end{pmatrix}_{x,i}, \tag{3.30}$$

$$U^2_{x,i} = \frac{1}{\sqrt{2}}\begin{pmatrix} 0 & 0 & 0 & 0 & -1 \\ 0 & 0 & 0 & 0 & 0 \\ 0 & 0 & 0 & 0 & 0 \\ 0 & 0 & 0 & 0 & -1 \\ -1 & 0 & 0 & -1 & 0 \end{pmatrix}_{x,i}, \qquad U^3_{x,i} = \frac{1}{\sqrt{2}}\begin{pmatrix} 0 & 0 & 0 & 0 & 0 \\ 0 & 0 & 0 & 0 & i \\ 0 & 0 & 0 & 0 & i \\ 0 & 0 & 0 & 0 & 0 \\ 0 & -i & -i & 0 & 0 \end{pmatrix}_{x,i}.$$

[7] The interested reader can again confirm, by direct calculations, that this set of operators satisfies the algebra of eqs. (3.11) and (3.22).

From the commutation relations of eq. (3.22)

$$\begin{aligned}
\left[L^3_{x,i}, U^{11}_{y,j}\right] &= -\delta_{xy}\delta_{ij}\frac{1}{2}U^{11}_{y,j}, & \left[L^3_{x,i}, U^{12}_{y,j}\right] &= -\delta_{xy}\delta_{ij}\frac{1}{2}U^{12}_{y,j}, \\
\left[L^3_{x,i}, U^{21}_{y,j}\right] &= \delta_{xy}\delta_{ij}\frac{1}{2}U^{21}_{y,j}, & \left[L^3_{x,i}, U^{22}_{y,j}\right] &= \delta_{xy}\delta_{ij}\frac{1}{2}U^{22}_{y,j}, \\
\left[R^3_{x,i}, U^{11}_{y,j}\right] &= \delta_{xy}\delta_{ij}\frac{1}{2}U^{11}_{y,j}, & \left[R^3_{x,i}, U^{12}_{y,j}\right] &= -\delta_{xy}\delta_{ij}\frac{1}{2}U^{12}_{y,j}, \\
\left[R^3_{x,i}, U^{21}_{y,j}\right] &= \delta_{xy}\delta_{ij}\frac{1}{2}U^{21}_{y,j}, & \left[R^3_{x,i}, U^{22}_{y,j}\right] &= -\delta_{xy}\delta_{ij}\frac{1}{2}U^{22}_{y,j},
\end{aligned} \tag{3.31}$$

which is independent of which representation we choose. Here $U^{ab}_{x,i}$ denotes the (a, b) entry of the 2×2 matrix $U_{x,i}$ in SU (2) space,

$$\begin{aligned}
U^{11}_{x,i} &= U^0_{x,i} + iU^3_{x,i}, & U^{12}_{x,i} &= U^2_{x,i} + iU^1_{x,i}, \\
U^{21}_{x,i} &= -U^2_{x,i} + iU^1_{x,i}, & U^{22}_{x,i} &= U^0_{x,i} - iU^3_{x,i}.
\end{aligned} \tag{3.32}$$

These commutation relations imply that $U^{ab}_{x,i}$ raises or lowers the colour charges at the ends of the links. Specifically, $U^{ab}_{x,i}$ lowers the colour charge at the left (right) end of the link by $1/2$ for $a = 1$ ($b = 2$). On the other hand, for $a = 2$ ($b = 1$) $U^{ab}_{x,i}$ raises the colour charge at left (right) end of the link by $1/2$. The colours at each end of a link are not independent. Raising or lowering the colour at one end of a link is always accompanied by another change at the other end of the link. Figure 3.5 shows the weight diagrams for the states, given in terms of their colour link operator eigenvalues. $R^3_{x,i}$ ($L^3_{x,i}$) is given on the horizontal (vertical) axis. States related by the raising or lowering operators are connected by an arrow in the direction of operation.[8]

As noted for the quantum spin models, different choices of representation may produce fundamentally different behaviour. To see this, let us consider Gauss' law, as given in eq. (3.13). Since a physical state $\left|\psi\right\rangle$ must satisfy Gauss' law at every site, each site must carry an overall $SU(2)$ colour singlet. This is only possible if an even number of colour $1/2$ charges associated with the in- and out-going links, are present at each site. For the $\{5\}$-representation there exists an "empty" link state, where both ends of the link simultaneously carry an SU (2) colour singlet. Therefore, a physical state can be constructed, without non-trivial charges anywhere on the lattice. Since all non-empty links in the $\{5\}$-representation have charges at both ends, non-empty link states can only be constructed by forming closed loops of flux strings, or flux strings connecting external charges. The situation is different for the $\{4\}$-representation. As can be seen in the weight diagram, no state has simultaneously a singlet on both ends of the link. We are therefore not able to construct an "empty" link state without colour charges anywhere on the lattice. Instead, any state must be constructed so that every lattice link contains exactly one colour $1/2$-charge either at its left or at its right end. All charges must be arranged so that an even number is present at each lattice site. These must then be combined to overall singlets. Including an external non-Abelian static charge at a lattice site implies a violation of Gauss' law at that site. This flux emanating from the external charge must be transported through the lattice and terminate at another charge. In contrast to the $\{5\}$-representation, the identification of the fluxes is far from straightforward, as we show in the next chapter.

[8] It should be noted that in addition to the raising and lowering of the colour at the ends of a link. The commutation relations of eq. 3.31 allows for an additional overall factor to be added to the state when performing the raising and lowering of the colour. In Figure 3.5 this factor is omitted.

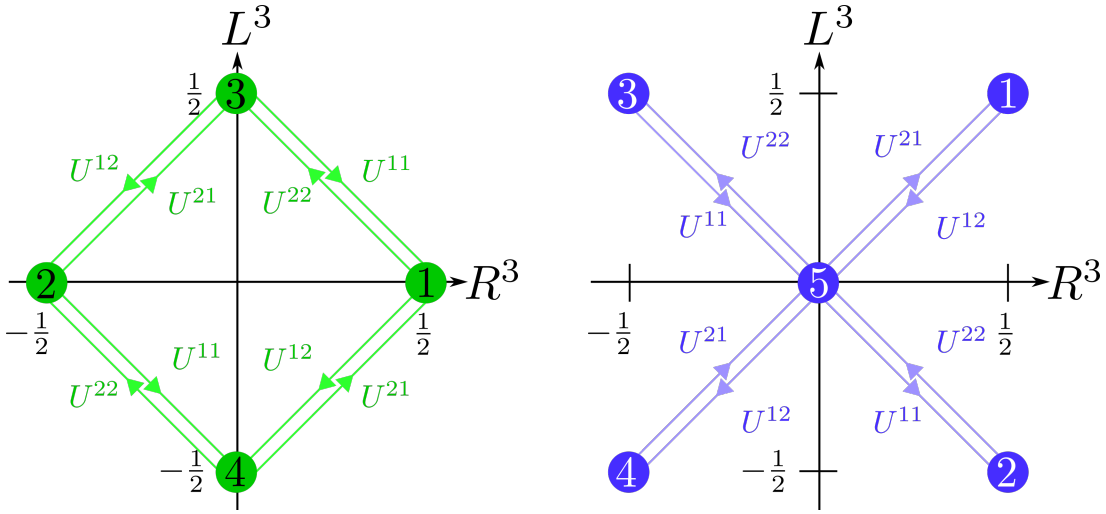

Figure 3.5: *Weight diagrams of (left) the* $\{4\}$*- and (right) the* $\{5\}$*-representation. States related by the raising or lowering operators* $U^{ab}_{x,i}$ *are connected by arrows.*

3.3 Rishon Representation of SU (2)-QLM

A general $SU(N)$ QLM, can be realized with an $su(2N)$ embedding algebra. In the case considered here, $SU(2)$ is realized with an $so(5)$ embedding algebra. We introduce so-called rishons by assigning two sets of N fermionic creation and annihilation operators to every link (x,i)[9]

$$\left(c^{a\dagger}_{x,i,S}, c^{b}_{x,i,S}\right). \tag{3.33}$$

Here a and b run from 1 to N, and denote different types of rishon. $S \in \{+,-\}$ denotes the ends of the links. We associate operators with $S=+$ ($S=-$) to the right (left) end of the link.[10] The two sets of operators each obey the standard creation and annihilation operator anticommutation relations:

$$\left\{c^{a\dagger}_{x,i,S_1}, c^{b}_{y,j,S_2}\right\} = \delta_{xy}\delta_{ij}\delta^{ab}\delta_{S_1S_2}, \quad \left\{c^{a\dagger}_{x,i,S_1}, c^{b\dagger}_{y,j,S_2}\right\} = 0, \quad \left\{c^{a}_{x,i,S_1}, c^{b}_{y,j,S_2}\right\} = 0. \tag{3.34}$$

We will refer to the "particles" created and annihilated by this set of operators as rishons [19]. Rishons are restricted to move along a single link. Since rishons are created and annihilated by a set of N different fermionic operators, a maximum of N rishons can reside at a given end of a link. All the above QLM operators can be expressed in terms of rishon operators. Below we present the rishon representation of the SU (2) QLM operators. It should be noted that this can be extended

[9] It should be noted that it is also possible to formulate rishons in terms of bosonic operators [19].

[10] In a more general sense $S=+$ denotes the positive direction, such that the $S=+$ end of a link (x,i) is near the lattice site $x+\hat{\imath}$, and the $S=-$ end of the link is near the lattice site x.

to a general $SU(N)$ QLM [19]. In the rishon formulation, the left and right colour operators are

$$
\begin{aligned}
R^1_{x,i} &= \frac{c^{1\dagger}_{x,i,+}c^2_{x,i,+} + c^{2\dagger}_{x,i,+}c^1_{x,i,+}}{2}, & L^1_{x,i} &= \frac{c^{1\dagger}_{x,i,-}c^2_{x,i,-} + c^{2\dagger}_{x,i,-}c^1_{x,i,-}}{2}, \\
R^2_{x,i} &= \frac{-ic^{1\dagger}_{x,i,+}c^2_{x,i,+} + ic^{2\dagger}_{x,i,+}c^1_{x,i,+}}{2}, & L^2_{x,i} &= \frac{-ic^{1\dagger}_{x,i,-}c^2_{x,i,-} + ic^{2\dagger}_{x,i,-}c^1_{x,i,-}}{2}, \\
R^3_{x,i} &= \frac{c^{1\dagger}_{x,i,+}c^1_{x,i,+} - c^{2\dagger}_{x,i,+}c^2_{x,i,+}}{2}, & L^3_{x,i} &= \frac{c^{1\dagger}_{x,i,-}c^1_{x,i,-} - c^{2\dagger}_{x,i,-}c^2_{x,i,-}}{2}.
\end{aligned}
\tag{3.35}
$$

We identify rishons of type 1 and 2 with a colour charge $+1/2$ and $-1/2$, respectively. We represent these two rishons pictorially with an upward arrow (♠) and a downward arrow (♥), respectively. We emphasize that the left (right) colour operator only includes rishon operators associated with the left (right) end of a link. Unlike the left and right operators, the U operators are constructed from rishons residing at opposite ends of a link

$$
U_{x,i} = \begin{pmatrix} c^{2\dagger}_{x,i,-}c^2_{x,i,+} + c^{1\dagger}_{x,i,+}c^1_{x,i,-} & -c^{2\dagger}_{x,i,-}c^1_{x,i,+} + c^{2\dagger}_{x,i,+}c^1_{x,i,-} \\ -c^{1\dagger}_{x,i,-}c^2_{x,i,+} + c^{1\dagger}_{x,i,+}c^2_{x,i,-} & c^{1\dagger}_{x,i,-}c^1_{x,i,+} + c^{2\dagger}_{x,i,+}c^2_{x,i,-} \end{pmatrix} \tag{3.36}
$$

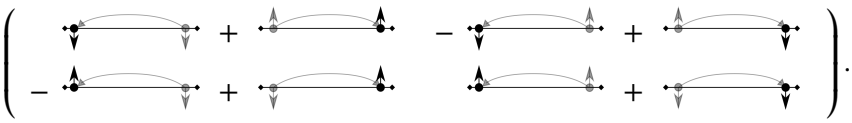

$$
U^\dagger_{x,i} = \begin{pmatrix} c^{2\dagger}_{x,i,+}c^2_{x,i,-} + c^{1\dagger}_{x,i,-}c^1_{x,i,+} & -c^{2\dagger}_{x,i,+}c^1_{x,i,-} + c^{2\dagger}_{x,i,-}c^1_{x,i,+} \\ -c^{1\dagger}_{x,i,+}c^2_{x,i,-} + c^{1\dagger}_{x,i,-}c^2_{x,i,+} & c^{1\dagger}_{x,i,+}c^1_{x,i,-} + c^{2\dagger}_{x,i,-}c^2_{x,i,+} \end{pmatrix} \tag{3.37}
$$

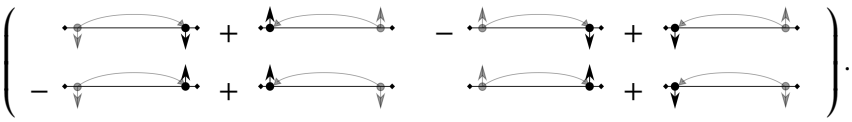

Above we have represented $U_{x,i}$ and $U^\dagger_{x,i}$ pictorially. The operators transport a rishon (semi-transparent) from one end of the link (along the semi-transparent arrow) to a rishon residing at the other end (black rishon), with an additional colour flip for the off-diagonal elements.[11]

In the rishon formulation there is another operator, not introduced above, namely the rishon-number operator [12]

$$
\mathcal{N}_{x,i} = \sum_{i=1}^{N} \left(c^{a\dagger}_{x,i,+}c^a_{x,i,+} + c^{a\dagger}_{x,i,-}c^a_{x,i,-} \right). \tag{3.38}
$$

This operator counts the total number of rishons on the link (x, i). Since it commutes with all the above link operators, the number of rishons per link is a conserved quantity.[13] We are thus able to define superselection sectors by specifying the number of rishons per link. The choice of number of rishons per lattice link corresponds to choosing a representation of the embedding algebra. The $\{4\}$-representation has one rishon per link, as illustrated in Figure 3.6. The $\{5\}$-representation

[11] The interested reader can easily confirm that this construction indeed satisfies the necessary link algebra of eqs. (3.11) and (3.22). By simply applying the rishon anticommutation relations of eq.(3.34).

[12] It should be noted that in the general $SU(N)$ case, when $N > 2$, there an additional operator needed on the links,

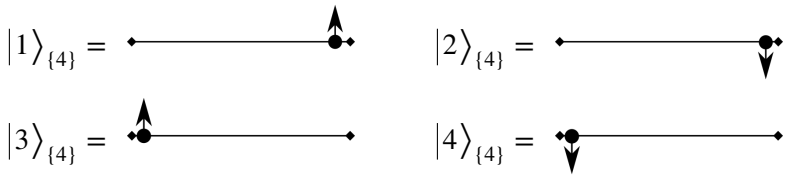

Figure 3.6: *The four link states for the* $\{4\}$*-representation, represented in terms of rishons.*

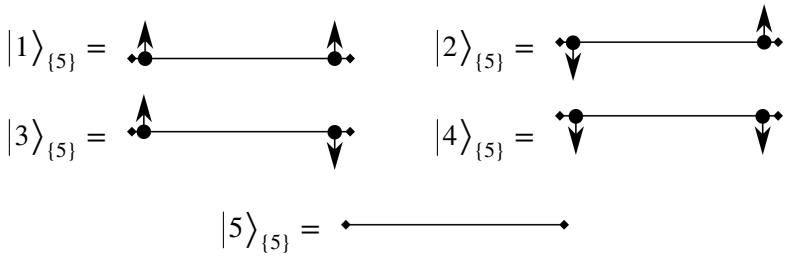

Figure 3.7: *The* $\{5\}$*-representation in terms of the colour charge at each end of a link. See appendix A for details.*

has two rishons per link, and is illustrated in Figure 3.7. There are two subtleties that should be addressed. First, since a link carries two rishons, we must fix the sign under exchange of the two rishons, to completely specify the states. Since the rishons are fermions, they must be in antisymmetrically states. Second, Figure 3.7 only shows the overall colour charge at each end of a link. This should be especially noted for the $|5\rangle$ state, which is represented by an empty link. This seems to contradict the conservation of rishons per link. This, however, is not the case. The empty link represents a state that is the superposition of two rishon singlet pairs, one at each end of the link. To maintain an overall antisymmetric state under the exchange of the two rishons, the two singlets are combined symmetrically under an exchange of left and right

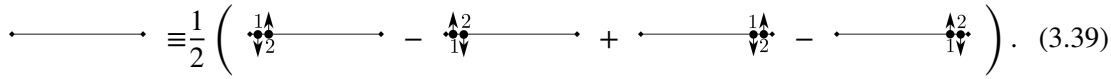

(3.39)

Since the rishons are bound into singlet pairs, we will often make a slight abuse of notation and simply refer to this state as containing no rishons. Appendix A contains a full description of both representations in the rishon formulation.

namely $\mathfrak{T}_{x,i} = \sum_a \left({c^a_{x,i,+}}^\dagger c^a_{x,i,+} - {c^a_{x,i,-}}^\dagger c^a_{x,i,-} \right)$. This operator is not needed here and will therefore not be presented in further details. The interested reader is referred to [19].

[13] This is not just for the current case of SU (2), but can be shown to be true for any SU (N) model.

3.4 $\mathbb{Z}(2)$ Center Symmetry

The center of $SU(2)$ is $\mathbb{Z}(2)$, which implies a $\mathbb{Z}(2)$ center symmetry for the $SU(2)$ QLM. The center transformation Z replaces a link variable $U_{x,i}$ with $-U_{x,i}$,

$$Z^{\dagger} U Z = -U. \tag{3.40}$$

In the $\{4\}$-representation we can identify this transformation with a matrix of the form

$$Z = \begin{pmatrix} \mathbb{1}_{2\times 2} & 0 \\ 0 & -\mathbb{1}_{2\times 2} \end{pmatrix}. \tag{3.41}$$

Here Z counts the number of rishons at the left (right) hand-side of the link with a factor -1 $(+1)$. This implies that the states of Figure 3.6 and Figure 3.7 are already eigenstates of the center symmetry, with either a $+1$ or -1 eigenvalue on the link. This will also be true in the next section, when we introduce a site-based basis, that the sites are already eigenstates of the center symmetry transformations. The total flux through a closed loop is found by taking the product of the individual center symmetry eigenvalues of each link intersected by the loop. When we are going to study the model, we implement the model in two spatial dimensions, where the lattice will be closed on a torus. This implies two non-trivial directions in which we can close a loop, and therefore $2^2 = 4$ distinct center symmetry sectors. We identify the sectors by the two center quantum numbers $Z_x = \pm 1$ and $Z_y = \pm 1$. These are calculated along a closed loop wrapping around the lattice in the x- and y-direction, respectively. An example of how to determine the center quantum number Z_y is given in Figure 3.19 for both the $\{4\}$- and the $\{5\}$-representation on the honeycomb lattice. It can trivially be shown that this value commutes with the Hamiltonian for any closed loop on any 2-dimensional lattice geometry. This is not just true for the Hamiltonian presented in eq. (3.24), but it is true for any general $SU(2)$ gauge-invariant Hamiltonian (this includes the general Hamiltonians we derive in Section 3.5).

We emphasize that we have chosen a convention of counting the rishons on the left with a -1. This is, however, a sign ambiguity, and we could just as well have chosen the rishons on the right, thereby shifting the fluxes to the other links. Since for a closed loop of even length, the number of left rishons equals the number of right rishons modulo 2, there is no difference in assigning -1 to the left or right rishons. For a closed loop of odd length this, however, plays a role, since the overall sign and thereby flux, is flipped between the two definitions. For computational reasons we only consider lattices of even-size, where the center symmetry sectors do not suffer from this sign ambiguity. We will, however, return to the flux ambiguity later, when we introduce charges and flux-strings in Chapter 4. We will see that the flux-strings fractionalize as a manifestation of the overall sign-ambiguity related to fluxes in the $\{4\}$-representation.

For the $\{5\}$-representation we similarly identify the center properties, by the number of rishons on either the left or the right side of the links. Since the $\{5\}$-representation always has the same number of rishons at both ends of a link, the sign ambiguity vanishes.[14] We emphasize that using Gauss' law, in the $\{5\}$-representation the flux is carried by links with one rishon at each end. In the $\{4\}$-representation no such identification can be made based on Gauss' law.

[14] Note that counting state $|5\rangle$ with two or zero rishons at each end gives the same result.

Figure 3.8: *Possible configurations for the colour* $1/2$ *charges on a link for the* $\{4\}$*-representation (left) and* $\{5\}$*-representation (right).*

3.5 Site-Based QLM Gauge Covariant Basis

So far, we have described the QLM in terms of a link-based algebra, where the fundamental degrees of freedom are defined on the links. This is similar to the Wilson formulation. In contrast to the algebra, Gauss' law, and hence also the charges, resides on the sites. Unlike the Wilson formulation, QLMs have a finite-dimensional Hilbert space per link and we can reformulate it as a site-based model. Since this will place the degrees of freedom on the sites, together with Gauss' law, the site basis is a more natural and versatile description of QLMs. Both the $\{4\}$- and the $\{5\}$-representation carry either a single rishon or no rishons at the link ends. Therefore, from the point of view of a single isolated lattice site, the two representations give rise to the same possible realizations of an overall singlet on the site, and therefore the site representations are only distinguished by how neighbouring sites are coupled together. We can thus construct a single set of site-states, which work as the basis states for both representations. In the link representation, we specify the explicit colour charges on the links, and afterwards we couple the colour charges together to overall singlets at each site. Since the site basis reside on the lattice sites, together with Gauss' law, we can reverse this process and demand that Gauss' law is already satisfied for all site basis states. We will therefore suppress the explicit colour charges and represent a single rishon of any type by a bullet $\bullet$. This reduces the number of configurations per link to just two, for both the $\{4\}$-, and the $\{5\}$-representation. These are presented Figure 3.8. These rishon configurations themselves are not defining a state on the lattice. To construct a lattice state, it is necessary to know how the colour charges are explicitly combined at each site. This is in contrast to the link states given in Figure 3.6 and Figure 3.7. Here a state is constructed by simply choosing and combining states on the individual links. Whether the resulting state is physical is another question. The possible singlet states that can be realized at a single lattice site, depend on the number of rishons that can be found on the given site. Since at most one rishon can reside at each end of a link, the maximum number of rishons at a lattice site is the same as the number of links joined together at a site. We consider two types of lattice geometry. These are the 2-dimensional square lattice, where four links meet at a lattice site, and the 2-dimensional honeycomb lattice, where three links meet at a lattice site. For now, we consider the case without external charges, such that all sites must carry a colour singlet. External charges will be introduced later, by coupling the rishons to non-singlet states.

3.5.1 Square Lattice

An example of a rishon configuration on a square lattice is presented in Figure 3.21. This lattice has several symmetries, which we demand the Hamiltonian to respect. The symmetries are translations by a single lattice spacing in both the x- and the y-direction: $\mathcal{T}_x$ and $\mathcal{T}_y$; 90°-rotation around a plaquette center p: $\mathcal{O}_p$; reflection at an axis in the x- and y-direction through the center of a plaquette p; R_{p_x} and R_{p_y}. We emphasize that reflections and rotations can alternatively be applied on a lattice site, in contrast to a plaquette center. These are, however, related to each other, and it thus suffices to

Symmetry	Operation	Independent
Translation: x	$\mathcal{T}_x$	Yes
Translation: y	$\mathcal{T}_y$	Yes
Rotation 90°: p	$\mathcal{O}_p$	Yes
Reflection: p_x	R_{p_x}	Yes
Reflection: p_y	R_{p_y}	No

Table 3.1: *Lattice symmetries for the square lattice geometry.*

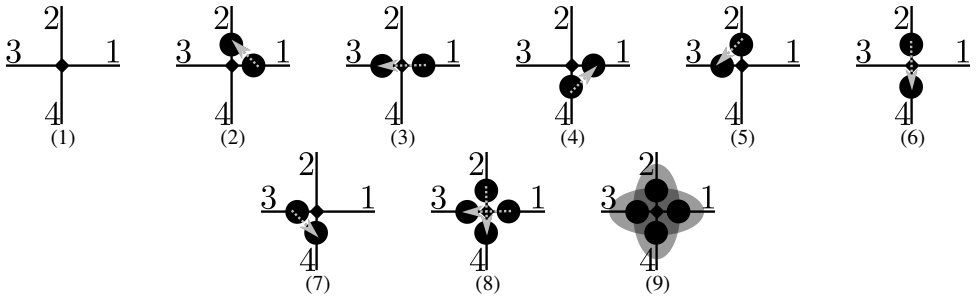

Figure 3.9: *Possible singlet configurations for rishons on a square lattice site. A grey arrow denotes two rishons combined into a singlet (the direction of the arrow denotes the overall sign). A semi-transparent oval denotes two rishons combined into a triplet. For state (9) the two triplet states are combined into an overall singlet.*

restrict ourself to the symmetries with respect to the plaquette centres.[15] The lattice symmetries are summarized in Table 3.1. Here independent means that the transformation cannot be constructed from operations listed above it.

On the square lattice four links come together at each lattice site, allowing for a maximum of four per site. A singlet can therefore be constructed with 0, 2, or 4 rishons residing near the site. The possible states are presented in Figure 3.9. Two rishons combined into an overall singlet is represented by a grey arrow connecting them. The direction of the arrow denotes the overall phase chosen for the state. The sign is defined such that the arrow points from the rishon that comes with a positive sign in front of the colour $+1/2$ term, and is going towards the charge that comes with a colour $-1/2$ in the same term

(3.42)

Later, when explicitly constructing the Hamiltonian in terms of plaquette transition, this sign will become important, since the Hamiltonian must explicitly display this change of sign between plaquette states. A semi-transparent oval represents two rishons combined into an overall triplet state. Appendix B.1 contains the explicit definitions of the site-states, in terms of the individual colour states on the separate links. By construction, the states in the site basis are gauge-invariant, such that any lattice state constructed in this basis automatically satisfies Gauss' law at each site. This

[15] The reflection through the x- and y-axis are similarly related by a rotation, but we include both.

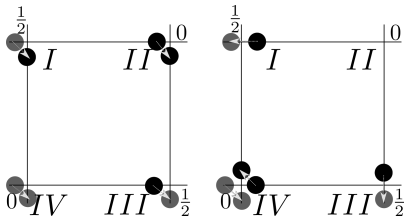

Figure 3.10: *Example of two elementary plaquette in the* $\{4\}$*-representation, with the same environment. Plaquettes (environment) rishons are marked in black (semi-transparent). The total magnitude of the environment charges is shown at each site.*

change of basis automatically enforces Gauss' law when constructing a lattice state. Since the links are constrained to carry a specific number of rishons (1 for the $\{4\}$-representation and 0 or 2 for the $\{5\}$-representation) a new constraint is imposed on the links. Neighbouring sites are constrained to states that have the correct number of rishons on the links connecting them. One could therefore be led to think that nothing has really been achieved by this change of basis. The new site basis is, however, more natural to consider. This is best illustrated with an example. Let us consider the magnetic part of the Hamiltonian in eq. (3.24). This is a sum of Hermitian elementary plaquette operators $\mathrm{Tr}\left(U_{\square_{x,i,j}} + U^{\dagger}_{\square_{x,i,j}}\right)$. The plaquette operators themselves act on the four links constituting a plaquette, leaving all other links unchanged, while also conserving the colour charges at each of the four corners of the plaquette. The plaquette operator commutes with the infinitesimal gauge transformation G_x on all sites. In the site basis a plaquette $U_{\square_{x,i,j}}$ is defined by the four states on the lattice sites residing at the four corners of the plaquette. Only the rishons residing on the four links constituting the plaquette can be affected by the plaquette operator. Figure 3.10 shows two examples of an elementary plaquette with four corners defined in the site basis. Here the rishons belong to the plaquette are marked in black. We refer to these as the plaquette rishons. Rishons residing on the corner states, but do not belong to the plaquette, are marked semi-transparent. These rishons are not affected by the plaquette operator. We refer to these as environment rishons. To construct an overall singlet at each plaquette site, the total charge of the environment rishons residing near a given site, must combine with the total charge of the plaquette rishons residing at the same site to create an overall colour singlet. Hence, the magnitude of the environment charges and the plaquette charges must be equal at each corner of the plaquette. Each plaquette corner is connected to two plaquette links and to two environment links.

Since, up to an overall sign, it is not important where the environment rishons reside,[16] we suppress the explicit link on which the environment charges reside, and simply specify the total environment charge at each site. In Figure 3.10 site I and III each contain an environment charge of $1/2$. Site II and IV each contain a vanishing environment charge. We emphasize that the state residing at the site IV is not included in the basis of Figure 3.9. For a plaquette corner containing 4 rishons, the two environment charges must be combined into a state of definite environment

[16]When constructing the Hamiltonian for the square lattice, the overall sign for a plaquette must explicitly be worked out for each plaquette. The sign rule for the plaquettes is defined such that, if an arrow points from an external rishon to a plaquette rishon, then the plaquette obtains an additional minus sign. It should be noted that, due to the site-states (3), (6), and (8), a plaquette-state can undergo a sign change under rotation. Note that the arrow, and thereby the overall sign, changes between the two plaquettes of Figure 3.10, from pointing into the plaquette to out of the plaquette at corner I. For more details, see appendix C.1.

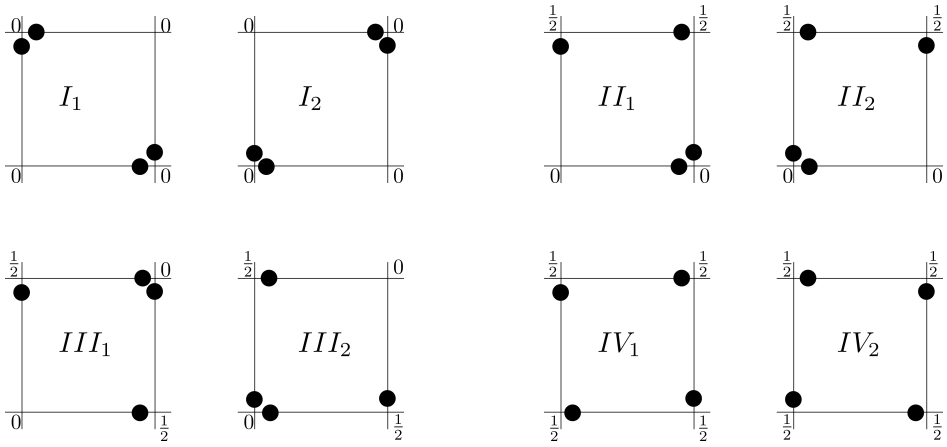

Figure 3.11: *The eight plaquettes for the four environments (I, II, III, and IV) that support a plaquette transitions in the* $\{4\}$*-representation. Each of the environments supports two distinct plaquette configurations, distinguished by a subscript.*

colour. This implies that the states (8) and (9) in Figure 3.9, must be rotated into states with charges combined along the diagonal. The direction in which two charges are combined depends on which of the plaquette corners the states reside. On site II and IV (I and III) in Figure 3.10 the charges must be combined in a direction of $\nwarrow\searrow$ ($\nearrow\swarrow$). The explicit rotations are given by (see appendix C.2 for an example),

$$\begin{pmatrix} \\ \end{pmatrix} = \begin{pmatrix} \frac{1}{2} & \frac{\sqrt{3}}{2} \\ \frac{\sqrt{3}}{2} & -\frac{1}{2} \end{pmatrix} \begin{pmatrix} \\ \end{pmatrix}, \qquad \begin{pmatrix} \\ \end{pmatrix} = \begin{pmatrix} -\frac{1}{2} & -\frac{\sqrt{3}}{2} \\ \frac{\sqrt{3}}{2} & -\frac{1}{2} \end{pmatrix} \begin{pmatrix} \\ \end{pmatrix}. \tag{3.43}$$

In Figure 3.10 the two plaquettes have the same environment charges, but different plaquette rishon configurations. We say that the two plaquettes are supported by the given environment. For the $\{4\}$-representation we identify 8 distinct environments, not related by rotation or reflection of the plaquettes, which supports a non-zero number of plaquettes. We denote these environments by Roman numerals I-VIII. Suppressing the explicit environment rishons, and the overall sign arrow for the singlets, the environments and their supported plaquettes are given in Figure 3.11 and Figure 3.12. We identify the example from Figure 3.10 to have an environment of type III. The environments of type I-IV each support two distinct plaquettes, distinguished by a subscript, and the four environments of type IV-VIII support a single plaquette each. To construct an overall singlet on a site, a triplet in the environment must be paired with another triplet pair on the plaquette. This necessarily implies that there is just a single plaquette supported by any environment with a triplet pair.[17]

Since the colours in the environment are unaffected by an operation on the plaquette, any SU (2) gauge-invariant plaquette operator, must conserve the colour for both the plaquette and the environment at each plaquette corner. Therefore, for a general SU (2) invariant plaquette Hamiltonian, only matrix elements between states supported by the same environment can be non-zero

[17]This would not be true for a lattice geometry that allows for a higher number of rishons residing at a lattice site, or higher representations.

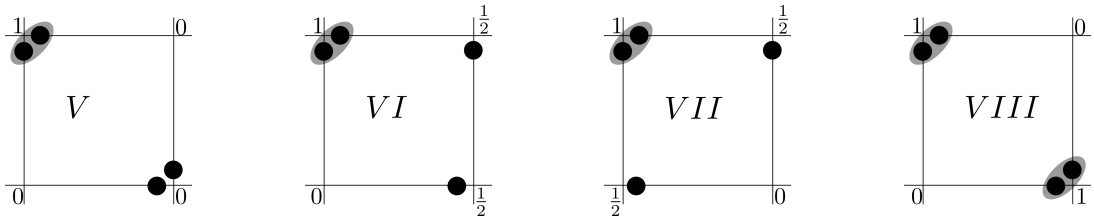

Figure 3.12: *The four plaquettes for the four environments (V, VI, VII, and VIII) containing a triplet pair and are hence not supporting a plaquette transitions in the* $\{4\}$*-representation.*

and the local plaquette Hamiltonian $\mathcal{H}_{\square_{x,i,j}}$ can be block-diagonalized in terms of the eight possible environment types,[18]

$$\mathcal{H}^{\{4\}}_{\square_{x,i,j}} = \begin{pmatrix} \mathcal{H}^{\{4\}}_{\square_I} & 0 & 0 & 0 & 0 & 0 & 0 & 0 \\ 0 & \mathcal{H}^{\{4\}}_{\square_{II}} & 0 & 0 & 0 & 0 & 0 & 0 \\ 0 & 0 & \mathcal{H}^{\{4\}}_{\square_{III}} & 0 & 0 & 0 & 0 & 0 \\ 0 & 0 & 0 & \mathcal{H}^{\{4\}}_{\square_{IV}} & 0 & 0 & 0 & 0 \\ 0 & 0 & 0 & 0 & \mathcal{H}^{\{4\}}_{\square_V} & 0 & 0 & 0 \\ 0 & 0 & 0 & 0 & 0 & \mathcal{H}^{\{4\}}_{\square_{VI}} & 0 & 0 \\ 0 & 0 & 0 & 0 & 0 & 0 & \mathcal{H}^{\{4\}}_{\square_{VII}} & 0 \\ 0 & 0 & 0 & 0 & 0 & 0 & 0 & \mathcal{H}^{\{4\}}_{\square_{VIII}} \end{pmatrix}. \tag{3.44}$$

Each $\mathcal{H}^{\{4\}}_{\square_{env}}$ describes the behaviour of the plaquettes supported by the given environment $env \in \{I, II, III, IV, V, VI, VII, VIII\}$. The four environments I-IV each support two plaquettes and the corresponding block Hamiltonians are 2×2 matrices, specifying the non-transitional weight W^a_{env} and the transitional weights T_{env} for the two states supported by the environment,[19]

$$\mathcal{H}^{\{4\}}_{env\in\{I,II,III,IV\}} = \begin{pmatrix} W^1_{env} & T_{env} \\ T^*_{env} & W^2_{env} \end{pmatrix}. \tag{3.45}$$

Since the plaquette Hamiltonian is Hermitian, we identify W^1_{env} and W^2_{env} as real parameters. T_{env} is in general complex.[20] Figure 3.11 implies that two plaquettes, supported by the same environment, are related by either a rotation or a reflection of the plaquette. Imposing rotation and reflection symmetry on the Hamiltonian, the transitional parameters T_{env} are restricted to real values $T^*_{env} = T_{env} \in \mathbb{R}$, and the non-transitional parameters are restricted to be equal for the two plaquette configurations $W^1_{env} = W^2_{env} \equiv W_{env}$. The remaining four environments V-VIII each support

[18] It is worth noting that when the Hamiltonian is constructed, it is more convenient not to block-diagonalize it in this form. As shown in eq. (3.43), the plaquettes are mixed together when they include site-states with four rishons residing at the same site. Therefore, states in e.g. $\mathcal{H}_{\square_{II}}$ are mixed with states in $\mathcal{H}_{\square_{VI}}$.

[19] The complete matrix contains copies of this block matrix for the distinct rotations and reflections of the possible explicit environment rishons.

[20] As noted above there are a non-trivial sign for the plaquette-states, defined through the singlet arrows. This sign gives rise to the possible appearance of an additional minus sign for the transition parameters T_{env} and T^*_{env} depending on the explicit state under consideration. This sign is important to consider, when implementing the full Hamiltonian in the calculations, but have been suppressed here. For more details see appendix C.1.

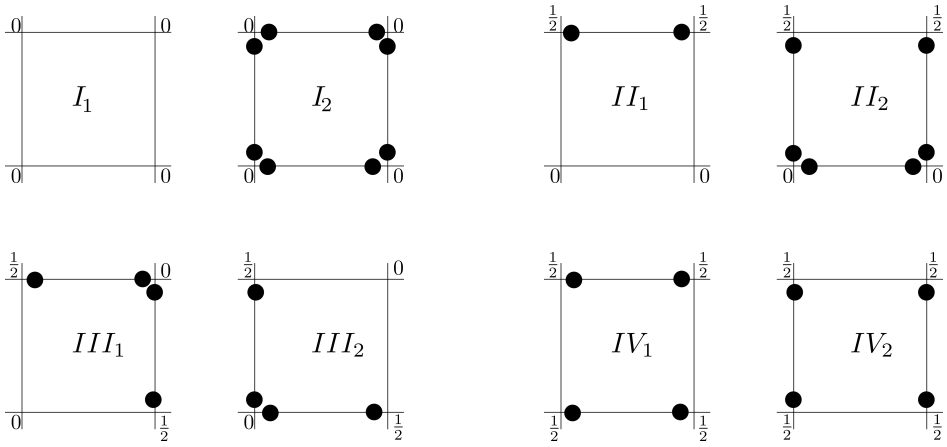

Figure 3.13: *The eight plaquettes for the four environments (I, II, III, and IV) that support plaquette transitions in the $\{5\}$-representation. Each of the environments supports two distinct plaquette configurations, distinguished by a subscript.*

a single plaquette-state and are therefore specified by a single parameter $W_{env} \in \mathbb{R}$. A general gauge-invariant single-plaquette ring-exchange Hamiltonian, that respects the lattice symmetries on the square lattice in the $\{4\}$-representation, is therefore represented by 12 real parameters.[21]

$$\begin{aligned} &\mathcal{H}^{\{4\}}_{\square_{x,i,j}}\left[W_{\square_{\{4\}}}, T_{\square_{\{4\}}}\right], \\ &W_{\square_{\{4\}}} = \left(W_I, W_{II}, W_{III}, W_{IV}, W_V, W_{VI}, W_{VII}, W_{VIII}\right), \\ &T_{\square_{\{4\}}} = \left(T_I, T_{II}, T_{III}, T_{IV}\right). \end{aligned} \tag{3.46}$$

The full Hamiltonian is a sum over all plaquettes,

$$H^{\{4\}} = \sum_{x,i>j} \mathcal{H}^{\{4\}}_{\square_{x,i,j}}. \tag{3.47}$$

Hence, by changing to the site basis, we have obtained a simple method to construct a completely general $SU(2)$ invariant ring-exchange Hamiltonian for the QLM, that respects the lattice symmetries.

By similar arguments, we identify all possible environments for the $\{5\}$-representation, together with the plaquettes supported by the environments. For the $\{5\}$-representation, we identify 12 distinct environments, enumerated with Roman numerals $I - XII$, that are not related by rotations or reflections of the plaquettes. As for the $\{4\}$-representation, four of these environments ($I - IV$) support exactly two plaquette configurations. These are presented in Figure 3.13. The remaining eight environments ($V - XII$) contain at least one triplet pair and each environment supports a single plaquette configuration. These are given in Figure 3.14. Due to the difference of the link constraints between the $\{4\}$- and the $\{5\}$-representation, there exist four additional plaquette environments in the $\{5\}$-representation (IX-XII). Each of these environments contains pairs of environment triplets on neighbouring sites. This necessitates a link with a rishon at both ends of the link. In contrast to the transitions found in the $\{4\}$-representation, the two

[21] Since there is an additive constant that can be removed from the Hamiltonian, there are actually only $12 - 1 = 11$ physical relevant parameters.

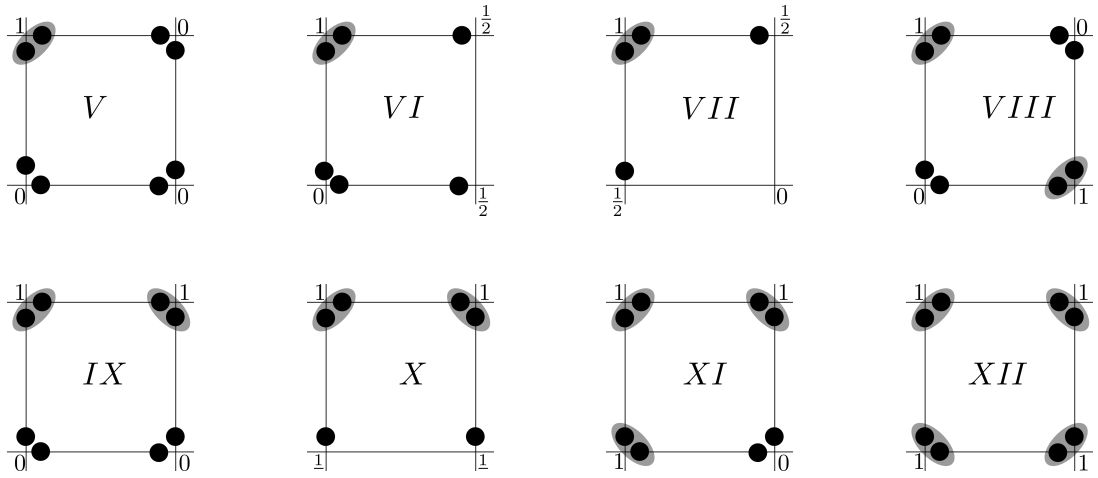

Figure 3.14: *The eight plaquettes for the environments (V-XII) contain a triplet pair and do therefore not support a plaquette transitions in the* $\{5\}$*-representation. Note that the four environments IX-XII are not allowed in the* $\{4\}$*-representation.*

supported states of environment I and II are not related by neither rotations nor reflections in the $\{5\}$-representation. Therefore, in general $W^1_{I,II} \neq W^2_{I,II}$, and $T_{I,II}$ are complex parameters for the $\{5\}$-representation. Hence, a general $SU(2)$-gauge-invariant ring-exchange Hamiltonian that respects the lattice symmetries is specified by 20 real parameters in the $\{5\}$-representation,[22]

$$\begin{aligned}
&\mathcal{H}^{\{5\}}_{\square_{x,i,j}}\left[W_{\square_{\{5\}}}, T_{\square_{\{5\}}}\right], \qquad (3.48)\\
&W_{\square_{\{5\}}} = \left(W^1_I, W^2_I, W^1_{II}, W^2_{II}, W_{III}, W_{IV}, W_V, W_{VI}, W_{VII}, W_{VIII}, W_{IX}, W_X, W_{XI}, W_{XII}\right),\\
&T_{\square_{\{5\}}} = \left(\Re T_I, \Im T_I, \Re T_{II}, \Im T_{II}, T_{III}, T_{IV}\right).
\end{aligned}$$

The full Hamiltonian is obtained as a sum over all plaquettes,

$$H^{\{5\}} = \sum_{x,i>j} \mathcal{H}^{\{5\}}_{\square_{x,i,j}} \qquad (3.49)$$

Several things should be noted for the states that we have considered here. First of all, including rotations and reflections of the plaquettes, the total number of distinct plaquette-states are 34 and 43 for the $\{4\}$- and $\{5\}$-representation, respectively. This should be seen in contrast to the link-based states, for which each link carries a 4- or a 5-dimensional Hilbert space for the $\{4\}$- and $\{5\}$-representation with 256 or 625 possible states per plaquette respectively. Furthermore, the states in the link-basis, are not necessarily gauge-invariant, and they would need to be combined into states satisfying Gauss' law at each lattice site.[23] In addition, the plaquettes states in our site basis are already block-diagonalized, into 2×2 matrices for the local elementary plaquette Hamiltonians $\mathcal{H}_{\square}$. This largely reduces the number of states to be considered when constructing

[22] Again an additive constant can be removed from the Hamiltonian leaving only $20-1=19$ parameters that specify the Hamiltonian.

[23] Of course, since the two basis are describing the same theory, the number of gauge-invariant states are the same.

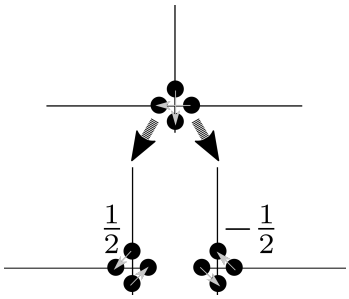

Figure 3.15: *Site-state 8 projected onto two different plaquette-states. Note that the two projected states differ by a sign.*

the Hamiltonian and it reduces the computational time for applying the Hamiltonian to a plaquette-state. The standard Hamiltonian of eq. (3.24), was taken directly from the standard Wilson formulation of SU (2) gauge theory. By using the newly constructed site basis, the model has been generalized to any SU (2) invariant single-plaquette Hamiltonian for the QLM in both the $\{4\}$- and $\{5\}$-representation. This opens a much richer parameter space to be explored.[24]

Sign Problem for the Square Lattice

The site basis on the square lattice, however, comes with some problems, that makes it unsuitable for Monte Carlo simulations. The basis gives rise to the notorious sign problem, which renders the Boltzmann factors unsuitable for interpretation as a positive probability distribution [110, 111]. Matrix elements of the transfer matrix may have negative, or even complex, values.[25] In this model the sign-problem originate from two sources. First, since for the states (3), (6), and (8) the rishons are coupled to singlets across the lattice site, and not with a neighbouring rishon, the states can obtain a sign change under rotations. Therefore, the given site basis necessarily gives rise to a sign change for plaquette-states containing these site-states are included in the full lattice, since a similar, but rotated, plaquette-state would come with an equal magnitude but opposite sign. Second, to obtain plaquette-states with definite environment and plaquette charges at the corners of the plaquette, the doublet of the two states (8) and (9) must be rotated in Hilbert-space to a doublet with define environment and plaquette charges (see eq. (3.43)). How the states are rotated in Hilbert-space depends on which plaquette corner the site-state occupies. Since the two rotations of eq. (3.43) differs in the signs, this creates a sign change, and thereby a possible sign problem, when considering the same site-state from the viewpoint of two neighbouring plaquettes. This is exemplified in Figure 3.15 for a site-state (8) projected onto the singlet environment charges, when viewed from the perspective of two neighbouring plaquettes. Since this model has a sign-problem, we will not pursue the construction of a Monte Carlo simulation. The QLM on the square lattice will instead be investigated by performing exact diagonalizations of the Hamiltonian, which we present in Section 3.6.

[24] The explicit magnetic part of the Hamiltonian in eq. (3.24) for both the $\{4\}$- and $\{5\}$-representation can be found to be identical to choosing the parameters of $T_I = 128J$, $T_{II} = -64J$, $T_{III} = -64J$, and $T_{IV} = 32J$ together with $W_{env} = 0$ for all environments

[25] It should be noted that the sign problem is not restricted to the use of the site basis, and would appear in most basis that we can use to describe the model.

Symmetry	Operation	Independent
Translation: $\hat{1}$	$\mathcal{T}_{\hat{1}}$	Yes
Translation: $\hat{2}$	$\mathcal{T}_{\hat{2}}$	Yes
Translation: $\hat{3}$	$\mathcal{T}_{\hat{3}}$	No
Rotation 60°: p	$\mathcal{O}_p$	Yes
Reflection: $p_{\hat{1}}$	$R_{p_{\hat{1}}}$	Yes
Reflection: $p_{\hat{2}}$	$R_{p_{\hat{2}}}$	No
Reflection: $p_{\hat{3}}$	$R_{p_{\hat{3}}}$	No

Table 3.2: *Lattice symmetries for the honeycomb lattice geometry.*

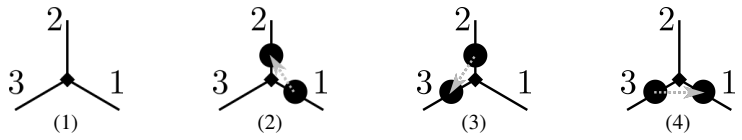

Figure 3.16: *Possible configurations of the colour* $1/2$ *charges on a single site for the honey-comb lattice. The light arrows denote the sign of the singlet, see appendix B.2 for the definitions. Note that each rishon configuration give rise to only one state and that under a* 120° *rotation the states are rotated into each other, without any sign changes.*

3.5.2 Honeycomb Lattice

One can circumvent the sign problem, by changing the lattice geometry to one where the problematical states cannot appear. This can be accomplished by choosing a lattice geometry where only three links are joined together at the sites, the simplest of which is the honeycomb lattice. Each site is connected to three links, separated by 120°, such that the elementary plaquette is a regular hexagon. An example of this is shown in Figure 4.6. As for the square lattice, this lattice geometry gives rise to several symmetries, which we demand the general Hamiltonian to respect. The symmetries are translations from one plaquette center to an adjacent plaquette center: $\mathcal{T}_{\hat{1}}$, $\mathcal{T}_{\hat{2}}$ and $\mathcal{T}_{\hat{3}}$.[26] 60°-rotation around a plaquette center p: $\mathcal{O}_p$ and reflections of any of the three axes going through the center of a plaquette p: $R_{p_{\hat{1}}}$, $R_{p_{\hat{2}}}$ and $R_{p_{\hat{3}}}$. As for the square lattice, the reflections and rotations can also be applied at a lattice site, in contrast to a plaquette center. These are again related to each other, and we will always consider the symmetries around the plaquette centres. The lattice symmetries are summarized in Table 3.2. With three links connected at a site, a singlet can be constructed either for an empty site, or for a site with exactly two adjacent rishons. These states are illustrated in Figure 3.16, where the overall sign for a singlet pair is again defined by the grey arrow.[27] Since the rishons are coupled to overall colour singlets with rishons residing on neighbouring links, all the non-empty site-states are now rotated into each other, without any additional sign changes.

In complete analogue to the square lattice, we specify every honeycomb plaquette according

[26] The three directions are illustrated in Figure 4.6. Note that the three directions are not independent.

[27] Since every other site is rotated by 45° degrees, the honeycomb lattice actually contains two types of lattice sites. This is, however, of no importance here.

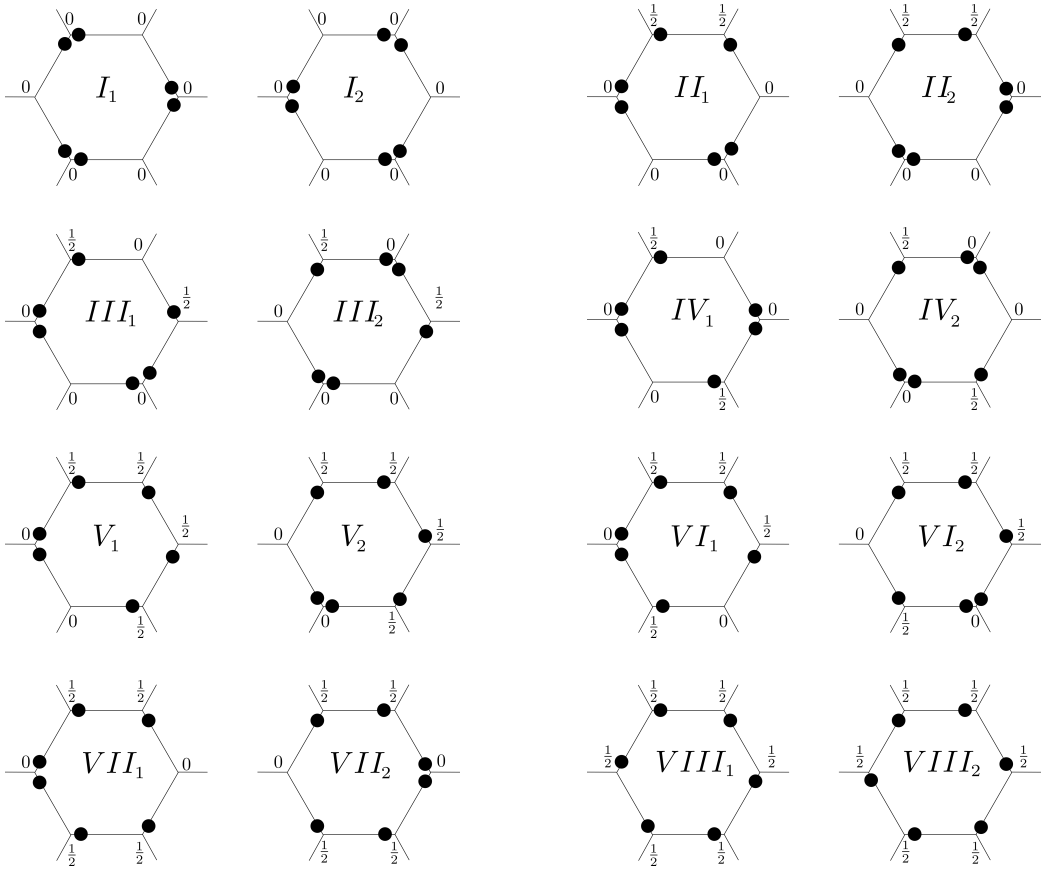

Figure 3.17: *All 16 plaquettes for the 8 environments (I, II, III, IV, V, VI, VII, and VIII) of the* $\{4\}$*-representation. Each of the 8 environments support exactly 2 different plaquettes configurations, distinguished by a subscript. Note that, except for environment III, the two supported plaquettes for each environment are related by rotations or reflections of the plaquette.*

to its supporting environment. In contrast to the square lattice, the sites on the honeycomb lattice cannot contain a triplet pair and all the environments are therefore supporting exactly two distinct plaquette configurations. We identify 8 distinct plaquette environments, not related by rotation nor reflection, with a total of 16 plaquette configurations for both representations. These are presented in Figure 3.17 and Figure 3.18 for the $\{4\}$- and $\{5\}$-representation, respectively. Again, we construct a single-plaquette Hamiltonian, that is block-diagonalized in terms of the environments. This

is given for the $\{4\}$-representation by

$$\mathcal{H}^{\{4\}}_{\hexagon_{x,i,j}} = \begin{pmatrix} \mathcal{H}^{\{4\}}_{\hexagon_I} & 0 & 0 & 0 & 0 & 0 & 0 & 0 \\ 0 & \mathcal{H}^{\{4\}}_{\hexagon_{II}} & 0 & 0 & 0 & 0 & 0 & 0 \\ 0 & 0 & \mathcal{H}^{\{4\}}_{\hexagon_{III}} & 0 & 0 & 0 & 0 & 0 \\ 0 & 0 & 0 & \mathcal{H}^{\{4\}}_{\hexagon_{IV}} & 0 & 0 & 0 & 0 \\ 0 & 0 & 0 & 0 & \mathcal{H}^{\{4\}}_{\hexagon_V} & 0 & 0 & 0 \\ 0 & 0 & 0 & 0 & 0 & \mathcal{H}^{\{4\}}_{\hexagon_{VI}} & 0 & 0 \\ 0 & 0 & 0 & 0 & 0 & 0 & \mathcal{H}^{\{4\}}_{\hexagon_{VII}} & 0 \\ 0 & 0 & 0 & 0 & 0 & 0 & 0 & \mathcal{H}^{\{4\}}_{\hexagon_{VIII}} \end{pmatrix}. \tag{3.50}$$

Each of the environments is again specified by a 2×2 Hermitian matrix containing four real parameters ($W^1_{env}, W^2_{env} \in \mathbb{R}$ and $T_{env} \in \mathbb{C}$),

$$\mathcal{H}^{\{4\}}_{env} = \begin{pmatrix} W^1_{env} & T_{env} \\ T^*_{env} & W^2_{env} \end{pmatrix}. \tag{3.51}$$

For the $\{4\}$-representation, plaquette pairs that are supported by a given environment, except for environment III, are again related by either a rotation or a reflection. Hence, demanding that the plaquette Hamiltonian respects the rotation and reflection symmetries of the lattice, the plaquette Hamiltonian can be fully specified by 18 real parameters,

$$\begin{aligned} &\mathcal{H}^{\{4\}}_{\hexagon}\left[W_{\hexagon_{\{4\}}}, T_{\hexagon_{\{4\}}}\right], \\ &W_{\hexagon_{\{4\}}} = \left(W_I, W_{II}, W^1_{III}, W^2_{III}, W_{IV}, W_V, W_{VI}, W_{VII}, W_{VIII}\right), \\ &T_{\hexagon_{\{4\}}} = \left(T_I, T_{II}, \Re T_{III}, \Im T_{III}, T_{IV}, T_V, T_{VI}, T_{VII}, T_{VIII}\right). \end{aligned} \tag{3.52}$$

The full Hamiltonian of the system is a sum over all plaquettes

$$H^{\{4\}} = \sum_{x,i>j} \mathcal{H}^{\{4\}}_{\hexagon_{x,i,j}}. \tag{3.53}$$

Interestingly $SU(2)$ QLM in the $\{4\}$-representation on the honeycomb lattice in the zero charge sector, turns out to be equivalent to the quantum dimer model [112, 113] on the Kagomé lattice. In the $\{4\}$-representation every link contains exactly one rishon, that must be combined with exactly one other rishon in order to be combined to a colour singlet. This implies that each link must be combined with exactly one other neighbouring link. This is equivalent to the dimer condition for a lattice connecting the centres of neighbouring links, which is exactly the Kagomé lattice, and the two models are therefore equivalent. A detailed description of how to map the corresponding Hamiltonians of the two models to each other, is presented in appendix D.

For the $\{5\}$-representation only the plaquette pairs supported by the environments IV, VI and VIII are related by either a rotation or a reflection. This gives a total of 26 real parameters that fully specify the general Hamiltonian,

$$\begin{aligned} &\mathcal{H}^{\{5\}}_{\hexagon}\left[W_{\hexagon_{\{5\}}}, T_{\hexagon_{\{5\}}}\right], \\ &W_{\hexagon_{\{5\}}} = \left(W^1_I, W^2_I, W^1_{II}, W^2_{II}, W^1_{III}, W^2_{III}, W_{IV}, W^1_V, W^2_V, W_{VI}, W^1_{VII}, W^2_{VII}, W_{VIII}\right), \\ &T_{\hexagon_{\{5\}}} = \left(\Re T_I, \Im T_I, \Re T_{II}, \Im T_{II}, \Re T_{III}, \Im T_{III}, T_{IV}, \Re T_V, \Im T_V, T_{VI}, \Re T_{VII}, \Im T_{VII}, T_{VIII}\right). \end{aligned} \tag{3.54}$$

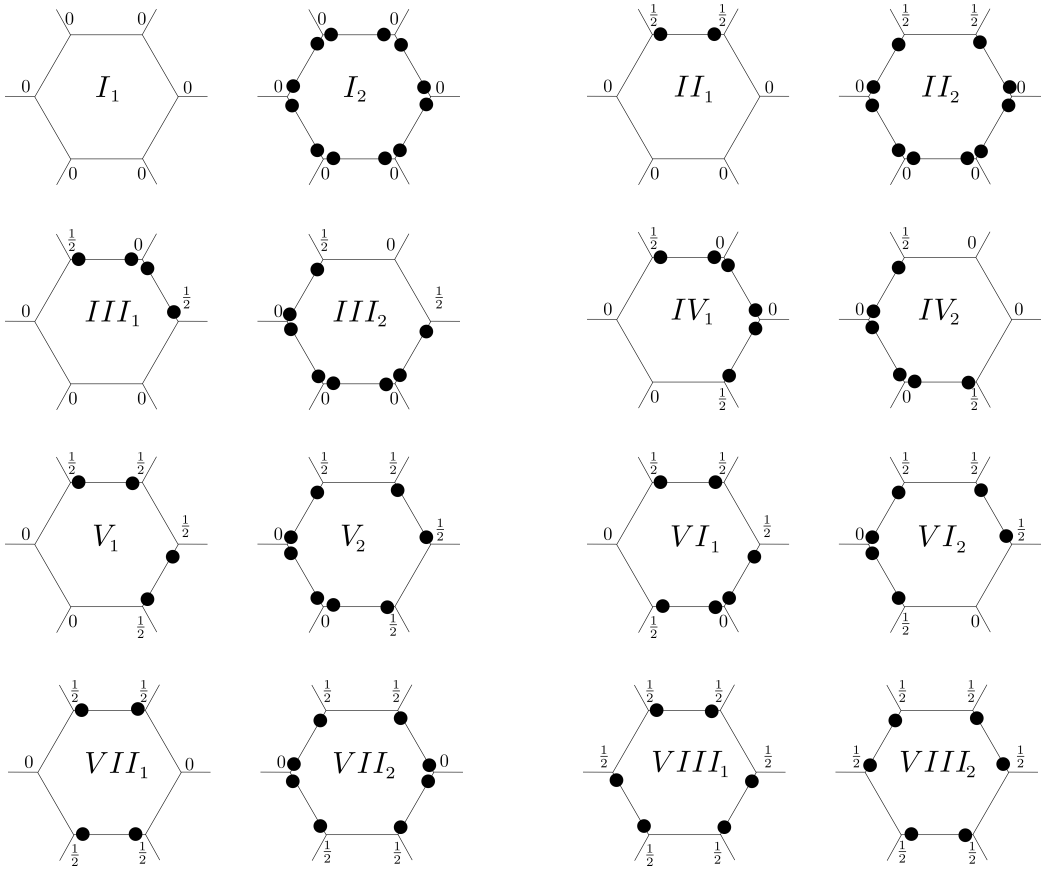

Figure 3.18: *All 16 plaquettes for the 8 environments (I, II, III, IV, V, VI, VII, and VIII) that support a plaquette transition in the* $\{5\}$*-representation. Each of the 8 environments support 2 different plaquettes, distinguished by a subscript. Note that for this representation only the two supported states of IV, VI, and VIII are related by rotations or reflections.*

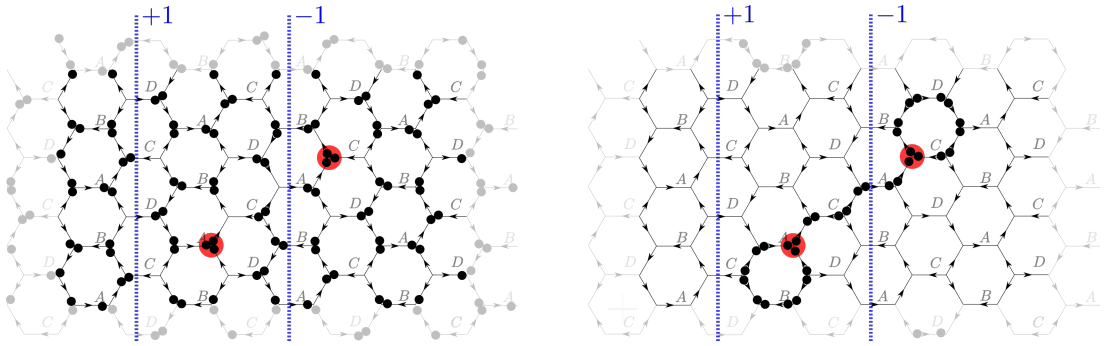

Figure 3.19: *Pairs of external non-Abelian static charges carrying a* $3/2$ *representation of* $SU(2)$ *(red filled circles) are included in the* $\{4\}$*-(left) and* $\{5\}$*-representation (right) on a periodic lattice. A flux is identified through the loops (blue lines), by a change in the center quantum number* Z_y *(*$+1$ *outside the charges and* -1 *between the charges).*

The full Hamiltonian is a sum over all plaquettes

$$H^{\{5\}} = \sum_{x,i>j} \mathcal{H}^{\{5\}}_{\hexagon_{x,i,j}}. \tag{3.55}$$

We emphasize that choosing the honeycomb lattice geometry, in combination with a representation allowing a maximum of a single rishon at each end of a link, effectively reduces the model to a $\mathbb{Z}(2)$ gauge theory, as long as no external charges are included. Since no site-states containing four or more colour charges can be constructed, Gauss' law is effectively reduced to a $\mathbb{Z}(2)$ Gauss' law, distinguishing between states with an even, i.e. 0 or 2 and an odd number of rishons residing at a given site. In later sections, when we apply Monte Carlo methods for simulating the model, we will introduce charges, thereby removing the non-Abelian nature of the model. In addition, it is important to note that, the $\{4\}$-representation does not contain any empty link-states. Although Gauss' law is effectively a $\mathbb{Z}(2)$ Gauss' law, it not the standard $\mathbb{Z}(2)$ gauge theory. In fact, it will turn out that the $\mathbb{Z}(2)$-flux of the model is delocalized, similar to what was observed in the $U(1)$ QLM in [14, 15]. This is in sharp contrast to the $\{5\}$-representation, which in the zero-charge sector is simply equivalent to a standard $\mathbb{Z}(2)$ gauge theory, where the flux resides on individual links. To see this, consider two charges, each carrying a $3/2$ representation of $SU(2)$. This is shown for the $\{4\}$- (left) and $\{5\}$-representation (right) in Figure 3.19 for a periodic honeycomb lattice. For both representation there is an unbreakable $\mathbb{Z}(2)$ flux-string connecting the charges, identified by the change in the center quantum number value through the closed loops marked in blue. In the $\{5\}$-representation we easily identify the $\mathbb{Z}(2)$-flux to reside on the links carrying a colour doublet at each end. The additional one-plaquette flux loop residing next to the two charges, are due to the $3/2$-representation (in contrast to the $1/2$-representation) carried by the external charges. This is, however, not the case for the $\{4\}$-representation, where every link carry exactly one colour doublet, and we cannot identify individual links that carry the $\mathbb{Z}(2)$-flux. In Section 4.4 we will see that in the $\{4\}$-representation the energy connecting the two charges is carried by two fractionalized flux strands connecting the charges.

3.6 Exact Diagonalization on the Square Lattice

Exact diagonalization of the full lattice Hamiltonian, allows us to directly obtain the spectrum of the lattice model and is not affected by the sign-problem. It is, however, computational heavy. Since the Hilbert space grows exponentially with the lattice size, the exact diagonalization method can only be applied to the smallest of lattice sizes. Nevertheless, it is still a valuable method that allows us to analyse the exact spectra of smaller lattices in great detail.

Since the Hilbert space of the $SU(2)$ QLM is finite-dimensional for any finite lattice size, one can explicitly construct the Hamiltonian matrix elements

$$\left\langle \psi' \right| \mathcal{H} \left| \psi \right\rangle, \tag{3.56}$$

relating two states $\left|\psi\right\rangle$ and $\left|\psi'\right\rangle$ through the Hamiltonian $\mathcal{H}$. We express the Hamiltonian as a $\mathcal{N} \times \mathcal{N}$ matrix, where $\mathcal{N}$ denotes the number of states. This matrix is then diagonalized, using standard algorithms. Since the computation time of diagonalization grows as a power function of the number of states,[28] it is often useful to first block-diagonalize the Hamiltonian by manually identifying eigenstates of symmetry operators that commute with the Hamiltonian.

For the general square lattice Hamiltonians of eq. (3.47) and eq. (3.49), we have constructed a code that performs exact diagonalization of any even-sized square lattice, up to a lattice size of 4×4, this is for both the $\{4\}$- and $\{5\}$-representation. The code is written with "Armadillo C++ Linear Algebra Library" [114]. This allows for a large Hamiltonian parameter space of 12- or 20-dimensions for the $\{4\}$- and $\{5\}$-representation, respectively, that can potentially be explored by exact diagonalization. The exact diagonalization of the square lattice Hamiltonian is, however, not the main focus of this thesis. We therefore only present a few of the results that can be obtained by exact diagonalization, and let the reader know that there is much more to be explored by exact diagonalization of the $SU(2)$ QLM. This section does not provide a comprehensive investigation of the $SU(2)$ QLM spectra on the square lattice, but merely serves as a presentation and a proof of concept of an interesting method that deserves attention in the future.

3.6.1 Lattice Setup

We close the lattice on a torus, with strictly periodic boundary conditions in both the x- and the y-direction. Since a site-state specifies the rishons on the four links connected to the site, we only need to specify the states on the even lattice sites.[29] For this reason, we only consider lattices of even-size in both dimensions. This allows us to put an upper bound on the number of states $\mathcal{N}$. For a lattice of even lengths L_x and L_y in the x- and y-direction respectively, there is $L_x L_y$ sites, which gives an upper bound on the number of states as $\mathcal{N} \leq 9^{\frac{L_x * L_y}{2}}$.[30]

By construction, the two Hamiltonians of eq. (3.47) and eq. (3.49) commute with lattice

[28] This grows $\sim \mathcal{O}\left(\mathcal{N}^3\right)$ where $\mathcal{N}$ is the number of states

[29] One must still be careful to only include states that satisfy the constraint for the number of rishons per link.

[30] The actual number of states is closer to $\mathcal{N} \approx 5^{\frac{L_x * L_y}{2}}$, depending on the chosen representation, and exact lattice geometry.

translation by one lattice spacing in both the x- and the y-direction, and with center transformations,

$$\left[H, \mathcal{T}_x\right] = \left[H, \mathcal{T}_y\right] = \left[H, Z_x\right] = \left[H, Z_y\right] = 0. \tag{3.57}$$

Since center transformations commute with translations in either direction, the full Hamiltonian can be block-diagonalized by identifying states with definite eigenvalues for both sets of operators. We classify the eigenvalues of the operator $\mathcal{T}_i$ by m_i, such that for an eigenstate $\left|\psi\right\rangle$

$$\mathcal{T}_i \left|\psi\right\rangle = e^{i\frac{2\pi m_i}{L_i}} \left|\psi\right\rangle. \tag{3.58}$$

Here L_i is the lattice size in the i-direction, m_i takes values in $\left\{0, 1, \ldots, L_i - 1\right\}$, and the momentum is $p_i = 2\pi m_i / L_i$.

3.6.2 Results

In Figure 3.20, we present the spectrum for the $\left\{4\right\}$-representation square lattice Hamiltonian of eq. (3.47). Here only T_I and T_{IV} are non-zero which represent plaquettes with only environment singlets and doubles at every plaquette corner, respectively. The entire spectrum for a 2×2 lattice is presented (top), together with the lowest laying states on a 4×4 lattice (bottom). For the 2×2 lattice we find that the spectrum is symmetric around zero. Such that for any eigenstate with an eigenvalue $-E$ there is another eigenstate with the same quantum numbers and eigenvalue $+E$. Here only states with center quantum numbers $Z_x = Z_y = -1$ and the same momentum in both directions ($m_x = m_y$), obtain a non-vanishing eigenvalue. The ground state has vanishing momentum in both directions (i.e. $m_x = m_y = 0$) and the first exited state has a non-vanishing momentum with $m_x = m_y = L_x/2 = L_y/2 = 1$. When the model is put on a 4×4 lattice (bottom), for $\lambda \lesssim 0.5$ the ground state is two-fold degenerated. Both states have trivial center quantum numbers of $Z_x = Z_y = +1$. The two states have momenta with $m_x = m_y = 0$ and, with $m_x = m_y = L_x/2 = L_y/2 = 2$. On the other hand, for $\lambda \gtrsim 0.5$ the second state with non-vanishing momentum, separates from the ground state and becomes the first excited state.

That the ground state shifts from a non-trivial to a trivial center quantum number, when changing the lattice size by a factor of two, may seem odd at first. This is, however, just a trivial consequence of the nature of the fluxes in the $\left\{4\right\}$-representation (see Section 3.4). To see this, let us consider the cartoon state shown in Figure 3.21. Here the red dashed lines mark a lattice of size 2×2. When calculating the center symmetry quantum number along the blue dashed line, this state obtains a quantum number $Z_y = -1$. On a 4×4 lattice, marked by the green dashed lines, the corresponding state, expanded to fill the entire lattice, now has a center quantum number of $Z_y = +1$, again obtained along the blue dashed line. From the explicit eigenstates found by the exact diagonalization of the Hamiltonian, it is confirmed that the cartoon state shown in Figure 3.21 is indeed a cartoon state of the ground state. Here the four rishon states on the sites represent a superposition of state (8) and (9). The true groundstate contains contributions from more cartoon states. Especially it is a superposition of the state in Figure 3.21, and the corresponding state with the rishons residing at the opposite sites. This shows that for the $\left\{4\right\}$-representation, there exists a crystalline confinement phase on the square lattice. Furthermore, on the 4×4 lattice, it shows that there is a phase transition at $T_I \approx T_{IV}$ where the degenerate crystalline confinement phase splits up to two distinct phases, with distinct momenta. The groundstate (first excited state) obtains a $+1$

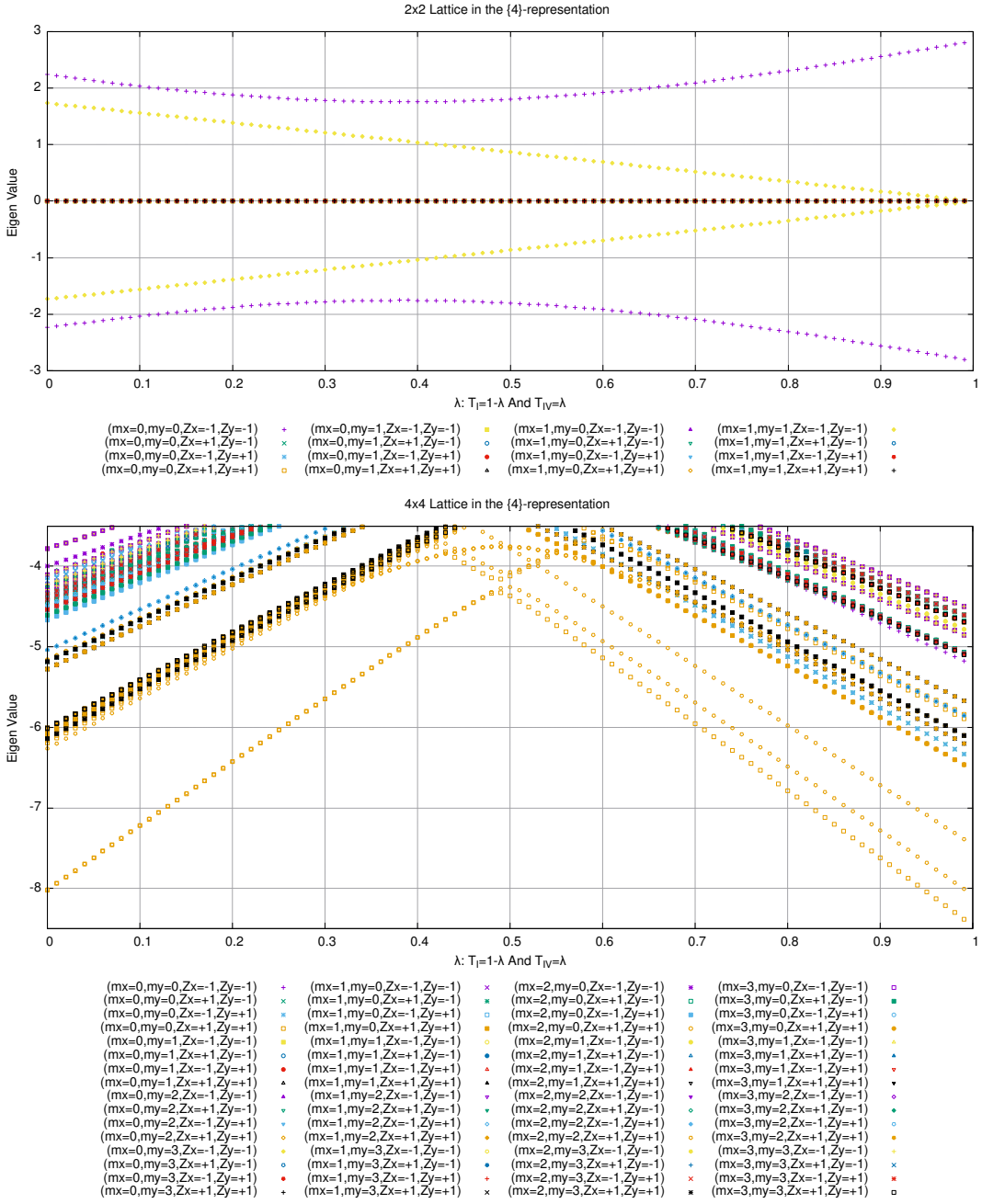

Figure 3.20: *Exact diagonalization results for a* 2×2 *(top) and a* 4×4 *(bottom) square lattice in the* $\{4\}$*-representation. The Hamiltonian parameters of eq. 3.47 are chosen as:* $W_{I-VIII} = 0$*,* $T_{II-III} = 0$*,* $T_I = \lambda$*, and* $T_{IV} = 1 - \lambda$*, where* λ *is given on the x-axis.*

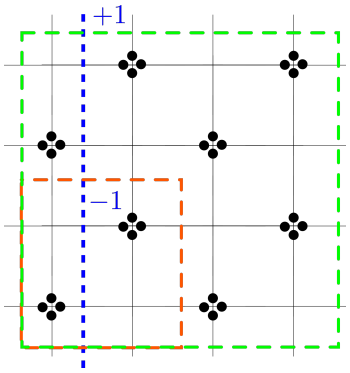

Figure 3.21: *The corresponding cartoon states on a* 2×2 *(orange boundary) and a* 4×4 *(green boundary) periodic square lattice cartoon have different center quantum numbers (obtained along the blue dashed line).*

(-1) factor under translation of half a lattice length. We will see more to crystalline confinement in Chapter 4, when we study the $\{4\}$-representation on the honeycomb lattice.

In Figure 3.22 we present the corresponding spectra for the $\{5\}$-representation. Here T_I and T_{IV} again represent plaquettes with only environment singlets and doubles at every plaquette corner, respectively, and they are again the only non-zero parameters. On the 2×2 lattice (top), the spectrum is similar to what we found for the $\{4\}$-representation and is again symmetric zero. Again the eigenstates with a non-vanishing eigenvalue have the same momentum in both directions ($m_x = m_y$). The ground state has a vanishing momentum in both directions (i.e. with $m_x = m_y = 0$), and the first exited state has a non-vanishing momentum with $m_x = m_y = L_x/2 = L_y/2 = 1$. In contrast to the $\{4\}$-representation, only states with a trivial center quantum numbers ($Z_x = Z_y = +1$) obtain a non-vanishing eigenvalue. On a 4×4 lattice (bottom), in contrast to the $\{4\}$-representation, the ground state is unique for all values of λ. The ground state and the first excited state have a momentum with $m_x = m_y = 0$ and with $m_x = m_y = L_x/2 = L_y/2 = 2$, respectively. Both states transform trivially in the center $Z_x = Z_y = +1$. This is similar to what we found for the $\{4\}$-representation for $\lambda \gtrsim 0.5$. We emphasize that for the $\{5\}$-representation the ground state and the first excited state, maintain the same trivial center quantum numbers for both lattice sizes. Since in contrast to the $\{4\}$-representation, the $\{5\}$-representation has the same number of rishons at both ends of a link, this is to be expected.

In this chapter, we have only made a short presentation of a few results obtained with exact diagonalization, and we have barely scratched the surface. It is clear that there are still a lot of interesting results to be found using this method. We believe that exact diagonalization of the general $SU(2)$ invariant ring-exchange Hamiltonians can become a valuable tool for analysing the model in the future. This method deserves more attention than what time has allowed here. This part of the thesis should just be viewed as a proof of concept, to show that the model is suitable for performing an exact diagonalization analysis.

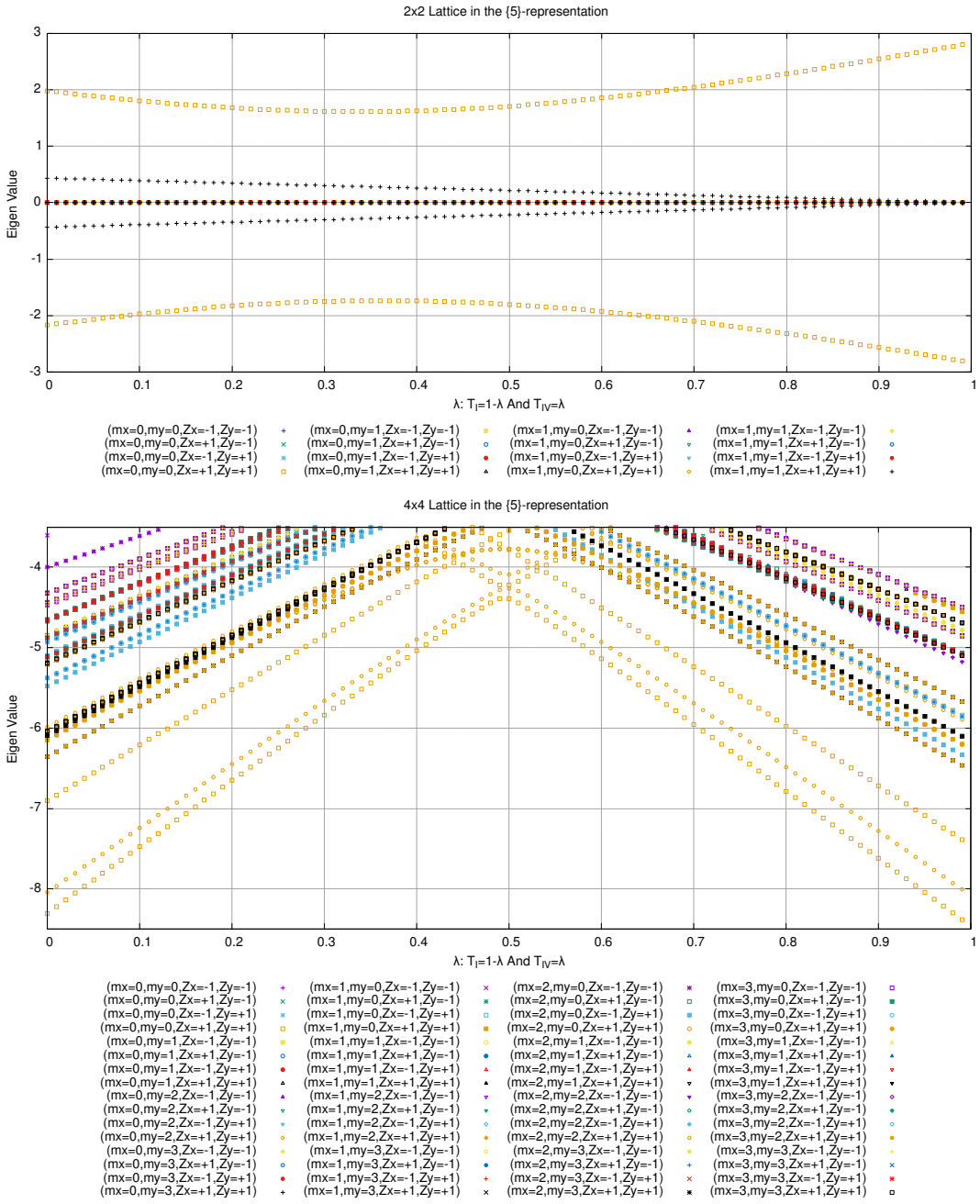

Figure 3.22: *Exact diagonalization results for a* 2×2 *(top) and a* 4×4 *(bottom) square lattice in the* $\{5\}$*-representation. The Hamiltonian parameters of eq. 3.49 are chosen as:* $W_{I-XII} = 0$, $T_{II-III} = 0$ *while* $T_I = \lambda$ *and* $T_{IV} = 1 - \lambda$*, where* λ *is shown on the x-axis.*

Chapter 4

Height Variable Monte Carlo on the Honeycomb Lattice

On the honeycomb lattice, we can reformulate the general $SU(2)$ Hamiltonian in the $\{4\}$-representation, see Figure 3.17, in terms of $\mathbb{Z}(2)$ height variables.[1] In a reduced parameter space, which, among other things, introduces three additional global $\mathbb{Z}(2)$ symmetries, it is possible to construct a highly-efficient Monte Carlo cluster algorithm acting on the height variables. In this chapter we first show in Section 4.1 how the height variables can be derived for the $SU(2)$ QLM model on the honeycomb lattice in the $\{4\}$-representation and how this naturally leads to a reduced parameter space. Furthermore, we will show how charges and Dirac-strings can be included in the height-variable formulation. In Section 4.2 we investigate several distinct phases and show how they can be distinguished in terms of order parameters. Finally, in Section 4.3, we introduce the Monte Carlo simulations. This includes the generally applicable but less efficient Metropolis algorithm in terms of the height variables, and the more efficient cluster algorithm that is applicable only in the reduced parameter space. Since the Metropolis algorithm works in a much larger parameter space than the cluster algorithm, it is useful to have both algorithms to simulate the model. The results of the simulations will be presented in Section 4.4.

4.1 Height Variables

In the rishon formulation, when Gauss' law is imposed at each site, each link effectively carries a 2-dimensional Hilbert space, where the rishon can be placed at either end of the link. When no charges are included on the honeycomb lattice, up to 120° rotations there are two valid site-states, i.e. states with either no rishons, or exactly two rishons residing near the site. These are shown in Figure 4.1. To describe the model in terms of height variables residing at the center of a plaquette, we introduce a standard orientation, shown by filled arrows on the links. On each link (x, i) we introduce a $\mathbb{Z}(2)$ variable $z_{x,i} = \pm 1$. Here i denotes a lattice link emanating from a site x. This

[1] It should be noted that we can similarly reformulate the model in the $\{5\}$-representation in terms of height variables. Here the height model can be constructed in a similar fashion as will be described here for the $\{4\}$-representation, but without the need for a lattice orientation and with the rule that the height variable changes sign when crossing a link that carries a flux.

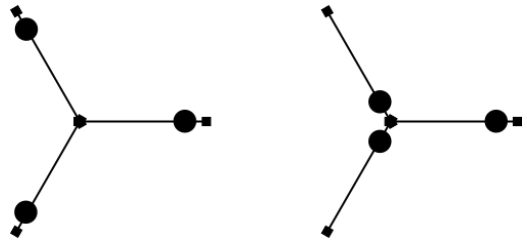

Figure 4.1: *The only two realizations (up to rotations) of Gauss' law at a honeycomb lattice site.*

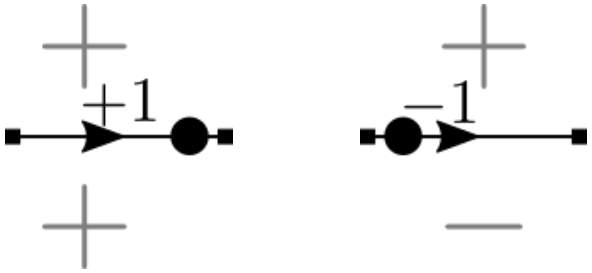

Figure 4.2: *Definition of the sign ($z_{x,i}$) on a link (x, i) in terms of the placements of the rishons with respect to a standard orientation, represented by a filled arrow on the link. $z_{x,i} = +1(-1)$ if the rishon is placed ahead (behind) the arrow, as illustrated in the left (right) figure. The height variables associated with the two hexagons adjacent to the link (semi-transparent) change sign over the link if $z_{x,i}$ is -1.*

takes the value of $z_{x,i} = +1$ ($z_{x,i} = -1$) if the rishon on the link, is placed ahead (behind) the arrow, representing the direction of the link (see Figure 4.2). Gauss' law is imposed on the product of the $\mathbb{Z}(2)$ link variables $z_{x,i}$, residing on the three links connected to the site x:

$$G_x^{\mathbb{Z}(2)} = \prod_i z_{x,i}. \tag{4.1}$$

Here i runs over all links connected to the site x. To be a physical state, we demand that the product equal $+1$. To describe the QLM, we demand that the two gauge-invariant states shown in Figure 4.1 satisfy Gauss' law, in terms of the $\mathbb{Z}(2)$ link variables $z_{x,i}$. This allows for two possible link orientations, which are presented in Figure 4.3. Figure 4.4 and Figure 4.5 show the possible gauge-

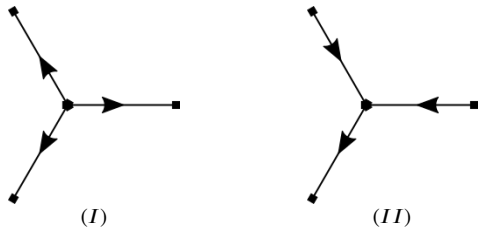

Figure 4.3: *The two link orientations connected to a single honeycomb lattice site, that gives rise to the correct Gauss' law.*

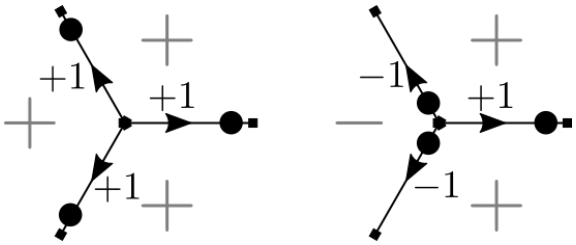

Figure 4.4: *The two possible rishon configurations that satisfy Gauss' law on the honeycomb lattice in the orientation (I). The sign $z_{x,i}$ of each link i is shown together with the corresponding height variables (up to an overall redundant flip of all height variables) in semi-transparent. Note that the product of all the $z_{x,i}$ is* $+1$.

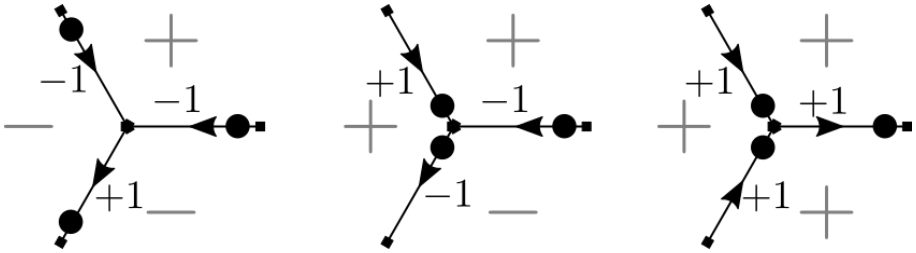

Figure 4.5: *The three possible rishon configurations that satisfy Gauss' law on the honeycomb lattice in the orientation (II). The sign $z_{x,i}$ of each link i is shown together with the corresponding height variables (up to an overall redundant flip of all height variables) in semi-transparent. Note that the product of all the $z_{x,i}$ is* $+1$.

invariant rishon states for orientation (I) and (II), respectively. They are presented in terms of both the rishons and the $\mathbb{Z}(2)$ link variables on each link. We emphasize that by construction, any state that obeys Gauss' law contains an even number of $z_{x,i} = -1$ factors on the links. This allows us to introduce a $\mathbb{Z}(2)$ height variable $m_p = \pm 1$ residing at the center of the plaquettes $p \in \tilde{\Lambda}$. We define the product of two neighbouring height variables as the value of the link separating them:

$$m_{(x,i)_+} m_{(x,i)_-} = z_{x,i}. \tag{4.2}$$

Here $(x,i)_\pm$ denotes the plaquettes on the two sides of the link (x,i). Crossing a link with $z_{x,i} = -1$ leads to a change of the height variable, otherwise they stay the same across the link. This is illustrated in Figure 4.2, where the height variables are shown as semi-transparent on each side of the link. Since the height variables are only defined through the difference between two neighbouring plaquettes, there is an overall sign ambiguity. Since all gauge-invariant states contain an even number links carrying $z_{x,i} = -1$, there is a direct correspondence between the rishon configuration and the height variables. For any rishon configuration satisfying Gauss' law there are two height variable configurations which differ by an overall global sign change.[2] This is illustrated in Figure 4.4 and Figure 4.5, where the height variables for the three hexagons touching a site are shown as semi-transparent. Since the site-orientation I contains three out-going arrows and orientation II contains one out-going with two in-going arrows. The sites must be combined in a 3:1 relation,

[2]There is a small caveat. When the lattice is closed on a torus, the height variables can only describe the sector with the center quantum number corresponding to the chosen boundary condition, that is periodic or antiperiodic for the height variables. This will be discussed in more details in Section 4.1.4.

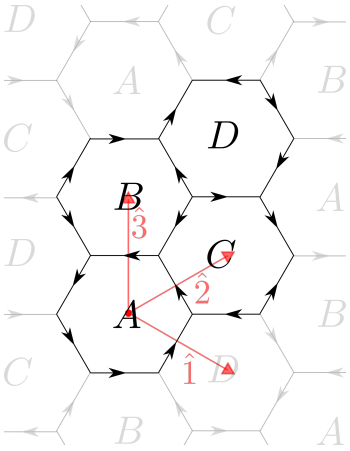

Figure 4.6: *Honeycomb unit cell (black) inserted in a larger lattice (semi transparent), that is divided into four sublattices (A,B,C, and D). The link orientations are indicated by black arrows. The red arrows denote the three unit-vectors;* $\hat{1}$, $\hat{2}$ *and* $\hat{3}$. *Note that* $\hat{1} + \hat{3} = \hat{2}$.

giving rise to four distinct plaquette sublattices A, B, C, and D. A single unit-cell, containing all plaquette types, is shown in Figure 4.6, together with the link orientations. We emphasize that the sublattices align not along the x-direction, but follow the natural directions of the hexagons, i.e. along directions of multiples of 60° with respect to the y-direction. These directions are represented by the vectors $(\pm\hat{1}, \pm\hat{2}, \pm\hat{3})$. The imposed link orientations do not respect the lattice symmetries and the translational and rotational symmetries are therefore not directly manifest in the height variables. Only the plaquettes of sublattice A preserve a manifest rotational symmetry in terms of the link orientations and hence the height variables. The link orientation of the plaquettes of sublattices B, C, and D rotate into each other. From the rules illustrated in Figure 4.2, we translate the plaquette environments of Figure 3.17 from the rishon representation to the corresponding height variables. These are shown in figures 4.7-4.10 for the four different sublattices. Since the three sublattice B, C, and D are rotated into each other, only a single orientation of each sublattice environment is shown. For the B, C, and D plaquettes, it is generally true that a rotation of the rishon configurations does not give rise to a corresponding rotation of the height variables. Instead, the rotation will, in general, induce a change of the signs for some of the height variables.[3]

Order Parameters

From the height variables we define a set of four magnetic order parameters $\left(M_A, M_B, M_C, M_D\right)$, defined as the sum of the height variables over the given sublattice:

$$M_X \equiv \sum_{p \in X} m_p, \quad X \in (A, B, C, D)\,. \tag{4.3}$$

This set of order parameters will be used to distinguish different crystalline phases appearing on the lattice. Several of these phases will be discussed in Section 4.2. A related order parameter that will become useful is the magnetic susceptibility χ_X. This is defined as the square of the magnetic

[3] See Table 4.1 for details.

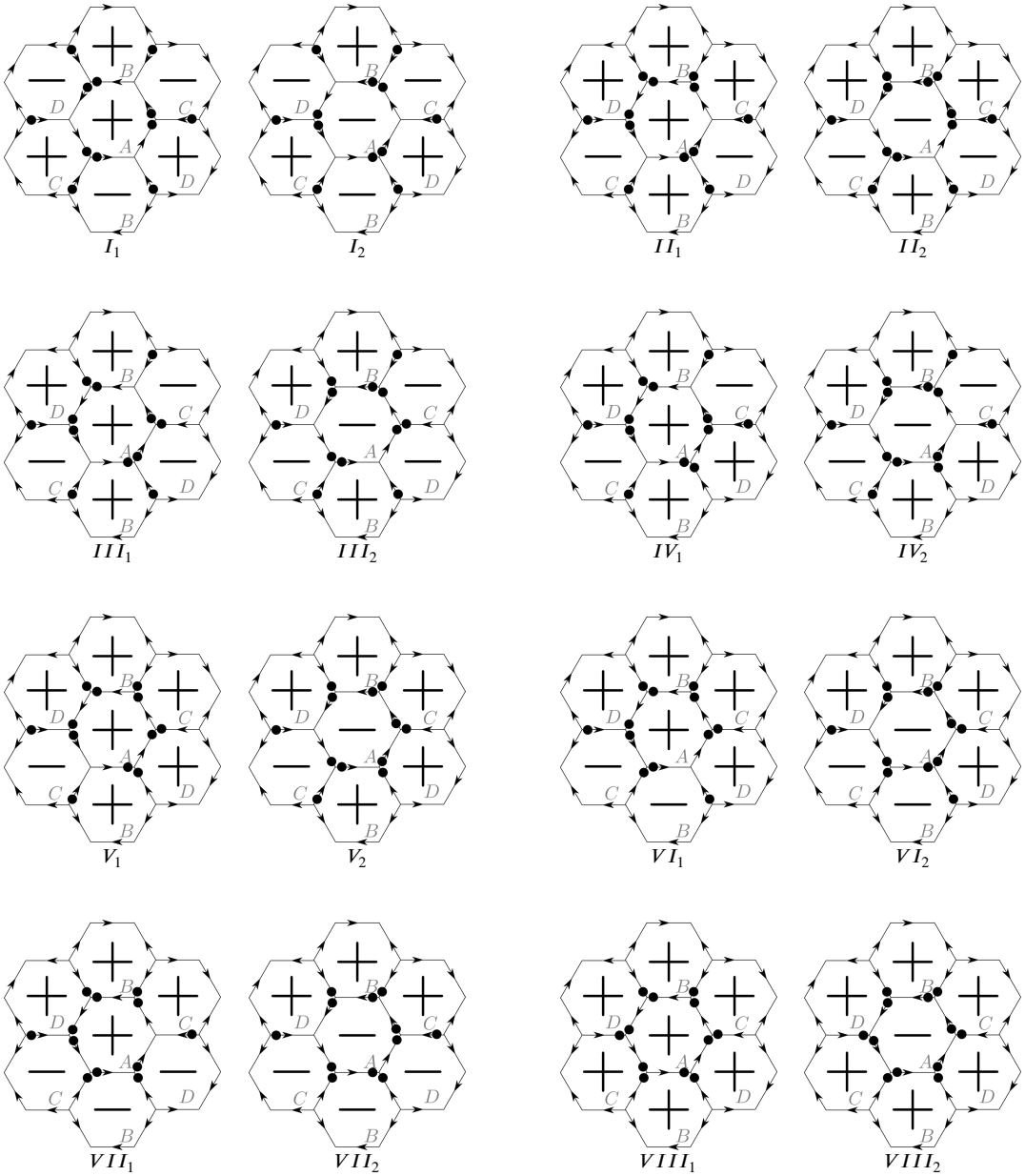

Figure 4.7: *The 16 plaquettes and environments of Figure 3.17 in terms of the height variables for the A sublattice. Each of the 8 environments supports two different plaquettes that are related by flipping the sign of the height variable at the central plaquette. Note that the height variables are affected by an overall sign ambiguity. Since sublattice A is rotationally symmetric, only a single orientation of the environments is shown.*

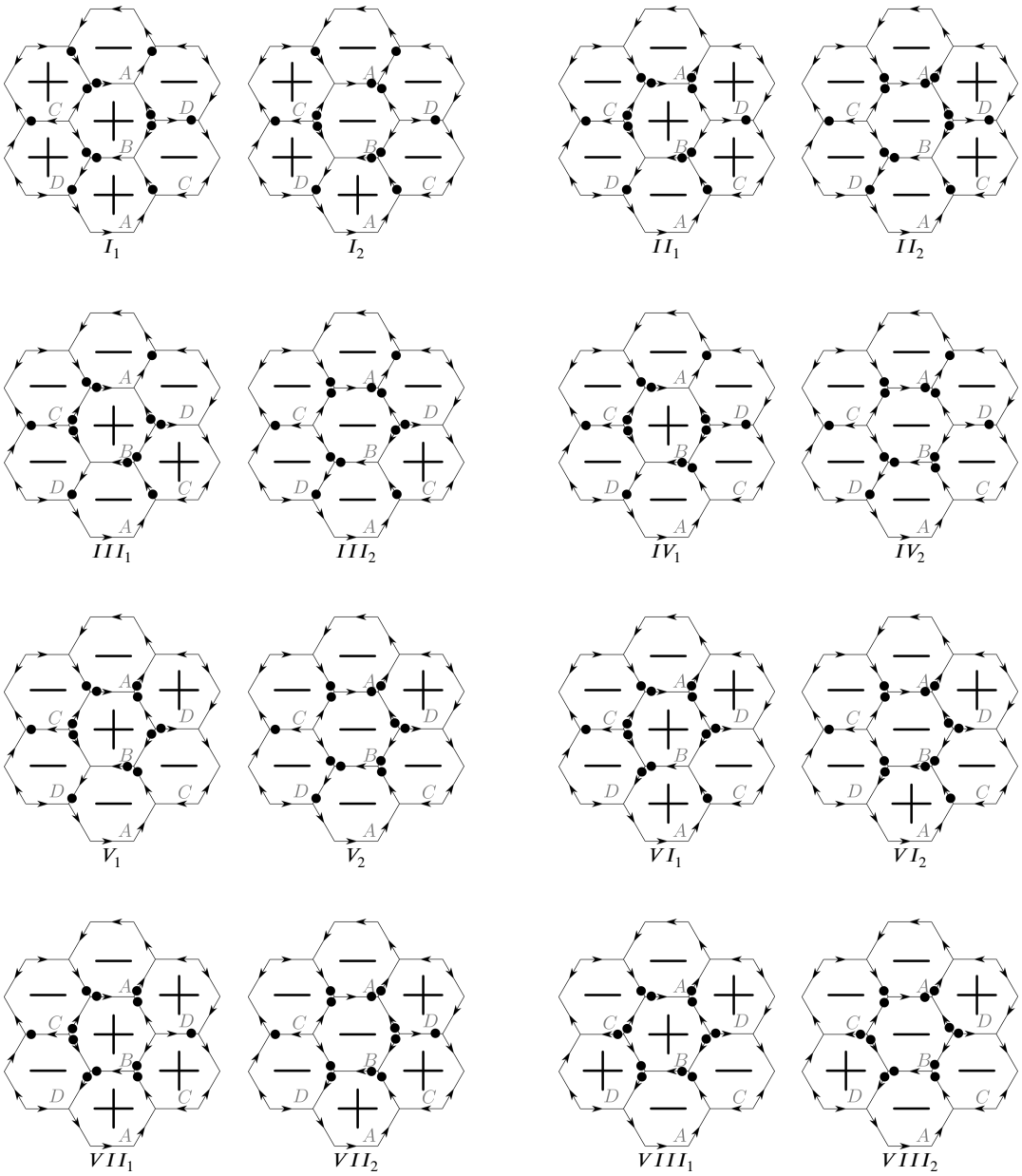

Figure 4.8: *The 16 plaquettes and environments of Figure 3.17 in terms of the height variables for the* **B** *sublattice. Each of the 8 environments supports two different plaquettes that are related by flipping the sign of the height variable at the central plaquette. Note that the height variables are affected by an overall sign ambiguity. Since the sublattices* **B**, **C**, *and* **D** *are related by rotations, only a single orientation of the environments is shown here.*

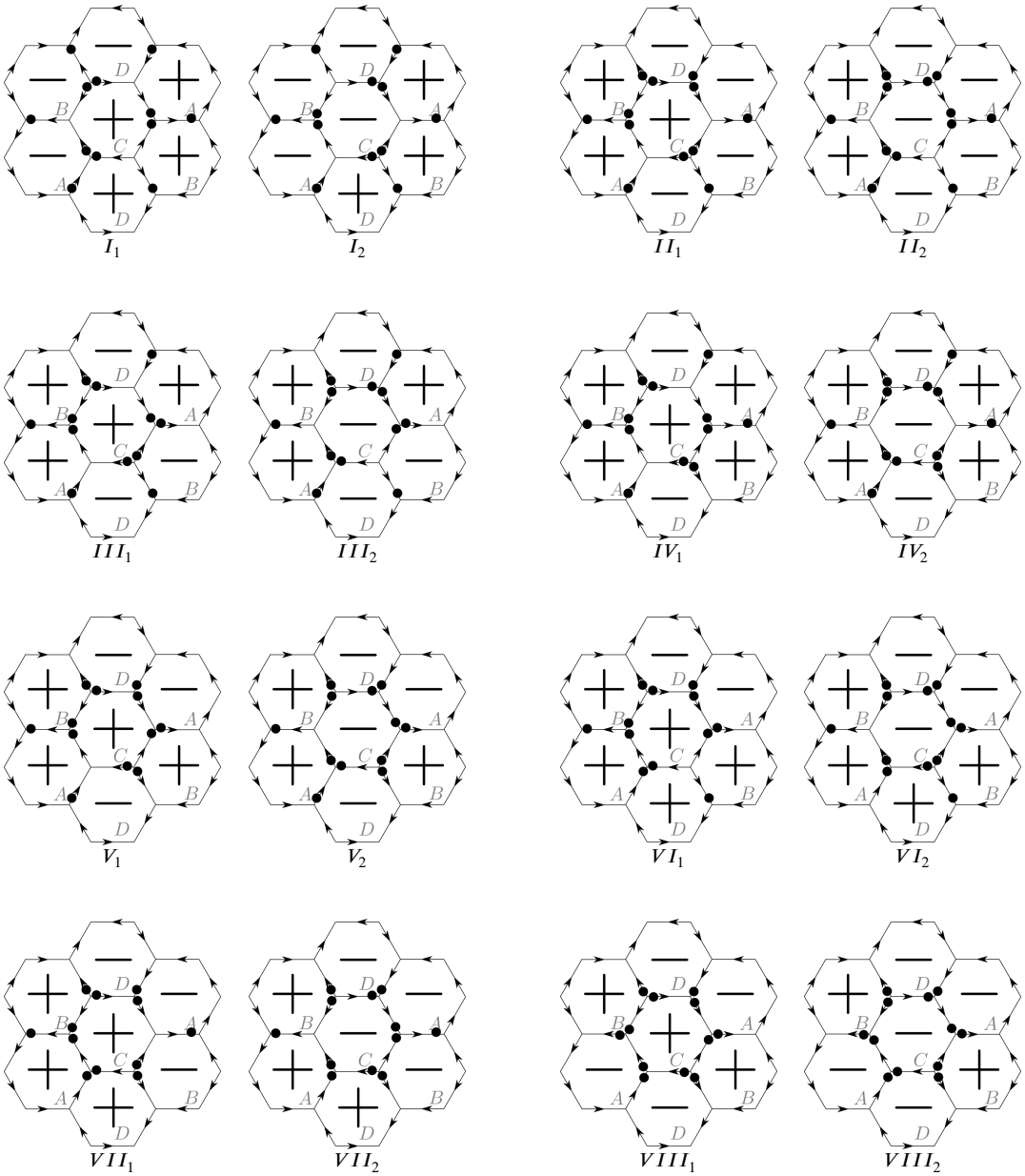

Figure 4.9: *The 16 plaquettes and environments of Figure 3.17 in terms of the height variables for the C sublattice. Each of the 8 environments supports two different plaquettes that are related by flipping the sign of the height variable at the central plaquette. Note that the height variables are affected by an overall sign ambiguity. Since the sublattices B, C, and D are related by rotations, only a single orientation of the environments is shown here.*

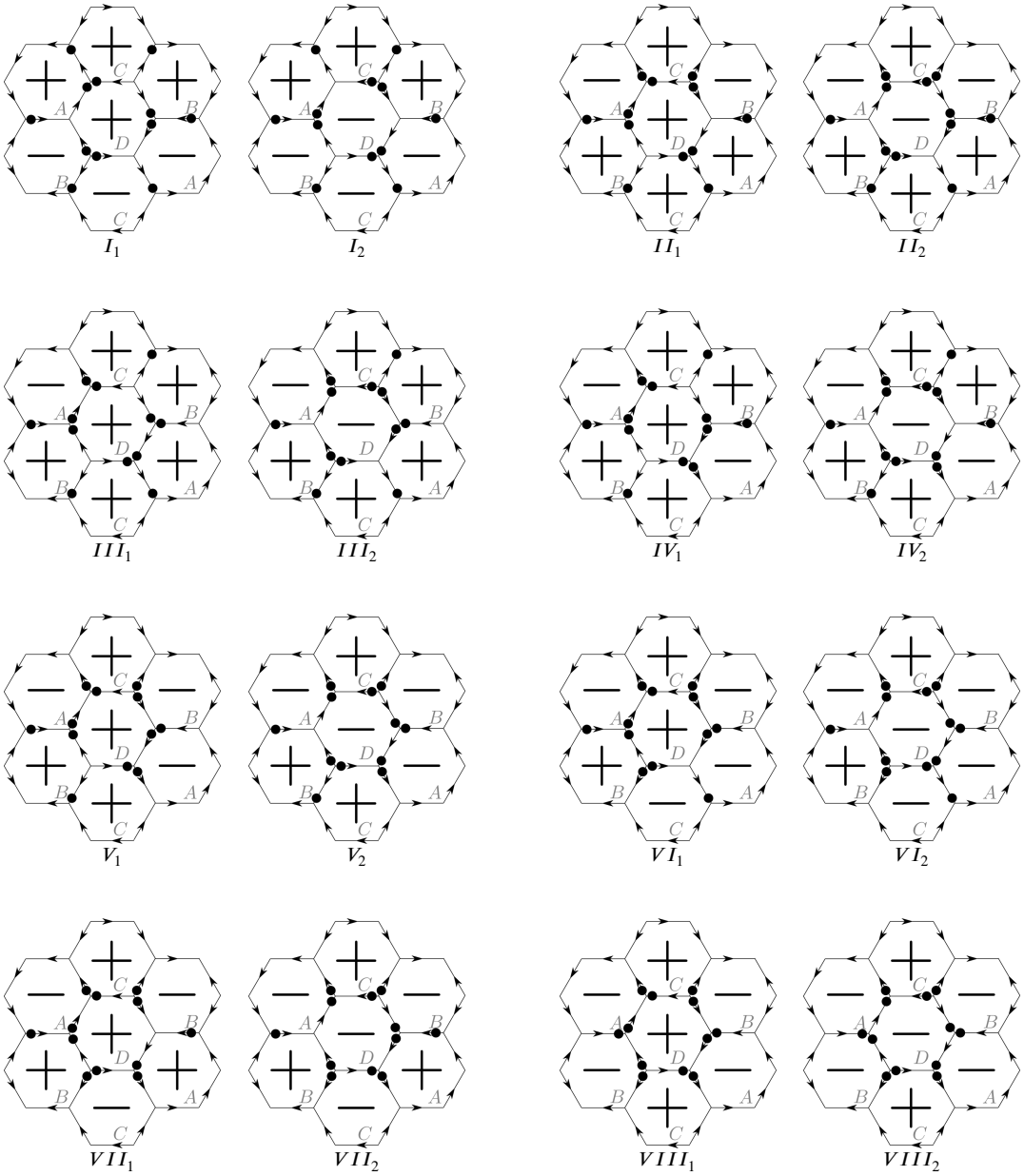

Figure 4.10: *The 16 plaquettes and environments of Figure 3.17 in terms of the height variables for the D sublattice. Each of the 8 environments supports two different plaquettes that are related by flipping the sign of the height variable at the central plaquette. Note that the height variables are affected by an overall sign ambiguity. Since the sublattices B, C, and D are related by rotations, only a single orientation of the environments is shown here.*

order parameter on the given sublattice X:

$$\chi_X \equiv M_X^2. \tag{4.4}$$

4.1.1 Reduced Hamiltonian Parameter Space

The apparent loss of manifest lattice symmetries for the height variable description, leads us to introduce a reduced parameter space for the Hamiltonian parameters of eq. (3.52), for which the symmetries are recovered in the height variable description. We emphasize that this reduction of the parameter space is not a necessity for performing Monte Carlo simulations of the QLM model. For the standard Metropolis algorithm the reduced parameter space merely simplifies the Hamiltonian, which makes it easier to handle numerically. The cluster algorithm, on the other hand, demands a symmetry for an overall sign change of the height variables on any one of the four sublattices. This is only realized in the reduced Hamiltonian parameter space, which is essential for the cluster algorithm to work efficiently. To see how the reduced parameter space is chosen, note that the height variable configuration of environment I for the A sublattice, is identical to the height variable configuration of environment VII for the D sublattice (or alternatively environment VII in the B and C environment, when properly rotated). Hence, by demanding that the Hamiltonian parameters related to environment I are equal to those of environment VII, i.e. $W_I = W_{VII} \equiv W_{17}$, and $T_I = T_{VII} \equiv T_{17}$, manifest translation and rotation symmetries have been recovered for the Hamiltonian in the height variable description, for the I and VII environments. Similar identifications can be made for the environment pairs of (II, VI), (III, V) and $(IV, VIII)$. The full rotation and translation symmetries are thereby recovered for the Hamiltonian in the height variable description by demanding that,

$$\begin{aligned}
W_{17} &\equiv W_I = W_{VII}, & T_{17} &\equiv T_I = T_{VII}, \\
W_{26} &\equiv W_{II} = W_{VI}, & T_{26} &\equiv T_{II} = T_{VI}, \\
W_{35} &\equiv W_{III} = W_V, & T_{35} &\equiv T_{III} = T_V, \\
W_{48} &\equiv W_{IV} = W_{VIII}, & T_{48} &\equiv T_{IV} = T_{VIII}.
\end{aligned} \tag{4.5}$$

In a plaquette environment, if two height variables on the same sublattice have the same sign, we say that they constitute a sign-pair in the given environment. E.g. for environment II in Figure 4.7, the two height variables on the B sublattice are both $+1$, thus giving rise to a single sign-pair on the B sublattice. The number of sign-pairs for an environment is directly linked to the environment pairs defined above,

env.	# sign-pairs
I,VII	0
II,VI	1
III,V	2
IV,VIII	3

Since the sign-pairs are-defined based on the relative sign for height variables on plaquettes on the same sublattice, an overall sign-flip on any of the four individual sublattices conserves the number of sign-pairs. Hence, by imposing the requirements of eq. (4.5), the model obtains four[4] global

[4]Since the model is affected by the redundancy of an overall flip of all the height variables, this represents three additional $\mathbb{Z}(2)$ symmetries .

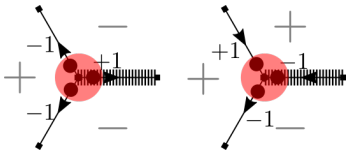

Figure 4.11: *Possible realizations of a* $3/2$*-charge on the lattice in terms of height variables. The Dirac-string can be placed on any of the 3 links connected to the site. Only a single Dirac-string configuration is shown here.*

Figure 4.12: *A Dirac-string along a link, marked by perpendicular lines, reverses the sign rules for the link orientation and the resulting height variables.*

$\mathbb{Z}(2)$-symmetries corresponding to an overall flip on any of the four sublattices. This is in contrast to the general case, where there is only a single $\mathbb{Z}(2)$ redundancy corresponding to a global flip of all the height variables.

4.1.2 Inclusion of Charges and Dirac-Strings

For the $\{4\}$-representation on the honeycomb lattice, three types of external charges exist. These are external charges carrying a $1/2$, 1, or $3/2$ representation of $SU(2)$ (i.e. doublet-, triplet-, or quadruplet-charges). In this thesis we focus on quadruplet charges. Since three links are coming together at a lattice site, a quadruplet colour charge can only be realized if all the link ends connected to the site, are populated with a colour doublet rishon. This is illustrated in Figure 4.11, for the two possible link orientations of the site. The external charges and the consequently odd number of rishons residing near the lattice site, alters the $\mathbb{Z}(2)$ Gauss' law of eq. (4.1) in terms of the link signs, and a Dirac-string must necessarily be included. The Dirac-string extends from one quadruplet colour charge to another quadruplet colour charge and transfers the flux between the two charges.[5] or it forms a closed loop. We emphasize that the Dirac-string itself is an unphysical object that is not gauge-invariant and cannot be observed, even though the flux transfer it imposes is physical. We represent the Dirac-string pictorially by perpendicular lines on the links, as shown in Figure 4.11. When crossing a Dirac-string the rules for assigning the $\mathbb{Z}(2)$ link variables and consequently the height variables are reversed.

This is illustrated in Figure 4.12. A flux closed around a periodic volume is constructed by first creating a pair of $3/2$ charges at a given lattice site. Then moving one of the charges over the lattice boundary, until it ends up at the original site where the two charges are annihilated, leaves behind a Dirac-string wrapping around the lattice. In Figure 4.13 two quadruplet charges are inserted into a background of -1 height variables. Note how the rishon configuration of plaquette A_1 gives

[5] Alternatively, the Dirac-string can end in $1/2$ charges, but we will not consider them here.

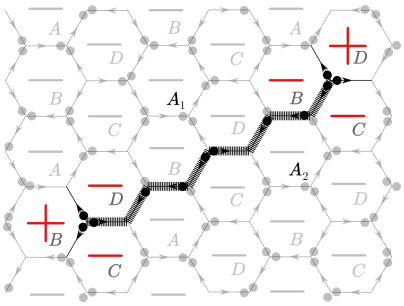

Figure 4.13: *Illustration of two external quadruplet-charges, marked in red circles, introduced into a pinwheel phase* $--\,--\,:\,A\circlearrowleft$ *(See Table 4.5). For each charge the surrounding height variables are locked (marked in red) and cannot be flipped. The two charges are connected by a Dirac-string (marked by perpendicular lines). In this cartoon state the physical flux string and the Dirac-string overlap.*

rise to a plaquette of environment type VIII, although plaquette A_2, with seemingly the same height variable configuration, gives rise to a rishon configuration of environment type VI. Since the quadruplet colour charge demands all the link-ends, that are coming together at the site, to be occupied by a rishon, there is a unique site-state that gives rise to a quadruplet charge on the honeycomb lattice. This implies that up to an overall sign there is only a single height variable configuration (at least when the Dirac-string and charge placement are specified), that gives rise to a quadruplet colour charge. These are marked in red in Figure 4.13. Changing the relative sign of the three height variables next to a quadruplet colour charge, would violate Gauss' law at the site. This is not true for neither the doublet nor the triplet external charges. For both of these, there are several rishon configurations near a site, that satisfy Gauss' law and consequently several height variable configurations that lead to a valid state. This is the reason why we only consider the $3/2$ charges.[6]

4.1.3 Height Variables on a Torus

To simulate the model, we wrap the honeycomb lattice around a torus. While for the square lattice we used boxed boundary conditions following the geometry of the square lattice, for the honeycomb lattice it is most natural to use a hexagonal geometry, i.e. the lattice is placed in a hexagonal domain and opposite sides of the hexagon are identified. This is illustrated in Figure 4.14 (left), where each of the hexagonal boundaries is coloured, such that sides of the same colour are identified with each other. This setup is equivalent to a square domain with periodic boundary conditions in the y-direction, and shifted periodic boundary conditions in the x-direction, as illustrated in Figure 4.14 (right). For computational reasons, we perform the simulations and present the results in terms of these boundary conditions. This construction allows for three directions in which a Dirac-string can be wrapped around the lattice. This is shown in Figure 4.14, where the Dirac-strings are coloured

[6]The two other types of external charges can be introduced similarly. To actually simulate the charges, one would, however, have to include transitions between the different height variable configurations that satisfy Gauss' law at the site. Even worse, in the case of the triplet charges, the height variable configurations would not be possible to use, since an external triplet charge, would be indistinguishable from a singlet in terms of the height variables and additional considerations would need to be taken into account.

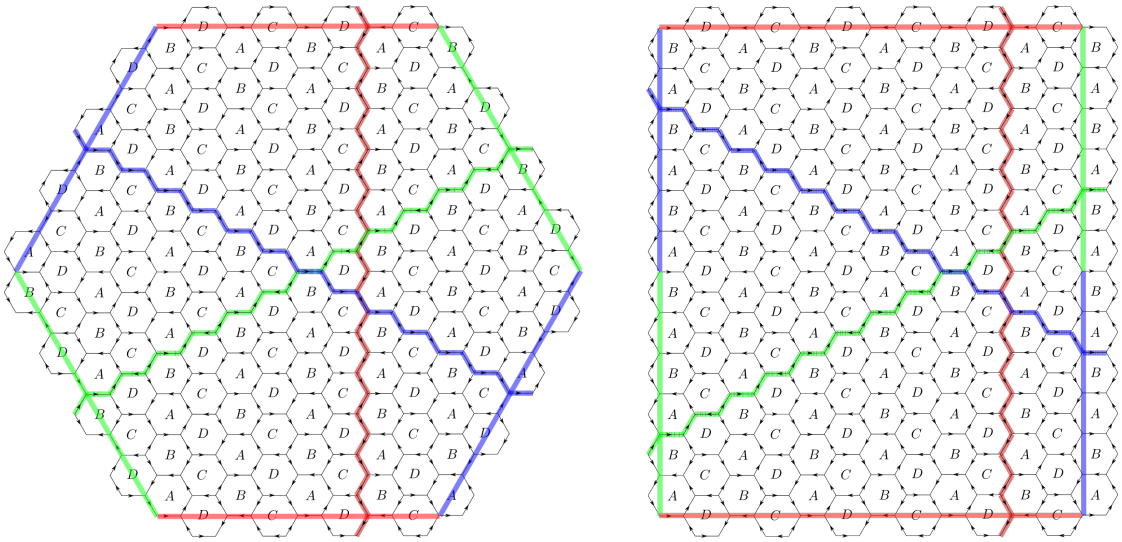

Figure 4.14: *Boundary conditions for the hexagonal lattice. Each boundary is represented by a colour (red, green, blue). The plaquettes are identified on boundaries with the same colour. Three possible Dirac-strings are included, coloured in the same way as the boundary that they wrap around. Left: Hexagonal periodic boundary conditions. Right: Corresponding shifted boundary conditions on a square domain.*

in the corresponding colour of the boundary, that they are wrapping around. Since wrapping a Dirac-string around in all three directions has no physical effect, the different Dirac-strings are not independent.

4.1.4 Symmetries of the Hamiltonian in Terms of Height Variables

Since the translation, rotation, and reflection symmetries of the lattice are not respected by the link orientation, the symmetries are not manifest in the height variable formulation. To find the corresponding symmetry operations in terms of the height variables, we introduce four operators $\mathcal{C}_{X\in\{A,B,C,D\}}$, that flip all the height variables on plaquettes belonging to a given sublattice X. It should be noted that the flip of all height variables on the entire lattice $\mathcal{C}_A\mathcal{C}_B\mathcal{C}_C\mathcal{C}_D$, is a trivial symmetry that reflects a $\mathbb{Z}(2)$ redundancy of the height variables. The height variable symmetries, corresponding to the symmetries of Table 3.2, are presented in Table 4.1. Several things should be noted. First of all, the link orientations and the related definition of the height variables depends on the sublattice. Here we have presented the rotations and reflections with respect to each type of sublattice. These are not independent, but are related to each other by translations.[7] Second, since the height variables are only defined up to an overall sign ambiguity, the symmetry operations are not unique. One is always free to introduce an overall flip of the height variables on all four sublattices. Furthermore, only a few of the operations are independent of each other. These are two of the translations, together with a single rotation and reflection. The other symmetry operations can be constructed from a combination of these. Under a symmetry operation, the order parameters

[7] Since the reflection axes intersect two types of sub-plaquettes, the reflections are double-counted. E.g. a reflection R_{A_i} is equivalent to a reflection R_{D_i}.

Symmetry	Operation	Independent	M'_A	M'_B	M'_C	M'_D
Translation: $\hat{1}$	$\mathcal{C}_A\mathcal{C}_B\mathcal{T}_{\hat{1}}$	Yes	$-M_D$	$-M_C$	M_B	M_A
Translation: $\hat{2}$	$\mathcal{C}_A\mathcal{C}_D\mathcal{T}_{\hat{2}}$	Yes	$-M_C$	M_D	M_A	$-M_B$
Translation: $\hat{3}$	$\mathcal{C}_A\mathcal{C}_C\mathcal{T}_{\hat{3}}$	No	$-M_B$	M_A	$-M_D$	M_C
Rotation: A	$\mathcal{O}_A$	Yes	M_A	M_C	M_D	M_B
Rotation: B	$\mathcal{C}_A\mathcal{C}_D\mathcal{O}_B$	No	$-M_D$	M_B	M_A	$-M_C$
Rotation: C	$\mathcal{C}_A\mathcal{C}_B\mathcal{O}_C$	No	$-M_B$	$-M_D$	M_C	M_A
Rotation: D	$\mathcal{C}_A\mathcal{C}_C\mathcal{O}_D$	No	$-M_C$	M_A	$-M_B$	M_D
Reflection: $A_{\hat{1}}$	$\mathcal{C}_A R_{A_{\hat{1}}}$	Yes	$-M_A$	M_C	M_B	M_D
Reflection: $A_{\hat{2}}$	$\mathcal{C}_A R_{A_{\hat{2}}}$	No	$-M_A$	M_D	M_C	M_B
Reflection: $A_{\hat{3}}$	$\mathcal{C}_A R_{A_{\hat{3}}}$	No	$-M_A$	M_B	M_D	M_C
Reflection: $B_{\hat{1}}$	$\mathcal{C}_C R_{B_{\hat{1}}}$	No	M_D	M_B	$-M_C$	M_A
Reflection: $B_{\hat{2}}$	$\mathcal{C}_B R_{B_{\hat{2}}}$	No	M_C	$-M_B$	M_A	M_D
Reflection: $B_{\hat{3}}$	$\mathcal{C}_A R_{B_{\hat{3}}}$	No	$-M_A$	M_B	M_D	M_C
Reflection: $C_{\hat{1}}$	$\mathcal{C}_C R_{C_{\hat{1}}}$	No	M_D	M_B	$-M_C$	M_A
Reflection: $C_{\hat{2}}$	$\mathcal{C}_A R_{C_{\hat{2}}}$	No	$-M_A$	M_D	M_C	M_B
Reflection: $C_{\hat{3}}$	$\mathcal{C}_D R_{C_{\hat{3}}}$	No	M_B	M_A	M_C	$-M_D$
Reflection: $D_{\hat{1}}$	$\mathcal{C}_A R_{D_{\hat{1}}}$	No	$-M_A$	M_C	M_B	M_D
Reflection: $D_{\hat{2}}$	$\mathcal{C}_B R_{D_{\hat{2}}}$	No	M_C	$-M_B$	M_A	M_D
Reflection: $D_{\hat{3}}$	$\mathcal{C}_D R_{D_{\hat{3}}}$	No	M_B	M_A	M_C	$-M_D$
Overall $\mathbb{Z}(2)$	$\mathcal{C}_A\mathcal{C}_B\mathcal{C}_C\mathcal{C}_D$	Yes	$-M_A$	$-M_B$	$-M_C$	$-M_D$

Table 4.1: *Lattice symmetries in terms of the height variables. $\mathcal{C}_X$ flips all the height variables on the X sublattice. The "Independent" column denotes whether the symmetry cannot be constructed from operations included in higher rows. The last columns show how the order parameters M_X are changed under the operation.*

are changed, and in the last column of the table we present the order parameters after the operation M'_X, in terms of the initial order parameters M_Y. In the reduced parameter space of eq. (4.5), there exist additional $\mathbb{Z}(2)$ symmetries corresponding to independent flips of the height variables, on each of the four sublattices. These are presented in Table 4.2.

Center Symmetries with Hexagonal Boundary Conditions on the Honeycomb Lattice

For the honeycomb lattice there exist three axes along which the center symmetry can be defined, see Figure 4.6. Only two of these are independent. We denote the center symmetry sectors according to the $\mathbb{Z}(2)$ value obtained in each of the three direction. These are shown in Table 4.3. Note that not all combinations are possible since the -1 values come in pairs. In the height variable description of the QLM, the center symmetry sectors are related to the choice of symmetric or antisymmetric boundary conditions for the height variables. We emphasize that the height variable description demands that the lattice has a length corresponding to an even number of plaquettes, thereby avoiding the ambiguities discussed in Section 3.4 in relation to odd-sized lattices. Strictly periodic boundary conditions for the height variables give rishon configurations in the trivial center symmetry sector. Antiperiodic boundary conditions along two directions change, the correspond-

Symmetry	Operation	Independent	M'_A	M'_B	M'_C	M'_D
Height-Variable Flip: A	$\mathcal{C}_A$	Yes	$-M_A$	M_B	M_C	M_D
Height-Variable Flip: B	$\mathcal{C}_B$	Yes	M_A	$-M_B$	M_C	M_D
Height-Variable Flip: C	$\mathcal{C}_C$	Yes	M_A	M_B	$-M_C$	M_D
Height-Variable Flip: D	$\mathcal{C}_D$	No	M_A	M_B	M_C	$-M_D$

Table 4.2: *In the reduced parameter space there exist additional* $\mathbb{Z}(2)$ *symmetries.*

Center Symmetry $(\hat{1}\hat{2}\hat{3})$	Boundary Conditions $(\hat{1}\hat{2}\hat{3})$	Dirac-String Direction
$+++$	$+++$	None
$--+$	$--+$	$\hat{3}$
$-+-$	$-+-$	$\hat{2}$
$+--$	$+--$	$\hat{1}$

Table 4.3: *Realizations of the four center symmetry sectors on the honeycomb lattice in the height variable description. The system is given in terms of the boundary conditions or equivalently Dirac-string wrapping around the lattice closed on a torus.*

ing center $\mathbb{Z}(2)$ values in those directions and is equivalent to creating a Dirac-string wrapping around the lattice in the remaining third direction. It should be noted that, since the three directions are not independent, it is not possible to impose antiperiodic boundary conditions in just a single direction. The relations between the center symmetry sectors, the boundary conditions, and the Dirac-strings are summarized in Table 4.3.

4.2 Different Confined Phases

In the 18-dimensional Hamiltonian parameter space, we will identify several distinct phases. In this section, we will discuss some of them in preparation for interpreting the results of the simulations. The different phases are distinguished by the sublattice magnetization order parameters M_X of eq. (4.3).

4.2.1 Mean Field Calculations in the Reduced Parameter Space

In the reduced parameter space there are four $\mathbb{Z}(2)$ symmetries, one for each of the order parameters M_X, compared to a single overall $\mathbb{Z}(2)$ symmetry, which respects the height variable redundancy, for the whole lattice in the general case. This allows the construction of a simple effective potential. Before specifying the different phases, we perform a mean field calculation in the reduced parameter space. In addition to the four $\mathbb{Z}(2)$-symmetries that the effective potential must respect, each of the order parameters M_X must also enter symmetrically in the effective potential. We construct

	M_A^2	M_B^2	M_C^2	M_D^2	$\chi_X = \sum_X M_X^2$	Min V_{eff}
I:	$\frac{1}{4}\sum_X M_X^2$	$\frac{1}{4}\sum_X M_X^2$	$\frac{1}{4}\sum_X M_X^2$	$\frac{1}{4}\sum_X M_X^2$	$-\frac{a}{2b+\frac{3}{4}c}$	$-\frac{a^2}{2(2b+\frac{3}{4}c)}$
II:	$\frac{1}{3}\sum_X M_X^2$	$\frac{1}{3}\sum_X M_X^2$	$\frac{1}{3}\sum_X M_X^2$	0	$-\frac{a}{2b+\frac{2}{3}c}$	$-\frac{a^2}{2(2b+\frac{2}{3}c)}$
III:	$\frac{1}{2}\sum_X M_X^2$	$\frac{1}{2}\sum_X M_X^2$	0	0	$-\frac{a}{2b+\frac{1}{2}c}$	$-\frac{a^2}{2(2b+\frac{1}{2}c)}$
IV:	$\sum_X M_X^2$	0	0	0	$-\frac{a}{2b}$	$-\frac{a^2}{2(2b)}$
V:	0	0	0	0	0	0

Table 4.4: *Results for the effective potential minimum and the corresponding magnetic susceptibility based in different assumptions. Only a single choice of sublattice ordering is shown here, but equivalent results are obtained for any permutation of the four sublattices.*

an effective potential to next-to-lowest-order in the order parameters M_X, $X \in \{A, B, C, D\}$, as

$$V_{eff}\left(M_A, M_B, M_C, M_D\right) = a\left(\sum_X M_X^2\right) + b\left(\sum_X M_X^2\right)^2 + c\left(\sum_{X\neq Y} M_X^2 M_Y^2\right). \tag{4.6}$$

Here a, b, and c are arbitrary real constants and the two variables X and Y are summed over the four sublattices (A, B, C, D). The minimum of the effective potential with respect to each of the M_X is obtained at

$$\begin{aligned} M_X\left(a + (2b+c)\sum_Y M_Y^2 - c M_X^2\right) &= 0 \qquad (4.7)\\ \Rightarrow \quad M_X = 0 \quad \vee \quad M_X &= \frac{1}{c}\left(a + (2b+c)\sum_Y M_Y^2\right). \end{aligned}$$

For the effective potential to result in spontaneous symmetry breaking, the a factor should be negative. Let us assume that, for any $X \in \{A, B, C, D\}$ the order parameters M_X^2 are either zero, or if non-zero, that the remaining order parameters appear symmetrically in the potential. The order parameters are then of equal magnitude, for each of the non-zero order parameters. We can set between zero and four order parameters to be equal to 0, which gives five possible results for the mean-field effective potential. These are presented in Table 4.4 together with the value of the effective potential extremum and the sum of the squared order parameters. Depending on the signs and magnitudes of the b and c parameters, the energetically most favourable state is either I, where all the sublattices are ordered, or IV, where only a single sublattice is ordered.[8] This implies that, in the mean-field approximation, there are only two possibilities for the phases in the reduced Hamiltonian parameter space. Either all 4 sublattices (A, B, C, D) order (I) or only a single out of the four sublattices orders (IV). Both of the phases that we will encounter in Monte Carlo simulations in the reduced Hamiltonian parameter space, will turn out to be ordered on all four sublattices.

Outside of the reduced parameter space, only the single $\mathbb{Z}(2)$ symmetry reflecting the redundancy of the height variables remains. This loss of symmetries complicates the construction of a

[8] For $b > 0$, I is the energetically most favourable state in the interval $-\frac{8}{3}b < c < 0$. For $b < 0$, state I is energetically most favourable in the regime $c \geq -\frac{8}{3}b$.

M_A	M_B	M_C	M_D	Pinwheel
+	+	+	+	A ↺
+	+	+	−	B ↻
+	+	−	+	D ↻
+	+	−	−	D ↺
+	−	+	+	C ↻
+	−	+	−	B ↺
+	−	−	+	C ↺
+	−	−	−	A ↻

Table 4.5: *Order parameter signatures for the 8 correlated pinwheel phases. The arrow denotes the orientation of the pinwheels. The height variables are affected by an overall sign redundancy, not included here.*

general effective potential, and we have not pursued the construction of the more general effective potential any further in this thesis. It could, however, be an interesting future project to generalize the effective action, since it could help to shine some light on the type of phase transitions we will observe in Section 4.3.

4.2.2 The Pinwheel Phase

As illustrated in Figure D.3 in the appendix, plaquettes supported by an environment with exactly one environment rishon at each site (environment VIII) give rise to a dimer pinwheel on the Kagomé lattice. We refer to this type of plaquette configurations as pinwheel plaquettes. In a cartoon state of the pinwheel phase, the pinwheel plaquettes completely cover one of the 4 sublattices (A, B, C, D), and the remaining 3 sublattices create an environment that support the pinwheel plaquettes. There exist two distinct types of pinwheel phases. A correlated pinwheel phase and an uncorrelated pinwheel phase, where correlation refers to the orientation of pinwheels on different plaquettes, but still on the same sublattice. In both phases, pinwheel plaquettes exist only in one of the four sublattices. In the correlated pinwheel phase, all pinwheels have the same (clockwise or counter-clockwise) orientation. This is not the case in the uncorrelated pinwheel phase.

Correlated Pinwheel Phase

In the correlated pinwheel phase all pinwheels are rotating in the same direction. Cartoon states of four realizations of the correlated pinwheel phase are shown in Figure 4.15. Here counter-clockwise rotating pinwheels are placed on each of the four sublattices. In the correlated pinwheel cartoon state, all plaquettes belonging to the sublattice carrying the pinwheels, are in the VIII environment. All remaining plaquettes are in the IV environment. If a pinwheel would be rotating in the opposite direction, this would change the plaquettes supporting that pinwheel away from the IV environment. Since the pinwheel can rotate in either direction, this give a total of 8 possible realizations of the correlated pinwheel phase. These are summarized in terms of their order parameters in Table 4.5. In this phase all four sublattices order, which agrees with the mean field

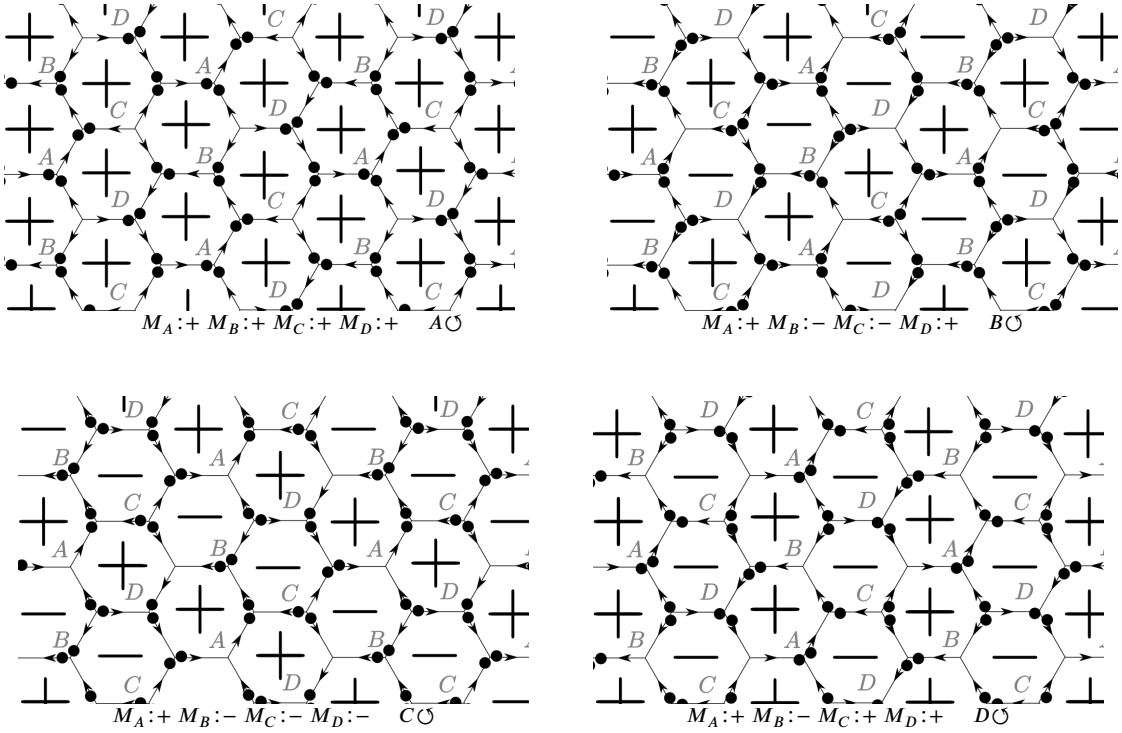

Figure 4.15: *Illustration of four pinwheel phases and their magnetic order parameters M_X. Here counter-clockwise oriented pinwheels are placed on each of the four sublattices.*

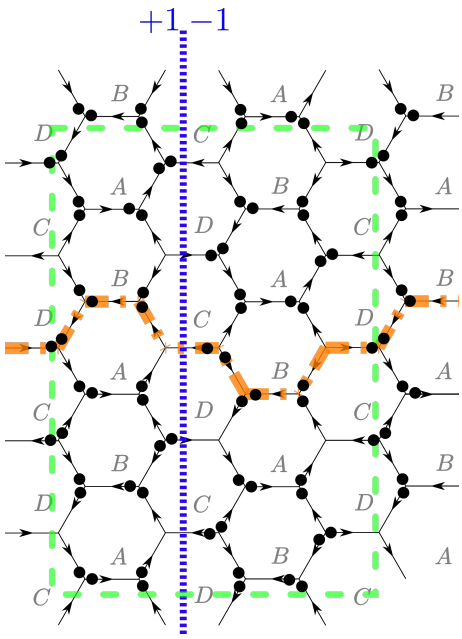

Figure 4.16: *An odd-sized lattice, periodic over the green dashed box, always contains a half-flux (measured over the dashed blue line), together with a single associated domain wall (orange), separating two realizations of a pinwheel phase. Note that the height variables do not fit onto an odd-sized lattice and they cannot close periodically over the green box in the y-direction.*

calculations for the reduced parameter space (see Table 4.4). The correlated pinwheel phase spontaneously breaks all the symmetries of Table 4.1 (and Table 4.2) in terms of the order parameters, except for rotations centred on the sublattice that carries the pinwheels.

$\mathbb{Z}(2)$ **Fluxes and Domain Walls**

Let us consider the behaviour of fluxes and domain walls in the correlated pinwheel phase. There are 8 possible realizations of the correlated pinwheel phase. Spatial regions that exist in different realizations of the pinwheel phase are separated by a domain wall. This is illustrated in Figure 4.16, where we have realized the correlated pinwheel phase on a lattice with odd-size in the y-direction. Since the lattice is odd-sized in the y-direction, it is not possible to close the pinwheel phase on itself. The upper pinwheels are therefore residing on the A sublattice and the lower pinwheels are residing on the B sublattice.[9] There exists a domain wall separating the two distinct realizations of a pinwheel phase, illustrated as an orange dashed line. As noted in Section 3.4, the flux going through a closed loop is determined by counting the number of rishons residing on either the left- or the right-hand side of the links crossed by the loop. In Figure 4.16 we calculate the flux through the dashed blue loop. Using the definition of a rishon to the left (right) gives a Z_y value of $+1$ (-1) across the blue loop. This is illustrated with the two values above the loop, where the left

[9] We emphasize that the lattice directions, and consequently the sublattice denominations, do not fit onto an odd-sized lattice. The sublattice denomination in Figure 4.16 does therefore strictly speaking not make sense. Here we are simply using them to indicate where the pinwheels are located. Later we double the size of the lattice, where we again are able to assign the orientations and consequently the sublattices.

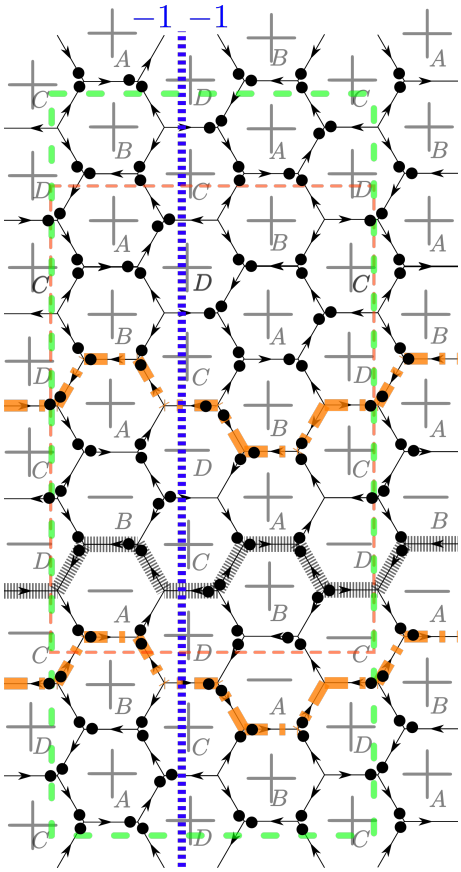

Figure 4.17: *The inclusion of a single Dirac-string (perpendicular lines), on an even-sized lattice, creates two domain walls. The green box is endowed with periodic boundary conditions. Notice that Figure 4.16 is included inside the red box.*

(right) is calculated with the left (right) flux definition. In addition to this, Z_y changes sign if we translate the loop by a single plaquette in the x-direction. Wrapping a flux line around the lattice in the x-direction, is equivalent to flipping all the rishons from the one end of a link to the other for all links along a strand going around the lattice in the x-direction (e.g. along the domain wall). This similarly flips the sign of the Z_y, as would be expected since a flux is added. It is important to note that this does not remove the flux, but simply flip the non-trivial center quantum number from the right to the left definition, or equivalently shifts the flux by one lattice translation in the x direction. We therefore interpret the loop to contain a single $1/2$-flux wrapping around the lattice in the x-direction, which is associated with a single domain wall wrapping around in the same direction. We emphasize that, based on the nature of the $\{4\}$-representation, we cannot determine where the $1/2$ flux is residing, but only that it exists in the same closed box as a single domain wall. On an even-sized lattice, this picture is fundamentally changed. This is illustrated in Figure 4.17, where the lattice is again periodic over the green dashed box. Since the link orientations can now be consistently extended over the periodic boundaries, we have reintroduced the height variables. Here we have introduced a single Dirac-string, as before illustrated by perpendicular lines, wrapping around the lattice in the x-direction. A realization of the correlated pinwheel phase cannot be maintained on the entire lattice with the inclusion of a Dirac-string and a correlated pinwheel

phase on the B sublattice appears. This is separated from the exterior by two domain walls (orange dashed lines). The flux is calculated through the closed blue loop and results in $Z_y = -1$ for both definitions. We interpret this as one unit of flux wrapping around the x-direction.[10] We emphasize that the odd-sized lattice of Figure 4.16, is identical to what is included inside the thin red box in Figure 4.17.[11] We therefore expect that the full 1-flux has fractionalized and there exists a $1/2$ flux inside this area of the lattice, together with another $1/2$ flux outside, each associated with a domain wall. Hence, introducing a Dirac-string to an even-sized lattice, creates a full 1-flux together with two domain walls. This is in contrast to the odd lattice, where there always exists exactly one domain wall together with a single $1/2$ flux. Considering an even-sized lattice with a set of $3/2$-charges, we obtain a similar picture. This is illustrated in Figure 4.18, where we have included two $3/2$-charges (red circles) into a background of correlated pinwheels on the A sublattice and connected the charges with a Dirac-string. Here we obtain two domain walls (orange dashed lines) separating the realization of the correlated pinwheels on the B sublattice from the exterior, where the correlated pinwheels are residing on the A sublattice. We measure the flux through closed loops (blue dashed lines) which in this case give rise to a Z_y value of -1 between the charges and $Z_y = +1$ beyond the charges.[12] This shows that there is a full 1-flux connecting the two charges. It is important to note that between the charges, where the flux is flowing, there are two domain walls. This picture is therefore similar to what we saw in Figure 4.17. It therefore seems natural that the flux would again fractionalize into two strands of $1/2$-flux, each associated with a domain wall. Although we have found that both the inclusion of a pair of $3/2$-charges and the inclusion of a flux, enforced by including a Dirac-string, each give rise to two domain walls separating distinct realizations of the pinwheel phase, the domain walls will not necessarily separate from each other, and open up a region on which another phase can exist. One could imagine that the two domain walls would stay together, and not let any phase grow in between them. with

Uncorrelated Pinwheel Phase

Cartoon states of the uncorrelated pinwheel phase are similar to those shown in Figure 4.15, except that the orientations of the pinwheel are uncorrelated. Consequently, the height variables can flip independently on the plaquettes that carry the pinwheels. The corresponding sublattice is therefore disordered such that the order parameter averages to zero. This reduces the number of distinct realizations of the phase from 8 to 4. These are characterized in Table 4.6, in terms of the order parameters. Since in the uncorrelated pinwheel phase only three of the sublattices order, according to the mean-filed analysis of Section 4.2.1 we do not expect this phase to show up in the reduced parameter space. Indeed, later we will find that this phase only appears when $T_{IV} \neq T_{VIII}$. For the uncorrelated pinwheel phase, both the rotation and reflection symmetries, centred on the sublattice that carries the pinwheels, are unbroken. The remaining symmetries in Table 4.1 (and Table 4.2) are spontaneously-broken. Concerning the fluxes, for the uncorrelated pinwheel phase we can make similar arguments and draw similar figures as for the correlated pinwheel phase in terms of the fluxes, except that the pinwheels are no longer necessarily oriented in the same direction.

[10] This value is independent of the translation of the loop along the x-direction. Introducing a flux string by flipping all rishons along a string that wraps around the lattice, flips the Z_y value for both definitions, which is expected for one unit of $\mathbb{Z}(2)$ flux of 1.

[11] This is the reason why we kept the sublattice denomination in the odd-sized lattice.

[12] Since we are still on an even-sized lattice, the left and right definition agree and we only show a single result in the figure.

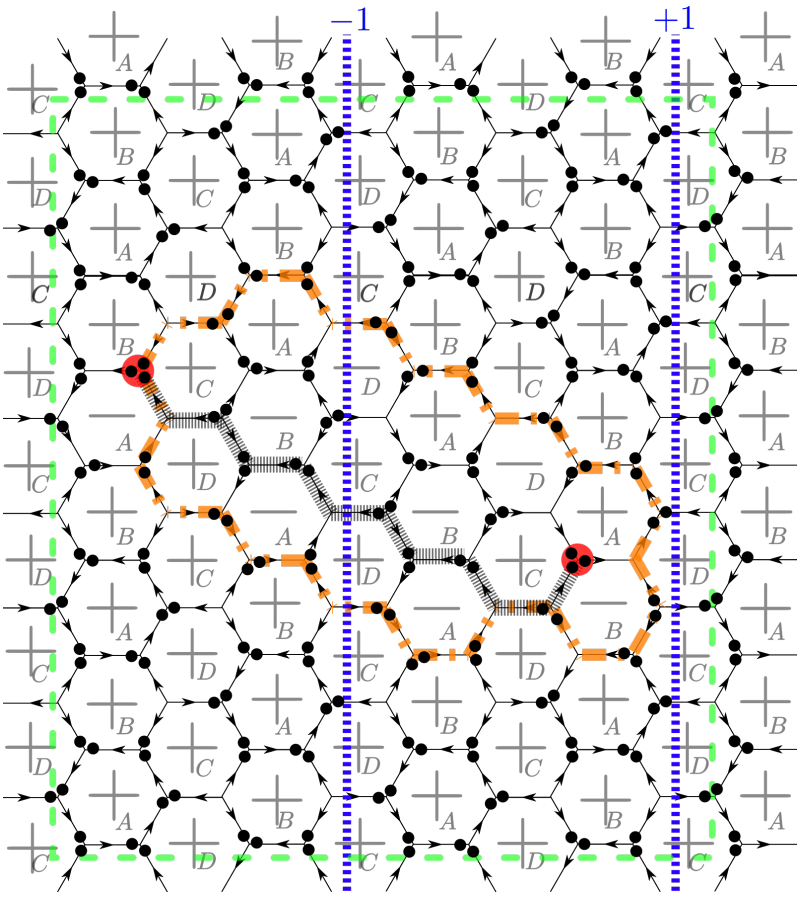

Figure 4.18: *The inclusion of two 3/2-charges connected by a Dirac-string (perpendicular lines) creates two domain walls (orange links) with a different pinwheel realization inside the domain walls compared to the bulk (See Figure 4.17). The green box is endowed with periodic boundary conditions.*

M_A	M_B	M_C	M_D	Pinwheel
0	+	+	+	***A***
+	0	+	−	***B***
+	−	0	+	***C***
+	+	−	0	***D***

Table 4.6: *Order parameter signatures for the cartoon states of the 4 uncorrelated pinwheel phases. The height variables are affected by an overall sign ambiguity, not included here.*

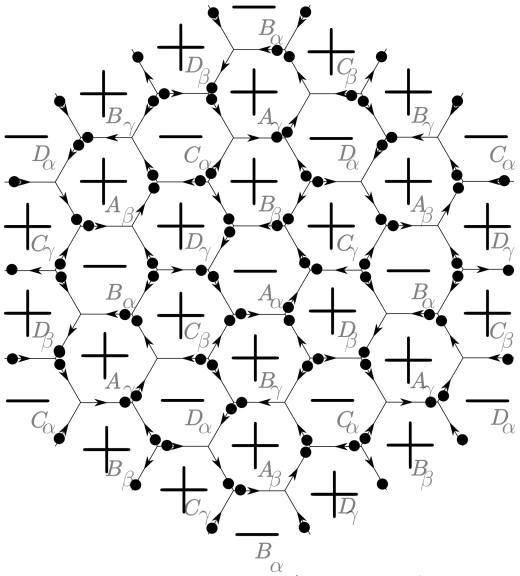

Figure 4.19: *Illustrations of the anti-pinwheel phase with the order parameters of* $M_{X_\alpha} = -M_{X_\beta} = -M_{X_\gamma}$*, where* X *is any of the sublattices* A*,* B*,* C*, or* D*.*

4.2.3 The Anti-Pinwheel Phase

In the reduced parameter space, the correlated pinwheel phase realizes the largest number of sign-pairs. The most different plaquette environments are I and VII, with no sign-pairs. We will denote the phase favoured by these environments as the anti-pinwheel phase. In contrast to the pinwheel phases, which live on the (A, B, C, D)-sublattices, the phase favoured by the environments I and VII, does not fit on the same four sublattice structure. Furthermore, no cartoon state can be constructed which realizes plaquettes belonging to the environments I or VII everywhere on the lattice. In a cartoon state of the anti-pinwheel phase, a maximum of two-thirds of each of the four sublattices can be covered by plaquettes in the environments I or VII, the last third of plaquettes must be in the environments IV or VIII. This implies that the anti-pinwheel phase lives on a tripartite lattice, denoted by Greek letters (α, β, γ). A cartoon state of this phase is shown in Figure 4.19. The height variables are defined in relation to the imposed link orientation, and we can therefore not relate the individual height variables on plaquettes belonging to different sublattices (A, B, C, D). Hence, we need to consider a total of 12 different sublattices, and their corresponding 12 order parameters, for the realization of this phase. To distinguish the 12 sublattices and order parameters, we endow the four (A, B, C, D) sublattices with an additional Greek subscript (α, β, γ). In the cartoon state shown in Figure 4.19, the sublattices β and γ are covered by plaquettes belonging to the environments I or VII, and plaquettes on the α sublattice are covered by plaquettes belonging to the environments IV or VIII. The anti-pinwheel phase is characterized by each of the four sublattice $X \in \{A, B, C, D\}$, are ordered with two of the additional $(X_\alpha, X_\beta, X_\gamma)$ sublattices having the same sign for the height variables, while the last is ordered with height variables with the opposite sign. It is important that it is the same $(X_\alpha, X_\beta, X_\gamma)$ sublattice that is carrying the opposite height variable sign, for all $X \in \{A, B, C, D\}$. E.g. in the cartoon state of Figure 4.19 the lattices are ordered such that $M_{X_\alpha} = -M_{X_\beta} = -M_{X_\gamma}$ for all $X \in \{A, B, C, D\}$. Since the (α, β, γ)

sublattice with the opposing sign for the height variables can be freely chosen, and the height variables on any of the four sublattice (A, B, C, D) can be flipped independently, this gives a total of $2^3 \times 3 = 24$ possible realizations of this phase (not counting the overall trivial flip of all height variables). Since there are now 12 magnetic order parameters, in contrast to the four encountered for the pinwheel phases, we will not present a complete symmetry analysis of the order parameters for this phase. Instead we will simply note that from Figure 4.19 one can convince oneself that all the symmetries of Table 4.1 and Table 4.2 are broken, with the exception of rotations centred on the plaquettes carrying the pinwheels. In Figure 4.19 these are the A_α plaquettes. The remaining plaquettes in the IV environment maintain a 120° rotation symmetry. These are the plaquettes belonging to the same sublattice (A, B, C, D) as the plaquettes which carry the pinwheels, but not the same sublattice (α, β, γ). In Figure 4.19 these are the A_β and A_γ plaquettes. Finally plaquettes belonging to the same sublattice (α, β, γ) as the plaquettes which carry the pinwheel, but not to the same (A, B, C, D), maintain a 180° rotation symmetry. In Figure 4.19 these are the B_α, C_α, and D_α plaquettes.

4.3 Monte Carlo Simulations

We are going to simulate the model using two different numerical methods. The first method is the standard Metropolis algorithm [115, 116]. Since on a closed torus, transitions must necessarily appear in pairs, the sign problem can be avoided, if all the transition have the same sign. This also implies that T_{III} must be a real parameter. The Metropolis algorithm is otherwise able to simulate the entire parameter space. It does, however, suffers from being inefficient and it is hard for the algorithm to tunnel between differently ordered configurations. For the simulations that we are going to perform, the parameters have been chosen such that the Metropolis algorithm works properly. The second method is a specialized cluster algorithm similar to the algorithm used in [14, 15]. This works for the correlated pinwheel phase in the reduced parameter space. The cluster algorithm is much more efficient than the Metropolis algorithm and can easily tunnel between different lattice phases.

For simulating the model, we perform a Suzuki-Trotter decomposition of the Hamiltonian [117, 118]. In the $SU(2)$ QLM, the partition function is given by

$$Z^{\{4\}}_{QLM} = \mathrm{Tr}\left[e^{-\beta H^{\{4\}}_{QLM}} P\right], \tag{4.8}$$

where $H^{\{4\}}$ is the QLM Hamiltonian of eq. (3.53) and P is a projector on Gauss' law. To perform the Suzuki-Trotter decomposition, the Hamiltonian is separated into sub-Hamiltonian parts, $H^{\{4\}}_{X\in\{A,B,C,D\}}$, where all the terms contributing to a given sub-Hamiltonian are commuting,

$$H^{\{4\}}_{QLM} = \sum_X H^{\{4\}}_X. \tag{4.9}$$

We split the Hamiltonian into a sum over the 4 sublattices introduced above (A, B, C, D), such that

$$\begin{aligned} H^{\{4\}} &= H^{\{4\}}_A + H^{\{4\}}_B + H^{\{4\}}_C + H^{\{4\}}_D, \\ H^{\{4\}}_X &\equiv \sum_{\hexagon\in X} \mathcal{H}^{\{4\}}_{\hexagon}. \end{aligned} \tag{4.10}$$

Although different sub-Hamiltonians do not commuter, it can easily be confirmed that all terms contributing to an individual sub-Hamiltonians are commuting, since a single sub-Hamiltonian does not contain any neighbouring plaquettes. It should be noted that this is not the minimal splitting of the Hamiltonian since one could alternatively have chosen a decomposition in a tripartite lattice, i.e. following the $\{\alpha, \beta, \gamma\}$ sublattices. The (A, B, C, D) sublattices are, however, the more natural choice for the height variables, which naturally live on this set of four sublattices. We rewrite the partition function in the Suzuki-Trotter expansion, where L_t Euclidean time-slices have been introduced together with a Euclidean time-step length $\epsilon \equiv \frac{\beta}{L_t}$, as

$$\begin{aligned} Z_{QLM}^{\{4\}} =& \mathrm{Tr}\left[\left(e^{-\epsilon H_A} e^{-\epsilon H_B} e^{-\epsilon H_C} e^{-\epsilon H_D}\right)^N P\right] + \mathcal{O}\left(\epsilon^2\right) \\ =& \sum_{S_1, S_2, \ldots, S_{4N-1}} \left\langle S_1 \middle| e^{-\epsilon H_A^{\{4\}}} \middle| S_2 \right\rangle \left\langle S_2 \middle| e^{-\epsilon H_B^{\{4\}}} \middle| S_3 \right\rangle \\ & \times \quad \left\langle S_3 \middle| e^{-\epsilon H_C^{\{4\}}} \middle| S_4 \right\rangle \left\langle S_4 \middle| e^{-\epsilon H_D^{\{4\}}} \middle| S_5 \right\rangle \left\langle S_5 \middle| \ldots \left\langle S_{4N-1} \middle| e^{-\epsilon H_D^{\{4\}}} \middle| S_1 \right\rangle + \mathcal{O}\left(\epsilon^2\right). \end{aligned} \tag{4.11}$$

We have introduced sums over complete sets of physical states for each of the $4N-1$ Trotter-slices, such that the theory is reformulated as a $(2+1)$-dimensional lattice theory. In this way it can be simulated in terms of standard Monte Carlo methods e.g. by the Metropolis algorithm or the cluster algorithm.

4.3.1 Cluster Algorithm

The cluster algorithm works by first identifying clusters of plaquettes belonging to a reference lattice configuration of the correlated pinwheel phase and then by flipping each cluster with a 50% probability. This process is repeated over all four sublattices, which constitutes a single sweep of the cluster algorithm. The rules for assigning plaquettes to a cluster are described below. For the algorithm to be able construct independent clusters on a single sublattice, and afterwards updating the sublattice, it is essential that there is a symmetry that allows an overall flip of all the height variables on an individual sublattice. This implies that the cluster algorithm works in the reduced Hamiltonian parameter space with the four $\mathbb{Z}(2)$ symmetries. In addition, since the cluster algorithm is constructed with the reference configuration of the correlated pinwheel phase, the Hamiltonian parameters must favour plaquette-states that belong to this configuration. This implies that a larger Boltzmann weight is given to plaquettes with a larger number of sign-pairs, and that the only allowed transition is the pinwheel transition, i.e. $T_{env} = 0$ for all environments except IV and VIII. Hence, to apply the cluster algorithm, the Hamiltonian parameters are restricted to

$$\begin{aligned} W_{17}^B \leq W_{26}^B \leq W_{35}^B \leq W_{48}^B, \\ T_{17}^B = T_{26}^B = T_{35}^B = 0, \quad T_{48}^B \geq 0, \end{aligned} \tag{4.12}$$

Here W_{env}^B and T_{env}^B are the Boltzmann weights associated with a continuation or a transition in Euclidean time for the environment *env*, respectively. In terms of the Hamiltonian parameters W_{env} and T_{env}, the Boltzmann weights are given by $W_{env}^B = exp(-\epsilon W_{env})\cosh(\epsilon T_{env})$ and $T_{env}^B = exp(-\epsilon W_{env})\sinh(\epsilon T_{env})$ for a continuation and a transition in Euclidean time, respectively.

The cluster algorithm can be realized either as a single-cluster algorithm, where a single cluster is constructed starting from a random plaquette on the sublattice, which is then definitely flipped, or alternatively as a multi-cluster algorithm, where the whole sublattice is covered by clusters and every cluster is flipped with 50% probability. We will only apply the multi-cluster algorithm.

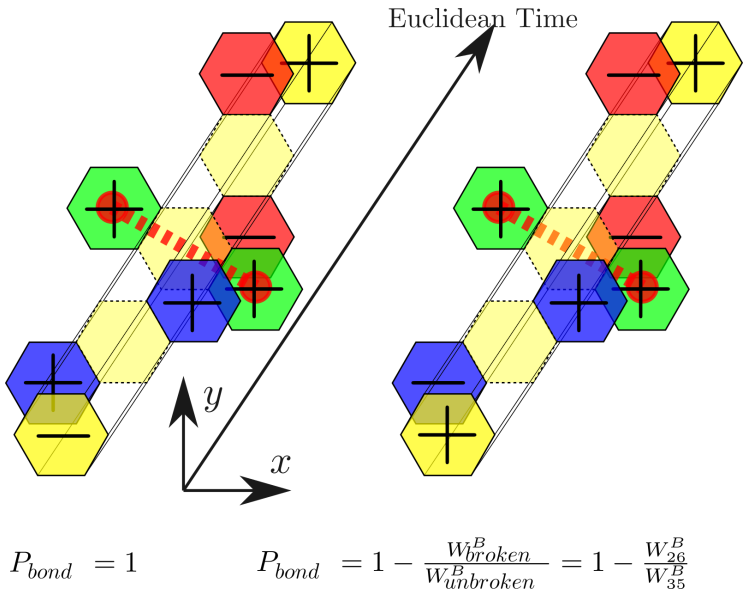

Figure 4.20: *Plaquette and environment expanded in Euclidean time. Cluster-bond (red dashed line) rules for plaquettes in the same Trotter-slice (green). Only plaquettes with the same value of the height variables can be bound together in a cluster. Left: If the plaquettes support a transition (yellow plaquette) a cluster-bond must be placed. Right: If no transition is supported, a cluster-bond is placed probabilistically.*

Cluster Rules

For the cluster algorithm to work, the clusters must be constructed in such a way that each cluster satisfies two conditions. First, under a flip of any cluster, no forbidden configurations can appear. Second, the clusters are constructed such that they can be flipped with a 50% probability.[13] We construct clusters by probabilistically assigning cluster-bonds between nearest-neighbour plaquettes of the same sublattice $X \in \{A, B, C, D\}$, with the same value of the height variables.

A cluster-bond is constructed between two plaquettes in the same Trotter slice according to two rules. First, if the two plaquettes are part of an environment that is supporting a transition on another sublattice, then a cluster-bond must be put between the two plaquettes. This is illustrated in Figure 4.20 (left) where 5 Trotter slices are shown. The plaquettes marked in yellow, undergo a transition which is possible since the remaining plaquettes (marked in blue, green, and red) together create an environment that supports transitions (IV or VIII environment). Flipping one but not the other plaquette marked in green, would destroy this environment. To avoid this, we must place the two plaquettes in the same cluster. We therefore connect the two plaquettes with a cluster-bond (red dashed line). Note that this would not be possible without a separate $\mathbb{Z}(2)$ symmetry for each of the 4 sublattices, since a flip of both of the green plaquettes would then induce a change in the energy. Second, if the two plaquettes are not part of an environment that is supporting a transition, a cluster-bond is placed probabilistically. The probability for placing a cluster-bond is a function of the Boltzmann weight of the environment that the plaquettes are currently part of, compared to

[13] This actually implies the first rule.

the Boltzmann weight that results if the sign-pair is broken up,

$$P_{bond} = 1 - \frac{W^B_{broken}}{W^B_{unbroken}}. \tag{4.13}$$

This is illustrated in Figure 4.20 (right) for the cluster-bond between the two green plaquettes. Here $W^B_{unbroken}$ is the Boltzmann weight of the current environment. For the yellow plaquettes this is W^B_{35}. W^B_{broken} is the Boltzmann weight for the yellow plaquette, if only a single one of the green plaquettes changes sign, i.e. the sign-pair is broken up. For the yellow plaquettes this is W^B_{26}. It is important to note that this set of cluster rules only works when one imposes requirements on the Boltzmann weights that favour the environments with a larger number of sign-pairs, i.e. eq. (4.12). Otherwise the above bond probability could take negative values.

For the construction of cluster-bonds in the Euclidean time direction, the cluster-bonds are similarly constructed according to two rules. First, if the two plaquettes are not supported by an environment allowing for a transition, i.e. neither the IV nor the VIII environment, the two plaquettes must be connected by a cluster-bond. This is illustrated in Figure 4.21 (left) for the green sublattice. Here the environment between the two green plaquettes is a III or a V environment. A cluster-bond must therefore be placed binding the two green plaquettes together, to avoid creating a transition that is not allowed. Second, if the environment supports a transition, a cluster-bond is placed probabilistically. This is done similarly as for the cluster-bonds in space, with the exception that the environment weight, when the pair is broken, is now a transition, i.e. the bond is constructed with a probability of $P_{bond} = 1 - \frac{T^B_{48}}{W^B_{48}}$. This is illustrated in Figure 4.21 (right) for the green sublattice. Here the environment between the two green plaquettes is a IV or a VIII environment, allowing for the transition of the green plaquette, and the cluster-bond is created probabilistically.

As discussed in Section 4.1.2, $3/2$-charges lock three neighbouring plaquettes together. Since the cluster algorithm is only updating a single sublattice at a time, it is therefore hampered by the inclusion of charges. Additionally, since the energy strands associated with domain walls between phase realizations are not residing on a single sublattice. It is also challenging for the cluster algorithm to update and hence move these strands around. This does not mean that we cannot use the cluster algorithm in the presence of charges and fluxes, but merely that the cluster algorithm is not as efficiently as in the absence.

4.4 Quantum Link Model Monte Carlo Results

This study is still ongoing, and a more complete analysis will be presented in a future publication in collaboration with D. Banerjee, F.-J. Jiang, P. Orland, and U.-J. Wiese. The results presented here are all obtained by either the Metropolis algorithm, or the cluster algorithm. Both are working in the height variable description of the $\{4\}$-representation on a honeycomb lattice, that is respecting the boundary conditions shown in Figure 4.14. These boundary conditions are demanding a lattice with the same number of plaquettes in the x-, and the y-directions (see Figure 4.14), and we are assuming this to be the case from here on forward.

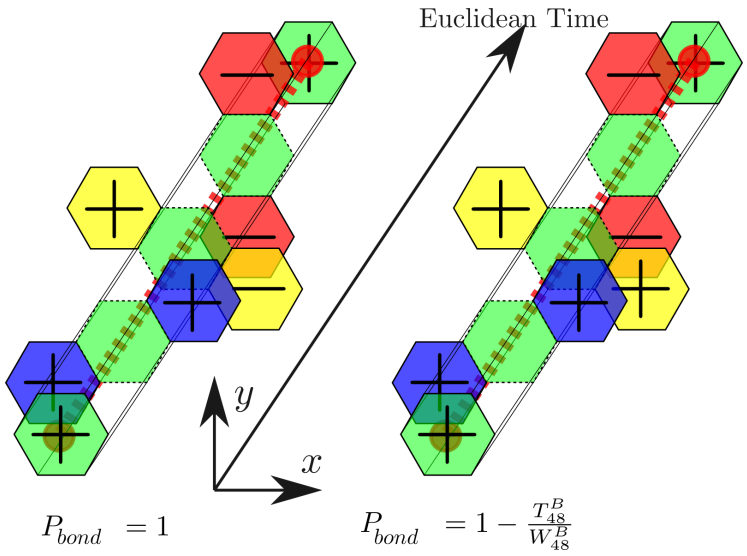

Figure 4.21: *Plaquette and environment expanded in Euclidean time. Cluster-bond (red dashed line) rules for the time direction (green plaquettes). Only plaquettes with the same value of the height variables can be bound together in a cluster. Left: If the environment is not supporting a transition, a cluster-bond is placed in Euclidean-time. Right: If a transition is supported, a cluster-bond is placed probabilistically.*

4.4.1 Pinwheel Phases

The correlated and uncorrelated pinwheel phases of Section 4.2.2 are favoured by different Hamiltonian parameters. We interpolate between the two phases by changing the relative values of T_{IV} and T_{VIII}. For simplicity, we fix T_{VIII} to 1 and only change T_{IV}. All the remaining Hamiltonian parameters of eq. (3.53) are set to zero.

Results Without Charges or Fluxes

To determine the transition between the correlated and uncorrelated pinwheel phases, we simulated lattice sizes from 12×12 up to 36×36 with Euclidean-time extend of $L_t = 50, 100, \ldots, 250$. Here the T_{IV} values are chosen between 0.5 and 1.25. A representative example of this is shown in Figure 4.22, where the magnetic susceptibilities χ_X are shown for each of the four sublattices $X \in \{A, B, C, D\}$ for a lattice size of $24\times24\times100$ with β-values between 3 and 15. Note that for all but the smallest β values, the results for different β values are lying on top of each other, such that they are hard to distinguish in the plot. Similarly, the B, C, and D sublattice results are lying on top of each other. Here $\chi_A \approx 0$ for $T_{IV} \lesssim 0.7$, while the remaining three $\chi_{X\in\{B,C,D\}}$ are all the same and non-zero.[14] This shows that the A sublattice is disordered, and the remaining three (B, C and D) are all ordered. I.e. for $T_{IV}/T_{VIII} \lesssim 0.7$, the uncorrelated pinwheel phase is realized, and in the case that is shown, the pinwheels are realized on the A sublattice. For larger values of T_{IV} all four sublattices obtain a non-zero magnetic susceptibility, and the correlated pinwheel phase is realized,

[14] In the figure all three $\chi_{X\in\{B,C,D\}}$ are lying on top of each other, such that only the blue line of χ_D is visible.

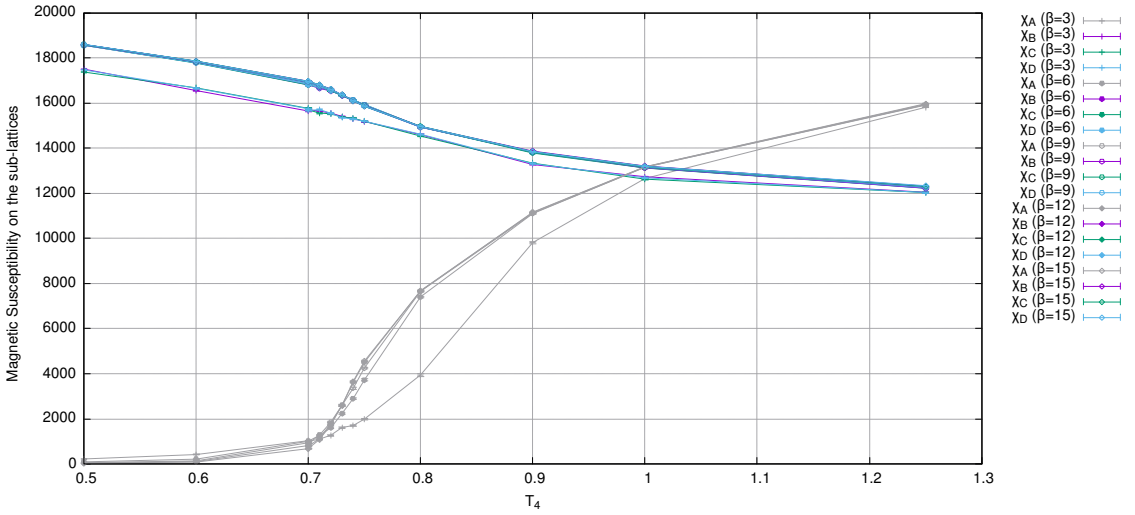

Figure 4.22: *Magnetic susceptibility for different choices of β on the four sublattices on a* 24×24 *honeycomb lattice with* $L_t = 100$*, as a function of* T_{IV}*, with* $T_{VIII} = 1$ *(see Figure 4.23). The other Hamiltonian parameters of eq.* (3.53) *are all set to zero.*

still with the pinwheels on the A sublattice in the case presented here. In the appendix, see figures E.1-E.6, we have included density histograms for the correlation between the four magnetization order parameters corresponding to the results presented in Figure 4.22, for $\beta = 6$. This shows that the magnetization of the sublattice that carries the pinwheels changes from being centred around $M_A \approx 0$, to spreading out when T_{IV} is increased, and finally to breaking apart into two distinct peaks (corresponding to pinwheels rotating either direction) when $T_{IV}/T_{VIII} \approx 0.70 - 0.80$. For larger values of T_{IV}, the Metropolis algorithm is not able to tunnel between distinct realizations of the correlated pinwheel phase. It should be noted that, at the point $T_{IV} = T_{VIII} = 1$, all four sublattices have the same values for the magnetic susceptibility. We emphasize that at this point, all four sublattices are ordered, in agreement with the mean-field calculations presented in Section 4.2.1.

The energy density averaged over Euclidean time is presented in Figure 4.23, for three sets of parameters ($T_{IV} = 0.50$, $T_{IV} = 1.00$ and $T_{IV} = 1.25$ all with $\beta = 3$). We find that in the uncorrelated pinwheel phase (at $T_{IV} = 0.50$) the energy is carried by the plaquettes surrounding the pinwheels, i.e. by the three sublattices B, C, and D. This continues to be the case in the correlated pinwheel phase, until one reaches $T_{IV} = T_{VIII} = 1$. Then the energy is evenly distributed over the entire lattice.[15] For $T_{IV} > T_{VIII}$ the energy is instead dominated by the plaquettes that carry the pinwheels, as shown for $T_{IV} = 1.25$ deep inside the correlated pinwheel phase.

We have here identified the parameter range where the phase transition between the uncorrelated and the correlated pinwheel phase takes place. It is, however, presently not possible to unambiguously determine the order of the phase transition. To determine the order of the phase

[15] Based on this picture one could be led to believe that there is no order on the lattice for $T_{IV} = T_{VIII}$. As confirmed by Figure 4.22, this is not the case.

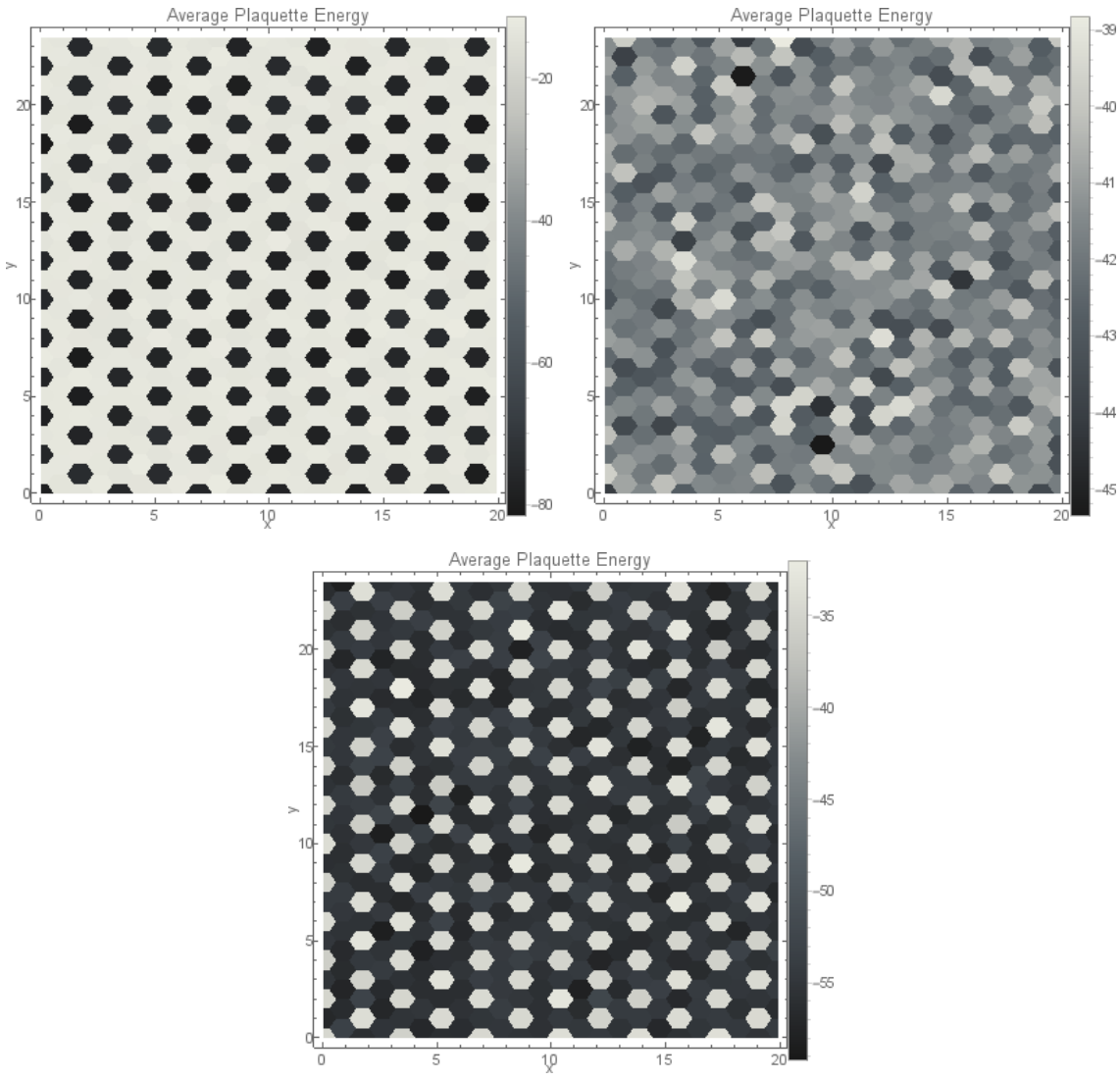

Figure 4.23: *Energy density for a* 24×24 *honeycomb lattice with* $L_t = 100$ *for* T_{IV} *values of* 0.50 *(left),* 1.00 *(right), and* 1.25 *(bottom) with* $T_{VIII} = 1$ *and* $\beta = 3$*, simulated with the Metropolis algorithm. Note the difference in scale for the energies, especially on the right plot the energy scale range is a factor 5 to 10 smaller than for the other plots.*

transition, we would need to obtain data from larger lattice sizes. The possibility for determining the order is within reach in the near future for the constructed algorithms and it will be presented in a future publication. Based on the results obtained so-far, we would expect the phase transition to be a first-order phase transition.

Results for a Single Dirac-String Wrapping Around the Torus

We introduce a flux by wrapping a Dirac-string around the lattice. The resulting energy densities on a 24×24 lattice with a single Dirac-string are shown in Figure 4.24 for three different values of T_{IV}. Here the T_{IV} values have been chosen similar to Figure 4.23, to obtain flux results from all three energy configurations. The two energy densities with $T_{IV} = 0.50$ (left) and $T_{IV} = 1.25$ (right) are both calculated with the Metropolis algorithm, on a lattice containing a Dirac-string wrapping around the $\hat{2}$-directions, with $\beta = 9$, and $L_t = 100$. The right plot is simulated with the cluster algorithm with $T_{IV} = T_{VIII} = 1$. Here a Dirac-string is wrapping around the lattice in the $\hat{3}$ (y) direction, with $\beta = 15$ and $L_t = 200$.

For $T_{IV} = 0.50$ (left) the lattice is in the uncorrelated pinwheel phase. By including the Dirac-string we obtain two domain walls, wrapping around the lattice in the same direction as the Dirac-string. The two domain walls enclose a realization of the uncorrelated pinwheel phase with pinwheels on the A sublattice from another realization with the pinwheels on the B sublattice on the other side of the domain walls. Each of the two domain walls is characterized by a higher energy density than the surrounding bulk pinwheel phases. A similar picture is obtained for $T_{IV} = T_{VIII} = 1$ (right). Here two energy strands are found to wrap around the lattice, in the same $\hat{3}$ direction as the Dirac-string. Since the energies are homogeneous over the phases,[16] we cannot directly determine what realizations of the correlated pinwheel phase that exist on either side of the domain walls. To decide this, we calculate the projected magnetization order parameters. By this we understand the value obtained by summing the magnetic order parameter m over a column of constant x-coordinate. This confirms that the strings are domain walls separating distinct realizations of the (correlated) pinwheel phases. A plot of the absolute value of the projected magnetic order parameters is shown in Figure 4.25.[17] For $T_{IV} = T_{VIII} = 1$ we use the efficient cluster algorithm to simulate the system to explore the evolution of the domain walls in simulation time. This is done by plotting the projected magnetic order parameters. In Figure 4.25, its absolute value (for the actual simulation of Figure 4.24 (right)) is plotted, as a function of simulation time. A dark spot denotes a lattice column with a vanishing magnetic order parameter, and therefore a low order on the sublattice. This is characteristic for a column with a domain walls, since the correlated pinwheel phase is no longer maintained in this region. By relating Figure 4.25 and Figure 4.24 (right), we indeed find that the dark lines of low order corresponds exactly to the location of the domain walls, which is to be expected. On the other hand, a light spot denotes a column of high order on the sublattice. We observe that two of the sublattices pair up (here A is together with B and C is together with D) and create a common domain wall. This domain wall can then be moved around on the lattice, but the sublattice pair is not broken up. At a domain wall, two of the sublattices

[16] This is not an artefact of using the cluster algorithm, but a physical property of the model. See Figure 4.23 (right).

[17] Since one would need information of the relative sign between the order parameters on different sublattice to determine the pinwheel realization, we emphasize that by the magnitude alone, one cannot determine the explicit realizations of the pinwheel phases. Since the cluster algorithm flips the sign of large clusters at every step, only the magnitude plot is included here, but the full information was used to manually determine the change in the realizations of the pinwheel phases over the domain walls.

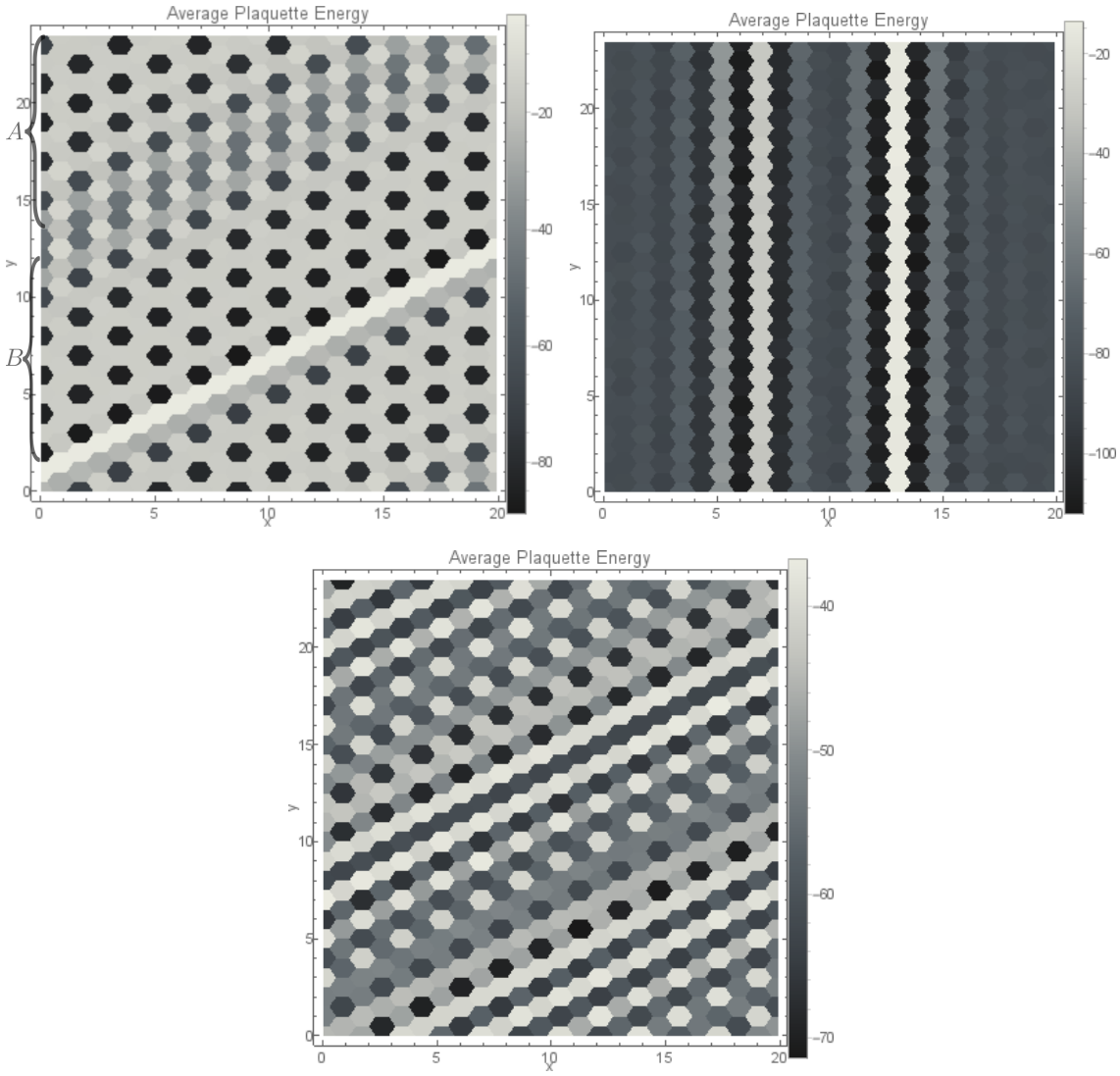

Figure 4.24: *Energy density on a* 24×24 *honeycomb lattice, with a single Dirac-string wrapping around the lattice in the* $\hat{2}$ *[*$\hat{3}$*] direction. Here* $L_t = 100$ *[*$L_t = 200$*] with* $T_{VIII} = 1$ *and* $\beta = 9$ *[*$\beta = 15$*]. The plots are for three* T_{IV} *values* 0.50 *(left),* 1.00 *(right), and* 1.50 *(bottom). The left and bottom [right] plots are produced using with the Metropolis [cluster] algorithm. Note the difference in scale for the energies.*

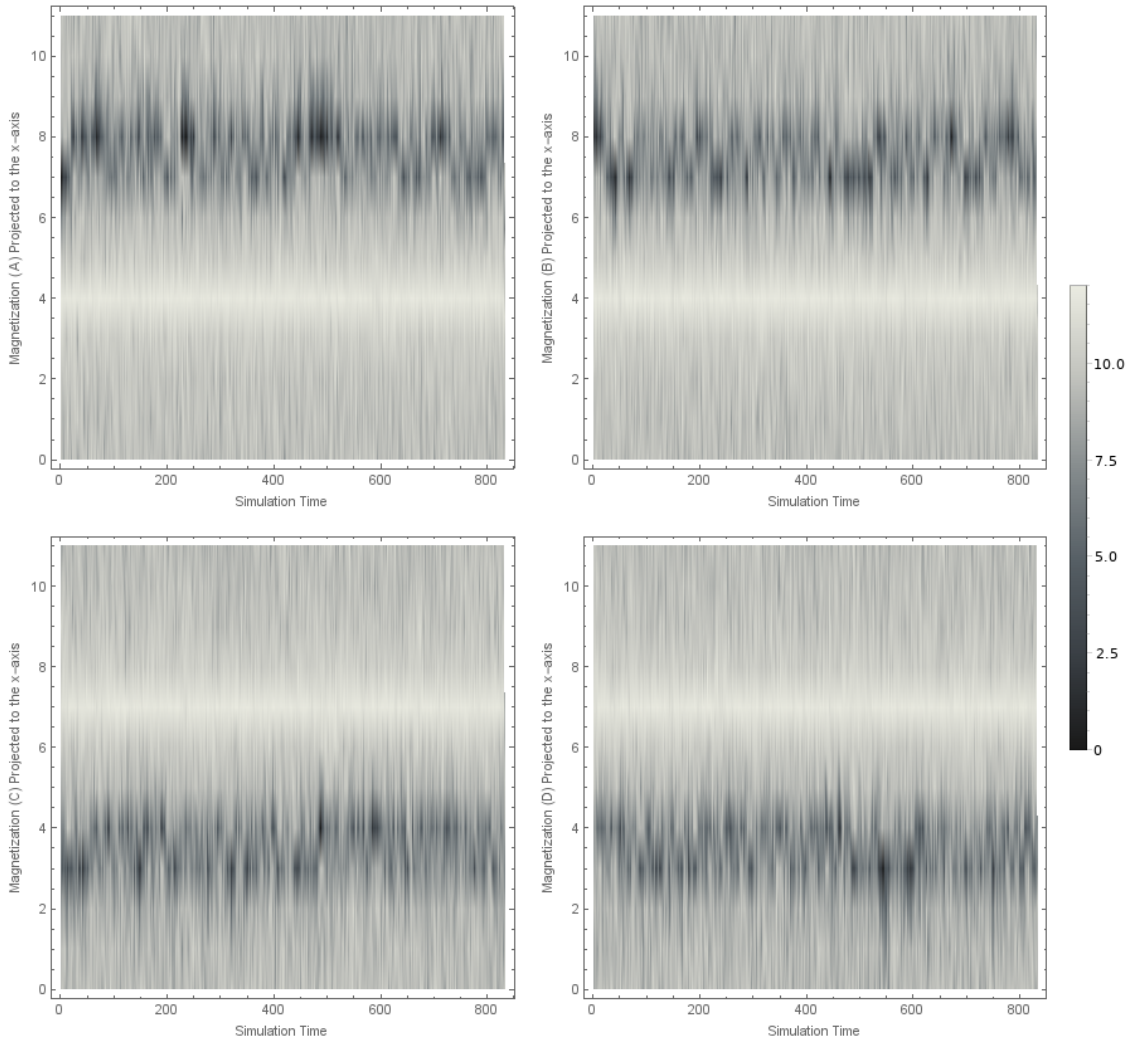

Figure 4.25: *Absolute value of the projected magnetic order parameters (top-left: M_A, top-right: M_B, bottom-left: M_C, and bottom-right: M_D), with the inclusion of a Dirac-string, as a function of simulation time. The horizontal axis shows the simulation time in cluster sweeps. The vertical axis shows the x-coordinate of the projected column, and the colour show the absolute value of the projected magnetic order parameters. Here $T_{IV} = T_{VIII} = 1$ and all other Hamiltonian parameters are set to zero (see Figure 4.24 (right)).*

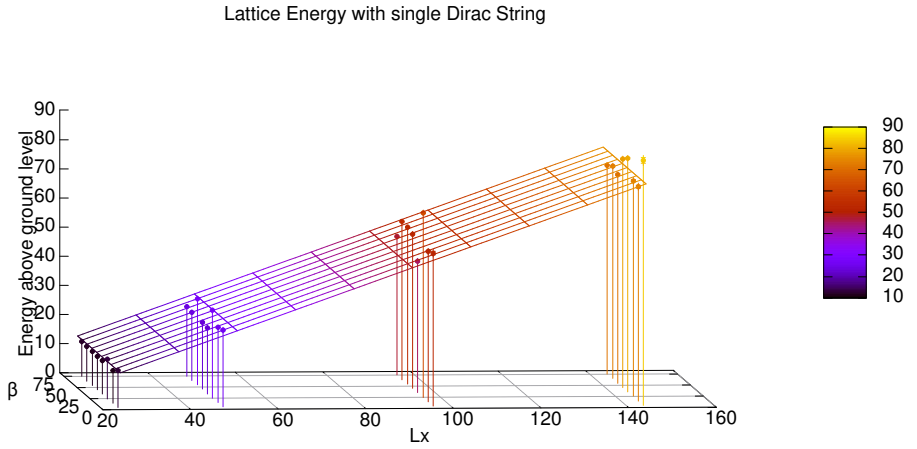

Figure 4.26: *Energies above the groundstate with a 1 flux and two domain walls, enforced by a Dirac-string wrapping around the lattice, as a function of lattice size, and consequently length of the flux or domain-walls, and β-values. The lattice has $L_t = 300$, and is simulated with the cluster algorithm, with $T_{IV} = T_{VIII} = 1$, and all other Hamiltonian parameters set to zero.*

disorder, while the other pair of sublattices order more strongly. This is represented by the light horizontal line in Figure 4.25. For $T_{IV} = 1.25$ we obtain two energy strands wrapping around the lattice, following the direction of the Dirac-string. It is, however, more difficult to determine the behaviour in between the two domain walls, and no clear phase seems to emerge in this case. It might be that the current lattice is simply too small for allowing the interior phases to appear properly. All three results agree with what we expect from the discussion about fluxes in Section 4.2. We therefore conclude that the 1-flux, enforced by the Dirac-string, fractionalizes into two half-fluxes, each associated with a domain wall as discussed in Section 4.2.

In Figure 4.26 we present the energies above the groundstate for a lattice with a single Dirac-string wrapping around the lattice. The energies are given relative to the groundstate, i.e. without a Dirac-string wrapping around the lattice. The energy gaps are presented as a function of the lattice size, and consequently the length of the Domain walls, on the x-axis. Since the energies are calculated for a finite lattice, with finite discretization in Euclidean time, the dependence on the inverse temperature β is also included in the figure on the y-axis. Due to the amount of computations needed to obtain the data, this is only calculated with the efficient cluster algorithm, and therefore only with $T_{IV} = T_{VIII} = 1$ (and all other Hamiltonian parameters set to zero) which puts us in the correlated pinwheel phase. We find that the domain-walls are confining, with an energy that grows linearly with their length. A simple plane forced to not depend on β is fitted to the data, and the energies in lattice units results as

$$\Delta E_{Dirac} = 0.53(\pm 0.01)L + 0.2(\pm 1.3), \tag{4.14}$$

where L is the length of the lattice, measured in lattice-spacings. We emphasize that the plane is not meant to be representing the true function describing the energy, but solely as a simple method

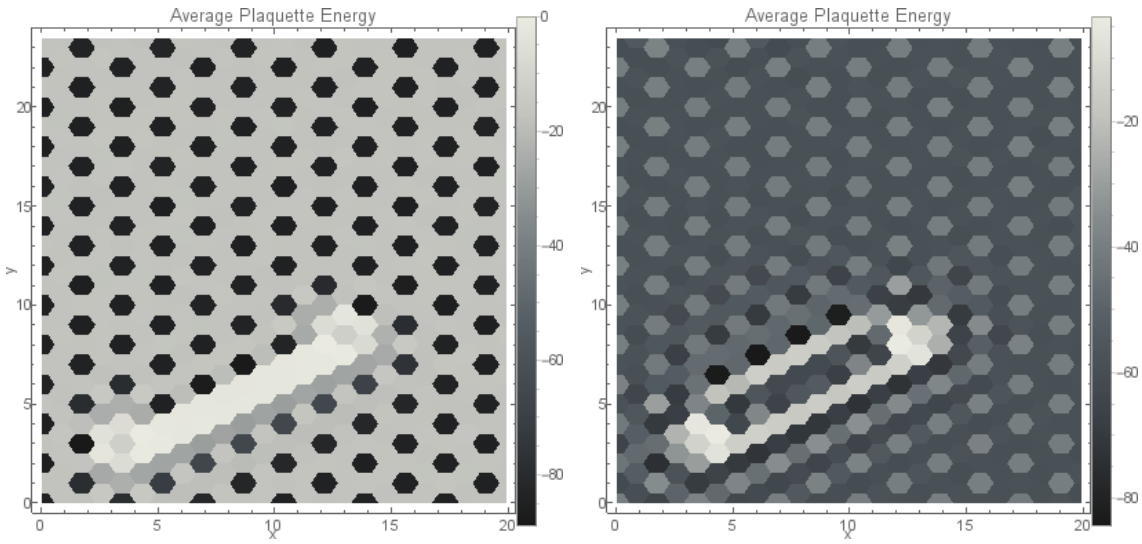

Figure 4.27: *Lattice energy density for a* 24×24 *lattice with* $\beta = 12$ *and* $L_t = 100$ *for two* $3/2$ *charges separated by 10 lattice spacings, simulated with the Metropolis algorithm. Left:* $T_{IV} = 0.50$ *and* $T_{VIII} = 1$. *Right:* $T_{IV} = 1.25$ *and* $T_{VIII} = 1$. *(All other Hamiltonian parameters are set to zero.)*

to quantify how the energies are growing with a linearly rising potential, as a function of the length of the flux string. The fit to the plane has $\chi^2/ndf = 14.5$, which shows that energy is not well described by a simple plane. We emphasize that the fit is consistent with a vanishing energy gap, for a vanishing lattice size, which is to be expected. We should point out two things in relation to this. First that since the simulations are carried out on a lattice with the same size in both dimensions, we are actually not just measuring the dependency on the length of the Domain walls, but also on the separation between them. If we would make the measurements all the way down to a vanishing lattice size, we would therefore expect some dependency on squeezing the two domain walls close together. For the lattice sizes used here, we would not expect to see this effect. Second, for fluxes enclosed in a very small volume, the linear dependency of the extension of the fluxes can break down and other effects can start to appear. We would in this case not obtain a vanishing energy gap, when linearly extending to a vanishing lattice size. In the lattice sizes used here, we do not see this.

Inclusion of $3/2$ Charges

Figure 4.27 presents the energy densities for a pair of $3/2$ charges separated by 10 lattice spacings on a 24×24 lattice. The charges are introduced as described in Section 4.1.2. Both plots are obtained with the Metropolis algorithm for $\beta = 12$ and $L_t = 100$, for the two cases of $T_{IV} = 0.50$ (left) and $T_{IV} = 1.25$ (right). All other Hamiltonian parameters are set to zero. We observe two rather distinct behaviours. For the plot on the right-hand side, the two charges are inserted into a background of correlated pinwheels on the A sublattice. The two charges are connected by two separate energy strands. This is what we would expect based on the discussion of Figure 4.18. This leads us to conclude that the 1-flux between the two charges, is fractionalized into two strands of

$1/2$-flux, each associated with a single energy strand. It should be noted that the energy in the bulk is carried by the pinwheels on the A sublattice. On the other hand, close to the upper energy strand the energy is instead carried by the plaquettes surrounding the C sublattice plaquettes. This is reminiscent of what we observed in Figure 4.23 (left), for the uncorrelated pinwheel phase. Since the area between the two energy strands is only a few lattice spacings wide, it is not possible to determine what phase is realized in there. Based on the discussion of Figure 4.18, we would expect this to be another realization of the correlated pinwheel phase. In the plot on the left-hand side, a pair of $3/2$ charges are included in the uncorrelated pinwheel phase. The two charges are simply joined together by a single thicker energy strand, while the rest of the lattice is completely covered by the uncorrelated pinwheel phase, with all the pinwheels residing on the A sublattice. Again, based on the discussion of Figure 4.18, we would expect a similar behaviour with two separated energy strands connecting the two charges. As we also noted there, depending on the energy cost of the domain wall, it is possible for the two domain walls to collapse together, and simply create a single doubled domain wall connecting the two charges. This seems to be what we observe here. We associate the entire unfractionalized flux with the single collapsed domain wall.

The above results for $T_{IV} \neq T_{VIII}$ are all obtained with the Metropolis algorithm. For $T_{IV} = T_{VIII} = 1$ we apply the cluster algorithm which gives results similar to what we observed above in the correlated pinwheel phase. Results for this are shown in Figure 4.28, for three different charge separations of 4, 10, and 16 lattice spacings for the plot on the left, right, and bottom, respectively. These simulations are performed on a 48×48 lattice with $\beta = 25$ and $L_t = 200$. We, again, observe that the two charges are connected by two separate energy strands. By closer inspection of specific snapshots of the height variable configurations during the simulation, we find that the correlated pinwheel phase between the strands that connect the charges, is indeed distinct from the phases in the bulk. This shows that the energy strands are indeed associated with domain walls separating distinct realizations of the correlated pinwheel phase, which is what we expected based on the discussion related to Figure 4.18.[18] We therefore identify each of the energy strands with the transport of a $1/2$-flux between the two charges. It should be noted that the two charges and their connecting energy strands are surrounded by a cloud of non-uniform energy density, where the energy strands have been sweeping out an area. This is similar to what was noted in Figure 4.27 (right). Since the cluster algorithm is more efficient, this is more pronounced here.[19]

In Figure 4.29 we present the energies above the groundstate for a 96×96 lattice containing pairs of $3/2$ charges. The energies are given above the groundstate, i.e. relative to a situation without external charges. The energy gaps are presented as a function of the charge separation on the x-axis. Since the energies are calculated for a finite lattice, with finite discretization in Euclidean time, the dependence on β is also included in the figure on the y-axis. Due to the amount of computations needed to obtain the data, this is only calculated with the efficient cluster algorithm, and therefore only with $T_{IV} = T_{VIII} = 1$ (and all other Hamiltonian parameters are set to zero) which puts us in the correlated pinwheel phase. We find that the charges are confined, with an energy that grows linearly with the separation of the charges. A simple plane not depending on β is again fitted to the data, and the energies in lattice units are given by

$$\Delta E_{\text{sep}} = 0.58(\pm 0.01)\Delta L + 3.5(\pm 0.1). \tag{4.15}$$

[18] This has been concluded by investigating several individual snapshots of configurations for certain points in simulation time, and by identifying the placement of the pinwheels inside and outside the domain walls.

[19] Since this effect was already observed in the Metropolis algorithm, we would expect to see a similar picture there, if we would allow the Metropolis algorithm to run for a much longer time.

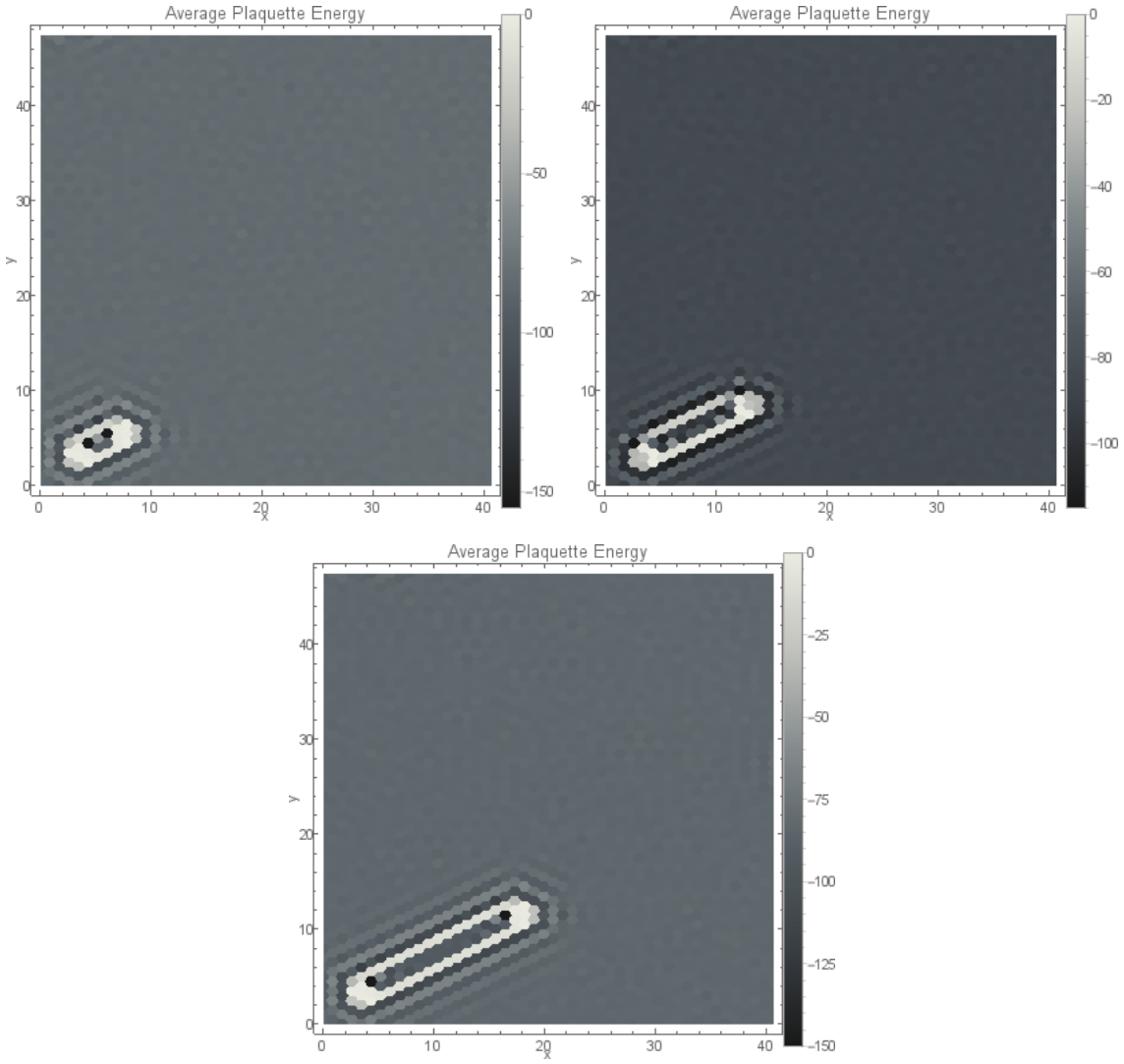

Figure 4.28: *Energy density for a* 48×48 *lattice with* $\beta = 25$ *and* $L_t = 200$ *with two* $3/2$ *charges separated by 4 (left), 10 (right), and 16 (bottom) plaquettes. These simulations were performed with the cluster algorithm with,* $T_{IV} = T_{VIII} = 1$*, and all other Hamiltonian parameters were set to zero.*

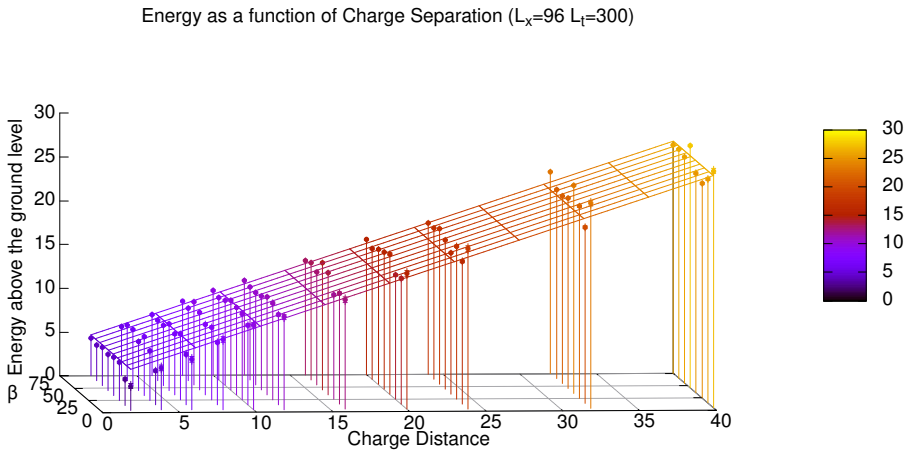

Figure 4.29: *Energies above the ground state, as a function of the charge separation between two* $3/2$ *charges, and of the* β*-values. The lattice size is* 96×96 *with* $L_t = 300$*. The simulations use the cluster algorithm with,* $T_{IV} = T_{VIII} = 1$*, and all other Hamiltonian parameters are set to zero.*

Here ΔL is the distance between the charges, measured in lattice spacings. Again, we emphasize that the plane is not meant to represent the true behaviour of the energies, but just as a rough demonstration that the energies define a linearly rising potential. The fit is, however, rather good and has a χ^2/ndf of 0.66. The energy as a function of the charge separation is $0.58(\pm0.01)$ per lattice spacing. This can be compared with the corresponding energy as a function of the length of the pair of domain-walls in eq. (4.14), which was found to be $0.53(\pm0.01)$ per lattice spacing. That there is no perfect agreement between these, should not come as a surprise. First of all, the simple fit is not very good to describe the true behaviour of the energies. Second, the flux strings connecting external charges are locked into place at the location of the charges. Since the fluxes cannot move freely, we would expect this to increase their energies, especially for shorter distances between the charges. It is also worth noting, that in the case of wrapping fluxes, the fit is consistent with a vanishing flux energy for a vanishing lattice size, which is to be expected. This is not the case for the charges, where a vanishing charge separation does not lead to a vanishing energy gap. For external charges there are two contributions to the energy. One is from the flux connecting the two external charges, and the other is from the intrinsic energy associated with creating a charge pair. Assuming that the linear energy dependency on the charge separation is valid for all distances, we find this energy for creating a pair of $3/2$ charges as 3.5 ± 0.1, based on eq. (4.15). We emphasize that for small separations of the charges, we expect the linearity to break down. Furthermore, the notion itself of a vanishing distance between charges breaks down, since it is not possible to neither separate a single charge or to create two charges at the same location. Therefore this should only be seen as a naive statement on the extra energy a pair of $3/2$ charges cost, in addition to the energy cost of the flux connecting them.

4.4.2 Anti-Pinwheel Phase

As discussed in Section 4.2, we expect to find a phase with tripartite sublattice order spontaneously breaking both the translation and rotation symmetries, when increasing the $T_I = T_{VII} \equiv T_{17}$ parameter in the Hamiltonian of eq. (3.53). We perform a set of simulations using the Metropolis algorithm, where all the Hamiltonian parameters are set to zero except for $T_{IV} = T_{VIII} \equiv T_{48} = 1$, and T_{17} which is varied between 0 and 1.5. Figure 4.30 shows the magnetic order parameters on the 12 sublattices M_{X_α}, M_{X_β}, and M_{X_γ} (with X taking values in (A,B,C, and D)) for a 24×24 lattice with $\beta = 25$ and $L_t = 250$. The top (bottom) plot of Figure 4.30 shows the results for a lattice initialized in the correlated pinwheel phase (anti-pinwheel phase). We find that for $T_{17} \lesssim 0.9$ all sublattices are ordered with a large negative magnetic order parameter, i.e. the lattice is in the correlated pinwheel phase with the pinwheels residing on the A sublattice. When T_{17} is increased to $T_{17} \gtrsim 1.2$, the magnetic order parameter for one of the three sublattices (α, β, and γ) obtains a sign opposite the other two. In this case the sign of the height variables on sublattice α (γ) is opposite the two remaining sublattices in the top (bottom) plot in Figure 4.30. As discussed in Section 4.2.3, this is exactly what we would expect for the anti-pinwheel phase. We therefore conclude that there exists a phase transition between the correlated pinwheel phase, and the anti-pinwheel phase for values of $0.9 \lesssim T_{17} \lesssim 1.2$.

We emphasize that it is harder for the Metropolis algorithm to tunnel between states in this parameter space, than in the previously considered pinwheel parameter space. For this reason, we initialized the states in both the anti-pinwheel phase (left), and in the correlated pinwheel phase (right). For the runs presented here, with an initial thermalization period of 25000 Metropolis sweeps, it was not possible to tunnel from the initial lattice phase to the other, in the parameter region $0.9 \lesssim T_{17} \lesssim 1.2$. The two distinct initializations are therefore not consistent with each other in this area, and we should not trust the simulations in this range. We cannot conclude where exactly the phase transition takes place, not to mention what type of phase transition it is. The pattern shown in the two figure are, however, reminiscent of a classical hysteresis loops. This could suggest that the phase transition is of first-order [119]. It is, however, only a possible suggestion towards the order of the phase transition and it is presently not possible to unambiguously determine the order.

Figure 4.31 shows the energy densities for two of the lattices used to obtain Figure 4.30 (top). These are for the parameters $T_{17} = 0.50$ (left) and $T_{17} = 1.50$ (right). We have chosen these parameter values to be in the range where the lattice initialization is of no importance, and both initializations lead to consistent results. For $T_{17} = 0.5$ we are in the correlated pinwheel phase and the energy density is similar to the one found in Figure 4.23 (right). We emphasize that the energy scales differ in the two plots, and that the energy density on the left is essentially uniform over the lattice. For $T_{17} = 1.25$ the energy density is ordered into a tripartite lattice, where the energy is dominated by the IV and VIII environments residing on the α sublattice. This corresponds to the cartoon state presented in Figure 4.19.

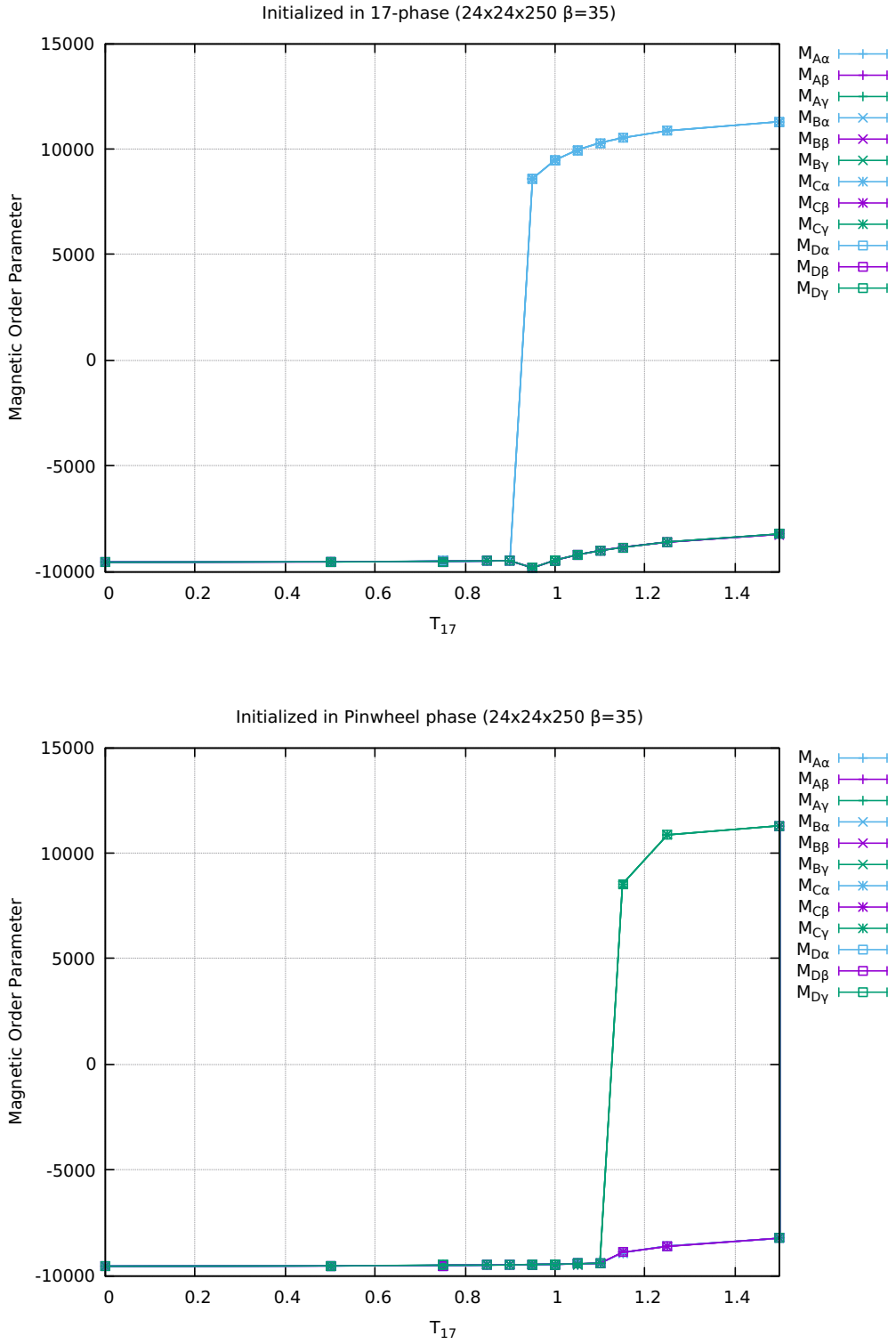

Figure 4.30: *Magnetic order parameters of the 12 sublattices (see Section 4.2.3) as a function of* T_{17} *on a* 24×24 *honeycomb lattice with* $L_t = 250$ *(see Figure 4.31). Here* $T_{48} = 1$ *and* $\beta = 35$*, and the remaining Hamiltonian parameters of eq.* (3.53) *are all set to zero. Top: Initialization with all height variables put to* -1*. Bottom: Initialization with all* α *(*β *and* γ*) height variables put to* $+1$ *(*-1*).*

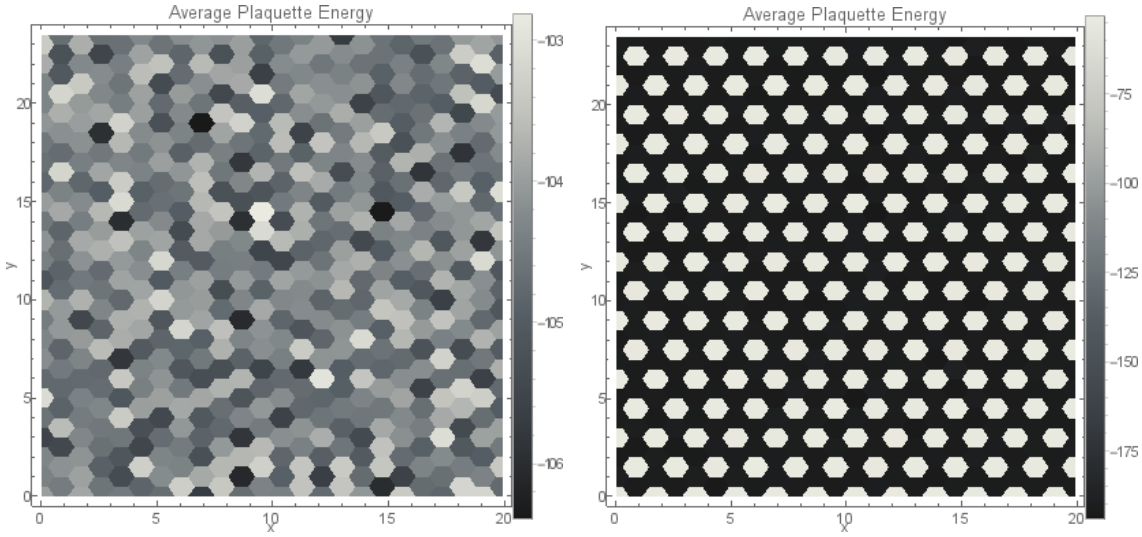

Figure 4.31: *Energy density on a* 24×24 *honeycomb lattice with* $L_t = 250$ *for two* T_{17} *values of* 0.50 *(left) and* 1.50 *(right), with* $T_{48} = 1$ *and* $\beta = 35$*. Note the difference in scale for the energies, especially on the left plot the energy scale range is a factor* ~ 25 *smaller than for the right.*

Part II

Doubled Lattice Chern-Simons Models

Chapter 5

Doubled Lattice Chern-Simons-Maxwell Theory

This chapter is organized as follows: In Section 5.1 the Chern-Simons-Maxwell gauge theory is introduced in the continuum. At first, we will use just a single Abelian gauge field and later we will add a dual gauge field to mimic the doubling once the theory is put on to the lattice. Then in Section 5.2 the doubled cross-based lattice is introduced and the doubled Chern-Simons-Maxwell theory is put on to this lattice geometry in a non-compact form. This section also includes a discussion of the mutual anyonic statistics of charges winding around each other on the direct and the dual lattice. In Section 5.3 the lattice gauge fields are compactified which consequently leads to the quantization of the level of the Chern-Simons theory, as well as to the generation of a non-dynamical background lattice gauge field formed by the self-adjoint extension parameters of the cross-based Hamiltonian. Finally, it will be shown how. in the limit of infinite "photon" mass, this theory reduces to the toric code. The results presented in this chapter, have previously been published in [23].

5.1 Chern-Simons-Maxwell Theory in the Continuum

Before moving on to Chern-Simons-Maxwell theory for the doubled lattice, let us get acquainted with the behaviour of the Chern-Simons-Maxwell model in the continuum. This will allow us to introduce many of the properties of the theory that will become important later on once the theory is put on to the lattice. Unlike for the Chern-Simons-Maxwell theory on the doubled lattice, which is necessarily doubled theory (similar to the famous fermionic doubling problem on the lattice [120, 121, 122]), the continuum gauge field is not automatically doubled. Let us therefore start by examining a single gauge field Chern-Simons-Maxwell theory.

5.1.1 Single Abelian Gauge Field Lagrangian

Here we consider a continuum in $(2+1)$-dimensions with a metric $g = \mathrm{diag}\,(1,-1,-1)$. The classical Lagrangian density for a single Abelian Chern-Simons-Maxwell gauge field $A_\mu(x)$ is

given by

$$\mathcal{L}_{CSM} = -\frac{1}{4e^2} F_{\mu\nu} F^{\mu\nu} + \frac{k}{4\pi} \epsilon_{\mu\nu\rho} A^{\mu} \partial^{\nu} A^{\rho}. \tag{5.1}$$

The first term in the Lagrangian is the standard Maxwell term while the second term is the Chern-Simons term. $F_{\mu\nu}$ is the field strength of the gauge field $F_{\mu\nu} \equiv \partial_{\mu} A_{\nu}(x) - \partial_{\nu} A_{\mu}(x)$ while e is the electric charge and k is the so-called level of the Chern-Simons theory. Without loss of generality, we can assume that $k \geq 0$. The model contains two extreme limits of interest to us. One is the standard Maxwell Lagrangian limit, which is recovered for $k = 0$, while the other is the pure Chern-Simons limit that is obtained as $e^2 \to \infty$. It is important to note that the Chern-Simons density is actually not a gauge-invariant quantity since under a gauge transformation of the field

$$A(x) \to A'(x) = A(x) - \partial_{\mu} \chi(x), \tag{5.2}$$

the Chern-Simons density picks up a total divergence,

$$\mathcal{L}_{CSM} \to \mathcal{L}'_{CSM} = \mathcal{L}_{CSM} - \partial^{\mu} \left(\frac{k}{4\pi} \epsilon_{\mu\nu\rho} \chi \partial^{\nu} A^{\rho} \right), \tag{5.3}$$

which is sent to the boundary when integrated, and can therefore be ignored in our case.[1] We emphasize that by introducing the Chern-Simons density we are explicitly breaking both time-reversal and parity symmetry, which are otherwise present in the standard Maxwell Lagrangian.[2]

Fixing the temporal gauge, i.e. $A_0\left(\vec{x}\right) = 0$ for all $\vec{x}$, we obtain a Lagrangian density of the form

$$\mathcal{L}_{CSM} = \frac{1}{2e^2} \dot{A}_i^2 - \frac{1}{2e^2} \left(\epsilon_{ij} \partial_i A_j \right)^2 + \frac{k}{4\pi} \epsilon_{ij} \dot{A}_i A_j. \tag{5.4}$$

From here we derive the canonically conjugate momentum Π_i of the gauge field A_i as

$$\Pi_i(x) \equiv \frac{\delta \mathcal{L}_{CSM}(x)}{\delta \dot{A}_i} = \frac{1}{e^2} \dot{A}_i(x) + \frac{k}{4\pi} \epsilon_{ij} A_j(x), \tag{5.5}$$

from which we construct the classical Hamilton density

$$\begin{aligned} \mathcal{H}_{CSM} &= \Pi_i \dot{A}_i - \mathcal{L}_{CSM} \\ &= \frac{1}{2e^2} \dot{A}_i^2 + \frac{1}{2e^2} \left(\epsilon_{ij} \partial_i A_j \right)^2 \\ &= \frac{e^2}{2} \left(\Pi_i - \frac{k}{4\pi} \epsilon_{ij} A_j \right)^2 + \frac{1}{2e^2} \left(\epsilon_{ij} \partial_i A_j \right)^2 \\ &= \frac{e^2}{2} E_i^2 + \frac{1}{2e^2} B^2. \end{aligned} \tag{5.6}$$

[1] We emphasize that, depending on the boundary conditions, this term might become of importance for other implementations of the theory.

[2] In 2 spatial dimensions one must take care when defining the parity operation. The operation must be an improper transformation, i.e. the determinant of the matrix representation of the operation must be -1 and therefore, in contrast to standard $(3+1)$-dimensional space-time one cannot choose to flip all the spacial coordinates. Instead, the parity operator in $(2+1)$-dimensional space-time is defined as a reflection through any spatial axis going through the origin. An appropriate choice, is to choose the parity operator to flip the x_1-coordinate $\left(x_1 \to -x_1\right)$ leaving x_2-coordinate unchanged.

In the last line we have introduced the electric field E_i together with the magnetic field B which we have identified as

$$E_i(x) \equiv \Pi_i(x) - \frac{k}{4\pi}\epsilon_{ij}A_j(x), \qquad B(x) \equiv \partial_1 A_2(x) - \partial_2 A_1(x). \tag{5.7}$$

For the classical model we derive the classical equations of motions as the Euler-Lagrange equations

$$\frac{d}{dt}\left(\frac{\partial_\mu \mathcal{L}_{CSM}}{\partial \dot{A}_\mu}\right) = \frac{\partial \mathcal{L}_{CSM}}{\partial A_\mu}, \tag{5.8}$$

for the Lagrangian of eq. (5.1). This gives us the following three equations of motion for the gauge field

$$\partial^\mu F_{\mu\nu}(x) + \frac{ke^2}{4\pi}\epsilon_{\nu\rho\sigma}F^{\rho\sigma}(x) = 0. \tag{5.9}$$

In addition, we note that the field strength $F_{\mu\nu}$ obeys the Bianchi identity,

$$\epsilon_{\mu\nu\rho}\partial^\mu F^{\nu\rho} = 0. \tag{5.10}$$

The equations of motion can be rewritten in terms of the electric and magnetic fields such that

$$\begin{aligned} &\dot{E}_i(x) + \frac{1}{e^2}\epsilon_{ij}\partial_j B(x) + \frac{ke^2}{2\pi}\epsilon_{ij}E_j(x) = 0, \\ &\partial_i E_i(x) + \frac{k}{2\pi}B(x) = 0. \end{aligned} \tag{5.11}$$

We recognize the last equation as Gauss' law for the Chern-Simons-Maxwell theory. It reduces to Gauss' law for the standard Maxwell theory in the limit $k = 0$. When $k > 0$ we observe from Gauss' law that a magnetic flux of $\frac{ke^2}{2\pi}$ is attached to each electric charge. This electrical flux will later turn out to give rise to the anyonic statistics of charges.

To solve the equations of motions let us consider a simple plane-wave ansatz for the electric field

$$E_i(x) = C_i \cos\left(\vec{p}\cdot\vec{x} - \omega t\right) + D_i \sin\left(\vec{p}\cdot\vec{x} - \omega t\right). \tag{5.12}$$

Substituting the ansatz into the equations of motion, we obtain that the ansatz parameters as

$$\begin{aligned} &C_i = c\epsilon_{ij}p_j - d\frac{M}{\omega}p_i, && D_i = d\epsilon_{ij}p_j + c\frac{M}{\omega}p_i, \\ &\omega = \sqrt{M^2 + p^2}, && M = \frac{ke^2}{2\pi}, \end{aligned} \tag{5.13}$$

where c and d are arbitrary real constants. We identify M as the topologically generated "photon" mass of the Abelian gauge field while ω determines the relativistic dispersion relation for the theory. From the explicit formulas of the two parameters C_i and D_i, we find the field contains a transverse part whose magnitude can be chosen freely, described by the parameters c and d, together with a longitudinal part that is proportional to the fraction

$$\frac{M}{\omega} = \frac{M}{\sqrt{M^2 + p^2}}. \tag{5.14}$$

We emphasize that the "photon" mass is proportional to the Chern-Simons level k and the squared electric charge e^2. This implies that in the pure Maxwell limit of $k \to 0$ the "photon" mass vanishes, such that the electromagnetic waves become purely transverse. In contrast, in the pure Chern-Simons limit of $e^2 \to \infty$ the "photon" becomes infinitely heavy and the longitudinal and transverse magnitudes of the wave appear on equal footing.

To quantize the classical Chern-Simons-Maxwell theory, we impose canonical commutation relations onto the gauge field A and the corresponding canonical momentum Π

$$\left[\Pi_i(x), A_j(x)\right] = -i\delta_{ij}\delta(x-y), \tag{5.15}$$

such that they are converted into quantum operators. The electric and magnetic fields are similarly converted into operators that are defined analogously to the classical case of eq. (5.7). We then rewrite the canonical commutation relations in terms of the electric and magnetic fields

$$\begin{aligned}\left[E_i(x), E_j(y)\right] &= -i\frac{k}{2\pi}\epsilon_{ij}\delta(x-y), \\ \left[B(x), B(y)\right] &= 0 \\ \left[E_i(x), B(y)\right] &= i\epsilon_{ij}\partial_j\delta(x-y).\end{aligned} \tag{5.16}$$

In the last commutation relation the derivative should be taken with respect to the variable x and not y, i.e. ∂_i should be read as $\frac{\partial}{\partial x^i}$. In contrast to the standard quantum Maxwell theory, here for a non-vanishing Chern-Simons density $k > 0$, the two components of the electric-field are non-commuting elements. The commutation relations between the magnetic fields themselves and between the electric fields and the magnetic field are identical to the pure Maxwell case. The full quantum Hamilton operator is derived directly from the classical counterpart

$$H = \int d^2x \left(\frac{e^2}{2}E_i^2 + \frac{1}{2e^2}B^2\right). \tag{5.17}$$

This can easily be shown to commute with the infinitesimal generators of local gauge transformations, that is the quantum Gauss operator,

$$\begin{aligned}G(x) &= \partial_i E_i(x) + \frac{k}{2\pi}B(x), \\ \left[G(x), H\right] &= 0.\end{aligned} \tag{5.18}$$

For a state $\left|\psi\right\rangle$ to be physical, it must satisfy Gauss' law everywhere, i.e.

$$G(x)\left|\psi\right\rangle = 0, \tag{5.19}$$

for any position x. When the theory is quantized the classical plane-wave solutions of eq. (5.12) are converted into free "photons" still with a "photon" mass of $M = \frac{ke^2}{2\pi}$.

5.1.2 Doubled Abelian Gauge Field Lagrangian

As we noted in the beginning, the theory is necessarily going to be doubled, once it is put on the lattice. Before moving on to the full doubled lattice model in the next section, let us first consider a doubled theory in the continuum.

We can construct this model directly from the single field continuum model by including a second dual Abelian gauge field in the Lagrangian. We denote this second dual gauge field by $\tilde{A}_\mu(x)$. We refer to the original gauge field A_μ as the direct field. The dual field comes with a standard Maxwell term that is simply added to the Lagrangian density. To couple the two gauge fields together, the Chern-Simons term is modified to include both gauge fields

$$\mathcal{L}_{D-CSM} = -\frac{1}{4e^2}F_{\mu\nu}F^{\mu\nu} - \frac{1}{4\widetilde{e}^2}\widetilde{F}_{\mu\nu}\widetilde{F}^{\mu\nu} + \frac{k}{4\pi}\epsilon_{\mu\nu\rho}\left(A^\mu\partial^\nu\widetilde{A}^\rho + \widetilde{A}^\mu\partial^\nu A^\rho\right). \tag{5.20}$$

Here $\widetilde{F}_{\mu\nu}$ is the field strength of the dual gauge field $\widetilde{F}_{\mu\nu} \equiv \partial_\mu\widetilde{A}_\nu - \partial_\nu\widetilde{A}_\mu$ and we have included a dual electric charge $\widetilde{e}$ for the dual field. Without loss of generality we assume the two electric charges to be equal $\widetilde{e} \equiv e$. If this is not the case a priori, we can obtain the equality of the two charges by a simple rescaling of the two fields. In contrast to the model with just a single Abelian gauge field, both time-reversal- and parity-symmetry are recovered in the doubled field model, since the dual field $\widetilde{A}_\mu(x)$ can be treated as a pseudo-vector. Again we are fixing the temporal gauge, i.e. $A_0(x) = 0$ and $\widetilde{A}_0(x) = 0$,

$$\mathcal{L}_{D-MSC} = \frac{1}{2e^2}\left(\dot{A}_i^2 - \left(\epsilon_{ij}\partial_i A_j\right)^2 + \dot{\widetilde{A}}_i^2 - \left(\epsilon_{ij}\partial_i\widetilde{A}_j\right)^2\right) + \frac{k}{4\pi}\epsilon_{ij}\left(\dot{A}_i\widetilde{A}_j + \dot{\widetilde{A}}_i A_j\right). \tag{5.21}$$

From here we identify the two conjugate momenta

$$\begin{aligned}\Pi_i(x) &\equiv \frac{\delta\mathcal{L}_{CSM}}{\delta\dot{A}_i} = \frac{1}{e^2}\dot{A}_i(x) + \frac{k}{4\pi}\epsilon_{ij}\widetilde{A}_j(x), \\ \widetilde{\Pi}_i(x) &\equiv \frac{\delta\mathcal{L}_{CSM}}{\delta\dot{\widetilde{A}}_i} = \frac{1}{e^2}\dot{\widetilde{A}}_i(x) + \frac{k}{4\pi}\epsilon_{ij}A_j(x),\end{aligned} \tag{5.22}$$

together with the classical Hamilton density

$$\begin{aligned}\mathcal{H}_{D-CSM} &= \Pi_i\dot{A}_i + \widetilde{\Pi}_i\dot{\widetilde{A}}_i - \mathcal{L}_{D-CSM} \\ &= \frac{1}{2e^2}\dot{A}_i^2 + \frac{1}{2e^2}\left(\epsilon_{ij}\partial_i A_j\right)^2 \frac{1}{2e^2}\dot{\widetilde{A}}_i^2 + \frac{1}{2e^2}\left(\epsilon_{ij}\partial_i\widetilde{A}_j\right)^2 \\ &= \frac{e^2}{2}\left(\Pi_i - \frac{k}{4\pi}\epsilon_{ij}\widetilde{A}_j\right)^2 + \frac{1}{2e^2}\left(\epsilon_{ij}\partial_i A_j\right)^2 \frac{e^2}{2}\left(\widetilde{\Pi}_i - \frac{k}{4\pi}\epsilon_{ij}A_j\right)^2 + \frac{1}{2e^2}\left(\epsilon_{ij}\partial_i\widetilde{A}_j\right)^2 \\ &= \frac{e^2}{2}E_i^2 + \frac{1}{2e^2}B^2 + \frac{e^2}{2}\widetilde{E}_i^2 + \frac{1}{2e^2}\widetilde{B}^2.\end{aligned} \tag{5.23}$$

In the last line we have identified the direct and dual electric (E_i and $\widetilde{E}_i$) and magnetic fields (B and $\widetilde{B}$) for the two gauge fields

$$\begin{aligned}E_i(x) &\equiv \Pi_i(x) - \frac{k}{4\pi}\epsilon_{ij}\widetilde{A}_j(x), & \widetilde{E}_i(x) &\equiv \widetilde{\Pi}_i(x) - \frac{k}{4\pi}\epsilon_{ij}A_j(x), \\ B(x) &\equiv \partial_1 A_2(x) - \partial_2 A_1(x), & \widetilde{B}(x) &\equiv \partial_1\widetilde{A}_2(x) - \partial_2\widetilde{A}_1(x).\end{aligned} \tag{5.24}$$

Again, we obtain the classical equations of motions as the Euler-Lagrange equations for the Lagrangian,

$$\partial^\mu F_{\mu\nu}(x) + \frac{ke^2}{4\pi}\epsilon_{\nu\rho\sigma}\widetilde{F}^{\rho\sigma}(x) = 0, \qquad \partial^\mu\widetilde{F}_{\mu\nu}(x) + \frac{ke^2}{4\pi}\epsilon_{\nu\rho\sigma}F^{\rho\sigma}(x) = 0. \tag{5.25}$$

Since both sets include the direct field strength $F_{\mu\nu}$ and the dual field strength $\widetilde{F}_{\mu\nu}$, The two sets of equations couple the two gauge fields together, but are otherwise similar to the equation of motions for the single field theory. We again rewrite the equations of motions in terms of the electric and magnetic fields

$$\begin{aligned} &\dot{E}_i(x) + \frac{1}{e^2}\epsilon_{ij}\partial_j B(x) + \frac{ke^2}{2\pi}\epsilon_{ij}\widetilde{E}_j(x) = 0, \quad \dot{\widetilde{E}}_i(x) + \frac{1}{e^2}\epsilon_{ij}\partial_j \widetilde{B}(x) + \frac{ke^2}{2\pi}\epsilon_{ij}E_j(x) = 0 \\ &\partial_i E_i(x) + \frac{k}{2\pi}\widetilde{B}(x) = 0, \qquad\qquad \partial_i \widetilde{E}_i(x) + \frac{k}{2\pi}B(x) = 0, \end{aligned} \tag{5.26}$$

where we recognize the two equations in the last line as Gauss' law for the direct and the dual gauge fields. Gauss' law for each of the two fields is identical to Gauss' law for the single gauge field theory, with the addition that for a non-vanishing Chern-Simons level $k > 0$. The electric charges are no longer bound to a magnetic flux, but instead to a dual magnetic flux, and vice versa for the dual electric charges. As for the single field theory we, find a solution to the equations of motion by constructing a plane-wave ansatz for each of the two gauge fields

$$\begin{aligned} E_i(x) &= C_i \cos\left(\vec{p}\cdot\vec{x} - \omega t\right) + D_i \sin\left(\vec{p}\cdot\vec{x} - \omega t\right), \\ \widetilde{E}_i(x) &= \widetilde{C}_i \cos\left(\vec{p}\cdot\vec{x} - \omega t\right) + \widetilde{D}_i \sin\left(\vec{p}\cdot\vec{x} - \omega t\right). \end{aligned} \tag{5.27}$$

Substituting the plane-wave ansatz into the equations of motion, we obtain a set of equations for the ansatz parameters in analogue to the single field model

$$\begin{aligned} C_i &= c\epsilon_{ij}p_j - \widetilde{d}\frac{M}{\omega}p_i, & \widetilde{C}_i &= \widetilde{c}\epsilon_{ij}p_j - d\frac{M}{\omega}p_i, \\ D_i &= d\epsilon_{ij}p_j + \widetilde{c}\frac{M}{\omega}p_i, & D_i &= \widetilde{d}\epsilon_{ij}p_j + c\frac{M}{\omega}p_i. \end{aligned} \tag{5.28}$$

Here c, $\widetilde{c}$, d, and $\widetilde{d}$ are four independent real variables corresponding to two "photon" modes each having a mass of $M = \frac{ke^2}{2\pi}$. The dispersion relation is again given by $\omega = \sqrt{M^2 + p^2}$ for both gauge fields. As in the single gauge field theory, it follows that in the pure Maxwell limit of $k \to 0$ the electric fields of the two photons becomes purely transverse and decouple from each other. To quantize the two gauge fields we promote the fields and their conjugate momenta to quantum operators by imposing the canonical commutation relations on the two fields separately

$$\begin{aligned} \left[\Pi_i(x), A_j(y)\right] &= \left[\widetilde{\Pi}_i(x), \widetilde{A}_j(y)\right] = -i\delta_{ij}\delta(x-y), \\ \left[\Pi_i(x), \widetilde{A}_j(y)\right] &= \left[\widetilde{\Pi}_i(x), A_j(y)\right] = 0. \end{aligned} \tag{5.29}$$

Again, we rewrite these relations in terms of the electric and magnetic fields

$$\begin{aligned} &\left[E_i(x), \widetilde{E}_j(y)\right] = \left[\widetilde{E}_i(x), E_j(y)\right] = -i\frac{k}{2\pi}\epsilon_{ij}\delta(x-y), \\ &\left[E_i(x), E_j(y)\right] = \left[\widetilde{E}_i(x), \widetilde{E}_j(y)\right] = 0, \\ &\left[B(x), B(y)\right] = \left[\widetilde{B}(x), \widetilde{B}(y)\right] = \left[B(x), \widetilde{B}(y)\right] = 0, \\ &\left[E(x), B(y)\right] = \left[\widetilde{E}(x), \widetilde{B}(y)\right] = i\epsilon_{ij}\partial_j\delta(x-y), \\ &\left[E(x), \widetilde{B}(y)\right] = \left[\widetilde{E}(x), B(y)\right] = 0. \end{aligned} \tag{5.30}$$

We then obtain the classical Hamilton operator

$$H_{D-CSM} = \int d^2x \left(\frac{e^2}{2}E_i^2 + \frac{1}{2e^2}B^2 + \frac{e^2}{2}\widetilde{E}_i^2 + \frac{1}{2e^2}\widetilde{B}^2\right), \tag{5.31}$$

which is commuting with the generators of infinitesimal local gauge transformations for both the direct and dual fields,

$$G(x) = \partial_i E_i(x) + \frac{k}{2\pi}\widetilde{B}(x), \qquad \left[G(x), H\right] = 0, \tag{5.32}$$
$$\widetilde{G}(x) = \partial_i \widetilde{E}_i(x) + \frac{k}{2\pi}B(x), \qquad \left[\widetilde{G}(x), H\right] = 0.$$

For a state $\left|\psi\right\rangle$ to be physical, it must satisfy Gauss' law everywhere. I.e. $G(x)\left|\psi\right\rangle = 0$ and $\widetilde{G}(x)\left|\psi\right\rangle = 0$ for any position x. Under quantization the two plane-wave solutions of the classical theory, eq. (5.27) are turned into two states of free "photons", still with a "photon" mass of $M = \frac{ke^2}{2\pi}$, associated with the direct and dual gauge field.

5.2 Non-Compact Doubled Chern-Simons-Maxwell Theory on Doubled Lattice Geometry

For simplicity, we only consider a doubled square lattice, but the generalization to other lattice geometries is straight forward. This will, however, not provide new insights into the model. We consider the lattice model in the Hamiltonian formulation, such that time is left as a continuous variable. Previous studies of Chern-Simons theory on the lattice have mainly focused on a description where all dynamical gauge degrees of freedom are residing on the links of a single lattice Λ with a link-based algebra. This means that the gauge field variables together with the corresponding canonically conjugate momenta are residing on the links of the lattice and the links are the basis for defining the operator algebra. Field operators residing on different links are then commuting with each other. As in the continuum description above, the canonically conjugate momenta for the direct gauge field $A_i(x)$ are given by $\Pi_i(x) = \frac{1}{e^2}\dot{A}_i + \frac{k}{4\pi}\epsilon_{ij}\widetilde{A}_j$. The 1-component of the conjugate momentum picks up a term of the 2-component of the dual field and vice versa. As we will confirm later, this implies that the field operators residing on different links, are no longer necessarily commuting. The standard link-based lattice representation is hence not a natural choice for this model. In contrast to a single lattice geometry, here we introduce an additional dual lattice $\widetilde{\Lambda}$, and we include independent gauge degrees of freedom simultaneously on the direct and on the dual lattice. We illustrate this lattice geometry in the left-hand side of Figure 5.1 where the direct (dual) lattice links are marked in solid black (dashed green) lines, and the lattice sites are marked by transparent black squares (green diamonds). The doubled lattice geometry gives rise to what we call lattice crosses. These are points of intersections between a direct and dual lattice link. It is important to note that the lattice crosses do not belong to either the direct (Λ) or the dual lattice ($\widetilde{\Lambda}$). Instead, the lattice crosses are forming two other sublattices, X and $\widetilde{X}$. This geometry is similar to the one that was previously considered in [92]. Depending on the orientation of the direct and dual lattice links there exist two different types of lattice crosses, one for each of the two lattice cross sublattices. In Figure 5.1 lattice crosses are marked by a red (blue) filled circle for lattice crosses of type I (II) $x \in X$ ($x \in \widetilde{X}$) and the boundary of the two lattice crosses have been marked by red (blue) dashed lines. The geometry of the two types of crosses are shown in the right-hand side of Figure 5.1. It should be noted that the type (I or II) that a lattice cross belongs to completely determines the direction of the direct and dual links. The lattice spacing for both the direct and the dual lattice is given by a which implies that the length of a cross side is $a/\sqrt{2}$ such that the area covered by a single-cross is $a^2/2$. On a single lattice cross x the vector potential of the direct gauge field $A_{x,i}$

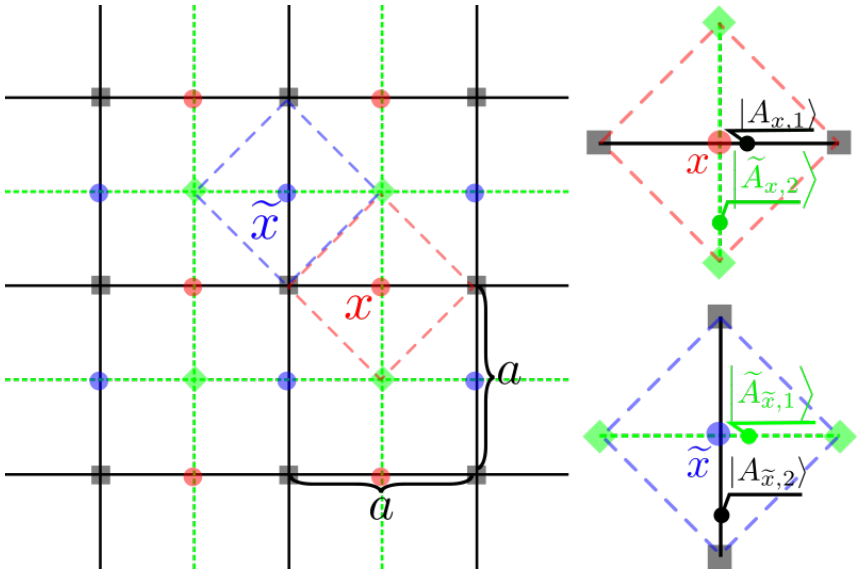

Figure 5.1: *Left: Illustration of the direct (black solid lines) lattice* Λ *and the dual (green dashed lines) lattice* $\widetilde{\Lambda}$*. Direct (dual) lattice sites are marked as black squares (green diamonds). The gauge fields* $A_{x,i}$ *and* $\widetilde{A}_{x,i}$ *are associated with the elementary lattice crosses. Cross type I (II) are marked by red (blue) filled circles. Right: The two types of elementary lattice crosses with the associated gauge field operators.*

is placed on the direct link meanwhile the corresponding dual vector potential $\epsilon_{ij}\widetilde{A}_{x,j}$ is placed on the dual link of the same cross. From the point of view of the Chern-Simons-Maxwell gauge fields, this is a natural lattice geometry, since the non-commutativity of the direct and dual gauge fields is incorporated into a single lattice cross algebra, and non-commuting elements are always residing on the same cross. Elements residing on different crosses are always commuting. This lattice geometry, however, comes with a price. It inevitably leads to the doubling of the gauge fields, thereby giving rise to two, instead of just a single, massive "photon" modes on the lattice. Due to the doubling problem we take the doubled model as the starting point for transferring the model on to the lattice. The single lattice gauge field model will not be considered on the lattice. Since the goal of this chapter is to connect Chern-Simons-Maxwell theory with Kitaev's toric-code, which corresponds to a doubled theory, the doubling of the gauge field is not a problem.

In the continuum we found the integrated Lagrange density for the doubled Chern-Simons-Maxwell theory in eq. (5.21), which we simplify to the form

$$L = \int d^2x \left(\frac{1}{2e^2}\dot{A}_i^2 - \frac{1}{2e^2}B^2 + \frac{1}{2e^2}\dot{\widetilde{A}}_i^2 - \frac{1}{2e^2}\widetilde{B}^2 + \frac{k}{4\pi}\epsilon_{ij}\left(\dot{A}_i\widetilde{A}_j + \dot{\widetilde{A}}_i A_j\right)\right), \tag{5.33}$$

by including the magnetic fields obtained for the continuum theory. We transfer this Lagrangian directly to the lattice by substituting the integration and the measure with a sum over the whole

lattice, and an area of a^2, $\int d^2x \to a^2 \sum$.[3] This gives the lattice Lagrangian

$$\begin{aligned} L = a^2 \sum_{x\in X} \left(\frac{1}{2e^2} \dot{A}_{x,1}^2 + \frac{1}{2e^2} \dot{\widetilde{A}}_{x,2}^2 + \frac{k}{4\pi} \left(\dot{A}_{x,1} \widetilde{A}_{x,2} - \dot{\widetilde{A}}_{x,2} A_{x,1} \right) \right) \\ + a^2 \sum_{x\in \widetilde{X}} \left(\frac{1}{2e^2} \dot{A}_{x,2}^2 + \frac{1}{2e^2} \dot{\widetilde{A}}_{x,1}^2 + \frac{k}{4\pi} \left(\dot{\widetilde{A}}_{x,1} A_{x,2} - \dot{A}_{x,2} \widetilde{A}_{x,1} \right) \right) \\ - a^2 \sum_{x\in \widetilde{X}} \frac{1}{2e^2} B_x^2 - a^2 \sum_{x\in X} \frac{1}{2e^2} \widetilde{B}_x^2, \end{aligned} \tag{5.34}$$

where we identify the magnetic fields on the lattice, B_x and $\widetilde{B}_x$, in analogue to the magnetic fields of the continuum:

$$\begin{aligned} B_x &\equiv \frac{1}{a} \left(A_{x-\frac{a}{2}\hat{2},1} + A_{x+\frac{a}{2}\hat{1},2} - A_{x+\frac{a}{2}\hat{2},1} - A_{x-\frac{a}{2}\hat{1},2} \right), \\ \widetilde{B}_x &\equiv \frac{1}{a} \left(\widetilde{A}_{x-\frac{a}{2}\hat{2},1} + \widetilde{A}_{x+\frac{a}{2}\hat{1},2} - \widetilde{A}_{x+\frac{a}{2}\hat{2},1} - \widetilde{A}_{x-\frac{a}{2}\hat{1},2} \right). \end{aligned} \tag{5.35}$$

Here $\hat{i}$ denotes the unit-vector in the i direction. It should be noted that the magnetic field associated with the direct gauge field variables $A_{x,i}$ resides on the dual lattice $x \in \widetilde{\Lambda}$ and vice versa. Both magnetic fields are invariant under a general lattice gauge transformations,

$$\begin{aligned} A_{x,i} \to A'_{x,i} &= A_{x,i} - \frac{1}{a} \left(\chi_{x+\frac{a}{2}\hat{i}} - \chi_{x-\frac{a}{2}\hat{i}} \right), \\ \widetilde{A}_{x,i} \to \widetilde{A}'_{x,i} &= \widetilde{A}_{x,i} - \frac{1}{a} \left(\widetilde{\chi}_{x+\frac{a}{2}\hat{i}} - \widetilde{\chi}_{x-\frac{a}{2}\hat{i}} \right). \end{aligned} \tag{5.36}$$

We obtain the canonically conjugate momenta on the lattice from the Lagrangian

$$\begin{aligned} \Pi_{x,i} &\equiv \frac{\partial L}{\partial \dot{A}_{x,i}} = a^2 \left(\frac{1}{e^2} \dot{A}_{x,i} + \frac{k}{4\pi} \epsilon_{ij} \widetilde{A}_{x,j} \right), \\ \widetilde{\Pi}_{x,i} &\equiv \frac{\partial L}{\partial \dot{\widetilde{A}}_{x,i}} = a^2 \left(\frac{1}{e^2} \dot{\widetilde{A}}_{x,i} + \frac{k}{4\pi} \epsilon_{ij} A_{x,j} \right). \end{aligned} \tag{5.37}$$

We emphasize that the dimensions of the canonically conjugate momenta on the lattice differ from the corresponding continuum momenta, since the lattice momenta contain an additional factor a^2. The classical Hamilton function on the lattice is similarly constructed

$$H = \sum_{x\in X} \left(\Pi_{x,1} \dot{A}_{x,1} + \widetilde{\Pi}_{x,2} \dot{\widetilde{A}}_{x,2} \right) + \sum_{x\in \widetilde{X}} \left(\Pi_{x,2} \dot{A}_{x,2} + \widetilde{\Pi}_{x,1} \dot{\widetilde{A}}_{x,1} \right) - L \tag{5.38}$$

$$= \frac{e^2}{2} a^2 \sum_{x\in X} \left(E_{x,1}^2 + \widetilde{E}_{x,2}^2 \right) + \frac{e^2}{2} a^2 \sum_{x\in \widetilde{X}} \left(E_{x,2}^2 + \widetilde{E}_{x,1}^2 \right) + \frac{1}{2e^2} a^2 \sum_{x\in \widetilde{X}} B_x^2 + \frac{1}{2e^2} a^2 \sum_{x\in X} B_x^2. \tag{5.39}$$

In analogue to the continuum theory, we identify the electric fields as

$$E_{x,i} = \frac{1}{a^2} \Pi_{x,i} - \frac{k}{4\pi} \epsilon_{ij} \widetilde{A}_{x,j}, \qquad \widetilde{E}_{x,i} = \frac{1}{a^2} \widetilde{\Pi}_{x,i} - \frac{k}{4\pi} \epsilon_{ij} A_{x,j}. \tag{5.40}$$

[3] That the area is a^2 instead of $a^2/2$ (as one might naively expect) comes from that both the direct and the dual field of the continuum theory are integrated over the entire volume.

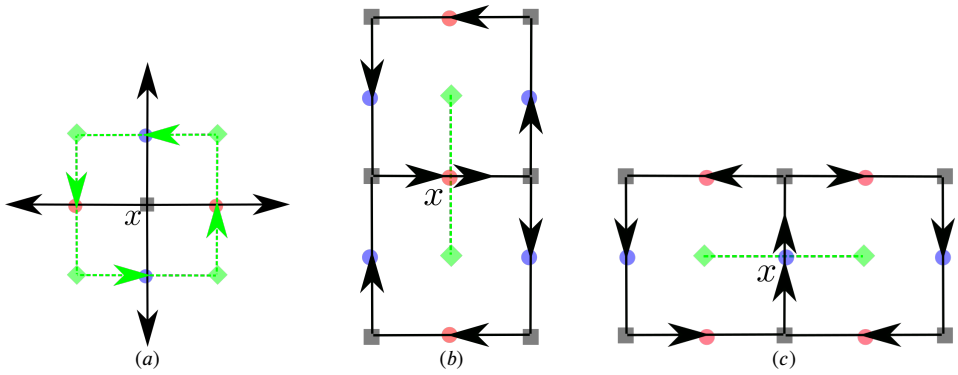

Figure 5.2: *Equations of motions for the doubled lattice Chern-Simons-Maxwell model. a: Gauss' law, eq.* (5.42)*. The divergence of the electric field (solid black arrows) on a lattice site x is coupled to the magnetic flux surrounding the site (green dashed lines). b-c: The equations of motion, eq.* (5.41)*. The difference in the magnetic flux (solid black arrows) across a link* (x, i) *is related to the time-derivative of the electric field* $\dot{E}_{x,i}$ *on the link, together with the dual electric field* $\epsilon_{ij}\widetilde{E}_{x,j}$ *associated with the same cross (dashed green line). Identical relations, that are not shown here, exist for the dual fields.*

As for the continuum theory, we obtain the classical equations of motion for the lattice Lagrangian of eq. (5.34) as its Euler-Lagrange equations,

$$\dot{E}_{x,i} + \frac{1}{ae^2}\epsilon_{ij}\left(B_{x+\frac{a}{2}\hat{j}} - B_{x-\frac{a}{2}\hat{j}}\right) + \frac{ke^2}{2\pi}\epsilon_{ij}\widetilde{E}_{x,j} = 0, \tag{5.41}$$

$$\dot{\widetilde{E}}_{x,i} + \frac{1}{ae^2}\epsilon_{ij}\left(\widetilde{B}_{x+\frac{a}{2}\hat{j}} - \widetilde{B}_{x-\frac{a}{2}\hat{j}}\right) + \frac{ke^2}{2\pi}\epsilon_{ij}E_{x,j} = 0,$$

$$\frac{1}{a}\sum_i \left(E_{x+\frac{a}{2}\hat{i},i} - E_{x-\frac{a}{2}\hat{i},i}\right) + \frac{k}{2\pi}\widetilde{B}_x = 0, \tag{5.42}$$

$$\frac{1}{a}\sum_i \left(\widetilde{E}_{x+\frac{a}{2}\hat{i},i} - \widetilde{E}_{x-\frac{a}{2}\hat{i},i}\right) + \frac{k}{2\pi}B_x = 0.$$

We recognize the last two equations as Gauss' law for the direct and dual lattice sites. We illustrate Gauss' law in Figure 5.2 (a) for a direct lattice site $x \in \Lambda$. As for the doubled Chern-Simons-Maxwell theory in the continuum, we find that the divergence of the electric field on a direct lattice site (black solid arrows) is coupled to the magnetic flux surrounding the direct lattice site (green dashed arrows), i.e. a dual magnetic flux is attached to the electric charges, and vice versa for the dual lattice sites. The two upper equations of motion are illustrated in Figure 5.2 (b-c) for a direct lattice link (x, i). The equations relate the time-derivative of the electric field $\dot{E}_{x,i}$ on a given link (x, i) to the difference of the magnetic fluxes (black solid arrows) across the same link, together with the dual electric field (green dashed lines) associated with the same lattice cross, $\epsilon_{ij}\widetilde{E}_{x,j}$.

We again apply two plane-wave ansatze to solve the classical equations of motion

$$E_{x,i} = C_i \cos(\vec{p}\cdot\vec{x} - \omega t) + D_i \sin(\vec{p}\cdot\vec{x} - \omega t), \tag{5.43}$$
$$\widetilde{E}_{x,i} = \widetilde{C}_i \cos(\vec{p}\cdot\vec{x} - \omega t) + \widetilde{D}_i \sin(\vec{p}\cdot\vec{x} - \omega t),$$

which when substituted into the equations of motion give

$$\begin{aligned} C_i &= c\epsilon_{ij}\hat{p}_j - \widetilde{d}\frac{M}{\omega}\hat{p}_i, & D_i &= d\epsilon_{ij}\hat{p}_j + \widetilde{c}\frac{M}{\omega}\hat{p}_i, \\ \widetilde{C}_i &= \widetilde{c}\epsilon_{ij}\hat{p}_j - d\frac{M}{\omega}\hat{p}_i, & \widetilde{D}_i &= \widetilde{d}\epsilon_{ij}\hat{p}_j + c\frac{M}{\omega}\hat{p}_i, \end{aligned} \tag{5.44}$$

where $\hat{p}$ denotes the lattice momentum defined by

$$\hat{p}_i = \frac{2}{a}\sin\frac{p_i a}{2}. \tag{5.45}$$

For small $p_i \ll \frac{1}{a}$ the lattice momentum agrees with the continuum momentum $\hat{p}_i \approx p_i$, and for p_i close to the edge of the Brillouin zone ($p_i \approx \pi/a$) the two values differ. As for the continuum model, we find that the theory contains four free parameters for the two ansatze, giving rise to two "photon" modes on the lattice. We find that the mass of the gauge fields is identical to the continuum case, and the energy-momentum dispersion relation is distorted by lattice artefacts when p comes close to the edge of the Brillouin zone

$$\omega = \sqrt{M^2 + \hat{p}^2}, \qquad M = \frac{ke^2}{2\pi}. \tag{5.46}$$

To quantize the theory, we impose the canonical commutation relations on the two gauge fields

$$\begin{aligned} [\Pi_{x,i}, A_{y,j}] &= [\widetilde{\Pi}_{x,i}, \widetilde{A}_{y,j}] = -i\delta_{ij}\delta_{xy}, \\ [\Pi_{x,i}, \widetilde{A}_{y,j}] &= [\widetilde{\Pi}_{x,i}, A_{y,j}] = 0. \end{aligned} \tag{5.47}$$

Before moving on to the commutation relations between the electric and magnetic fields, let us first examine the similarities between this theory and the classical mechanical system of a particle in a constant magnetic field. To do this, let us consider the commutation relations between the electric fields $E_{x,i}$ and $\widetilde{E}_{x,i}$ and the vector potentials $A_{x,i}$ and $\widetilde{A}_{x,i}$.
We identify these relations as

$$\begin{aligned} &[A_{x,i}, A_{y,j}] = [\widetilde{A}_{x,i}, \widetilde{A}_{y,j}] = [A_{x,i}, \widetilde{A}_{y,j}] = 0, \\ &[E_{x,i}, A_{y,j}] = [\widetilde{E}_{x,i}, \widetilde{A}_{y,j}] = -\frac{i}{a^2}\delta_{ij}\delta_{xy}, \\ &[E_{x,i}, \widetilde{A}_{y,j}] = [\widetilde{E}_{x,i}, A_{y,j}] = 0, \\ &[E_{x,i}, \widetilde{E}_{y,j}] = -i\frac{k}{2\pi a^2}\epsilon_{ij}\delta_{xy}, \\ &[E_{x,i}, E_{y,j}] = [\widetilde{E}_{x,i}, \widetilde{E}_{y,j}] = 0. \end{aligned} \tag{5.48}$$

In the naive continuum limit of $a \to 0$, $\frac{1}{a^2}\delta_{xy}$ approaches $\delta(x-y)$.[4] This set of commutation relations on a single lattice cross is identical to the commutation relations of a charged particle moving in a 2-dimensional plane, with a constant magnetic field perpendicular to the plane. The strength of the magnetic field is proportional to the Chern-Simons level $\frac{k}{2\pi}$. This classical system works as a "mechanical analogue" for the Chern-Simons-Maxwell theory on a single lattice cross. In the mechanical analogue the two gauge fields $A_{x,i}$ and $\epsilon_{ij}\widetilde{A}_{x,j}$ act as the x- and y-coordinates of

[4] Remembering that the discrete lattice integration measure is a^2, this is seen to give the correct result.

the mechanical particle, respectively. $E_{x,i}$ and $\epsilon_{ij}\widetilde{E}_{x,j}$ act as the corresponding momenta. In the mechanical analogue the non-zero commutators for the momenta arise from a non-zero magnetic flux in the plane, while in the Chern-Simons-Maxwell theory the non-zero commutators originates from the Chern-Simons level, which we interpret as an abstract "magnetic" field on the lattice cross. In the next section we are going to compactify the gauge fields on the lattice crosses from being real valued to an element in $U(1)$. This leads to a Dirac quantization of the abstract "magnetic" field in integer units, i.e. $k \in \mathbb{Z}$. For now, we let the Chern-Simons strength k be any positive real value.

The commutation relations between the electric and magnetic fields take the form

$$\begin{aligned}
&[E_{x,i}, B_y] = [\widetilde{E}_{x,i}, \widetilde{B}_y] = i\epsilon_{ij}\frac{1}{a^3}(\delta_{x,y+\frac{a}{2}\hat{j}} - \delta_{x,y-\frac{a}{2}\hat{j}}), \\
&[E_{x,i}, \widetilde{B}_y] = [\widetilde{E}_{x,i}, B_y] = 0, \\
&[B_x, B_y] = [\widetilde{B}_x, \widetilde{B}_y] = [B_x, \widetilde{B}_y] = 0.
\end{aligned} \tag{5.49}$$

As in the continuum, the classical plane-wave states from the ansatze considered above turn into two massive "photon" modes, when the theory is quantized. The mass of the "photons" is still given by $M = \frac{ke^2}{2\pi}$, and the lattice dispersion relation is identical to the classical case, $E(p) = \sqrt{M^2 + \hat{p}^2}$, where again $\hat{p}_i \equiv \frac{2}{a}\sin\frac{p_i a}{2}$.

The lattice Hamiltonian takes the form of the classical lattice Hamilton of eq. (5.38), where the fields are promoted to operators on which the above commutation relations are imposed. The Hamiltonian again commutes with the lattice generators of infinitesimal local gauge transformations for both the direct and the dual lattice,

$$\begin{aligned}
\frac{G_x}{a^2} &= \sum_i \frac{1}{a}(E_{x+\frac{a}{2}\hat{i},i} - E_{x-\frac{a}{2}\hat{i},i}) + \frac{k}{2\pi}\widetilde{B}_x, \qquad [G_x, H] = 0, \quad \forall \quad x \in \Lambda, \\
\frac{\widetilde{G}_x}{a^2} &= \sum_i \frac{1}{a}(\widetilde{E}_{x+\frac{a}{2}\hat{i},i} - \widetilde{E}_{x-\frac{a}{2}\hat{i},i}) + \frac{k}{2\pi}B_x, \qquad [\widetilde{G}_x, H] = 0, \quad \forall \quad x \in \widetilde{\Lambda}.
\end{aligned} \tag{5.50}$$

It should be noted that, just as for the lattice momenta, the dimensions of the lattice gauge transformation generators G_x and $\widetilde{G}_x$ differ from those of the corresponding operators in the continuum.

The gauge transformation generators associated with the different sites of the same lattice are commuting with each other, i.e. $[G_x, G_y] = 0$, for any $x, y \in \Lambda$, and $[\widetilde{G}_x, \widetilde{G}_y] = 0$, for any $x, y \in \widetilde{\Lambda}$. This follows trivially since the two generators are constructed from elements that are already commuting among themselves. For two generators residing on different sublattices, G_x and $\widetilde{G}_{x'}$ for $x \in \Lambda$ and $x' \in \widetilde{\Lambda}$, the generators are still commuting with each other. This is a non-trivial property of the operators, since the direct and dual generators now share two lattice crosses if the two generators are placed at a neighbouring site- and dual site. I.e. for $\widetilde{x} = x \pm \frac{1}{2}\hat{1} \pm \frac{1}{2}\hat{2}$. This is illustrated in Figure 5.3 where the lattice links residing in lattice crosses shared between the two generators are shown as bold links. Since the direct and dual fields on the same lattice cross are in general non-commuting, it is not a priori clear that the two generators of the gauge transformations are commuting. By explicitly calculating the commutators of the two generators for the case of $\widetilde{x} = x + \frac{1}{2}\hat{1} + \frac{1}{2}\hat{2}$, we find that the non-commutativity picked up from each of the two crosses that

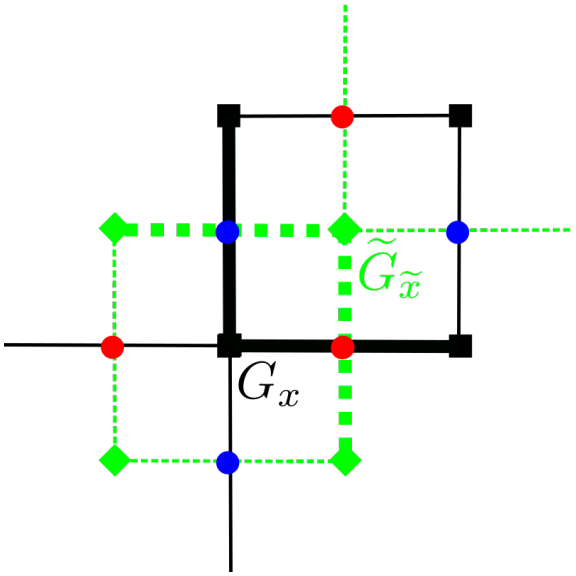

Figure 5.3: *Two neighbouring direct G_x and dual gauge generators $\widetilde{G}_{\widetilde{x}}$ are commuting, $\left[G_x, \widetilde{G}_{\widetilde{x}}\right] = 0$, even though they are sharing two lattice crosses with non-commuting electric fields $E_{x+\frac{a}{2}\hat{1},1}$ and $\widetilde{E}_{\widetilde{x}-\frac{a}{2}\hat{2},2}$ (bold lattice links).*

are shared between the generator, exactly cancel each other

$$\begin{aligned}\left[G_x, \widetilde{G}_{x+\frac{a}{2}\hat{1}+\frac{a}{2}\hat{2}}\right] &= -a^2[E_{x+\frac{a}{2}\hat{1},1}, \widetilde{E}_{x+\frac{a}{2}\hat{1},2}] - a^2[E_{x+\frac{a}{2}\hat{2},2}, \widetilde{E}_{x+\frac{a}{2}\hat{2},1}] \\ &\quad + \frac{ka^3}{2\pi}[E_{x+\frac{a}{2}\hat{1},1}, B_{x+\frac{a}{2}\hat{1}+\frac{a}{2}\hat{2}}] + \frac{ka^3}{2\pi}[E_{x+\frac{a}{2}\hat{2},2}, B_{x+\frac{a}{2}\hat{1}+\frac{a}{2}\hat{2}}] \\ &\quad + \frac{ka^3}{2\pi}[\widetilde{E}_{x+\frac{a}{2}\hat{2},1}, \widetilde{B}_x] + \frac{ka^3}{2\pi}[\widetilde{E}_{x+\frac{a}{2}\hat{1},2}, \widetilde{B}_x] \\ &= -\frac{ka^3}{2\pi}\frac{i}{a^3} + \frac{ka^3}{2\pi}\frac{i}{a^3} + \frac{ka^3}{2\pi}\frac{i}{a^3} - \frac{ka^3}{2\pi}\frac{i}{a^3} = 0.\end{aligned} \tag{5.51}$$

The other cases of neighbouring direct and dual sites can be shown to commute by similar calculations. Hence, generators of local lattice gauge transformations are guaranteed to always commute with each other. We define the vacuum state $\left|0\right\rangle$ to be the groundstate without charges, i.e. $Q_x = 0$ for every $x \in \Lambda$ and $\widetilde{Q}_x = 0$ for every $x \in \widetilde{\Lambda}$. This state is gauge-invariant and satisfies Gauss' law everywhere such that $G_x\left|0\right\rangle = 0$ and $\widetilde{G}_x\left|0\right\rangle = 0$. In addition to the vacuum state we will later consider states containing charges. Since the infinitesimal gauge transformation generators are always commuting with each other, we can specify a lattice state by the charges residing simultaneously on the direct lattice Q and the dual lattice $\widetilde{Q}$. We denote such a state by $|Q, \widetilde{Q}\rangle$. This state contains static direct and dual charges $Q_x \in \mathbb{Z}$ and $\widetilde{Q}_x \in \mathbb{Z}$,

$$G_x|Q, \widetilde{Q}\rangle = Q_x|Q, \widetilde{Q}\rangle, \quad x \in \Lambda, \qquad \widetilde{G}_x|Q, \widetilde{Q}\rangle = \widetilde{Q}_x|Q, \widetilde{Q}\rangle, \quad x \in \widetilde{\Lambda}. \tag{5.52}$$

In addition, using the above commutation relations, it can easily be shown that the electric and magnetic fields on both the direct and dual lattice are gauge-invariant objects, i.e. both are

commuting with the two generators of infinitesimal local gauge transformations,

$$\begin{aligned} &\left[E_{x,i}, G_y\right] = 0, \quad &&\left[E_{x,i}, \widetilde{G}_y\right] = 0, \quad &&\left[\widetilde{E}_{x,i}, G_y\right] = 0, \quad &&\left[\widetilde{E}_{x,i}, \widetilde{G}_y\right] = 0, \\ &\left[B_x, G_y\right] = 0, \quad &&\left[B_x, \widetilde{G}_y\right] = 0, \quad &&\left[\widetilde{B}_x, G_y\right] = 0, \quad &&\left[\widetilde{B}_x, \widetilde{G}_y\right] = 0. \end{aligned} \tag{5.53}$$

5.2.1 Anyonic Statistics of the Direct and Dual Charges

On the direct and dual lattice links (x, i) Wilson's parallel transporter is given by $U_{x,i} = \exp(iaA_{x,i})$ and $\widetilde{U}_{x,i} = \exp(ia\widetilde{A}_{x,i})$, respectively. Under a general unitary transformation on the direct lattice sites,

$$V = \prod_{x\in\Lambda} V_x = \prod_{x\in\Lambda} \exp(i\chi_x G_x), \tag{5.54}$$

which implements a general gauge transformation in the Hilbert space. The parallel transporter on a direct link is transformed according to,

$$U'_{x,i} = VU_{x,i}V^\dagger = \exp(i\chi_{x-\frac{a}{2}\hat{i}})U_{x,i}\exp(-i\chi_{x+\frac{a}{2}\hat{i}}), \quad x \in X, \widetilde{X}. \tag{5.55}$$

We find the commutation relation between the parallel transporter and the gauge transformation to be

$$[G_y, U_{x,i}] = \frac{1}{a}\sum_j [\Pi_{y+\frac{a}{2}\hat{j},j} - \Pi_{y-\frac{a}{2}\hat{j},j}, U_{x,i}] = \left(\delta_{y+\frac{a}{2}\hat{i},x} - \delta_{y-\frac{a}{2}\hat{i},x}\right) U_{x,i}. \tag{5.56}$$

Here the electric and magnetic fields contributing to the gauge transformation generator G_x have been rewritten in terms of the gauge fields and momenta by equations (5.35) and (5.40) and we have suppressed the trivially commuting terms. With this commutation relation we are able to find the charge distribution on the lattice before and after acting on a general charged state $|Q, \widetilde{Q}\rangle$ with Wilson's parallel transporter $U_{x,i}$,

$$\begin{aligned} G_y|Q', \widetilde{Q}\rangle &= G_y U_{x,i}|Q, \widetilde{Q}\rangle \\ &= U_{x,i}G_y|Q, \widetilde{Q}\rangle + \left(\delta_{y+\frac{a}{2}\hat{i},x} - \delta_{y-\frac{a}{2}\hat{i},x}\right) U_{x,i}|Q, \widetilde{Q}\rangle \\ &= \left(Q_y + \delta_{y+\frac{a}{2}\hat{i},x} - \delta_{y-\frac{a}{2}\hat{i},x}\right)|Q', \widetilde{Q}\rangle. \end{aligned} \tag{5.57}$$

As expected this shows that $U_{x,i}$ transports a single charge along the link (x, i). It should be noted that the operator $U_{x,i}$ actually transports a -1 charge from $x - \frac{a}{2}\hat{i}$ to $x + \frac{a}{2}\hat{i}$, and a charge of $+1$ is transported in the opposite direction, i.e. the state $|Q', \widetilde{Q}\rangle = U_{x,i}|Q, \widetilde{Q}\rangle$ contains the charge configuration of,

$$Q'_y = Q_y + \delta_{y+\frac{a}{2}\hat{i},x} - \delta_{y-\frac{a}{2}\hat{i},x}. \tag{5.58}$$

Similarly, we can show that the dual operator $\widetilde{U}_{x,i}$ transports a dual charge along the link analogously. Hence, we are able to transport a single charge along a curve on the lattice by combining Wilson's parallel transporters together. A special case of interest is transporting a charge around a

closed loop C, where the set of Wilson's transporters is called a Wilson-loop. This is defined on the direct and dual lattice as,

$$W_C = \prod_{(x,i)\in C} U_{x,i}, \qquad \widetilde{W}_C = \prod_{(x,i)\in C} \widetilde{U}_{x,i}. \tag{5.59}$$

Under the operation of a direct Wilson-loop on a charged lattice state $\left|Q, \widetilde{Q}\right\rangle$ we can show that the state is transformed according to

$$W_C|Q,\widetilde{Q}\rangle = \prod_{(x,i)\in C} U_{x,i}|Q,\widetilde{Q}\rangle = \exp(i\Phi_C)|Q,\widetilde{Q}\rangle, \tag{5.60}$$

where we find the phase Φ_C to be given by

$$\Phi_C = \sum_{x\in S\subset\widetilde{\Lambda}} a^2 B_x = \sum_{x\in S\subset\widetilde{\Lambda}} \frac{2\pi}{k}\widetilde{G}_x - \sum_C \frac{2\pi a}{k}\epsilon_{ij}\widetilde{E}_{x,j}. \tag{5.61}$$

Here x denotes a point on the dual lattice at the center of a plaquette on the original lattice which belongs to the surface S. That is, we find that the state picks up a phase given by the magnetic flux through the surface S bounded by the loop $C = \partial S$. The last equality follows from Stoke's theorem on the lattice as well as from the definitions for the gauge transformation generators in eq. (5.50). The first term in the last line counts — with an additional weight factor of $\frac{2\pi}{k}$ — the dual charges encircled by the loop C, along which the direct charge is transported around $\widetilde{Q}_S = \sum_{x\in S\subset\widetilde{\Lambda}} \widetilde{G}_x$. In a pure Chern-Simons theory when $e^2 \to \infty$, this is the only term contributing to the phase. [5] In this limit the phase Φ_C is therefore solely given by the total dual charge encircled by the loop C, such that the wave function picks up a topological phase $\exp(\frac{2\pi\widetilde{Q}_S}{k}i)$. This means that the direct charges and the dual charges have mutual anyonic statistics with the statistics angle given by the Chern-Simons level as $\frac{2\pi}{k}$. This is illustrated in Figure 5.4 where a charge is transported around a Wilson-loop (bold black directed links) which is encircling four dual charges (bold diamond outlines). The topological phase Φ_C is an adiabatic Berry phase, that, in contrast to generic Berry phases, is even insensitive to the shape of the curve C, as long as it encircles the same total charge $\widetilde{Q}_S$ on the dual lattice. By symmetry, we find analogous rules for the dual lattice and the corresponding operators.

Since the "photon" obtains a finite mass, in the general Chern-Simons-Maxwell theory, away from the pure Chern-Simons limit. The additional term in eq. (5.61) changes the above result slightly This creates a finite-size "photon" cloud surrounding each dual charge. Since the "photon" is massive, the effect of this term is exponentially suppressed at large distances compared to the mass, i.e. at distances $d \gg M^{-1}$, [79]. Still, it slightly affects the topological nature of the Berry phase, and gives rise to a small sensitivity to the precise location of the curve C, when the curve is close to the photon cloud surrounding the dual charges. The core result that the direct and dual charges have mutual anyonic statistics, with a statistics angle of $\frac{2\pi}{k}$, is, however, still valid as long as the charges are transported around each other in such a way that their "photon" clouds have a negligible overlap, that is to say at distances of $d \gg M^{-1}$.

[5] To see this, recall from eqs. (5.37) and (5.40), that the electric fields contain a hidden $\frac{1}{e^2}$ dependency and vanish in the pure Chern-Simons limit of $e^2 \to \infty$.

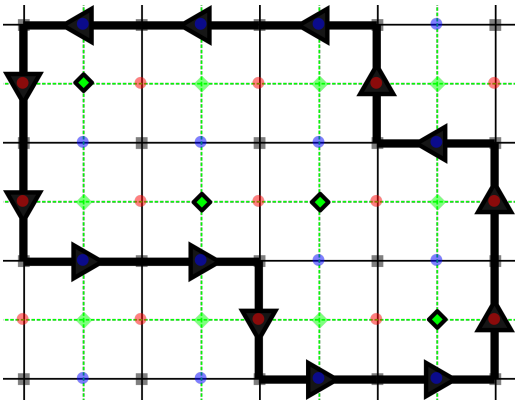

Figure 5.4: *A Wilson-loop W_C (bold black lines) on the direct lattice encircles a set of four dual charges $\widetilde{Q}_x$ (bold black diamond outlines). Up to exponentially suppressed corrections due to the finite "photon" mass, the vacuum expectation value of the Wilson-loop depends only on the total encircled dual charge, and not on further details of the geometry of the closed loop C.*

5.3 Compact Doubled Chern-Simons-Maxwell Theory on the Lattice

As found in eq. (5.48), the local degrees of freedom on a single lattice cross have a "mechanical analogue" in the form of a charged "particle" moving in the 2-dimensional plane $\mathbb{R}^2$ with an abstract "magnetic" field of strength $k/(2\pi)$ perpendicular to the plane. We are now going to compactify the gauge fields from the real numbers $\mathbb{R}$ to the gauge group $U(1)$. In terms of the "mechanical analogue", this corresponds to the motion of a "particle" in the same constant abstract "magnetic" field, but now restricted to the torus $U(1)^2$ instead of the plane $\mathbb{R}^2$. As for an actual magnetic field, we will find that this leads to the Dirac quantization of the abstract "magnetic" field. That is the Chern-Simons level k will be quantized in integer units, i.e. $k \in \mathbb{Z}$. We will further find that the compactification leads to a two-parameter family of self-adjoint extensions for the electric part of the Hamiltonian and the fixing of these self-adjoint extension parameters explicitly breaks the manifest $U(1)$ gauge symmetry down to just a $\mathbb{Z}(k)$ symmetry.

5.3.1 Compact Fields and Relations

To compactify the theory we turn the two direct and dual link variables $A_{x,i}$ and $\widetilde{A}_{x,i}$ into phases of Wilson's parallel transporters

$$\begin{aligned} U_{x,i} &= \exp(iaA_{x,i}) = \exp(i\varphi_{x,i}) \in U(1), \\ \widetilde{U}_{x,i} &= \exp(ia\widetilde{A}_{x,i}) = \exp(i\widetilde{\varphi}_{x,i}) \in U(1). \end{aligned} \tag{5.62}$$

In the compact theory these phases are the truly fundamental degrees of freedom. In terms of the compact parameters we now find that the electric fields are

$$aE_{x,i} = -i\partial_{\varphi_{x,i}} - \frac{k}{4\pi}\epsilon_{ij}\widetilde{\varphi}_{x,j}, \qquad a\widetilde{E}_{x,i} = -i\partial_{\widetilde{\varphi}_{x,i}} - \frac{k}{4\pi}\epsilon_{ij}\varphi_{x,j}. \tag{5.63}$$

We construct a plaquette term by group multiplication of the four link variables around an elementary plaquette

$$\begin{aligned} U_{\square_x} &\equiv U_{x-\frac{a}{2}\hat{2},1} U_{x+\frac{a}{2}\hat{1},2} U^{-1}_{x+\frac{a}{2}\hat{2},1} U^{-1}_{x-\frac{a}{2}\hat{1},2}, \quad x \in \widetilde{\Lambda} \\ &= \exp\left(i\varphi_{x-\frac{a}{2}\hat{2},1} + i\varphi_{x+\frac{a}{2}\hat{1},2} - i\varphi_{x+\frac{a}{2}\hat{2},1} - i\varphi_{x-\frac{a}{2}\hat{1},2} \right), \end{aligned} \tag{5.64}$$

$$\begin{aligned} \widetilde{U}_{\square_x} &\equiv \widetilde{U}_{x-\frac{a}{2}\hat{2},1} \widetilde{U}_{x+\frac{a}{2}\hat{1},2} \widetilde{U}^{-1}_{x+\frac{a}{2}\hat{2},1} \widetilde{U}^{-1}_{x-\frac{a}{2}\hat{1},2}, \quad x \in \Lambda \\ &= \exp\left(i\widetilde{\varphi}_{x-\frac{a}{2}\hat{2},1} + i\widetilde{\varphi}_{x+\frac{a}{2}\hat{1},2} - i\widetilde{\varphi}_{x+\frac{a}{2}\hat{2},1} - i\widetilde{\varphi}_{x-\frac{a}{2}\hat{1},2} \right), \end{aligned} \tag{5.65}$$

and we identify the plaquette magnetic fields with the plaquette terms by

$$\begin{aligned} \exp\left(ia^2 B_x\right) &= \exp\left(i\left(\varphi_{x-\frac{a}{2}\hat{2},1} + \varphi_{x+\frac{a}{2}\hat{1},2} - \varphi_{x+\frac{a}{2}\hat{2},1} - \varphi_{x-\frac{a}{2}\hat{1},2} \right)\right), \quad x \in \widetilde{\Lambda}, \\ \exp\left(ia^2 \widetilde{B}_x\right) &= \exp\left(i\left(\widetilde{\varphi}_{x-\frac{a}{2}\hat{2},1} + \widetilde{\varphi}_{x+\frac{a}{2}\hat{1},2} - \widetilde{\varphi}_{x+\frac{a}{2}\hat{2},1} - \widetilde{\varphi}_{x-\frac{a}{2}\hat{1},2} \right)\right), \quad x \in \Lambda. \end{aligned} \tag{5.66}$$

The commutation relations of eqs. (5.48) now take the form of

$$\begin{aligned} &[U_{x,i}, U_{y,j}] = [\widetilde{U}_{x,i}, \widetilde{U}_{y,j}] = [U_{x,i}, \widetilde{U}_{y,j}] = 0, \\ &[E_{x,i}, U_{y,j}] = \frac{1}{a}\delta_{ij}\delta_{xy} U_{x,i}, \\ &[\widetilde{E}_{x,i}, \widetilde{U}_{y,j}] = \frac{1}{a}\delta_{ij}\delta_{xy} \widetilde{U}_{x,i}, \\ &[E_{x,i}, \widetilde{U}_{y,j}] = [\widetilde{E}_{x,i}, U_{y,j}] = 0, \\ &[E_{x,i}, \widetilde{E}_{y,j}] = [\widetilde{E}_{x,i}, E_{y,j}] = -i\frac{k}{2\pi a^2}\epsilon_{ij}\delta_{xy}, \\ &[E_{x,i}, E_{y,j}] = [\widetilde{E}_{x,i}, \widetilde{E}_{y,j}] = 0. \end{aligned} \tag{5.67}$$

The commutation relations between the electric- and magnetic-fields are unchanged and are identical to what we found in eq. (5.49). Unlike the non-compact variables $A_{x,i}$ and $\widetilde{A}_{x,i}$, the compact variables $\varphi_{x,i}$ and $\widetilde{\varphi}_{x,i}$ are angles and are therefore not representing self-adjoint quantum mechanical operators. We are therefore not able to directly include the magnetic fields — as defined above — into the Hamiltonian. Instead, we must include the corresponding self-adjoint quantum operators. The solution to this problem is to construct a self-adjoint operator as $U_{\square} + U^{\dagger}_{\square} = 2\cos\left(a^2 B_x\right)$ such that the Hamiltonian of the corresponding theory is given by[6],

$$\begin{aligned} H = &\frac{e^2}{2}\sum_{x\in X}\left[\left(-i\partial_{\varphi_{x,1}} - \frac{k}{4\pi}\widetilde{\varphi}_{x,2} \right)^2 + \left(-i\partial_{\widetilde{\varphi}_{x,2}} + \frac{k}{4\pi}\varphi_{x,1} \right)^2 \right] \\ &+ \frac{e^2}{2}\sum_{x\in\widetilde{X}}\left[\left(-i\partial_{\varphi_{x,2}} + \frac{k}{4\pi}\widetilde{\varphi}_{x,1} \right)^2 + \left(-i\partial_{\widetilde{\varphi}_{x,1}} - \frac{k}{4\pi}\varphi_{x,2} \right)^2 \right] \\ &- \frac{1}{e^2 a^2}\sum_{x\in\Lambda}\cos(a^2\widetilde{B}_x) - \frac{1}{e^2 a^2}\sum_{x\in\widetilde{\Lambda}}\cos(a^2 B_x). \end{aligned} \tag{5.68}$$

[6]It can easily be shown that the two results agree to first-order since $\frac{1}{e^2 a^2}\cos\left(a^2 B_x^2\right) = 1 - \frac{a^2}{e^2}B_x^2 + \mathcal{O}\left(a^4 B_x^2\right)$ which equals the non-compact term $\frac{a^2}{2e^2}B_x^2$ up to an unimportant constant. Similar results are trivially found for the dual magnetic field by substituting B_x by $\widetilde{B}_x$.

5.3.2 Behaviour on a Single Lattice Cross

Before we move on to consider the behaviour of the model on the full lattice, let us start by just considering the behaviour on a single lattice cross. For concreteness, we will consider a lattice cross of type I (see Figure 5.1) that is $x \in X$, but the results presented here can be translated into analogous results for a lattice cross of type II. On the lattice cross of type I, the direct variable φ is associated with the link in the 1-direction, and the dual variable $\widetilde{\varphi}$ is associated with the link in the 2-direction. To ease the notation we are going to suppress the explicit link indices (x, i) as long as we are just considering a single-cross of type I.

Different lattice crosses are coupled together through the magnetic terms of the lattice Hamiltonian in eq. (5.38). Therefore, as long as we are just considering the behaviour on a single lattice cross, we ignore the magnetic terms. The "mechanical analogue" of the single-cross problem then corresponds to a charged "particle" with "spatial" coordinates $(\varphi, \widetilde{\varphi})$ moving in the 2-dimensional group space subject to the single-cross Hamiltonian,

$$H_+ = \frac{e^2a^2}{2}(E_{x,1}^2 + \widetilde{E}_{x,2}^2) = \frac{e^2a^2}{2}(E^2 + \widetilde{E}^2). \tag{5.69}$$

We emphasize that in the compactified theory, one can no longer achieve $\widetilde{e} = e$ through a rescaling of the fields. To maintain the symmetry between the original and the dual lattice we instead impose this condition by hand.

Self-adjoint Extensions of the Electric Contribution to the Hamiltonian

For a single lattice cross we introduce two abstract vector potentials a and $\widetilde{a}$. These vector potentials live on the group space torus $U(1)^2$ and are parametrized by the two variables φ and $\widetilde{\varphi}$

$$a(\varphi, \widetilde{\varphi}) = -\frac{k}{4\pi}\widetilde{\varphi}, \qquad \widetilde{a}(\varphi, \widetilde{\varphi}) = \frac{k}{4\pi}\varphi. \tag{5.70}$$

Using eq. (5.63) we rewrite the electric fields belonging to the lattice cross in terms of the new abstract vector potentials as

$$aE = -i\partial_\varphi + a\left(\varphi, \widetilde{\varphi}\right) \qquad a\widetilde{E} = -i\partial_{\widetilde{\varphi}} + \widetilde{a}\left(\varphi, \widetilde{\varphi}\right). \tag{5.71}$$

From the two abstract vector potentials we find that the lattice cross contains a constant abstract "magnetic" field

$$b(\varphi, \widetilde{\varphi}) = \partial_\varphi \widetilde{a}(\varphi, \widetilde{\varphi}) - \partial_{\widetilde{\varphi}} a(\varphi, \widetilde{\varphi}) = \frac{k}{2\pi}, \tag{5.72}$$

which is completely determined by the Chern-Simons level k. It is important to note that this abstract "magnetic" field $b(\varphi, \widetilde{\varphi})$ is unrelated to the actual magnetic fields of the theory, i.e. the B_x and $\widetilde{B}_x$, and these should not be confused with $b\left(\phi, \widetilde{\phi}\right)$.

The square of the direct and dual electric fields E^2 and $\widetilde{E}^2$ are included in the Hamiltonian H_+ in eq. (5.69). Since the Hamiltonian is necessarily a self-adjoint operator so must the squared electric fields also be self-adjoint operators. For a mathematical description detailing the theory of

self-adjoint extensions the reader is referred to [123, 124]. The problem of finding the self-adjoint extensions of H_+ has already been discussed for the "mechanical analogue" of the system, i.e. for a charged particle moving on a torus in a constant magnetic field in [125] and we apply the same mathematical solution here to the compactified CSM on a single lattice cross.

The state on a single-cross is described by a wave function $\Psi(\varphi, \widetilde{\varphi})$. We will later extend this to the wave functional of the full lattice field theory, once all the crosses are combined to form the entire lattice. The self-adjoint extension parameters enter the boundary conditions for this single-cross wave function on the group space torus $U(1)^2$. In contrast to the abstract "magnetic" field $b\left(\phi, \widetilde{\phi}\right)$, that is constant and thus trivially a periodic function over the group space torus, the abstract vector potentials themselves, i.e. $a\left(\phi, \widetilde{\phi}\right)$ and $\widetilde{a}\left(\phi, \widetilde{\phi}\right)$, are not strictly periodic functions. Eq. (5.70) implies that the explicit boundary conditions for the two vector potentials take the form

$$\begin{aligned} a(\varphi + 2\pi, \widetilde{\varphi}) &= -\frac{k}{4\pi}\widetilde{\varphi} = a(\varphi, \widetilde{\varphi}), \\ a(\varphi, \widetilde{\varphi} + 2\pi) &= -\frac{k}{4\pi}\widetilde{\varphi} - \frac{k}{2} = a(\varphi, \widetilde{\varphi}) - \frac{k}{2}, \\ \widetilde{a}(\varphi + 2\pi, \widetilde{\varphi}) &= \frac{k}{4\pi}\varphi + \frac{k}{2} = \widetilde{a}(\varphi, \widetilde{\varphi}) + \frac{k}{2}, \\ \widetilde{a}(\varphi, \widetilde{\varphi} + 2\pi) &= \frac{k}{4\pi}\varphi = \widetilde{a}(\varphi, \widetilde{\varphi}). \end{aligned} \tag{5.73}$$

By introducing two so-called transition functions, which play the role of gauge transformations of the boundary,

$$\alpha(\widetilde{\varphi}) = -\frac{k}{2}\widetilde{\varphi} + \widetilde{\theta}, \qquad \widetilde{\alpha}(\varphi) = \frac{k}{2}\varphi + \theta, \tag{5.74}$$

we rewrite the boundary conditions as twisted periodic boundary conditions over the group space torus $U(1)^2$,

$$\begin{aligned} a\left(\varphi + 2\pi, \widetilde{\varphi}\right) &= a\left(\varphi, \widetilde{\varphi}\right) - \partial_{\varphi}\alpha\left(\widetilde{\varphi}\right), \\ a\left(\varphi, \widetilde{\varphi} + 2\pi\right) &= a\left(\varphi, \widetilde{\varphi}\right) - \partial_{\varphi}\widetilde{\alpha}\left(\varphi\right), \\ \widetilde{a}\left(\varphi + 2\pi, \widetilde{\varphi}\right) &= \widetilde{a}\left(\varphi, \widetilde{\varphi}\right) - \partial_{\widetilde{\varphi}}\alpha\left(\widetilde{\varphi}\right), \\ \widetilde{a}\left(\varphi, \widetilde{\varphi} + 2\pi\right) &= \widetilde{a}\left(\varphi, \widetilde{\varphi}\right) - \partial_{\widetilde{\varphi}}\widetilde{\alpha}\left(\varphi\right). \end{aligned} \tag{5.75}$$

This shows that α and $\widetilde{\alpha}$ play the role of abstract gauge transformations. Here we have introduced θ and $\widetilde{\theta}$ as two real-valued angular parameters, i.e. they are both restricted to take values in $[0, 2\pi[$. We will later see that these parameters are self-adjoint extension parameters. Again, we emphasize that these abstract "gauge fields" should not be confused with the original lattice gauge symmetry. In order for the wave function $\Psi\left(\varphi, \widetilde{\varphi}\right)$ to respect the abstract gauge structure, it is necessary that it obeys boundary conditions that are consistent with the twisted boundary conditions for the abstract "gauge fields"

$$\begin{aligned} \Psi\left(\varphi + 2\pi, \widetilde{\varphi}\right) &= \exp\left(i\alpha\left(\widetilde{\varphi}\right)\right)\Psi\left(\varphi, \widetilde{\varphi}\right) \\ &= \exp\left(-i\frac{k}{2}\widetilde{\varphi} + i\widetilde{\theta}\right)\Psi\left(\varphi, \widetilde{\varphi}\right), \end{aligned} \tag{5.76}$$

$$\begin{aligned} \Psi\left(\varphi, \widetilde{\varphi} + 2\pi\right) &= \exp\left(i\widetilde{\alpha}\left(\varphi\right)\right)\Psi\left(\varphi, \widetilde{\varphi}\right) \\ &= \exp\left(i\frac{k}{2}\varphi + i\theta\right)\Psi\left(\varphi, \widetilde{\varphi}\right). \end{aligned} \tag{5.77}$$

These equations are valid for a cross of type I ($x \in X$). For a cross of type II the corresponding boundary conditions are obtained by changing the signs of θ and $\widetilde{\theta}$. Both θ and $\widetilde{\theta}$ enter the boundary conditions of the wave function, which is typical for self-adjoint extension parameters.

By applying the above boundary conditions to the wave function in opposite orders

$$\begin{aligned}\Psi\left(\varphi+2\pi,\widetilde{\varphi}+2\pi\right) &= \exp\left(-i\frac{k}{2}\left(\widetilde{\varphi}+2\pi\right)+i\widetilde{\theta}\right)\Psi\left(\varphi,\widetilde{\varphi}+2\pi\right) \qquad (5.78)\\ &= \exp\left(-i\frac{k}{2}\left(\widetilde{\varphi}+2\pi\right)+i\widetilde{\theta}+i\frac{k}{2}\varphi+i\theta\right)\Psi\left(\varphi,\widetilde{\varphi}\right),\\ \Psi\left(\varphi+2\pi,\widetilde{\varphi}+2\pi\right) &= \exp\left(i\frac{k}{2}\left(\varphi+2\pi\right)+i\theta\right)\Psi\left(\varphi+2\pi,\widetilde{\varphi}\right) \qquad (5.79)\\ &= \exp\left(i\frac{k}{2}\left(\varphi+2\pi\right)+i\theta-i\frac{k}{2}\widetilde{\varphi}+i\widetilde{\theta}\right)\Psi\left(\varphi,\widetilde{\varphi}\right),\end{aligned}$$

we obtain a consistency relation

$$\exp\left(-ik\pi\right)=\exp\left(ik\pi\right). \qquad (5.80)$$

This implies that the Chern-Simons level must be quantized in integer units $k \in \mathbb{Z}$. The abstract "magnetic" flux through the group space torus $U(1)^2$ is quantized as well

$$\int_0^{2\pi} d\varphi \int_0^{2\pi} d\widetilde{\varphi}\, b(\varphi,\widetilde{\varphi}) = 2\pi k. \qquad (5.81)$$

The quantization of the level k is thus a Dirac quantization condition for the abstract "magnetic" flux through the group space torus.

In addition to the two abstract gauge fields a and $\widetilde{a}$ and their associated abstract magnetic field b, there exist two additional gauge-invariant quantities on the group space torus $U(1)^2$. These are the two Polyakov loops ϕ and $\widetilde{\phi}$

$$\begin{aligned}\phi\left(\widetilde{\varphi}\right) &= \int_0^{2\pi} d\varphi\, a\left(\varphi,\widetilde{\varphi}\right)+\alpha\left(\widetilde{\varphi}\right) = -k\widetilde{\varphi}+\widetilde{\theta}, \qquad (5.82)\\ \widetilde{\phi}\left(\varphi\right) &= \int_0^{2\pi} d\widetilde{\varphi}\,\widetilde{a}\left(\varphi,\widetilde{\varphi}\right)+\widetilde{\alpha}\left(\varphi\right) = k\varphi+\theta.\end{aligned}$$

which arise from the non-trivial holonomies of the torus. The two Polyakov loops give rise to two separate complex Aharonov-Bohm phases

$$\exp\left(i\phi\left(\widetilde{\varphi}\right)\right)=\exp\left(-ik\widetilde{\varphi}+i\widetilde{\theta}\right), \qquad \exp\left(i\widetilde{\phi}\left(\varphi\right)\right)=\exp\left(ik\varphi+i\theta\right). \qquad (5.83)$$

In contrast to the classical theory, the quantum CSM theory is sensitive to these Aharonov-Bohm phases. The two Aharonov-Bohm phases are invariant only under shifts of the φ and $\widetilde{\varphi}$ parameters by integer multiples of $\frac{2\pi}{k}$. Therefore, we find that the two continuous $U(1)$ gauge transformations of the direct and dual lattice are each broken down to a discrete $\mathbb{Z}(k)$ gauge-invariance, by the two Polyakov loops. Hence, the Aharonov-Bohm phases are breaking the original and dual lattice $U(1)$ gauge symmetries down to a manifest $\mathbb{Z}(k)$ symmetry for each lattice.

Fate of the Original and Dual $U(1)$ Gauge Symmetries

Since gauge symmetries are not actual physical symmetries but merely redundancies in the theoretical description of the theory, we should ask what happened to the redundancy associated with the continuous $U(1)$ gauge symmetries in the classical model, when the gauge theory is broken explicitly to $\mathbb{Z}(k)$ at the quantum level. To understand what is going on here let us consider a continuous $U(1)$ gauge transformation for both the direct and dual link variables

$$\begin{aligned} U_{x,i} \to U'_{x,i} &= \exp\left(i\varphi'_{x,i}\right) \\ &= \exp\left(i\chi_{x-\frac{a}{2}\hat{\imath}}\right) U_{x,i} \exp\left(-i\chi_{x+\frac{a}{2}\hat{\imath}}\right) \\ &= \exp\left(i\left(\varphi_{x,i} - \chi_{x+\frac{a}{2}\hat{\imath}} + \chi_{x-\frac{a}{2}\hat{\imath}}\right)\right), \end{aligned} \tag{5.84}$$

$$\begin{aligned} \widetilde{U}_{x,i} \to \widetilde{U}'_{x,i} &= \exp\left(i\widetilde{\varphi}'_{x,i}\right) \\ &= \exp\left(i\widetilde{\chi}_{x-\frac{a}{2}\hat{\imath}}\right) \widetilde{U}_{x,i} \exp\left(-i\widetilde{\chi}_{x+\frac{a}{2}\hat{\imath}}\right) \\ &= \exp\left(i\left(\widetilde{\varphi}_{x,i} - \widetilde{\chi}_{x+\frac{a}{2}\hat{\imath}} + \widetilde{\chi}_{x-\frac{a}{2}\hat{\imath}}\right)\right). \end{aligned} \tag{5.85}$$

As we noted in the case of the non-compact theory in the previous section, both the electric ($E_{x,i}$ and $\widetilde{E}_{x,i}$) and magnetic fields (B_x and $\widetilde{B}_x$) on both the direct and dual lattice turn out to be gauge-invariant objects, i.e. they are both commuting with local gauge transformations on both a direct lattice site (G_x) and on a dual lattice site ($\widetilde{G}_x$). In the compact theory this is not as simple as for the non-compact theory. Let us consider a general finite gauge transformation that is represented in the Hilbert space by a unitary transformation of the form

$$V = \prod_{x\in\Lambda} \exp\left(i\chi_x G_x\right) \prod_{x\in\widetilde{\Lambda}} \exp\left(i\widetilde{\chi}_x \widetilde{G}_x\right). \tag{5.86}$$

The link variables of eq. (5.84) and (5.85) then transform according to

$$V U_{x,i} V^\dagger = U'_{x,i}, \qquad\qquad V \widetilde{U}_{x,i} V^\dagger = \widetilde{U}'_{x,i}, \tag{5.87}$$

where the transformed fields are given in eqs. (5.84) and (5.85). Similarly, we find that, when solely considering the superficial algebraic form of the electric and Hamiltonian operators,

$$V E_{x,i} V^\dagger = E_{x,i}, \qquad V \widetilde{E}_{x,i} V^\dagger = \widetilde{E}_{x,i}, \qquad V H V^\dagger = H. \tag{5.88}$$

So far this seems to be identical to what we found in the non-compact case, which suggests that there should still exist an $U(1)$ gauge symmetry on each of the links of a lattice cross. There is, however, a caveat concerning the results of eq. (5.88) that we have so far ignored. The gauge transformation V does leave the explicit algebraic form of the three operators E, $\widetilde{E}$, and H unchanged. This is, however, not the case for the domain of these operators, which is changed by the transformation V. To see this let us consider the wave functional of the full theory $\Psi'[\varphi, \widetilde{\varphi}] = V\Psi[\varphi, \widetilde{\varphi}]$ which depends on the entire lattice gauge field $[\varphi, \widetilde{\varphi}]$ on all crosses. As noted above the wave functional needs to satisfy boundary conditions consistent with the twisted boundary conditions for the two "abstract gauge" fields a and $\widetilde{a}$, as given in eqs. (5.78) and (5.79). When the wave functional is

transformed by V, it no longer automatically satisfies these boundary conditions. Under a general gauge transformation V, the wave functional is transformed by

$$\begin{aligned}\Psi'[\varphi,\widetilde{\varphi}] &= V\Psi[\varphi,\widetilde{\varphi}] \\ &= \prod_{x\in\Lambda}\exp\left(i\frac{ka^2}{4\pi}\chi_x\widetilde{B}_x\right)\prod_{x\in\widetilde{\Lambda}}\exp\left(i\frac{ka^2}{4\pi}\widetilde{\chi}_x B_x\right)\Psi[\varphi',\widetilde{\varphi}'].\end{aligned} \tag{5.89}$$

Here φ' and $\widetilde{\varphi}'$ are the gauge transformed fields of eqs. (5.84) and (5.85). Applying the unitary transformation V to the wave function for just a single lattice cross we find that the boundary conditions for the wave function get transformed to

$$\begin{aligned}\Psi'\left(\varphi+2\pi,\widetilde{\varphi}\right) &= \exp\left(-i\frac{k}{2}\widetilde{\varphi}+i\widetilde{\theta}'\right)\Psi'\left(\varphi,\widetilde{\varphi}\right), \\ \Psi'\left(\varphi,\widetilde{\varphi}+2\pi\right) &= \exp\left(i\frac{k}{2}\varphi+i\theta'\right)\Psi'\left(\varphi,\widetilde{\varphi}\right),\end{aligned} \tag{5.90}$$

where the two self-adjoint extension parameters θ and $\widetilde{\theta}$ are themselves transformed according to

$$\begin{aligned}\exp\left(i\theta'_{x,i}\right) &= \exp\left(i\left(\theta_{x,i}+k\chi_{x+\frac{a}{2}\hat{i}}-k\chi_{x-\frac{a}{2}\hat{i}}\right)\right), \\ \exp\left(i\widetilde{\theta}'_{x,i}\right) &= \exp\left(i\left(\widetilde{\theta}_{x,i}+k\widetilde{\chi}_{x+\frac{a}{2}\hat{i}}-k\widetilde{\chi}_{x-\frac{a}{2}\hat{i}}\right)\right).\end{aligned} \tag{5.91}$$

Hence, the self-adjoint extension parameters $\exp\left(i\theta_{x,i}\right)$ and $\exp\left(i\widetilde{\theta}_{x,i}\right)$ themselves transform under V as $U(1)$ gauge fields. If we compare the transformation of the two self-adjoint extension parameters with the link variables $U_{x,i}$ and $\widetilde{U}_{x,i}$, see eqs. (5.84) and (5.85), we find that the self-adjoint extension parameters transport k units of charge. Hence, the phases $\exp\left(i\theta_{x,i}\right)$ and $\exp\left(i\widetilde{\theta}_{x,i}\right)$ are invariant only under $\mathbb{Z}(k)$ gauge transformations.

A general $U(1)$ gauge transformation necessarily also changes the two self-adjoint extension parameters θ and $\widetilde{\theta}$. This in turn changes the boundary conditions and hence the domain of the Hamiltonian. Thus, even though the algebraic form of the Hamiltonian is unchanged by the gauge transformation V, the domain on which the Hamiltonian can operate is changed. Therefore, only the $\mathbb{Z}(k)$ subgroup of the $U(1)$ symmetry, which simultaneously leaves the algebraic form of the Hamiltonian and its domain unchanged, remains a symmetry of the theory.

The original redundancies associated with the $U(1)$ gauge symmetries of the classical theory are therefore still present at the quantum level. It is just that the continuous $U(1)$ gauge transformations are leading from one domain of the Hamiltonian, which is characterized by θ and $\widetilde{\theta}$, to another unitarily equivalent domain, characterized by the transformed parameters θ' and $\widetilde{\theta}'$.

Since the self-adjoint extension parameters θ and $\widetilde{\theta}$ are transformed under gauge transformations the physical content of the theory cannot be characterized by the self-adjoint extension parameters themselves. Instead, we must construct a gauge-invariant plaquette field strengths of the self-adjoint parameters

$$\begin{aligned}\exp\left(i\eta_x\right) &= \exp\left(i\left(\theta_{x-\frac{a}{2}\hat{2},1}+\theta_{x+\frac{a}{2}\hat{1},2}-\theta_{x+\frac{a}{2}\hat{2},1}-\theta_{x-\frac{a}{2}\hat{1},2}\right)\right), \quad x\in\widetilde{\Lambda}, \\ \exp\left(i\widetilde{\eta}_x\right) &= \exp\left(i\left(\widetilde{\theta}_{x-\frac{a}{2}\hat{2},1}+\widetilde{\theta}_{x+\frac{a}{2}\hat{1},2}-\widetilde{\theta}_{x+\frac{a}{2}\hat{2},1}-\widetilde{\theta}_{x-\frac{a}{2}\hat{1},2}\right)\right), \quad x\in\Lambda,\end{aligned} \tag{5.92}$$

which are gauge-invariant quantities. We have two natural choices $\eta_x = \widetilde{\eta}_x = 0$ or $\eta_x = \widetilde{\eta}_x = \pi$ everywhere on the lattice. Both of these leave the charge conjugation symmetry C intact, while any other choice would explicitly break C. It should be noted that the parity symmetry P is already explicitly broken by the Chern-Simons term. We emphasize that in contrast to the link variables $U_{x,i}$ and $\widetilde{U}_{x,i}$ the self-adjoint parameters $\exp\left(i\theta_{x,i}\right)$ and $\exp\left(i\widetilde{\theta}_{x,i}\right)$ are not dynamical gauge degrees of freedom but merely parameters defining a super-selection sector. In this way the parameters resemble the θ vacuum angle in 4-dimensional non-Abelian gauge theories. For both cases different values of the parameters define different vacuum sectors. As for the η and $\widetilde{\eta}$ values, a choice of the vacuum θ-angle in non-Abelian gauge theories different from to 0 or π, is explicitly breaking a symmetry of the theory, in this case the CP-symmetry.

Local Magnetic Translation Group on a Single Lattice Cross

To investigate the behaviour of the reduced $\mathbb{Z}(k)$ gauge symmetry of the Hamiltonian, we introduce two unitary operators

$$\begin{aligned} T &= \exp\left(\frac{2\pi i}{k}\left(-i\partial_\varphi + \frac{k}{4\pi}\widetilde{\varphi} - \frac{\widetilde{\theta}}{2\pi}\right)\right) = \exp\left(\frac{2\pi}{k}\partial_\varphi + \frac{i}{2}\widetilde{\varphi} - \frac{i}{k}\widetilde{\theta}\right), \\ \widetilde{T} &= \exp\left(\frac{2\pi i}{k}\left(-i\partial_{\widetilde{\varphi}} - \frac{k}{4\pi}\varphi - \frac{\theta}{2\pi}\right)\right) = \exp\left(\frac{2\pi}{k}\partial_{\widetilde{\varphi}} - \frac{i}{2}\varphi - \frac{i}{k}\theta\right), \end{aligned} \tag{5.93}$$

The operators translate the direct and the dual link angles for the wave function on a single lattice cross by $2\pi/k$, while simultaneously inducing an abstract gauge transformation of the wave function,

$$\begin{aligned} T\Psi(\varphi,\widetilde{\varphi}) &= \exp\left(i\frac{\widetilde{\varphi}}{2} - \frac{i}{k}\widetilde{\theta}\right)\Psi\left(\varphi + \frac{2\pi}{k},\widetilde{\varphi}\right), \\ \widetilde{T}\Psi(\varphi,\widetilde{\varphi}) &= \exp\left(-i\frac{\varphi}{2} - \frac{i}{k}\theta\right)\Psi\left(\varphi,\widetilde{\varphi} + \frac{2\pi}{k}\right). \end{aligned} \tag{5.94}$$

We then rewrite the boundary condition for the wave function on a single lattice cross (see eqs. (5.76) and (5.77)) in terms of these two unitary operators

$$T^k\Psi(\varphi,\widetilde{\varphi}) = \Psi(\varphi,\widetilde{\varphi}), \qquad \widetilde{T}^k\Psi(\varphi,\widetilde{\varphi}) = \Psi(\varphi,\widetilde{\varphi}). \tag{5.95}$$

Since the domain of a single-cross Hamiltonian H_+ is defined via the boundary conditions for the wave function which can be expressed in terms of the two unitary operators T and $\widetilde{T}$ it is clear that the operators are preserving the domain of the single-cross Hamiltonian.

The two operators T and $\widetilde{T}$ are not commuting with each other. Under an exchange of the two operators we obtain an overall factor W,

$$\widetilde{T}T = WT\widetilde{T}, \tag{5.96}$$

where $W = \exp\left(\frac{2\pi i}{k}\right)$. The two operators generates the so-called discrete magnetic translation group (see [126, 127]) which is defined as

$$\mathcal{G}_T = \left\{ g(n,\widetilde{n},m) = \exp\left(\frac{2\pi i m}{k}\right)\widetilde{T}^{\widetilde{n}}T^n | n,\widetilde{n},m \in \{0,1,\ldots,k-1\} \right\}. \tag{5.97}$$

We obtain the multiplication rule for the group from the definition of the two generators

$$g\left(n,\widetilde{n},m\right)g\left(n',\widetilde{n}',m'\right)=g\left(\left[n+n'\right]_k,\left[\widetilde{n}+\widetilde{n}'\right]_k,\left[m+m'-n\widetilde{n}'\right]_k\right), \tag{5.98}$$

where $\left[\cdots\right]_k$ denotes modulo k. The unit element of the group is given by

$$\mathbb{1}=g\left(0,0,0\right), \tag{5.99}$$

while the inverse of an element $g(n,\widetilde{n},m)$ is given by

$$g\left(n,\widetilde{n},m\right)^{-1}=g\left(-n,-\widetilde{n},-m-n\widetilde{n}\right). \tag{5.100}$$

That follows from,

$$g\left(n,\widetilde{n},m\right)g\left(-n,-\widetilde{n},-m-n\widetilde{n}\right)=g\left(0,0,-n\widetilde{n}+n\widetilde{n}\right)=g(0,0,0)=\mathbb{1}. \tag{5.101}$$

The center of the discrete magnetic translation group is formed by the cyclic Abelian subgroup $Z\left(\mathcal{G}_T\right)=\mathbb{Z}(k)\subset\mathcal{G}_T$. Multiplication of a group element by a center element, amounts to a $\mathbb{Z}\left(k\right)$ gauge transformation. Using the multiplication rule, the conjugacy class of a given group element $g(n,\widetilde{n},m)$ is identified as the elements,

$$\begin{aligned}g\left(n',\widetilde{n}',m'\right)g\left(n,\widetilde{n},m\right)g\left(n',\widetilde{n}',m'\right)^{-1}&=g\left(n'+n,\widetilde{n}'+\widetilde{n},m'+m-n'\widetilde{n}\right)g\left(-n',-\widetilde{n}',-m'-n'\widetilde{n}'\right)\\&=g\left(n,\widetilde{n},m-n'\left(\widetilde{n}+\widetilde{n}'\right)+\left(n'+n\right)\widetilde{n}'\right)\\&=g\left(n,\widetilde{n},m+n\widetilde{n}'-n'\widetilde{n}\right),\end{aligned} \tag{5.102}$$

for all $n',m'\in\{0,1,\ldots,k-1\}$. This implies that the conjugacy classes consists of elements related by gauge transformations and that the conjugacy classes therefore corresponds to gauge equivalence classes. As for any group, the individual elements of the center form conjugacy classes of a single element. The center forms a normal subgroup which can be factored out. This is equivalent to identifying gauge equivalence classes.

As noted above, a single direct T and a single dual $\widetilde{T}$ operator obtain a phase W under commutation. For the general case of n direct and m dual operators we find the more general factor

$$\widetilde{T}^mT^n=W\left(T^n,\widetilde{T}^m\right)T^n\widetilde{T}^m, \tag{5.103}$$

given by

$$W\left(T^n,\widetilde{T}^m\right)=\exp\left(\frac{2\pi i}{k}nm\right). \tag{5.104}$$

The general factor $W\left(T^n,\widetilde{T}^m\right)$ can be constructed from two separate functions. One related to the direct links ω and one related to the dual links $\widetilde{\omega}$. These two functions are each assigning a value to every element of the magnetic translation group, such that factor W is given as the product of the two functions,

$$W\left(T^n,\widetilde{T}^m\right)=\widetilde{\omega}\left(\widetilde{T}^m,T^n\right)\omega\left(T^n,\widetilde{T}^m\right)^{-1}. \tag{5.105}$$

An especially simple choice for this is to choose the following set of functions,

$$\begin{aligned} \omega\left(T^n, \widetilde{T}^m\right) &= \exp\left(-\frac{2\pi i}{k} nm\right), \\ \widetilde{\omega}\left(\widetilde{T}^m, T^m\right) &= \mathbb{1}. \end{aligned} \tag{5.106}$$

Both of these functions satisfy the one-cocycle condition of eq. (2.36) in relation to the first variable. This is trivially seen in case of $\widetilde{\omega}$. In case of ω, noting that

$$T^n T^{n'} = T^{\left[n+n\right]_k}, \tag{5.107}$$

it follows that

$$\begin{aligned} &\omega\left(T^n T^{n'}, \widetilde{T}^m\right) = \exp\left(-\frac{2\pi i}{k}\left[n+n'\right]_k m\right), \\ &\omega\left(T^n, \widetilde{T}^m\right) \cdot \left(\alpha\left(T^n, \omega\left(T^{n'}, \widetilde{T}^m\right)\right)\right) = \exp\left(-\frac{2\pi i}{k} nm\right) \alpha\left(T^n, \exp\left(-\frac{2\pi i}{k} n'm\right)\right). \end{aligned} \tag{5.108}$$

The right-hand side of the two equations becomes identical if we choose the trivial action, such that $\alpha\left(T^n, U\right) = U$ for all T^n. This shows that ω satisfies the one-cocycle condition with respect to the first variable.

In this example the one-cocycle condition plays a minor role and that the phase $W\left(T^n, \widetilde{T}^m\right)$ can be reduced to the factor of two one-cocycles seems more like a curiosity. In the next chapter, it will, however, be shown how the one-cocycles can be used as the starting point to construct the generally allowed W factors. For the remainder of this chapter we only make use of W as given eq. (5.104).

The single-cross Hamiltonian H_+ commutes with both the T and the $\widetilde{T}$ operators, and the two operators are clearly non-commuting among themselves. We can therefore construct simultaneous eigenstates of H_+ and T, but these are not simultaneous eigenstates of $\widetilde{T}$.[7] Since $T^k = \mathbb{1}$, it is clear that the eigenvalues of T are elements of $\mathbb{Z}(k)$, i.e. $\exp(2\pi i l/k)$, where $l \in \{0, 1, \ldots, k-1\}$. We obtain the eigenvalues of H_+ directly from the Landau levels of the well-known "mechanical analogue" of the model. These are given by $E_n = M(n + \frac{1}{2})$ where $n \in \{0, 1, 2, \ldots\}$ [128, 129] and M is again the "photon" mass. We will denote the simultaneous eigenstates of H_+ and T as $\left|n, l\right\rangle$ such that

$$H_+\left|n,l\right\rangle = M\left(n+\frac{1}{2}\right)\left|n,l\right\rangle, \qquad T\left|n,l\right\rangle = \exp\left(\frac{2\pi i l}{k}\right)\left|n,l\right\rangle. \tag{5.109}$$

As a consequence of the commutation relation between T and $\widetilde{T}$ in eq.(5.96), we find that $\widetilde{T}$ acts as a lowering operator of l,

$$\begin{aligned} T\widetilde{T}\left|n,l\right\rangle &= \exp\left(-\frac{2\pi i}{k}\right)\widetilde{T}T\left|n,l\right\rangle \\ &= \exp\left(\frac{2\pi i(l-1)}{k}\right)\widetilde{T}\left|n,l\right\rangle, \end{aligned} \tag{5.110}$$

[7] We could, of course, alternatively choose eigenstates of H_+ and $\widetilde{T}$, which would not simultaneously be eigenstates of T.

which implies

$$\widetilde{T}\left|n,l\right\rangle = |n,\left[l-1\right]_k\rangle. \tag{5.111}$$

Since the Hamiltonian for the single-cross is commuting with the lowering operator $\widetilde{T}$, the energy must be independent of the value of l. Hence, the k different states $\left|n,l\right\rangle$ with $l \in \left\{0,1,\ldots,k-1\right\}$ are degenerate and forms an irreducible representation of the magnetic translation group $\mathcal{G}_T$. We are able to explicitly construct the eigenfunctions as

$$\begin{aligned}\Psi^{\theta,\widetilde{\theta}}_{n,l}(\varphi,\widetilde{\varphi}) &= \langle\varphi\widetilde{\varphi}\left|n,l\right\rangle \\ &= \frac{1}{\sqrt{2\pi}}\sum_{m\in\mathbb{Z}}\psi_n\left(\widetilde{\varphi}-2\pi\left[m+\frac{l}{k}+\frac{\widetilde{\theta}}{2\pi k}\right]\right)\exp\left(i(k\varphi+\theta)\left[m+\frac{l}{k}+\frac{\widetilde{\theta}}{2\pi k}\right]-i\frac{k\varphi\widetilde{\varphi}}{4\pi}\right),\end{aligned} \tag{5.112}$$

where,

$$\psi_n(\xi) = \sqrt[4]{\frac{k}{2\pi}}\frac{1}{\sqrt{2^n n!\sqrt{\pi}}}\exp\left(-\frac{k}{2\pi}\frac{\xi^2}{2}\right)H_n\left(\sqrt{\frac{k}{2\pi}}\xi\right), \tag{5.113}$$

and $H_n\left(\sqrt{\frac{k}{2\pi}}\right)$ are the Hermite polynomials, i.e. the eigenfunctions for a 1-dimensional harmonic oscillator with a characteristic frequency related to the "photon" mass of $M = \frac{ke^2}{2\pi}$. The eigenfunctions satisfy the correct boundary conditions of (5.76) and (5.77), as one can verify by direct calculations. In addition, by shifting the self-adjoint extension parameters θ and $\widetilde{\theta}$ by 2π, we find that the corresponding boundary conditions for the two extension parameters can be identified as

$$\begin{aligned}\Psi^{\theta+2\pi,\widetilde{\theta}}_{n,l}\left(\varphi,\widetilde{\varphi}\right) &= \exp\left(i\frac{2\pi l+\widetilde{\theta}}{k}\right)\Psi^{\theta,\widetilde{\theta}}_{nl}\left(\varphi,\widetilde{\varphi}\right) \\ &= \Omega_{ll'}\Psi^{\theta,\widetilde{\theta}}_{n,l'}\left(\varphi,\widetilde{\varphi}\right),\end{aligned} \tag{5.114}$$

$$\begin{aligned}\Psi^{\theta,\widetilde{\theta}+2\pi}_{n,l}\left(\varphi,\widetilde{\varphi}\right) &= \Psi^{\theta,\widetilde{\theta}}_{n,l+1}\left(\varphi,\widetilde{\varphi}\right) \\ &= \widetilde{\Omega}_{ll'}\Psi^{\theta,\widetilde{\theta}}_{n,l'}\left(\varphi,\widetilde{\varphi}\right).\end{aligned} \tag{5.115}$$

Here we have introduced two matrices, Ω and $\widetilde{\Omega}$, such that we can express the boundary conditions as a sum over the matrices in terms of the l parameter, where the explicit matrix elements are

$$\Omega_{ll'} = \exp\left(i\frac{2\pi l+\widetilde{\theta}}{k}\right)\delta_{ll'}, \qquad \widetilde{\Omega}_{ll'} = \delta_{\left[l+1\right]_k,l'}. \tag{5.116}$$

We recognize the boundary conditions as 't Hooft's $U(k)$ twisted boundary conditions [130, 131]. The two transition functions Ω and $\widetilde{\Omega}$ each live in the group space $U(k)$ and are each playing the role of an $U(k)$ gauge transformation. This is analogous to how the T and $\widetilde{T}$ operators are transformations in the group $U\,(k=1)$ space and the two sets of functions turn out to obey the identical commutation relation

$$\Omega\widetilde{\Omega} = \exp\left(\frac{2\pi i}{k}\right)\widetilde{\Omega}\Omega. \tag{5.117}$$

Ω and $\widetilde{\Omega}$ are hence also generators of a representation of the magnetic translation group and therefore also satisfy the cocycle consistency condition of (2.36). This is characterized by the $U(k)$ gauge-invariant twist-factor $\exp(2\pi i/k) \in \mathbb{Z}(k)$, which belongs to the center of the group $Z(U(k)) = U(1)$. As we increase $\widetilde{\theta}$ by 2π, we see that the $\mathbb{Z}(k)$ electric flux quantum number l is shifted to $\left[l+1\right]_k$. Hence, an adiabatic change of the self-adjoint extension parameters allows for a continuous interpolation between the different discrete $\mathbb{Z}(k)$ electric flux sectors of the model. Using the energy levels on a single-cross, as given in (5.109), the splitting between the different levels, are seen to be proportional to the "photon" mass. Therefore, by sending the "photon" mass to infinity $M \to \infty$, all but the lowest Landau levels are eliminated from the model. This limit is achieved by sending $e^2 \to \infty$, which, as noted earlier, is the limit of the pure Chern-Simons model. In the pure Chern-Simons limit, the different energy levels decouple and the local Hilbert space of a cross is k-dimensional. Later we will show how the doubled Chern-Simons-Maxwell theory reduces to a $\mathbb{Z}(k)$ variant of the toric code in this limit.

$U(k)$ Berry Gauge Fields

A natural question to ask is how the wave functions on a single-cross respond to an adiabatic change of the two extension parameters θ and $\widetilde{\theta}$. Since each energy level contains k degenerate states, that is each of the states $\left|n,l\right\rangle$ with the same n value and with $l \in \{0,1,\ldots,k-1\}$ belong to the same energy level. This gives rise to an abstract $U(k)$ non-Abelian Berry gauge field on the torus $U(1)^2$ that is parametrized by θ and $\widetilde{\theta}$,

$$g_{ll'}(\theta,\widetilde{\theta}) = \left\langle n,l\right|\mathcal{W}^\dagger\partial_\theta\mathcal{W}\left|n,l'\right\rangle = 0, \quad \widetilde{g}_{ll'}(\theta,\widetilde{\theta}) = \left\langle n,l\right|\mathcal{W}^\dagger\partial_{\widetilde{\theta}}\mathcal{W}\left|n,l'\right\rangle = i\frac{\theta}{2\pi k}\delta_{ll'}, \quad (5.118)$$

where

$$\mathcal{W} = \exp\left(-\frac{i}{2\pi}(\theta\widetilde{\varphi}+\widetilde{\theta}\varphi)\right). \quad (5.119)$$

To account for the fact that different values of θ and $\widetilde{\theta}$ correspond to different domains of the Hamiltonian, it is important to include the unitary transformation $\mathcal{W}$ in the definition of the Berry connection. The $g_{ll'}$ and $\widetilde{g}_{ll'}$ are elements of two $k\times k$ antihermitean matrix-valued fields denoted by g and $\widetilde{g}$ respectively, which play the role of abstract $U(k)$ Berry vector potentials. In the gauge that is chosen, here it turns out that $\widetilde{g}$ is Abelian and that g even vanishes. The corresponding Berry field strength, i.e. the abstract "magnetic" field, is given by,

$$h\left(\theta,\widetilde{\theta}\right) = \partial_\theta\widetilde{g}\left(\theta,\widetilde{\theta}\right) - \partial_{\widetilde{\theta}}g\left(\theta,\widetilde{\theta}\right) + \left[g\left(\theta,\widetilde{\theta}\right),\widetilde{g}\left(\theta,\widetilde{\theta}\right)\right], \quad h_{ll'}\left(\theta,\widetilde{\theta}\right) = \frac{i}{2\pi k}\delta_{ll'}. \quad (5.120)$$

As for the abstract magnetic field that arose from the abstract vector potentials a and $\widetilde{a}$ parametrized by ϕ and $\widetilde{\phi}$ above, the abstract magnetic field h is both Abelian and constant over the 2-dimensional torus parametrized by θ and $\widetilde{\theta}$. Since the field strength is simply the unit-matrix multiplied by a constant factor, is invariant under a general non-Abelian $U(k)$ gauge transformation, resulting from a basis change in the subspace of the degenerate states $\left|n,l\right\rangle$. This implies that it is reduced to an Abelian $U(1)$ Berry field strength. Since the field strength is non-zero, it can, however, still give rise to non-trivial Berry phases. Since the phases must necessarily be Abelian, the use of the Berry phases for quantum information processing will be of limited use. The total "magnetic" flux that threads the torus is given by $2\pi/k$ which is consistent with the twist factor $\exp(2\pi i/k) \in \mathbb{Z}(k)$ of eq.(5.117) that characterizes 't Hooft's twisted boundary conditions [130].

In addition to the Berry field strength there exist two gauge-invariant Berry Polyakov loops Φ and $\widetilde{\Phi}$, resulting from the holonomies of the torus that are parametrized by the periodic self-adjoint extension parameters θ and $\widetilde{\theta}$. Integrating the Berry connection along a straight line wrapping around the torus gives

$$\int_0^{2\pi} d\theta\, g_{ll}(\theta,\widetilde{\theta}) = 0, \qquad \int_0^{2\pi} d\widetilde{\theta}\, \widetilde{g}_{ll}(\theta,\widetilde{\theta}) = i\frac{\theta}{k}. \tag{5.121}$$

The Polyakov loop matrices Φ and $\widetilde{\Phi}$ both are $U(k)$ matrices that describe parallel transport around the torus. The two Polyakov loops receive contributions from the two transition functions Ω and $\widetilde{\Omega}$ such that,

$$\Phi_{ll'}(\widetilde{\theta}) = \Omega_{ll'} = \exp\left(i\frac{2\pi l+\widetilde{\theta}}{k}\right)\delta_{ll'}, \quad \widetilde{\Phi}_{ll'}(\theta) = \exp\left(i\frac{\theta}{k}\right)\widetilde{\Omega}_{ll'} = \exp\left(i\frac{\theta}{k}\right)\delta_{l+1,l'}. \tag{5.122}$$

We will see later that this allows for the derivation of the mutual statistics angle between direct and dual charges of $\frac{2\pi}{k}$ in the compact Chern-Simons theory.

5.3.3 $\mathbb{Z}(k)$ Gauge Symmetry and Gauss' Law

So far we have only considered a single lattice cross of type I ($x \in X$), where the two operators T and $\widetilde{T}$ are associated with the direct and the dual link, respectively. Now we are going to consider both the $\mathbb{Z}(k)$ gauge symmetry and Gauss' law. Since these operators are relating neighbouring lattice crosses, it is necessary to generalize the above results for the T and $\widetilde{T}$ operators to the lattice crosses of type II ($x \in \widetilde{X}$). Reintroducing the explicit link subscripts, the general $T_{x,i}$ and $\widetilde{T}_{x,i}$ are given by

$$\begin{aligned} T_{x,i} &= \exp\left(\frac{2\pi}{k}\partial_{\varphi_{x,i}} + \frac{i}{2}\epsilon_{ij}\widetilde{\varphi}_{x,j} - \frac{i}{k}\epsilon_{ij}\widetilde{\theta}_{x,j}\right), \\ \widetilde{T}_{x,i} &= \exp\left(\frac{2\pi}{k}\partial_{\widetilde{\varphi}_{x,i}} + \frac{i}{2}\epsilon_{ij}\varphi_{x,j} + \frac{i}{k}\epsilon_{ij}\theta_{x,j}\right). \end{aligned} \tag{5.123}$$

A $\mathbb{Z}(k)$ Gauss' law on a direct (dual) lattice site x combines the T ($\widetilde{T}$) operators residing on the direct (dual) links that are attached to the direct (dual) lattice site. The operators are combined to form a unitary operator, V ($\widetilde{V}$) that represents local $\mathbb{Z}(k)$ gauge transformations at the lattice site,

$$V_x = \prod_{i=1}^{2} T_{x+\frac{a}{2}\hat{i},i} T^{\dagger}_{x-\frac{a}{2}\hat{i},i}, \quad x \in \Lambda, \qquad \widetilde{V}_x = \prod_{i=1}^{2} \widetilde{T}_{x+\frac{a}{2}\hat{i},i} \widetilde{T}^{\dagger}_{x-\frac{a}{2}\hat{i},i}, \quad x \in \widetilde{\Lambda}. \tag{5.124}$$

The two unitary operators V_x and $\widetilde{V}_x$ represent the manifest $\mathbb{Z}(k)$ gauge symmetries of the full Hamiltonian, i.e. the gauge symmetries of the full CSM Hamiltonian which include both the electric cross together with the magnetic plaquette contributions.

Since the two unitary operators are constructed from the T and $\widetilde{T}$ operators, they both respect the domain structure of the full Hamiltonian, defined by the values of the self-adjoint extension parameters θ and $\widetilde{\theta}$. Although T and $\widetilde{T}$ themselves are not commuting when residing on the same

lattice cross, the direct and dual gauge transformations are always described by commuting operators,

$$\begin{aligned} V_x \widetilde{V}_{x+\frac{a}{2}\hat{1}+\frac{a}{2}\hat{2}} &= T_{x+\frac{a}{2}\hat{1},1} T_{x+\frac{a}{2}\hat{2},2} T^{\dagger}_{x-\frac{a}{2}\hat{1},1} T^{\dagger}_{x-\frac{a}{2}\hat{2},2} \widetilde{T}_{x+a\hat{1}+\frac{a}{2}\hat{2},1} \widetilde{T}_{x+\frac{a}{2}\hat{1}+a\hat{2},2} \widetilde{T}^{\dagger}_{x+\frac{a}{2}\hat{2},1} \widetilde{T}^{\dagger}_{x+\frac{a}{2}\hat{1},2} \\ &= \widetilde{T}_{x+a\hat{1}+\frac{a}{2}\hat{2},1} \widetilde{T}_{x+\frac{a}{2}\hat{1}+a\hat{2},2} \widetilde{T}^{\dagger}_{x+\frac{a}{2}\hat{2},1} \widetilde{T}^{\dagger}_{x+\frac{a}{2}\hat{1},2} T_{x+\frac{a}{2}\hat{1},1} T_{x+\frac{a}{2}\hat{2},2} T^{\dagger}_{x-\frac{a}{2}\hat{1},1} T^{\dagger}_{x-\frac{a}{2}\hat{2},2} \\ &= \widetilde{V}_{x+\frac{a}{2}\hat{1}+\frac{a}{2}\hat{2}} V_x. \end{aligned} \tag{5.125}$$

Here the commutation relations between the operators have been used for both of the lattice crosses, i.e.,

$$\begin{aligned} T_{x+\frac{a}{2}\hat{1},1} \widetilde{T}^{\dagger}_{x+\frac{a}{2}\hat{1},2} &= \exp\left(\frac{2\pi i}{k}\right) \widetilde{T}^{\dagger}_{x+\frac{a}{2}\hat{1},2} T_{x+\frac{a}{2}\hat{1},1}, \\ T_{x+\frac{a}{2}\hat{2},2} \widetilde{T}^{\dagger}_{x+\frac{a}{2}\hat{2},1} &= \exp\left(-\frac{2\pi i}{k}\right) \widetilde{T}^{\dagger}_{x+\frac{a}{2}\hat{2},1} T_{x+\frac{a}{2}\hat{2},2}. \end{aligned} \tag{5.126}$$

This is analogous to the non-compact case, see eq. (5.51) and Figure 5.3, where the generators of infinitesimal gauge transformations on the direct and dual lattice sites are commuting, even though the individual components are not commuting. As for the non-compact case, physical states without external charges from the corresponding domain of H (defined by a given set of θ and $\widetilde{\theta}$) must obey the $\mathbb{Z}(k)$ Gauss' law at every lattice site and dual site,

$$V_x \big|\Psi\big\rangle = \big|\Psi\big\rangle, \quad \forall \quad x \in \Lambda, \qquad\qquad \widetilde{V}_x \big|\Psi\big\rangle = \big|\Psi\big\rangle, \quad \forall \quad x \in \widetilde{\Lambda}. \tag{5.127}$$

Introducing external charges $Q_x, \widetilde{Q}_x \in 0, 1, \ldots, k-1$ on a direct or dual lattice site, give rise to an additional $\mathbb{Z}\,(k)$ phase under a gauge transformation at the site,

$$\begin{aligned} V_x \big|Q, \widetilde{Q}\big\rangle &= \exp\left(\frac{2\pi i}{k} Q_x\right) \big|Q, \widetilde{Q}\big\rangle, \quad \forall \quad x \in \Lambda, \\ \widetilde{V}_x \big|Q, \widetilde{Q}\big\rangle &= \exp\left(\frac{2\pi i}{k} \widetilde{Q}_x\right) \big|Q, \widetilde{Q}\big\rangle, \quad \forall \quad x \in \widetilde{\Lambda}. \end{aligned} \tag{5.128}$$

It is important to remember – as was shown above – that θ and $\widetilde{\theta}$ represent external non-dynamical $U(1)$ lattice gauge fields and when an $U(1)$ gauge transformation is performed, it may change the values of θ and $\widetilde{\theta}$. This in turn leads to an unitarily equivalent domain of H leaving the physics invariant. The physics, however, depends on the gauge-invariant plaquette field strengths of $\exp(i\eta_x)$ and $\exp(i\widetilde{\eta}_x)$ that we defined in eq. (5.92).

5.3.4 Pure Chern-Simons Limit

As already noted above, in the pure Chern-Simons limit of $e^2 \to \infty$, the "photon" mass $M = \frac{ke^2}{2\pi}$ goes to infinity and is thus removed from the spectrum. The system reduces to a pure Chern-Simons theory, such that the low-energy physics is restricted to the lowest Landau level $n = 0$ which leaves k states on each individual lattice cross. Again we choose an electric flux basis such that the local Hilbert space is characterized by the fluxes $l \in \{0, 1, \ldots, k-1\}$ on the links of the original lattice. The electric field energy on a single-cross is then simply given by a constant $M/2$ which implies that the dynamics is controlled by the magnetic field energy as well as by Gauss' law. The magnetic field enters the Hamiltonian of (5.38) with a factor of e^{-2} which implies that

the magnetic contribution to the energy can be treated in first-order degenerate perturbation theory in the limit of a pure Chern-Simons theory. This is achieved by evaluating the matrix elements of the magnetic energy term between the degenerate eigenstates for the electric flux, i.e. $\left|0,l\right\rangle$. To evaluate these matrix elements we consider

$$\begin{aligned}\left\langle 0,l\right|\exp\left(\pm i\varphi\right)\left|0,l'\right\rangle &= C\exp\left(\pm\frac{i\theta}{k}\right)\delta_{l,l'\pm 1} \qquad (5.129)\\ &= C\exp\left(\pm\frac{i\theta}{k}\right)\left\langle 0,l\right|\widetilde{T}^{\mp 1}\left|0,l'\right\rangle,\\ \left\langle 0,l\right|\exp\left(\pm i\widetilde{\varphi}\right)\left|0,l'\right\rangle &= C\exp\left(\pm\frac{i\widetilde{\theta}}{k}\right)\exp\left(\pm\frac{2\pi il}{k}\right)\delta_{ll'} \qquad (5.130)\\ &= C\exp\left(\pm\frac{i\widetilde{\theta}}{k}\right)\left\langle 0,l\right|T^{\pm 1}\left|0,l'\right\rangle,\end{aligned}$$

where the states $\left|n=0,l\right\rangle$ have been obtained directly from eq. (5.112). Here C is an overall constant,

$$C=\exp\left(-\frac{\pi}{2k}\right). \qquad (5.131)$$

Recalling that $\widetilde{T}$ acts as a lowering operator for the flux, i.e. $\widetilde{T}|0,l\rangle = |0,(l-1)\rangle$, this implies that, up to a trivial additive constant, the effective low-energy pure Chern-Simons Hamiltonian of eq. (5.68) is given by,

$$\begin{aligned}H_{\text{eff}} = &-\frac{C^4}{2e^2a^2}\sum_{x\in\widetilde{\Lambda}}\left(\exp\left(\frac{i\eta_x}{k}\right)\widetilde{V}_x+\exp\left(-\frac{i\eta_x}{k}\right)\widetilde{V}_x^{\dagger}\right) \qquad (5.132)\\ &-\frac{C^4}{2e^2a^2}\sum_{x\in\Lambda}\left(\exp\left(\frac{i\widetilde{\eta}_x}{k}\right)V_x^{\dagger}+\exp\left(-\frac{i\widetilde{\eta}_x}{k}\right)V_x\right),\end{aligned}$$

where η and $\widetilde{\eta}$ are the plaquette field strength variables associated with the non-dynamical gauge fields θ and $\widetilde{\theta}$ of eq. (5.92). The contribution in the first line results from a $\cos(a^2B_x)$ term on the direct plaquettes. The term in the second line is a contribution that results from a dual plaquette term $\cos(a^2\widetilde{B}_x)$ in the Hamiltonian of (5.68). Eq. (5.52) implies that the Hamiltonian acting on an electric flux eigenstate $|Q,\widetilde{Q}\rangle$, with charges Q_x and $\widetilde{Q}_x$ on the direct and the dual lattice respectively, is given by,

$$H_{\text{eff}}\left|Q,\widetilde{Q}\right\rangle = -\frac{C^4}{e^2a^2}\left(\sum_{x\in\widetilde{\Lambda}}\cos\left(\frac{2\pi\widetilde{Q}_x+\eta_x}{k}\right)+\sum_{x\in\Lambda}\cos\left(\frac{2\pi Q_x-\widetilde{\eta}_x}{k}\right)\right)\left|Q,\widetilde{Q}\right\rangle. \qquad (5.133)$$

This implies that the effective Hamiltonian is energetically punishing violations of the $\mathbb{Z}(k)$ Gauss' law on both the direct and on the dual lattice. In the special case of a vanishing plaquette field strength for all plaquettes, i.e. $\eta_x = 0$ and $\widetilde{\eta}_{x'} = 0$ for all $x \in \widetilde{\Lambda}$ and $x' \in \Lambda$, the ground state is simply the state with a vanishing charge at every site, that is to say that $V_x|\Psi\rangle = |\Psi\rangle$ for all $x \in \Lambda$ and $\widetilde{V}_{x'}|\Psi\rangle = |\Psi\rangle$ for all $x' \in \widetilde{\Lambda}$. For other choices of η_x and $\widetilde{\eta}_{x'}$, other charge configurations are energetically favoured and the ground state is no longer the zero charge state. The charged eigenstates $\left|Q,\widetilde{Q}\right\rangle$ can be constructed explicitly. For this construction we introduce the dual charge projection operators which project onto a state of definite dual charge $\widetilde{Q}$ at the dual lattice site x,

$$P_{\widetilde{Q}_x}=\frac{1}{k}\sum_{m=0}^{k-1}\exp\left(-\frac{2\pi mi}{k}\widetilde{Q}_x\right)\widetilde{V}_x^m. \qquad (5.134)$$

It can easily be shown that this operator obeys,

$$P_{\widetilde{Q}_x} P_{\widetilde{Q}_{x'}} = \delta_{\widetilde{Q}_x,\widetilde{Q}_{x'}} P_{\widetilde{Q}_x}, \qquad \widetilde{V}_x P_{\widetilde{Q}_x} = \exp\left(\frac{2\pi i}{k}\widetilde{Q}_x\right) P_{\widetilde{Q}_x}, \tag{5.135}$$

which shows that it is indeed an operator that projects onto a state of definite dual charge $\widetilde{Q}_x$ at the given site x. Let $\big|[l]\big\rangle$ denote a state with a specific electric flux configuration $[l]$ that obeys Gauss' law in the presence of direct charges $Q_x \in \mathbb{Z}(k)$ on the original lattice, $x \in \Lambda$. Hence, modulo k, the sum of fluxes at a direct site is equal to the charge at the site,

$$\sum_i (l_{x+\frac{a}{2}\hat{i},i} - l_{x-\frac{a}{2}\hat{i},i}) \bmod k = Q_x. \tag{5.136}$$

By construction, we obtain

$$V_x \big|[l]\big\rangle = \exp\left(\frac{2\pi i}{k} Q_x\right) \big|[l]\big\rangle, \quad \forall \quad x \in \Lambda. \tag{5.137}$$

This flux configuration specifies the direct charges on all direct lattice sites. To specify the dual charge, we apply the charge projection operator to every dual sites

$$\big|Q, \widetilde{Q}\big\rangle = \mathcal{N} \prod_{x\in\widetilde{\Lambda}} P_{\widetilde{Q}_x} \big|[l]\big\rangle, \tag{5.138}$$

where $\mathcal{N}$ is a normalization factor. Using the properties of the projection operator one can show that this state indeed satisfies

$$\widetilde{V}_x \big|Q, \widetilde{Q}\big\rangle = \exp\left(\frac{2\pi i}{k} \widetilde{Q}_x\right) \big|Q, \widetilde{Q}\big\rangle, \quad \forall \quad x \in \widetilde{\Lambda}. \tag{5.139}$$

In the non-compact theory we found that the direct and the dual charges are showing a mutually anyonic statistics, with a statistics angle of $\frac{2\pi}{k}$. We derive a similar result here for the compact theory. To show this, we construct a Wilson-loop operator for the compact theory. As in the non-compact case, we construct this in terms of parallel transporters,

$$W_C = \prod_{(x,i)\in C} U_{x,i} = \prod_{(x,i)\in C} \exp\left(i\varphi_{x,i}\right). \tag{5.140}$$

By using the results of eqs. (5.129) and (5.130) this implies that for a charged state $\big|Q, \widetilde{Q}\big\rangle$,

$$\begin{aligned} W_C \big|Q, \widetilde{Q}\big\rangle &= C^{L_C} \sum_{x\in S\subset\widetilde{\Lambda}} \widetilde{V}_x \prod_{(x,i)\in C} \exp(i\frac{\theta_{x,i}}{k}) \big|Q, \widetilde{Q}\big\rangle \\ &= C^{L_C} \exp\left(\frac{2\pi\widetilde{Q}_S}{k} i\right) \exp\left(\frac{\eta_S}{k} i\right) \big|Q, \widetilde{Q}\big\rangle. \end{aligned} \tag{5.141}$$

Here L_C is the total length of the closed loop, and S denotes the surface bounded by the loop C. $\widetilde{Q}_S$ and $\widetilde{\eta}_S$ are the sum of the dual charges and plaquette field strengths on the surface respectively,

$$\widetilde{Q}_S = \sum_{x\in S\subset\widetilde{\Lambda}} \widetilde{Q}_x, \qquad \eta_S = \sum_{x\in S\subset\widetilde{\Lambda}} \eta_x. \tag{5.142}$$

The total phase obtained from the Wilson-loop consists of two parts. In analogue to the non-compact case the first part of the phase contains a $\widetilde{Q}_S$-term, which implies that the direct and dual charges have mutually anyonic statistics, with a statistics angle $2\pi/k$. In addition to this anyonic phase, there is a second contribution to the overall Wilson-loop phase that originates from the flux of the non-trivial background gauge field strength through the enclosed surface. By choosing $\eta_x = 0$ for every plaquette this term vanishes.

The Wilson-loop describes the instantaneous transport of a charge around a loop. We can alternatively consider a much slower adiabatic process in which a charge-anticharge pair is created and then transported around a loop to finally be annihilated. As noted below eq. (5.117), a change of the self-adjoint extension parameters allows for a continuous interpolation between the discrete electrical fluxes, which allows us to calculate the adiabatic process by computing the Berry phase that is accumulated when the background field $\widetilde{\theta}$ is gradually changed from 0 to 2π on all dual links intersecting the loop. According to the results obtained in eq. (5.122) a factor $\exp(i\theta_{x,i}/k)$ is obtained for every link that belongs to the loop C. By imposing the lattice version of Stokes' theorem this gives an overall phase of $\exp(i\eta_S/k)$. In addition to this, the factor $\delta_{l+1,l'}$ in eq. (5.122) shifts all electric flux variables along the loop by 1. This gives rise to an additional phase $\exp(2\pi i\widetilde{Q}_S/k)$ when one returns to the initial state $\left|Q,\widetilde{Q}\right\rangle$ at the very end of the adiabatic charge transport process. The total phase for the adiabatic process is therefore identical to the total phase obtained from the Wilson-loop, which shows explicitly that the anyon statistics angle of $2\pi/k$ is insensitive to whether the charge transport is an adiabatic or an instantaneous process.

Since the direct and dual charges again show Abelian anyonic behaviour, the anyons obtained for this model are only of limited use for quantum computation. This was only to be expected since we explicitly constructed a model with an Abelian gauge group. In the next chapter we will move on to explore the behaviour of several non-Abelian gauge theories.

5.3.5 Relation to the Toric Code

As previously mentioned, Kitaev's toric code is a $\mathbb{Z}(2)$ lattice gauge theory with a degenerate ground state that can be used as a storage device for topologically protected quantum information. Here the fundamental degrees of freedom on each link (x,i) of a square lattice are quantum spins $\frac{1}{2}$, described by operators $\vec{S}_{x,i}$ and the Hamiltonian is given by,

$$H = -J\sum_{x\in\widetilde{\Lambda}} U_{\square_x} - G\sum_{x\in\Lambda} V_x. \tag{5.143}$$

In fact, the toric code is an example of a $\mathbb{Z}(2)$ quantum link model, whose $SU(2)$ variant we considered in the first part of the thesis. Here the first term is a plaquette term constructed from four $\mathbb{Z}(2)$ quantum link operators $U_{x,i} = S^1_{x,i}$ around a plaquette

$$U_{\square_x} = S^1_{x-\frac{a}{2}\hat{2},1} S^1_{x+\frac{a}{2}\hat{1},2} S^1_{x+\frac{a}{2}\hat{2},1} S^1_{x-\frac{a}{2}\hat{1},2}, \quad x\in\widetilde{\Lambda}, \tag{5.144}$$

which is invariant under discrete $\mathbb{Z}(2)$ gauge transformations $\Omega_x = \pm 1$. The second term combines the 3-component of the spin for the four links joined at the site,

$$V_x = \prod_i \exp\left(i\pi S^3_{x+\frac{a}{2}\hat{i}}\right)\exp\left(-i\pi S^3_{x-\frac{a}{2}\hat{i}}\right), \tag{5.145}$$

For $G > 0$ this term is energetically punishing violations of the $\mathbb{Z}(2)$ Gauss' law $V_x\big|\Psi\big\rangle = \big|\Psi\big\rangle$. It should be noted that in the case considered here, i.e. for the $\mathbb{Z}(2)$ toric code, $U_x = U_x^\dagger$ and $V_x = V_x^\dagger$. Similar to the Chern-Simons limit of the doubled CSM model above, the dynamics of the toric code can be described in a basis of electric flux states residing on the lattice links. These flux states are given in terms of the third component of the spin operators $S^3_{x,i} = \pm 1/2$. The $\pm 1/2$ value of the $S^3_{x,i}$ operator can then be associated with two possible directions of the electric flux. The quantum link operator $U_{x,i} = S^1_{x,i}$ flips the flux direction, which implies that the plaquette operator, $U_{\square_x}$ flips the direction of the electric flux around an elementary plaquette loop. This holds for the $\mathbb{Z}(2)$ toric code, but it can be generalized to the general $\mathbb{Z}(k)$ toric code by increasing the possible electric flux states per link to k states. The quantum link operator is then generalized to increase the flux by 1 modulo k, instead of just flipping between $\pm 1/2$. Gauss' law of eq. (5.145) is similarly modified in such a way that it ensures that the fluxes entering a common lattice point add up to zero modulo k,

$$V_x = \prod_i \exp\left(i\frac{2\pi}{k} S^3_{x+\frac{a}{2}\hat{i}}\right) \exp\left(-i\frac{2\pi}{k} S^3_{x-\frac{a}{2}\hat{i}}\right), \tag{5.146}$$

This is similar to the case of the doubled compact Chern-Simons-Maxwell theory considered above, when we take the pure Chern-Simons limit of infinite "photon" mass. In this case, the T operators play a role similar as the electric flux, i.e. the S^3 operators for the toric code (see (5.124)). The $\widetilde{T}$ plays a role similar to the flux raising operator in the toric code (see eq. (5.111), and the $\mathbb{Z}(k)$-variant of the toric code is exactly identified with the above doubled compact Chern-Simons-Maxwell in the pure Chern-Simons limit. To see this we identify both the J and G parameters of eq. (5.143) with $C^4/(e^2)$, where C is the overall constant given in eq. (5.131). This opens up the possibility that this model can be useful for quantum information processing. As was already noted when the anyonic phases were considered, the model, however, only contains Abelian anyons, which necessarily limits the usefulness of the model in applications to general quantum computation devices.

5.3.6 Rotating θ and $\widetilde{\theta}$ into the Hamiltonian

The two external background gauge fields θ and $\widetilde{\theta}$ originally entered the theory in terms of the boundary conditions for the wave functions on a single lattice cross, and we originally defined them through eqs. (5.76) and (5.77). As an alternative, we can rotate the two background fields into the Hamiltonian. This is achieved by a unitary transformation of the form,

$$\mathcal{W} = \prod_{x\in X} \exp\left(-\frac{i}{2\pi}(\theta_{x,1}\widetilde{\varphi}_{x,2} + \widetilde{\theta}_{x,2}\varphi_{x,1})\right) \prod_{x\in\widetilde{X}} \exp\left(\frac{i}{2\pi}(\theta_{x,2}\widetilde{\varphi}_{x,1} + \widetilde{\theta}_{x,1}\varphi_{x,2})\right), \tag{5.147}$$

which rotates the Hamiltonian as well as the state,

$$H' = \mathcal{W} H \mathcal{W}^\dagger \qquad\qquad \big|\Psi'\big\rangle = \mathcal{W}\big|\Psi\big\rangle. \tag{5.148}$$

The original Hamiltonian from eq. (5.68) comes with the original boundary conditions, which for a cross of type I ($x \in X$) are

$$\begin{aligned} \Psi(\varphi + 2\pi, \widetilde{\varphi}) &= \exp\left(-i\frac{k}{2}\widetilde{\varphi} + i\widetilde{\theta}\right)\Psi(\varphi,\widetilde{\varphi}), \\ \Psi(\varphi, \widetilde{\varphi} + 2\pi) &= \exp\left(i\frac{k}{2}\varphi + i\theta\right)\Psi(\varphi,\widetilde{\varphi}). \end{aligned} \tag{5.149}$$

Under the unitary transformation, the Hamiltonian is rotated into a new Hamiltonian

$$\begin{aligned} H' = \frac{e^2}{2}\sum_{x\in X}\left[\left(-i\partial_{\varphi_{x,1}} - \frac{k}{4\pi}\widetilde{\varphi}_{x,2} + \frac{\widetilde{\theta}_{x,2}}{2\pi}\right)^2 + \left(-i\partial_{\widetilde{\varphi}_{x,2}} + \frac{k}{4\pi}\varphi_{x,1} + \frac{\theta_{x,1}}{2\pi}\right)^2\right] \\ + \frac{e^2}{2}\sum_{x\in\widetilde{X}}\left[\left(-i\partial_{\varphi_{x,2}} + \frac{k}{4\pi}\widetilde{\varphi}_{x,1} - \frac{\widetilde{\theta}_{x,1}}{2\pi}\right)^2 + \left(-i\partial_{\widetilde{\varphi}_{x,1}} - \frac{k}{4\pi}\varphi_{x,2} - \frac{\theta_{x,2}}{2\pi}\right)^2\right] \\ - \frac{1}{e^2a^2}\sum_{x\in\Lambda}\cos(a^2\widetilde{B}_x) - \frac{1}{e^2a^2}\sum_{x\in\widetilde{\Lambda}}\cos(a^2B_x), \end{aligned} \tag{5.150}$$

which directly depends on the two external background gauge fields θ and $\widetilde{\theta}$. The wave function $\big|\Psi\big\rangle$ has simultaneously been rotated into a new wave function. On a single-cross $x \in X$ it takes the explicit form

$$\begin{aligned} \Psi'^{\theta,\widetilde{\theta}}_{nl}(\varphi,\widetilde{\varphi}) &= \big\langle\varphi,\widetilde{\varphi}\big|n,l\big\rangle \\ &= \frac{1}{\sqrt{2\pi}}\sum_{m\in\mathbb{Z}}\psi_n\left(\widetilde{\varphi} - 2\pi\big[m + \frac{l}{k} + \frac{\widetilde{\theta}}{2\pi k}\big]\right) \\ &\quad\times\exp\left(i\varphi\big[km + l - \frac{k\widetilde{\varphi}}{4\pi}\big] + i\big[m + \frac{l}{k} + \frac{\widetilde{\theta}}{2\pi k} - \frac{\widetilde{\varphi}}{2\pi}\big]\theta\right), \end{aligned} \tag{5.151}$$

where the dependencies of the two background gauge fields have been rotated out of the boundary conditions. We thereby obtain that the new wave function obeys simplified boundary conditions, which are independent of both θ and $\widetilde{\theta}$,

$$\begin{aligned} \Psi'(\varphi + 2\pi,\widetilde{\varphi}) &= \exp\left(-i\frac{k}{2}\widetilde{\varphi}\right)\Psi'(\varphi,\widetilde{\varphi}), \\ \Psi'(\varphi,\widetilde{\varphi} + 2\pi) &= \exp\left(i\frac{k}{2}\varphi\right)\Psi'(\varphi,\widetilde{\varphi}). \end{aligned} \tag{5.152}$$

This also simplifies the definition of the Berry connection which no longer requires the insertion of $\mathcal{W}$ since this has now been rotated into the Hamiltonian. Using that $\big|n,l\big\rangle' = \mathcal{W}\big|n,l\big\rangle$ we find that the definition of the Berry phase is changed from eq. (5.118) to simply

$$g_{ll'}(\theta,\widetilde{\theta}) = {}'\langle n,l|\partial_\theta|n,l'\rangle', \qquad \widetilde{g}_{ll'}(\theta,\widetilde{\theta}) = {}'\langle n,l|\partial_{\widetilde{\theta}}|n,l'\rangle'. \tag{5.153}$$

This does not change the resulting values of the Berry connection which are still the same as in eq. (5.118).

In this chapter, we have seen how the self-adjoint extension parameters θ and $\widetilde{\theta}$, break the $U(1)$ gauge symmetry of the classical theory down to a manifest $\mathbb{Z}(k)$ in the quantum theory, with a corresponding $\mathbb{Z}(k)$ Gauss' law, given in terms of the T and $\widetilde{T}$ operators. This raises the question about the significance of the reduction of the manifest gauge symmetry at the quantum level, and in particular, whether we should interpret this explicit quantum mechanical symmetry breaking as an anomaly of the theory. To answer this question, one should ask what we mean by an anomaly. In this model, unlike the classical theory, the quantum theory is sensitive to the external parameters, i.e. the gauge fields θ and $\widetilde{\theta}$ representing the Aharonov-Bohm phases, which suggest that it is an anomaly. At the same time the external parameters are, however, themselves transformed under

the full $U(1)$ gauge transformations (see eq. (5.91)). This leads to an equivalent theory, where the domain of the Hamiltonian is shifted. Still, under a $\mathbb{Z}(k)$ gauge transformation, the domain is shifted by the exact amount to recover the original domain again, and the theory is therefore maintains the $\mathbb{Z}(k)$ gauge symmetry. This suggest to us that the symmetry breaking is indeed some form of an anomaly, but not necessarily what we would normally know as an anomaly.

Chapter 6

Doubled Lattice Chern-Simons-Yang-Mills Theories with Discrete Gauge Group

In this chapter we extend the investigation of the previous chapter to more general theories with a discrete Abelian or non-Abelian gauge group on the same doubled lattice. The discrete nature of the gauge groups gives finite local Hilbert spaces on the lattice, which, as we also noted for the QLM in the first part of the thesis, lends itself well for being realized in an experimental setup with ultracold atoms in an optical lattice. This allows for the possibility of mapping the theories onto atomic gauge simulators. In this chapter we consider four discrete gauge groups, the cyclic group $\mathbb{Z}(k) \subset U(1)$, the symmetric group $S_3 \subset O(2)$ (i.e., the permutation group of three objects), the binary dihedral (quaternion) group $\bar{D}_2 \subset SU(2)$, and the 27-element group $\Delta(27) \subset SU(3)$ (see e.g. [132, 133, 134, 135]). The gauge group $\mathbb{Z}(k)$ was already discussed in the previous chapter, but we include it here to highlight the relation to the previous chapter and to show how the results extend to non-Abelian gauge groups. As we noted in the previous chapter, we impose the one-cocycles onto the different gauge groups to generalize the lattice cross algebra to a more general algebra.

This chapter is ordered as follows: In Section 6.1 we generalize the single direct lattice Hamiltonian of the previous chapter to a general finite gauge group. This includes the link-based operator algebra, gauge symmetry, and Gauss' law, as well as the electric and magnetic contributions to the Hamiltonian. In Section 6.2 we generalize the direct lattice to the doubled lattice construction, similar to what was introduced in the previous chapter, but with the inclusion of the more general lattice cross algebra defined in terms of a one-cocycle. In Section 6.3 we finally apply the model to concrete examples of finite gauge groups. This also includes a discussion of the special role of center symmetry for the confinement for the different gauge groups. The results presented in this chapter, have previously been published in [24].

6.1 Hamiltonian Formulation of Standard Lattice Gauge Theories with Discrete Gauge Group

Let us start by introducing the theory in the standard formulation using single undoubled lattice with a link-based operator algebra. In particular, we like to familiarize ourselves with the standard formulation before we reintroduce the doubled lattice and the cross-based operator algebra. We again consider the model in the Hamiltonian formulation, thus leaving time as a continuous parameter. As before, we split the Hamiltonian into two parts, a link-based electric Hamiltonian H_E and a plaquette-based magnetic Hamiltonian H_B:

$$H = H_E + H_B. \tag{6.1}$$

6.1.1 Link-Based Operator Algebra

We introduce a square lattice identical to the one in Figure 5.1. The link-based theories reside on just the direct lattice Λ, and the dual lattice $\widetilde{\Lambda}$ can be ignored for the remainder of this section. We will, however, reintroduce the dual lattice in Section 6.2. As for the Chern-Simons-Maxwell theory, it is straightforward to generalize the models to other lattice geometries. Again this will not add much to the understanding of these theories.

As we noted in the previous chapter, the basic dynamical variables of a lattice gauge theory are the parallel transporters $U_{x,i}$ residing on the lattice links (x, i). The parallel transporters take values in the gauge group of the theory, i.e. that $U \in \mathcal{G}$. Here we have suppressed the explicit link subscript of the parallel transporter, and we will continue to do so as long as no confusion may arise. On a single lattice link we define an orthonormal basis for the link Hilbert space $\mathcal{H}$ in terms of the parallel transporters residing on the link:

$$\mathcal{B} = \left\{ \left| U \right\rangle \mid U \in \mathcal{G} \right\}. \tag{6.2}$$

We identify the single-link Hilbert space with a vector space having a dimension equal to the order of the group $\mathrm{Ord}\,(\mathcal{G})$, where the vector space is freely generated by the elements of the gauge group, i.e., $\mathcal{H} \cong \mathbb{C}[G]$. We view the states of parallel transporters $\left| U_{x,i} \right\rangle$ as the "coordinate" eigenstates in the Hilbert space, similar to the φ phases, which were used as the coordinates in the group space in the previous chapter. In addition to the "coordinate" states we can define the conjugate "momentum" states $\left| \Gamma_P, ab \right\rangle$ which are also residing on the links. Here Γ_p is a unitary irreducible representation of the gauge group while a and b each take values in $\left\{ 1, 2, \ldots, d_{\Gamma_P} \right\}$, and d_{Γ_P} is the dimension of the irreducible representation Γ_p of the gauge group. The conjugate "momentum" states define a flux basis which we obtain by a Fourier transformation in the gauge group:

$$\left| \Gamma_p, ab \right\rangle = \sum_{U \in \mathcal{G}} \left| U \right\rangle \left\langle U \middle| \Gamma_p, ab \right\rangle. \tag{6.3}$$

The matrix elements in the sum, are defined as

$$\left\langle U \middle| \Gamma_p, ab \right\rangle = \frac{\sqrt{d_{\Gamma_p} d_{\Gamma_q}}}{\mathrm{Ord}\,(\mathcal{G})} \Gamma_p\,(U)_{ab}\,. \tag{6.4}$$

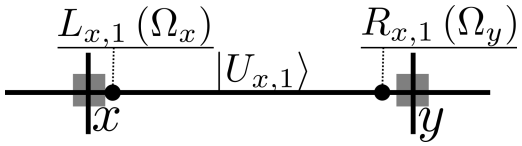

Figure 6.1: *Single direct lattice link connecting the sites x and* $y = x + \hat{1}$. *In addition to the link state* $\left|U\right\rangle$ *the link also carries the left* $L\left(\Omega_L\right)$ *and right operators* $R\left(\Omega_R\right)$ *inducing a left- and right-multiplication of the link variable with a group element* $\Omega \in \mathcal{G}$.

The group orthogonality theorem of eq. (2.15) implies that the matrix elements are unitary, i.e. $\Gamma_p(U)^*_{ba} = \Gamma_p\left(U^{-1}\right)_{ab}$. As in the previous chapter, we find that the conjugate momentum variables are associated with the electric field degrees of freedom. In the previous chapter we defined a T operator for every direct lattice-link, which upon matrix multiplication induced a $\mathbb{Z}(k)$ gauge transformation of the direct link variable. For a non-Abelian gauge group it is necessary to introduce two distinct unitary operators on every link, L and R, which we associate with the left and right end of the link, respectively, as shown in figure (6.1). In terms of the coordinate link states $\left|U\right\rangle$ the two operators represent multiplications of the link state with a group element $\Omega \in \mathcal{G}$ from the left and right end of the link, respectively:

$$L(\Omega)\left|U\right\rangle \equiv \left|\Omega U\right\rangle, \qquad R(\Omega)\left|U\right\rangle \equiv \left|U\Omega^{-1}\right\rangle. \tag{6.5}$$

For an Abelian gauge group it is clear that there is no difference between multiplication from the left and right side, and the link construction reduces to what was considered in the previous chapter, with just a single operator $T(\Omega)$ such that

$$T(\Omega) = L(\Omega) = R\left(\Omega^{-1}\right), \qquad T(\Omega)\left|U\right\rangle = \left|\Omega U\right\rangle = \left|U\Omega\right\rangle. \tag{6.6}$$

In the flux basis $\left|\Gamma_p, ab\right\rangle$ we represent the left L and right R operators by applying the Fourier transformation of eq. (6.3)

$$L\left(\Omega_L\right)\left|\Gamma_p, ab\right\rangle = \sum_c \Gamma_p\left(\Omega_L\right)^*_{ca}\left|\Gamma_p, cb\right\rangle, \quad R\left(\Omega_R\right)\left|\Gamma_p, ab\right\rangle = \sum_c \left|\Gamma_p, ac\right\rangle \Gamma_p\left(\Omega_R\right)_{cb}. \tag{6.7}$$

We demand that link operators on different links always commute [1],

$$\left[L_{x,i}\left(\Omega_L\right), L_{y,j}\left(\Omega'_L\right)\right] = \left[L_{x,i}\left(\Omega_L\right), R_{y,j}\left(\Omega_R\right)\right] = \left[R_{x,i}\left(\Omega_R\right), R_{y,j}\left(\Omega'_R\right)\right] = 0. \tag{6.8}$$

On a single link the left and right operators are trivially commuting (based on the associativity property of groups)

$$\begin{aligned} L\left(\Omega_L\right) R\left(\Omega_R\right)\left|U\right\rangle &= \left|\Omega_L\left(U\Omega_R^{-1}\right)\right\rangle = \left|\Omega_L U\Omega_R^{-1}\right\rangle, \\ R\left(\Omega_R\right) L\left(\Omega_L\right)\left|U\right\rangle &= \left|\left(\Omega_L U\right)\Omega_R^{-1}\right\rangle = \left|\Omega_L U\Omega_R^{-1}\right\rangle. \end{aligned} \tag{6.9}$$

Furthermore, on a single link both the left and the right operators obey the multiplication law:

$$\begin{aligned} L(\Omega)\,L\left(\Omega'\right)\left|U\right\rangle = \left|\Omega\Omega' U\right\rangle, \quad & L\left(\Omega\Omega'\right)\left|U\right\rangle = \left|\Omega\Omega' U\right\rangle, \\ & \Rightarrow \quad L(\Omega)\,L\left(\Omega'\right) = L\left(\Omega\Omega'\right), \\ R(\Omega)\,R\left(\Omega'\right)\left|U\right\rangle = \left|U\Omega'^{-1}\Omega^{-1}\right\rangle, \quad & R\left(\Omega\Omega'\right)\left|U\right\rangle = \left|U\left(\Omega\Omega'\right)^{-1}\right\rangle = \left|U\Omega'^{-1}\Omega^{-1}\right\rangle \\ & \Rightarrow \quad R(\Omega)\,R\left(\Omega'\right) = R\left(\Omega\Omega'\right). \end{aligned} \tag{6.10}$$

[1] Note that this will not be the case once the dual lattice is introduced in the next section, since operators on a direct lattice link will not commute with operators on a dual link residing on the same lattice cross.

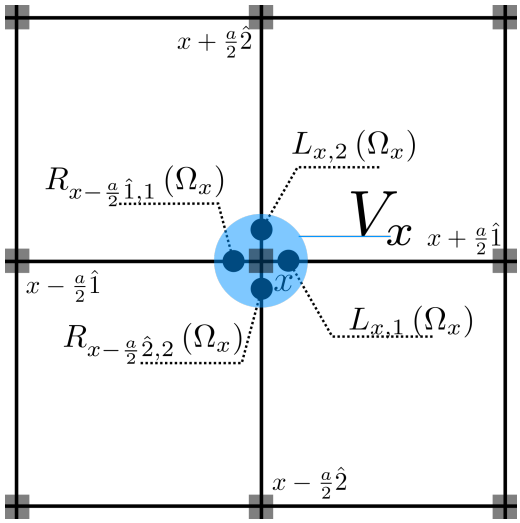

Figure 6.2: *The unitary operator of discrete gauge transformations V_x, for a general discrete gauge group is constructed from the link operators L and R residing next to the site.*

In addition to the left and right operators, on every link we introduce an operator P which projects onto a given coordinate state Ω, such that for a state $\left|U\right\rangle$,

$$P(\Omega)\left|U\right\rangle \equiv \delta_{\Omega,U}\left|U\right\rangle. \tag{6.11}$$

Since P projects the link states onto a group element Ω, it is clear that P is a complete orthonormal projector:

$$P\left(\Omega'\right)P(\Omega) = \delta_{\Omega',\Omega}P(\Omega). \tag{6.12}$$

It should be noted that the projection operator does not commute with the left and right operators on the same link, and in fact

$$L\left(\Omega_L\right)P(\Omega) = P\left(\Omega_L\Omega\right)L\left(\Omega_L\right), \qquad R\left(\Omega_R\right)P(\Omega) = P\left(\Omega\Omega_R^{-1}\right)R\left(\Omega_R\right). \tag{6.13}$$

6.1.2 Gauge Symmetry and Gauss' Law

In analogue to how we constructed Gauss' law in terms of the T operators in eq. (5.124) on the direct links we construct a Gauss operator for a non-Abelian group in terms of the L and R operators residing next to a given site,

$$V_x \equiv \prod_{i=1}^{2} L_{x+\frac{a}{2}\hat{\imath},i}\left(\Omega_x\right)R_{x-\frac{a}{2}\hat{\imath},i}\left(\Omega_x\right). \tag{6.14}$$

This is illustrated in Figure 6.2 for a Gauss' operator on the direct lattice site x, where the left and right operators are represented by filled circles residing near the site x. The general gauge transformation of the entire lattice is then given as a direct product over all lattice sites,

$$V = \prod_{x\in\Lambda} V_x(\Omega), \tag{6.15}$$

Under gauge transformations the parallel transporters are transformed by gauge transformations residing at the two ends of the link

$$U_{x,i} \to \Omega_{x-\frac{a}{2}\hat{i}} U_{x,i} \Omega^{-1}_{x+\frac{a}{2}\hat{i}}. \tag{6.16}$$

Again, for a state $\left|\Psi\right\rangle$ to be a physical, it must satisfy Gauss' law everywhere

$$V\left|\Psi\right\rangle = \left|\Psi\right\rangle. \tag{6.17}$$

6.1.3 Hamiltonian Formulation

Before constructing the full Hamiltonian for a general gauge group, it is useful to first define two sets of orthonormal basis states for the entire lattice. These are both defined for the direct lattice links, and are simply the direct product of the two different link-bases considered above. We refer to the first set as the link-basis

$$|\Psi_U\rangle \equiv \bigotimes_{(x,i)\in\text{all links}} \left|U_{x,i}\right\rangle, \tag{6.18}$$

and to the second as the flux-basis

$$|\Psi_\Gamma\rangle \equiv \bigotimes_{(x,i)\in\text{all links}} \left|\Gamma_{p;x,i}, ab\right\rangle. \tag{6.19}$$

Ψ_U and Ψ_Γ each denote a single state of parallel transporters (for $\left|\Psi_U\right\rangle$) or of fluxes (for $\left|\Psi_\Gamma\right\rangle$). The $\left|\Psi_U\right\rangle$- and the $\left|\Psi_\Gamma\right\rangle$-basis states are useful to construct the magnetic and electric parts of the Hamiltonian, respectively. The magnetic Hamiltonian H_B is diagonal in the link-basis, and we express it as a projection onto the parallel transporter states,

$$H_B = \sum_{\Psi_U} H_B\left(\Psi_U\right) \left|\Psi_U\right\rangle\left\langle\Psi_U\right|. \tag{6.20}$$

At the same time, the electric contribution H_E is diagonal in the flux-basis, and we express it as a projection onto the flux states,

$$H_E = \sum_{\Psi_\Gamma} H_E\left(\Psi_\Gamma\right) |\Psi_\Gamma\rangle\langle\Psi_\Gamma|. \tag{6.21}$$

Although diagonalizing the individual terms contributing to the Hamiltonian is a trivial task, it is non-trivial to diagonalize the full Hamiltonian.

Plaquette-Based Magnetic Hamiltonian

We introduce the plaquette variables by group multiplication of four link variables around an elementary plaquette:

$$U_{\square_x} \equiv U_{x-\frac{a}{2}\hat{2},1} U_{x+\frac{a}{2}\hat{1},2} U^{-1}_{x+\frac{a}{2}\hat{2},1} U^{-1}_{x-\frac{a}{2}\hat{1},2}, \quad x \in \widetilde{\Lambda}. \tag{6.22}$$

Here $\widetilde{\Lambda}$ is again a dual site at the center of the plaquette. We will later reintroduced the full dual lattice which will carry the dual fields. Under a gauge transformation at the initial site of the plaquette, $\Omega_{x-\frac{a}{2}\hat{2}} \in G$, the plaquette variable transforms as

$$U'_{\square_x} = \Omega_{x-\frac{a}{2}\hat{2}} U_{\square_x} \Omega^{-1}_{x-\frac{a}{2}\hat{2}}. \tag{6.23}$$

The magnetic energy of a state is represented by $H_B(\Psi_U)$, where the link configuration Ψ_U is expressed in terms of the elementary plaquette variables:

$$H_B\left(\Psi_U\right) = \frac{2}{(ea)^2} \sum_{x\in\widetilde{\Lambda}} h_B(U_{\square_x}). \tag{6.24}$$

Here e is again the unit of electric charge and $h_B(U_{\square_x})$ is the magnetic energy of a single plaquette.[2] This is a generalization of the magnetic energy of eq. (5.68) and we recover the results of eq. (5.68) by identifying $h_B\left(U_{\square_x}\right)$ with $-\frac{1}{4}\left(U_{\square_x} + U^{\dagger}_{\square_x}\right) = -\frac{1}{2}\cos\left(a^2 B_x\right)$. We observed that the breaking of the $U(1)$ symmetry down to $\mathbb{Z}(k)$ implies that the magnetic field can only take values $B_x = \frac{2\pi n}{k}$.

The magnetic contribution to the Hamiltonian is a physical quantity and must therefore be gauge-invariant. From the gauge transformation of the plaquette variable, eq. (6.22), it therefore follows that h_B must take constant values over the conjugacy classes of the gauge group $\mathcal{G}$.[3] Therefore, instead of specifying the magnetic energy for single group elements $\Omega \in \mathcal{G}$, we simply specify it in terms of the characters χ_{Γ_P},[4]

$$\chi_{\Gamma_p}(U_{\square,x}) = \mathrm{Tr}\left[\Gamma_p(U_{\square,x})\right], \tag{6.25}$$

where the subscript Γ_p characterizes the representation of the group. We are free to choose any representation of the group, but a natural choice is a "fundamental" irreducible representation Γ_p from which we can construct other representations.[5] Furthermore, if the gauge group has a non-trivial center, the chosen irreducible representation should also transform non-trivially under the center $Z(G)$. To normalize the magnetic energy, such that a vanishing magnetic flux of $U_{\square_x} = \mathbb{1}$ gives rise to a vanishing magnetic energy, we set the magnetic energy of a single plaquette to

$$a h_B(U_\square) = d_{\Gamma_p} - \Re\left[\chi_{\Gamma_p}(U_\square)\right]. \tag{6.26}$$

It follows from $\chi_{\Gamma_p}(\mathbb{1}) = d_{\Gamma_p}$, that this choice gives the correct vanishing magnetic energy

Link-Based Electric Hamiltonian

We define the electric energy on a single link as a hopping term between group elements which are nearest-neighbours in the gauge group. To determine these nearest-neighbours, we introduce a pseudo-metric

$$\mu(\Omega,\Omega') = 1 - \frac{1}{d_\Gamma}\Re\left\{\mathrm{Tr}\left[\Gamma(\Omega')\Gamma(\Omega)^{\dagger}\right]\right\}, \quad \left(\Omega,\Omega'\right) \in \mathcal{G}, \tag{6.27}$$

[2] We emphasize that here we use a definition of e that differs from [24], but agrees with [23]. The two definitions are related by shifting $e^2 \to e^2 a$ in [24].

[3] See Section 2.1.3.

[4] See Section 2.1.4.

[5] See Section 2.1.4.

that determines the distance between two group elements. Γ is a unitary irreducible representation of $\mathcal{G}$ that can be freely chosen. It is natural to choose the same representation as for the magnetic energy above. We will assume this choice from here on. μ is a pseudo-metric since it satisfies

$$\mu(\Omega, \Omega) = 0, \quad \forall \quad \Omega \in \mathcal{G}. \tag{6.28}$$

It is, however, not a full metric since $\mu\left(\Omega, \Omega'\right) = 0$ does not necessarily imply that $\Omega = \Omega'$. The electrical energy of a flux configuration $\left|\Psi_{\Gamma_p}\right\rangle$ is given by the sum over the electric energies on the individual links:

$$H_E(\Psi_{\Gamma_p}) = \frac{(ea)^2}{2} \sum_{x\in\Lambda} \sum_{i\in\{1,2\}} h_E\left(\Gamma_{p;x,i}\right), \tag{6.29}$$

where $h_E\left(\Gamma_{p;x,i}\right)$ defines the electric energy of a single link (x, i) with a flux state Γ_p, and the single-link Hamiltonian

$$H_E^{\text{single-link}} = \frac{(ea)^2}{2} \sum_{\Gamma_p, ab} h_E(\Gamma_p) \left|\Gamma_p, ab\right\rangle\left\langle\Gamma_p, ab\right|, \tag{6.30}$$

describes the hopping between nearest-neighbour elements of the gauge group, as defined by the pseudo-metric μ. Changing to the link-basis, we rewrite this as

$$\begin{aligned}
\left\langle U'\right| H_E^{\text{single-link}} \left|U\right\rangle &= \frac{e^2 a}{2} \sum_p \sum_{ab} h_E\left(\Gamma_p\right) \left\langle U'\middle|\Gamma_p, ab\right\rangle\left\langle\Gamma_p, ab\middle|U\right\rangle \\
&= \frac{e^2 a}{2} \sum_p h_E\left(\Gamma_p\right) d_{\Gamma_p} \frac{1}{\text{Ord}\left(\mathcal{G}\right)} \sum_{ab} \Gamma_p\left(U'\right)_{ab} \Gamma_p^*(U)_{ba} \\
&= \frac{e^2 a}{2} \frac{1}{\text{Ord}\left(\mathcal{G}\right)} \sum_{\Gamma_p} d_{\Gamma_p} h_E\left(\Gamma_p\right) \chi_{\Gamma_p}(U'U^{-1}).
\end{aligned} \tag{6.31}$$

In the second line we have used eq. (6.4) together with the fact that the matrix elements themselves are unitary, to rewrite the matrix elements in terms the representations of the group element, and in the third line we have identified the sum on the right-hand side with the character of the group elements. Requiring that the single-link Hamiltonian is described by a discrete Laplacian on the gauge group, i.e.,

$$\left\langle U'\right| H_E^{\text{single-link}} \left|U\right\rangle = \frac{e^2}{2}\left(-\delta_{\langle U,U'\rangle} + N_U \delta_{U,U'}\right), \tag{6.32}$$

we obtain a condition for the single-link energies. Here $\langle U, U'\rangle$ denotes a pair of nearest-neighbour group elements U and U' such that $\delta_{\langle U,U'\rangle}$ equals 1 if U and U', are nearest-neighbours and otherwise equals 0. N_U denotes the number of nearest-neighbours of the group element U. This choice of electric energy per link matches with the electric energy defined in the previous chapter. There we considered the continuous $U(1)$ and the discrete $\mathbb{Z}(k)$ gauge groups, for which the concept of nearest-neighbours are trivial. In the previous chapter, the lattice model was not considered for an undoubled lattice, but from eq. (5.63) we easily identify the corresponding electric field as $E_{x,i} = -i\frac{1}{a}\partial_{\varphi_{x,i}}$. This provides the single link electric energy from eq. (5.69) for the continuous $U(1)$ as

$$H_{E_{CSM}}^{\text{Single-Link}} = \frac{e^2 a^2}{2}\left(-i\frac{1}{a}\partial_{\varphi_{x,i}}\right)^2 = -\frac{e^2}{2}\left(\partial_{\varphi_{x,i}}\right)\left(\partial_{\varphi_{x,i}}\right). \tag{6.33}$$

The most symmetric way to discretize this $U(1)$ result to the discrete group $\mathbb{Z}(k)$ is to let the first (second) derivative operator act as a forward (backward) difference operator in group space. Denoting an operator that shifts z_l to $z_{\left[l\pm1\right]_k}$ by $\delta_\pm$. For $\mathbb{Z}(k)$ we obtain the single link electric energy as

$$\begin{aligned} H_{E_{CSM}}^{\text{Single-Link}} &= -\frac{e^2}{2}\left(\delta_+ - \mathbb{1}\right)\left(\mathbb{1} - \delta_-\right) \\ &= -\frac{e^2}{2}\left(\delta_+ + \delta_- - 2\mathbb{1}\right), \quad \because \quad \delta_\pm\delta_\mp = \mathbb{1}. \end{aligned} \tag{6.34}$$

Acting with this operator between two link states $\left|z_n\right\rangle$ and $\left|z_m\right\rangle$, we obtain

$$\left\langle z_m\right| H_{E_{CSM}}^{\text{single-link}} \left|z_n\right\rangle = \frac{e^2}{2}\left(-\delta_{\left[m\pm1\right]_k,n} - 2\delta_{mn}\right), \tag{6.35}$$

which agrees with the expression in eq. (6.32) since each element in the group has exactly 2 nearest-neighbours (at least for $k > 2$).

It should be noted that the single-link electric Hamiltonian of eq.(6.30) is commuting with both the left and right link operator,

$$[L(\Omega_L), H_E^{\text{single-link}}] = 0, \qquad [R(\Omega_R), H_E^{\text{single-link}}] = 0. \tag{6.36}$$

This follows directly from eq. (6.7).

6.1.4 Standard $\mathbb{Z}(k)$ Lattice Gauge Theory

As noted in Section 2.3.1, the group elements of the cyclic group $\mathbb{Z}(k)$ can be represented as the kth roots of unity:

$$\mathbb{Z}(k) = \left\{ e^{\frac{2\pi n}{k}i} \mid n \in \left\{0, 1, \ldots, k-1\right\} \right\}. \tag{6.37}$$

$\mathbb{Z}(k)$ is an Abelian group and every group element defines its own conjugacy class C_p, with $p = 1, 2, \ldots, k$ such that there exist k 1-dimensional representations Γ_p, $p = 1, 2, \ldots, k$. A representation Γ_p describes single-particle excitations with $(p-1)$ units of charge, i.e., $\Gamma_p(z_n) = z_n^{p-1}$. As considered above, the magnetic energy of an elementary plaquette is defined through the irreducible representation with a unit-charge, i.e. Γ_2, such that,

$$h_B(U_\square = z_n) = \frac{1 - \cos(2\pi n/k)}{a}. \tag{6.38}$$

By using the pseudo-metric as defined in eq. (6.27) with the representation carrying a unit charge, the distance between two group elements is given by

$$\mu(z_m, z_n) = 1 - \cos\left(\frac{2\pi(m-n)}{k}\right). \tag{6.39}$$

This explicitly shows that the nearest-neighbours of the group element z_m are the two group elements $\left[z_{m\pm1}\right]_k$.[6] The electric energy for a single link is then given by,

$$\left\langle z_m \middle| H_E^{\text{single-link}} \middle| z_n \right\rangle = \frac{e^2}{2}\left(-\delta_{m,[n+1]_k} - \delta_{m,[n-1]_k} + 2\delta_{m,n}\right). \tag{6.40}$$

By diagonalization, we obtain the spectrum of the single-link Hamiltonian as

$$h_E(\Gamma_p) = \frac{2}{a}\left(1 - \cos\left(\frac{2\pi(p-1)}{k}\right)\right), \tag{6.41}$$

which implies that the lowest-energy link state has a Γ_1 flux,

$$h_E\left(\Gamma_1\right) = \frac{2}{a}\left(1 - \cos\left(\frac{2\pi(1-1)}{k}\right)\right) = 0. \tag{6.42}$$

The spectrum is thus bounded from below for any k. The case $k = 2$ is special since the two neighbouring group elements $\left[z_{m\pm1}\right]_k$ are the same element. In this case the electric energy on a single-link is changed to

$$\left\langle z_m \middle| H_E^{\text{single-link}} \middle| z_n \right\rangle = \frac{e^2}{2}\left(-\delta_{m,[n+1]_2} + \delta_{m,n}\right). \tag{6.43}$$

The diagonalization of the $\mathbb{Z}(2)$ single-link Hamiltonian gives the two eigenvalues $h_E(\Gamma_1) = 0$ and $h_E(\Gamma_2) = 2/a$.

6.1.5 Standard S_3 Lattice Gauge Theory

The non-Abelian symmetric group S_3 consists of the six permutations on the set $\left\{1,2,3\right\}$, see Section 2.3.2. This group has 3 conjugacy classes,

$$\mathcal{C}_1 = \left\{\mathbb{1}\right\}, \qquad \mathcal{C}_2 = \left\{P_{12}, P_{23}, P_{31}\right\}, \qquad \mathcal{C}_3 = \left\{P_{231}, P_{312}\right\}, \tag{6.44}$$

which give rise to two 1-dimensional representations Γ_1 and Γ_2 and a single 2-dimensional representation Γ_3. To define the magnetic energy, the 2-dimensional fundamental representation Γ_3 is used, i.e.,

$$h_B(U_\square) = \frac{2 - \chi_{\Gamma_3}(U_\square)}{a}. \tag{6.45}$$

For the three conjugacy classes, the magnetic energy of a single plaquette is hence given by

$$h_B(\mathcal{C}_1) = 0, \qquad h_B(\mathcal{C}_2) = \frac{2}{a}, \qquad h_B(\mathcal{C}_3) = \frac{3}{a}. \tag{6.46}$$

The 2-dimensional Γ_3-representation of the group consists of the six orthogonal matrices shown in Table 6.1. Similarly, using this representation to specify the distances between different group elements Ω and Ω', we obtain

$$\mu(\Omega,\Omega') = 1 - \frac{1}{2}\mathrm{Tr}\left(\Gamma_3\left(\Omega'\right)\Gamma_3\left(\Omega\right)^T\right), \tag{6.47}$$

$\mathbb{1}$	P_{231}	P_{312}	P_{12}	P_{23}	P_{31}
$\begin{pmatrix} 1 & 0 \\ 0 & 1 \end{pmatrix}$	$\begin{pmatrix} -\frac{1}{2} & -\frac{\sqrt{3}}{2} \\ \frac{\sqrt{3}}{2} & -\frac{1}{2} \end{pmatrix}$	$\begin{pmatrix} -\frac{1}{2} & \frac{\sqrt{3}}{2} \\ -\frac{\sqrt{3}}{2} & -\frac{1}{2} \end{pmatrix}$	$\begin{pmatrix} 1 & 0 \\ 0 & -1 \end{pmatrix}$	$\begin{pmatrix} -\frac{1}{2} & \frac{\sqrt{3}}{2} \\ \frac{\sqrt{3}}{2} & \frac{1}{2} \end{pmatrix}$	$\begin{pmatrix} -\frac{1}{2} & -\frac{\sqrt{3}}{2} \\ -\frac{\sqrt{3}}{2} & \frac{1}{2} \end{pmatrix}$

Table 6.1: *The 2-dimensional Γ_3-representation of the S_3 group. This is the representation that is used to determine the magnetic energies and the distances between the elements of S_3.*

	$\mathbb{1}$	P_{231}	P_{312}	P_{12}	P_{23}	P_{31}
$\mathbb{1}$	0	$\frac{3}{2}$	$\frac{3}{2}$	1	1	1
P_{231}	$\frac{3}{2}$	0	$\frac{3}{2}$	1	1	1
P_{312}	$\frac{3}{2}$	$\frac{3}{2}$	0	1	1	1
P_{12}	1	1	1	0	$\frac{3}{2}$	$\frac{3}{2}$
P_{23}	1	1	1	$\frac{3}{2}$	0	$\frac{3}{2}$
P_{31}	1	1	1	$\frac{3}{2}$	$\frac{3}{2}$	0

Table 6.2: *Distances between group elements of S_3 calculated with the 2-dimensional Γ_3-representation.*

where the superscript T denotes the matrix transpose. The distances between different group elements are summarized in Table 6.2. For the single-link electric energy, there is no difference between the conjugacy classes C_1 and C_3. This implies that two elements that belong to distinct sets C_{13} and C_2, are nearest-neighbours.[7] This identification of conjugacy classes in terms of the electric energies is not just true for the group S_3, but will turn out to hold for the remaining finite discrete non-Abelian groups considered in this chapter, as long as the representation Γ, that is used to define the distance between group elements, is an irreducible representation of maximal degree. Hence, the identification of different conjugacy classes seems to be a general feature of these theories. We define the nearest-neighbour delta-function in mathematical terms, which generally holds for any discrete gauge group considered here,

$$\delta_{\langle U,U'\rangle} = (1-\delta_{C(U),C(U')})\big[1-\Big(1-\delta_{\mathrm{Ord}(C(U)),\mathrm{Ord}_p^{max}(C(U_p))}\Big)\Big(1-\delta_{\mathrm{Ord}(C(U')),\mathrm{Ord}_p^{max}(C(U_p))}\Big)\big]. \tag{6.48}$$

Here $\mathrm{Ord}_p^{max}\left(C\left(U_p\right)\right)$ denotes the order of the largest conjugacy class. It is still true that this function simply gives 1 when U and U' are nearest-neighbours in group space and otherwise 0. This implies that the electric energy of a single link is given by,

$$\left\langle U'\right| H_E^{\text{single-link}} \left|U\right\rangle = \frac{e^2}{2}\left(-\delta_{\langle U,U'\rangle}+3\delta_{U,U'}\right), \tag{6.49}$$

[6]This is the explicit form of the nearest-neighbour condition that we stated as trivial above.

[7]The set C_{13} is defined as the union of the two conjugacy classes C_1 and C_3, as defined in Section 2.3.2.

which we rewrite in matrix form

$$\left\langle U' \middle| h_E \middle| U \right\rangle = \begin{pmatrix} 3 & -1 & -1 & -1 & 0 & 0 \\ -1 & 3 & 0 & 0 & -1 & -1 \\ -1 & 0 & 3 & 0 & -1 & -1 \\ -1 & 0 & 0 & 3 & -1 & -1 \\ 0 & -1 & -1 & -1 & 3 & 0 \\ 0 & -1 & -1 & -1 & 0 & 3 \end{pmatrix}. \tag{6.50}$$

By diagonalizing the matrix we obtain the spectrum of the electric energy for a single link

$$h_E(\Gamma_p) = \frac{3}{a}\left(1 - \chi_{\Gamma_p}(C_2)\right), \tag{6.51}$$

which gives the following three values for the 3 irreducible representations of the group,

$$h_E(\Gamma_1) = 0, \qquad h_E(\Gamma_2) = \frac{6}{a}, \qquad h_E(\Gamma_3) = \frac{3}{a}. \tag{6.52}$$

6.1.6 Standard $\bar{D}_2$ Lattice Gauge Theory

We define the binary dihedral group $\bar{D}_2$ in terms of four pairs of 2×2 matrices, (see Section 2.3.3):

$$\bar{D}_2 = \left\{ \pm \mathbb{1}, \pm i\sigma_1, \pm i\sigma_2, \pm i\sigma_3 \right\}. \tag{6.53}$$

The group has 5 conjugacy classes

$$C_1 = \left\{\mathbb{1}\right\}, \quad C_2 = \left\{-\mathbb{1}\right\}, \quad C_3 = \left\{\pm\sigma_1\right\}, \quad C_4 = \left\{\pm\sigma_2\right\}, \quad C_5 = \left\{\pm\sigma_3\right\}, \tag{6.54}$$

and therefore four 1-dimensional irreducible representation $\left\{\Gamma_1, \Gamma_2, \Gamma_3, \Gamma_4\right\}$, together with a single 2-dimensional irreducible representation Γ_5. The magnetic energy for an elementary plaquette is defined by the use of the 2-dimensional fundamental representation Γ_5

$$h_B(U_\square) = \frac{2 - \Re\left[\chi_{\Gamma_5}(U_\square)\right]}{a}. \tag{6.55}$$

For each of the 5 conjugacy classes this gives magnetic energies of the form

$$h_B(C_1) = 0, \qquad h_B(C_2) = \frac{4}{a}, \qquad h_B(C_3) = \frac{2}{a}, \qquad h_B(C_4) = \frac{2}{a}, \qquad h_B(C_5) = \frac{2}{a}. \tag{6.56}$$

Still using the 2-dimensional Γ_5-representation, the distances between group elements in $\bar{D}_2$ are given by

$$\mu(\Omega, \Omega') = 1 - \frac{1}{2}\Re\left(\mathrm{Tr}\left[\Gamma_5(\Omega')\Gamma_5(\Omega)^\dagger\right]\right), \tag{6.57}$$

and are summarized in Table 6.3. The nearest-neighbours are elements belonging to different sets $\left\{C_{12}, C_3, C_4, C_5\right\}$.[8] Using the same definition as in eq. (6.48) we obtain the electric Hamiltonian for a single link

$$\left\langle U' \middle| H_E^{\text{single-link}} \middle| U \right\rangle = \frac{e^2}{2}\left(-\delta_{\langle U,U'\rangle} + 6\delta_{U,U'}\right), \tag{6.58}$$

[8]The set C_{12} is defined as the union of the two conjugacy classes C_1 and C_2, see Section 2.3.3.

	$\mathbb{1}$	$-\mathbb{1}$	σ_1	$-\sigma_1$	σ_2	$-\sigma_2$	σ_3	$-\sigma_3$
$\mathbb{1}$	0	2	1	1	1	1	1	1
$-\mathbb{1}$	2	0	1	1	1	1	1	1
σ_1	1	1	0	2	1	1	1	1
$-\sigma_1$	1	1	2	0	1	1	1	1
σ_2	1	1	1	1	0	2	1	1
$-\sigma_2$	1	1	1	1	2	0	1	1
σ_3	1	1	1	1	1	1	0	2
$-\sigma_3$	1	1	1	1	1	1	2	0

Table 6.3: *Distances between group elements of $\bar{D}_2$ calculated with the 2-dimensional Γ_5-representation.*

which in matrix notation takes the form

$$\left\langle U' \middle| h_E \middle| U \right\rangle = \begin{pmatrix} 6 & 0 & -1 & -1 & -1 & -1 & -1 & -1 \\ 0 & 6 & -1 & -1 & -1 & -1 & -1 & -1 \\ -1 & -1 & 6 & 0 & -1 & -1 & -1 & -1 \\ -1 & -1 & 0 & 6 & -1 & -1 & -1 & -1 \\ -1 & -1 & -1 & -1 & 6 & 0 & -1 & -1 \\ -1 & -1 & -1 & -1 & 0 & 6 & -1 & -1 \\ -1 & -1 & -1 & -1 & -1 & -1 & 6 & 0 \\ -1 & -1 & -1 & -1 & -1 & -1 & 0 & 6 \end{pmatrix}. \tag{6.59}$$

Upon diagonalization, we find the spectrum of the electric Hamiltonian

$$h_E(\Gamma_p) = \frac{6 - 2\left(\chi_{\Gamma_p}(C_3) + \chi_{\Gamma_p}(C_4) + \chi_{\Gamma_p}(C_5)\right)}{a}. \tag{6.60}$$

For the 5 irreducible representations this implies

$$h_E(\Gamma_1) = 0, \qquad h_E(\Gamma_2) = \frac{8}{a}, \qquad h_E(\Gamma_3) = \frac{8}{a}, \qquad h_E(\Gamma_4) = \frac{8}{a}, \qquad h_E(\Gamma_5) = \frac{6}{a}. \tag{6.61}$$

6.1.7 Standard $\Delta(27)$ Lattice Gauge Theory

The group $\Delta(27)$ consists of 27 elements that we define by three types of 3×3 matrices $D(a,b)$, $U(a,b)$, and $L(a,b)$ (see Section 2.3.3):

$$\Delta(27) = \left\{ D(a,b), U(a,b), L(a,b) \mid a, b \in \left\{1, e^{\frac{2\pi}{3}i}, e^{-\frac{2\pi}{3}i}\right\}\right\}. \tag{6.62}$$

The group has 11 conjugacy classes and therefore nine 1-dimensional representation $\left\{\Gamma_1, \ldots, \Gamma_9\right\}$ together with two 3-dimensional representations Γ_{10} and Γ_{11}. The magnetic energy is defined through the 3-dimensional fundamental representation Γ_{10}, or alternatively the antifundamental representation $\Gamma_{11} = \overline{\Gamma}_{10}$,

$$h_B(U_\square) = \frac{3 - \mathfrak{R}\left[\chi_{\Gamma_{10}}(U_\square)\right]}{a}. \tag{6.63}$$

	$\mathcal{C}_{123}$	$\mathcal{C}_4$	$\mathcal{C}_5$	$\mathcal{C}_6$	$\mathcal{C}_7$	$\mathcal{C}_8$	$\mathcal{C}_9$	$\mathcal{C}_{10}$	$\mathcal{C}_{11}$
$\mathcal{C}_{123}$	$M_{D(27)}$	$J_{3\times3}$	$J_{3\times3}$	$J_{3\times3}$	$J_{3\times3}$	$J_{3\times3}$	$J_{3\times3}$	$J_{3\times3}$	$J_{3\times3}$
$\mathcal{C}_4$	$J_{3\times3}$	$M_{D(27)}$	$J_{3\times3}$	$J_{3\times3}$	$J_{3\times3}$	$J_{3\times3}$	$J_{3\times3}$	$J_{3\times3}$	$J_{3\times3}$
$\mathcal{C}_5$	$J_{3\times3}$	$J_{3\times3}$	$M_{D(27)}$	$J_{3\times3}$	$J_{3\times3}$	$J_{3\times3}$	$J_{3\times3}$	$J_{3\times3}$	$J_{3\times3}$
$\mathcal{C}_6$	$J_{3\times3}$	$J_{3\times3}$	$J_{3\times3}$	$M_{D(27)}$	$J_{3\times3}$	$J_{3\times3}$	$J_{3\times3}$	$J_{3\times3}$	$J_{3\times3}$
$\mathcal{C}_7$	$J_{3\times3}$	$J_{3\times3}$	$J_{3\times3}$	$J_{3\times3}$	$M_{D(27)}$	$J_{3\times3}$	$J_{3\times3}$	$J_{3\times3}$	$J_{3\times3}$
$\mathcal{C}_8$	$J_{3\times3}$	$J_{3\times3}$	$J_{3\times3}$	$J_{3\times3}$	$J_{3\times3}$	$M_{D(27)}$	$J_{3\times3}$	$J_{3\times3}$	$J_{3\times3}$
$\mathcal{C}_9$	$J_{3\times3}$	$J_{3\times3}$	$J_{3\times3}$	$J_{3\times3}$	$J_{3\times3}$	$J_{3\times3}$	$M_{D(27)}$	$J_{3\times3}$	$J_{3\times3}$
$\mathcal{C}_{10}$	$J_{3\times3}$	$J_{3\times3}$	$J_{3\times3}$	$J_{3\times3}$	$J_{3\times3}$	$J_{3\times3}$	$J_{3\times3}$	$M_{D(27)}$	$J_{3\times3}$
$\mathcal{C}_{11}$	$J_{3\times3}$	$J_{3\times3}$	$J_{3\times3}$	$J_{3\times3}$	$J_{3\times3}$	$J_{3\times3}$	$J_{3\times3}$	$J_{3\times3}$	$M_{D(27)}$

Table 6.4: *Distances between group elements of* $\Delta(27)$ *calculated with the 3-dimensional* Γ_{10}*-representation. Here* $J_{3\times3}$ *denotes a* 3×3 *matrix where all the entries are* 1 *and* $M_{D(27)} = \frac{3}{2}\left(J_{3\times3} - \mathbb{1}_{3\times3}\right)$.

For the conjugacy classes this gives

$$h_B(\mathcal{C}_1) = 0, \qquad h_B(\mathcal{C}_2) = \frac{9}{2a}, \qquad h_B(\mathcal{C}_3) = \frac{9}{2a}, \tag{6.64}$$

$$h_B(\mathcal{C}_i) = \frac{3}{a}, \quad \forall \quad i \in \{4, 5, \ldots, 11\}. \tag{6.65}$$

Using the same 3-dimensional representation, the distances between the individual elements are given by,

$$\mu(\Omega, \Omega') = 1 - \frac{1}{3}\Re\left(\mathrm{Tr}\left[\Gamma_{10}(\Omega')\Gamma_{10}(\Omega)^\dagger\right]\right). \tag{6.66}$$

Again, group elements belonging to distinct sets $\{\mathcal{C}_{123}, \mathcal{C}_4, \mathcal{C}_5, \mathcal{C}_6, \mathcal{C}_7, \mathcal{C}_8, \mathcal{C}_9, \mathcal{C}_{10}, \mathcal{C}_{11}\}$ are nearest-neighbours.[9] We summarize the distances between group elements in Table 6.4 where the distances are shown in a 27×27 matrix, which is reduced to blocks of 3×3 corresponding to the elements of the nine sets of $\mathcal{C}$. This implies that the single link electric Hamiltonian is given by

$$\frac{2}{e^2}\left\langle U' \middle| H_E^{\text{single-link}} \middle| U \right\rangle = -\delta_{\langle U,U'\rangle} + 24\delta_{U,U'}. \tag{6.67}$$

where $\delta_{\langle U,U'\rangle}$ is again defined in eq. (6.48). In matrix notation one obtains

$$\left\langle U' \middle| h_E \middle| U \right\rangle = \tag{6.68}$$

$$\begin{pmatrix}
24\mathbb{1}_{3\times3} & -J_{3\times3} & -J_{3\times3} & -J_{3\times3} & -J_{3\times3} & -J_{3\times3} & -J_{3\times3} & -J_{3\times3} & -J_{3\times3} \\
-J_{3\times3} & 24\mathbb{1}_{3\times3} & -J_{3\times3} & -J_{3\times3} & -J_{3\times3} & -J_{3\times3} & -J_{3\times3} & -J_{3\times3} & -J_{3\times3} \\
-J_{3\times3} & -J_{3\times3} & 24\mathbb{1}_{3\times3} & -J_{3\times3} & -J_{3\times3} & -J_{3\times3} & -J_{3\times3} & -J_{3\times3} & -J_{3\times3} \\
-J_{3\times3} & -J_{3\times3} & -J_{3\times3} & 24\mathbb{1}_{3\times3} & -J_{3\times3} & -J_{3\times3} & -J_{3\times3} & -J_{3\times3} & -J_{3\times3} \\
-J_{3\times3} & -J_{3\times3} & -J_{3\times3} & -J_{3\times3} & 24\mathbb{1}_{3\times3} & -J_{3\times3} & -J_{3\times3} & -J_{3\times3} & -J_{3\times3} \\
-J_{3\times3} & -J_{3\times3} & -J_{3\times3} & -J_{3\times3} & -J_{3\times3} & 24\mathbb{1}_{3\times3} & -J_{3\times3} & -J_{3\times3} & -J_{3\times3} \\
-J_{3\times3} & -J_{3\times3} & -J_{3\times3} & -J_{3\times3} & -J_{3\times3} & -J_{3\times3} & 24\mathbb{1}_{3\times3} & -J_{3\times3} & -J_{3\times3} \\
-J_{3\times3} & -J_{3\times3} & -J_{3\times3} & -J_{3\times3} & -J_{3\times3} & -J_{3\times3} & -J_{3\times3} & 24\mathbb{1}_{3\times3} & -J_{3\times3} \\
-J_{3\times3} & -J_{3\times3} & -J_{3\times3} & -J_{3\times3} & -J_{3\times3} & -J_{3\times3} & -J_{3\times3} & -J_{3\times3} & 24\mathbb{1}_{3\times3}
\end{pmatrix}. \tag{6.69}$$

[9] The set $\mathcal{C}_{123}$ is defined as the union of the three conjugacy classes $\mathcal{C}_1$, $\mathcal{C}_2$, and $\mathcal{C}_3$, see Section 2.3.3.

Here $J_{3\times3}$ is a 3×3 matrix where all the entries equal 1. Upon diagonalization, we obtain the single-link electric energy spectrum as

$$h_E(\Gamma_p) = \frac{24 - 3\sum_{i=4}^{11} \chi_{\Gamma_p}(C_i)}{a}. \tag{6.70}$$

For the different flux states this implies

$$h_E(\Gamma_1) = 0, \qquad h_E(\Gamma_{10}) = \frac{24}{a}, \qquad h_E(\Gamma_{11}) = \frac{24}{a}, \tag{6.71}$$

$$h_E(\Gamma_p) = \frac{27}{a}, \quad \forall \quad p \in \{2, 3, \dots, 9\}.$$

6.2 Hamiltonian Formulation of Doubled Lattice Gauge Theories with Discrete Gauge Group

Let us now reintroduce the dual lattice $\widetilde{\Lambda}$ of the previous chapter and generalize the cross-based algebra to a more general non-commuting algebra of group multiplication operators. This is in contrast to the previous chapter where only a single algebra was considered on a lattice cross. As we saw there, the cross-based algebra can be described in terms of one-cocycles, see eq. (5.105). Similarly, here we will see that we can specify the non-commuting algebra in terms of one-cocycles. We will follow a more general approach to the cocycles which will form the basis for constructing a more general cross-based algebra. For a full characterization of one-cocycles for arbitrary discrete groups the reader is referred to [136].

6.2.1 Cross-Based Operator Algebra

Let us consider a lattice geometry identical to the one introduced in Figure 5.1. The basic dynamical variables are pairs of direct and dual parallel transporters, denoted by $U_{x,i}$ and $\widetilde{U}_{x,\epsilon_{ij}j}$ respectively, which are defined on the lattice crosses. As in the Chern-Simons-Maxwell theory on the doubled lattice, there are two different types of crosses, which have opposite orientation of the direct and dual lattice links. Each type of lattice cross constitutes its own sublattice, X and $\widetilde{X}$. In contrast to the Chern-Simons-Maxwell theory, where the link operators were Abelian ($T(\Omega)$ and $\widetilde{T}(\Omega)$), here the link operators will in general be non-Abelian. We therefore consider the left and right operators separately on both the direct and the dual links. As in the standard lattice gauge theories above, the two unitary operators L and R ($\widetilde{L}$ and $\widetilde{R}$) on a direct (dual) link realizes a left and a right multiplication of the associated link variable. Again, we additionally introduce a projection operator P ($\widetilde{P}$) for each direct (dual) link, which implements projections, analogous to the projection operator for a single link considered in the previous section. Since the operators on each direct (dual) link are defined as in the previous section, it is clear that each sets of direct (dual) operators satisfies the operator algebra of Section 6.1.1. The lattice crosses together with the link operators (excluding the projection operators) are illustrated in Figure 6.3. We express the states on a single cross as linear combinations of the orthonormal basis states on the direct and the dual link, i.e. $|U\rangle \otimes |\widetilde{U}\rangle$ where $|U\rangle$ and $|\widetilde{U}\rangle$ belong to the local Hilbert space of the direct link $\mathcal{H}$ and the dual

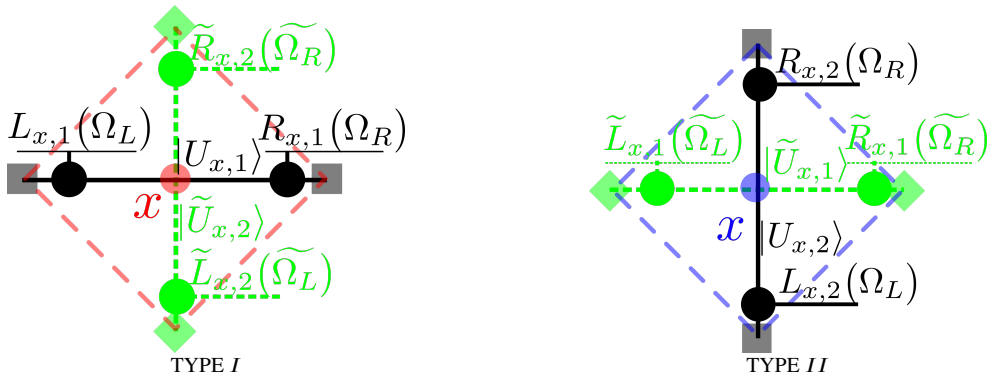

Figure 6.3: *The two types of lattice crosses for the doubled lattice. These are the non-Abelian generalization of the crosses in Figure 5.1, where the Abelian T ($\widetilde{T}$) operators have been replaced by the non-Abelian left L ($\widetilde{L}$) and right operators R ($\widetilde{R}$). The two crosses differ in the orientation of the direct and dual links.*

link $\widetilde{\mathcal{H}}$, respectively. In addition to the operator algebra for the single direct and dual links we need to specify the algebra between the direct and dual operators residing on the same lattice cross. The two projection operators P and $\widetilde{P}$ commute

$$[P(\Omega), \widetilde{P}(\widetilde{\Omega})] = 0. \tag{6.72}$$

As in the Chern-Simons-Maxwell case, the left and right operators are in general not commuting when they are residing on different links of the same lattice cross. To describe this, we introduce a phase similar to W in the previous chapter. For the two left operators this is defined by

$$\widetilde{L}(\widetilde{\Omega})L(\Omega) = W_{L\widetilde{L}}(\Omega, \widetilde{\Omega})L(\Omega)\widetilde{L}(\widetilde{\Omega}). \tag{6.73}$$

It is clear from the definition of the W factor that $W_{\widetilde{L}L}(\widetilde{\Omega}, \Omega) = W_{L\widetilde{L}}(\Omega, \widetilde{\Omega})^{-1}$. Since there exist two operators per link, we need to specify four of these factors to fully specify the cross-based algebra. With an obvious adaptation of notation, these are denoted by $\left\{W_{L\widetilde{L}}, W_{L\widetilde{R}}, W_{R\widetilde{L}}, W_{L\widetilde{R}}\right\}$. The four W factors are, however, in general not independent of each other. For the Chern-Simons-Maxwell model we only needed to specify a single independent W factor, which was given by (see eq. (5.104)),

$$W_{T\widetilde{T}} = e^{-\frac{2\pi}{k}i}. \tag{6.74}$$

We present a more general operator algebra, where the four W factors will be determined in terms of one-cocycles of the groups. We add an $U(1)$ phase ω, which will later turn out to be the one-cocycles, such that when operating on a link state with, e.g., the right direct link operator $R\left(\Omega_R\right)$, the direct link state is again multiplied from the right by Ω_R. In addition to this, the state receives an overall phase factor $\omega_R\left(\Omega_R, U\right)$, which is a function of both the group element Ω_R and the dual link state, $\widetilde{U}$. An analogous phase exists for the left link operator as well as for the corresponding

dual operators. These relations can be summarized as

$$\begin{aligned}
L\left(\Omega_L\right)\left|U\right\rangle \otimes \left|\widetilde{U}\right\rangle &= \omega_L\left(\Omega_L, \widetilde{U}\right)\left|\Omega_L U\right\rangle \otimes \left|\widetilde{U}\right\rangle, \\
R\left(\Omega_R\right)\left|U\right\rangle \otimes \left|\widetilde{U}\right\rangle &= \omega_R\left(\Omega_R, \widetilde{U}\right)\left|U\Omega_R^{-1}\right\rangle \otimes \left|\widetilde{U}\right\rangle, \\
\widetilde{L}\left(\widetilde{\Omega}_L\right)\left|U\right\rangle \otimes \left|\widetilde{U}\right\rangle &= \omega_{\widetilde{L}}\left(\widetilde{\Omega}_L, U\right)\left|U\right\rangle \otimes \left|\widetilde{\Omega}_L\widetilde{U}\right\rangle, \\
\widetilde{R}\left(\widetilde{\Omega}_R\right)\left|U\right\rangle \otimes \left|\widetilde{U}\right\rangle &= \omega_{\widetilde{R}}\left(\widetilde{\Omega}_R, U\right)\left|U\right\rangle \otimes \left|\widetilde{U}\widetilde{\Omega}_R^{-1}\right\rangle.
\end{aligned} \tag{6.75}$$

This gives four $U(1)$ phase factors ω_L, ω_R, $\omega_{\widetilde{L}}$, and $\omega_{\widetilde{R}}$, which may lead to non-trivial W factor when combined. These factors are therefore defining the possible realizations of non-commuting operator algebras for the left and right multiplication operators.[10]

As for the direct link in the previous section, there exist a dual link basis $\left|\widetilde{U}\right\rangle$, and a dual flux basis $\left|\Gamma_p, ab\right\rangle$, which are defined in complete analogue to the direct basis in Section 6.1.1. Due to the non-commuting nature of the operators, it is not possible to define a basis on a lattice cross that simultaneously specifying the flux Γ_p on both the direct and the dual link. Instead, on a single lattice cross we define three types of base, which are the direct link dual link basis $\left|U\right\rangle \otimes \left|\widetilde{U}\right\rangle$, the direct flux dual link basis $\left|\Gamma_p, ab\right\rangle \otimes \left|\widetilde{U}\right\rangle$, and finally, the direct link dual flux basis $\left|U\right\rangle \otimes \left|\widetilde{\Gamma}_p, ab\right\rangle$. This is similar to how the direct operator T and dual operator $\widetilde{T}$ were non-commuting in the Chern-Simons-Maxwell case. There a lattice cross basis was chosen in which the states were eigenstates of the T operator, but not of the $\widetilde{T}$ operator. In the notation introduced here this corresponds to the direct flux dual link basis. Alternatively, one can choose a basis of $\widetilde{T}$ eigenstates instead, which corresponds to a direct link dual flux basis. It should be noted that this is in contrast to a trivially doubled YM theory where the operators are commuting, and we can specify the flux simultaneously on both lattices. Later on we will use the direct flux dual link basis as the standard basis. It is useful to explicitly specify the operation of the left and right operators on a cross in this basis

$$\begin{aligned}
&L(\Omega_L)\left|\Gamma_p, ab\right\rangle \otimes \left|\widetilde{U}\right\rangle = \omega_L(\Omega_L, \widetilde{U})\left(\sum_c \Gamma_p(\Omega_L)^*_{ca}\left|\Gamma_p, cb\right\rangle\right) \otimes \left|\widetilde{U}\right\rangle, \\
&R(\Omega_R)\left|\Gamma_p, ab\right\rangle \otimes \left|\widetilde{U}\right\rangle = \omega_R(\Omega_R, \widetilde{U})\left(\sum_c \left|\Gamma_p, ac\right\rangle\Gamma_p(\Omega_R)_{cb}\right) \otimes \left|\widetilde{U}\right\rangle, \\
&\widetilde{L}(\Omega_L)\left|\Gamma_p, ab\right\rangle \otimes \left|\widetilde{U}\right\rangle \\
&\quad = \frac{\sqrt{d_p}}{\mathrm{Ord}\left(\mathcal{G}\right)}\left(\sum_{\Gamma_q, cd}\sqrt{d_q}\left(\sum_{\widetilde{U}'\in\mathcal{G}} \omega_{\widetilde{L}}(\Omega_L, \widetilde{U}')\Gamma_p(\widetilde{U}')_{ab}\Gamma_q(\widetilde{U}')^*_{cd}\right)\left|\Gamma_q, cd\right\rangle\right) \otimes \left|\Omega_L\widetilde{U}\right\rangle, \\
&\widetilde{R}(\Omega_R)\left|\Gamma_p, ab\right\rangle \otimes \left|\widetilde{U}\right\rangle \\
&\quad = \frac{\sqrt{d_p}}{\mathrm{Ord}\left(\mathcal{G}\right)}\left(\sum_{\Gamma_q, cd}\sqrt{d_q}\left(\sum_{\widetilde{U}'\in\mathcal{G}} \omega_{\widetilde{R}}(\Omega_R, \widetilde{U}')\Gamma_p(\widetilde{U}')_{ab}\Gamma_q(\widetilde{U}')^*_{cd}\right)\left|\Gamma_q, cd\right\rangle\right) \otimes \left|\widetilde{U}\Omega_R^{-1}\right\rangle,
\end{aligned} \tag{6.76}$$

[10] This is not necessarily the most general form of ω.

6.2.2 One-Cocycles and Non-Commuting Operator Algebra

Let us consider a single lattice cross in the direct link dual link basis $|U\rangle \otimes |U'\rangle$, where we apply two L operators to obtain

$$L(\Omega_L)L(\Omega'_L)\left|U\right\rangle \otimes \left|\widetilde{U}\right\rangle = \omega_L(\Omega_L,\widetilde{U})\omega_L(\Omega'_L,\widetilde{U})\left|\Omega_L\Omega'_L U\right\rangle \otimes \left|\widetilde{U}\right\rangle. \tag{6.77}$$

Since the operators satisfy the group multiplication (see eq. (6.10)) we obtain

$$\begin{aligned} L(\Omega_L)L(\Omega'_L)\left|U\right\rangle \otimes \left|\widetilde{U}\right\rangle &= L(\Omega_L\Omega'_L)\left|U\right\rangle \otimes \left|\widetilde{U}\right\rangle \\ &= \omega_L(\Omega_L\Omega'_L,\widetilde{U})\left|(\Omega_L\Omega'_L)U\right\rangle \otimes \left|\widetilde{U}\right\rangle, \end{aligned} \tag{6.78}$$

from which we obtain a consistency condition for the ω_L phase factor,

$$\omega_L(\Omega_L\Omega'_L,\widetilde{U}) = \omega_L(\Omega_L,\widetilde{U})\omega_L(\Omega'_L,\widetilde{U}). \tag{6.79}$$

This consistency condition is identical to the one-cocycle condition of eq. (2.36) in the first variable, with a trivial group action, $\alpha\left(g,\omega\left(g'\right)\right) = \omega\left(g'\right)$. We obtain similar relations for the remaining three phase factors ω_R, $\omega_{\widetilde{L}}$, and $\omega_{\widetilde{R}}$, which shows that all four phase factors are one-cocycles of the gauge group. Since the four phase factors satisfy the same one-cocycle relation, we will often suppress the explicit subscripts to ease the notation, and we will refer to the phase factors themselves as the one-cocycles. As we saw in Section 2.2.3, a one-cocycle with a trivial action leads to the effective Abelianization of the group. We will explicitly see this at work when we consider specific discrete gauge groups in the next section. We will find that the conjugacy classes that define the commutator groups $\left[\mathcal{G},\mathcal{G}\right]$ are always ascribed the same representation by the cocycles. From the consistency condition of eq. (6.79) and the corresponding consistency conditions for the three other phases, we conclude that ω must be a 1-dimensional representation of the gauge group $\mathcal{G}$. I.e. $\omega(\Omega,U)$ assigns a 1-dimensional representation $\Gamma_{p(U)}$ to every element $U \in \mathcal{G}$,

$$\omega(\Omega,U) = \Gamma_{p(U)}(\Omega). \tag{6.80}$$

Distinct one-cocycles ω_i then differ from each other in how the functions p_i, $i = 1,2,\ldots$ are assigning different 1-dimensional representations to a given group element. The next question is how the one-cocycles are related to the W-factors. By applying the two L and $\widetilde{L}$ operators in opposite order to a given lattice cross state $\left|U\right\rangle \otimes \left|\widetilde{U}\right\rangle$, we find that

$$\begin{aligned} \widetilde{L}\left(\widetilde{\Omega}\right)L\left(\Omega\right)\left|U\right\rangle \otimes \left|\widetilde{U}\right\rangle &= \widetilde{L}\left(\widetilde{\Omega}\right)\omega_L\left(\Omega,\widetilde{U}\right)\left|\Omega U\right\rangle \otimes \left|\widetilde{U}\right\rangle \\ &= \omega_{\widetilde{L}}\left(\widetilde{\Omega},\Omega U\right)\omega_L\left(\Omega,\widetilde{U}\right)\left|\Omega U\right\rangle \otimes \left|\widetilde{\Omega}\widetilde{U}\right\rangle, \\ L\left(\Omega\right)\widetilde{L}\left(\widetilde{\Omega}\right)\left|U\right\rangle \otimes \left|\widetilde{U}\right\rangle &= L\left(\Omega\right)\omega_{\widetilde{L}}\left(\widetilde{\Omega},U\right)\left|U\right\rangle \otimes \left|\widetilde{\Omega}\widetilde{U}\right\rangle \\ &= \omega_L\left(\Omega,\widetilde{\Omega}\widetilde{U}\right)\omega_{\widetilde{L}}\left(\widetilde{\Omega},U\right)\left|\Omega U\right\rangle \otimes \left|\widetilde{\Omega}\widetilde{U}\right\rangle. \end{aligned} \tag{6.81}$$

From the defining equation of the W factor (eq. (6.73)) it follows that

$$W_{L\widetilde{L}}(\Omega,\widetilde{\Omega}) = \omega_{\widetilde{L}}(\widetilde{\Omega},\Omega U)\omega_{\widetilde{L}}(\widetilde{\Omega},U)^{-1}\omega_L(\Omega,\widetilde{U})\omega_L(\Omega,\widetilde{\Omega}\widetilde{U})^{-1}. \tag{6.82}$$

The right-hand side of this equation contains a dependency on the link states, $\left|U\right\rangle$ and $\left|\widetilde{U}\right\rangle$. This will, however, turn out to be a superficial dependence that will disappear when we impose additional consistency requirements below. Again, imposing the group multiplication law for the left

operators L and $\widetilde{L}$ implies that $W_{L\widetilde{L}}(\Omega,\Omega')$ must satisfy the group composition law with respect to both of its arguments

$$W_{L\widetilde{L}}(\Omega,\widetilde{\Omega})W_{L\widetilde{L}}(\Omega',\widetilde{\Omega}) = W_{L\widetilde{L}}(\Omega\Omega',\widetilde{\Omega}), \quad W_{L\widetilde{L}}(\Omega,\widetilde{\Omega})W_{L\widetilde{L}}(\Omega,\widetilde{\Omega}') = W_{L\widetilde{L}}(\Omega,\widetilde{\Omega}\widetilde{\Omega}'). \tag{6.83}$$

Inserting $W_{L\widetilde{L}}$ in the form of eq. (6.82) into the second line above implies an additional consistency condition for the cocycle,

$$\omega_L\left(\Omega,\widetilde{\Omega}\widetilde{U}\right)\omega_L\left(\Omega,\widetilde{\Omega}'\widetilde{U}\right) = \omega_L\left(\Omega,\widetilde{U}\right)\omega_L\left(\Omega,\widetilde{\Omega}\widetilde{\Omega}'\widetilde{U}\right). \tag{6.84}$$

This relation is satisfied for any ω_L which obeys

$$\omega_L(\Omega,\widetilde{U})\omega_L(\Omega,\widetilde{U}') = \omega_L(\Omega,\widetilde{U}\widetilde{U}'). \tag{6.85}$$

It should be noted that this consistency condition can also be expressed in terms of the 1-dimensional group representations from which the one-cocycles are constructed. Using eq. (6.80), this condition is equivalent to

$$\Gamma_{p(\widetilde{U})}(\Omega)\otimes\Gamma_{p(\widetilde{U}')}(\Omega) = \Gamma_{p(\widetilde{U}\widetilde{U}')}(\Omega), \tag{6.86}$$

It is important to note that this implies that the function $p\left(\widetilde{U}\right)$ does not depend on the group element itself, but merely on its associated conjugacy class. This can be shown by repeated use of the above condition together with the fact that 1-dimensional representations are always commuting,

$$\begin{aligned}
\Gamma_{p\left(\widetilde{U}'^{-1}\widetilde{U}\widetilde{U}'\right)}(\Omega) &= \Gamma_{p\left(\widetilde{U}'^{-1}\right)}(\Omega)\otimes\Gamma_{p\left(\widetilde{U}\right)}(\Omega)\otimes\Gamma_{p\left(\widetilde{U}'\right)}(\Omega) \\
&= \Gamma_{p\left(\widetilde{U}'^{-1}\right)}(\Omega)\otimes\Gamma_{p\left(\widetilde{U}'\right)}(\Omega)\otimes\Gamma_{p\left(\widetilde{U}\right)}(\Omega) \\
&= \Gamma_{p\left(\widetilde{U}'^{-1}\widetilde{U}'\right)}(\Omega)\otimes\Gamma_{p\left(\widetilde{U}\right)}(\Omega) \\
&= \Gamma_{p(\mathbb{1})}(\Omega)\otimes\Gamma_{p\left(\widetilde{U}\right)}(\Omega) \\
&= \Gamma_{p\left(\widetilde{U}\right)}(\Omega)
\end{aligned} \tag{6.87}$$

Similar arguments imply that $p\left(\widetilde{U}\right)$ is a function of the gauge group Abelianization, $\mathcal{A}_{\mathcal{G}} = \mathcal{G}/\left[\mathcal{G},\mathcal{G}\right]$. This follows since for any group element $U_{[U_1,U_2]}$ that is obtained as the commutator of two other group elements U_1 an U_2, i.e. $U_{[U_1,U_2]} = U_1^{-1}U_2^{-1}U_1U_2$ one obtains,

$$\begin{aligned}
\Gamma_{p\left(U_{[U_1,U_2]}\right)}(\Omega) &= \Gamma_{p(U_1^{-1}U_2^{-1}U_1U_2)}(\Omega) \\
&= \Gamma_{p(U_1^{-1})}(\Omega)\otimes\Gamma_{p(U_2^{-1})}(\Omega)\otimes\Gamma_{p(U_1)}(\Omega)\otimes\Gamma_{p(U_2)}(\Omega) \\
&= \Gamma_{p(U_1^{-1})}(\Omega)\otimes\Gamma_{p(U_1)}(\Omega)\otimes\Gamma_{p(U_2^{-1})}(\Omega)\otimes\Gamma_{p(U_2)}(\Omega) \\
&= \Gamma_{p(U_1^{-1}U_1U_2^{-1}U_2)}(\Omega) \\
&= \Gamma_{p(\mathbb{1})}(\Omega)
\end{aligned} \tag{6.88}$$

Solutions to eq. (6.85) provide all possible ω_L cocycles, up to an overall phase factor that corresponds to a specific gauge choice, which we can therefore set to 1. This give a manifestly state-independent W factor of the form

$$\begin{aligned}
W_{L\widetilde{L}}(\Omega,\widetilde{\Omega}) &= \omega_{\widetilde{L}}(\widetilde{\Omega},\Omega)\omega_{\widetilde{L}}(\widetilde{\Omega},U)\omega_{\widetilde{L}}(\widetilde{\Omega},U)^{-1}\omega_L(\Omega,\widetilde{U})\omega_L(\Omega,\widetilde{U})^{-1}\omega_L(\Omega,\widetilde{\Omega})^{-1} \\
&= \omega_{\widetilde{L}}(\widetilde{\Omega},\Omega)\omega_L(\Omega,\widetilde{\Omega})^{-1}.
\end{aligned} \tag{6.89}$$

Analogous expressions can be derived for the remaining three coefficients $W_{L\widetilde{R}}$, $W_{R\widetilde{L}}$, and $W_{R\widetilde{R}}$. It will turn out that, once a gauge has been chosen, one can derive a relation between the different W factors. We will return to this in eq. (6.115).

6.2.3 Gauge Transformations and Gauss' Law

For the direct lattice we already introduced the unitary operator that realizes the gauge transformation in eq. (6.14). A similar operator, which is constructed by the corresponding dual operators, exists for the dual lattice

$$\widetilde{V} = \bigotimes_{\widetilde{x}\in\widetilde{\Lambda}} \widetilde{V}_x\left(\Omega\right). \tag{6.90}$$

This operator acts on the entire dual lattice and it implements gauge transformations on the single dual sites $\widetilde{x} \in \widetilde{\Lambda}$, where a single dual site operator is given by

$$\widetilde{V}_x \equiv \prod_{i=1}^{2} \widetilde{L}_{x+\frac{a}{2}\hat{i}}\left(\widetilde{\Omega}_x\right) \widetilde{R}_{x-\frac{a}{2}\hat{i}}\left(\widetilde{\Omega}_x\right). \tag{6.91}$$

To perform a gauge transformation, that is on both the direct and the dual lattice, we successively operate with the operators $(V \otimes \mathbb{1})$ and $(\mathbb{1} \otimes \widetilde{V})$ on the direct and dual lattice, respectively. We have expressed the operators in terms of the direct and dual lattice parts, such that they operate in the entire Hilbert space given by $\mathcal{H} \otimes \widetilde{\mathcal{H}}$. As for the Chern-Simons-Maxwell theory (see eq. (5.125)) the individual gauge transformation operators on a direct and on dual site are always commuting. This is trivially obeyed for direct and dual sites that are not neighbouring sites, while for neighbouring sites it follows directly from the symmetries imposed on the lattice. This in turn give rise to the relations between the different W factors that will be presented in eq. (6.115) below, after we impose a gauge fixing. The V and $\widetilde{V}$ operators are illustrated in Figure 6.4, for the operation on a pair of neighbouring direct site and dual site. For a full lattice state $\left|\Psi\right\rangle \in \mathcal{H} \otimes \widetilde{\mathcal{H}}$ to be physical, Gauss' law must be satisfied on both the direct and the dual lattice sites,

$$(V \otimes \mathbb{1})|\Psi\rangle = (\mathbb{1} \otimes \widetilde{V})|\Psi\rangle = |\Psi\rangle. \tag{6.92}$$

6.2.4 Hamiltonian Formulation

Before moving on to the full Hamiltonian for a general non-commuting cross algebra, let us start by first considering the trivially doubled Yang-Mills Hamiltonian, which is equivalent to choosing all the one-cocycles to be equal to 1. The magnetic Hamiltonian is naturally constructed by adding a magnetic term for the dual links, similar to the one used for the single direct lattice in eq. (6.20). The magnetic Hamiltonian is expressed as a sum of different plaquette contributions, both from the direct and from the dual lattice, i.e.,

$$H_B = \sum_{\Psi_U} \left\{ H_B(\Psi_U)\, |\Psi_U\rangle\langle\Psi_U| \otimes \mathbb{1} + \widetilde{H}_B(\Psi_U)\, \mathbb{1} \otimes |\Psi_U\rangle\langle\Psi_U| \right\}. \tag{6.93}$$

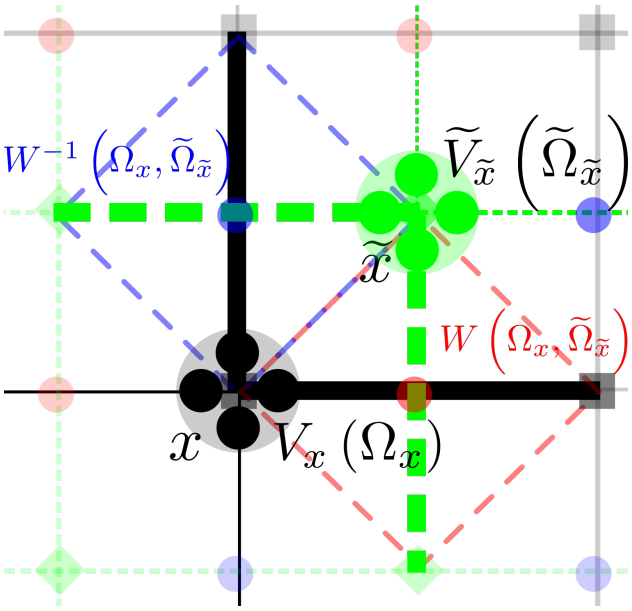

Figure 6.4: *Two gauge transformation generators, V_x and $\widetilde{V}_{\widetilde{x}}$, on a direct x and a dual site $\widetilde{x}$ respectively, are always commuting. This is non-trivial, since the links marked in bold contain non-commutativity operators. The total non-community factor picks up two factors of W and W^{-1} from the two crosses, which cancel each other out.*

Here $H_B(\Psi_U)$ is defined as above, i.e. eq. (6.24), and the dual $\widetilde{H}_B$ is defined as

$$\widetilde{H}_B(\Psi_U) = \frac{2}{(ea)^2} \sum_{x \in \widetilde{\Lambda}} h\left(U_{\square,x}\right). \tag{6.94}$$

As for the Chern-Simons-Maxwell case, the direct and dual magnetic energies have the same form. It should be noted that this is not a necessary condition for the Hamiltonian and one could define a Hamiltonian with different magnetic energies for the direct and the dual lattice. Similarly, a dual term is added for the electrical part of the Hamiltonian, which is again analogous to the direct electrical part,

$$H_E = \sum_{\Psi_\Gamma} \left(H_E(\Psi_\Gamma) \left|\Psi_\Gamma\right\rangle\left\langle\Psi_\Gamma\right| \otimes \mathbb{1} + \widetilde{H}_E(\Psi_\Gamma) \mathbb{1} \otimes \left|\Psi_\Gamma\right\rangle\left\langle\Psi_\Gamma\right| \right). \tag{6.95}$$

$H_E(\Psi_U)$ is given by eq. (6.29) and the dual electric Hamiltonian, $\widetilde{H}_E$, is again defined as

$$\widetilde{H}_E(\Psi_U) = \frac{(ea)^2}{2} \sum_{x \in \widetilde{\Lambda}} \sum_{i \in \{1,2\}} h_E\left(\Gamma_{p;x,i}\right). \tag{6.96}$$

Before moving on to the full lattice Hamiltonian, it is again convenient to familiarize ourselves with the behaviour of the Hamiltonian on just a single lattice cross,

$$H_{E_+} = \frac{(ea)^2}{2} \sum_{\Gamma_p, ab} h_E(\Gamma_p) \left(\left|\Gamma_p, ab\right\rangle\left\langle\Gamma_p, ab\right| \otimes \mathbb{1} + \mathbb{1} \otimes \left|\Gamma_p, ab\right\rangle\left\langle\Gamma_p, ab\right| \right). \tag{6.97}$$

Changing to the direct link dual link basis the electric Hamiltonian is given by,

$$\begin{aligned}
&\left\langle U' \right| \otimes \left\langle \widetilde{U}' \right| H_{E_+} \left| U \right\rangle \otimes \left| \widetilde{U} \right\rangle \\
&= \frac{(ea)^2}{2\mathrm{Ord}\,(\mathcal{G})} \sum_{\Gamma_p} d_{\Gamma_p} h_E\left(\Gamma_p\right) \left(\delta_{\widetilde{U},\widetilde{U}'} \chi_{\Gamma_p}(U'U^{-1}) + \delta_{U,U'} \chi_{\Gamma_p}(\widetilde{U}'\widetilde{U}^{-1}) \right) \\
&= \left(-\delta_{\langle U,U' \rangle} + N_U \delta_{U,U'} \right) \delta_{\widetilde{U},\widetilde{U}'} + \left(-\delta_{\langle \widetilde{U},\widetilde{U}' \rangle} + \widetilde{N}_{\widetilde{U}} \delta_{\widetilde{U},\widetilde{U}'} \right) \delta_{U,U'}.
\end{aligned} \tag{6.98}$$

In analogue to eq. (6.32), N_U and $\widetilde{N}_{\widetilde{U}}$ denote the number of nearest-neighbour elements of U and $\widetilde{U}$, in their respective group spaces. As in the previous chapter, the dynamics governed by the electric Hamiltonian admits a simple quantum mechanical analogy, not different from the analogy, in terms of the motion of an abstract charged "particle" in the presence of an abstract $U(1) \otimes U(1)$ gauge field, which implements parallel transport between nearest-neighbours in group space. By successive hopping in the discrete group space of the doubled theory, this abstract "particle" can accumulate an Aharonov-Bohm phase [137], which determines the degeneracies of the states in the Hilbert space of a single lattice cross.

As expected, the trivially doubled YM theory just corresponds to two decoupled copies of an undoubled theory (see eq. (6.32)), the hopping on one link leaves the state of the dual link unchanged.[11]

We are now moving on to the non-trivial Chern-Simons type theories where $\omega \neq 1$. The magnetic part of the Hamiltonian remains the same as before, although the electric part of the Hamiltonian must be modified to incorporate the non-commutativity of the lattice cross operators. The cocycles of eq. (6.75) depend on the link states on the lattice cross. For non-trivial cocycles, it is expected the hopping on the direct link depends on the state of the dual link, and vice versa. To describe this, let us consider a Hamiltonian of the form,

$$\begin{aligned}
&\left\langle U' \right| \otimes \left\langle \widetilde{U}' \right| H_{E_+} \left| U \right\rangle \otimes \left| \widetilde{U} \right\rangle \\
&= \frac{(ea)^2}{2} \left(\left(-e^{i\varphi(\Omega,\widetilde{U})} \delta_{\langle U,U' \rangle} + N_U \delta_{U,U'} \right) \delta_{\widetilde{U},\widetilde{U}'} + \left(-e^{i\widetilde{\varphi}(\widetilde{\Omega},U)} \delta_{\langle \widetilde{U},\widetilde{U}' \rangle} + \widetilde{N}_{\widetilde{U}} \delta_{\widetilde{U},\widetilde{U}'} \right) \delta_{U,U'} \right),
\end{aligned} \tag{6.99}$$

where $\Omega = U'U^{-1}$ and $\widetilde{\Omega} = \widetilde{U}'\widetilde{U}^{-1}$. We have added two additional complex phase factors to the Hamiltonian, to describe the non-commuting nature of the theory. In a similar manner to the Maxwell-Chern-Simons theory we interpret the two phases as two independent abstract $U(1)$ gauge fields, which provide parallel transporters connecting nearest-neighbour group elements. The two phase factors $e^{i\varphi}$ and $e^{i\widetilde{\varphi}}$ each satisfy the group composition law and define a one-cocycle

$$\begin{aligned}
e^{i\varphi(\Omega,\widetilde{U})} e^{i\varphi(\Omega',\widetilde{U})} &= e^{i\varphi(\Omega\Omega',\widetilde{U})}, \quad \forall \quad \left(\Omega, \Omega', \widetilde{U}\right) \in \mathcal{G}, \\
e^{i\varphi(\widetilde{\Omega},U)} e^{i\varphi(\widetilde{\Omega}',U)} &= e^{i\varphi(\widetilde{\Omega}\widetilde{\Omega}',U)}, \quad \forall \quad \left(\widetilde{\Omega}, \widetilde{\Omega}', U\right) \in \mathcal{G}.
\end{aligned} \tag{6.100}$$

Again, the dynamics of the electric Hamiltonian on a single lattice cross give rise to a simple mechanical analogue in terms of a charged particle in the presence of an $U(1) \otimes U(1)$ gauge field. The successive hopping in the discrete group space $\mathcal{G} \otimes \mathcal{G}$ define the motion of the mechanical

[11] We can recover the single lattice electric energy of eq. (6.32), up to a constant term, by demanding a constant dual lattice.

analogue particle in the $U(1) \otimes U(1)$ background gauge field. The particle can cumulate a phase, just as in the mechanical analogue described in the previous chapter for the doubled Chern-Simons-Maxwell theory.

The individual phase factors are not directly physical objects, but we accumulate an Aharonov-Bohm physical phase [137], denoted by $\Phi\big(\Omega, \widetilde{\Omega}\big)$, as a sequence of non-trivial group transformations Ω and $\widetilde{\Omega}$,

$$e^{i\varphi(\Omega,\widetilde{U})} e^{i\widetilde{\varphi}(\widetilde{\Omega},\Omega U)} e^{i\varphi(\Omega^{-1},\widetilde{\Omega}\widetilde{U})} e^{i\widetilde{\varphi}(\widetilde{\Omega}^{-1},U)} = e^{i\Phi(\Omega,\widetilde{\Omega})}. \tag{6.101}$$

We emphasize that it is not possible to accumulate this phase on just one of the direct or dual lattices. The phase must necessarily be accumulated on both lattices simultaneously. This follows from the group property in eq. (6.100),

$$e^{i\varphi(\Omega_1,U)} e^{i\varphi(\Omega_2,U)} \dots e^{i\varphi(\Omega_n,U)} = e^{i\varphi(\prod_{l=1}^{n}\Omega_l,U)} = 1, \tag{6.102}$$

for group elements $\Omega_l \neq \mathbb{1}$, $l = 1, 2, \dots, n$, with $\prod_{l=1}^{n} \Omega_l = \mathbb{1}$. Hence, trying to impose a transformation solely on the direct lattice i.e. $\widetilde{\Omega} = \mathbb{1}$ implies

$$\begin{aligned} e^{i\Phi(\Omega,\mathbb{1})} &= e^{i\varphi(\Omega,\widetilde{U})} e^{i\widetilde{\varphi}(\mathbb{1},\Omega U)} e^{i\varphi(\Omega^{-1},\mathbb{1}\widetilde{U})} e^{i\widetilde{\varphi}(\mathbb{1}^{-1},U)} \\ &= e^{i\varphi(\Omega,\widetilde{U})} e^{i\varphi(\Omega^{-1},\widetilde{U})} \qquad \because \quad (6.102) \\ &= 1. \end{aligned} \tag{6.103}$$

This shows that in this case no phase can be accumulated. A similar result exists for $\Omega = 1$. We identify the above Aharonov-Bohm phase factor $e^{i\Phi\left(\Omega,\widetilde{\Omega}\right)}$ as the phases $W\left(\Omega, \widetilde{\Omega}\right)$, that we introduced in the previous section. These are similarly defined as a product of one-cocycles. Any Hamiltonian for a single-cross of the form given in eq. (6.99) gives rise to a distinct Aharonov-Bohm phase Φ, that is characterized by the allowed one-cocycles of the theory. All the allowed W factors for a given gauge group $\mathcal{G}$ are associated with the allowed one-cocycles. This implies that the complete set of distinct doubled theories, be it Yang-Mills or Chern-Simons type, can be constructed in the framework that we have introduced here. The remainder of this chapter is devoted to specify the possible doubled theories for the different specific gauge groups. Before constructing all possible theories, we note that we are always able to choose a gauge, such that the accumulated phases can be expressed by a single one-cocycle. To choose a proper gauge, the consistency condition of eq. (6.85) is imposed on the phases, i.e.

$$e^{i\varphi(\Omega,U)} e^{i\varphi(\Omega,U')} = e^{i\varphi(\Omega,UU')}. \tag{6.104}$$

This condition eliminates the lattice cross state-dependence (i.e. U and $\widetilde{U}$), from the Aharonov-Bohm phase,

$$\begin{aligned} e^{i\Phi(\Omega,\widetilde{\Omega})} &= e^{i\varphi(\Omega,\widetilde{U})} e^{i\widetilde{\varphi}(\widetilde{\Omega},\Omega U)} e^{i\varphi(\Omega^{-1},\widetilde{\Omega}\widetilde{U})} e^{i\widetilde{\varphi}(\widetilde{\Omega}^{-1},U)} \\ &= e^{i\varphi(\Omega,\widetilde{U})} e^{i\widetilde{\varphi}(\widetilde{\Omega},\Omega)} e^{i\widetilde{\varphi}(\widetilde{\Omega},U)} e^{i\varphi(\Omega^{-1},\widetilde{\Omega})} e^{i\varphi(\Omega^{-1},\widetilde{U})} e^{i\widetilde{\varphi}(\widetilde{\Omega}^{-1},U)} \\ &= e^{i\widetilde{\varphi}(\Omega_2,\Omega_1)} e^{i\varphi(\Omega_1^{-1},\Omega_2)}. \end{aligned} \tag{6.105}$$

It further follows from eq. (6.100) that,

$$e^{i\varphi(\Omega_1^{-1},\Omega_2)} = e^{-i\varphi(\Omega_1,\Omega_2)}. \tag{6.106}$$

It may seem that a natural gauge choice would correspond to the symmetric gauge

$$\varphi(\Omega_1, \Omega_2) = \widetilde{\varphi}(\Omega_2, \Omega_1) \mod (2\pi). \tag{6.107}$$

This gauge does, however, not constitute a valid choice in these models, since inserting eq. (6.107) into eq. (6.105) gives,

$$\begin{aligned} e^{i\Phi(\Omega_1,\Omega_2)} &= e^{i\widetilde{\varphi}(\Omega_2,\Omega_1)} e^{i\varphi(\Omega_1^{-1},\Omega_2)} \\ &= e^{i\varphi(\Omega_1,\Omega_2)} e^{i\varphi(\Omega_1^{-1},\Omega_2)} = 1. \end{aligned} \tag{6.108}$$

Instead, we choose a gauge in which the direct phase φ vanishes,[12]

$$e^{i\varphi(\Omega,U)} = 1, \tag{6.109}$$

such that the Aharonov-Bohm phase is simply given by the dual phase,

$$e^{i\Phi(\Omega_1,\Omega_2)} = e^{\widetilde{\varphi}(\Omega_2,\Omega_1)}. \tag{6.110}$$

This choice corresponds to a complete gauge fixing that leaves no residual gauge degrees of freedom. The gauge fixing of eq. (6.109) implies that the cocycle resides on the dual, and not on the direct, link. This gauge fixing turns out to constrain the action of the left and right operators on a lattice cross. To see this we impose the requirement that the Hamiltonian is invariant under gauge transformations, i.e.

$$\left[L(\Omega_L), H_{E_+}\right] = 0, \quad \left[R(\Omega_R), H_{E_+}\right] = 0, \quad \left[\widetilde{L}(\widetilde{\Omega}_L), H_{E_+}\right] = 0, \quad \left[\widetilde{R}(\widetilde{\Omega}_R), H_{E_+}\right] = 0. \tag{6.111}$$

For a given $e^{i\widetilde{\varphi}}$, the one-cocycles associated with left- and right-multiplications are then given by,

$$\omega_L(\Omega, U) = \omega_R(\Omega, U)^* = e^{i\widetilde{\varphi}(\Omega,U)}. \tag{6.112}$$

This in turns implies that

$$\omega_L(\Omega, U)\omega_R(\Omega', U) = \omega_L(\Omega\Omega'^{-1}, U) = \omega_R(\Omega^{-1}\Omega', U), \tag{6.113}$$

together with

$$\omega_{\widetilde{L}}(\Omega, U) = \omega_{\widetilde{R}}(\Omega, U)^* = 1. \tag{6.114}$$

Through the definitions of the W phase factors in eq. (6.82), together with the corresponding equations for the remaining operators, this finally provides a relation between the different W factors, such that,

$$W_{L\widetilde{L}}(\Omega, \Omega') = W_{R\widetilde{L}}(\Omega, \Omega')^{-1} = W_{L\widetilde{R}}(\Omega, \Omega') = W_{R\widetilde{R}}(\Omega, \Omega')^{-1} = e^{-i\widetilde{\varphi}(\Omega,\Omega')}. \tag{6.115}$$

Therefore, any choice of group multiplication operator algebra, consistent with the gauge fixing of eq. (6.109), determines a corresponding Hamiltonian, and vice versa. Furthermore, the allowed theories can be specified by a single independent W factor, from which the individual phase factors for the lattice cross operators are determined through eq. (6.115). This is equivalent to specifying a single one-cocycle $\omega \equiv \omega_L = \omega_R^{-1} = e^{i\widetilde{\varphi}}$ that determines the complete lattice cross algebra of the theory. This relation implies that the two operators V and $\widetilde{V}$ in Figure 6.4 commutes.

[12] An equally valid choice would, of course, be to choose $\widetilde{\varphi} = 0$.

6.3 Explicit Calculations for the Specific Discrete Gauge Groups Examples

Having introduced the general Hamiltonian formulation of the theory we are ready to describe the spectrum of the Hamiltonian for the specific discrete finite gauge groups. We will do this in the strong-coupling regime, where the magnetic contribution to the Hamiltonian can be neglected. The dynamics are then fully characterized by the electric part of the Hamiltonian, which is described by a hopping between nearest-neighbour group elements. As for the Chern-Simons theory in the previous chapter, the hopping amplitude for a general Chern-Simons theory is in general complex and arises through the coupling to an abstract $U(1) \otimes U(1)$ gauge field.

Distinct theories are defined in terms of the corresponding Aharonov-Bohm phase, which is accumulated by a non-trivial set of group transformations on a single link and the intersecting dual link. We will specify the spectrum of these theories on a single cross. The energy eigenstates will be specified in terms of the energies E_n, $n = 0, 1, \ldots$, together with the properties of the ground state and the first excited states. We are only going to consider the two lowest energy levels, which are separated by a spectral gap $\Delta = E_1 - E_0$. The gap becomes infinitely large in the strong-coupling limit $(ea)^2 \to \infty$. Since the four W phases are related to each other through the relation in eq. (6.115), we only specify the $W_{L\tilde{L}}$ in this section. To ease the notation, and since a single W factor specifies the entire algebra on a lattice cross, from here on we will use W to refer to the $W_{L\tilde{L}}$ factor.

6.3.1 Doubled $\mathbb{Z}(k)$ Lattice Gauge Theory

One-Cocycles and W Factors

From eq. (6.80) the one-cocycle ω assigns a 1-dimensional representation Γ_p to every conjugacy class in $\mathbb{Z}(k)$. Since $\mathbb{Z}(k)$ is an Abelian group every group element constitutes its own conjugacy class. In Section 2.3.1 $\mathbb{Z}(k)$ was shown to contain k 1-dimensional representations, such that for $p = 1, 2, \ldots, k$

$$\omega(z_m, z_n) = \Gamma_{p(z_n)}(z_m) = z_m^{p(z_n)-1}. \tag{6.116}$$

$p\left(z_n\right)$ assigns one of the k 1-dimensional representations as a function of the value of z_n, which has k possible values, providing a total of k^k possible functions p and therefore a similar number of possible candidate one-cocycles. Not all the candidates are allowed, since they must in addition satisfy the consistency condition eq. (6.85). For the $\mathbb{Z}(k)$ gauge group this takes the form of

$$z_m^{p(z_n)-1} z_m^{p(z_{n'})-1} = z_m^{p(z_n z_{n'})-1}. \tag{6.117}$$

In terms of the function $p\left(z_n\right)$ this implies

$$\left[p\left(z_n z_{n'}\right) - p\left(z_n\right) - p\left(z_{n'}\right) + 1\right]_k = 0. \tag{6.118}$$

We solve this equation by choosing a function p of the form

$$p(n) = \left[an\right]_k + 1, \tag{6.119}$$

where a takes k distinct values $a = 0, 1, 2, \ldots, k-1$, providing a total of k distinct one-cocycles that satisfy the consistency condition. Denoting the different choices of a by a subscript $i = 1, 2, \ldots, k$, we express the general one-cocycle as

$$\omega_i(z_m, z_n) = z_m^{[a_i n]_k} = e^{2\pi i a_i mn/k}. \tag{6.120}$$

The general W-factors, on which the gauge fixing of eq. (6.109) has not yet been imposed, are obtained by substituting this result into eq. (6.89),

$$W(z_m, z_n) = \omega_i(z_n, z_m)\omega_j(z_m, z_n)^{-1} = e^{2\pi i a_{ij} mn/k}. \tag{6.121}$$

The W factors depend only on the difference $a_{ij} \equiv [a_i - a_j]_k$, and not on a_i and a_j themselves. Since both coefficients a_i and a_j take their values in the set $\{0, 1, \ldots, k-1\}$, so does a_{ij}. Hence, there is a redundancy in the formula that we like to fix, i.e. we need a gauge fixing. A simple gauge choose is $a_j = 0$, i.e.,

$$\omega_i(\Omega, U) = \omega_1(\Omega, U) = \Gamma_1(\Omega) = 1, \tag{6.122}$$

which is the same as the gauge imposed in eq. (6.109). This finally implies that for the $\mathbb{Z}(k)$ all possible W phases are specified as

$$W(z_m, z_n) = \widetilde{\omega}_i(z_n, z_m) = e^{2\pi i a_i mn/k}. \tag{6.123}$$

From this formula we explicitly see that there is a one-to-one correspondence between the one-cocycles and the W phases, which characterize the in-equivalent doubled lattice gauge theories which are distinguished by different W phases.

Trivial One-Cocycle

In the trivially doubled theory with $W = 1$ we obtain a single unique ground state for the single-cross Hamiltonian H_{E_+} with an energy $E_0 = 0$. In the flux-dual link basis the ground state is explicitly given by

$$\big|E_0\big\rangle = \frac{1}{\sqrt{k}} \sum_{n=0}^{k-1} \big|\Gamma_1\big\rangle \otimes \big|z_n\big\rangle, \tag{6.124}$$

For $k > 2$ the first excited state is a four-fold degenerate, and for $k = 2$ the degeneracy is only two-fold.

Non-Trivial One-Cocycles

When a non-trivial one-cocycle is introduced to the doubled $\mathbb{Z}(k)$ gauge theory, the ground state becomes degenerate. The properties of the degenerate ground states depend on the corresponding one-cocycle and whether the order of the group k is a prime. For any Chern-Simons type theory, where k is a prime number the ground state is k-fold degenerate.

	C_1	C_2	C_3
ω_1	Γ_1	Γ_1	Γ_1
ω_2	Γ_1	Γ_2	Γ_1

Table 6.5: *Allowed one-cocycles ω_1 and ω_2 for the symmetric group S_3. The group representations can be found in Section 2.3.2*

As an example, let us consider the $\mathbb{Z}(2)$ case. Since $k = 2$ is a prime number the ground state is two-fold degenerate and the two ground states are given by,

$$\left|E_0, a\right\rangle = \frac{1}{\sqrt{2\left(2+\sqrt{2}\right)}}\left(\left(1+\sqrt{2}\right)\left|\Gamma_1\right\rangle \otimes \left|z_{[a]_2}\right\rangle + \left|\Gamma_2\right\rangle \otimes \left|z_{[a+1]_2}\right\rangle\right), \tag{6.125}$$

where a takes values in $\{1, 2\}$. In addition, the first excited states are also modified when we introduce a non-trivial one-cocycle. The explicit form of these states depends on the particular case and is only of limited interest, and the states are therefore not listed here. A list of all eigenstates for $k \leq 3$ is included in appendix F.

6.3.2 Doubled S_3 Lattice Gauge Theory

6.3.3 One-Cocycles and W Factors

An S_3 one-cocycle ω assigns one of the two possible 1-dimensional representations, Γ_1 or Γ_2, to each conjugacy class C in S_3,

$$\omega(\Omega, U) = \Gamma_{p(C)}(\Omega). \tag{6.126}$$

With two 1-dimensional representations and three conjugacy classes there exist $2^3 = 8$ possible one-cocycles candidates. Explicitly testing all possible cocycle candidates against the condition in eq. (6.85) we find that two of them, presented in Table 6.5, are valid one-cocycles. The two allowed one-cocycles ω_1 and ω_2 associate the same representation to the two conjugacy classes C_1 and C_3, which together form the set $C_{13} = C_1 \cup C_3$, i.e.,

$$\omega_i(C_1) = \omega_i(C_3) = \omega_i(C_{13}), \quad i = 1, 2. \tag{6.127}$$

This follows from eq. (6.88), that the cocycles descend to a representation of the Abelianization of the group $A_{S_3} = S_3/\left[S_3, S_3\right] \cong \mathbb{Z}(2)$. This is further elaborated in [136]. With these two cocycles we can construct a set of corresponding W factors

$$W(\Omega, \Omega') = \omega_i(\Omega', \Omega)\omega_j(\Omega, \Omega')^{-1}. \tag{6.128}$$

Again this is affected by redundancies and to remove these we impose the gauge fixing of eq. (6.109)

$$W(\Omega, \Omega') = \Gamma_{p_i(C)}(\Omega'), \quad i = 1, 2. \tag{6.129}$$

	$n=0$	$n=1$	$n=2$	$n=3$	$n=4$
$E_n/(e^2)$	0	$\frac{3}{2}$	3	$\frac{9}{2}$	6
g_n	1	8	18	8	1

Table 6.6: *Eigenvalues E_n and their degeneracies g_n, $n = 0, 1, \ldots$, of the single-cross electric Hamiltonian H_{E_+} for the trivially doubled S_3 lattice YM theory. Note that the ground state is unique.*

This yields two distinct W factors, and therefore two distinct types of theories. The trivial YM theory is obtained from ω_1, which implies

$$W(\Omega, \Omega') = 1, \tag{6.130}$$

for all $\Omega, \Omega' \in S_3$. The second is obtained from ω_2 which gives rise to a doubled Chern-Simons type theory, with a lattice cross algebra defined by

$$W(\Omega, \Omega') = \begin{cases} -1 & | \quad \Omega, \Omega' \in C_2 \\ +1 & | \quad \text{otherwise} \end{cases} . \tag{6.131}$$

Trivial One-Cocycle

We summarize, the spectrum for the trivially doubled YM theory with $W = 1$ in Table 6.6, where the degeneracy of energy level n is denoted by g_n. The YM theory has a unique ground state with an energy of $E_0/(e^2) = 0$. The ground state is the totally symmetric superposition of the direct $\left|\Gamma_1\right\rangle$-flux with all the dual links,

$$\left|E_0\right\rangle = \frac{1}{\sqrt{6}} \sum_{\widetilde{U} \in S_3} \left|\Gamma_1\right\rangle \otimes \left|\widetilde{U}\right\rangle. \tag{6.132}$$

As expected, this state can easily be shown to be invariant under group multiplication on the direct and dual link.

The first excited state comes with an energy gap $\Delta/(e^2) = 3/2$, which goes to infinity in the limit of $e^2 \to \infty$· This energy level has an eight-fold degeneracy, with states that naturally fall into two categories, specified by the fluxes of the states. Four of the states are modified by the introduction of a non-trivial one-cocycle. These eigenstates are explicitly given by

$$\left|E_1, ab\right\rangle = \frac{1}{\sqrt{6}} \sum_{\widetilde{U} \in S_3} \left|\Gamma_3^{ab}\right\rangle \otimes \left|\widetilde{U}\right\rangle, \tag{6.133}$$

where a and b each take values in $\{1, 2\}$, corresponding to the 2-dimensional irreducible Γ_3 representation. In addition to these, there are four more states with the same energy, which are not

	$n=0$	$n=1$	$n=2$	$n=3$	$n=4$
$E_n/(e^2)$	$3/2(2-\sqrt{2})$	$3/2$	3	$9/2$	$3/2(2+\sqrt{2})$
g_n	2	8	16	8	2

Table 6.7: *Eigenvalues E_n and the corresponding degeneracies g_n, $n = 0, 1, \ldots$, of the single-cross electric Hamiltonian H_{E_+} for the doubled S_3 lattice CSYM theory. Note that the ground state is two-fold degenerate.*

changed under the inclusion of a non-trivial cocycle. These are given by

$$\begin{aligned}
\big|E_1,5\big\rangle &= \frac{1}{\sqrt{6}}\Big(2\big|\Gamma_1\big\rangle\otimes\big|\widetilde{1}\big\rangle - \big|\Gamma_1\big\rangle\otimes\big|\widetilde{P_{231}}\big\rangle - \big|\Gamma_1\big\rangle\otimes\big|\widetilde{P_{312}}\big\rangle\Big), \qquad (6.134)\\
\big|E_1,6\big\rangle &= \frac{1}{\sqrt{2}}\Big(\big|\Gamma_1\big\rangle\otimes\big|\widetilde{P_{231}}\big\rangle - \big|\Gamma_1\big\rangle\otimes\big|\widetilde{P_{312}}\big\rangle\Big),\\
\big|E_1,7\big\rangle &= \frac{1}{\sqrt{2}}\Big(\big|\Gamma_1\big\rangle\otimes\big|\widetilde{P_{12}}\big\rangle - \big|\Gamma_1\big\rangle\otimes\big|\widetilde{P_{31}}\big\rangle\Big),\\
\big|E_1,8\big\rangle &= \frac{1}{\sqrt{6}}\Big(\big|\Gamma_1\big\rangle\otimes\big|\widetilde{P_{12}}\big\rangle - 2\big|\Gamma_1\big\rangle\otimes\big|\widetilde{P_{23}}\big\rangle + \big|\Gamma_1\big\rangle\otimes\big|\widetilde{P_{31}}\big\rangle\Big).
\end{aligned}$$

We specify the action of the left and right operators for each eigenstate in appendix F. It is worth noting that for the states $\big|E_1, ab\big\rangle$ the dual link operators simply act as the identity operator,

$$\widetilde{L}(\Omega_L)\big|E_1,ab\big\rangle = \big|E_1,ab\big\rangle, \qquad \widetilde{R}(\Omega_R)\big|E_1,ab\big\rangle = \big|E_1,ab\big\rangle. \qquad (6.135)$$

It is also interesting to note how the ground state only contains Γ_1 direct fluxes in a symmetric sum, while the first excited states are split into two categories. One only contains Γ_1 direct fluxes and the other only contains Γ_3 direct fluxes.

Non-Trivial One-Cocycle

For the S_3 gauge theory there exist a single non-trivial cocycle and therefore a single Chern-Simons type theory. The spectrum for this non-trivial doubled CSYM theory is summarized in Table 6.7. It should be noted how the energy spectrum is changed under the inclusion of a non-trivial cocycle. Both the ground state and the highest energy level then shift their energies and merge with a state previously belonging to the $n = 2$ energy level. The ground state energy is shifted up to $E_0/(e^2) = 3/2(2-\sqrt{2}) \approx 0.879$, with corresponding orthonormal ground states given by,

$$\begin{aligned}
\big|E_0,1\big\rangle &= \frac{1}{\sqrt{6\left(2+\sqrt{2}\right)}}\Big[\left(1+\sqrt{2}\right)\sum_{\widetilde{U}\in C_2}\big|\Gamma_1\big\rangle\otimes\big|\widetilde{U}\big\rangle + \sum_{U\in C_{13}}|\Gamma_2\rangle\otimes\big|\widetilde{U}\big\rangle\Big], \qquad (6.136)\\
\big|E_0,2\big\rangle &= \frac{1}{\sqrt{6\left(2+\sqrt{2}\right)}}\Big[\left(1+\sqrt{2}\right)\sum_{\widetilde{U}\in C_{13}}\big|\Gamma_1\big\rangle\otimes\big|\widetilde{U}\big\rangle + \sum_{U\in C_2}\big|\Gamma_2\big\rangle\otimes\big|\widetilde{U}\big\rangle\Big].
\end{aligned}$$

We should emphasize that the ground states are now a mixture of states with both a Γ_1 and a Γ_2 direct flux. This is in contrast to the YM type theory above. For the doubled CS type theory, the action of the left and right operators with a group element in C_{13} are still trivial. With $a \in \{1, 2\}$, one obtains

$$\begin{aligned} L\left(C_{13}\right)\left|E_0, a\right\rangle &= \left|E_0, a\right\rangle, & R\left(C_{13}\right)\left|E_0, a\right\rangle &= \left|E_0, a\right\rangle, \\ \widetilde{L}\left(C_{13}\right)\left|E_0, a\right\rangle &= \left|E_0, a\right\rangle, & \widetilde{R}\left(C_{13}\right)\left|E_0, a\right\rangle &= \left|E_0, a\right\rangle. \end{aligned} \tag{6.137}$$

This is, however, not true for the operators with group elements in C_2. For these the actions are given by,

$$\begin{aligned} L(C_2)\left|E_0, a\right\rangle &= R(C_2)\left|E_0, a\right\rangle = (-1)^a\left|E_0, a\right\rangle, \\ \widetilde{L}(C_2)\left|E_0, a\right\rangle &= \widetilde{R}(C_2)\left|E_0, a\right\rangle = \left|E_0, [a]_2 + 1\right\rangle, \end{aligned} \tag{6.138}$$

The notation in the last line on the right-hand side simply states that the dual link operators flips between the two ground states. From here it follows that

$$L(C_2)\widetilde{L}(C_2) = -\widetilde{L}(C_2)L(C_2). \tag{6.139}$$

This is identical to the $\mathbb{Z}(2)$ algebra discussed for the toric code in Chapter 5 which shows that the non-commuting algebra of group multiplication operators yields the $\mathbb{Z}(2)$ toric code if the model is restricted to the set of ground states, that is for $e^2 \to \infty$. The non-Abelian S_3 lattice gauge theory of CS type therefore effectively Abelianizes when it is projected to the lowest energy level.

As noted for the trivial cocycle, four of the first excited states are deformed under the inclusion of a non-trivial cocycle. These are now given by,

$$\begin{aligned} \left|E_1, 11\right\rangle &= \frac{1}{\sqrt{6}}\left(\sum_{\widetilde{U}\in C_{13}}\left|\Gamma_3^{12}\right\rangle \otimes \left|\widetilde{U}\right\rangle - \sum_{\widetilde{U}\in C_2}\left|\Gamma_3^{21}\right\rangle \otimes \left|U\right\rangle\right), \\ \left|E_1, 12\right\rangle &= \frac{1}{\sqrt{6}}\left(\sum_{\widetilde{U}\in C_{13}}\left|\Gamma_3^{11}\right\rangle \otimes \left|\widetilde{U}\right\rangle + \sum_{\widetilde{U}\in C_2}\left|\Gamma_3^{22}\right\rangle \otimes \left|\widetilde{U}\right\rangle\right), \\ \left|E_1, 21\right\rangle &= \frac{1}{\sqrt{6}}\left(\sum_{\widetilde{U}\in C_{13}}\left|\Gamma_3^{22}\right\rangle \otimes \left|\widetilde{U}\right\rangle + \sum_{\widetilde{U}\in C_2}\left|\Gamma_3^{11}\right\rangle \otimes \left|\widetilde{U}\right\rangle\right), \\ \left|E_1, 22\right\rangle &= \frac{1}{\sqrt{6}}\left(\sum_{\widetilde{U}\in C_{13}}\left|\Gamma_3^{21}\right\rangle \otimes \left|\widetilde{U}\right\rangle - \sum_{\widetilde{U}\in C_2}\left|\Gamma_3^{12}\right\rangle \otimes \left|\widetilde{U}\right\rangle\right), \end{aligned} \tag{6.140}$$

with an energy gap to the ground state of $\Delta/(e^2) = 3/2(\sqrt{2} - 1) \approx 0.621$. The dual operators are mixing the four states when acting with a group element in C_2. In contrast to the lowest level, these states are all carrying a 2-dimensional (non-Abelian) representation Γ_3 and the actions of the left and right operators are clearly different. It is again interesting to note that the eigenstates sort themselves into categories of specific direct fluxes. The ground state is a mixture between the two 1-dimensional direct fluxes of Γ_1 and Γ_2, and the first excited states are separated into two categories of Γ_1 and Γ_3 direct fluxes. Although the direct and dual fluxes cannot be specified

simultaneously, there still exists a relation between them. Changing the basis of ground states to the direct link dual flux basis, we find that the states are given by

$$\begin{aligned}\left|E_0,1\right\rangle = \frac{1}{\sqrt{6(4+2\sqrt{2})}}\Big(&\left(1+\sqrt{2}\right)\left|1\right\rangle\otimes\left|\widetilde{\Gamma_1}\right\rangle - \left|1\right\rangle\otimes\left|\widetilde{\Gamma_2}\right\rangle \\ &-\left(1+\sqrt{2}\right)\left|P_{12}\right\rangle\otimes\left|\widetilde{\Gamma_1}\right\rangle + \left|P_{12}\right\rangle\otimes\left|\widetilde{\Gamma_2}\right\rangle \\ &-\left(1+\sqrt{2}\right)\left|P_{23}\right\rangle\otimes\left|\widetilde{\Gamma_1}\right\rangle + \left|P_{23}\right\rangle\otimes\left|\widetilde{\Gamma_2}\right\rangle \\ &-\left(1+\sqrt{2}\right)\left|P_{31}\right\rangle\otimes\left|\widetilde{\Gamma_1}\right\rangle + \left|P_{31}\right\rangle\otimes\left|\widetilde{\Gamma_2}\right\rangle \\ &+\left(1+\sqrt{2}\right)\left|P_{231}\right\rangle\otimes\left|\widetilde{\Gamma_1}\right\rangle - \left|P_{231}\right\rangle\otimes\left|\widetilde{\Gamma_2}\right\rangle \\ &+\left(1+\sqrt{2}\right)\left|P_{312}\right\rangle\otimes\left|\widetilde{\Gamma_1}\right\rangle - \left|P_{312}\right\rangle\otimes\left|\widetilde{\Gamma_2}\right\rangle\Big),\end{aligned} \tag{6.141}$$

$$\begin{aligned}\left|E_0,2\right\rangle = \frac{1}{\sqrt{6(4+2\sqrt{2})}}\Big(&\left(1+\sqrt{2}\right)\left|1\right\rangle\otimes\left|\widetilde{\Gamma_1}\right\rangle + \left|1\right\rangle\otimes\left|\widetilde{\Gamma_2}\right\rangle \\ &+\left(1+\sqrt{2}\right)\left|P_{12}\right\rangle\otimes\left|\widetilde{\Gamma_1}\right\rangle + \left|P_{12}\right\rangle\otimes\left|\widetilde{\Gamma_2}\right\rangle \\ &+\left(1+\sqrt{2}\right)\left|P_{23}\right\rangle\otimes\left|\widetilde{\Gamma_1}\right\rangle + \left|P_{23}\right\rangle\otimes\left|\widetilde{\Gamma_2}\right\rangle \\ &+\left(1+\sqrt{2}\right)\left|P_{31}\right\rangle\otimes\left|\widetilde{\Gamma_1}\right\rangle + \left|P_{31}\right\rangle\otimes\left|\widetilde{\Gamma_2}\right\rangle \\ &+\left(1+\sqrt{2}\right)\left|P_{231}\right\rangle\otimes\left|\widetilde{\Gamma_1}\right\rangle + 1\left|P_{231}\right\rangle\otimes\left|\widetilde{\Gamma_2}\right\rangle \\ &+\left(1+\sqrt{2}\right)\left|P_{312}\right\rangle\otimes\left|\widetilde{\Gamma_1}\right\rangle + \left|P_{312}\right\rangle\otimes\left|\widetilde{\Gamma_2}\right\rangle\Big).\end{aligned} \tag{6.142}$$

This shows that the ground state only includes the 1-dimensional Γ_1 and Γ_2 dual fluxes. This can similarly be done for the first excited states (see appendix F for explicit expressions for these states). The two categories of first excited states also come with specific dual fluxes. The states $\left|E_1,ab\right\rangle$, which has a Γ_3 direct flux, all comes with a Γ_1 dual flux, when the same states are expressed in the direct link dual flux basis. Similarly, the first excited states $\left|E_1,a\right\rangle$ with $a\in\left\{5,6,7,8\right\}$, i.e. with a Γ_1 direct flux, all contain a Γ_3 dual flux in the direct link dual flux basis. Similar results can be obtained for the higher energy eigenstates together with the energy eigenstates for the trivial cocycle. This implies that even though the flux cannot be specified on both the direct and the dual lattice simultaneously it is still possible to specify to what category the flux belongs in both the direct and the dual lattice. The energies are summarized for all the energy eigenstates of the S_3 theory in Figure 6.5 for both the trivial and the non-trivial cocycle. The energy levels are denoted in terms of their direct and dual flux categories $\left\{\Gamma\right\}\leftrightarrow\left\{\widetilde{\Gamma}\right\}$, as described above. The states containing a Γ_3 direct flux, marked in blue, are all unchanged by the inclusion of a non-trivial cocycle. It should be noted that the ground-states all contain 1-dimensional representations, the first excited states all contain a Γ_3 representation on either the direct or the dual lattice, and the second excited states all contain a Γ_3 representation on both the direct and the dual lattice – and a mixture of both 1-dimensional representations in the case of the trivial cocycle. This will become important when we consider the charged states for the group S_3 in Section 6.3.8. The higher-level states are a mirror of these states, with the roles of Γ_1 and Γ_2 interchanged. Appendix F contains a list of all the non-trivial cocycle eigenstates.

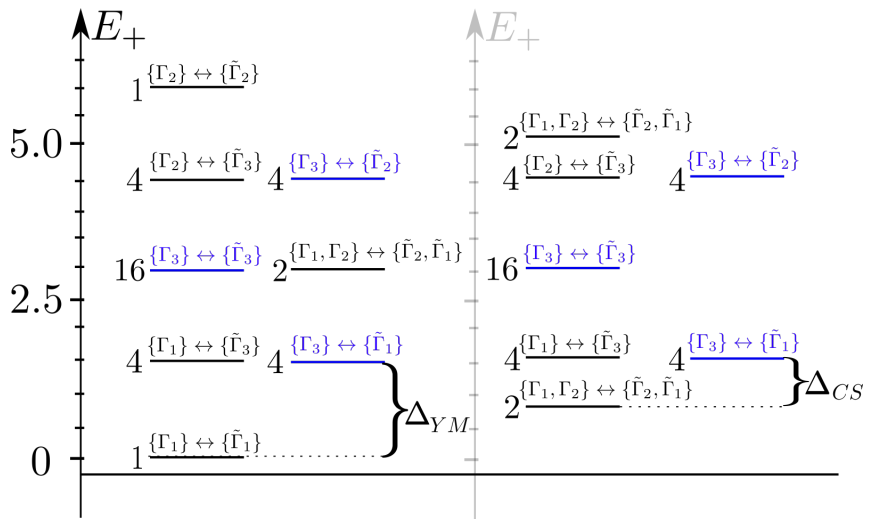

Figure 6.5: *Energy eigenstates with their respective degeneracies for the S_3 theory for both the trivial YM type (left) and the non-trivial CS type (right). The energies are specified by their direct and dual flux categories $\{\Gamma\} \leftrightarrow \{\tilde{\Gamma}\}$. States marked in blue are unaffected by the inclusion of a non-trivial cocycle. The two energy gaps are given by $\Delta_{YM} = 3/2$ and $\Delta_{CS} = 3\left(\sqrt{2}-1\right)/2 \approx 0.621$.*

6.3.4 Doubled $\bar{D}_2$ Lattice Gauge Theory

6.3.5 One-Cocycles and W Factors

The one-cocycle ω assigns a 1-dimensional representation Γ_p, $p = 1,2,3,4$, to each conjugacy class of $\bar{D}_2$, i.e.,

$$\omega(\Omega, U) = \Gamma_{p(C)}(\Omega), \tag{6.143}$$

The group $\bar{D}_2$ has four 1-dimensional representations together with five conjugacy classes C_q, $q = 1,2,\ldots,5$, which gives a $4^5 = 1024$ possible one-cocycle candidates. Again, for the candidates to represent a valid one-cocycle they need to satisfy the consistency condition of eq. (6.109), which leaves 16 one-cocycles $\omega_{i\in\{1,2,\ldots,16\}}$. These are summarized in Table 6.8. The two conjugacy classes C_1 and C_2 which combined make up the commutator sub-group (that is here equal to the center), are again associated with the same representation, i.e., $p(C_1) = p(C_2)$, such that C_1 and C_2 can be combined to $C_{12} = C_1 \cup C_2 = Z\left(\bar{D}_2\right)$. From the 16 allowed one-cocycles we find the corresponding W factors

$$W(\Omega, \Omega') = \omega_i(\Omega', \Omega)\omega_j(\Omega, \Omega')^{-1}. \tag{6.144}$$

As before, we impose a gauge fixing of $\omega_j(\Omega, \Omega') = 1$, by which

$$W(\Omega, \Omega') = \Gamma_{p_i(C)}(\Omega'), \quad i = 1,2,\ldots,16. \tag{6.145}$$

This provides a total of 16 distinct W factors corresponding to 16 distinct doubled $\bar{D}_2$ lattice gauge theories. Only one of them, $\omega_i = \omega_1$, gives rise to a doubled YM theory with a trivial W factor,

$$W(\Omega, \Omega') = 1, \quad \forall \quad \Omega, \Omega' \in \bar{D}_2. \tag{6.146}$$

	C_1	C_2	C_3	C_4	C_5
ω_1	Γ_1	Γ_1	Γ_1	Γ_1	Γ_1
ω_2	Γ_1	Γ_1	Γ_1	Γ_2	Γ_2
ω_3	Γ_1	Γ_1	Γ_1	Γ_3	Γ_3
ω_4	Γ_1	Γ_1	Γ_1	Γ_4	Γ_4
ω_5	Γ_1	Γ_1	Γ_2	Γ_1	Γ_2
ω_6	Γ_1	Γ_1	Γ_2	Γ_2	Γ_1
ω_7	Γ_1	Γ_1	Γ_3	Γ_1	Γ_3
ω_8	Γ_1	Γ_1	Γ_3	Γ_3	Γ_1
ω_9	Γ_1	Γ_1	Γ_4	Γ_1	Γ_4
ω_{10}	Γ_1	Γ_1	Γ_4	Γ_4	Γ_1
ω_{11}	Γ_1	Γ_1	Γ_2	Γ_3	Γ_4
ω_{12}	Γ_1	Γ_1	Γ_2	Γ_4	Γ_3
ω_{13}	Γ_1	Γ_1	Γ_3	Γ_2	Γ_4
ω_{14}	Γ_1	Γ_1	Γ_3	Γ_4	Γ_2
ω_{15}	Γ_1	Γ_1	Γ_4	Γ_2	Γ_3
ω_{16}	Γ_1	Γ_1	Γ_4	Γ_3	Γ_2

Table 6.8: *Allowed one-cocycles for the binary dihedral group* $\bar{D}_2$.

	$n=0$	$n=1$	$n=2$	$n=3$	$n=4$	$n=5$
$E_n/(e^2)$	0	3	4	6	7	8
g_n	1	8	6	16	24	9

Table 6.9: *Eigenvalues* E_n *and their degeneracies* g_n, $n = 0, 1, \ldots$, *of the single-cross electric Hamiltonian* H_{E_+} *for the doubled* $\bar{D}_2$ *lattice YM theory. Note that the ground state is a unique state.*

The remaining 15 one-cocycles ω_i, $i \in \{2, 3, \ldots, 16\}$ all give rise to CS type theories with non-trivial W factors of the form,

$$W(C, C') \in \{\pm 1\}. \tag{6.147}$$

It should be noted that $W\left(\Omega, \Omega'\right)$ is always 1 when either Ω or Ω' belongs to the set C_{12}. We can separate the 15 non-trivial cocycles into two sets $\omega_{i\in\{2,3,\ldots,10\}}$ and $\omega_{i\in\{11,12,\ldots,16\}}$. The energy spectra are identical for the cocycles in the same set. Hence, the group $\bar{D}_2$ contains two distinct energy spectra for the CS type theories. Furthermore, these theories Abelianize, similarly as for the group S_3, when they are projected to the lowest energy eigenstate. The properties of the low-energy states are therefore not discussed at length. Only the level structure will be presented together with the degeneracies of the different levels.

Trivial One-Cocycle

The energy levels of the YM type theory are presented in Table 6.9. As we saw in the case of S_3, the ground state of the trivially doubled lattice YM theory is non-degenerate and has an energy

	$n=0$	$n=1$	$n=2$	$n=3$	$n=4$	$n=5$	$n=6$
$E_n/(e^2)$	$2(2-\sqrt{2})$	3	4	6	$2(2+\sqrt{2})$	7	8
g_n	2	8	4	16	2	24	8

Table 6.10: *Eigenvalue E_n and their degeneracies g_n of the single-cross electric Hamiltonian H_{E_+} for the doubled $\bar{D}_2$ lattice theory constructed from the first set of cocycles. Note that the ground state is two-fold degenerate.*

$E_0/(e^2) = 0$. The ground state is again given by the totally symmetric superposition involving the Γ_1 representation,

$$\left|E_0\right\rangle = \frac{1}{\sqrt{8}} \sum_{\widetilde{U}\in\bar{D}_2} \left|\Gamma_1\right\rangle \otimes \left|\widetilde{U}\right\rangle. \tag{6.148}$$

The first excited state is eight-fold degenerate and separated from the ground state by an energy gap $\Delta/(e^2) = 3$.

Non-Trivial One-Cocycles

For the first set of non-trivial one-cocycles,

$$\omega_L(\Omega, U) = \omega_R(\Omega, U)^* \quad \in \quad \left\{\omega_i(\Omega, U) \,|\, i = 2, 3, \ldots, 10\right\}, \tag{6.149}$$

we obtain a spectrum that has a two-fold degenerate ground state, in contrast to the unique ground state of the YM theory, together with an energy gap of $\Delta/(e^2) = 2\sqrt{2} - 1 \approx 1.828$ to the first excited energy level. The energy levels and their corresponding degeneracies are summarized in table 6.10. The eigenstates for this theory are presented in appendix F for a particular choice of ω. It should be noted that although the spectrum of the theory is the same for each of the above cocycles, the eigenstates are not necessarily identical.

For the second set of non-trivial one-cocycles

$$\omega_L(\Omega, U) = \omega_R(\Omega, U)^* \quad \in \quad \left\{\omega_i(\Omega, U) \,|\, i = 11, 12, \ldots, 16\right\}, \tag{6.150}$$

we obtain a spectrum for which the ground state is four-fold degenerate. This is in contrast to both the YM theory and the other set of cocycles. The theory has an energy gap of $\Delta/(e^2) = 1$ between the ground state and the eight-fold degenerate first excited state. We summarize the entire spectrum of the model in Table 6.11. The explicit eigenstates for the two lowest energy levels of this theory are presented in appendix F for a particular choice of ω.

	$n=0$	$n=1$	$n=2$	$n=3$	$n=4$
$E_n/(e^2)$	2	3	6	7	8
g_n	4	8	20	24	8

Table 6.11: *Eigenvalues E_n and their degeneracies g_n, of the single-cross electric Hamiltonian H_{E_+} for the doubled $\bar{D}_2$ lattice theory constructed from the second set of cocycles. Note that the ground state is four-fold degenerated.*

	$\mathcal{C}_1$	$\mathcal{C}_2$	$\mathcal{C}_3$	$\mathcal{C}_4$	$\mathcal{C}_5$	$\mathcal{C}_6$	$\mathcal{C}_7$	$\mathcal{C}_8$	$\mathcal{C}_9$	$\mathcal{C}_{10}$	$\mathcal{C}_{11}$
$\omega_1(\Omega,U)=\omega_1(\Omega,U)^*$	Γ_1	Γ_1	Γ_1	Γ_1	Γ_1	Γ_1	Γ_1	Γ_1	Γ_1	Γ_1	Γ_1
$\omega_2(\Omega,U)=\omega_3(\Omega,U)^*$	Γ_1	Γ_1	Γ_1	Γ_1	Γ_1	Γ_2	Γ_2	Γ_2	Γ_3	Γ_3	Γ_3
$\omega_4(\Omega,U)=\omega_7(\Omega,U)^*$	Γ_1	Γ_1	Γ_1	Γ_4	Γ_7	Γ_1	Γ_4	Γ_7	Γ_1	Γ_4	Γ_7
$\omega_5(\Omega,U)=\omega_9(\Omega,U)^*$	Γ_1	Γ_1	Γ_1	Γ_5	Γ_9	Γ_5	Γ_9	Γ_1	Γ_9	Γ_1	Γ_5
$\omega_6(\Omega,U)=\omega_8(\Omega,U)^*$	Γ_1	Γ_1	Γ_1	Γ_6	Γ_8	Γ_8	Γ_1	Γ_6	Γ_6	Γ_8	Γ_1
$\omega_{10}(\Omega,U)=\omega_{11}(\Omega,U)^*$	Γ_1	Γ_1	Γ_1	Γ_6	Γ_8	Γ_9	Γ_2	Γ_4	Γ_5	Γ_7	Γ_3
$\omega_{12}(\Omega,U)=\omega_{13}(\Omega,U)^*$	Γ_1	Γ_1	Γ_1	Γ_2	Γ_3	Γ_4	Γ_5	Γ_6	Γ_7	Γ_8	Γ_9
$\omega_{14}(\Omega,U)=\omega_{15}(\Omega,U)^*$	Γ_1	Γ_1	Γ_1	Γ_2	Γ_3	Γ_5	Γ_6	Γ_4	Γ_9	Γ_7	Γ_8
$\omega_{16}(\Omega,U)=\omega_{17}(\Omega,U)^*$	Γ_1	Γ_1	Γ_1	Γ_2	Γ_3	Γ_6	Γ_4	Γ_5	Γ_8	Γ_9	Γ_7
$\omega_{18}(\Omega,U)=\omega_{19}(\Omega,U)^*$	Γ_1	Γ_1	Γ_1	Γ_4	Γ_7	Γ_2	Γ_5	Γ_8	Γ_3	Γ_6	Γ_9
$\omega_{20}(\Omega,U)=\omega_{21}(\Omega,U)^*$	Γ_1	Γ_1	Γ_1	Γ_4	Γ_7	Γ_3	Γ_6	Γ_9	Γ_2	Γ_5	Γ_8
$\omega_{22}(\Omega,U)=\omega_{23}(\Omega,U)^*$	Γ_1	Γ_1	Γ_1	Γ_5	Γ_9	Γ_4	Γ_8	Γ_3	Γ_7	Γ_2	Γ_6
$\omega_{24}(\Omega,U)=\omega_{25}(\Omega,U)^*$	Γ_1	Γ_1	Γ_1	Γ_5	Γ_9	Γ_6	Γ_7	Γ_2	Γ_8	Γ_3	Γ_4
$\omega_{26}(\Omega,U)=\omega_{27}(\Omega,U)^*$	Γ_1	Γ_1	Γ_1	Γ_6	Γ_8	Γ_7	Γ_3	Γ_5	Γ_4	Γ_9	Γ_2

Table 6.12: *27 (among the 81) allowed one-cocycles for the group $\Delta(27)$, which are related to each other by complex conjugation.*

6.3.6 Doubled $\Delta(27)$ Lattice Gauge Theory

6.3.7 One-Cocycles and W Factors

The one-cocycles ω of $\Delta\,(27)$ assign a 1-dimensional representation Γ_p (with $p = 1, 2, \ldots, 9$), to each conjugacy class of the group,

$$\omega(\Omega, U) = \Gamma_{p(C)}(\Omega). \tag{6.151}$$

$\Delta(27)$ has nine 1-dimensional representations and 11 conjugacy classes giving a total of $9^{11} \approx 31 \cdot 10^9$ possible one-cocycle candidates. The three conjugacy classes $\mathcal{C}_1$, $\mathcal{C}_2$, and $\mathcal{C}_3$, which together constitute the commutator subgroup (which again equals the center) $\mathcal{C}_{123} = \mathcal{C}_1 \cup \mathcal{C}_2 \cup \mathcal{C}_3 = Z\,(\Delta\,(27))$, are always associated with the same representation. Of the 9^{11} candidate one-cocycles there are 81 which satisfy the consistency condition of eq. (6.85). A representative subset of these are summarized in Table 6.12. Note that, since the representations of $\Delta\,(27)$ are related by complex conjugation, the one-cocycles are also related in this way. As for the previous groups, the W factors are in one-to-one correspondence with the one-cocycles. Again applying the gauge choice

	$n=0$	$n=1$	$n=2$	$n=3$	$n=4$	$n=5$
$E_n/(e^2)$	0	12	27/2	24	51/2	27
g_n	1	36	16	324	288	64

Table 6.13: *Eigenvalues E_n and their degeneracies g_n, of the single-cross electric Hamiltonian H_{E_+} for the doubled $\Delta(27)$ lattice YM theory. Note that the ground state is unique.*

of eq. (6.109) a single trivial doubled YM theory is associated with the cocycle ω_1, which yields

$$W(\Omega, \Omega') = 1. \tag{6.152}$$

The remaining one-cocycles ω_i, for $i = 2, 3, \ldots, 81$ give rise to non-trivial W factors which are of the form,

$$W(C, C') \in \{1, e^{2\pi i/3}, e^{-2\pi i/3}\}. \tag{6.153}$$

These are again split into two sets of theories with distinct spectra. As for the $\bar{D}_2$ case, it is worth to note that $W\left(\Omega, \Omega'\right) = 1$ when either Ω or Ω' belongs to the set C_{123}.

Trivial One-Cocycle

The energy levels for the trivial cocycle are presented in Table 6.13. The ground state of the trivially doubled lattice YM theory with energy $E_0/(e^2) = 0$ is non-degenerate and is given by the totally symmetric superposition involving the Γ_1 representation,

$$\left|E_0\right\rangle = \frac{1}{\sqrt{27}} \sum_{\widetilde{U} \in \Delta(27)} \left|\Gamma_1^{11}\right\rangle \otimes \left|\widetilde{U}\right\rangle. \tag{6.154}$$

The first excited energy level is 36-fold degenerate and is separated from the ground state by an energy gap of $\Delta/(e^2) = 12$.

Non-Trivial One-Cocycles

The energy levels for the first set of cocycles in Table 6.12,

$$\omega_L(\Omega, U) = \omega_R(\Omega, U)^* = \omega_i(\Omega, U), \quad i \in \left\{2, 3, \ldots, 9\right\}, \tag{6.155}$$

are summarized in Table 6.14. In contrast to the YM theory, the ground state is three-fold degenerate, and the first excited states are is again a 36-fold degenerate. Now separated from the ground state by an energy gap $\Delta/(e^2) = \sqrt{3}/2(9 - \sqrt{3}) \approx 6.294$. For a particular choice of cocycle, the explicit form of the three ground states is presented in appendix F.

The energy levels for the second set of non-trivial cocycles in Table 6.12 of,

$$\omega_L(\Omega, U) = \omega_R(\Omega, U)^* = \omega_i(\Omega, U), \quad i \in \left\{10, 11, \ldots, 27\right\}, \tag{6.156}$$

are summarized in Table 6.15. In contrast to both the YM and the other CS type theories, here the ground state is nine-fold degenerate, with an energy gap $\Delta/(e^2) = 3$ to the 36 fold degenerate first excited states. For a specific choice of cocycle, the explicit form of the nine ground states are presented in appendix F.

	$n=0$	$n=1$	$n=2$	$n=3$	$n=4$	$n=5$	$n=6$
$E_n/(e^2)$	$9/2(3-\sqrt{3})$	12	27/2	$9/2(3+\sqrt{3})$	24	51/2	27
g_n	3	36	12	3	324	288	63

Table 6.14: *Eigenvalues E_n and their degeneracies g_n of the single-cross electric Hamiltonian H_{E_+} for the doubled $\Delta(27)$ lattice CS type theory constructed from the first set of one-cocycles. Note that the ground state is three-fold degenerated.*

	$n=0$	$n=1$	$n=2$	$n=3$	$n=4$	$n=5$
$E_n/(e^2)$	9	12	18	24	51/2	27
g_n	9	36	9	324	288	63

Table 6.15: *Eigenvalues E_n and their degeneracies g_n of the single-cross electric Hamiltonian H_{E_+} for the doubled $\Delta(27)$ lattice CS type theory constructed from the second set of one-cocycles. Note that the ground state is nine-fold degenerate.*

6.3.8 Center Symmetry and Confinement

Using the energy spectra and applying the center symmetries of the different gauge groups, we are able to paint a picture of how external charge configurations behave in the strong-coupling regime. In particular, it is possible to construct different charge states and identify their energies. This allows us to decide whether these states exhibit charge confinement. The full analysis of the charges, that is an analysis that also includes the description of the relative statistical phases between charges, will, however, have to wait for a future study [136].

Charged States in the Doubled S_3 Lattice Gauge Theory

The doubled lattice gauge theory with gauge group S_3 has a trivial center $Z\left(S_3\right)=\left\{\mathbb{1}\right\}$ and contains both an Abelian and a non-Abelian charge, in the Γ_2 and Γ_3 representation, respectively. In addition to these two charges, the theory has a representation Γ_1, which is associated with a vanishing charge. We can uniquely specify any physical state by the corresponding charge assignments at every direct and dual lattice site. This gives rise to an electric flux configuration, for which we can determine the energies from the results in Table 6.6 and Table 6.7. We find that a lattice cross with either a single direct or dual Γ_3-flux has an energy Δ above the ground state where Δ is $3e^2/2$ and $3\left(\sqrt{2}-1\right)e^2/2\approx 0.621e^2$ for the YM and CS type theory, respectively. A lattice cross with both a direct and a dual Γ_3 flux, as described in Section 6.3.2, has an energy $\Delta+3e^2/2$. In the absence of the magnetic part of the Hamiltonian, states in the non-trivial CS type theory, which only contain Abelian Γ_2 charges, carry the same energy as the vacuum, since the ground state is a mixture of Γ_1 and Γ_2 fluxes. This is not the case for the YM type theory. States that contain a non-Abelian Γ_3 charge, on the other hand, are separated from the ground state by multiples of the energy gap Δ. In the strong coupling limit, this gap goes to infinity, and we only have to consider the lowest-energy states for any charge sector. Since the group S_3 has a trivial center, flux strings with the gauge group S_3 theories can be broken and reconnected into closed loops. In both the YM

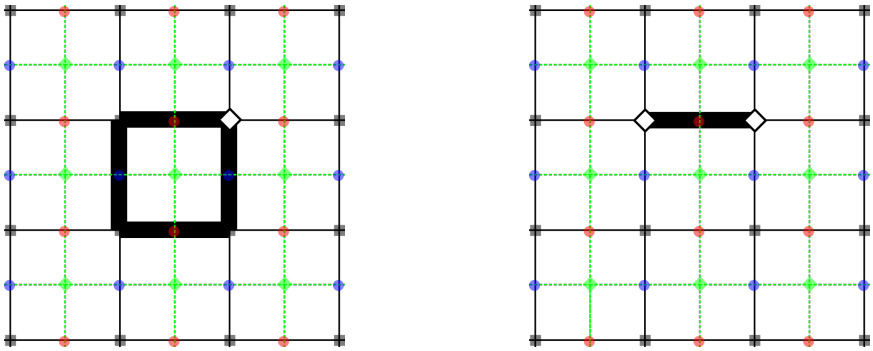

Figure 6.6: *(Left) S_3 has a trivial center and can therefore support a single Γ_3 charge. For a single Γ_3 charge, the energetically favourable electric-flux configuration has four units of Γ_3 electric flux along an elementary plaquette. (Right) Two non-Abelian Γ_3 charges connected by a single Γ_3 flux string.*

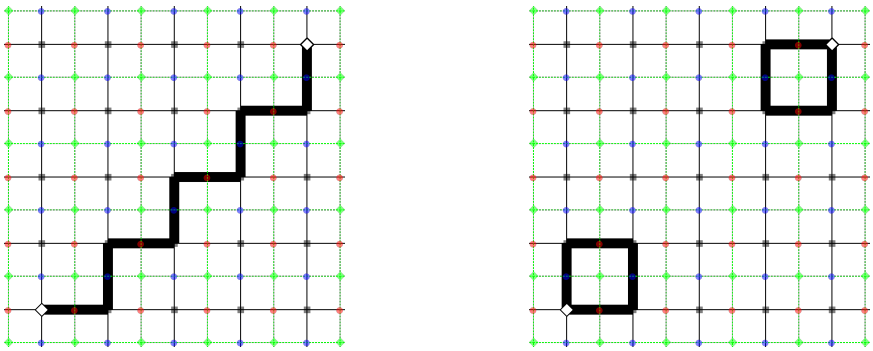

Figure 6.7: *Flux string breaking is possible since S_3 has a trivial center. Left: Two direct Γ_3 charges joined by a string of length 8 with $E = 8\Delta$. Right: Two direct Γ_3 charges no longer confined to each other with the same energy $E = 8\Delta$.*

and the CS theories with gauge group S_3, we are therefore able to construct states that only contain a single charge connected to a closed loop of Γ_3 electric flux. Representing a direct Γ_3-charge by an open diamond and a Γ_3 direct flux by a bold link, the realization of such a state is shown in Figure 6.6 (left). A state consisting of two direct or dual Γ_3 charges, separated by one lattice spacing and connected by a single link flux string, costs an additional energy Δ above the ground state. This is illustrated in Figure 6.6 (right) for the case of two direct Γ_3-charges. Since the energy of such a state grows by Δ for every link carrying a Γ_3-flux, the energy grows linearly with the number of connecting Γ_3 electric flux links. This implies that at short distances, the lowest energy state of two Γ_3 contains a confining string. When the charges are separated by eight or more lattice spacings, the string can break and is replaced by two separate flux loops attached to the individual charges. This is illustrated in Figure 6.7 where the states on the left- and on the right-hand side have the same flux energy of $E = 8\Delta$ above the ground state. Therefore, from this picture, two Γ_3-charges are confined by a flux string, only as long as they are not separated by more than eight lattice spacings. At larger separations the charges are deconfined and can move freely. This is how the charges behave in the strong coupling limit. To obtain a complete picture beyond that limit, one

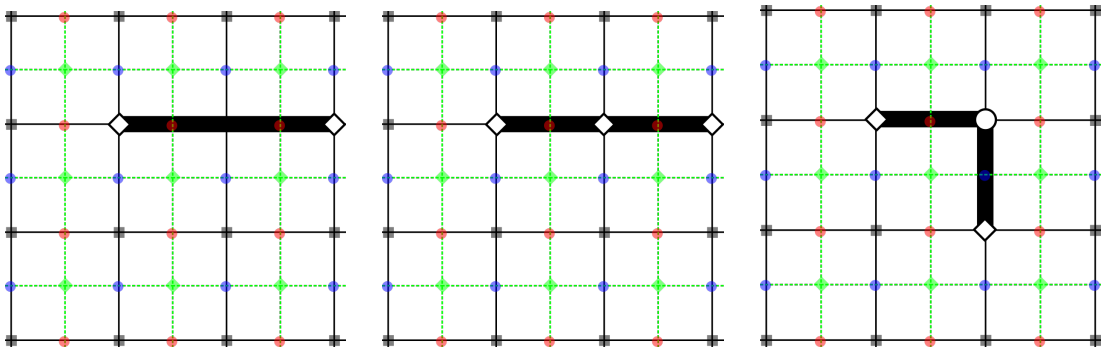

Figure 6.8: *Possible realizations of states with two* Γ_3 *direct fluxes. In the CS type theory all three configurations have an energy of* 2Δ*. In the YM type theory only the left and the center configurations have an energy of* 2Δ*, while the right configuration has a higher energy. Left: Two direct* Γ_3 *charges connected by two* Γ_3 *direct fluxes. Center: Three direct* Γ_3 *charges connected by two* Γ_3 *direct fluxes. Right: For the CS type theory a* Γ_2 *charge (open circle) can be inserted at no additional energy cost.*

would have to perform Monte Carlo simulations, which would be an interesting challenge for the future. It should be noted that a state containing a fixed number of Γ_3 fluxes, all of them on either the direct or the dual, can be realized in different ways. This is illustrated in Figure 6.8 (left) where a state with two Γ_3 fluxes (and therefore an energy of 2Δ) is illustrated. For both the YM and the CS type theories, we can insert an additional Γ_3 charges along the flux lines. This is illustrated in Figure 6.8 (center) where an additional Γ_3 direct charge has been inserted without additional energy cost. In the CS type theory the additional Γ_2 charges can be inserted at no additional cost in energy. In Figure 6.8 (right) we have inserted an additional direct Γ_2-charge (open circle) between the two direct Γ_3 charges. This cost additional energy in the YM type theory, but not in the CS type theory. In addition to the charge configurations considered above, where all the charges were residing on the same sublattice, it is also possible to have a single Γ_3 direct charge together with a Γ_3 dual charge. For a pair of direct and dual Γ_3-charges there are two distinct flux configurations. These are distinguished by whether the direct and dual flux loops are crossing each other on a single lattice cross. A state with crossed fluxes is illustrated in Figure 6.9 (left), where a pair of neighbouring direct and dual Γ_3 charges contains a flux encircling the other charge. Using Table 6.6 and Table 6.7 this flux configuration is found to have an energy of $E_{\square} = 6\Delta + 6e^2$. As an alternative to this flux configuration, the same set of charges can be realized without flux crossing. This is illustrated in Figure 6.9 (right). Again the energy of this configuration follows from the results in Table 6.6 and Table 6.7 and is given by $E_{\square\,\square} = 8\Delta$. For the YM type theory $\Delta_{YM} = 3e^2$, which implies that the two flux configurations have the same energy. For the CS type theory we have $\Delta_{CS} < 3e^2$ which implies the right-hand side of Figure 6.9 is energetically favourable. This means that a pair of direct and dual charges does not stick together, but is repulsive in the CS type theory.

We obtain a similar result when considering flux-strings connecting a pair of Γ_3 direct charges and a pair of Γ_3 dual charges. Again in the CS type theory the non-crossing direct and dual string-fluxes are energetically favoured. In the YM type theory there is no energetic distinction between states with crossing or non-crossing direct and dual flux-strings.

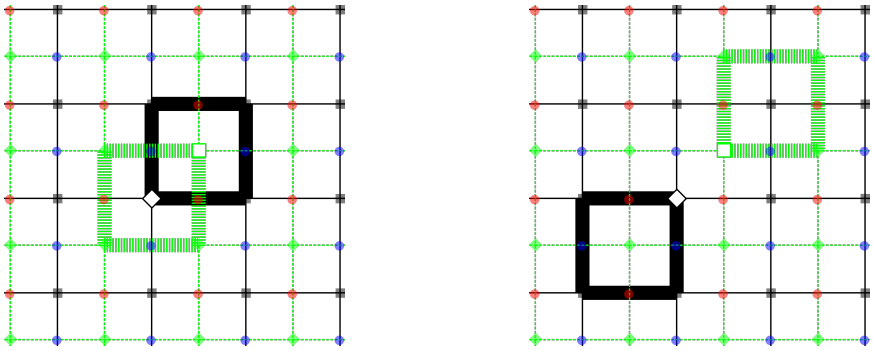

Figure 6.9: *Flux dual flux repulsion. Left: Joined charge and dual charge;* $E_{\square\!\square} = 6\Delta + 6e^2$. *Right: Free charge and dual charge;* $E_{\square\ \square} = 8\Delta$.

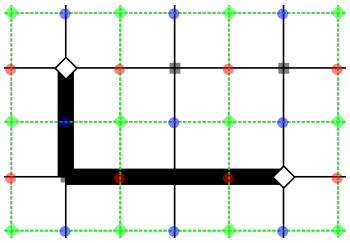

Figure 6.10: *Charged excitation for gauge group* $\bar{D}_2$*, consisting of two* Γ_5 *charges connected by a confining electric flux string.*

Charged States in the Doubled $\bar{D}_2$ Lattice Gauge Theory

The doubled $\bar{D}_2$ gauge theory has a center $Z\left(\bar{D}_2\right) = \mathbb{Z}(2) = \left\{\pm\mathbb{1}\right\}$ and contains three types of Abelian charges, associated with the 1-dimensional representations Γ_2, Γ_3, and Γ_4, together with a single non-Abelian charge associated with the 2-dimensional Γ_5 representation, which transforms non-trivially under the $\mathbb{Z}(2)$ center. Since, unlike for the group S_3, the center of $\bar{D}_2$ is non-trivial, we cannot have a single Γ_5-charge in this theory. Two Γ_5-charges are always connected by an unbreakable Γ_5 flux string, which costs an energy Δ per link (see Table 6.9, Table 6.10 and Table 6.11). This is illustrated in Figure 6.10 for two direct Γ_5-charges (open diamonds) connected by three links carrying a Γ_5 flux (bold link). Since the electric flux string cannot break, and the energy grows linearly with the length, the theory is confining.

Charged States in the Doubled $\Delta(27)$ Lattice Gauge Theory

The center of $\Delta(27)$ is $Z(\Delta(27)) \cong \mathbb{Z}(3)$ and the theory admits eight Abelian charges, associated with the 1-dimensional representations Γ_2, Γ_3, …, Γ_9. In addition, there are two non-Abelian charges associated with the 3-dimensional representations Γ_{10} and Γ_{11}, which transform non-trivially under the center. Since the theory has a non-trivial center, no single Γ_{10}- or Γ_{11}-charge excitation can exist in the $\Delta(27)$-theory. Since the center is complex, the electric flux lines are directed and the lowest-energy charge excitations are therefore a pair of Γ_{10} and $\Gamma_{11} = \overline{\Gamma}_{10}$ charges connected by a string of electric flux. This is illustrated in Figure 6.11 (left), where the two charges

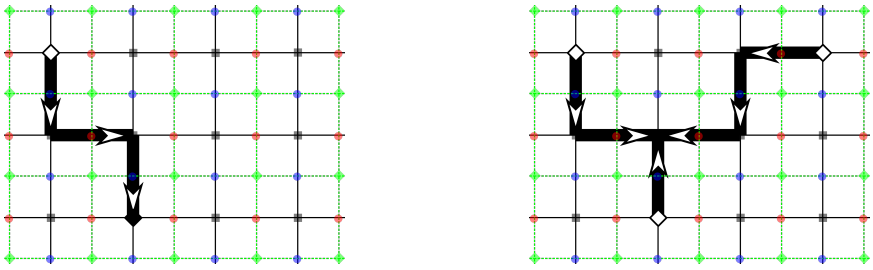

Figure 6.11: Γ_{10}- *(open diamond) and* Γ_{11}*-charge (black diamond) excitations for the gauge group* $\Delta(27)$*. Due to the non-trivial center* $Z(\Delta(27)) \cong \mathbb{Z}(3)$ *charges which transform non-trivially under the center are bound into either antiparticle particle (left), or three-particle states (right), where the individual components are confined by a directed electric flux string.*

are separated by three links, each with an electric flux directed from the Γ_{10} (open diamond) to the Γ_{11} (black diamond). The energy cost of each link carrying an electric flux results from Table 6.13, Table 6.14 and Table 6.15. The center also admits the possibility of joining three charges (either Γ_{10} or Γ_{11}) together such that three electric-flux strings meet at a lattice site. This is illustrated in Figure 6.11 (right) for three Γ_{10} charges.

Chapter 7

Conclusion

In this thesis, we have studied two different aspects of lattice QFT, both concerning theories with discrete Hilbert spaces in relation to quantum information. Since a discrete Hilbert space can be mapped to ultracold atoms trapped in an optical lattice, these theories lends themselves well to a possible realization in the laboratory.

In the first part of the thesis we studied the $SU(2)$ QLM. We started in Chapter 3 by constructing the $SU(2)$ QLM in the rishon formulation, and created a site-based basis for the model. We used this basis to construct the most general gauge-invariant ring-exchange Hamiltonian associated with an elementary plaquette, that respects the lattice symmetries. We did this for both the honeycomb, and the square lattice for the two lowest representations (the $\{4\}$-, and $\{5\}$-representation) of the $so(5)$ embedding algebra, corresponding to one or two rishons residing on each link, respectively. We parametrized these Hamiltonians in terms of 12 and 20 parameters for the $\{4\}$- and $\{5\}$-representation, respectively. For the square lattice we constructed a method for performing exact diagonalizations for lattice sizes up to 4×4. As a proof of concept, we presented data for two Hamiltonians. One for the $\{4\}$- and one for the $\{5\}$-representation. Here we interpolated from a Hamiltonian transition with only environment singlets to a Hamiltonian transition with only environment doublets. For the $\{4\}$-representation we found that the spectrum is symmetric around zero. The ground state on the 2×2 lattice has center quantum numbers $Z_x = Z_y = -1$, and comes with a vanishing momentum. The first excited state comes with the same center quantum numbers, and with a momentum of $(\pi/a, \pi/a)$. On the 4×4 lattice the ground state and the first excited state have the same momentum. The center quantum numbers are here both changed to a trivial $Z_x = Z_y = +1$. This change was found to be an effect of the $\{4\}$-representations. On the 4×4 lattice, the two states were found to be degenerate for Hamiltonians favouring environment singlet transitions, and splitting up into two levels when the Hamiltonian is favouring doublet transitions. The ground state is still the state with vanishing momentum. In the $\{5\}$-representation a similar spectrum was found. Again the spectrum is symmetric around zero. In contrast to the $\{4\}$-representation, the ground state and the first excited state both have trivial center quantum numbers $Z_x = Z_y = +1$, for both the 2×2, and the 4×4 lattice. The lowest state comes with vanishing momentum and the first excited state with a momentum $(\pi/a, \pi/a)$. The states are not degenerate in the $\{5\}$-representation. There is a very large parameter space for which the exact diagonalization method can be employed, and we have barely scratched the surface here. The algorithm for exact diagonalization is fast enough to perform quick scans of parameter space. It would

be most interesting for a future study to perform a more detailed investigation of the parameter space. Additionally, here we have only employed the exact diagonalization on even-size lattices, and it would be interesting to investigate the behaviour of odd-sizes lattice as well. With a bit more ingenuity and work, it should also be possible to extend the analysis to larger lattices, than what have been employed here. There is clearly much more to be found here, and this is a method that deserves more attention in the future.

In Chapter 4, we constructed a $\mathbb{Z}(2)$ height-variable description of the $SU(2)$ QLM on the honeycomb lattice for the lowest $\{4\}$-representation, which corresponds to the dimer model on the Kagomé lattice in the zero-charge sector. We constructed both a standard Metropolis algorithm, and an efficient cluster algorithm for simulating the model. We identified three different phases. Two distinct pinwheel phases, with correlated and uncorrelated pinwheel rotations, defined on four sublattices, and an anti-pinwheel phase living on a larger sublattice division. For the pinwheel phases, we identified the parameter region on which the phase transition takes place, although based on our Monte Carlo data it is presently impossible to unambiguously identify the order of the phase transition. In addition, for both pinwheel phases we found that a single $\mathbb{Z}(2)$ flux splits into two domain walls, each associated with a fractionalized flux. Introducing external charges, we observed two fractionalized flux strands connecting the two charges in the correlated pinwheel phase, but not in the uncorrelated pinwheel phase, at least not for the lattice sizes and charge separations considered here. The charges are confined by a linearly rising potential as a function of the charge separation. For the anti-pinwheel phase we identified the parameter region in which the phase transition, between the correlated pinwheel phase and the anti-pinwheel phase, takes place. At the moment, it is again not possible to determine the order of the phase transition. The results presented here are currently being prepared for publication.

In this part of the thesis we have only considered the two lowest representations of the $SU(2)$ QLM. The method for constructing higher representations is straightforward in the rishon formulation, and it would be interesting to consider the model with higher representations. The height variable formulation will, however, not be applicable for any but the two lowest representations, and one would have to make use of a different technique for simulating higher representations. Likewise, it would be most interesting to extend the analysis to an $SU(3)$ QLM.

In the second part of the thesis we have constructed Chern-Simons models on a doubled lattice consisting of the direct lattice and its dual lattice. In standard lattice gauge theory, where the fundamental degrees of freedom are based on the lattice links, there exists a "mechanical" analogue for a lattice link. This is given by a "particle" moving in the group space, i.e. a "particle" moving on a circle for a compact Abelian $U(1)$ lattice gauge theory. For our doubled compact Chern-Simons-Maxwell theory, where the fundamental degrees of freedom are based on the cross formed by a link and its intersecting dual link, we found that the "mechanical" analogue is a charged "particle" moving on a torus $U(1)^2$, threaded by an abstract "magnetic" flux proportional to the Chern-Simons level k. This led to the Dirac quantization condition of the abstract "magnetic" field, and implied that the Chern-Simons level must be quantized in integer units $k \in \mathbb{Z}$. We were further able to show that a $\mathbb{Z}(k)$ variant of the toric code is intricately related to this model. The toric code is obtained in the infinite "photon" mass limit of the model.

We furthermore found that the cross-based electric contribution to the Hamiltonian possesses two self-adjoint extension parameters θ and $\widetilde{\theta}$, which form two non-dynamical background $U(1)$ lattice gauge fields. For a fixed background field the two self-adjoint extension parameters specify

a domain of the Hamiltonian, where only $\mathbb{Z}(k)$ gauge symmetry was found to remain as a manifest remnant of the $U(1)$ gauge symmetry. Only a $\mathbb{Z}(k)$, in contrast to the full $U(1)$ Gauss' law, must be imposed on physical states in a given domain of the Hamiltonian. The explicit symmetry breaking from $U(1)$ to $\mathbb{Z}(k)$ is not present at the classical level, which is not sensitive to the external self-adjoint extension parameters which results from Aharonov-Bohm phases, and the symmetry breaking is of quantum mechanical origin. This led us to ask whether this quantum mechanical gauge symmetry breaking should be viewed as an "anomaly". The description of this symmetry breaking as an anomaly is, however, not completely appropriate, and this breaking is something more than just a standard anomaly. As was noted in Section 5.3.2, when we considered the symmetry breaking the original redundancy associated with the $U(1)$ gauge symmetry of the classical theory still persists at the quantum level. Here it manifests itself in the $U(1)$ gauge redundancy of the external background lattice gauge fields, formed by the two self-adjoint extension parameters. We have made no attempt to take the continuum limit by sending $e^2a \to 0$. The full $U(1)$ gauge symmetry may in fact re-emerge dynamically from the manifest $\mathbb{Z}(k)$ symmetry in the continuum limit. This would reduce the lattice theory to the non-compact doubled Chern-Simons-Maxwell continuum theory that we started out with in Section 5.1.2.

Only the magnetic, and not the electric, field energy depends on the self-adjoint extension parameters. As we noted, for the $\mathbb{Z}(k)$ toric code in the infinite "photon" mass limit $e^2 \to \infty$, the magnetic field energy is suppressed by a factor of $\left(e^2a^2\right)^{-1}$, and the dependence of the energy on the self-adjoint extension parameters disappears. Although in this limit the energy is independent of the extension parameters, the wave function itself still depends on θ and $\widetilde{\theta}$. As a result, we found that the toric code possesses a large variety of hidden self-adjoint extension parameters, that form two $U(1)$ gauge fields associated with the direct and the dual lattice.

It was further found that under adiabatic changes of the parameters θ and $\widetilde{\theta}$, an $U(k)$ Berry gauge field arises with a non-trivial Berry curvature. This Berry field strength turned out to be gauge equivalent to an Abelian field strength, and the corresponding Berry phases will therefore not allow universal topological quantum computation, and will thus be of limited use. Still, it is interesting to further investigate whether manipulating these parameters can be utilized for other forms of quantum information processing. This is a subject for future investigations.

In Chapter 5 we encountered numerous (abstract) gauge fields. First of all, the non-compact Chern-Simons-Maxwell theory was introduced in terms of the Abelian gauge fields A and $\widetilde{A}$. Upon compactification of the gauge group, the two fields were replaced by the compact $U(1)$ lattice gauge fields φ and $\widetilde{\varphi}$. The group space of an original and a dual cross-based link-pair $U(1)^2$ was endowed with an abstract vector potential $(a, \widetilde{a})$ that describes the quantized "magnetic" flux represented by the level $k \in \mathbb{Z}$. The two Polyakov loops winding around the group space torus $U(1)^2$ then gave rise to two self-adjoint extension parameters θ and $\widetilde{\theta}$, each playing the role of Aharonov-Bohm phases for the "particle" in the "mechanical" analogue moving in the group space. At the classical level these parameters are invisible, although at the quantum level the two parameters break the manifest gauge symmetry from $U(1)$ down to $\mathbb{Z}(k)$. The self-adjoint extension parameters themselves turned out to be non-dynamical background lattice gauge fields, associated with the original and the dual lattice. The full $U(1)$ redundancy of the gauge description is still present in the theory. An extended version of the toric code emerged at low energies, as a $\mathbb{Z}(k)$ lattice gauge theory. Finally, by considering adiabatic changes of the self-adjoint extension parameters $U(k)$ Berry gauge fields appeared, which are defined over the base space of the lattice gauge fields θ and $\widetilde{\theta}$. All these different gauge structures are closely related to each other, and they deserve to

be studied further in the future. In particular, it is worth to study them in the context of quantum information processing.

Throughout Chapter 5, we repeatedly stated how the systems can be described in terms a corresponding "mechanical" analogue. For the compact doubled lattice Chern-Simons-Maxwell theory this is as a "particle" moving in the cross-based group space torus $U(1)^2$, threaded by k units of quantized "magnetic" flux. An interesting question is whether such a mechanical analogue might be possible to construct in the laboratory. This would lead to an interesting method to investigate the behaviour of such a system, in order to manipulate quantum information. Actually building a real physical torus with the required properties seems like a difficult task, but one might be able to construct a similar system using trapped ions. Already by using digital quantum simulations with up to 100 quantum gate operations [138], this has been achieved for a single plaquette of the standard $\mathbb{Z}(2)$ toric code [139]. Inspired by the ingenuity of experimentalists we wonder whether it is possible to obtain similar results for the extended toric code described here.

In Chapter 6, we extended several results from the previous chapter to the non-Abelian case. It was shown how to realize Hamiltonians for non-Abelian lattice gauge theories, that are compatible with a non-commuting algebra of group multiplication operators, and therefore lead to theories of the Chern-Simons type. The construction considered here relies on the identification of one-cocycles of the gauge group, which represent the action of gauge transformations on quantum states. We found that these cocycles are in one-to-one correspondence with an Aharonov-Bohm phase, which is introduced in the group space on a lattice cross. Here we defined all the possible theories within the considered class of Hamiltonians. We furthermore constructed the explicit Hamiltonians for the finite Abelian gauge group $\mathbb{Z}(k) \subset U(1)$, and for three finite non-Abelian gauge groups $S_3 \subset O(2)$, $\bar{D}_2 \subset SU(2)$, and $\Delta(27) \subset SU(3)$. For these gauge groups we characterized the behaviour in the strong coupling limit for which the theory can be solved exactly. In particular, we showed that the doubled lattice theories of the Chern-Simons type, when projected onto the lowest-energy eigenstates are mapped to a (generalized) toric code. Finally, it was shown how the two gauge groups $\bar{D}_2$ and $\Delta(27)$, which both have a non-trivial center, lead to confining gauge theories. For the S_3 gauge group the flux string connecting two charges, is energetically favoured to break when the charges are separated by 8 or more lattice spacings, but otherwise holds the charges together. This is potentially useful to control finite temperature errors [42, 140, 141, 142, 143, 144, 145] in quantum information processing. The question whether the charges considered here are indeed anyons, let alone non-Abelian anyons, have not yet been answered conclusively and an analysis of their braiding properties, awaits further investigations [136].

Appendix A

States with 0, 1, or 2 Rishons per Link

Here we present the explicit link states, for all representations containing up to two rishons per link. This includes both fermionic and bosonic rishons. Weight diagrams are included for each representation, which show how the different states are related through the U^{ij} operators of eq. (3.36). We include the factors that the states obtain under the U^{ij} operators. The states are presented in the tables in pictorial form, where a rishon of type 1(2) is presented as an upward(downward) arrow. The overall colour charge at each end of the link is presented for each of the states, together with the total colour charge magnitude on the lattice link.

A.1 Fermionic Rishons

The states must be antisymmetric under exchange of two rishons.

A.1.1 0 Rishons $\{1\}_1$-Representation

A link with no rishons can only be in the trivial vacuum state, $\left|1\right\rangle_{\{1\}_1}$. This state is presented in Table A.1 and the corresponding weight diagram is presented in Figure A.1.

A.1.2 1 Rishon $\{4\}$-Representation

A single rishon gives rise to four independent states on a link. The rishon can either be of type 1 or 2 and can reside on either end of the link. The total colour charge-magnitude on the link is

State	$\lvert L\rvert$	$\lvert R\rvert$	L^3	R^3	$\lvert L\rvert+\lvert R\rvert$
$\left\|1\right\rangle_{\{1\}_1}$ ≡	0	0	0	0	0

Table A.1: *States with 0 rishons on a link.*

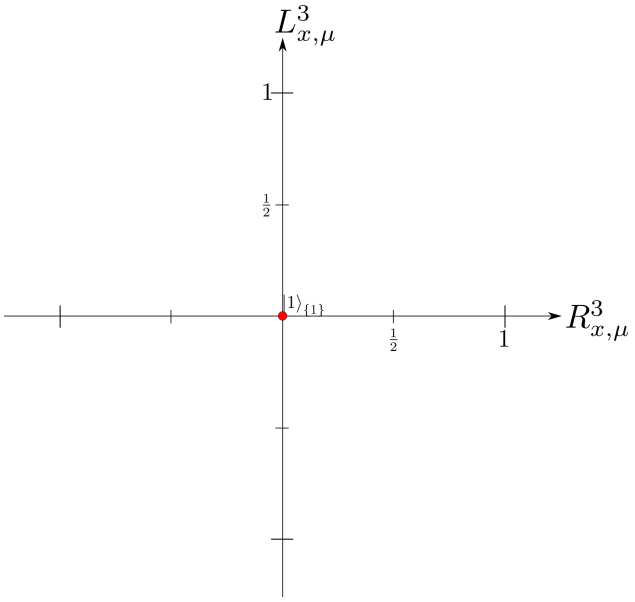

Figure A.1: *Weight diagram for the* $\{0\}$*-representation of a link without rishons on the link, as given in Table A.1.*

State			$\lvert L\rvert$	$\lvert R\rvert$	L^3	R^3	$\lvert L\rvert + \lvert R\rvert$
$\lvert 1\rangle_{\{4\}}$	$\equiv$	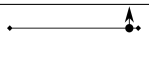	0	$\frac{1}{2}$	0	$+\frac{1}{2}$	$\frac{1}{2}$
$\lvert 2\rangle_{\{4\}}$	$\equiv$		0	$\frac{1}{2}$	0	$-\frac{1}{2}$	$\frac{1}{2}$
$\lvert 3\rangle_{\{4\}}$	$\equiv$	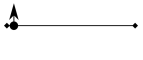	$\frac{1}{2}$	0	$+\frac{1}{2}$	0	$\frac{1}{2}$
$\lvert 4\rangle_{\{4\}}$	$\equiv$		$\frac{1}{2}$	0	$-\frac{1}{2}$	0	$\frac{1}{2}$

Table A.2: *States with 1 rishons on a link.*

thus always $\frac{1}{2}$. These states are presented in Table A.2 and the corresponding weight diagram is presented in Figure A.2.

A.1.3 2 Rishons $\{5\}$-Representation

Two rishons on a single link allow for five independent states. Four states, $\big|1\big\rangle_{\{5\}}$ to $\big|4\big\rangle_{\{5\}}$, have one rishon at each end of the link. These states have a total spin magnitude 1 with a spin $\frac{1}{2}$ at each end. In addition to these four states, a single state $\big|5\big\rangle_{\{5\}}$ exists, which is a superposition of states with two rishons combined to a singlet at each end of the link. This state has a spin magnitude of 0 at each end. These states are presented in Table A.3 and the corresponding weight diagram is presented in Figure A.3.

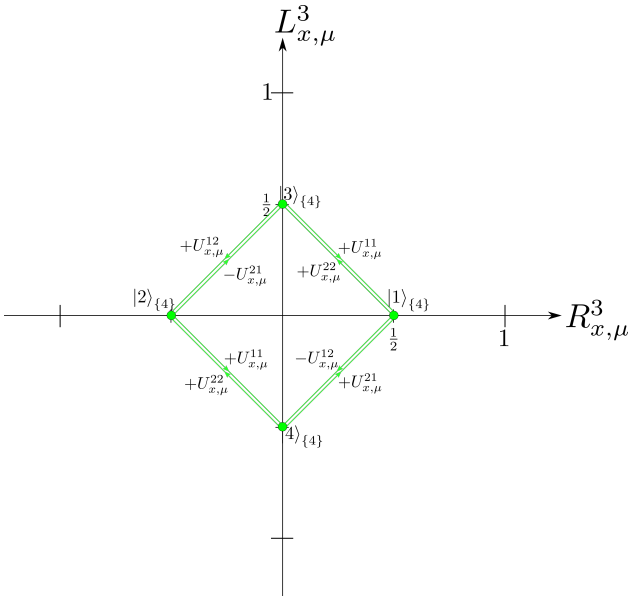

Figure A.2: *Weight diagram for the* $\{4\}$*-representation with a single rishon on the link, as given in Table A.2.*

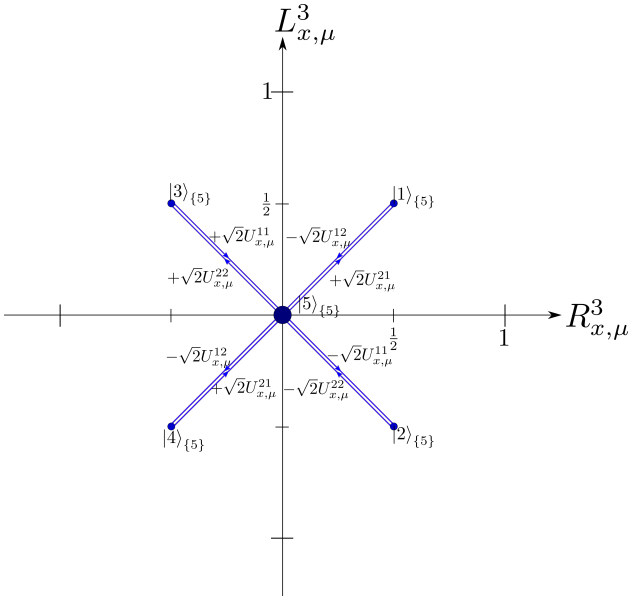

Figure A.3: *Weight diagram for the* $\{5\}$*-representation with two rishons on the link, as given in Table A.3.*

State	$\|L\|$	$\|R\|$	L^3	R^3	$\|L\|+\|R\|$
$\|1\rangle_{\{5\}} \equiv$ 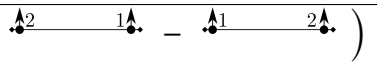	$\frac{1}{2}$	$\frac{1}{2}$	$+\frac{1}{2}$	$+\frac{1}{2}$	1
$\|2\rangle_{\{5\}} \equiv$ 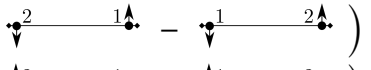	$\frac{1}{2}$	$\frac{1}{2}$	$-\frac{1}{2}$	$+\frac{1}{2}$	1
$\|3\rangle_{\{5\}} \equiv$ 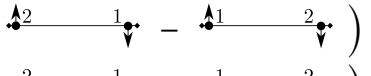	$\frac{1}{2}$	$\frac{1}{2}$	$+\frac{1}{2}$	$-\frac{1}{2}$	1
$\|4\rangle_{\{5\}} \equiv$ 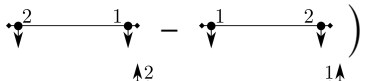	$\frac{1}{2}$	$\frac{1}{2}$	$-\frac{1}{2}$	$-\frac{1}{2}$	1
$\|5\rangle_{\{5\}} \equiv$ 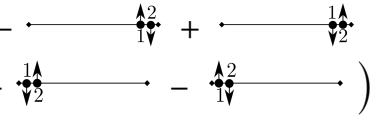	0	0	0	0	0

Table A.3: *States of 2 antisymmetric rishons on a link, i.e. the* $\{5\}$*-Representation.*

State	$\|L\|$	$\|R\|$	L^3	R^3	$\|L\|+\|R\|$
$\|1\rangle_{\{1\}_2} \equiv$ 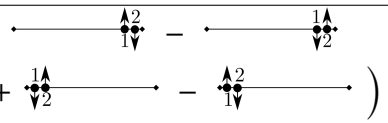	0	0	0	0	0

Table A.4: *States of two symmetric colour singlets on a link.*

A.2 Bosonic Rishons

For completeness, let us also consider for bosonic rishons (see [19]). Then there are two additional representations with two rishon on a link. These are states that are symmetric under the exchange of the two rishons.

A.2.1 2 Rishons Singlet $\{1\}_2$-Representation

Two singlets at each end of the link can be combined symmetrically under exchange, providing a bosonic representation with a single state. This state is presented in Table A.4, and the corresponding weight diagram is given in Figure A.4.

A.2.2 2 Rishons Triplet $\{10\}$-Representation

The two rishons on a link can be combined to a colour triplet, giving rise to 10 possible states. These states are presented in Table A.5 and the corresponding weight diagram is presented in Figure A.5.

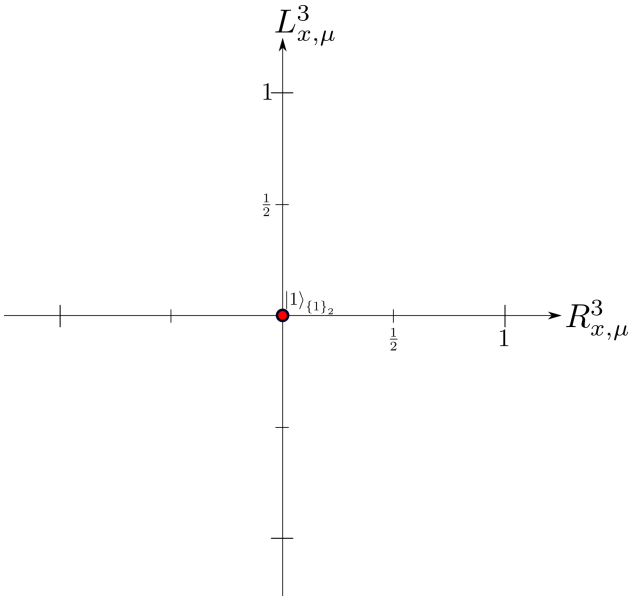

Figure A.4: *Weight diagram for the* $\{1\}_2$*-representation with two rishons on the link, as given in Table A.4.*

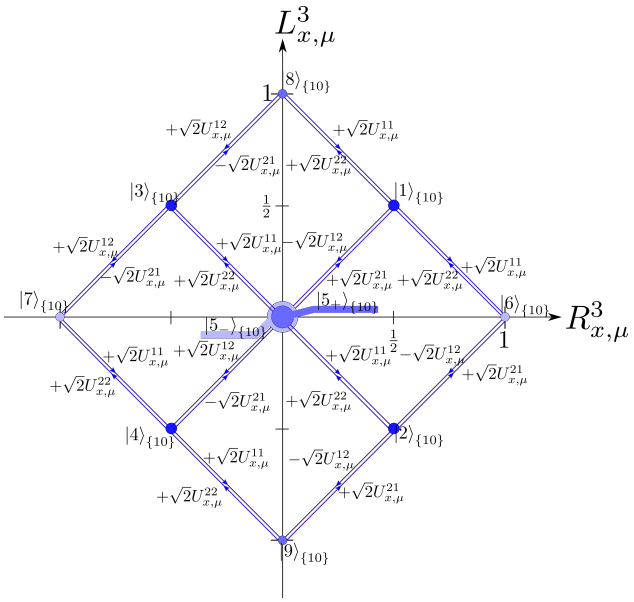

Figure A.5: *Weight diagram for the* $\{10\}$*-representation with two rishons on the link, as given in Table A.5.*

State			$\|L\|$	$\|R\|$	L^3	R^3	$\|L\|+\|R\|$
$\|1\rangle_{\{10\}}$	$\equiv$	$\frac{1}{\sqrt{2}}\Big($ $\Big)$	$\frac{1}{2}$	$\frac{1}{2}$	$+\frac{1}{2}$	$+\frac{1}{2}$	1
$\|2\rangle_{\{10\}}$	$\equiv$	$\frac{1}{\sqrt{2}}\Big($ $\Big)$	$\frac{1}{2}$	$\frac{1}{2}$	$-\frac{1}{2}$	$+\frac{1}{2}$	1
$\|3\rangle_{\{10\}}$	$\equiv$	$\frac{1}{\sqrt{2}}\Big($ $\Big)$	$\frac{1}{2}$	$\frac{1}{2}$	$+\frac{1}{2}$	$-\frac{1}{2}$	1
$\|4\rangle_{\{10\}}$	$\equiv$	$\frac{1}{\sqrt{2}}\Big($ $\Big)$	$\frac{1}{2}$	$\frac{1}{2}$	$-\frac{1}{2}$	$-\frac{1}{2}$	1
$\|5_+\rangle_{\{10\}}$	$\equiv$	$\frac{1}{2}\Big($ 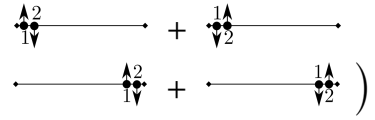 $\Big)$	-	-	-	-	1
$\|5_-\rangle_{\{10\}}$	$\equiv$	$\frac{1}{2}\Big($ 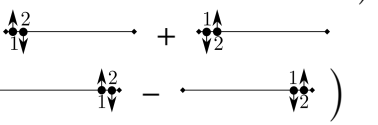 $\Big)$	-	-	-	-	1
$\|6\rangle_{\{10\}}$	$\equiv$		0	1	0	1	1
$\|7\rangle_{\{10\}}$	$\equiv$	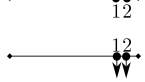	0	1	0	-1	1
$\|8\rangle_{\{10\}}$	$\equiv$	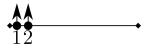	1	0	1	0	1
$\|9\rangle_{\{10\}}$	$\equiv$	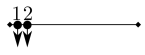	1	0	-1	0	1

Table A.5: *States of 2 symmetric rishons combined to triplets on a link.*

Appendix B

Site-Based States

The states of the $\{4\}$- and $\{5\}$-representation of the $SU(2)$ QLM can be constructed in both a link-based and a site-based representation. To obtain a physical state in the link-based representation, Gauss' law is imposed on each lattice site. In the site-based representation, Gauss' law is built directly into the states residing on the sites. Here each site-state is explicitly constructed as a colour singlet. This, however, introduces a new constraint into the system: the number of rishons per link must satisfy the constraint imposed by the chosen representation. For the $\{4\}$-representation there must be exactly 1 rishon on each link and for the $\{5\}$-representation there must be either 0 or 2 rishons on each link.[1]

The explicit formulas for the site-states are given below for the square and the honeycomb lattice sites. Here the subscripts represent the link that the rishon is residing on. The $|0\rangle$ state represents that there are no rishon residing on the site from that link. In other words, for the $\{4\}$-representation the rishon is residing at the other end of the link, and for the $\{5\}$-representation that there are no rishons residing on the link. The up (down) arrow represent the standard rishon notation introduced in Chapter 3. For each singlet pair there is an overall phase factor, this phase is represented by a light arrow.

B.1 Square Lattice

On the square lattice an overall singlet state can be obtained by either 0, 2, or 4 rishons residing at the site. The state of 0 rishons is trivially a singlet. For two rishons on a site the state is uniquely defined up to the overall phase. Note that state (3) and (6) obtain a change of sign under a 180° rotation. The remaining 4 states rotates into each other. For 4 rishons residing on a site there are two possible method to construct an overall singlet. State (8) is constructed by combining link 1 and 3 (2 and 4) into singlets, and then trivially combine the two singlets into an overall singlet on the site. State (9) is constructed by combining link 1 and 3 (2 and 4) into triplets represented by light ovals. These triplets are then combined into an overall singlet on the site. These states are presented in Table B.1.

[1] Recalling that a link carrying a superposition of two rishons combined into overall singlets at each end of the link, is also said to have no rishons.

#	Picture	Explicit Formula
(1)	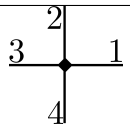	$\|0\rangle_1\|0\rangle_2\|0\rangle_3\|0\rangle_4$
(2)	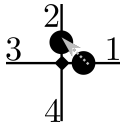	$\frac{1}{\sqrt{2}}\left(\|\uparrow\rangle_1\|\downarrow\rangle_2\|0\rangle_3\|0\rangle_4 - \|\downarrow\rangle_1\|\uparrow\rangle_2\|0\rangle_3\|0\rangle_4\right)$
(3)	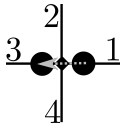	$\frac{1}{\sqrt{2}}\left(\|\uparrow\rangle_1\|0\rangle_2\|\downarrow\rangle_3\|0\rangle_4 - \|\downarrow\rangle_1\|0\rangle_2\|\uparrow\rangle_3\|0\rangle_4\right)$
(4)	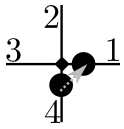	$\frac{1}{\sqrt{2}}\left(\|\downarrow\rangle_1\|0\rangle_2\|0\rangle_3\|\uparrow\rangle_4 - \|\uparrow\rangle_1\|0\rangle_2\|0\rangle_3\|\downarrow\rangle_4\right)$
(5)	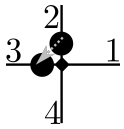	$\frac{1}{\sqrt{2}}\left(\|0\rangle_1\|\uparrow\rangle_2\|\downarrow\rangle_3\|0\rangle_4 - \|0\rangle_1\|\downarrow\rangle_2\|\uparrow\rangle_3\|0\rangle_4\right)$
(6)	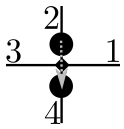	$\frac{1}{\sqrt{2}}\left(\|0\rangle_1\|\uparrow\rangle_2\|0\rangle_3\|\downarrow\rangle_4 - \|0\rangle_1\|\downarrow\rangle_2\|0\rangle_3\|\uparrow\rangle_4\right)$
(7)	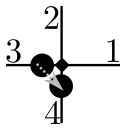	$\frac{1}{\sqrt{2}}\left(\|0\rangle_1\|0\rangle_2\|\uparrow\rangle_3\|\downarrow\rangle_4 - \|0\rangle_1\|0\rangle_2\|\downarrow\rangle_3\|\uparrow\rangle_4\right)$
(8)	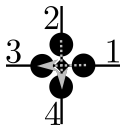	$\frac{1}{2}\left(\|\uparrow\rangle_1\|\uparrow\rangle_2\|\downarrow\rangle_3\|\downarrow\rangle_4 - \|\uparrow\rangle_1\|\downarrow\rangle_2\|\downarrow\rangle_3\|\uparrow\rangle_4 - \|\downarrow\rangle_1\|\uparrow\rangle_2\|\uparrow\rangle_3\|\downarrow\rangle_4 + \|\downarrow\rangle_1\|\downarrow\rangle_2\|\uparrow\rangle_3\|\uparrow\rangle_4\right)$
(9)	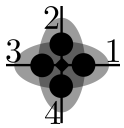	$\frac{1}{2\sqrt{3}}\left(2\|\uparrow\rangle_1\|\downarrow\rangle_2\|\uparrow\rangle_3\|\downarrow\rangle_4 + 2\|\downarrow\rangle_1\|\uparrow\rangle_2\|\downarrow\rangle_3\|\uparrow\rangle_4 - \|\uparrow\rangle_1\|\uparrow\rangle_2\|\downarrow\rangle_3\|\downarrow\rangle_4 - \|\uparrow\rangle_1\|\downarrow\rangle_2\|\downarrow\rangle_3\|\uparrow\rangle_4 - \|\downarrow\rangle_1\|\uparrow\rangle_2\|\uparrow\rangle_3\|\downarrow\rangle_4 - \|\downarrow\rangle_1\|\downarrow\rangle_2\|\uparrow\rangle_3\|\uparrow\rangle_4\right)$

Table B.1: *Possible singlet states at a square lattice site. The filled circles represent coloured rishons residing near the lattice site. The light arrows represent the overall sign for singlet pairs.*

#	Picture	Explicit Formula
1	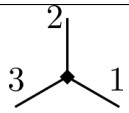	$\|0\rangle_1\|0\rangle_2\|0\rangle_3$
2	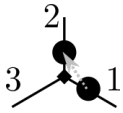	$\frac{1}{\sqrt{2}}\left(\|\uparrow\rangle_1\|\downarrow\rangle_2\|0\rangle_3 - \|\downarrow\rangle_1\|\uparrow\rangle_2\|0\rangle_3\right)$
3	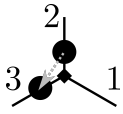	$\frac{1}{\sqrt{2}}\left(\|0\rangle_1\|\uparrow\rangle_2\|\downarrow\rangle_3 - \|0\rangle_1\|\downarrow\rangle_2\|\uparrow\rangle_3\right)$
4	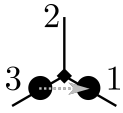	$\frac{1}{\sqrt{2}}\left(\|\downarrow\rangle_1\|0\rangle_2\|\uparrow\rangle_3 - \|\uparrow\rangle_1\|0\rangle_2\|\downarrow\rangle_3\right)$

Table B.2: *Possible singlet states at a honeycomb lattice site. The filled circles represent coloured rishons residing near the lattice site. The light arrows represent the overall sign for singlet pairs.*

B.2 Honeycomb Lattice

On the honeycomb lattice three links are joined at each site. A singlet can therefore only be constructed with either 0 or 2 rishons residing at a site. Note that this lattice geometry removes both the problem of states changing sign under a 180° rotation and the singlet-triplet ambiguity for states with 4 rishons residing at a site. These states are presented in Table B.2.

Appendix C

Square Plaquette Hamiltonian

C.1 Overall Sign

A plaquette is constructed from the individual site-state at the corners of the plaquette. Each site comes with a definite sign, which implies an overall sign for the entire plaquette state. When constructing the explicit single plaquette Hamiltonian, it is important to keep track on the relative signs between plaquettes that can make a transition to each other, since the 2×2 block Hamiltonian for the given plaquettes must include the relative sign into the off-diagonal elements. As was noted in Section 3.5, the arrow denotes the sign of the individual site-states making up the plaquette-states. An overall sign of the plaquette can thus be defined through the arrows. If a site contains a rishon pair arrow from an environment rishon towards a plaquette rishon, then the site obtains a factor -1, and otherwise a factor $+1$. The overall sign of the plaquette is then taken as the product of the signs associated with the individual sites. It should be pointed out, that, since we are constructing the Hamiltonian with the site-states rotated to give definite environment charges, the site-states with four rishons always give rise to a factor of $+1$. An example of how the signs are assigned is shown in Figure C.1 in the case of a transition between two plaquettes in the II environment, including the associated plaquette in the VI environment. Here plaquette *a* has three

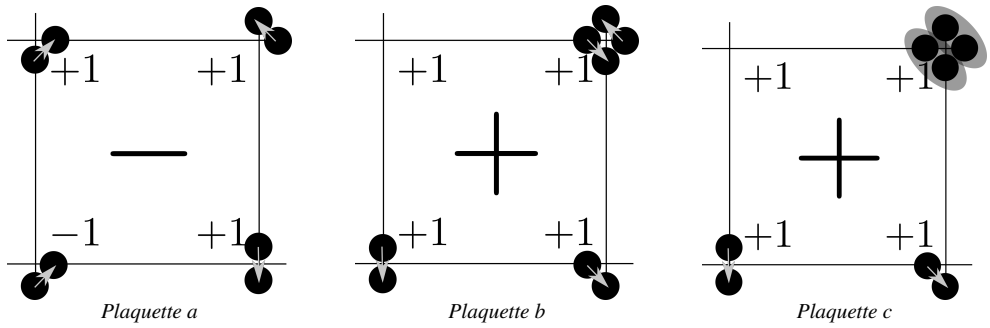

Figure C.1: *Three plaquettes making up a* 3×3 *block on the diagonal of the full Hamiltonian in eq.* (3.44) *(see footnote 18 on page 41). The states are given with their corresponding sign-factors at each lattice site, and the total plaquette sign is shown in the center of the plaquette.*

sites with a factor $+1$ and a single site with a factor -1. This gives an overall plaquette sign of -1. The two remaining plaquettes both have an overall sign $+1$. Since the signs on plaquette a and b differs, an additional -1 must be included in the transition between the two states. Note that no transition can be made to plaquette c and the sign for this plaquette is therefore of no importance. The block Hamiltonian for the three plaquettes is therefore given by,

$$\mathcal{H}^{\{4\}}_{II,VI} = \begin{pmatrix} W_{II} & -T_{II} & 0 \\ -T_{II} & W_{II} & 0 \\ 0 & 0 & W_{VI} \end{pmatrix}, \tag{C.1}$$

where the basis is understood to be ordered as plaquette $\{a, b, c\}$.

C.2 Symmetric Basis

To apply the above block Hamiltonian to a full lattice state, it is more convenient to choose site-states that are more symmetric on the full lattice, as given in Figure 3.9. For the example shown in Figure C.1, the two plaquettes b and c are rotated into each other, according to the rules given in eq. (3.43). For this example, the rotation is given by the matrix

$$V = \begin{pmatrix} 1 & 0 & 0 \\ 0 & \frac{1}{2} & \frac{\sqrt{3}}{2} \\ 0 & \frac{\sqrt{3}}{2} & -\frac{1}{2} \end{pmatrix}, \tag{C.2}$$

such that,

$$\mathcal{H}^{\{4\}-sym.}_{II,VI} = V\mathcal{H}^{\{4\}}_{II,VI}V^{\dagger} = \begin{pmatrix} W_{II} & -\frac{T_{II}}{2} & -\frac{\sqrt{3}T_{II}}{2} \\ -\frac{T_{II}}{2} & \frac{W_{II}+3W_{VI}}{4} & \frac{\sqrt{3}(W_{II}-W_{VI})}{4} \\ -\frac{\sqrt{3}T_{II}}{2} & \frac{\sqrt{3}(W_{II}-W_{VI})}{4} & \frac{3W_{II}+W_{VI}}{4} \end{pmatrix}. \tag{C.3}$$

Similar rotations can easily be found for any other set of plaquette-states by applying eq. (3.43).

Appendix D

Map Between the $SU(2)$ QLM on the Honeycomb Lattice with the $\{4\}$-Representation and the Quantum Dimer Model on the Kagomé Lattice

Without external charges the $SU(2)$ QLM on the honeycomb lattice with the $\{4\}$-representation is equivalent to the quantum dimer model on the Kagomé lattice. The Kagomé lattice can be constructed from the honeycomb lattice by connecting the center of neighbouring links. This is illustrated in Figure D.1. Here the Kagomé lattice is shown as black dotted lines overlaid on the honeycomb lattice, which is represented by full black lines. For the $\{4\}$-representation without external charges, every link contains exactly one rishon. To construct an overall singlet at each lattice site, this rishon must be coupled to exactly one other neighbouring rishon. Since each link carries exactly one rishon, the coupling of rishons to singlets is equivalent to coupling neighbouring links together. I.e. every link must be coupled to exactly one neighbouring link. This is illustrated

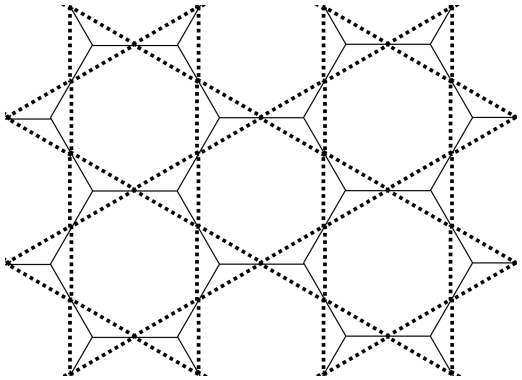

Figure D.1: *The Kagomé lattice (black dotted lines) is constructed from the honeycomb lattice (full black lines) by connecting the centers of neighbouring links.*

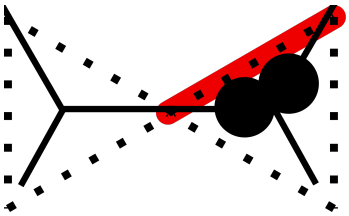

Figure D.2: *Two rishons on the honeycomb lattice (full black lines), forming a singlet pair, is identified with a corresponding dimer (red bold line) on the Kagomé lattice (dotted black lines).*

in Figure D.2. Here a singlet rishon pair is identified with a dimer (bold red) on the Kagomé lattice link, that connects the two honeycomb lattice links on which the two rishons reside. We can therefore reformulate the theory in terms of dimers on the Kagomé lattice. There every site on the Kagomé lattice contains exactly one dimer, connecting the site to any of the neighbouring Kagomé sites. This dimer formulation is mapped to the rishon configurations of the original QLM in the $\{4\}$-representation, as illustrated in Figure D.3. Here we mark the Kagomé dimers related to the corresponding rishon singlet pairs by bold red links. Each of the transitions is identified with a specific geometry of closed dimer loops on the Kagomé lattice. To highlight this, we include the Kagomé dimers after a transition, which are shown in bold semi-transparent blue.

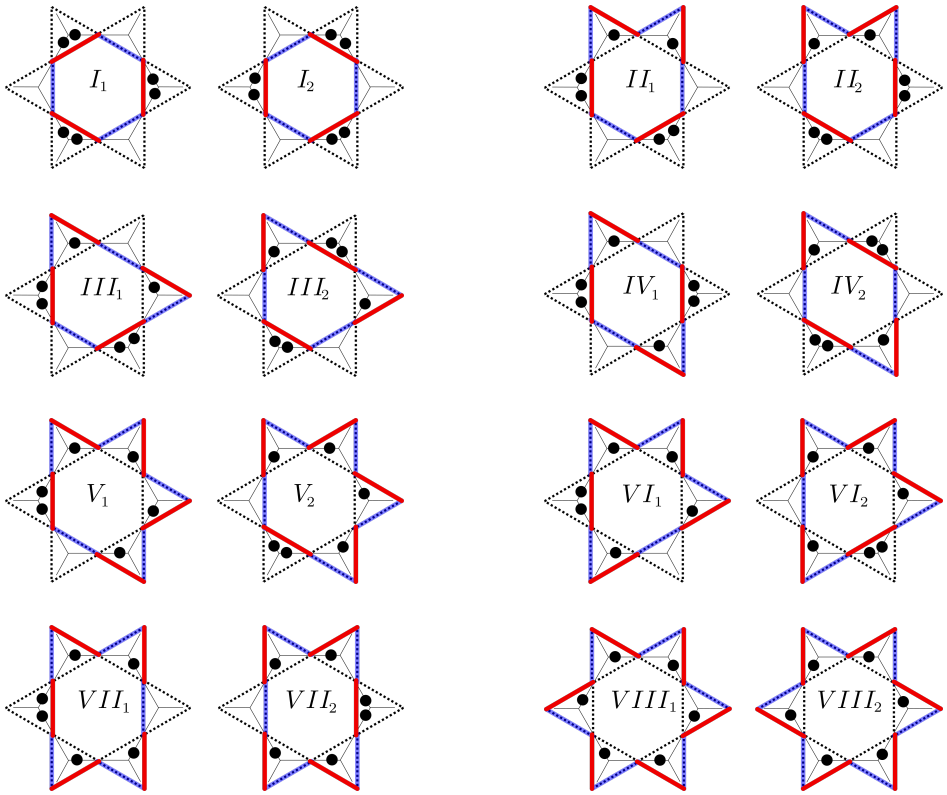

Figure D.3: *Map between the plaquettes of the quantum dimer model on the Kagomé lattice and the* SU (2) *QLM in the* $\{4\}$*-representation on the honeycomb lattice. A colour singlet rishon-pair on the honeycomb lattice (full black lines) is identified with a dimer (bold red link) on the Kagomé lattice (dotted black lines). A transition flips the dimers from the red to the transparent blue state thus closing the dimer loop.*

Appendix E

QLM Additional Plots

E.1 Magnetic Order Parameters for the Pinwheel Phase Transition

Here we present the normalized density histograms across the pinwheel phase transition. In other words, all the Hamiltonian parameters of eq. (3.53) are set to zero, except for T_{IV} and T_{VIII}. We choose T_{IV} between 0.5 and 1.0, and T_{VIII} is set to 1.0. The order parameters are presented as 2-dimensional plots, thus illustrating the correlations between the different order parameters. The axes of the histograms are each scaled to the maximal possible magnetization on the given sublattice (in this case ± 150). The 16 histograms in each plot are ordered such that the (x, y) axes of the histograms are given by;

$$\begin{array}{cccc} (M_A, M_A) & (M_A, M_B) & (M_A, M_C) & (M_A, M_D) \\ (M_B, M_A) & (M_B, M_B) & (M_B, M_C) & (M_B, M_D) \\ (M_C, M_A) & (M_C, M_B) & (M_C, M_C) & (M_C, M_D) \\ (M_D, M_A) & (M_D, M_B) & (M_D, M_C) & (M_D, M_D) \end{array} . \tag{E.1}$$

Figure E.1-E.6 shows the results for a 12×12 lattice with $\beta = 6$ and $L_t = 100$ simulated with the Metropolis algorithm. This is identical to the lattice presented in Figure 4.22 and Figure 4.23. Figure E.7 shows the results for a 12×12 lattice with $\beta = 5$ and $L_t = 100$ simulated with the cluster algorithm, hence $T_{IV} = T_{VIII} = 1$.

It should be noted that in the uncorrelated pinwheel phase, the A-sublattice has a magnetic order parameter centred tightly around $M_A = 0$ (see Figure E.1). When T_{IV} is increased, the order parameter spreads out, until one reaches $T_{IV}/T_{VIII} \approx 0.7 - 0.8$ (see Figure E.3 and Figure E.4). Here the order parameter splits into two separate peaks. Then it is impossible for the Metropolis algorithm to tunnel between these peaks. Finally, when $T_{IV} = T_{VIII}$ all four magnetic order parameters are the same (see Figure E.6 and Figure E.7). In contrast to the Metropolis algorithm, the cluster algorithm is very efficient in tunnelling between distinct realizations of the correlated pinwheel phase. This is illustrated in Figure E.7.

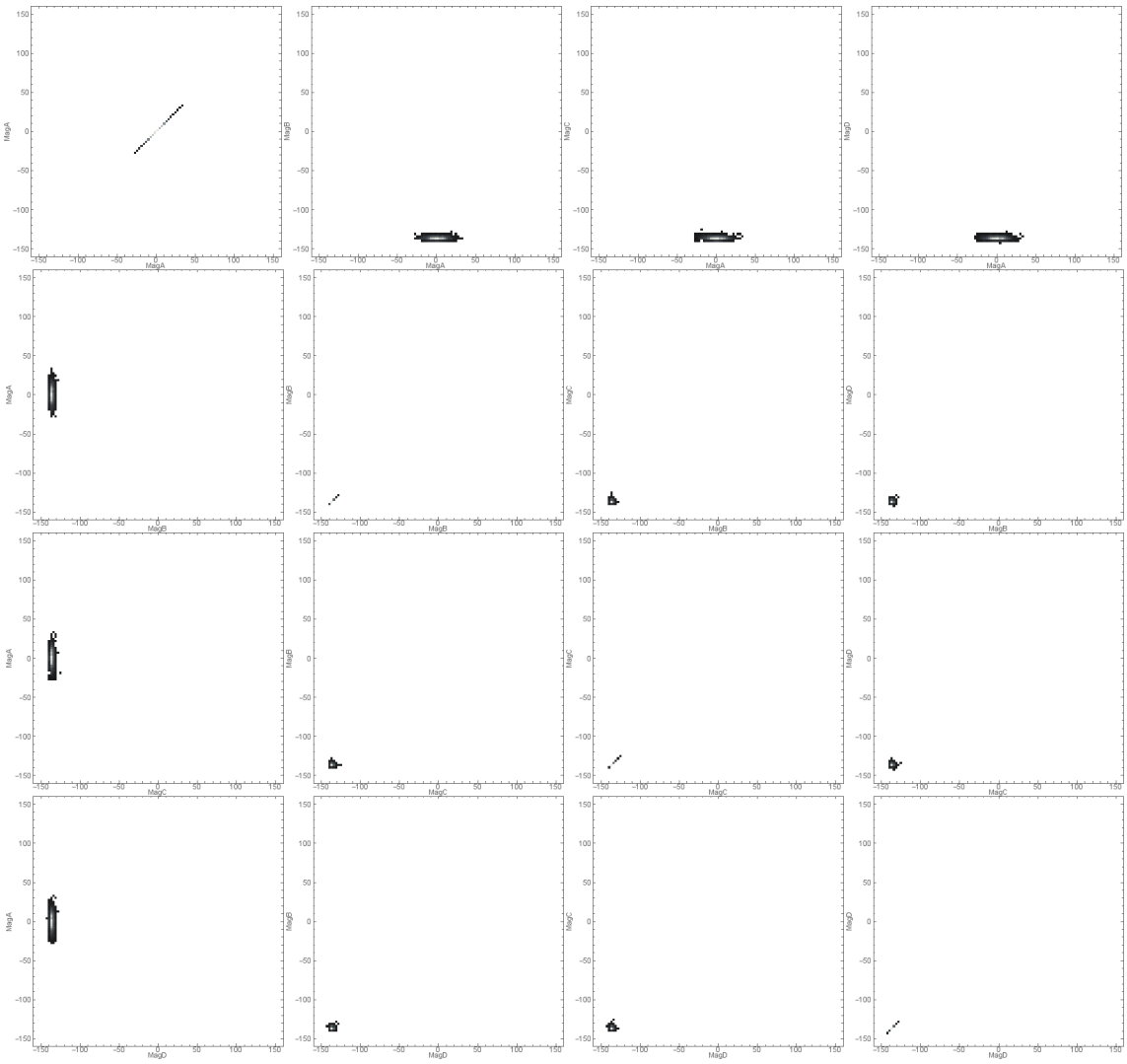

Figure E.1: *Normalized density histograms (lighter colours corresponds to higher values) of the correlations between the four magnetic order parameters for the Hamiltonian parameters* $T_{IV} = 0.5$ *and* $T_{VIII} = 1$ *(all remaining parameters are set to zero), with* $\beta = 6$ *and* $L_t = 100$ *— see Figure 4.22.*

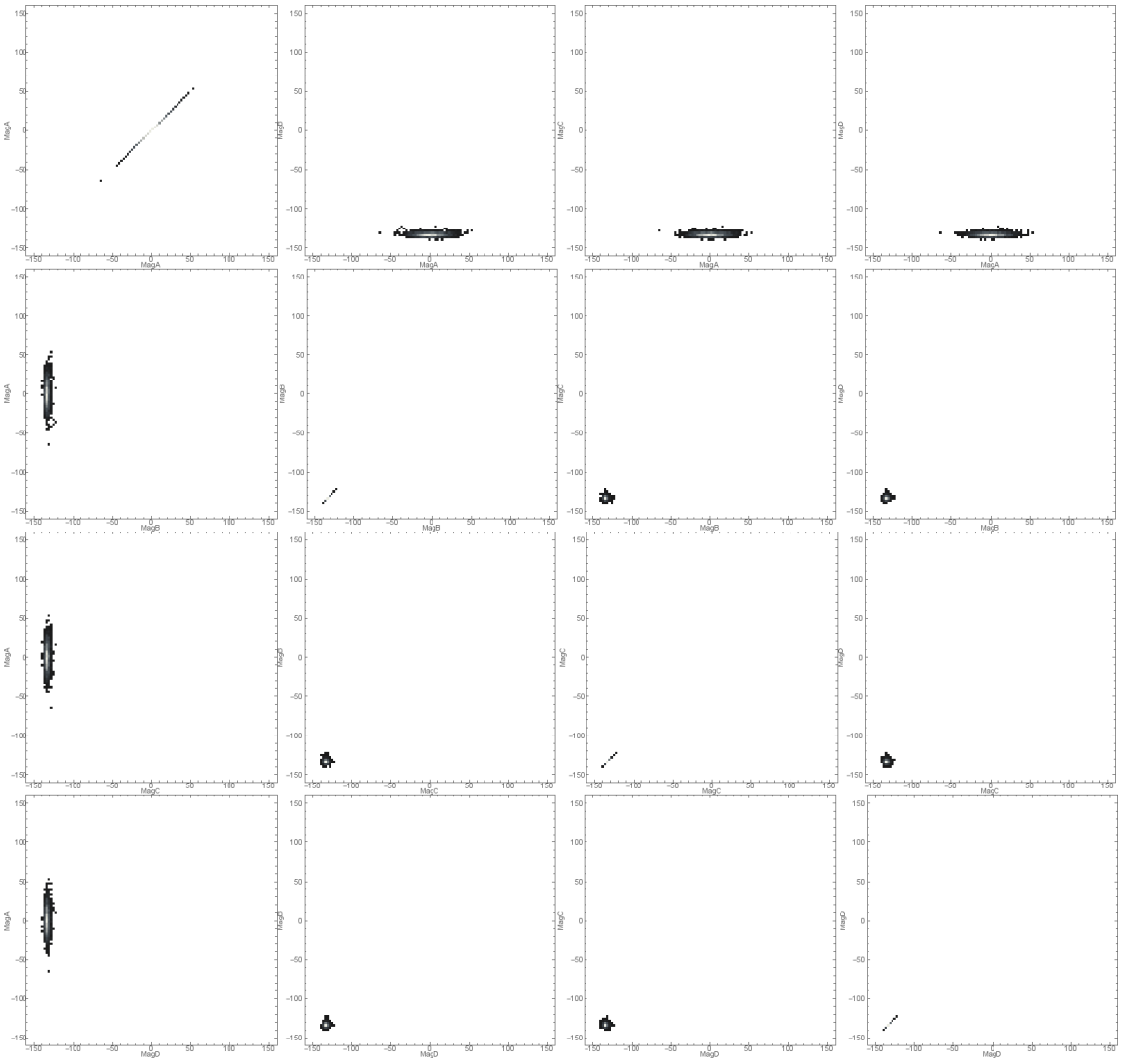

Figure E.2: *Normalized density histograms (lighter colours corresponds to higher values) of the correlations between the four magnetic order parameters for the Hamiltonian parameters* $T_{IV} = 0.6$ *and* $T_{VIII} = 1$ *(all remaining parameters are set to zero), with* $\beta = 6$ *and* $L_t = 100$ *— see Figure 4.22.*

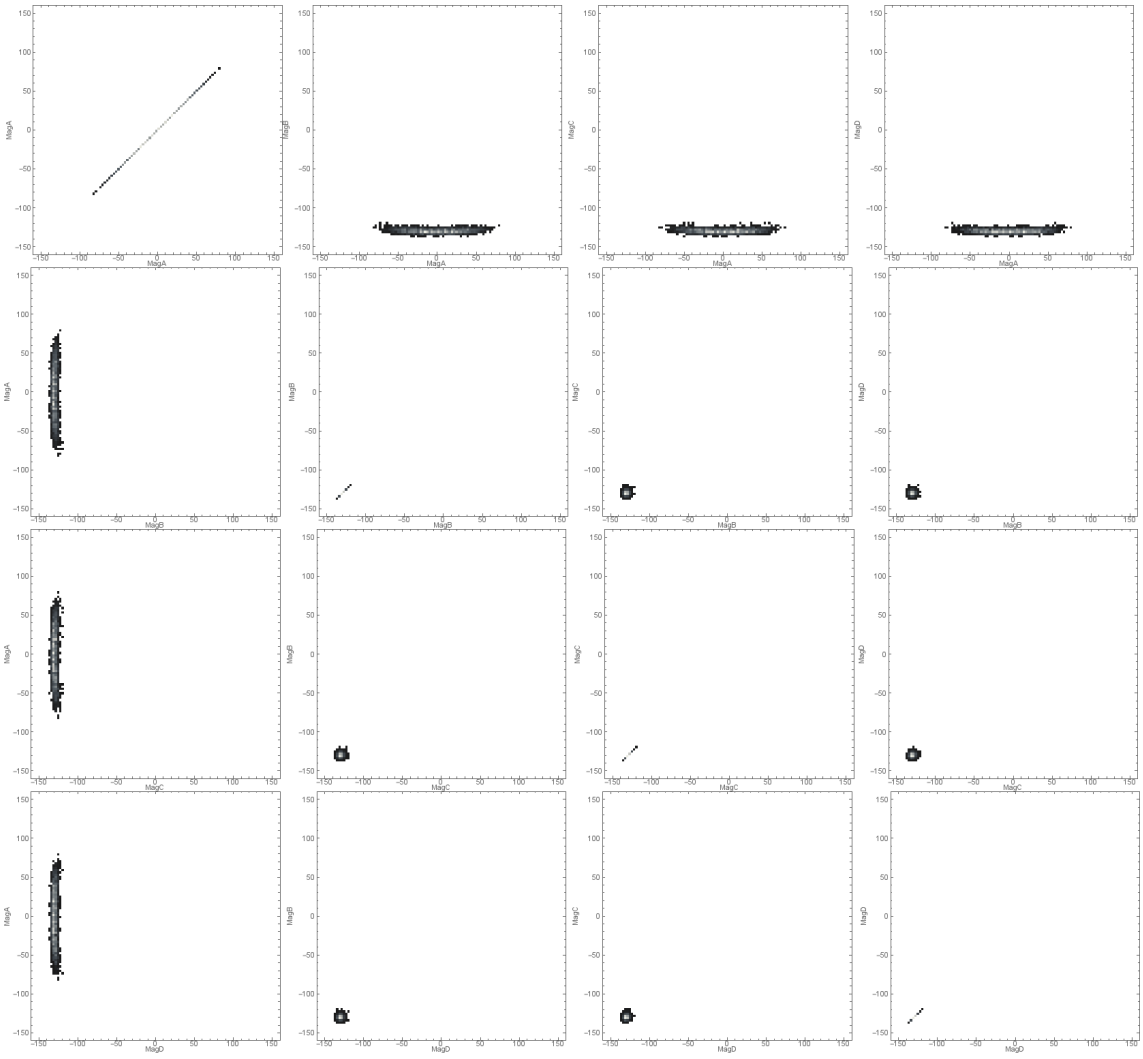

Figure E.3: *Normalized density histograms (lighter colours corresponds to higher values) of the correlations between the four magnetic order parameters for the Hamiltonian parameters* $T_{IV} = 0.7$ *and* $T_{VIII} = 1$ *(all remaining parameters are set to zero), with* $\beta = 6$ *and* $L_t = 100$ *— see Figure 4.22.*

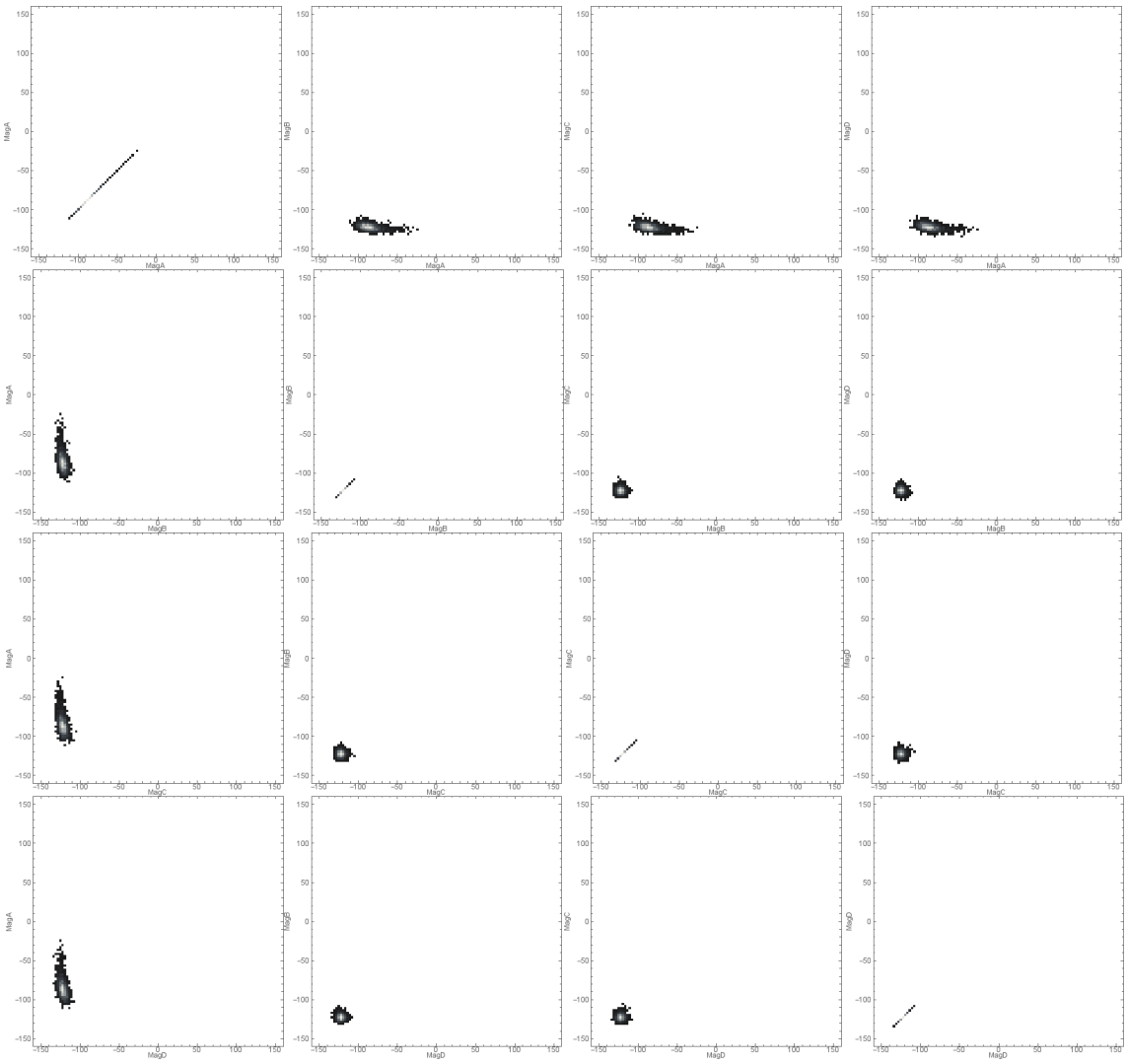

Figure E.4: *Normalized density histograms (lighter colours corresponds to higher values) of the correlations between the four magnetic order parameters for the Hamiltonian parameters* $T_{IV} = 0.8$ *and* $T_{VIII} = 1$ *(all remaining parameters are set to zero), with* $\beta = 6$ *and* $L_t = 100$ *— see Figure 4.22.*

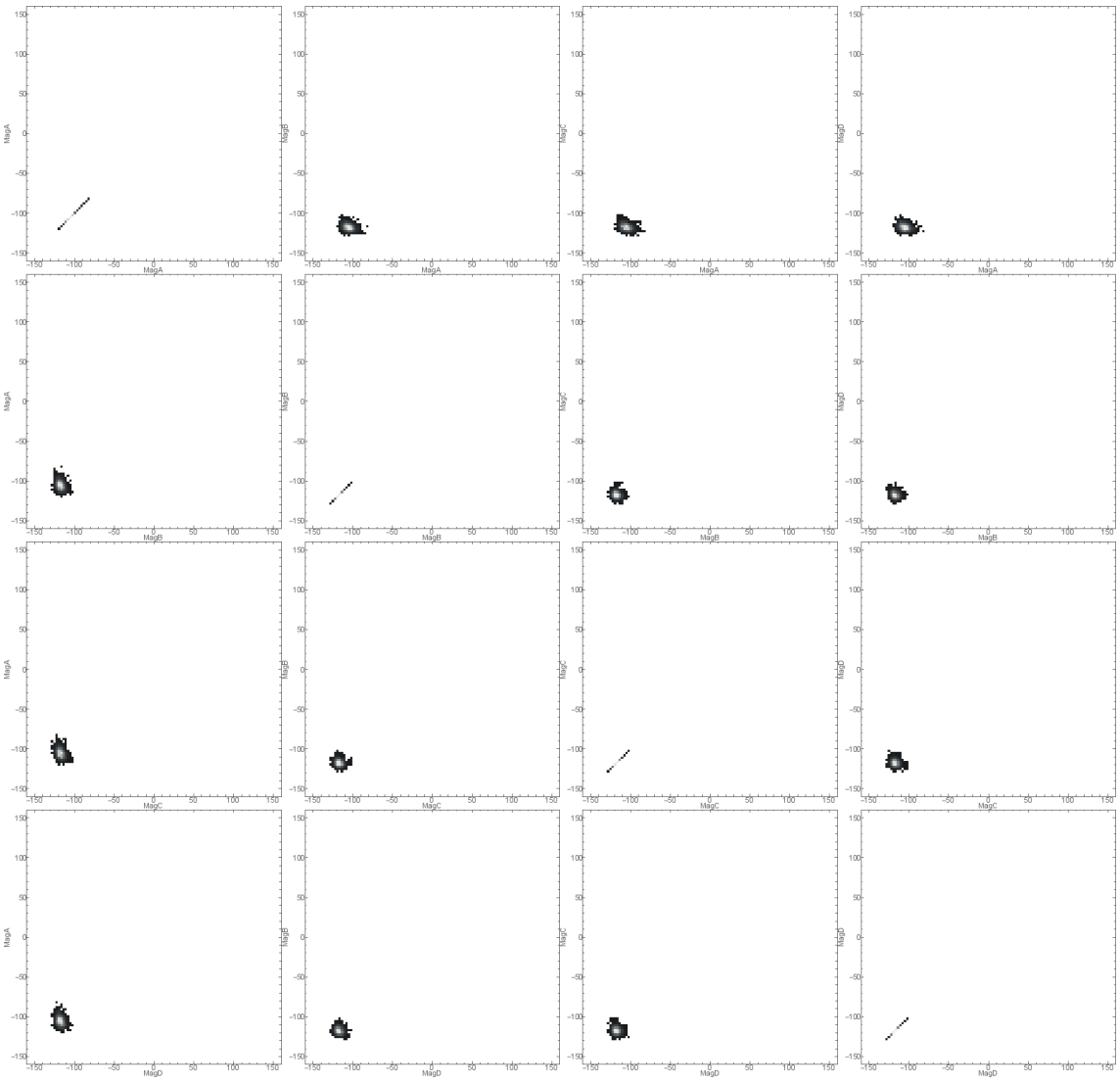

Figure E.5: *Normalized density histograms (lighter colours corresponds to higher values) of the correlations between the four magnetic order parameters for the Hamiltonian parameters* $T_{IV} = 0.9$ *and* $T_{VIII} = 1$ *(all remaining parameters are set to zero), with* $\beta = 6$ *and* $L_t = 100$ *— see Figure 4.22.*

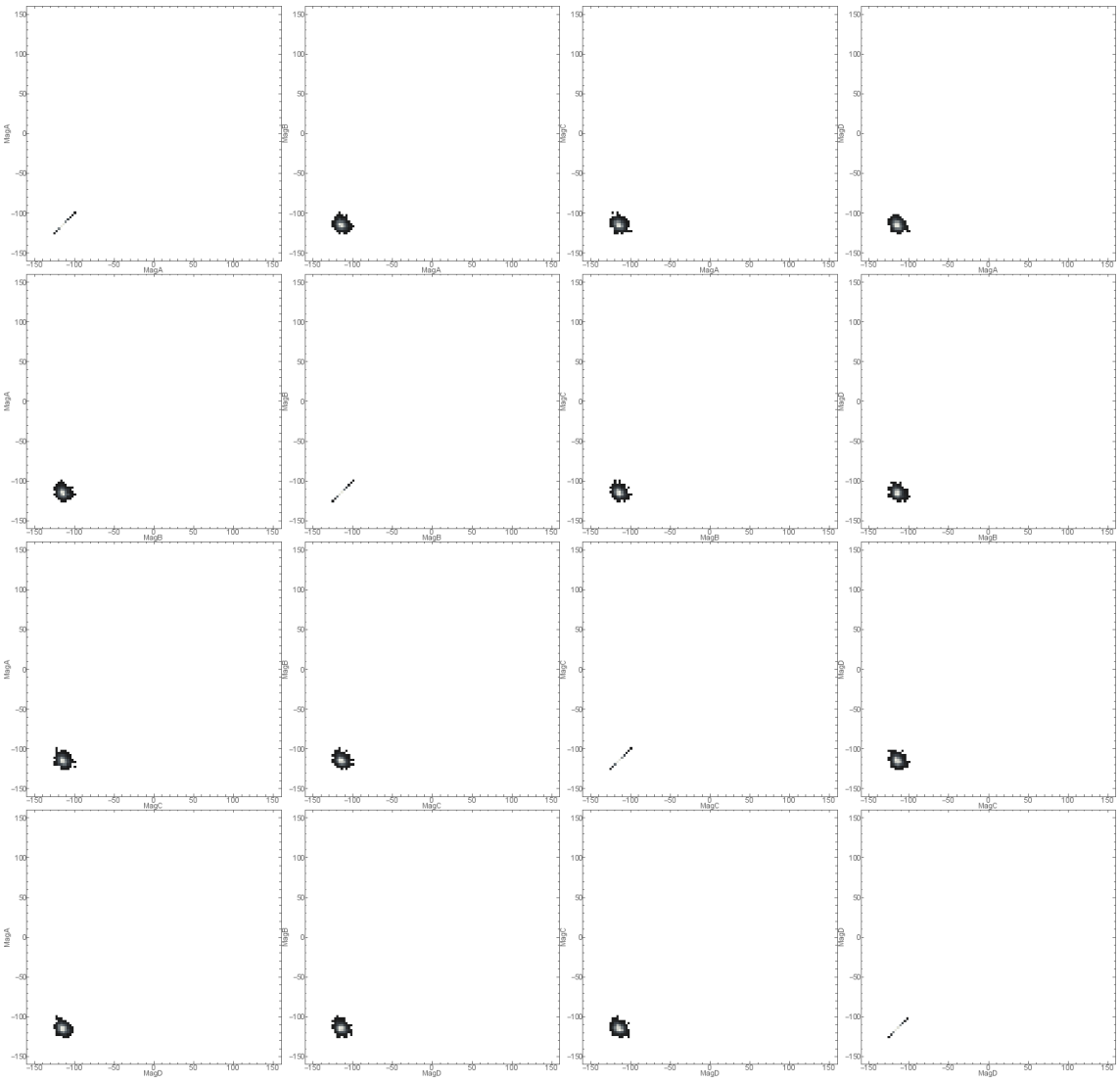

Figure E.6: *Normalized density histograms (lighter colours corresponds to higher values) of the correlations between the four magnetic order parameters for the Hamiltonian parameters* $T_{IV} = 1.0$ *and* $T_{VIII} = 1$ *(all remaining parameters are set to zero), with* $\beta = 6$ *and* $L_t = 100$ *— see Figure 4.22.*

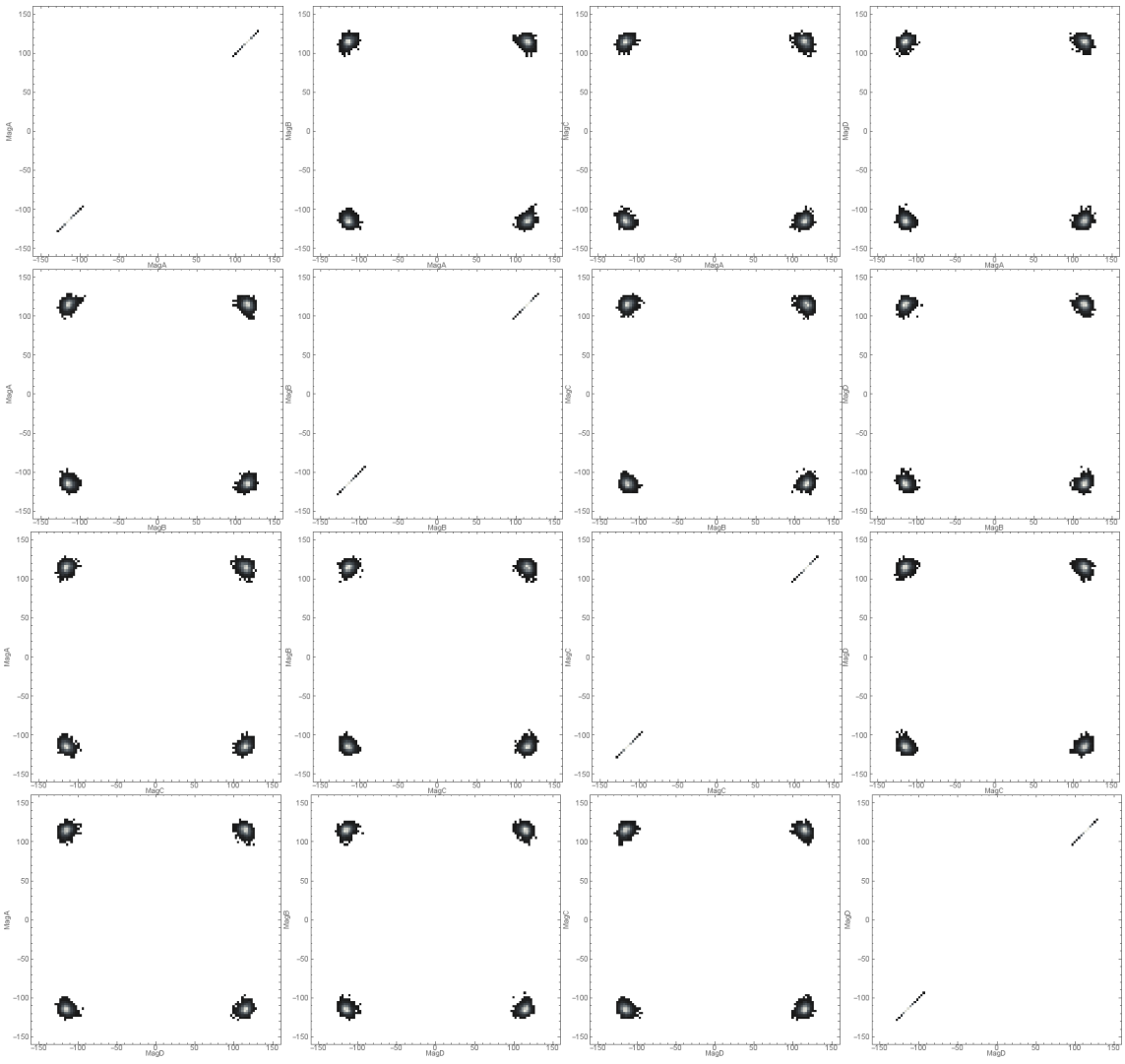

Figure E.7: *Normalized density histograms (lighter colours corresponds to higher values) of the correlations between the four magnetic order parameters for the Hamiltonian parameters* $T_{IV} = 1.0$ *and* $T_{VIII} = 1$ *(all remaining parameters are set to zero), with* $\beta = 5$ *and* $L_t = 100$*, simulated with the cluster algorithm. Note the tunnelling between the distinct realizations of the correlated pinwheel phases.*

Appendix F

Explicit Energy Eigenstates for Specific Doubled CSYM Theories

Here we present several energy eigenstates of a single-cross Hamiltonian, for specific doubled CSYM theories (as presented in Chapter 6). It is a straightforward, but tedious, process to obtain the explicit form of the eigenstates for the different theories, and therefore only a representative subset of eigenstates are presented here. In agreement with the gauge choice of eq. (6.109), $\widetilde{\omega}$ is always chosen to be 1 and the theories will be specified by the direct cocycles represented by a single parameter $\omega \equiv \omega_L = \omega_R^{-1}$. Except for the $\mathbb{Z}(k)$ theories, only the non-trivial cocycles are presented here. As in Chapter 6, the main focus will be on the gauge group S_3, where the eigenstates are presented in both the direct flux dual link basis and the direct link dual flux basis. Furthermore, for this gauge group we will also present the left and right operators in a basis of the direct flux dual link eigenstates.

F.1 $\mathbb{Z}(k)$ Energy-Eigenstates

Here energy eigenstates are presented for the $\mathbb{Z}(2)$ and $\mathbb{Z}(3)$ theories.

F.1.1 $\mathbb{Z}(2)$ with a Trivial Cocycle: ω_1

Lowest Energy Eigenstates: $E_0 = 0$

In the lowest energy level, there is a single energy eigenstate that is given by

$$\left|E_0, 1\right\rangle = \frac{1}{\sqrt{2}}\left(\left|\Gamma_1\right\rangle \otimes \left|\widetilde{z}_0\right\rangle + \left|\Gamma_1\right\rangle \otimes \left|\widetilde{z}_1\right\rangle\right). \tag{F.1}$$

First Excited Energy Eigenstates: $E_1 = 2$

In the first excited energy level, there are two energy eigenstates which are given by

$$\begin{aligned} \left|E_1, 1\right\rangle &= \frac{1}{\sqrt{2}}\left(\left|\Gamma_1\right\rangle \otimes \left|\widetilde{z}_0\right\rangle - \left|\Gamma_1\right\rangle \otimes \left|\widetilde{z}_1\right\rangle\right), \\ \left|E_1, 2\right\rangle &= \frac{1}{\sqrt{2}}\left(\left|\Gamma_2\right\rangle \otimes \left|\widetilde{z}_0\right\rangle + \left|\Gamma_2\right\rangle \otimes \left|\widetilde{z}_1\right\rangle\right). \end{aligned} \tag{F.2}$$

Second Excited Energy Eigenstates: $E_2 = 4$

In the second excited energy level, there is a single energy eigenstate that is given by

$$\left|E_2, 1\right\rangle = \frac{1}{\sqrt{2}}\left(\left|\Gamma_2\right\rangle \otimes \left|\widetilde{z}_0\right\rangle - \left|\Gamma_2\right\rangle \otimes \left|\widetilde{z}_1\right\rangle\right). \tag{F.3}$$

F.1.2 $\mathbb{Z}(2)$ with a Non-Trivial Cocycle: ω_2

Lowest Energy Eigenstates: $E_0 = (2 - \sqrt{2})$

In the lowest energy level, there are two energy eigenstates which are given by

$$\begin{aligned} \left|E_0, 1\right\rangle &= \frac{1}{2\left(2+\sqrt{2}\right)}\left(\left(1+\sqrt{2}\right)\left|\Gamma_1\right\rangle \otimes \left|\widetilde{z}_1\right\rangle + \left|\Gamma_2\right\rangle \otimes \left|\widetilde{z}_0\right\rangle\right), \\ \left|E_0, 2\right\rangle &= \frac{1}{2\left(2+\sqrt{2}\right)}\left(\left(1+\sqrt{2}\right)\left|\Gamma_1\right\rangle \otimes \left|\widetilde{z}_0\right\rangle + \left|\Gamma_2\right\rangle \otimes \left|\widetilde{z}_1\right\rangle\right). \end{aligned} \tag{F.4}$$

First Excited Energy Eigenstates: $E_1 = (2 + \sqrt{2})$

In the first excited energy level, there are two energy eigenstates which are given by

$$\begin{aligned} \left|E_1, 1\right\rangle &= \frac{1}{2\left(2+\sqrt{2}\right)}\left(\left|\Gamma_1\right\rangle \otimes \left|\widetilde{z}_0\right\rangle - \left(1+\sqrt{2}\right)\left|\Gamma_2\right\rangle \otimes \left|\widetilde{z}_1\right\rangle\right), \\ \left|E_1, 2\right\rangle &= \frac{1}{2\left(2+\sqrt{2}\right)}\left(\left|\Gamma_1\right\rangle \otimes \left|\widetilde{z}_1\right\rangle - \left(1+\sqrt{2}\right)\left|\Gamma_2\right\rangle \otimes \left|\widetilde{z}_0\right\rangle\right). \end{aligned} \tag{F.5}$$

F.1.3 $\mathbb{Z}(3)$ with a Trivial Cocycle: ω_1

Lowest Energy Eigenstates: $E_0 = 0$

In the lowest energy level, there is a single energy eigenstate that is given by

$$\left|E_0, 1\right\rangle = \frac{1}{\sqrt{3}}\left(\left|\Gamma_1\right\rangle \otimes \left|\widetilde{z_0}\right\rangle + \left|\Gamma_1\right\rangle \otimes \left|\widetilde{z_1}\right\rangle + \left|\Gamma_1\right\rangle \otimes \left|\widetilde{z_2}\right\rangle\right). \tag{F.6}$$

First Excited Energy Eigenstates: $E_1 = \frac{3}{2}$

In the first excited energy level, there are four energy eigenstates which are given by

$$\begin{aligned}
\left|E_1, 1\right\rangle &= \frac{1}{\sqrt{3}}\left(\left|\Gamma_2\right\rangle \otimes \left|\widetilde{z_0}\right\rangle + \left|\Gamma_2\right\rangle \otimes \left|\widetilde{z_1}\right\rangle + \left|\Gamma_2\right\rangle \otimes \left|\widetilde{z_2}\right\rangle\right), \\
\left|E_1, 2\right\rangle &= \frac{1}{\sqrt{3}}\left(\left|\Gamma_3\right\rangle \otimes \left|\widetilde{z_0}\right\rangle + \left|\Gamma_3\right\rangle \otimes \left|\widetilde{z_1}\right\rangle + \left|\Gamma_3\right\rangle \otimes \left|\widetilde{z_2}\right\rangle\right), \\
\left|E_1, 3\right\rangle &= \frac{1}{\sqrt{6}}\left(2\left|\Gamma_1\right\rangle \otimes \left|\widetilde{z_0}\right\rangle - \left|\Gamma_1\right\rangle \otimes \left|\widetilde{z_1}\right\rangle - \left|\Gamma_1\right\rangle \otimes \left|\widetilde{z_2}\right\rangle\right), \\
\left|E_1, 4\right\rangle &= \frac{1}{\sqrt{2}}\left(\left|\Gamma_1\right\rangle \otimes \left|\widetilde{z_1}\right\rangle - \left|\Gamma_1\right\rangle \otimes \left|\widetilde{z_2}\right\rangle\right).
\end{aligned} \tag{F.7}$$

Second Excited Energy Eigenstates: $E_2 = 3$

In the second excited energy level, there are four energy eigenstate which are given by

$$\begin{aligned}
\left|E_2, 1\right\rangle &= \frac{1}{\sqrt{2}}\left(\left|\Gamma_3\right\rangle \otimes \left|\widetilde{z_1}\right\rangle - \left|\Gamma_3\right\rangle \otimes \left|\widetilde{z_2}\right\rangle\right), \\
\left|E_2, 2\right\rangle &= \frac{1}{\sqrt{6}}\left(2\left|\Gamma_3\right\rangle \otimes \left|\widetilde{z_0}\right\rangle - \left|\Gamma_3\right\rangle \otimes \left|\widetilde{z_1}\right\rangle - \left|\Gamma_3\right\rangle \otimes \left|\widetilde{z_2}\right\rangle\right), \\
\left|E_2, 3\right\rangle &= \frac{1}{\sqrt{2}}\left(\left|\Gamma_2\right\rangle \otimes \left|\widetilde{z_1}\right\rangle - \left|\Gamma_2\right\rangle \otimes \left|\widetilde{z_2}\right\rangle\right), \\
\left|E_2, 4\right\rangle &= \frac{1}{\sqrt{6}}\left(2\left|\Gamma_2\right\rangle \otimes \left|\widetilde{z_0}\right\rangle - \left|\Gamma_2\right\rangle \otimes \left|\widetilde{z_1}\right\rangle - \left|\Gamma_2\right\rangle \otimes \left|\widetilde{z_2}\right\rangle\right).
\end{aligned} \tag{F.8}$$

F.1.4 $\mathbb{Z}(3)$ with a Non-Trivial Cocycle: ω_2

Lowest Energy Eigenstates: $E_0 = \frac{3-\sqrt{3}}{2}$

In the lowest energy level, there are three energy eigenstates which are given by

$$\left|E_0, 1\right\rangle = \frac{1}{2\left(3+\sqrt{3}\right)}\left(\left(3+\sqrt{3}\right)\left|\Gamma_1\right\rangle \otimes \left|\widetilde{z_0}\right\rangle + \left|\Gamma_2\right\rangle \otimes \left|\widetilde{z_1}\right\rangle + \left|\Gamma_3\right\rangle \otimes \left|\widetilde{z_2}\right\rangle\right), \tag{F.9}$$

$$|E_0,2\rangle = \frac{1}{2\left(3+\sqrt{3}\right)}\left(\left(3+\sqrt{3}\right)|\Gamma_1\rangle\otimes|\widetilde{z_1}\rangle + |\Gamma_2\rangle\otimes|\widetilde{z_2}\rangle + |\Gamma_3\rangle\otimes|\widetilde{z_0}\rangle\right),$$
$$|E_0,3\rangle = \frac{1}{2\left(3+\sqrt{3}\right)}\left(\left(3+\sqrt{3}\right)|\Gamma_1\rangle\otimes|\widetilde{z_2}\rangle + |\Gamma_2\rangle\otimes|\widetilde{z_0}\rangle + |\Gamma_3\rangle\otimes|\widetilde{z_1}\rangle\right).$$

First Excited Energy Eigenstates: $E_1 = \frac{3+\sqrt{3}}{2}$

In the first excited energy level, there are three energy eigenstates which are given by

$$|E_1,1\rangle = \frac{1}{4\left(3+\sqrt{3}\right)}\left(2|\Gamma_1\rangle\otimes|\widetilde{z_0}\rangle - \left(3+\sqrt{3}\right)\left(|\Gamma_2\rangle\otimes|\widetilde{z_1}\rangle + |\Gamma_3\rangle\otimes|\widetilde{z_2}\rangle\right)\right), \quad \text{(F.10)}$$
$$|E_1,2\rangle = \frac{1}{4\left(3+\sqrt{3}\right)}\left(2|\Gamma_1\rangle\otimes|\widetilde{z_1}\rangle - \left(3+\sqrt{3}\right)\left(|\Gamma_2\rangle\otimes|\widetilde{z_2}\rangle + |\Gamma_3\rangle\otimes|\widetilde{z_0}\rangle\right)\right),$$
$$|E_1,3\rangle = \frac{1}{4\left(3+\sqrt{3}\right)}\left(2|\Gamma_1\rangle\otimes|\widetilde{z_2}\rangle - \left(3+\sqrt{3}\right)\left(|\Gamma_2\rangle\otimes|\widetilde{z_0}\rangle + |\Gamma_3\rangle\otimes|\widetilde{z_1}\rangle\right)\right).$$

Second Excited Energy Eigenstates: $E_2 = 3$

In the second excited energy level, there are three energy eigenstates which given by

$$|E_2,1\rangle = \frac{1}{2}\left(|\Gamma_1\rangle\otimes|\widetilde{z_2}\rangle - |\Gamma_2\rangle\otimes|\widetilde{z_0}\rangle\right), \quad \text{(F.11)}$$
$$|E_2,2\rangle = \frac{1}{2}\left(|\Gamma_1\rangle\otimes|\widetilde{z_1}\rangle - |\Gamma_2\rangle\otimes|\widetilde{z_2}\rangle\right),$$
$$|E_2,3\rangle = \frac{1}{2}\left(|\Gamma_1\rangle\otimes|\widetilde{z_0}\rangle - |\Gamma_2\rangle\otimes|\widetilde{z_1}\rangle\right).$$

F.2 S_3 with a Non-Trivial Cocycle: ω_2

Ground State: $E_0 = \frac{3\left(2-\sqrt{2}\right)}{2}$

In the lowest energy level, there are two energy eigenstates which are given in the direct flux dual link basis as

$$|E_0,1\rangle = \frac{1}{\sqrt{3(4+2\sqrt{2})}}\left(\left(1+\sqrt{2}\right)|\Gamma_1\rangle\otimes|\widetilde{P_{12}}\rangle + \left(1+\sqrt{2}\right)|\Gamma_1\rangle\otimes|\widetilde{P_{23}}\rangle\right. \quad \text{(F.12)}$$
$$\left. + \left(1+\sqrt{2}\right)|\Gamma_1\rangle\otimes|\widetilde{P_{31}}\rangle + |\Gamma_2\rangle\otimes|\widetilde{1}\rangle + |\Gamma_2\rangle\otimes|\widetilde{P_{231}}\rangle + |\Gamma_2\rangle\otimes|\widetilde{P_{312}}\rangle\right),$$
$$|E_0,2\rangle = \frac{1}{\sqrt{3(4+2\sqrt{2})}}\left(\left(1+\sqrt{2}\right)|\Gamma_1\rangle\otimes|\widetilde{1}\rangle + \left(1+\sqrt{2}\right)|\Gamma_1\rangle\otimes|\widetilde{P_{231}}\rangle\right.$$

$$+\left(1+\sqrt{2}\right)\left|\Gamma_1\right\rangle\otimes\left|\widetilde{P_{312}}\right\rangle+\left|\Gamma_2\right\rangle\otimes\left|\widetilde{P_{12}}\right\rangle+\left|\Gamma_2\right\rangle\otimes\left|\widetilde{P_{23}}\right\rangle+\left|\Gamma_2\right\rangle\otimes\left|\widetilde{P_{31}}\right\rangle\Big).$$

In the basis of the two eigenstates, the left and right operators on a cross are given by

$$\begin{aligned}
\widetilde{L}\left(C_{13}\right)&=\begin{pmatrix}1&0\\0&1\end{pmatrix}, & \widetilde{R}\left(C_{13}\right)&=\begin{pmatrix}1&0\\0&1\end{pmatrix},\\
\widetilde{L}\left(C_{2}\right)&=\begin{pmatrix}0&1\\1&0\end{pmatrix}, & \widetilde{R}\left(C_{2}\right)&=\begin{pmatrix}0&1\\1&0\end{pmatrix},\\
L\left(C_{13}\right)&=\begin{pmatrix}1&0\\0&1\end{pmatrix}, & R\left(C_{13}\right)&=\begin{pmatrix}1&0\\0&1\end{pmatrix},\\
L\left(C_{2}\right)&=\begin{pmatrix}-1&0\\0&1\end{pmatrix}, & R\left(C_{2}\right)&=\begin{pmatrix}-1&0\\0&1\end{pmatrix}.
\end{aligned}\tag{F.13}$$

Changing to the direct link dual flux basis the same states are given by

$$\begin{aligned}
\left|E_0,1\right\rangle=&\frac{1}{\sqrt{6(4+2\sqrt{2})}}\Big(\left(1+\sqrt{2}\right)\left|1\right\rangle\otimes\left|\widetilde{\Gamma_1}\right\rangle-\left|1\right\rangle\otimes\left|\widetilde{\Gamma_2}\right\rangle\\
&-\left(1+\sqrt{2}\right)\left|P_{12}\right\rangle\otimes\left|\widetilde{\Gamma_1}\right\rangle+\left|P_{12}\right\rangle\otimes\left|\widetilde{\Gamma_2}\right\rangle\\
&-\left(1+\sqrt{2}\right)\left|P_{23}\right\rangle\otimes\left|\widetilde{\Gamma_1}\right\rangle+\left|P_{23}\right\rangle\otimes\left|\widetilde{\Gamma_2}\right\rangle\\
&-\left(1+\sqrt{2}\right)\left|P_{31}\right\rangle\otimes\left|\widetilde{\Gamma_1}\right\rangle+\left|P_{31}\right\rangle\otimes\left|\widetilde{\Gamma_2}\right\rangle\\
&+\left(1+\sqrt{2}\right)\left|P_{231}\right\rangle\otimes\left|\widetilde{\Gamma_1}\right\rangle-\left|P_{231}\right\rangle\otimes\left|\widetilde{\Gamma_2}\right\rangle\\
&+\left(1+\sqrt{2}\right)\left|P_{312}\right\rangle\otimes\left|\widetilde{\Gamma_1}\right\rangle-\left|P_{312}\right\rangle\otimes\left|\widetilde{\Gamma_2}\right\rangle\Big),\\
\left|E_0,2\right\rangle=&\frac{1}{\sqrt{6(4+2\sqrt{2})}}\Big(\left(1+\sqrt{2}\right)\left|1\right\rangle\otimes\left|\widetilde{\Gamma_1}\right\rangle+\left|1\right\rangle\otimes\left|\widetilde{\Gamma_2}\right\rangle\\
&+\left(1+\sqrt{2}\right)\left|P_{12}\right\rangle\otimes\left|\widetilde{\Gamma_1}\right\rangle+\left|P_{12}\right\rangle\otimes\left|\widetilde{\Gamma_2}\right\rangle\\
&+\left(1+\sqrt{2}\right)\left|P_{23}\right\rangle\otimes\left|\widetilde{\Gamma_1}\right\rangle+\left|P_{23}\right\rangle\otimes\left|\widetilde{\Gamma_2}\right\rangle\\
&+\left(1+\sqrt{2}\right)\left|P_{31}\right\rangle\otimes\left|\widetilde{\Gamma_1}\right\rangle+\left|P_{31}\right\rangle\otimes\left|\widetilde{\Gamma_2}\right\rangle\\
&+\left(1+\sqrt{2}\right)\left|P_{231}\right\rangle\otimes\left|\widetilde{\Gamma_1}\right\rangle+1\left|P_{231}\right\rangle\otimes\left|\widetilde{\Gamma_2}\right\rangle\\
&+\left(1+\sqrt{2}\right)\left|P_{312}\right\rangle\otimes\left|\widetilde{\Gamma_1}\right\rangle+\left|P_{312}\right\rangle\otimes\left|\widetilde{\Gamma_2}\right\rangle\Big).
\end{aligned}\tag{F.14}$$

First Excited States: $E_1=\frac{3}{2}$

In the first excited energy level, there are eight states, that can be divided into two sets, depending on their fluxes. The first set is given in the direct flux dual link basis by

$$\left|E_1,12\right\rangle=\frac{1}{\sqrt{6}}\Big(\left|\Gamma_3^{11}\right\rangle\otimes\left|\widetilde{1}\right\rangle+\left|\Gamma_3^{11}\right\rangle\otimes\left|\widetilde{P_{231}}\right\rangle+\left|\Gamma_3^{11}\right\rangle\otimes\left|\widetilde{P_{312}}\right\rangle\tag{F.15}$$

$$
\begin{aligned}
&+\left|\Gamma_3^{22}\right\rangle \otimes \left|\widetilde{P_{12}}\right\rangle + \left|\Gamma_3^{22}\right\rangle \otimes \left|\widetilde{P_{23}}\right\rangle + \left|\Gamma_3^{22}\right\rangle \otimes \left|\widetilde{P_{31}}\right\rangle\Big), \\
\left|E_1, 21\right\rangle = \frac{1}{\sqrt{6}}\Big(&\left|\Gamma_3^{11}\right\rangle \otimes \left|\widetilde{P_{12}}\right\rangle + \left|\Gamma_3^{11}\right\rangle \otimes \left|\widetilde{P_{23}}\right\rangle + \left|\Gamma_3^{11}\right\rangle \otimes \left|\widetilde{P_{31}}\right\rangle \\
&+\left|\Gamma_3^{22}\right\rangle \otimes \left|\widetilde{1}\right\rangle + \left|\Gamma_3^{22}\right\rangle \otimes \left|\widetilde{P_{231}}\right\rangle + \left|\Gamma_3^{22}\right\rangle \otimes \left|\widetilde{P_{312}}\right\rangle\Big), \\
\left|E_1, 11\right\rangle = \frac{1}{\sqrt{6}}\Big(&\left|\Gamma_3^{12}\right\rangle \otimes \left|\widetilde{1}\right\rangle + \left|\Gamma_3^{12}\right\rangle \otimes \left|\widetilde{P_{231}}\right\rangle + \left|\Gamma_3^{12}\right\rangle \otimes \left|\widetilde{P_{312}}\right\rangle \\
&-\left|\Gamma_3^{21}\right\rangle \otimes \left|\widetilde{P_{12}}\right\rangle - \left|\Gamma_3^{21}\right\rangle \otimes \left|\widetilde{P_{23}}\right\rangle - \left|\Gamma_3^{21}\right\rangle \otimes \left|\widetilde{P_{31}}\right\rangle\Big), \\
\left|E_1, 22\right\rangle = \frac{1}{\sqrt{6}}\Big(&\left|\Gamma_3^{21}\right\rangle \otimes \left|\widetilde{1}\right\rangle + \left|\Gamma_3^{21}\right\rangle \otimes \left|\widetilde{P_{231}}\right\rangle + \left|\Gamma_3^{21}\right\rangle \otimes \left|\widetilde{P_{312}}\right\rangle \\
&-\left|\Gamma_3^{12}\right\rangle \otimes \left|\widetilde{P_{12}}\right\rangle - \left|\Gamma_3^{12}\right\rangle \otimes \left|\widetilde{P_{23}}\right\rangle - \left|\Gamma_3^{12}\right\rangle \otimes \left|\widetilde{P_{31}}\right\rangle\Big).
\end{aligned}
$$

In a basis of $\left\{\left|E_1, 12\right\rangle, \left|E_1, 21\right\rangle, \left|E_1, 11\right\rangle, \left|E_1, 22\right\rangle\right\}$ the left and right operators are represented by

$$
\widetilde{L}\left(\mathbb{1}\right) = \begin{pmatrix} 1 & 0 & 0 & 0 \\ 0 & 1 & 0 & 0 \\ 0 & 0 & 1 & 0 \\ 0 & 0 & 0 & 1 \end{pmatrix}, \qquad \widetilde{R}\left(\mathbb{1}\right) = \begin{pmatrix} 1 & 0 & 0 & 0 \\ 0 & 1 & 0 & 0 \\ 0 & 0 & 1 & 0 \\ 0 & 0 & 0 & 1 \end{pmatrix}, \tag{F.16}
$$

$$
\widetilde{L}\left(P_{12}\right) = \begin{pmatrix} 0 & 1 & 0 & 0 \\ 1 & 0 & 0 & 0 \\ 0 & 0 & 0 & -1 \\ 0 & 0 & -1 & 0 \end{pmatrix}, \qquad \widetilde{R}\left(P_{12}\right) = \begin{pmatrix} 0 & 1 & 0 & 0 \\ 1 & 0 & 0 & 0 \\ 0 & 0 & 0 & -1 \\ 0 & 0 & -1 & 0 \end{pmatrix},
$$

$$
\widetilde{L}\left(P_{23}\right) = \begin{pmatrix} 0 & 1 & 0 & 0 \\ 1 & 0 & 0 & 0 \\ 0 & 0 & 0 & -1 \\ 0 & 0 & -1 & 0 \end{pmatrix}, \qquad \widetilde{R}\left(P_{23}\right) = \begin{pmatrix} 0 & 1 & 0 & 0 \\ 1 & 0 & 0 & 0 \\ 0 & 0 & 0 & -1 \\ 0 & 0 & -1 & 0 \end{pmatrix},
$$

$$
\widetilde{L}\left(P_{31}\right) = \begin{pmatrix} 0 & 1 & 0 & 0 \\ 1 & 0 & 0 & 0 \\ 0 & 0 & 0 & -1 \\ 0 & 0 & -1 & 0 \end{pmatrix}, \qquad \widetilde{R}\left(P_{31}\right) = \begin{pmatrix} 0 & 1 & 0 & 0 \\ 1 & 0 & 0 & 0 \\ 0 & 0 & 0 & -1 \\ 0 & 0 & -1 & 0 \end{pmatrix},
$$

$$
\widetilde{L}\left(P_{231}\right) = \begin{pmatrix} 1 & 0 & 0 & 0 \\ 0 & 1 & 0 & 0 \\ 0 & 0 & 1 & 0 \\ 0 & 0 & 0 & 1 \end{pmatrix}, \qquad \widetilde{R}\left(P_{231}\right) = \begin{pmatrix} 1 & 0 & 0 & 0 \\ 0 & 1 & 0 & 0 \\ 0 & 0 & 1 & 0 \\ 0 & 0 & 0 & 1 \end{pmatrix},
$$

$$
\widetilde{L}\left(P_{312}\right) = \begin{pmatrix} 1 & 0 & 0 & 0 \\ 0 & 1 & 0 & 0 \\ 0 & 0 & 1 & 0 \\ 0 & 0 & 0 & 1 \end{pmatrix}, \qquad \widetilde{R}\left(P_{312}\right) = \begin{pmatrix} 1 & 0 & 0 & 0 \\ 0 & 1 & 0 & 0 \\ 0 & 0 & 1 & 0 \\ 0 & 0 & 0 & 1 \end{pmatrix},
$$

$$L(\mathbb{1}) = \begin{pmatrix} 1 & 0 & 0 & 0 \\ 0 & 1 & 0 & 0 \\ 0 & 0 & 1 & 0 \\ 0 & 0 & 0 & 1 \end{pmatrix}, \qquad R(\mathbb{1}) = \begin{pmatrix} 1 & 0 & 0 & 0 \\ 0 & 1 & 0 & 0 \\ 0 & 0 & 1 & 0 \\ 0 & 0 & 0 & 1 \end{pmatrix}, \tag{F.17}$$

$$L\left(P_{12}\right) = \begin{pmatrix} 1 & 0 & 0 & 0 \\ 0 & -1 & 0 & 0 \\ 0 & 0 & -1 & 0 \\ 0 & 0 & 0 & 1 \end{pmatrix}, \qquad R\left(P_{12}\right) = \begin{pmatrix} 1 & 0 & 0 & 0 \\ 0 & -1 & 0 & 0 \\ 0 & 0 & 1 & 0 \\ 0 & 0 & 0 & -1 \end{pmatrix},$$

$$L\left(P_{23}\right) = \begin{pmatrix} -\frac{1}{2} & 0 & \frac{\sqrt{3}}{2} & 0 \\ 0 & \frac{1}{2} & 0 & \frac{\sqrt{3}}{2} \\ \frac{\sqrt{3}}{2} & 0 & \frac{1}{2} & 0 \\ 0 & \frac{\sqrt{3}}{2} & 0 & -\frac{1}{2} \end{pmatrix}, \qquad R\left(P_{23}\right) = \begin{pmatrix} -\frac{1}{2} & 0 & 0 & \frac{\sqrt{3}}{2} \\ 0 & \frac{1}{2} & \frac{\sqrt{3}}{2} & 0 \\ 0 & \frac{\sqrt{3}}{2} & -\frac{1}{2} & 0 \\ \frac{\sqrt{3}}{2} & 0 & 0 & \frac{1}{2} \end{pmatrix},$$

$$L\left(P_{31}\right) = \begin{pmatrix} -\frac{1}{2} & 0 & -\frac{\sqrt{3}}{2} & 0 \\ 0 & \frac{1}{2} & 0 & -\frac{\sqrt{3}}{2} \\ -\frac{\sqrt{3}}{2} & 0 & \frac{1}{2} & 0 \\ 0 & -\frac{\sqrt{3}}{2} & 0 & -\frac{1}{2} \end{pmatrix}, \qquad R\left(P_{31}\right) = \begin{pmatrix} -\frac{1}{2} & 0 & 0 & -\frac{\sqrt{3}}{2} \\ 0 & \frac{1}{2} & -\frac{\sqrt{3}}{2} & 0 \\ 0 & -\frac{\sqrt{3}}{2} & -\frac{1}{2} & 0 \\ -\frac{\sqrt{3}}{2} & 0 & 0 & \frac{1}{2} \end{pmatrix},$$

$$L\left(P_{231}\right) = \begin{pmatrix} -\frac{1}{2} & 0 & -\frac{\sqrt{3}}{2} & 0 \\ 0 & -\frac{1}{2} & 0 & \frac{\sqrt{3}}{2} \\ \frac{\sqrt{3}}{2} & 0 & -\frac{1}{2} & 0 \\ 0 & -\frac{\sqrt{3}}{2} & 0 & -\frac{1}{2} \end{pmatrix}, \qquad R\left(P_{231}\right) = \begin{pmatrix} -\frac{1}{2} & 0 & 0 & -\frac{\sqrt{3}}{2} \\ 0 & -\frac{1}{2} & \frac{\sqrt{3}}{2} & 0 \\ 0 & -\frac{\sqrt{3}}{2} & -\frac{1}{2} & 0 \\ \frac{\sqrt{3}}{2} & 0 & 0 & -\frac{1}{2} \end{pmatrix},$$

$$L\left(P_{312}\right) = \begin{pmatrix} -\frac{1}{2} & 0 & \frac{\sqrt{3}}{2} & 0 \\ 0 & -\frac{1}{2} & 0 & -\frac{\sqrt{3}}{2} \\ -\frac{\sqrt{3}}{2} & 0 & -\frac{1}{2} & 0 \\ 0 & \frac{\sqrt{3}}{2} & 0 & -\frac{1}{2} \end{pmatrix}, \qquad R\left(P_{312}\right) = \begin{pmatrix} -\frac{1}{2} & 0 & 0 & \frac{\sqrt{3}}{2} \\ 0 & -\frac{1}{2} & -\frac{\sqrt{3}}{2} & 0 \\ 0 & \frac{\sqrt{3}}{2} & -\frac{1}{2} & 0 \\ -\frac{\sqrt{3}}{2} & 0 & 0 & -\frac{1}{2} \end{pmatrix}.$$

In terms of the direct link dual flux basis the same energy eigenstates are represented by

$$\begin{aligned} \left|E_1, 12\right\rangle &= \frac{1}{\sqrt{12}}\Big(2\left|1\right\rangle \otimes \left|\widetilde{\Gamma_1}\right\rangle + 2\left|P_{12}\right\rangle \otimes \left|\widetilde{\Gamma_1}\right\rangle - \left|P_{23}\right\rangle \otimes \left|\widetilde{\Gamma_1}\right\rangle - \left|P_{31}\right\rangle \otimes \left|\widetilde{\Gamma_1}\right\rangle \\ &\quad -\left|P_{231}\right\rangle \otimes \left|\widetilde{\Gamma_1}\right\rangle - \left|P_{312}\right\rangle \otimes \left|\widetilde{\Gamma_1}\right\rangle\Big), \\ \left|E_1, 21\right\rangle &= \frac{1}{\sqrt{12}}\Big(2\left|1\right\rangle \otimes \left|\widetilde{\Gamma_1}\right\rangle - 2\left|P_{12}\right\rangle \otimes \left|\widetilde{\Gamma_1}\right\rangle + \left|P_{23}\right\rangle \otimes \left|\widetilde{\Gamma_1}\right\rangle + \left|P_{31}\right\rangle \otimes \left|\widetilde{\Gamma_1}\right\rangle \\ &\quad -\left|P_{231}\right\rangle \otimes \left|\widetilde{\Gamma_1}\right\rangle - \left|P_{312}\right\rangle \otimes \left|\widetilde{\Gamma_1}\right\rangle\Big), \\ \left|E_1, 11\right\rangle &= \frac{1}{2}\Big(\left|P_{23}\right\rangle \otimes \left|\widetilde{\Gamma_1}\right\rangle - \left|P_{31}\right\rangle \otimes \left|\widetilde{\Gamma_1}\right\rangle + \left|P_{231}\right\rangle \otimes \left|\widetilde{\Gamma_1}\right\rangle - \left|P_{312}\right\rangle \otimes \left|\widetilde{\Gamma_1}\right\rangle\Big), \end{aligned} \tag{F.18}$$

$$\left|E_1, 22\right\rangle = \frac{1}{2}\left(-\left|P_{23}\right\rangle \otimes \left|\widetilde{\Gamma_1}\right\rangle + \left|P_{31}\right\rangle \otimes \left|\widetilde{\Gamma_1}\right\rangle + \left|P_{231}\right\rangle \otimes \left|\widetilde{\Gamma_1}\right\rangle - \left|P_{312}\right\rangle \otimes \left|\widetilde{\Gamma_1}\right\rangle\right).$$

The second set of first excited energy eigenstates is given in the direct flux dual link basis by

$$\begin{aligned}
\left|E_1, 5\right\rangle &= \frac{1}{\sqrt{6}}\left(2\left|\Gamma_1\right\rangle \otimes \left|\widetilde{1}\right\rangle - \left|\Gamma_1\right\rangle \otimes \left|\widetilde{P_{231}}\right\rangle - \left|\Gamma_1\right\rangle \otimes \left|\widetilde{P_{312}}\right\rangle\right), \\
\left|E_1, 6\right\rangle &= \frac{1}{\sqrt{2}}\left(\left|\Gamma_1\right\rangle \otimes \left|\widetilde{P_{231}}\right\rangle - \left|\Gamma_1\right\rangle \otimes \left|\widetilde{P_{312}}\right\rangle\right), \\
\left|E_1, 7\right\rangle &= \frac{1}{\sqrt{2}}\left(\left|\Gamma_1\right\rangle \otimes \left|\widetilde{P_{12}}\right\rangle - \left|\Gamma_1\right\rangle \otimes \left|\widetilde{P_{31}}\right\rangle\right), \\
\left|E_1, 8\right\rangle &= \frac{1}{\sqrt{6}}\left(\left|\Gamma_1\right\rangle \otimes \left|\widetilde{P_{12}}\right\rangle - 2\left|\Gamma_1\right\rangle \otimes \left|\widetilde{P_{23}}\right\rangle + \left|\Gamma_1\right\rangle \otimes \left|\widetilde{P_{31}}\right\rangle\right).
\end{aligned} \tag{F.19}$$

In a basis of these four eigenstates, the left and right operators are given by

$$\widetilde{L}(\mathbb{1}) = \begin{pmatrix} 1 & 0 & 0 & 0 \\ 0 & 1 & 0 & 0 \\ 0 & 0 & 1 & 0 \\ 0 & 0 & 0 & 1 \end{pmatrix}, \qquad \widetilde{R}(\mathbb{1}) = \begin{pmatrix} 1 & 0 & 0 & 0 \\ 0 & 1 & 0 & 0 \\ 0 & 0 & 1 & 0 \\ 0 & 0 & 0 & 1 \end{pmatrix}, \tag{F.20}$$

$$\widetilde{L}\left(P_{12}\right) = \begin{pmatrix} 0 & 0 & \frac{\sqrt{3}}{2} & \frac{1}{2} \\ 0 & 0 & -\frac{1}{2} & \frac{\sqrt{3}}{2} \\ \frac{\sqrt{3}}{2} & -\frac{1}{2} & 0 & 0 \\ \frac{1}{2} & \frac{\sqrt{3}}{2} & 0 & 0 \end{pmatrix}, \qquad \widetilde{R}\left(P_{12}\right) = \begin{pmatrix} 0 & 0 & \frac{\sqrt{3}}{2} & \frac{1}{2} \\ 0 & 0 & \frac{1}{2} & -\frac{\sqrt{3}}{2} \\ \frac{\sqrt{3}}{2} & \frac{1}{2} & 0 & 0 \\ \frac{1}{2} & -\frac{\sqrt{3}}{2} & 0 & 0 \end{pmatrix},$$

$$\widetilde{L}\left(P_{23}\right) = \begin{pmatrix} 0 & 0 & 0 & -1 \\ 0 & 0 & 1 & 0 \\ 0 & 1 & 0 & 0 \\ -1 & 0 & 0 & 0 \end{pmatrix}, \qquad \widetilde{R}\left(P_{23}\right) = \begin{pmatrix} 0 & 0 & 0 & -1 \\ 0 & 0 & -1 & 0 \\ 0 & -1 & 0 & 0 \\ -1 & 0 & 0 & 0 \end{pmatrix},$$

$$\widetilde{L}\left(P_{31}\right) = \begin{pmatrix} 0 & 0 & -\frac{\sqrt{3}}{2} & \frac{1}{2} \\ 0 & 0 & -\frac{1}{2} & -\frac{\sqrt{3}}{2} \\ -\frac{\sqrt{3}}{2} & -\frac{1}{2} & 0 & 0 \\ \frac{1}{2} & -\frac{\sqrt{3}}{2} & 0 & 0 \end{pmatrix}, \qquad \widetilde{R}\left(P_{31}\right) = \begin{pmatrix} 0 & 0 & -\frac{\sqrt{3}}{2} & \frac{1}{2} \\ 0 & 0 & \frac{1}{2} & \frac{\sqrt{3}}{2} \\ -\frac{\sqrt{3}}{2} & \frac{1}{2} & 0 & 0 \\ \frac{1}{2} & \frac{\sqrt{3}}{2} & 0 & 0 \end{pmatrix},$$

$$\widetilde{L}\left(P_{231}\right) = \begin{pmatrix} -\frac{1}{2} & -\frac{\sqrt{3}}{2} & 0 & 0 \\ \frac{\sqrt{3}}{2} & -\frac{1}{2} & 0 & 0 \\ 0 & 0 & -\frac{1}{2} & \frac{\sqrt{3}}{2} \\ 0 & 0 & -\frac{\sqrt{3}}{2} & -\frac{1}{2} \end{pmatrix}, \qquad \widetilde{R}\left(P_{231}\right) = \begin{pmatrix} -\frac{1}{2} & \frac{\sqrt{3}}{2} & 0 & 0 \\ -\frac{\sqrt{3}}{2} & -\frac{1}{2} & 0 & 0 \\ 0 & 0 & -\frac{1}{2} & \frac{\sqrt{3}}{2} \\ 0 & 0 & -\frac{\sqrt{3}}{2} & -\frac{1}{2} \end{pmatrix},$$

$$\widetilde{L}\left(P_{312}\right)=\begin{pmatrix} -\frac{1}{2} & \frac{\sqrt{3}}{2} & 0 & 0 \\ -\frac{\sqrt{3}}{2} & -\frac{1}{2} & 0 & 0 \\ 0 & 0 & -\frac{1}{2} & -\frac{\sqrt{3}}{2} \\ 0 & 0 & \frac{\sqrt{3}}{2} & -\frac{1}{2} \end{pmatrix}, \qquad \widetilde{R}\left(P_{312}\right)=\begin{pmatrix} -\frac{1}{2} & -\frac{\sqrt{3}}{2} & 0 & 0 \\ \frac{\sqrt{3}}{2} & -\frac{1}{2} & 0 & 0 \\ 0 & 0 & -\frac{1}{2} & -\frac{\sqrt{3}}{2} \\ 0 & 0 & \frac{\sqrt{3}}{2} & -\frac{1}{2} \end{pmatrix},$$

$$L\left(\mathbb{1}\right)=\begin{pmatrix} 1 & 0 & 0 & 0 \\ 0 & 1 & 0 & 0 \\ 0 & 0 & 1 & 0 \\ 0 & 0 & 0 & 1 \end{pmatrix}, \qquad R\left(\mathbb{1}\right)=\begin{pmatrix} 1 & 0 & 0 & 0 \\ 0 & 1 & 0 & 0 \\ 0 & 0 & 1 & 0 \\ 0 & 0 & 0 & 1 \end{pmatrix}, \tag{F.21}$$

$$L\left(P_{12}\right)=\begin{pmatrix} 1 & 0 & 0 & 0 \\ 0 & 1 & 0 & 0 \\ 0 & 0 & -1 & 0 \\ 0 & 0 & 0 & -1 \end{pmatrix}, \qquad R\left(P_{12}\right)=\begin{pmatrix} 1 & 0 & 0 & 0 \\ 0 & 1 & 0 & 0 \\ 0 & 0 & -1 & 0 \\ 0 & 0 & 0 & -1 \end{pmatrix},$$

$$L\left(P_{23}\right)=\begin{pmatrix} 1 & 0 & 0 & 0 \\ 0 & 1 & 0 & 0 \\ 0 & 0 & -1 & 0 \\ 0 & 0 & 0 & -1 \end{pmatrix}, \qquad R\left(P_{23}\right)=\begin{pmatrix} 1 & 0 & 0 & 0 \\ 0 & 1 & 0 & 0 \\ 0 & 0 & -1 & 0 \\ 0 & 0 & 0 & -1 \end{pmatrix},$$

$$L\left(P_{31}\right)=\begin{pmatrix} 1 & 0 & 0 & 0 \\ 0 & 1 & 0 & 0 \\ 0 & 0 & -1 & 0 \\ 0 & 0 & 0 & -1 \end{pmatrix}, \qquad R\left(P_{31}\right)=\begin{pmatrix} 1 & 0 & 0 & 0 \\ 0 & 1 & 0 & 0 \\ 0 & 0 & -1 & 0 \\ 0 & 0 & 0 & -1 \end{pmatrix},$$

$$L\left(P_{231}\right)=\begin{pmatrix} 1 & 0 & 0 & 0 \\ 0 & 1 & 0 & 0 \\ 0 & 0 & 1 & 0 \\ 0 & 0 & 0 & 1 \end{pmatrix}, \qquad R\left(P_{231}\right)=\begin{pmatrix} 1 & 0 & 0 & 0 \\ 0 & 1 & 0 & 0 \\ 0 & 0 & 1 & 0 \\ 0 & 0 & 0 & 1 \end{pmatrix},$$

$$L\left(P_{312}\right)=\begin{pmatrix} 1 & 0 & 0 & 0 \\ 0 & 1 & 0 & 0 \\ 0 & 0 & 1 & 0 \\ 0 & 0 & 0 & 1 \end{pmatrix}, \qquad R\left(P_{312}\right)=\begin{pmatrix} 1 & 0 & 0 & 0 \\ 0 & 1 & 0 & 0 \\ 0 & 0 & 1 & 0 \\ 0 & 0 & 0 & 1 \end{pmatrix}.$$

Changing to the direct link dual flux basis the same states are given by

$$\begin{aligned} \left|E_1,5\right\rangle = \frac{1}{\sqrt{12}}\Big(&\left|1\right\rangle\otimes\left|\widetilde{\Gamma_3^{11}}\right\rangle+\left|1\right\rangle\otimes\left|\widetilde{\Gamma_3^{22}}\right\rangle+\left|P_{12}\right\rangle\otimes\left|\widetilde{\Gamma_3^{11}}\right\rangle+\left|P_{12}\right\rangle\otimes\left|\widetilde{\Gamma_3^{22}}\right\rangle \\ &+\left|P_{21}\right\rangle\otimes\left|\widetilde{\Gamma_3^{11}}\right\rangle+\left|P_{21}\right\rangle\otimes\left|\widetilde{\Gamma_3^{22}}\right\rangle+\left|P_{31}\right\rangle\otimes\left|\widetilde{\Gamma_3^{11}}\right\rangle+\left|P_{31}\right\rangle\otimes\left|\widetilde{\Gamma_3^{22}}\right\rangle \\ &+\left|P_{231}\right\rangle\otimes\left|\widetilde{\Gamma_3^{11}}\right\rangle+\left|P_{231}\right\rangle\otimes\left|\widetilde{\Gamma_3^{22}}\right\rangle+\left|P_{312}\right\rangle\otimes\left|\widetilde{\Gamma_3^{11}}\right\rangle+\left|P_{312}\right\rangle\otimes\left|\widetilde{\Gamma_3^{22}}\right\rangle\Big), \\ \left|E_1,6\right\rangle = \frac{1}{\sqrt{12}}\Big(&\left|1\right\rangle\otimes\left|\widetilde{\Gamma_3^{11}}\right\rangle-\left|1\right\rangle\otimes\left|\widetilde{\Gamma_3^{22}}\right\rangle+\left|P_{12}\right\rangle\otimes\left|\widetilde{\Gamma_3^{11}}\right\rangle-\left|P_{12}\right\rangle\otimes\left|\widetilde{\Gamma_3^{22}}\right\rangle \\ &+\left|P_{21}\right\rangle\otimes\left|\widetilde{\Gamma_3^{11}}\right\rangle-\left|P_{21}\right\rangle\otimes\left|\widetilde{\Gamma_3^{22}}\right\rangle+\left|P_{31}\right\rangle\otimes\left|\widetilde{\Gamma_3^{11}}\right\rangle-\left|P_{31}\right\rangle\otimes\left|\widetilde{\Gamma_3^{22}}\right\rangle \\ &+\left|P_{231}\right\rangle\otimes\left|\widetilde{\Gamma_3^{11}}\right\rangle-\left|P_{231}\right\rangle\otimes\left|\widetilde{\Gamma_3^{22}}\right\rangle+\left|P_{312}\right\rangle\otimes\left|\widetilde{\Gamma_3^{11}}\right\rangle-\left|P_{312}\right\rangle\otimes\left|\widetilde{\Gamma_3^{22}}\right\rangle\Big), \end{aligned} \tag{F.22}$$

$$
\begin{aligned}
|E_1,7\rangle = \frac{1}{\sqrt{12}}\Big(&\sqrt{3}|1\rangle\otimes|\widetilde{\Gamma_3^{11}}\rangle + |1\rangle\otimes|\widetilde{\Gamma_3^{12}}\rangle + |1\rangle\otimes|\widetilde{\Gamma_3^{21}}\rangle - \sqrt{3}|1\rangle\otimes|\widetilde{\Gamma_3^{22}}\rangle \\
&- \sqrt{3}|P_{12}\rangle\otimes|\widetilde{\Gamma_3^{11}}\rangle - |P_{12}\rangle\otimes|\widetilde{\Gamma_3^{12}}\rangle - |P_{12}\rangle\otimes|\widetilde{\Gamma_3^{21}}\rangle + \sqrt{3}|P_{12}\rangle\otimes|\widetilde{\Gamma_3^{22}}\rangle \\
&- \sqrt{3}|P_{23}\rangle\otimes|\widetilde{\Gamma_3^{11}}\rangle - |P_{23}\rangle\otimes|\widetilde{\Gamma_3^{12}}\rangle - |P_{23}\rangle\otimes|\widetilde{\Gamma_3^{21}}\rangle + \sqrt{3}|P_{23}\rangle\otimes|\widetilde{\Gamma_3^{22}}\rangle \\
&- \sqrt{3}|P_{31}\rangle\otimes|\widetilde{\Gamma_3^{11}}\rangle - |P_{31}\rangle\otimes|\widetilde{\Gamma_3^{12}}\rangle - |P_{31}\rangle\otimes|\widetilde{\Gamma_3^{21}}\rangle + \sqrt{3}|P_{31}\rangle\otimes|\widetilde{\Gamma_3^{22}}\rangle \\
&+ \sqrt{3}|P_{231}\rangle\otimes|\widetilde{\Gamma_3^{11}}\rangle + |P_{231}\rangle\otimes|\widetilde{\Gamma_3^{12}}\rangle + |P_{231}\rangle\otimes|\widetilde{\Gamma_3^{21}}\rangle - \sqrt{3}|P_{231}\rangle\otimes|\widetilde{\Gamma_3^{22}}\rangle \\
&+\sqrt{3}|P_{312}\rangle\otimes|\widetilde{\Gamma_3^{11}}\rangle + |P_{312}\rangle\otimes|\widetilde{\Gamma_3^{12}}\rangle + |P_{312}\rangle\otimes|\widetilde{\Gamma_3^{21}}\rangle - \sqrt{3}|P_{312}\rangle\otimes|\widetilde{\Gamma_3^{22}}\rangle\Big), \\
|E_1,8\rangle = \frac{1}{\sqrt{12}}\Big(&|1\rangle\otimes|\widetilde{\Gamma_3^{11}}\rangle - \sqrt{3}|1\rangle\otimes|\widetilde{\Gamma_3^{12}}\rangle - \sqrt{3}|1\rangle\otimes|\widetilde{\Gamma_3^{21}}\rangle - |1\rangle\otimes|\widetilde{\Gamma_3^{22}}\rangle \\
&- |P_{12}\rangle\otimes|\widetilde{\Gamma_3^{11}}\rangle + \sqrt{3}|P_{12}\rangle\otimes|\widetilde{\Gamma_3^{12}}\rangle + \sqrt{3}|P_{12}\rangle\otimes|\widetilde{\Gamma_3^{21}}\rangle + |P_{12}\rangle\otimes|\widetilde{\Gamma_3^{22}}\rangle \\
&- |P_{23}\rangle\otimes|\widetilde{\Gamma_3^{11}}\rangle + \sqrt{3}|P_{23}\rangle\otimes|\widetilde{\Gamma_3^{12}}\rangle + \sqrt{3}|P_{23}\rangle\otimes|\widetilde{\Gamma_3^{21}}\rangle + |P_{23}\rangle\otimes|\widetilde{\Gamma_3^{22}}\rangle \\
&- |P_{31}\rangle\otimes|\widetilde{\Gamma_3^{11}}\rangle + \sqrt{3}|P_{31}\rangle\otimes|\widetilde{\Gamma_3^{12}}\rangle + \sqrt{3}|P_{31}\rangle\otimes|\widetilde{\Gamma_3^{21}}\rangle + |P_{31}\rangle\otimes|\widetilde{\Gamma_3^{22}}\rangle \\
&+ |P_{231}\rangle\otimes|\widetilde{\Gamma_3^{11}}\rangle - \sqrt{3}|P_{231}\rangle\otimes|\widetilde{\Gamma_3^{12}}\rangle - \sqrt{3}|P_{231}\rangle\otimes|\widetilde{\Gamma_3^{21}}\rangle - |P_{231}\rangle\otimes|\widetilde{\Gamma_3^{22}}\rangle \\
&+|P_{312}\rangle\otimes|\widetilde{\Gamma_3^{11}}\rangle - \sqrt{3}|P_{312}\rangle\otimes|\widetilde{\Gamma_3^{12}}\rangle - \sqrt{3}|P_{312}\rangle\otimes|\widetilde{\Gamma_3^{21}}\rangle - |P_{312}\rangle\otimes|\widetilde{\Gamma_3^{22}}\rangle\Big).
\end{aligned}
$$

Second Excited Energy Eigenstates: $E_2 = 3$

The second excited energy level contains 16 states that are given by

$$
\begin{aligned}
|E_2,1\rangle &= \frac{1}{\sqrt{6}}\Big(2|\Gamma_3^{11}\rangle\otimes|\widetilde{1}\rangle - |\Gamma_3^{11}\rangle\otimes|\widetilde{P_{231}}\rangle - |\Gamma_3^{11}\rangle\otimes|\widetilde{P_{312}}\rangle\Big), \qquad \text{(F.23)}\\
|E_2,2\rangle &= \frac{1}{\sqrt{2}}\Big(|\Gamma_3^{11}\rangle\otimes|\widetilde{P_{231}}\rangle - |\Gamma_3^{11}\rangle\otimes|\widetilde{P_{312}}\rangle\Big),\\
|E_2,3\rangle &= \frac{1}{\sqrt{2}}\Big(|\Gamma_3^{11}\rangle\otimes|\widetilde{P_{12}}\rangle - |\Gamma_3^{11}\rangle\otimes|\widetilde{P_{31}}\rangle\Big),\\
|E_2,4\rangle &= \frac{1}{\sqrt{6}}\Big(|\Gamma_3^{11}\rangle\otimes|\widetilde{P_{12}}\rangle - 2|\Gamma_3^{11}\rangle\otimes|\widetilde{P_{23}}\rangle + |\Gamma_3^{11}\rangle\otimes|\widetilde{P_{31}}\rangle\Big),\\
\\
|E_2,5\rangle &= \frac{1}{\sqrt{6}}\Big(2|\Gamma_3^{12}\rangle\otimes|\widetilde{1}\rangle - |\Gamma_3^{12}\rangle\otimes|\widetilde{P_{231}}\rangle - |\Gamma_3^{12}\rangle\otimes|\widetilde{P_{312}}\rangle\Big),\\
|E_2,6\rangle &= \frac{1}{\sqrt{2}}\Big(|\Gamma_3^{12}\rangle\otimes|\widetilde{P_{231}}\rangle - |\Gamma_3^{12}\rangle\otimes|\widetilde{P_{312}}\rangle\Big),\\
|E_2,7\rangle &= \frac{1}{\sqrt{2}}\Big(|\Gamma_3^{12}\rangle\otimes|\widetilde{P_{12}}\rangle - |\Gamma_3^{12}\rangle\otimes|\widetilde{P_{31}}\rangle\Big),\\
|E_2,8\rangle &= \frac{1}{\sqrt{6}}\Big(|\Gamma_3^{12}\rangle\otimes|\widetilde{P_{12}}\rangle - 2|\Gamma_3^{12}\rangle\otimes|\widetilde{P_{23}}\rangle + |\Gamma_3^{12}\rangle\otimes|\widetilde{P_{31}}\rangle\Big),
\end{aligned}
$$

$$
\begin{aligned}
\big|E_2,9\big\rangle &= \frac{1}{\sqrt{6}}\Big(2\big|\Gamma_3^{21}\big\rangle\otimes\big|\widetilde{1}\big\rangle-\big|\Gamma_3^{21}\big\rangle\otimes\big|\widetilde{P_{231}}\big\rangle-\big|\Gamma_3^{21}\big\rangle\otimes\big|\widetilde{P_{312}}\big\rangle\Big)\,.\\
\big|E_2,10\big\rangle &= \frac{1}{\sqrt{2}}\Big(\big|\Gamma_3^{21}\big\rangle\otimes\big|\widetilde{P_{231}}\big\rangle-\big|\Gamma_3^{21}\big\rangle\otimes\big|\widetilde{P_{312}}\big\rangle\Big),\\
\big|E_2,11\big\rangle &= \frac{1}{\sqrt{2}}\Big(\big|\Gamma_3^{21}\big\rangle\otimes\big|\widetilde{P_{12}}\big\rangle-\big|\Gamma_3^{21}\big\rangle\otimes\big|\widetilde{P_{31}}\big\rangle\Big),\\
\big|E_2,12\big\rangle &= \frac{1}{\sqrt{6}}\Big(\big|\Gamma_3^{21}\big\rangle\otimes\big|\widetilde{P_{12}}\big\rangle-2\big|\Gamma_3^{21}\big\rangle\otimes\big|\widetilde{P_{23}}\big\rangle+\big|\Gamma_3^{21}\big\rangle\otimes\big|\widetilde{P_{31}}\big\rangle\Big),\\
\\
\big|E_2,13\big\rangle &= \frac{1}{\sqrt{6}}\Big(2\big|\Gamma_3^{22}\big\rangle\otimes\big|\widetilde{1}\big\rangle-\big|\Gamma_3^{22}\big\rangle\otimes\big|\widetilde{P_{231}}\big\rangle-\big|\Gamma_3^{22}\big\rangle\otimes\big|\widetilde{P_{312}}\big\rangle\Big),\\
\big|E_2,14\big\rangle &= \frac{1}{\sqrt{2}}\Big(\big|\Gamma_3^{22}\big\rangle\otimes\big|\widetilde{P_{231}}\big\rangle-\big|\Gamma_3^{22}\big\rangle\otimes\big|\widetilde{P_{312}}\big\rangle\Big),\\
\big|E_2,15\big\rangle &= \frac{1}{\sqrt{2}}\Big(\big|\Gamma_3^{22}\big\rangle\otimes\big|\widetilde{P_{12}}\big\rangle-\big|\Gamma_3^{22}\big\rangle\otimes\big|\widetilde{P_{31}}\big\rangle\Big),\\
\big|E_2,16\big\rangle &= \frac{1}{\sqrt{6}}\Big(\big|\Gamma_3^{22}\big\rangle\otimes\big|\widetilde{P_{12}}\big\rangle-2\big|\Gamma_3^{22}\big\rangle\otimes\big|\widetilde{P_{23}}\big\rangle+\big|\Gamma_3^{22}\big\rangle\otimes\big|\widetilde{P_{31}}\big\rangle\Big)\,.
\end{aligned}
$$

In terms of the above energy eigenstates, the left and right operators are given by

$$
\widetilde{L}\,(1)=\mathbb{1}_{4\times4}\otimes\mathbb{1}_{4\times4},\qquad
\widetilde{L}\,(P_{12})=\begin{pmatrix}0&0&\frac{\sqrt3}{2}&\frac12\\0&0&-\frac12&\frac{\sqrt3}{2}\\\frac{\sqrt3}{2}&-\frac12&0&0\\\frac12&\frac{\sqrt3}{2}&0&0\end{pmatrix}\otimes\mathbb{1}_{4\times4},
$$

$$
\widetilde{L}\,(P_{23})=\begin{pmatrix}0&0&0&-1\\0&0&1&0\\0&1&0&0\\-1&0&0&0\end{pmatrix}\otimes\mathbb{1}_{4\times4},\qquad
\widetilde{L}\,(P_{31})=\begin{pmatrix}0&0&-\frac{\sqrt3}{2}&\frac12\\0&0&-\frac12&-\frac{\sqrt3}{2}\\-\frac{\sqrt3}{2}&-\frac12&0&0\\\frac12&-\frac{\sqrt3}{2}&0&0\end{pmatrix}\otimes\mathbb{1}_{4\times4},
$$

$$
\widetilde{L}\,(P_{231})=\begin{pmatrix}-\frac12&-\frac{\sqrt3}{2}&0&0\\\frac{\sqrt3}{2}&-\frac12&0&0\\0&0&-\frac12&\frac{\sqrt3}{2}\\0&0&-\frac{\sqrt3}{2}&-\frac12\end{pmatrix}\otimes\mathbb{1}_{4\times4},\quad
\widetilde{L}\,(P_{312})=\begin{pmatrix}-\frac12&\frac{\sqrt3}{2}&0&0\\-\frac{\sqrt3}{2}&-\frac12&0&0\\0&0&-\frac12&-\frac{\sqrt3}{2}\\0&0&\frac{\sqrt3}{2}&-\frac12\end{pmatrix}\otimes\mathbb{1}_{4\times4},
$$

$$
\widetilde{R}\,(1)=\mathbb{1}_{4\times4}\otimes\mathbb{1}_{4\times},\qquad
\widetilde{R}\,(P_{12})=\begin{pmatrix}0&0&\frac{\sqrt3}{2}&\frac12\\0&0&\frac12&-\frac{\sqrt3}{2}\\\frac{\sqrt3}{2}&-\frac12&0&0\\\frac12&-\frac{\sqrt3}{2}&0&0\end{pmatrix}\otimes\mathbb{1}_{4\times4},
$$

$$\widetilde{R}\left(P_{23}\right)=\begin{pmatrix}0&0&0&-1\\0&0&-1&0\\0&-1&0&0\\-1&0&0&0\end{pmatrix}\otimes\mathbb{1}_{4\times4},\qquad \widetilde{R}\left(P_{31}\right)=\begin{pmatrix}0&0&-\frac{\sqrt{3}}{2}&\frac{1}{2}\\0&0&\frac{1}{2}&\frac{\sqrt{3}}{2}\\-\frac{\sqrt{3}}{2}&\frac{1}{2}&0&0\\\frac{1}{2}&\frac{\sqrt{3}}{2}&0&0\end{pmatrix}\otimes\mathbb{1}_{4\times4},$$

$$\widetilde{R}\left(P_{231}\right)=\begin{pmatrix}-\frac{1}{2}&\frac{\sqrt{3}}{2}&0&0\\-\frac{\sqrt{3}}{2}&-\frac{1}{2}&0&0\\0&0&-\frac{1}{2}&\frac{\sqrt{3}}{2}\\0&0&-\frac{\sqrt{3}}{2}&-\frac{1}{2}\end{pmatrix}\otimes\mathbb{1}_{4\times4},\quad \widetilde{R}\left(P_{312}\right)=\begin{pmatrix}-\frac{1}{2}&-\frac{\sqrt{3}}{2}&0&0\\\frac{\sqrt{3}}{2}&-\frac{1}{2}&0&0\\0&0&-\frac{1}{2}&-\frac{\sqrt{3}}{2}\\0&0&\frac{\sqrt{3}}{2}&-\frac{1}{2}\end{pmatrix}\otimes\mathbb{1}_{4\times4},$$

$$L\left(1\right)=\mathbb{1}_{4\times4}\otimes\mathbb{1}_{4\times4}$$

$$L\left(P_{12}\right)=\begin{pmatrix}\mathbb{1}_{2\times2}&0\\0&-\mathbb{1}_{2\times2}\end{pmatrix}\otimes\begin{pmatrix}1&0&0&0\\0&-1&0&0\\0&0&1&0\\0&0&0&-1\end{pmatrix},$$

$$L\left(P_{23}\right)=\begin{pmatrix}\mathbb{1}_{2\times2}&0\\0&-\mathbb{1}_{2\times2}\end{pmatrix}\otimes\begin{pmatrix}-\frac{1}{2}&\frac{\sqrt{3}}{2}&0&0\\\frac{\sqrt{3}}{2}&\frac{1}{2}&0&0\\0&0&-\frac{1}{2}&\frac{\sqrt{3}}{2}\\0&0&\frac{\sqrt{3}}{2}&\frac{1}{2}\end{pmatrix},$$

$$L\left(P_{31}\right)=\begin{pmatrix}\mathbb{1}_{2\times2}&0\\0&-\mathbb{1}_{2\times2}\end{pmatrix}\otimes\begin{pmatrix}-\frac{1}{2}&-\frac{\sqrt{3}}{2}&0&0\\-\frac{\sqrt{3}}{2}&\frac{1}{2}&0&0\\0&0&-\frac{1}{2}&-\frac{\sqrt{3}}{2}\\0&0&-\frac{\sqrt{3}}{2}&\frac{1}{2}\end{pmatrix},$$

$$L\left(P_{231}\right)=\begin{pmatrix}\mathbb{1}_{2\times2}&0\\0&\mathbb{1}_{2\times2}\end{pmatrix}\otimes\begin{pmatrix}-\frac{1}{2}&-\frac{\sqrt{3}}{2}&0&0\\\frac{\sqrt{3}}{2}&-\frac{1}{2}&0&0\\0&0&-\frac{1}{2}&-\frac{\sqrt{3}}{2}\\0&0&\frac{\sqrt{3}}{2}&-\frac{1}{2}\end{pmatrix},$$

$$L\left(P_{312}\right)=\begin{pmatrix}\mathbb{1}_{2\times2}&0\\0&\mathbb{1}_{2\times2}\end{pmatrix}\otimes\begin{pmatrix}-\frac{1}{2}&\frac{\sqrt{3}}{2}&0&0\\-\frac{\sqrt{3}}{2}&-\frac{1}{2}&0&0\\0&0&-\frac{1}{2}&+\frac{\sqrt{3}}{2}\\0&0&-\frac{\sqrt{3}}{2}&-\frac{1}{2}\end{pmatrix},$$

$$R\left(1\right)=\mathbb{1}_{4\times4}\otimes\mathbb{1}_{4\times4},$$

$$R\left(P_{12}\right) = \begin{pmatrix} \mathbb{1}_{2\times2} & 0 \\ 0 & -\mathbb{1}_{2\times2} \end{pmatrix} \otimes \begin{pmatrix} 1 & 0 & 0 & 0 \\ 0 & 1 & 0 & 0 \\ 0 & 0 & -1 & 0 \\ 0 & 0 & 0 & -1 \end{pmatrix},$$

$$R\left(P_{23}\right) = \begin{pmatrix} \mathbb{1}_{2\times2} & 0 \\ 0 & -\mathbb{1}_{2\times2} \end{pmatrix} \otimes \begin{pmatrix} -\frac{1}{2} & 0 & \frac{\sqrt{3}}{2} & 0 \\ 0 & -\frac{1}{2} & 0 & \frac{\sqrt{3}}{2} \\ \frac{\sqrt{3}}{2} & 0 & \frac{1}{2} & 0 \\ 0 & \frac{\sqrt{3}}{2} & 0 & \frac{1}{2} \end{pmatrix},$$

$$R\left(P_{31}\right) = \begin{pmatrix} \mathbb{1}_{2\times2} & 0 \\ 0 & -\mathbb{1}_{2\times2} \end{pmatrix} \otimes \begin{pmatrix} -\frac{1}{2} & 0 & -\frac{\sqrt{3}}{2} & 0 \\ 0 & -\frac{1}{2} & 0 & -\frac{\sqrt{3}}{2} \\ -\frac{\sqrt{3}}{2} & 0 & \frac{1}{2} & 0 \\ 0 & -\frac{\sqrt{3}}{2} & 0 & \frac{1}{2} \end{pmatrix},$$

$$R\left(P_{231}\right) = \begin{pmatrix} \mathbb{1}_{2\times2} & 0 \\ 0 & \mathbb{1}_{2\times2} \end{pmatrix} \otimes \begin{pmatrix} -\frac{1}{2} & 0 & -\frac{\sqrt{3}}{2} & 0 \\ 0 & -\frac{1}{2} & 0 & -\frac{\sqrt{3}}{2} \\ \frac{\sqrt{3}}{2} & 0 & -\frac{1}{2} & 0 \\ 0 & \frac{\sqrt{3}}{2} & 0 & -\frac{1}{2} \end{pmatrix},$$

$$R\left(P_{312}\right) = \begin{pmatrix} \mathbb{1}_{2\times2} & 0 \\ 0 & \mathbb{1}_{2\times2} \end{pmatrix} \otimes \begin{pmatrix} -\frac{1}{2} & 0 & \frac{\sqrt{3}}{2} & 0 \\ 0 & -\frac{1}{2} & 0 & \frac{\sqrt{3}}{2} \\ -\frac{\sqrt{3}}{2} & 0 & -\frac{1}{2} & 0 \\ 0 & -\frac{\sqrt{3}}{2} & 0 & -\frac{1}{2} \end{pmatrix},$$

Changing to the direct link dual flux basis the same energy eigenstates are represented as

$$\begin{aligned}
\left|E_2,1\right\rangle = \frac{1}{\sqrt{24}}\Big(&2\left|1\right\rangle\otimes\left|\widetilde{\Gamma_3^{11}}\right\rangle + 2\left|1\right\rangle\otimes\left|\widetilde{\Gamma_3^{22}}\right\rangle + 2\left|P_{12}\right\rangle\otimes\left|\widetilde{\Gamma_3^{11}}\right\rangle + \left|P_{12}\right\rangle\otimes\left|\widetilde{\Gamma_3^{22}}\right\rangle \\
&- \left|P_{23}\right\rangle\otimes\left|\widetilde{\Gamma_3^{11}}\right\rangle - \left|P_{23}\right\rangle\otimes\left|\widetilde{\Gamma_3^{22}}\right\rangle - \left|P_{31}\right\rangle\otimes\left|\widetilde{\Gamma_3^{11}}\right\rangle - \left|P_{31}\right\rangle\otimes\left|\widetilde{\Gamma_3^{22}}\right\rangle \\
&- \left|P_{231}\right\rangle\otimes\left|\widetilde{\Gamma_3^{11}}\right\rangle - \left|P_{231}\right\rangle\otimes\left|\widetilde{\Gamma_3^{22}}\right\rangle - \left|P_{312}\right\rangle\otimes\left|\widetilde{\Gamma_3^{11}}\right\rangle - \left|P_{312}\right\rangle\otimes\left|\widetilde{\Gamma_3^{22}}\right\rangle\Big), \\
\left|E_2,2\right\rangle = \frac{1}{\sqrt{24}}\Big(&2\left|1\right\rangle\otimes\left|\widetilde{\Gamma_3^{12}}\right\rangle - 2\left|1\right\rangle\otimes\left|\widetilde{\Gamma_3^{21}}\right\rangle + 2\left|P_{12}\right\rangle\otimes\left|\widetilde{\Gamma_3^{12}}\right\rangle - \left|P_{12}\right\rangle\otimes\left|\widetilde{\Gamma_3^{21}}\right\rangle \\
&- \left|P_{23}\right\rangle\otimes\left|\widetilde{\Gamma_3^{12}}\right\rangle + \left|P_{23}\right\rangle\otimes\left|\widetilde{\Gamma_3^{21}}\right\rangle - \left|P_{31}\right\rangle\otimes\left|\widetilde{\Gamma_3^{12}}\right\rangle + \left|P_{31}\right\rangle\otimes\left|\widetilde{\Gamma_3^{21}}\right\rangle \\
&- \left|P_{231}\right\rangle\otimes\left|\widetilde{\Gamma_3^{12}}\right\rangle + \left|P_{231}\right\rangle\otimes\left|\widetilde{\Gamma_3^{21}}\right\rangle - \left|P_{312}\right\rangle\otimes\left|\widetilde{\Gamma_3^{12}}\right\rangle + \left|P_{312}\right\rangle\otimes\left|\widetilde{\Gamma_3^{21}}\right\rangle\Big), \\
\left|E_2,3\right\rangle = \frac{1}{\sqrt{96}}\Big(&2\sqrt{3}\left|1\right\rangle\otimes\left|\widetilde{\Gamma_3^{1}}\right\rangle + 2\left|1\right\rangle\otimes\left|\widetilde{\Gamma_3^{12}}\right\rangle + 2\left|1\right\rangle\otimes\left|\widetilde{\Gamma_3^{21}}\right\rangle - 2\sqrt{3}\left|1\right\rangle\otimes\left|\widetilde{\Gamma_3^{22}}\right\rangle \\
&- 2\sqrt{3}\left|P_{12}\right\rangle\otimes\left|\widetilde{\Gamma_3^{1}}\right\rangle - 2\left|P_{12}\right\rangle\otimes\left|\widetilde{\Gamma_3^{12}}\right\rangle - 2\left|P_{12}\right\rangle\otimes\left|\widetilde{\Gamma_3^{21}}\right\rangle + 2\sqrt{3}\left|P_{12}\right\rangle\otimes\left|\widetilde{\Gamma_3^{22}}\right\rangle
\end{aligned} \tag{F.24}$$

$$
\begin{aligned}
&+\sqrt{3}|P_{23}\rangle\otimes|\widetilde{\Gamma^{1}_{3}}\rangle+|P_{23}\rangle\otimes|\widetilde{\Gamma^{12}_{3}}\rangle+|P_{23}\rangle\otimes|\widetilde{\Gamma^{21}_{3}}\rangle-\sqrt{3}|P_{23}\rangle\otimes|\widetilde{\Gamma^{22}_{3}}\rangle\\
&+\sqrt{3}|P_{31}\rangle\otimes|\widetilde{\Gamma^{1}_{3}}\rangle+|P_{31}\rangle\otimes|\widetilde{\Gamma^{12}_{3}}\rangle+|P_{31}\rangle\otimes|\widetilde{\Gamma^{21}_{3}}\rangle-\sqrt{3}|P_{31}\rangle\otimes|\widetilde{\Gamma^{22}_{3}}\rangle\\
&-\sqrt{3}|P_{231}\rangle\otimes|\widetilde{\Gamma^{1}_{3}}\rangle-|P_{231}\rangle\otimes|\widetilde{\Gamma^{12}_{3}}\rangle-|P_{231}\rangle\otimes|\widetilde{\Gamma^{21}_{3}}\rangle+\sqrt{3}|P_{231}\rangle\otimes|\widetilde{\Gamma^{22}_{3}}\rangle\\
&-\sqrt{3}|P_{312}\rangle\otimes|\widetilde{\Gamma^{1}_{3}}\rangle-|P_{312}\rangle\otimes|\widetilde{\Gamma^{12}_{3}}\rangle-|P_{312}\rangle\otimes|\widetilde{\Gamma^{21}_{3}}\rangle+\sqrt{3}|P_{312}\rangle\otimes|\widetilde{\Gamma^{22}_{3}}\rangle\Big),
\end{aligned}
$$

$$
\begin{aligned}
|E_2,4\rangle=\frac{1}{\sqrt{96}}\Big(&2\sqrt{3}|1\rangle\otimes|\widetilde{\Gamma^{1}_{3}}\rangle-2|1\rangle\otimes|\widetilde{\Gamma^{12}_{3}}\rangle-2|1\rangle\otimes|\widetilde{\Gamma^{21}_{3}}\rangle-2\sqrt{3}|1\rangle\otimes|\widetilde{\Gamma^{22}_{3}}\rangle\\
&-2\sqrt{3}|P_{12}\rangle\otimes|\widetilde{\Gamma^{1}_{3}}\rangle+2|P_{12}\rangle\otimes|\widetilde{\Gamma^{12}_{3}}\rangle+2|P_{12}\rangle\otimes|\widetilde{\Gamma^{21}_{3}}\rangle+2\sqrt{3}|P_{12}\rangle\otimes|\widetilde{\Gamma^{22}_{3}}\rangle\\
&+\sqrt{3}|P_{23}\rangle\otimes|\widetilde{\Gamma^{1}_{3}}\rangle-|P_{23}\rangle\otimes|\widetilde{\Gamma^{12}_{3}}\rangle-|P_{23}\rangle\otimes|\widetilde{\Gamma^{21}_{3}}\rangle-\sqrt{3}|P_{23}\rangle\otimes|\widetilde{\Gamma^{22}_{3}}\rangle\\
&+\sqrt{3}|P_{31}\rangle\otimes|\widetilde{\Gamma^{1}_{3}}\rangle-|P_{31}\rangle\otimes|\widetilde{\Gamma^{12}_{3}}\rangle-|P_{31}\rangle\otimes|\widetilde{\Gamma^{21}_{3}}\rangle-\sqrt{3}|P_{31}\rangle\otimes|\widetilde{\Gamma^{22}_{3}}\rangle\\
&-\sqrt{3}|P_{231}\rangle\otimes|\widetilde{\Gamma^{1}_{3}}\rangle+|P_{231}\rangle\otimes|\widetilde{\Gamma^{12}_{3}}\rangle+|P_{231}\rangle\otimes|\widetilde{\Gamma^{21}_{3}}\rangle+\sqrt{3}|P_{231}\rangle\otimes|\widetilde{\Gamma^{22}_{3}}\rangle\\
&-\sqrt{3}|P_{312}\rangle\otimes|\widetilde{\Gamma^{1}_{3}}\rangle+|P_{312}\rangle\otimes|\widetilde{\Gamma^{12}_{3}}\rangle+|P_{312}\rangle\otimes|\widetilde{\Gamma^{21}_{3}}\rangle+\sqrt{3}|P_{312}\rangle\otimes|\widetilde{\Gamma^{22}_{3}}\rangle\Big),
\end{aligned}
$$

$$
\begin{aligned}
|E_2,5\rangle=\frac{1}{\sqrt{8}}\Big(&|P_{23}\rangle\otimes|\widetilde{\Gamma^{11}_{3}}\rangle+|P_{23}\rangle\otimes|\widetilde{\Gamma^{22}_{3}}\rangle-|P_{3}1\rangle\otimes|\widetilde{\Gamma^{11}_{3}}\rangle-|P_{31}\rangle\otimes|\widetilde{\Gamma^{22}_{3}}\rangle\\
&+|P_{231}\rangle\otimes|\widetilde{\Gamma^{11}_{3}}\rangle+|P_{231}\rangle\otimes|\widetilde{\Gamma^{22}_{3}}\rangle-|P_{312}\rangle\otimes|\widetilde{\Gamma^{11}_{3}}\rangle-|P_{312}\rangle\otimes|\widetilde{\Gamma^{22}_{3}}\rangle\Big),\\
|E_2,6\rangle=\frac{1}{\sqrt{8}}\Big(&|P_{23}\rangle\otimes|\widetilde{\Gamma^{11}_{3}}\rangle-|P_{23}\rangle\otimes|\widetilde{\Gamma^{22}_{3}}\rangle-|P_{31}\rangle\otimes|\widetilde{\Gamma^{11}_{3}}\rangle+|P_{31}\rangle\otimes|\widetilde{\Gamma^{22}_{3}}\rangle\\
&+|P_{231}\rangle\otimes|\widetilde{\Gamma^{11}_{3}}\rangle-|P_{231}\rangle\otimes|\widetilde{\Gamma^{22}_{3}}\rangle-|P_{312}\rangle\otimes|\widetilde{\Gamma^{11}_{3}}\rangle+|P_{312}\rangle\otimes|\widetilde{\Gamma^{22}_{3}}\rangle\Big),\\
|E_2,7\rangle=\frac{1}{\sqrt{32}}\Big(&-\sqrt{3}|P_{23}\rangle\otimes|\widetilde{\Gamma^{11}_{3}}\rangle-|P_{23}\rangle\otimes|\widetilde{\Gamma^{12}_{3}}\rangle-|P_{23}\rangle\otimes|\widetilde{\Gamma^{21}_{3}}\rangle+\sqrt{3}|P_{23}\rangle\otimes|\widetilde{\Gamma^{22}_{3}}\rangle\\
&+\sqrt{3}|P_{31}\rangle\otimes|\widetilde{\Gamma^{11}_{3}}\rangle+|P_{31}\rangle\otimes|\widetilde{\Gamma^{12}_{3}}\rangle+|P_{31}\rangle\otimes|\widetilde{\Gamma^{21}_{3}}\rangle-\sqrt{3}|P_{31}\rangle\otimes|\widetilde{\Gamma^{22}_{3}}\rangle\\
&+\sqrt{3}|P_{231}\rangle\otimes|\widetilde{\Gamma^{11}_{3}}\rangle+|P_{231}\rangle\otimes|\widetilde{\Gamma^{12}_{3}}\rangle+|P_{231}\rangle\otimes|\widetilde{\Gamma^{21}_{3}}\rangle-\sqrt{3}|P_{231}\rangle\otimes|\widetilde{\Gamma^{22}_{3}}\rangle\\
&-\sqrt{3}|P_{312}\rangle\otimes|\widetilde{\Gamma^{11}_{3}}\rangle-|P_{312}\rangle\otimes|\widetilde{\Gamma^{12}_{3}}\rangle-|P_{312}\rangle\otimes|\widetilde{\Gamma^{21}_{3}}\rangle+\sqrt{3}|P_{312}\rangle\otimes|\widetilde{\Gamma^{22}_{3}}\rangle\Big),\\
|E_2,8\rangle=\frac{1}{\sqrt{32}}\Big(&-|P_{23}\rangle\otimes|\widetilde{\Gamma^{11}_{3}}\rangle+\sqrt{3}|P_{23}\rangle\otimes|\widetilde{\Gamma^{12}_{3}}\rangle+\sqrt{3}|P_{23}\rangle\otimes|\widetilde{\Gamma^{21}_{3}}\rangle+|P_{23}\rangle\otimes|\widetilde{\Gamma^{22}_{3}}\rangle\\
&+|P_{31}\rangle\otimes|\widetilde{\Gamma^{11}_{3}}\rangle-\sqrt{3}|P_{31}\rangle\otimes|\widetilde{\Gamma^{12}_{3}}\rangle-\sqrt{3}|P_{31}\rangle\otimes|\widetilde{\Gamma^{21}_{3}}\rangle-|P_{31}\rangle\otimes|\widetilde{\Gamma^{22}_{3}}\rangle\\
&+|P_{231}\rangle\otimes|\widetilde{\Gamma^{11}_{3}}\rangle-\sqrt{3}|P_{231}\rangle\otimes|\widetilde{\Gamma^{12}_{3}}\rangle-\sqrt{3}|P_{231}\rangle\otimes|\widetilde{\Gamma^{21}_{3}}\rangle-|P_{231}\rangle\otimes|\widetilde{\Gamma^{22}_{3}}\rangle\\
&-|P_{312}\rangle\otimes|\widetilde{\Gamma^{11}_{3}}\rangle+\sqrt{3}|P_{312}\rangle\otimes|\widetilde{\Gamma^{12}_{3}}\rangle+\sqrt{3}|P_{312}\rangle\otimes|\widetilde{\Gamma^{21}_{3}}\rangle+|P_{312}\rangle\otimes|\widetilde{\Gamma^{22}_{3}}\rangle\Big),
\end{aligned}
$$

$$
\begin{aligned}
|E_2,9\rangle=\frac{1}{\sqrt{8}}\Big(&|P_{23}\rangle\otimes|\widetilde{\Gamma^{11}_{3}}\rangle+|P_{23}\rangle\otimes|\widetilde{\Gamma^{22}_{3}}\rangle-|P_{31}\rangle\otimes|\widetilde{\Gamma^{11}_{3}}\rangle-|P_{31}\rangle\otimes|\widetilde{\Gamma^{22}_{3}}\rangle\\
&-|P_{231}\rangle\otimes|\widetilde{\Gamma^{11}_{3}}\rangle-|P_{231}\rangle\otimes|\widetilde{\Gamma^{22}_{3}}\rangle+|P_{312}\rangle\otimes|\widetilde{\Gamma^{11}_{3}}\rangle+|P_{312}\rangle\otimes|\widetilde{\Gamma^{22}_{3}}\rangle\Big),
\end{aligned}
$$

$$
\begin{aligned}
|E_2,10\rangle = \frac{1}{\sqrt{8}}\Big(&|P_{23}\rangle\otimes|\widetilde{\Gamma_3^{12}}\rangle - |P_{23}\rangle\otimes|\widetilde{\Gamma_3^{21}}\rangle - |P_{31}\rangle\otimes|\widetilde{\Gamma_3^{12}}\rangle + |P_{31}\rangle\otimes|\widetilde{\Gamma_3^{21}}\rangle \\
&-|P_{231}\rangle\otimes|\widetilde{\Gamma_3^{12}}\rangle + |P_{231}\rangle\otimes|\widetilde{\Gamma_3^{21}}\rangle + |P_{312}\rangle\otimes|\widetilde{\Gamma_3^{12}}\rangle - |P_{312}\rangle\otimes|\widetilde{\Gamma_3^{21}}\rangle\Big),\\
|E_2,11\rangle = \frac{1}{\sqrt{32}}\Big(&-\sqrt{3}|P_{23}\rangle\otimes|\widetilde{\Gamma_3^{11}}\rangle - |P_{23}\rangle\otimes|\widetilde{\Gamma_3^{12}}\rangle - |P_{23}\rangle\otimes|\widetilde{\Gamma_3^{21}}\rangle + \sqrt{3}|P_{23}\rangle\otimes|\widetilde{\Gamma_3^{22}}\rangle \\
&+\sqrt{3}|P_{31}\rangle\otimes|\widetilde{\Gamma_3^{11}}\rangle + |P_{31}\rangle\otimes|\widetilde{\Gamma_3^{12}}\rangle + |P_{31}\rangle\otimes|\widetilde{\Gamma_3^{21}}\rangle - \sqrt{3}|P_{31}\rangle\otimes|\widetilde{\Gamma_3^{22}}\rangle \\
&-\sqrt{3}|P_{231}\rangle\otimes|\widetilde{\Gamma_3^{11}}\rangle - |P_{231}\rangle\otimes|\widetilde{\Gamma_3^{12}}\rangle - |P_{231}\rangle\otimes|\widetilde{\Gamma_3^{21}}\rangle + \sqrt{3}|P_{231}\rangle\otimes|\widetilde{\Gamma_3^{22}}\rangle \\
&+\sqrt{3}|P_{312}\rangle\otimes|\widetilde{\Gamma_3^{11}}\rangle + |P_{312}\rangle\otimes|\widetilde{\Gamma_3^{12}}\rangle + |P_{312}\rangle\otimes|\widetilde{\Gamma_3^{21}}\rangle - \sqrt{3}|P_{312}\rangle\otimes|\widetilde{\Gamma_3^{22}}\rangle\Big),\\
|E_2,12\rangle = \frac{1}{\sqrt{32}}\Big(&-|P_{23}\rangle\otimes|\widetilde{\Gamma_3^{11}}\rangle + \sqrt{3}|P_{23}\rangle\otimes|\widetilde{\Gamma_3^{12}}\rangle + \sqrt{3}|P_{23}\rangle\otimes|\widetilde{\Gamma_3^{21}}\rangle + |P_{23}\rangle\otimes|\widetilde{\Gamma_3^{22}}\rangle \\
&+|P_{31}\rangle\otimes|\widetilde{\Gamma_3^{11}}\rangle - \sqrt{3}|P_{31}\rangle\otimes|\widetilde{\Gamma_3^{12}}\rangle - \sqrt{3}|P_{31}\rangle\otimes|\widetilde{\Gamma_3^{21}}\rangle - |P_{31}\rangle\otimes|\widetilde{\Gamma_3^{22}}\rangle \\
&-|P_{231}\rangle\otimes|\widetilde{\Gamma_3^{11}}\rangle + \sqrt{3}|P_{231}\rangle\otimes|\widetilde{\Gamma_3^{12}}\rangle + \sqrt{3}|P_{231}\rangle\otimes|\widetilde{\Gamma_3^{21}}\rangle + |P_{231}\rangle\otimes|\widetilde{\Gamma_3^{22}}\rangle \\
&+|P_{312}\rangle\otimes|\widetilde{\Gamma_3^{11}}\rangle - \sqrt{3}|P_{312}\rangle\otimes|\widetilde{\Gamma_3^{12}}\rangle - \sqrt{3}|P_{312}\rangle\otimes|\widetilde{\Gamma_3^{21}}\rangle - |P_{312}\rangle\otimes|\widetilde{\Gamma_3^{22}}\rangle\Big),
\end{aligned}
$$

$$
\begin{aligned}
|E_2,13\rangle = \frac{1}{\sqrt{24}}\Big(&2|1\rangle\otimes|\widetilde{\Gamma_3^{11}}\rangle + 2|1\rangle\otimes|\widetilde{\Gamma_3^{22}}\rangle - 2|P_{12}\rangle\otimes|\widetilde{\Gamma_3^{11}}\rangle - |P_{12}\rangle\otimes|\widetilde{\Gamma_3^{22}}\rangle \\
&+|P_{23}\rangle\otimes|\widetilde{\Gamma_3^{11}}\rangle + |P_{23}\rangle\otimes|\widetilde{\Gamma_3^{22}}\rangle + |P_{31}\rangle\otimes|\widetilde{\Gamma_3^{11}}\rangle + |P_{31}\rangle\otimes|\widetilde{\Gamma_3^{22}}\rangle \\
&-|P_{231}\rangle\otimes|\widetilde{\Gamma_3^{11}}\rangle - |P_{231}\rangle\otimes|\widetilde{\Gamma_3^{22}}\rangle - |P_{312}\rangle\otimes|\widetilde{\Gamma_3^{11}}\rangle - |P_{312}\rangle\otimes|\widetilde{\Gamma_3^{22}}\rangle\Big),\\
|E_2,14\rangle = \frac{1}{\sqrt{24}}\Big(&2|1\rangle\otimes|\widetilde{\Gamma_3^{12}}\rangle - 2|1\rangle\otimes|\widetilde{\Gamma_3^{21}}\rangle - 2|P_{12}\rangle\otimes|\widetilde{\Gamma_3^{12}}\rangle + |P_{12}\rangle\otimes|\widetilde{\Gamma_3^{21}}\rangle \\
&+|P_{23}\rangle\otimes|\widetilde{\Gamma_3^{12}}\rangle - |P_{23}\rangle\otimes|\widetilde{\Gamma_3^{21}}\rangle + |P_{31}\rangle\otimes|\widetilde{\Gamma_3^{12}}\rangle - |P_{31}\rangle\otimes|\widetilde{\Gamma_3^{21}}\rangle \\
&-|P_{231}\rangle\otimes|\widetilde{\Gamma_3^{12}}\rangle + |P_{231}\rangle\otimes|\widetilde{\Gamma_3^{21}}\rangle - |P_{312}\rangle\otimes|\widetilde{\Gamma_3^{12}}\rangle + |P_{312}\rangle\otimes|\widetilde{\Gamma_3^{21}}\rangle\Big),\\
|E_2,15\rangle = \frac{1}{\sqrt{96}}\Big(&2\sqrt{3}|1\rangle\otimes|\widetilde{\Gamma_3^{1}}\rangle + 2|1\rangle\otimes|\widetilde{\Gamma_3^{12}}\rangle + 2|1\rangle\otimes|\widetilde{\Gamma_3^{21}}\rangle - 2\sqrt{3}|1\rangle\otimes|\widetilde{\Gamma_3^{22}}\rangle \\
&+2\sqrt{3}|P_{12}\rangle\otimes|\widetilde{\Gamma_3^{1}}\rangle + 2|P_{12}\rangle\otimes|\widetilde{\Gamma_3^{12}}\rangle + 2|P_{12}\rangle\otimes|\widetilde{\Gamma_3^{21}}\rangle - 2\sqrt{3}|P_{12}\rangle\otimes|\widetilde{\Gamma_3^{22}}\rangle \\
&-\sqrt{3}|P_{23}\rangle\otimes|\widetilde{\Gamma_3^{1}}\rangle - |P_{23}\rangle\otimes|\widetilde{\Gamma_3^{12}}\rangle - |P_{23}\rangle\otimes|\widetilde{\Gamma_3^{21}}\rangle + \sqrt{3}|P_{23}\rangle\otimes|\widetilde{\Gamma_3^{22}}\rangle \\
&-\sqrt{3}|P_{31}\rangle\otimes|\widetilde{\Gamma_3^{1}}\rangle - |P_{31}\rangle\otimes|\widetilde{\Gamma_3^{12}}\rangle - |P_{31}\rangle\otimes|\widetilde{\Gamma_3^{21}}\rangle + \sqrt{3}|P_{31}\rangle\otimes|\widetilde{\Gamma_3^{22}}\rangle \\
&-\sqrt{3}|P_{231}\rangle\otimes|\widetilde{\Gamma_3^{1}}\rangle - |P_{231}\rangle\otimes|\widetilde{\Gamma_3^{12}}\rangle - |P_{231}\rangle\otimes|\widetilde{\Gamma_3^{21}}\rangle + \sqrt{3}|P_{231}\rangle\otimes|\widetilde{\Gamma_3^{22}}\rangle \\
&-\sqrt{3}|P_{312}\rangle\otimes|\widetilde{\Gamma_3^{1}}\rangle - |P_{312}\rangle\otimes|\widetilde{\Gamma_3^{12}}\rangle - |P_{312}\rangle\otimes|\widetilde{\Gamma_3^{21}}\rangle + \sqrt{3}|P_{312}\rangle\otimes|\widetilde{\Gamma_3^{22}}\rangle\Big),\\
|E_2,16\rangle = \frac{1}{\sqrt{96}}\Big(&2\sqrt{3}|1\rangle\otimes|\widetilde{\Gamma_3^{1}}\rangle - 2|1\rangle\otimes|\widetilde{\Gamma_3^{12}}\rangle - 2|1\rangle\otimes|\widetilde{\Gamma_3^{21}}\rangle - 2\sqrt{3}|1\rangle\otimes|\widetilde{\Gamma_3^{22}}\rangle \\
&+2\sqrt{3}|P_{12}\rangle\otimes|\widetilde{\Gamma_3^{1}}\rangle - 2|P_{12}\rangle\otimes|\widetilde{\Gamma_3^{12}}\rangle - 2|P_{12}\rangle\otimes|\widetilde{\Gamma_3^{21}}\rangle - 2\sqrt{3}|P_{12}\rangle\otimes|\widetilde{\Gamma_3^{22}}\rangle \\
&-\sqrt{3}|P_{23}\rangle\otimes|\widetilde{\Gamma_3^{1}}\rangle + |P_{23}\rangle\otimes|\widetilde{\Gamma_3^{12}}\rangle + |P_{23}\rangle\otimes|\widetilde{\Gamma_3^{21}}\rangle + \sqrt{3}|P_{23}\rangle\otimes|\widetilde{\Gamma_3^{22}}\rangle
\end{aligned}
$$

$$
\begin{aligned}
&- \sqrt{3}\left|P_{31}\right\rangle \otimes \left|\widetilde{\Gamma_3^1}\right\rangle + \left|P_{31}\right\rangle \otimes \left|\widetilde{\Gamma_3^{12}}\right\rangle + \left|P_{31}\right\rangle \otimes \left|\widetilde{\Gamma_3^{21}}\right\rangle + \sqrt{3}\left|P_{31}\right\rangle \otimes \left|\widetilde{\Gamma_3^{22}}\right\rangle \\
&- \sqrt{3}\left|P_{231}\right\rangle \otimes \left|\widetilde{\Gamma_3^1}\right\rangle + \left|P_{231}\right\rangle \otimes \left|\widetilde{\Gamma_3^{12}}\right\rangle + \left|P_{231}\right\rangle \otimes \left|\widetilde{\Gamma_3^{21}}\right\rangle + \sqrt{3}\left|P_{231}\right\rangle \otimes \left|\widetilde{\Gamma_3^{22}}\right\rangle \\
&- \sqrt{3}\left|P_{312}\right\rangle \otimes \left|\widetilde{\Gamma_3^1}\right\rangle + \left|P_{312}\right\rangle \otimes \left|\widetilde{\Gamma_3^{12}}\right\rangle + \left|P_{312}\right\rangle \otimes \left|\widetilde{\Gamma_3^{21}}\right\rangle + \sqrt{3}\left|P_{312}\right\rangle \otimes \left|\widetilde{\Gamma_3^{22}}\right\rangle \Big).
\end{aligned}
$$

F.3 $\bar{D}_2$ Energy Eigenstates

F.3.1 $\bar{D}_2$ with a Non-Trivial Cocycle: ω_2

Lowest Energy Eigenstates: $E_0 = 2\left(2 - \sqrt{2}\right)$

In the lowest energy level, there are two energy eigenstates which are given by

$$
\begin{aligned}
\left|E_0, 1\right\rangle = \frac{1}{\sqrt{8\left(2+\sqrt{2}\right)}} \Big(&\left(1+\sqrt{2}\right)\left|\Gamma_1\right\rangle \otimes \left|\widetilde{\mathbb{1}}\right\rangle + \left(1+\sqrt{2}\right)\left|\Gamma_1\right\rangle \otimes \left|\widetilde{-\mathbb{1}}\right\rangle \\
&+ \left(1+\sqrt{2}\right)\left|\Gamma_1\right\rangle \otimes \left|\widetilde{i\sigma_1}\right\rangle + \left(1+\sqrt{2}\right)\left|\Gamma_1\right\rangle \otimes \left|\widetilde{-i\sigma_1}\right\rangle \\
&+ \left|\Gamma_2\right\rangle \otimes \left|\widetilde{i\sigma_2}\right\rangle + \left|\Gamma_2\right\rangle \otimes \left|\widetilde{-i\sigma_2}\right\rangle + \left|\Gamma_2\right\rangle \otimes \left|\widetilde{i\sigma_3}\right\rangle + \left|\Gamma_2\right\rangle \otimes \left|\widetilde{-i\sigma_3}\right\rangle \Big),
\end{aligned}
\tag{F.25}
$$

$$
\begin{aligned}
\left|E_0, 2\right\rangle = \frac{1}{\sqrt{8\left(2+\sqrt{2}\right)}} \Big(&\left|\Gamma_2\right\rangle \otimes \left|\widetilde{\mathbb{1}}\right\rangle + \left|\Gamma_2\right\rangle \otimes \left|\widetilde{-\mathbb{1}}\right\rangle + \left|\Gamma_2\right\rangle \otimes \left|\widetilde{i\sigma_1}\right\rangle + \left|\Gamma_2\right\rangle \otimes \left|\widetilde{-i\sigma_1}\right\rangle \\
&+ \left(1+\sqrt{2}\right)\left|\Gamma_1\right\rangle \otimes \left|\widetilde{i\sigma_2}\right\rangle + \left(1+\sqrt{2}\right)\left|\Gamma_1\right\rangle \otimes \left|\widetilde{-i\sigma_2}\right\rangle \\
&+ \left(1+\sqrt{2}\right)\left|\Gamma_1\right\rangle \otimes \left|\widetilde{i\sigma_3}\right\rangle + \left(1+\sqrt{2}\right)\left|\Gamma_1\right\rangle \otimes \left|\widetilde{-i\sigma_3}\right\rangle \Big).
\end{aligned}
\tag{F.26}
$$

First Excited Energy Eigenstates: $E_1 = 3$

In the first excited energy level, there are eight energy eigenstates, that can be separated into two sets of four, depending on the representations. The first set contains states with a direct Γ_5-flux. These energy eigenstates are given by

$$
\begin{aligned}
\left|E_1, 1\right\rangle = \frac{1}{\sqrt{8}} \Big(&\left|\Gamma_5^{11}\right\rangle \otimes \left|\widetilde{\mathbb{1}}\right\rangle + \left|\Gamma_5^{11}\right\rangle \otimes \left|\widetilde{-\mathbb{1}}\right\rangle + \left|\Gamma_5^{11}\right\rangle \otimes \left|\widetilde{i\sigma_1}\right\rangle + \left|\Gamma_5^{11}\right\rangle \otimes \left|\widetilde{-i\sigma_1}\right\rangle \\
&+ \left|\Gamma_5^{22}\right\rangle \otimes \left|\widetilde{i\sigma_2}\right\rangle + \left|\Gamma_5^{22}\right\rangle \otimes \left|\widetilde{-i\sigma_2}\right\rangle + \left|\Gamma_5^{22}\right\rangle \otimes \left|\widetilde{i\sigma_3}\right\rangle + \left|\Gamma_5^{22}\right\rangle \otimes \left|\widetilde{-i\sigma_2}\right\rangle \Big),
\end{aligned}
\tag{F.27}
$$

$$
\begin{aligned}
\left|E_1, 2\right\rangle = \frac{1}{\sqrt{8}} \Big(&\left|\Gamma_5^{22}\right\rangle \otimes \left|\widetilde{\mathbb{1}}\right\rangle + \left|\Gamma_5^{22}\right\rangle \otimes \left|\widetilde{-\mathbb{1}}\right\rangle + \left|\Gamma_5^{22}\right\rangle \otimes \left|\widetilde{i\sigma_1}\right\rangle + \left|\Gamma_5^{22}\right\rangle \otimes \left|\widetilde{-i\sigma_1}\right\rangle \\
&+ \left|\Gamma_5^{11}\right\rangle \otimes \left|\widetilde{i\sigma_2}\right\rangle + \left|\Gamma_5^{11}\right\rangle \otimes \left|\widetilde{-i\sigma_2}\right\rangle + \left|\Gamma_5^{11}\right\rangle \otimes \left|\widetilde{i\sigma_3}\right\rangle + \left|\Gamma_5^{11}\right\rangle \otimes \left|\widetilde{-i\sigma_2}\right\rangle \Big),
\end{aligned}
$$

$$
\begin{aligned}
\big|E_1,3\big\rangle = \frac{1}{\sqrt{8}}\Big(&\big|\Gamma_5^{12}\big\rangle\otimes\big|\widetilde{\mathbb{1}}\big\rangle + \big|\Gamma_5^{12}\big\rangle\otimes\big|\widetilde{-\mathbb{1}}\big\rangle + \big|\Gamma_5^{12}\big\rangle\otimes\big|\widetilde{i\sigma_1}\big\rangle + \big|\Gamma_5^{12}\big\rangle\otimes\big|\widetilde{-i\sigma_1}\big\rangle \\
&+\big|\Gamma_5^{12}\big\rangle\otimes\big|\widetilde{i\sigma_2}\big\rangle + \big|\Gamma_5^{12}\big\rangle\otimes\big|\widetilde{-i\sigma_2}\big\rangle + \big|\Gamma_5^{12}\big\rangle\otimes\big|\widetilde{i\sigma_3}\big\rangle + \big|\Gamma_5^{12}\big\rangle\otimes\big|\widetilde{-i\sigma_2}\big\rangle\Big), \\
\big|E_1,4\big\rangle = \frac{1}{\sqrt{8}}\Big(&\big|\Gamma_5^{21}\big\rangle\otimes\big|\widetilde{\mathbb{1}}\big\rangle + \big|\Gamma_5^{21}\big\rangle\otimes\big|\widetilde{-\mathbb{1}}\big\rangle + \big|\Gamma_5^{21}\big\rangle\otimes\big|\widetilde{i\sigma_1}\big\rangle + \big|\Gamma_5^{21}\big\rangle\otimes\big|\widetilde{-i\sigma_1}\big\rangle \\
&+\big|\Gamma_5^{21}\big\rangle\otimes\big|\widetilde{i\sigma_2}\big\rangle + \big|\Gamma_5^{21}\big\rangle\otimes\big|\widetilde{-i\sigma_2}\big\rangle + \big|\Gamma_5^{21}\big\rangle\otimes\big|\widetilde{i\sigma_3}\big\rangle + \big|\Gamma_5^{21}\big\rangle\otimes\big|\widetilde{-i\sigma_2}\big\rangle\Big).
\end{aligned}
$$

The second set contains states with a direct Γ_1 flux, and the energy eigenstates are given by

$$
\begin{aligned}
\big|E_1,5\big\rangle &= \frac{1}{\sqrt{2}}\Big(\big|\Gamma_1\big\rangle\otimes\big|\widetilde{\mathbb{1}}\big\rangle - \big|\Gamma_1\big\rangle\otimes\big|\widetilde{-\mathbb{1}}\big\rangle\Big), \\
\big|E_1,6\big\rangle &= \frac{1}{\sqrt{2}}\Big(\big|\Gamma_1\big\rangle\otimes\big|\widetilde{i\sigma_1}\big\rangle - \big|\Gamma_1\big\rangle\otimes\big|\widetilde{-i\sigma_1}\big\rangle\Big), \\
\big|E_1,7\big\rangle &= \frac{1}{\sqrt{2}}\Big(\big|\Gamma_1\big\rangle\otimes\big|\widetilde{i\sigma_2}\big\rangle - \big|\Gamma_1\big\rangle\otimes\big|\widetilde{-i\sigma_2}\big\rangle\Big), \\
\big|E_1,8\big\rangle &= \frac{1}{\sqrt{2}}\Big(\big|\Gamma_1\big\rangle\otimes\big|\widetilde{i\sigma_3}\big\rangle - \big|\Gamma_1\big\rangle\otimes\big|\widetilde{-i\sigma_3}\big\rangle\Big).
\end{aligned}
\tag{F.28}
$$

Second Excited Energy Eigenstates: $E_2 = 4$

In the second excited energy level, there are four energy eigenstates that are given by

$$
\begin{aligned}
\big|E_2,1\big\rangle &= \frac{1}{2}\Big(\big|\Gamma_1\big\rangle\otimes\big|\widetilde{\mathbb{1}}\big\rangle + \big|\Gamma_1\big\rangle\otimes\big|\widetilde{-\mathbb{1}}\big\rangle - \big|\Gamma_1\big\rangle\otimes\big|\widetilde{i\sigma_1}\big\rangle - \big|\Gamma_1\big\rangle\otimes\big|\widetilde{-i\sigma_1}\big\rangle\Big), \\
\big|E_2,2\big\rangle &= \frac{1}{2}\Big(\big|\Gamma_1\big\rangle\otimes\big|\widetilde{i\sigma_2}\big\rangle + \big|\Gamma_1\big\rangle\otimes\big|\widetilde{-i\sigma_2}\big\rangle - \big|\Gamma_1\big\rangle\otimes\big|\widetilde{i\sigma_3}\big\rangle - \big|\Gamma_1\big\rangle\otimes\big|\widetilde{-i\sigma_3}\big\rangle\Big), \\
\big|E_2,3\big\rangle = \frac{1}{\sqrt{8}}\Big(&\big|\Gamma_3\big\rangle\otimes\big|\widetilde{\mathbb{1}}\big\rangle + \big|\Gamma_3\big\rangle\otimes\big|\widetilde{-\mathbb{1}}\big\rangle + \big|\Gamma_3\big\rangle\otimes\big|\widetilde{i\sigma_3}\big\rangle + \big|\Gamma_3\big\rangle\otimes\big|\widetilde{-i\sigma_1}\big\rangle \\
&+\big|\Gamma_4\big\rangle\otimes\big|\widetilde{i\sigma_2}\big\rangle + +\big|\Gamma_4\big\rangle\otimes\big|\widetilde{-i\sigma_2}\big\rangle + \big|\Gamma_4\big\rangle\otimes\big|\widetilde{i\sigma_3}\big\rangle + \big|\Gamma_4\big\rangle\otimes\big|\widetilde{-i\sigma_3}\big\rangle\Big), \\
\big|E_2,4\big\rangle = \frac{1}{\sqrt{8}}\Big(&\big|\Gamma_4\big\rangle\otimes\big|\widetilde{\mathbb{1}}\big\rangle + \big|\Gamma_4\big\rangle\otimes\big|\widetilde{-\mathbb{1}}\big\rangle + \big|\Gamma_4\big\rangle\otimes\big|\widetilde{i\sigma_3}\big\rangle + \big|\Gamma_4\big\rangle\otimes\big|\widetilde{-i\sigma_1}\big\rangle \\
&+\big|\Gamma_3\big\rangle\otimes\big|\widetilde{i\sigma_2}\big\rangle + +\big|\Gamma_3\big\rangle\otimes\big|\widetilde{-i\sigma_2}\big\rangle + \big|\Gamma_3\big\rangle\otimes\big|\widetilde{i\sigma_3}\big\rangle + \big|\Gamma_3\big\rangle\otimes\big|\widetilde{-i\sigma_3}\big\rangle\Big).
\end{aligned}
\tag{F.29}
$$

Third Excited Energy Eigenstates: $E_3 = 6$

In the third excited energy level, there are 16 energy eigenstates that are given by

$$
\begin{aligned}
\big|E_3,1\big\rangle &= \frac{1}{\sqrt{2}}\Big(\big|\Gamma_5^{11}\big\rangle\otimes\big|\widetilde{\mathbb{1}}\big\rangle - \big|\Gamma_5^{11}\big\rangle\otimes\big|\widetilde{-\mathbb{1}}\big\rangle\Big), \\
\big|E_3,2\big\rangle &= \frac{1}{\sqrt{2}}\Big(\big|\Gamma_5^{11}\big\rangle\otimes\big|\widetilde{i\sigma_1}\big\rangle - \big|\Gamma_5^{11}\big\rangle\otimes\big|\widetilde{-i\sigma_1}\big\rangle\Big),
\end{aligned}
\tag{F.30}
$$

$$
\begin{aligned}
\left|E_3,3\right\rangle &= \frac{1}{\sqrt{2}}\left(\left|\Gamma_5^{11}\right\rangle \otimes \left|\widetilde{i\sigma_2}\right\rangle - \left|\Gamma_5^{11}\right\rangle \otimes \left|\widetilde{-i\sigma_2}\right\rangle\right),\\
\left|E_3,4\right\rangle &= \frac{1}{\sqrt{2}}\left(\left|\Gamma_5^{11}\right\rangle \otimes \left|\widetilde{i\sigma_3}\right\rangle - \left|\Gamma_5^{11}\right\rangle \otimes \left|\widetilde{-i\sigma_3}\right\rangle\right),\\
\left|E_3,5\right\rangle &= \frac{1}{\sqrt{2}}\left(\left|\Gamma_5^{12}\right\rangle \otimes \left|\widetilde{\mathbb{1}}\right\rangle - \left|\Gamma_5^{12}\right\rangle \otimes \left|\widetilde{-\mathbb{1}}\right\rangle\right),\\
\left|E_3,6\right\rangle &= \frac{1}{\sqrt{2}}\left(\left|\Gamma_5^{12}\right\rangle \otimes \left|\widetilde{i\sigma_1}\right\rangle - \left|\Gamma_5^{12}\right\rangle \otimes \left|\widetilde{-i\sigma_1}\right\rangle\right),\\
\left|E_3,7\right\rangle &= \frac{1}{\sqrt{2}}\left(\left|\Gamma_5^{12}\right\rangle \otimes \left|\widetilde{i\sigma_2}\right\rangle - \left|\Gamma_5^{12}\right\rangle \otimes \left|\widetilde{-i\sigma_2}\right\rangle\right),\\
\left|E_3,8\right\rangle &= \frac{1}{\sqrt{2}}\left(\left|\Gamma_5^{12}\right\rangle \otimes \left|\widetilde{i\sigma_3}\right\rangle - \left|\Gamma_5^{12}\right\rangle \otimes \left|\widetilde{-i\sigma_3}\right\rangle\right),\\
\left|E_3,9\right\rangle &= \frac{1}{\sqrt{2}}\left(\left|\Gamma_5^{21}\right\rangle \otimes \left|\widetilde{\mathbb{1}}\right\rangle - \left|\Gamma_5^{21}\right\rangle \otimes \left|\widetilde{-\mathbb{1}}\right\rangle\right),\\
\left|E_3,10\right\rangle &= \frac{1}{\sqrt{2}}\left(\left|\Gamma_5^{21}\right\rangle \otimes \left|\widetilde{i\sigma_1}\right\rangle - \left|\Gamma_5^{21}\right\rangle \otimes \left|\widetilde{-i\sigma_1}\right\rangle\right),\\
\left|E_3,11\right\rangle &= \frac{1}{\sqrt{2}}\left(\left|\Gamma_5^{21}\right\rangle \otimes \left|\widetilde{i\sigma_2}\right\rangle - \left|\Gamma_5^{21}\right\rangle \otimes \left|\widetilde{-i\sigma_2}\right\rangle\right),\\
\left|E_3,12\right\rangle &= \frac{1}{\sqrt{2}}\left(\left|\Gamma_5^{21}\right\rangle \otimes \left|\widetilde{i\sigma_3}\right\rangle - \left|\Gamma_5^{21}\right\rangle \otimes \left|\widetilde{-i\sigma_3}\right\rangle\right),\\
\left|E_3,13\right\rangle &= \frac{1}{\sqrt{2}}\left(\left|\Gamma_5^{22}\right\rangle \otimes \left|\widetilde{\mathbb{1}}\right\rangle - \left|\Gamma_5^{22}\right\rangle \otimes \left|\widetilde{-\mathbb{1}}\right\rangle\right),\\
\left|E_3,14\right\rangle &= \frac{1}{\sqrt{2}}\left(\left|\Gamma_5^{22}\right\rangle \otimes \left|\widetilde{i\sigma_1}\right\rangle - \left|\Gamma_5^{22}\right\rangle \otimes \left|\widetilde{-i\sigma_1}\right\rangle\right),\\
\left|E_3,15\right\rangle &= \frac{1}{\sqrt{2}}\left(\left|\Gamma_5^{22}\right\rangle \otimes \left|\widetilde{i\sigma_2}\right\rangle - \left|\Gamma_5^{22}\right\rangle \otimes \left|\widetilde{-i\sigma_2}\right\rangle\right),\\
\left|E_3,16\right\rangle &= \frac{1}{\sqrt{2}}\left(\left|\Gamma_5^{22}\right\rangle \otimes \left|\widetilde{i\sigma_3}\right\rangle - \left|\Gamma_5^{22}\right\rangle \otimes \left|\widetilde{-i\sigma_3}\right\rangle\right).
\end{aligned}
$$

Fourth Excited Energy Eigenstates: $E_4 = 2\left(2+\sqrt{2}\right)$

In the fourth excited energy level, there are two energy eigenstates that are given by

$$
\begin{aligned}
\left|E_4,1\right\rangle = \frac{1}{\sqrt{8\left(2+\sqrt{2}\right)}}\Big(&\left|\Gamma_1\right\rangle \otimes \left|\widetilde{\mathbb{1}}\right\rangle + \left|\Gamma_1\right\rangle \otimes \left|\widetilde{-\mathbb{1}}\right\rangle + \left|\Gamma_1\right\rangle \otimes \left|\widetilde{i\sigma_1}\right\rangle + \left|\Gamma_1\right\rangle \otimes \left|\widetilde{-i\sigma_1}\right\rangle\\
&-\left(1+\sqrt{2}\right)\left|\Gamma_2\right\rangle \otimes \left|\widetilde{i\sigma_2}\right\rangle - \left(1+\sqrt{2}\right)\left|\Gamma_2\right\rangle \otimes \left|\widetilde{-i\sigma_2}\right\rangle\\
&-\left(1+\sqrt{2}\right)\left|\Gamma_2\right\rangle \otimes \left|\widetilde{i\sigma_3}\right\rangle - \left(1+\sqrt{2}\right)\left|\Gamma_2\right\rangle \otimes \left|\widetilde{-i\sigma_3}\right\rangle\Big),
\end{aligned}
\tag{F.31}
$$

$$
\begin{aligned}
\left|E_4,2\right\rangle = \frac{1}{\sqrt{8\left(2+\sqrt{2}\right)}} \Big(& \left|\Gamma_1\right\rangle \otimes \left|\widetilde{i\sigma_2}\right\rangle + \left|\Gamma_1\right\rangle \otimes \left|\widetilde{-i\sigma_2}\right\rangle + \left|\Gamma_1\right\rangle \otimes \left|\widetilde{i\sigma_3}\right\rangle + \left|\Gamma_1\right\rangle \otimes \left|\widetilde{-i\sigma_3}\right\rangle \\
& - \left(1+\sqrt{2}\right)\left|\Gamma_2\right\rangle \otimes \left|\widetilde{\mathbb{1}}\right\rangle - \left(1+\sqrt{2}\right)\left|\Gamma_2\right\rangle \otimes \left|\widetilde{-\mathbb{1}}\right\rangle \\
& - \left(1+\sqrt{2}\right)\left|\Gamma_2\right\rangle \otimes \left|\widetilde{i\sigma_1}\right\rangle - \left(1+\sqrt{2}\right)\left|\Gamma_2\right\rangle \otimes \left|\widetilde{-i\sigma_1}\right\rangle \Big).
\end{aligned}
$$

Fifth Excited Energy Eigenstates: $E_5 = 7$

In the fifth excited energy level, there are 24 energy eigenstates that can be separated into two sets of 12 states each. The 12 states of the first set all contain a 1-dimensional direct flux and they are given by

$$
\begin{aligned}
\left|E_5,1\right\rangle &= \frac{1}{\sqrt{2}}\left(\left|\Gamma_2\right\rangle \otimes \left|\widetilde{\mathbb{1}}\right\rangle + \left|\Gamma_2\right\rangle \otimes \left|\widetilde{-\mathbb{1}}\right\rangle\right), \qquad \text{(F.32)} \\
\left|E_5,2\right\rangle &= \frac{1}{\sqrt{2}}\left(\left|\Gamma_2\right\rangle \otimes \left|\widetilde{i\sigma_1}\right\rangle + \left|\Gamma_2\right\rangle \otimes \left|\widetilde{-i\sigma_1}\right\rangle\right), \\
\left|E_5,3\right\rangle &= \frac{1}{\sqrt{2}}\left(\left|\Gamma_2\right\rangle \otimes \left|\widetilde{i\sigma_2}\right\rangle + \left|\Gamma_2\right\rangle \otimes \left|\widetilde{-i\sigma_2}\right\rangle\right), \\
\left|E_5,4\right\rangle &= \frac{1}{\sqrt{2}}\left(\left|\Gamma_2\right\rangle \otimes \left|\widetilde{i\sigma_3}\right\rangle + \left|\Gamma_2\right\rangle \otimes \left|\widetilde{-i\sigma_3}\right\rangle\right), \\
\left|E_5,5\right\rangle &= \frac{1}{\sqrt{2}}\left(\left|\Gamma_3\right\rangle \otimes \left|\widetilde{\mathbb{1}}\right\rangle + \left|\Gamma_3\right\rangle \otimes \left|\widetilde{-\mathbb{1}}\right\rangle\right), \\
\left|E_5,6\right\rangle &= \frac{1}{\sqrt{2}}\left(\left|\Gamma_3\right\rangle \otimes \left|\widetilde{i\sigma_1}\right\rangle + \left|\Gamma_3\right\rangle \otimes \left|\widetilde{-i\sigma_1}\right\rangle\right), \\
\left|E_5,7\right\rangle &= \frac{1}{\sqrt{2}}\left(\left|\Gamma_3\right\rangle \otimes \left|\widetilde{i\sigma_2}\right\rangle + \left|\Gamma_3\right\rangle \otimes \left|\widetilde{-i\sigma_2}\right\rangle\right), \\
\left|E_5,8\right\rangle &= \frac{1}{\sqrt{2}}\left(\left|\Gamma_3\right\rangle \otimes \left|\widetilde{i\sigma_3}\right\rangle + \left|\Gamma_3\right\rangle \otimes \left|\widetilde{-i\sigma_3}\right\rangle\right), \\
\left|E_5,9\right\rangle &= \frac{1}{\sqrt{2}}\left(\left|\Gamma_4\right\rangle \otimes \left|\widetilde{\mathbb{1}}\right\rangle + \left|\Gamma_4\right\rangle \otimes \left|\widetilde{-\mathbb{1}}\right\rangle\right), \\
\left|E_5,10\right\rangle &= \frac{1}{\sqrt{2}}\left(\left|\Gamma_4\right\rangle \otimes \left|\widetilde{i\sigma_1}\right\rangle + \left|\Gamma_4\right\rangle \otimes \left|\widetilde{-i\sigma_1}\right\rangle\right), \\
\left|E_5,11\right\rangle &= \frac{1}{\sqrt{2}}\left(\left|\Gamma_4\right\rangle \otimes \left|\widetilde{i\sigma_2}\right\rangle + \left|\Gamma_4\right\rangle \otimes \left|\widetilde{-i\sigma_2}\right\rangle\right), \\
\left|E_5,12\right\rangle &= \frac{1}{\sqrt{2}}\left(\left|\Gamma_4\right\rangle \otimes \left|\widetilde{i\sigma_3}\right\rangle + \left|\Gamma_4\right\rangle \otimes \left|\widetilde{-i\sigma_3}\right\rangle\right).
\end{aligned}
$$

The 12 states of the second set all contain a direct Γ_5-flux and they are given by

$$
\left|E_5,13\right\rangle = \frac{1}{2}\left(\left|\Gamma_5^{22}\right\rangle \otimes \left|\widetilde{i\sigma_2}\right\rangle + \left|\Gamma_5^{22}\right\rangle \otimes \left|\widetilde{-i\sigma_2}\right\rangle - \left|\Gamma_5^{22}\right\rangle \otimes \left|\widetilde{i\sigma_3}\right\rangle - \left|\Gamma_5^{22}\right\rangle \otimes \left|\widetilde{-i\sigma_3}\right\rangle\right), \quad \text{(F.33)}
$$

$$
\begin{aligned}
|E_5,14\rangle &= \frac{1}{2}\Big(|\Gamma_5^{11}\rangle\otimes|\widetilde{\mathbb{1}}\rangle + |\Gamma_5^{11}\rangle\otimes|\widetilde{-\mathbb{1}}\rangle - |\Gamma_5^{11}\rangle\otimes|\widetilde{i\sigma_1}\rangle - |\Gamma_5^{11}\rangle\otimes|\widetilde{-i\sigma_1}\rangle\Big),\\
|E_5,15\rangle &= \frac{1}{\sqrt{8}}\Big(|\Gamma_5^{11}\rangle\otimes|\widetilde{\mathbb{1}}\rangle + |\Gamma_5^{11}\rangle\otimes|\widetilde{-\mathbb{1}}\rangle + |\Gamma_5^{11}\rangle\otimes|\widetilde{i\sigma_1}\rangle + |\Gamma_5^{11}\rangle\otimes|\widetilde{-i\sigma_1}\rangle\\
&\quad -|\Gamma_5^{22}\rangle\otimes|\widetilde{i\sigma_2}\rangle - |\Gamma_5^{22}\rangle\otimes|\widetilde{-i\sigma_2}\rangle - |\Gamma_5^{22}\rangle\otimes|\widetilde{i\sigma_3}\rangle - |\Gamma_5^{22}\rangle\otimes|\widetilde{-i\sigma_3}\rangle\Big),\\
|E_5,16\rangle &= \frac{1}{2}\Big(|\Gamma_5^{11}\rangle\otimes|\widetilde{i\sigma_2}\rangle + |\Gamma_5^{11}\rangle\otimes|\widetilde{-i\sigma_2}\rangle - |\Gamma_5^{11}\rangle\otimes|\widetilde{i\sigma_3}\rangle - |\Gamma_5^{11}\rangle\otimes|\widetilde{-i\sigma_3}\rangle\Big),\\
|E_5,17\rangle &= \frac{1}{2}\Big(|\Gamma_5^{22}\rangle\otimes|\widetilde{\mathbb{1}}\rangle + |\Gamma_5^{22}\rangle\otimes|\widetilde{-\mathbb{1}}\rangle - |\Gamma_5^{22}\rangle\otimes|\widetilde{i\sigma_1}\rangle - |\Gamma_5^{22}\rangle\otimes|\widetilde{-i\sigma_1}\rangle\Big),\\
|E_5,18\rangle &= \frac{1}{\sqrt{8}}\Big(|\Gamma_5^{22}\rangle\otimes|\widetilde{\mathbb{1}}\rangle + |\Gamma_5^{22}\rangle\otimes|\widetilde{-\mathbb{1}}\rangle + |\Gamma_5^{22}\rangle\otimes|\widetilde{i\sigma_1}\rangle + |\Gamma_5^{22}\rangle\otimes|\widetilde{-i\sigma_1}\rangle\\
&\quad -|\Gamma_5^{11}\rangle\otimes|\widetilde{i\sigma_2}\rangle - |\Gamma_5^{11}\rangle\otimes|\widetilde{-i\sigma_2}\rangle - |\Gamma_5^{11}\rangle\otimes|\widetilde{i\sigma_3}\rangle - |\Gamma_5^{11}\rangle\otimes|\widetilde{-i\sigma_3}\rangle\Big),\\
|E_5,19\rangle &= \frac{1}{2}\Big(|\Gamma_5^{21}\rangle\otimes|\widetilde{i\sigma_2}\rangle + |\Gamma_5^{21}\rangle\otimes|\widetilde{-i\sigma_2}\rangle - |\Gamma_5^{21}\rangle\otimes|\widetilde{i\sigma_3}\rangle - |\Gamma_5^{21}\rangle\otimes|\widetilde{-i\sigma_3}\rangle\Big),\\
|E_5,20\rangle &= \frac{1}{2}\Big(|\Gamma_5^{12}\rangle\otimes|\widetilde{\mathbb{1}}\rangle + |\Gamma_5^{12}\rangle\otimes|\widetilde{-\mathbb{1}}\rangle - |\Gamma_5^{12}\rangle\otimes|\widetilde{i\sigma_1}\rangle - |\Gamma_5^{12}\rangle\otimes|\widetilde{-i\sigma_1}\rangle\Big),\\
|E_5,21\rangle &= \frac{1}{\sqrt{8}}\Big(|\Gamma_5^{12}\rangle\otimes|\widetilde{\mathbb{1}}\rangle + |\Gamma_5^{12}\rangle\otimes|\widetilde{-\mathbb{1}}\rangle + |\Gamma_5^{12}\rangle\otimes|\widetilde{i\sigma_1}\rangle + |\Gamma_5^{12}\rangle\otimes|\widetilde{-i\sigma_1}\rangle\\
&\quad -|\Gamma_5^{21}\rangle\otimes|\widetilde{i\sigma_2}\rangle - |\Gamma_5^{21}\rangle\otimes|\widetilde{-i\sigma_2}\rangle - |\Gamma_5^{21}\rangle\otimes|\widetilde{i\sigma_3}\rangle - |\Gamma_5^{21}\rangle\otimes|\widetilde{-i\sigma_3}\rangle\Big),\\
|E_5,22\rangle &= \frac{1}{2}\Big(|\Gamma_5^{12}\rangle\otimes|\widetilde{i\sigma_2}\rangle + |\Gamma_5^{12}\rangle\otimes|\widetilde{-i\sigma_2}\rangle - |\Gamma_5^{12}\rangle\otimes|\widetilde{i\sigma_3}\rangle - |\Gamma_5^{12}\rangle\otimes|\widetilde{-i\sigma_3}\rangle\Big),\\
|E_5,23\rangle &= \frac{1}{2}\Big(|\Gamma_5^{21}\rangle\otimes|\widetilde{\mathbb{1}}\rangle + |\Gamma_5^{21}\rangle\otimes|\widetilde{-\mathbb{1}}\rangle - |\Gamma_5^{21}\rangle\otimes|\widetilde{i\sigma_1}\rangle - |\Gamma_5^{21}\rangle\otimes|\widetilde{-i\sigma_1}\rangle\Big),\\
|E_5,24\rangle &= \frac{1}{\sqrt{8}}\Big(|\Gamma_5^{21}\rangle\otimes|\widetilde{\mathbb{1}}\rangle + |\Gamma_5^{21}\rangle\otimes|\widetilde{-\mathbb{1}}\rangle + |\Gamma_5^{21}\rangle\otimes|\widetilde{i\sigma_1}\rangle + |\Gamma_5^{21}\rangle\otimes|\widetilde{-i\sigma_1}\rangle\\
&\quad -|\Gamma_5^{12}\rangle\otimes|\widetilde{i\sigma_2}\rangle - |\Gamma_5^{12}\rangle\otimes|\widetilde{-i\sigma_2}\rangle - |\Gamma_5^{12}\rangle\otimes|\widetilde{i\sigma_3}\rangle - |\Gamma_5^{12}\rangle\otimes|\widetilde{-i\sigma_3}\rangle\Big).
\end{aligned}
$$

Sixth Excited Energy Eigenstates: $E_6 = 8$

In the sixth and highest excited energy level, there are eight energy eigenstate which are given by

$$
\begin{aligned}
|E_6,1\rangle &= \frac{1}{2}\Big(|\Gamma_2\rangle\otimes|\widetilde{\mathbb{1}}\rangle + |\Gamma_2\rangle\otimes|\widetilde{-\mathbb{1}}\rangle - |\Gamma_2\rangle\otimes|\widetilde{i\sigma_1}\rangle - |\Gamma_2\rangle\otimes|\widetilde{-i\sigma_1}\rangle\Big), \qquad \text{(F.34)}\\
|E_6,2\rangle &= \frac{1}{2}\Big(|\Gamma_2\rangle\otimes|\widetilde{i\sigma_2}\rangle + |\Gamma_2\rangle\otimes|\widetilde{-i\sigma_2}\rangle - |\Gamma_2\rangle\otimes|\widetilde{i\sigma_3}\rangle - |\Gamma_2\rangle\otimes|\widetilde{-i\sigma_3}\rangle\Big),\\
|E_6,3\rangle &= \frac{1}{2}\Big(|\Gamma_3\rangle\otimes|\widetilde{\mathbb{1}}\rangle + |\Gamma_3\rangle\otimes|\widetilde{-\mathbb{1}}\rangle - |\Gamma_3\rangle\otimes|\widetilde{i\sigma_1}\rangle - |\Gamma_3\rangle\otimes|\widetilde{-i\sigma_1}\rangle\Big),\\
|E_6,4\rangle &= \frac{1}{2}\Big(|\Gamma_3\rangle\otimes|\widetilde{i\sigma_2}\rangle + |\Gamma_3\rangle\otimes|\widetilde{-i\sigma_2}\rangle - |\Gamma_3\rangle\otimes|\widetilde{i\sigma_3}\rangle - |\Gamma_3\rangle\otimes|\widetilde{-i\sigma_3}\rangle\Big),\\
|E_6,5\rangle &= \frac{1}{2}\Big(|\Gamma_4\rangle\otimes|\widetilde{\mathbb{1}}\rangle + |\Gamma_4\rangle\otimes|\widetilde{-\mathbb{1}}\rangle - |\Gamma_4\rangle\otimes|\widetilde{i\sigma_1}\rangle - |\Gamma_4\rangle\otimes|\widetilde{-i\sigma_1}\rangle\Big),\\
|E_6,6\rangle &= \frac{1}{2}\Big(|\Gamma_4\rangle\otimes|\widetilde{i\sigma_2}\rangle + |\Gamma_4\rangle\otimes|\widetilde{-i\sigma_2}\rangle - |\Gamma_4\rangle\otimes|\widetilde{i\sigma_3}\rangle - |\Gamma_4\rangle\otimes|\widetilde{-i\sigma_3}\rangle\Big),
\end{aligned}
$$

$$
\begin{aligned}
\left|E_6,7\right\rangle = \frac{1}{\sqrt{8}}\Big(&\left|\Gamma_3\right\rangle\otimes\left|\widetilde{\mathbb{1}}\right\rangle + \left|\Gamma_3\right\rangle\otimes\left|\widetilde{-\mathbb{1}}\right\rangle + \left|\Gamma_3\right\rangle\otimes\left|\widetilde{i\sigma_1}\right\rangle + \left|\Gamma_3\right\rangle\otimes\left|\widetilde{-i\sigma_1}\right\rangle \\
&-\left|\Gamma_4\right\rangle\otimes\left|\widetilde{i\sigma_2}\right\rangle - \left|\Gamma_4\right\rangle\otimes\left|\widetilde{-i\sigma_2}\right\rangle - \left|\Gamma_4\right\rangle\otimes\left|\widetilde{i\sigma_3}\right\rangle - \left|\Gamma_4\right\rangle\otimes\left|\widetilde{-i\sigma_3}\right\rangle\Big), \\
\left|E_6,8\right\rangle = \frac{1}{\sqrt{8}}\Big(&\left|\Gamma_4\right\rangle\otimes\left|\widetilde{\mathbb{1}}\right\rangle + \left|\Gamma_4\right\rangle\otimes\left|\widetilde{-\mathbb{1}}\right\rangle + \left|\Gamma_4\right\rangle\otimes\left|\widetilde{i\sigma_1}\right\rangle + \left|\Gamma_4\right\rangle\otimes\left|\widetilde{-i\sigma_1}\right\rangle \\
&-\left|\Gamma_3\right\rangle\otimes\left|\widetilde{i\sigma_2}\right\rangle - \left|\Gamma_3\right\rangle\otimes\left|\widetilde{-i\sigma_2}\right\rangle - \left|\Gamma_3\right\rangle\otimes\left|\widetilde{i\sigma_3}\right\rangle - \left|\Gamma_3\right\rangle\otimes\left|\widetilde{-i\sigma_3}\right\rangle\Big).
\end{aligned}
$$

F.3.2 $\bar{D}_2$ with a Non-Trivial Cocycle: ω_{11}

Lowest Energy Eigenstates: $E_0 = 2$

In the lowest energy level, there are four energy eigenstates that are given by

$$
\begin{aligned}
\left|E_0,1\right\rangle &= \frac{1}{\sqrt{24}}\left(3\sum_{\widetilde{U}\in C_5}\left|\Gamma_1\right\rangle\otimes\left|\widetilde{U}\right\rangle + \sum_{\widetilde{U}\in C_4}\left|\Gamma_2\right\rangle\otimes\left|\widetilde{U}\right\rangle + \sum_{\widetilde{U}\in C_3}\left|\Gamma_3\right\rangle\otimes\left|\widetilde{U}\right\rangle + \sum_{\widetilde{U}\in C_{12}}\left|\Gamma_4\right\rangle\otimes\left|\widetilde{U}\right\rangle\right), \\
\left|E_0,2\right\rangle &= \frac{1}{\sqrt{24}}\left(3\sum_{\widetilde{U}\in C_4}\left|\Gamma_1\right\rangle\otimes\left|\widetilde{U}\right\rangle + \sum_{\widetilde{U}\in C_5}\left|\Gamma_2\right\rangle\otimes\left|\widetilde{U}\right\rangle + \sum_{\widetilde{U}\in C_{12}}\left|\Gamma_3\right\rangle\otimes\left|\widetilde{U}\right\rangle + \sum_{\widetilde{U}\in C_3}\left|\Gamma_4\right\rangle\otimes\left|\widetilde{U}\right\rangle\right), \\
\left|E_0,3\right\rangle &= \frac{1}{\sqrt{24}}\left(3\sum_{\widetilde{U}\in C_3}\left|\Gamma_1\right\rangle\otimes\left|\widetilde{U}\right\rangle + \sum_{\widetilde{U}\in C_{12}}\left|\Gamma_2\right\rangle\otimes\left|\widetilde{U}\right\rangle + \sum_{\widetilde{U}\in C_5}\left|\Gamma_3\right\rangle\otimes\left|\widetilde{U}\right\rangle + \sum_{\widetilde{U}\in C_4}\left|\Gamma_4\right\rangle\otimes\left|\widetilde{U}\right\rangle\right), \\
\left|E_0,4\right\rangle &= \frac{1}{\sqrt{24}}\left(3\sum_{\widetilde{U}\in C_{12}}\left|\Gamma_1\right\rangle\otimes\left|\widetilde{U}\right\rangle + \sum_{\widetilde{U}\in C_3}\left|\Gamma_2\right\rangle\otimes\left|\widetilde{U}\right\rangle + \sum_{\widetilde{U}\in C_4}\left|\Gamma_3\right\rangle\otimes\left|\widetilde{U}\right\rangle + \sum_{\widetilde{U}\in C_5}\left|\Gamma_4\right\rangle\otimes\left|\widetilde{U}\right\rangle\right).
\end{aligned}
$$

First Excited Energy Eigenstates: $E_1 = 3$

In the first excited energy level, there are eight energy eigenstates. The first four are identical to the first set considered above. The states are given by

$$
\begin{aligned}
\left|E_1,1\right\rangle &= \frac{1}{\sqrt{8}}\left(\sum_{\widetilde{U}\in C_4,C_5}\left|\Gamma_5^{11}\right\rangle\otimes\left|\widetilde{U}\right\rangle + \sum_{\widetilde{U}\in C_{12},C_3}\left|\Gamma_5^{22}\right\rangle\otimes\left|\widetilde{U}\right\rangle\right), \qquad \text{(F.35)} \\
\left|E_1,2\right\rangle &= \frac{1}{\sqrt{8}}\left(\sum_{\widetilde{U}\in C_4,C_5}\left|\Gamma_5^{12}\right\rangle\otimes\left|\widetilde{U}\right\rangle + \sum_{\widetilde{U}\in C_{12},C_3}\left|\Gamma_5^{21}\right\rangle\otimes\left|\widetilde{U}\right\rangle\right), \\
\left|E_1,3\right\rangle &= \frac{1}{\sqrt{8}}\left(\sum_{\widetilde{U}\in C_4,C_5}\left|\Gamma_5^{21}\right\rangle\otimes\left|\widetilde{U}\right\rangle + \sum_{\widetilde{U}\in C_{12},C_3}\left|\Gamma_5^{21}\right\rangle\otimes\left|\widetilde{U}\right\rangle\right),
\end{aligned}
$$

$$
\begin{aligned}
\left|E_1,4\right\rangle &= \frac{1}{\sqrt{8}}\left(\sum_{\widetilde{U}\in\mathcal{C}_4,\mathcal{C}_5}\left|\Gamma_5^{22}\right\rangle\otimes\left|\widetilde{U}\right\rangle+\sum_{\widetilde{U}\in\mathcal{C}_{12},\mathcal{C}_3}\left|\Gamma_5^{11}\right\rangle\otimes\left|\widetilde{U}\right\rangle\right),\\
\left|E_1,5\right\rangle &= \frac{1}{\sqrt{8}}\left(\sum_{\widetilde{U}\in\mathcal{C}_{12},\mathcal{C}_5}\left|\Gamma_5^{11}\right\rangle\otimes\left|\widetilde{U}\right\rangle+\sum_{\widetilde{U}\in\mathcal{C}_3,\mathcal{C}_4}\left|\Gamma_5^{22}\right\rangle\otimes\left|\widetilde{U}\right\rangle\right),\\
\left|E_1,6\right\rangle &= \frac{1}{\sqrt{8}}\left(\sum_{\widetilde{U}\in\mathcal{C}_{12},\mathcal{C}_5}\left|\Gamma_5^{22}\right\rangle\otimes\left|\widetilde{U}\right\rangle+\sum_{\widetilde{U}\in\mathcal{C}_3,\mathcal{C}_4}\left|\Gamma_5^{11}\right\rangle\otimes\left|\widetilde{U}\right\rangle\right),\\
\left|E_1,7\right\rangle &= a\sum_{\widetilde{U}\in\mathcal{C}_{12}}\left|\Gamma_5^{12}\right\rangle\otimes\left|\widetilde{U}\right\rangle-a\sum_{\widetilde{U}\in\mathcal{C}_5}\left|\Gamma_5^{12}\right\rangle\otimes\left|\widetilde{U}\right\rangle+b\sum_{\widetilde{U}\in\mathcal{C}_3}\left|\Gamma_5^{12}\right\rangle\otimes\left|\widetilde{U}\right\rangle-b\sum_{\widetilde{U}\in\mathcal{C}_4}\left|\Gamma_5^{12}\right\rangle\otimes\left|\widetilde{U}\right\rangle\\
&\quad+b\sum_{\widetilde{U}\in\mathcal{C}_{12}}\left|\Gamma_5^{21}\right\rangle\otimes\left|\widetilde{U}\right\rangle+a\sum_{\widetilde{U}\in\mathcal{C}_3}\left|\Gamma_5^{21}\right\rangle\otimes\left|\widetilde{U}\right\rangle-a\sum_{\widetilde{U}\in\mathcal{C}_4}\left|\Gamma_5^{21}\right\rangle\otimes\left|\widetilde{U}\right\rangle-b\sum_{\widetilde{U}\in\mathcal{C}_5}\left|\Gamma_5^{21}\right\rangle\otimes\left|\widetilde{U}\right\rangle,\\
\left|E_1,8\right\rangle &= b\sum_{\widetilde{U}\in\mathcal{C}_{12}}\left|\Gamma_5^{12}\right\rangle\otimes\left|\widetilde{U}\right\rangle-b\sum_{\widetilde{U}\in\mathcal{C}_5}\left|\Gamma_5^{12}\right\rangle\otimes\left|\widetilde{U}\right\rangle-a\sum_{\widetilde{U}\in\mathcal{C}_3}\left|\Gamma_5^{12}\right\rangle\otimes\left|\widetilde{U}\right\rangle+a\sum_{\widetilde{U}\in\mathcal{C}_4}\left|\Gamma_5^{12}\right\rangle\otimes\left|\widetilde{U}\right\rangle\\
&\quad-a\sum_{\widetilde{U}\in\mathcal{C}_{12}}\left|\Gamma_5^{21}\right\rangle\otimes\left|\widetilde{U}\right\rangle+b\sum_{\widetilde{U}\in\mathcal{C}_3}\left|\Gamma_5^{21}\right\rangle\otimes\left|\widetilde{U}\right\rangle-b\sum_{\widetilde{U}\in\mathcal{C}_4}\left|\Gamma_5^{21}\right\rangle\otimes\left|\widetilde{U}\right\rangle+a\sum_{\widetilde{U}\in\mathcal{C}_5}\left|\Gamma_5^{21}\right\rangle\otimes\left|\widetilde{U}\right\rangle.
\end{aligned}
$$

where $a = 0.10369\ldots$ and $b = 0.33801\ldots$.

F.4 $\Delta\,(27)$ Energy-Eigenstates

Here we present the ground states for the $\Delta\,(27)$ CSYM theory for two non-trivial cocycles.

F.4.1 $\Delta\,(27)$ with a Non-Trivial Cocycle: ω_2

Lowest Energy Eigenstates: $E_0 = \frac{9\left(3-\sqrt{3}\right)}{2}$

In the lowest energy level, there are three energy eigenstates which are given by

$$
\begin{aligned}
\left|E_0,1\right\rangle &= \frac{1}{\sqrt{18\left(3+\sqrt{3}\right)}}\left(\left(1+\sqrt{3}\right)\sum_{z_i,z_j\in\mathbb{Z}(3)}\left|\Gamma_1\right\rangle\otimes\left|\widetilde{L\left(z_i,z_j\right)}\right\rangle\right.\\
&\quad\left.+\sum_{z_i,z_j\in\mathbb{Z}(3)}\left|\Gamma_1\right\rangle\otimes\left|\widetilde{D\left(z_i,z_j\right)}\right\rangle+\sum_{z_i,z_j\in\mathbb{Z}(3)}\left|\Gamma_1\right\rangle\otimes\left|\widetilde{U\left(z_i,z_j\right)}\right\rangle\right),\\
\left|E_0,2\right\rangle &= \frac{1}{\sqrt{18\left(3+\sqrt{3}\right)}}\left(\left(1+\sqrt{3}\right)\sum_{z_i,z_j\in\mathbb{Z}(3)}\left|\Gamma_1\right\rangle\otimes\left|\widetilde{U\left(z_i,z_j\right)}\right\rangle\right.
\end{aligned}
\tag{F.36}
$$

$$+\sum_{z_i,z_j\in\mathbb{Z}(3)}\left|\Gamma_1\right\rangle\otimes\left|L\widetilde{(z_i,z_j)}\right\rangle+\sum_{z_i,z_j\in\mathbb{Z}(3)}\left|\Gamma_1\right\rangle\otimes\left|D\widetilde{(z_i,z_j)}\right\rangle\Bigg),$$

$$\left|E_0,3\right\rangle=\frac{1}{\sqrt{18\left(3+\sqrt{3}\right)}}\Bigg(\left(1+\sqrt{3}\right)\sum_{z_i,z_j\in\mathbb{Z}(3)}\left|\Gamma_1\right\rangle\otimes\left|D\widetilde{(z_i,z_j)}\right\rangle$$

$$+\sum_{z_i,z_j\in\mathbb{Z}(3)}\left|\Gamma_1\right\rangle\otimes\left|U\widetilde{(z_i,z_j)}\right\rangle+\sum_{z_i,z_j\in\mathbb{Z}(3)}\left|\Gamma_1\right\rangle\otimes\left|L\widetilde{(z_i,z_j)}\right\rangle\Bigg).$$

F.4.2 Δ (27) with a Non-Trivial Cocycle: ω_4

Lowest Energy Eigenstates: $E_0 = 9$

In the lowest energy level, there are nine energy eigenstates which are given by

$$\left|E_0,1\right\rangle=\frac{1}{\sqrt{72}}\Bigg(4\sum_{\widetilde{U}\in\mathcal{C}_{10}}\left|\Gamma_1\right\rangle\otimes\left|\widetilde{U}\right\rangle+\sum_{\widetilde{U}\in\mathcal{C}_{11}}\left|\Gamma_2\right\rangle\otimes\left|\widetilde{U}\right\rangle+\sum_{\widetilde{U}\in\mathcal{C}_9}\left|\Gamma_3\right\rangle\otimes\left|\widetilde{U}\right\rangle \tag{F.37}$$
$$+\sum_{\widetilde{U}\in\mathcal{C}_4}\left|\Gamma_4\right\rangle\otimes\left|\widetilde{U}\right\rangle+\sum_{\widetilde{U}\in\mathcal{C}_5}\left|\Gamma_5\right\rangle\otimes\left|\widetilde{U}\right\rangle+\sum_{\widetilde{U}\in\mathcal{C}_{123}}\left|\Gamma_6\right\rangle\otimes\left|\widetilde{U}\right\rangle$$
$$+\sum_{\widetilde{U}\in\mathcal{C}_7}\left|\Gamma_7\right\rangle\otimes\left|\widetilde{U}\right\rangle+\sum_{\widetilde{U}\in\mathcal{C}_8}\left|\Gamma_8\right\rangle\otimes\left|\widetilde{U}\right\rangle+\sum_{\widetilde{U}\in\mathcal{C}_6}\left|\Gamma_9\right\rangle\otimes\left|\widetilde{U}\right\rangle\Bigg),$$

$$\left|E_0,2\right\rangle=\frac{1}{\sqrt{72}}\Bigg(4\sum_{\widetilde{U}\in\mathcal{C}_7}\left|\Gamma_1\right\rangle\otimes\left|\widetilde{U}\right\rangle+\sum_{\widetilde{U}\in\mathcal{C}_8}\left|\Gamma_2\right\rangle\otimes\left|\widetilde{U}\right\rangle+\sum_{\widetilde{U}\in\mathcal{C}_6}\left|\Gamma_3\right\rangle\otimes\left|\widetilde{U}\right\rangle$$
$$+\sum_{\widetilde{U}\in\mathcal{C}_{10}}\left|\Gamma_4\right\rangle\otimes\left|\widetilde{U}\right\rangle+\sum_{\widetilde{U}\in\mathcal{C}_{11}}\left|\Gamma_5\right\rangle\otimes\left|\widetilde{U}\right\rangle+\sum_{\widetilde{U}\in\mathcal{C}_9}\left|\Gamma_6\right\rangle\otimes\left|\widetilde{U}\right\rangle$$
$$+\sum_{\widetilde{U}\in\mathcal{C}_4}\left|\Gamma_7\right\rangle\otimes\left|\widetilde{U}\right\rangle+\sum_{\widetilde{U}\in\mathcal{C}_5}\left|\Gamma_8\right\rangle\otimes\left|\widetilde{U}\right\rangle+\sum_{\widetilde{U}\in\mathcal{C}_{123}}\left|\Gamma_9\right\rangle\otimes\left|\widetilde{U}\right\rangle\Bigg),$$

$$\left|E_0,3\right\rangle=\frac{1}{\sqrt{72}}\Bigg(4\sum_{\widetilde{U}\in\mathcal{C}_{11}}\left|\Gamma_1\right\rangle\otimes\left|\widetilde{U}\right\rangle+\sum_{\widetilde{U}\in\mathcal{C}_9}\left|\Gamma_2\right\rangle\otimes\left|\widetilde{U}\right\rangle+\sum_{\widetilde{U}\in\mathcal{C}_{10}}\left|\Gamma_3\right\rangle\otimes\left|\widetilde{U}\right\rangle$$
$$+\sum_{\widetilde{U}\in\mathcal{C}_5}\left|\Gamma_4\right\rangle\otimes\left|\widetilde{U}\right\rangle+\sum_{\widetilde{U}\in\mathcal{C}_{123}}\left|\Gamma_5\right\rangle\otimes\left|\widetilde{U}\right\rangle+\sum_{\widetilde{U}\in\mathcal{C}_4}\left|\Gamma_6\right\rangle\otimes\left|\widetilde{U}\right\rangle$$
$$+\sum_{\widetilde{U}\in\mathcal{C}_8}\left|\Gamma_7\right\rangle\otimes\left|\widetilde{U}\right\rangle+\sum_{\widetilde{U}\in\mathcal{C}_6}\left|\Gamma_8\right\rangle\otimes\left|\widetilde{U}\right\rangle+\sum_{\widetilde{U}\in\mathcal{C}_7}\left|\Gamma_9\right\rangle\otimes\left|\widetilde{U}\right\rangle\Bigg),$$

$$
\begin{aligned}
\left|E_0,4\right\rangle = \frac{1}{\sqrt{72}}\Bigg(&4\sum_{\widetilde{U}\in\mathcal{C}_9}\left|\Gamma_1\right\rangle\otimes\left|\widetilde{U}\right\rangle+\sum_{\widetilde{U}\in\mathcal{C}_{10}}\left|\Gamma_2\right\rangle\otimes\left|\widetilde{U}\right\rangle+\sum_{\widetilde{U}\in\mathcal{C}_{11}}\left|\Gamma_3\right\rangle\otimes\left|\widetilde{U}\right\rangle\\
&+\sum_{\widetilde{U}\in\mathcal{C}_{123}}\left|\Gamma_4\right\rangle\otimes\left|\widetilde{U}\right\rangle+\sum_{\widetilde{U}\in\mathcal{C}_4}\left|\Gamma_5\right\rangle\otimes\left|\widetilde{U}\right\rangle+\sum_{\widetilde{U}\in\mathcal{C}_5}\left|\Gamma_6\right\rangle\otimes\left|\widetilde{U}\right\rangle\\
&+\sum_{\widetilde{U}\in\mathcal{C}_6}\left|\Gamma_7\right\rangle\otimes\left|\widetilde{U}\right\rangle+\sum_{\widetilde{U}\in\mathcal{C}_7}\left|\Gamma_8\right\rangle\otimes\left|\widetilde{U}\right\rangle+\sum_{\widetilde{U}\in\mathcal{C}_8}\left|\Gamma_9\right\rangle\otimes\left|\widetilde{U}\right\rangle\Bigg),\\
\left|E_0,5\right\rangle = \frac{1}{\sqrt{72}}\Bigg(&4\sum_{\widetilde{U}\in\mathcal{C}_8}\left|\Gamma_1\right\rangle\otimes\left|\widetilde{U}\right\rangle+\sum_{\widetilde{U}\in\mathcal{C}_6}\left|\Gamma_2\right\rangle\otimes\left|\widetilde{U}\right\rangle+\sum_{\widetilde{U}\in\mathcal{C}_7}\left|\Gamma_3\right\rangle\otimes\left|\widetilde{U}\right\rangle\\
&+\sum_{\widetilde{U}\in\mathcal{C}_{11}}\left|\Gamma_4\right\rangle\otimes\left|\widetilde{U}\right\rangle+\sum_{\widetilde{U}\in\mathcal{C}_9}\left|\Gamma_5\right\rangle\otimes\left|\widetilde{U}\right\rangle+\sum_{\widetilde{U}\in\mathcal{C}_{10}}\left|\Gamma_6\right\rangle\otimes\left|\widetilde{U}\right\rangle\\
&+\sum_{\widetilde{U}\in\mathcal{C}_5}\left|\Gamma_7\right\rangle\otimes\left|\widetilde{U}\right\rangle+\sum_{\widetilde{U}\in\mathcal{C}_{123}}\left|\Gamma_8\right\rangle\otimes\left|\widetilde{U}\right\rangle+\sum_{\widetilde{U}\in\mathcal{C}_4}\left|\Gamma_9\right\rangle\otimes\left|\widetilde{U}\right\rangle\Bigg),\\
\left|E_0,6\right\rangle = \frac{1}{\sqrt{72}}\Bigg(&4\sum_{\widetilde{U}\in\mathcal{C}_6}\left|\Gamma_1\right\rangle\otimes\left|\widetilde{U}\right\rangle+\sum_{\widetilde{U}\in\mathcal{C}_7}\left|\Gamma_2\right\rangle\otimes\left|\widetilde{U}\right\rangle+\sum_{\widetilde{U}\in\mathcal{C}_8}\left|\Gamma_3\right\rangle\otimes\left|\widetilde{U}\right\rangle\\
&+\sum_{\widetilde{U}\in\mathcal{C}_9}\left|\Gamma_4\right\rangle\otimes\left|\widetilde{U}\right\rangle+\sum_{\widetilde{U}\in\mathcal{C}_{10}}\left|\Gamma_5\right\rangle\otimes\left|\widetilde{U}\right\rangle+\sum_{\widetilde{U}\in\mathcal{C}_{11}}\left|\Gamma_6\right\rangle\otimes\left|\widetilde{U}\right\rangle\\
&+\sum_{\widetilde{U}\in\mathcal{C}_{123}}\left|\Gamma_7\right\rangle\otimes\left|\widetilde{U}\right\rangle+\sum_{\widetilde{U}\in\mathcal{C}_4}\left|\Gamma_8\right\rangle\otimes\left|\widetilde{U}\right\rangle+\sum_{\widetilde{U}\in\mathcal{C}_5}\left|\Gamma_9\right\rangle\otimes\left|\widetilde{U}\right\rangle\Bigg),\\
\left|E_0,7\right\rangle = \frac{1}{\sqrt{72}}\Bigg(&4\sum_{\widetilde{U}\in\mathcal{C}_5}\left|\Gamma_1\right\rangle\otimes\left|\widetilde{U}\right\rangle+\sum_{\widetilde{U}\in\mathcal{C}_{123}}\left|\Gamma_2\right\rangle\otimes\left|\widetilde{U}\right\rangle+\sum_{\widetilde{U}\in\mathcal{C}_4}\left|\Gamma_3\right\rangle\otimes\left|\widetilde{U}\right\rangle\\
&+\sum_{\widetilde{U}\in\mathcal{C}_8}\left|\Gamma_4\right\rangle\otimes\left|\widetilde{U}\right\rangle+\sum_{\widetilde{U}\in\mathcal{C}_6}\left|\Gamma_5\right\rangle\otimes\left|\widetilde{U}\right\rangle+\sum_{\widetilde{U}\in\mathcal{C}_7}\left|\Gamma_6\right\rangle\otimes\left|\widetilde{U}\right\rangle\\
&+\sum_{\widetilde{U}\in\mathcal{C}_{11}}\left|\Gamma_7\right\rangle\otimes\left|\widetilde{U}\right\rangle+\sum_{\widetilde{U}\in\mathcal{C}_9}\left|\Gamma_8\right\rangle\otimes\left|\widetilde{U}\right\rangle+\sum_{\widetilde{U}\in\mathcal{C}_{10}}\left|\Gamma_9\right\rangle\otimes\left|\widetilde{U}\right\rangle\Bigg),\\
\left|E_0,8\right\rangle = \frac{1}{\sqrt{72}}\Bigg(&4\sum_{\widetilde{U}\in\mathcal{C}_4}\left|\Gamma_1\right\rangle\otimes\left|\widetilde{U}\right\rangle+\sum_{\widetilde{U}\in\mathcal{C}_5}\left|\Gamma_2\right\rangle\otimes\left|\widetilde{U}\right\rangle+\sum_{\widetilde{U}\in\mathcal{C}_{123}}\left|\Gamma_3\right\rangle\otimes\left|\widetilde{U}\right\rangle\\
&+\sum_{\widetilde{U}\in\mathcal{C}_7}\left|\Gamma_4\right\rangle\otimes\left|\widetilde{U}\right\rangle+\sum_{\widetilde{U}\in\mathcal{C}_8}\left|\Gamma_5\right\rangle\otimes\left|\widetilde{U}\right\rangle+\sum_{\widetilde{U}\in\mathcal{C}_6}\left|\Gamma_6\right\rangle\otimes\left|\widetilde{U}\right\rangle\\
&+\sum_{\widetilde{U}\in\mathcal{C}_{10}}\left|\Gamma_7\right\rangle\otimes\left|\widetilde{U}\right\rangle+\sum_{\widetilde{U}\in\mathcal{C}_{11}}\left|\Gamma_8\right\rangle\otimes\left|\widetilde{U}\right\rangle+\sum_{\widetilde{U}\in\mathcal{C}_9}\left|\Gamma_9\right\rangle\otimes\left|\widetilde{U}\right\rangle\Bigg),
\end{aligned}
$$

$$\begin{aligned}\left|E_0, 9\right\rangle = \frac{1}{\sqrt{72}}\Bigg(4 \sum_{\widetilde{U}\in\mathcal{C}_{123}} \left|\Gamma_1\right\rangle \otimes \left|\widetilde{U}\right\rangle + \sum_{\widetilde{U}\in\mathcal{C}_4} \left|\Gamma_2\right\rangle \otimes \left|\widetilde{U}\right\rangle + \sum_{\widetilde{U}\in\mathcal{C}_5} \left|\Gamma_3\right\rangle \otimes \left|\widetilde{U}\right\rangle \\ + \sum_{\widetilde{U}\in\mathcal{C}_6} \left|\Gamma_4\right\rangle \otimes \left|\widetilde{U}\right\rangle + \sum_{\widetilde{U}\in\mathcal{C}_7} \left|\Gamma_5\right\rangle \otimes \left|\widetilde{U}\right\rangle + \sum_{\widetilde{U}\in\mathcal{C}_8} \left|\Gamma_6\right\rangle \otimes \left|\widetilde{U}\right\rangle \\ + \sum_{\widetilde{U}\in\mathcal{C}_9} \left|\Gamma_7\right\rangle \otimes \left|\widetilde{U}\right\rangle + \sum_{\widetilde{U}\in\mathcal{C}_{10}} \left|\Gamma_8\right\rangle \otimes \left|\widetilde{U}\right\rangle + \sum_{\widetilde{U}\in\mathcal{C}_{11}} \left|\Gamma_9\right\rangle \otimes \left|\widetilde{U}\right\rangle\Bigg).\end{aligned}$$

List of Figures

2.1 Visualization of $U(1)$ and $\mathbb{Z}(5)$. 13

2.2 Visualization of $O(2)$. 14

3.1 Classical $O(3)$ spin model. 26

3.2 Wilson's link. 28

3.3 $SU(2)$ Gauss' law. 28

3.4 Wilson's square plaquette. 29

3.5 Weight diagrams of $\{4\}$ and $\{5\}$. 33

3.6 Link states of $\{4\}$. 35

3.7 Link states of $\{5\}$. 35

3.8 Reduced link states. 37

3.9 Square lattice site states. 38

3.10 Square lattice site basis plaquette example. 39

3.11 Square lattice plaquette environments (I-IV) in $\{4\}$. 40

3.12 Square lattice plaquette environments (V-VIII) in $\{4\}$. 41

3.13 Square lattice plaquette environments (I-IV) in $\{5\}$. 42

3.14 Square lattice plaquette environments (V-XII) in $\{5\}$. 43

3.15 Square lattice site-state (8) projection. 44

3.16 Honeycomb lattice site-states. 45

3.17 Honeycomb lattice plaquette environments in the $\{4\}$-representation. 46

3.18 Honeycomb lattice plaquette environments in the $\{5\}$-representation. 48

3.19 Honeycomb lattice flux strings. 49
3.20 Exact diagonalization in the $\{4\}$-representation with varying T_I and T_{IV}. 52
3.21 Square lattice cartoon state. 53
3.22 Exact diagonalization in the $\{5\}$-representation with varying T_I and T_{IV}. 54

4.1 Honeycomb lattice Gauss' law. 56
4.2 $\mathbb{Z}(2)$ link- and height-variables. 56
4.3 Honeycomb lattice site orientation. 56
4.4 Honeycomb lattice site orientation (I) with $Z(2)$ variables. 57
4.5 Honeycomb lattice site orientation (II) with $Z(2)$ variables. 57
4.6 Honeycomb lattice orientation unit-cell. 58
4.7 Height variable environment: A. 59
4.8 Height variable environment: B. 60
4.9 Height variable environment: C. 61
4.10 Height variable environment: D. 62
4.11 Height variable $3/2$-charge. 64
4.12 Height variable Dirac-string. 64
4.13 Height variable connected $3/2$-charges. 65
4.14 Hexagonal boundary conditions. 66
4.15 Cartoon pinwheel phases. 71
4.16 Single domain wall on an odd honeycomb lattice. 72
4.17 Two domain walls on an even honeycomb lattice. 73
4.18 Domain walls for charges on a honeycomb lattice. 75
4.19 Cartoon anti-pinwheel phase. 76
4.20 Cluster-bonds in space. 79
4.21 Cluster-bonds in Euclidean time. 81
4.22 Magnetic susceptibility for the pinwheel phase transition. 82
4.23 Pinwheel phases energy densities. 83

4.24 Energy densities on the honeycomb lattice with a Dirac-string, for the pinwheel phases. . . . 85

4.25 Projected magnetic order parameters with a Dirac-string in the correlated pinwheel phase. . . . 86

4.26 Dirac-string energies in the correlated pinwheel phase. . . . 87

4.27 Energy densities for the pinwheel phases on a honeycomb lattice with two $3/2$ charges. . . . 88

4.28 Energy densities on the honeycomb lattice for different charge separation, for the correlated pinwheel phase. . . . 90

4.29 Charge separation energies in the correlated pinwheel phase. . . . 91

4.30 Anti-pinwheel phase order parameters. . . . 93

4.31 Energy densities for the anti-pinwheel phase on the honeycomb lattice. . . . 94

5.1 Lattice crosses. . . . 104

5.2 Equations of motion of doubled lattice Chern-Simons-Maxwell theory. . . . 106

5.3 Gauss' law on direct and dual lattice sites. . . . 109

5.4 Wilson-loop encircling dual charges. . . . 112

6.1 Non-Abelian link operators. . . . 135

6.2 Non-Abelian Gauss' law. . . . 136

6.3 Non-Abelian lattice crosses. . . . 147

6.4 Non-Abelian Gauss' law on the direct and dual lattice. . . . 152

6.5 S_3 energy spectrum. . . . 163

6.6 S_3 Γ_3-charges. . . . 169

6.7 S_3 flux string breaking. . . . 169

6.8 S_3 charges with the same energy. . . . 170

6.9 Γ_3 direct dual charge energies. . . . 171

6.10 $\bar{D}_2$ Γ_5-charges. . . . 171

6.11 $\Delta(27)$ Γ_{10}- and Γ_{11}-charges. . . . 172

A.1 Weight diagram of $\{1\}_1$. . . . 178

A.2 Weight diagram of $\{4\}$. 179

A.3 Weight diagram of $\{5\}$. 179

A.4 Weight diagram of $\{1\}_2$. 181

A.5 Weight diagram of $\{10\}$. 181

C.1 Square lattice plaquettes in a 3×3 Hamiltonian block matrix. 187

D.1 Kagomé honeycomb lattice relation. 189

D.2 Kagomé dimer and honeycomb rishons. 190

D.3 Plaquette environments with honeycomb lattice rishon and Kagomé dimer. 191

E.1 Magnetic order parameters for the pinwheel phases: $T_{IV} = 0.5$ and $T_{VIII} = 1$. . 194

E.2 Magnetic order parameters for the pinwheel phases: $T_{IV} = 0.6$ and $T_{VIII} = 1$. . 195

E.3 Magnetic order parameters for the pinwheel phases: $T_{IV} = 0.7$ and $T_{VIII} = 1$. . 196

E.4 Magnetic order parameters for the pinwheel phases: $T_{IV} = 0.8$ and $T_{VIII} = 1$. . 197

E.5 Magnetic order parameters for the pinwheel phases: $T_{IV} = 0.9$ and $T_{VIII} = 1$. . 198

E.6 Magnetic order parameters for the pinwheel phases: $T_{IV} = T_{VIII} = 1$. 199

E.7 Magnetic order parameters for the pinwheel phases: $T_{IV} = T_{VIII} = 1$ (cluster algorithm). 200

List of Tables

2.1 Cayley table of S_3. 15

2.2 Cayley table of $S_3/[S_3, S_3]$. 16

2.3 Character table of S_3 16

2.4 Product rules for S_3 irreducible representations. 16

2.5 Cayley table of $\bar{D}_2$. 17

2.6 Cayley table of $\bar{D}_2/[\bar{D}_2, \bar{D}_2]$. 18

2.7 Character table of $\bar{D}_2$. 18

2.8 Product rules for $\bar{D}_2$ irreducible representations. 18

2.9 Cayley table of $\Delta(27)$. 19

2.10 Multiplication table of $\Delta(27)/[\Delta(27), \Delta(27)]$. 20

2.11 Character table of $\Delta(27)$. 20

2.12 Product table of $\Delta(27)$ irreducible representations. 21

3.1 Lattice symmetries for the square lattice geometry. 38

3.2 Lattice symmetries for the honeycomb lattice geometry. 45

4.1 Height variable symmetries. 67

4.2 Height variable symmetries (reduced parameter space). 68

4.3 Height variable center symmetry and boundary conditions. 68

4.4 Mean field results. 69

4.5 Correlated pinwheel phase signatures. 70

4.6 Uncorrelated pinwheel phase signatures. 75

6.1 S_3 2-dimensional irreducible representation. 142
6.2 S_3 element distances. 142
6.3 $\bar{D}_2$ element distances. 144
6.4 $\Delta(27)$ element distances. 145
6.5 S_3 one-cocycles. 158
6.6 S_3 YM spectrum. 159
6.7 S_3 CS spectrum. 160
6.8 $\bar{D}_2$ one-cocycles. 164
6.9 $\bar{D}_2$ YM spectrum. 164
6.10 $\bar{D}_2$ first CS spectrum. 165
6.11 $\bar{D}_2$ second CS spectrum. 166
6.12 $\Delta(27)$ one-cocycles. 166
6.13 $\Delta(27)$ YM spectrum. 167
6.14 $\Delta(27)$ first CS spectrum. 168
6.15 $\Delta(27)$ second CS spectrum. 168

A.1 States with 0 rishons on a link. 177
A.2 States with 1 rishons on a link. 178
A.3 States of 2 antisymmetric rishons on a link, i.e. the $\{5\}$-Representation. 180
A.4 States of two symmetric colour singlets on a link. 180
A.5 States of 2 symmetric rishons combined to triplets on a link. 182

B.1 Square lattice site-states definition. 184
B.2 Honeycomb lattice site-states definition. 185

Bibliography

[1] K. G. Wilson, "Confinement of quarks," *Phys. Rev. D*, vol. 10, pp. 2445–2459, Oct 1974.

[2] J. I. Cirac and P. Zoller, "Quantum computations with cold trapped ions," *Phys. Rev. Lett.*, vol. 74, pp. 4091–4094, May 1995.

[3] S. Lloyd, "Universal quantum simulators," *Science*, vol. 273, no. 5278, pp. 1073–1078, 1996.

[4] D. Jaksch, C. Bruder, J. I. Cirac, C. W. Gardiner, and P. Zoller, "Cold bosonic atoms in optical lattices," *Phys. Rev. Lett.*, vol. 81, pp. 3108–3111, Oct 1998.

[5] E. Zohar and B. Reznik, "Confinement and lattice quantum-electrodynamic electric flux tubes simulated with ultracold atoms," *Phys. Rev. Lett.*, vol. 107, p. 275301, Dec 2011.

[6] G. Szirmai, E. Szirmai, A. Zamora, and M. Lewenstein, "Gauge fields emerging from time-reversal symmetry breaking for spin-5/2 fermions in a honeycomb lattice," *Phys. Rev. A*, vol. 84, p. 011611, Jul 2011.

[7] Y. Liu, Y. Meurice, and S. W. Tsai, "Local gauge symmetry on optical lattices?," in *Proceedings of the 30th International Symposium on Lattice Field Theory. June 24-29, 2012. Cairns, Australia. Published online at* `http://pos.sissa.it/cgi-bin/reader/conf.cgi?confid=164''>http://pos.sissa.it/cgi-bin/reader/conf.cgi?confid=164`, p. 246, 2012.

[8] E. Zohar, J. I. Cirac, and B. Reznik, "Simulating compact quantum electrodynamics with ultracold atoms: Probing confinement and nonperturbative effects," *Phys. Rev. Lett.*, vol. 109, p. 125302, Sep 2012.

[9] D. Banerjee, M. Dalmonte, M. Müller, E. Rico, P. Stebler, U.-J. Wiese, and P. Zoller, "Atomic quantum simulation of dynamical gauge fields coupled to fermionic matter: From string breaking to evolution after a quench," *Phys. Rev. Lett.*, vol. 109, p. 175302, Oct 2012.

[10] D. Banerjee, M. Bögli, M. Dalmonte, E. Rico, P. Stebler, U.-J. Wiese, and P. Zoller, "Atomic quantum simulation of $\mathbf{U}(n)$ and $\mathrm{SU}(n)$ non-abelian lattice gauge theories," *Phys. Rev. Lett.*, vol. 110, p. 125303, Mar 2013.

[11] E. Zohar, J. I. Cirac, and B. Reznik, "Cold-atom quantum simulator for su(2) Yang-Mills lattice gauge theory," *Phys. Rev. Lett.*, vol. 110, p. 125304, Mar 2013.

[12] E. Zohar, J. I. Cirac, and B. Reznik, "Quantum simulations of gauge theories with ultracold atoms: Local gauge invariance from angular-momentum conservation," *Phys. Rev. A*, vol. 88, p. 023617, Aug 2013.

[13] U.-J. Wiese, "Ultracold quantum gases and lattice systems: quantum simulation of lattice gauge theories," *Annalen der Physik*, vol. 525, pp. 777–796, Nov. 2013.

[14] D. Banerjee, P. Widmer, F. J. Jiang, and U. J. Wiese, "Crystalline confinement," 2013.

[15] D. Banerjee, F. J. Jiang, P. Widmer, and U. J. Wiese, "The (2 + 1)-d U(1) quantum link model masquerading as deconfined criticality," *J. Stat. Mech.*, vol. 1312, p. P12010, 2013.

[16] D. Horn, "Finite matrix models with continuous local gauge invariance," *Physics Letters B*, vol. 100, no. 2, pp. 149 – 151, 1981.

[17] P. Orland and D. Rohrlich, "Lattice gauge magnets: Local isospin from spin," *Nuclear Physics B*, vol. 338, no. 3, pp. 647 – 672, 1990.

[18] S. Chandrasekharan and U.-J. Wiese, "Quantum link models: A discrete approach to gauge theories," *Nuclear Physics B*, vol. 492, no. 1, pp. 455 – 471, 1997.

[19] R. Brower, S. Chandrasekharan, and U.-J. Wiese, "QCD as a quantum link model," *Phys. Rev. D*, vol. 60, p. 094502, Sep 1999.

[20] P. Orland, "A reintroduction of dynamical SU(2) gauge fields in Hubbard models," *ArXiv e-prints:1207.0455*.

[21] J. M. Leinaas and J. Myrheim, "On the theory of identical particles," *Il Nuovo Cimento B (1971-1996)*, vol. 37, pp. 1–23, Jan 1977.

[22] F. Wilczek, "Quantum mechanics of fractional-spin particles," *Phys. Rev. Lett.*, vol. 49, pp. 957–959, Oct 1982.

[23] T. Olesen, N. Vlasii, and U.-J. Wiese, "From doubled Chern–Simons–Maxwell lattice gauge theory to extensions of the toric code," *Annals of Physics*, vol. 361, pp. 303 – 329, 2015.

[24] S. Caspar, D. Mesterházy, T. Olesen, N. Vlasii, and U.-J. Wiese, "Doubled lattice Chern–Simons–Yang–Mills theories with discrete gauge group," *Annals of Physics*, vol. 374, pp. 255 – 290, 2016.

[25] R. Feynman, "Simulating physics with computers," *International Journal of Theoretical Physics*, vol. 21, no. 6-7, pp. 467–488, 1982.

[26] I. Bloch, J. Dalibard, and W. Zwerger, "Many-body physics with ultracold gases," *Reviews of Modern Physics*, vol. 80, no. 3, pp. 885–964, 2008.

[27] M. Lewenstein, A. Sanpera, and V. Ahufinger, *Ultracold Atoms in Optical Lattices: Simulating Quantum Many-Body Systems*. 2012.

[28] A. Kitaev, "Fault-tolerant quantum computation by anyons," *Annals of Physics*, vol. 303, no. 1, pp. 2–30, 2003.

[29] P. Shor, "Fault-tolerant quantum computation," *arXiv:quant-ph/9605011*, p. 56, 1996.

[30] D. Gottesman, "Theory of fault-tolerant quantum computation," *Physical Review A - Atomic, Molecular, and Optical Physics*, vol. 57, no. 1, pp. 127–137, 1998.

[31] J. Preskill, "Fault-tolerant quantum computation," *arXiv:quant-ph/9712048*, 1997.

[32] F. Wilczek and A. Zee, "Linking numbers, spin, and statistics of solitons," *Physical Review Letters*, vol. 51, no. 25, pp. 2250–2252, 1983.

[33] J. Fröhlich and P.-A. Marchetti, "Quantum field theory of anyons," *Letters in Mathematical Physics*, vol. 16, no. 4, pp. 347–358, 1988.

[34] J. Fröhlich and P. Marchetti, "Quantum field theories of vortices and anyons," *Communications in Mathematical Physics*, vol. 121, no. 2, pp. 177–223, 1989.

[35] F. Wilczek and D. S. Rokhsar, "Fractional statistics and anyon superconductivity," vol. 45, pp. 101–, 01 1992.

[36] D. Deutsch, "Quantum theory, the church-turing principle and the universal quantum computer.," *Proceedings of The Royal Society of London, Series A: Mathematical and Physical Sciences*, vol. 400, no. 1818, pp. 97–117, 1985.

[37] J. Cirac and P. Zoller, "Quantum computations with cold trapped ions," *Physical Review Letters*, vol. 74, no. 20, pp. 4091–4094, 1995.

[38] P. Shor, "Polynomial-time algorithms for prime factorization and discrete logarithms on a quantum computer," *SIAM Journal on Computing*, vol. 26, no. 5, pp. 1484–1509, 1997.

[39] A. Kitaev, "Anyons in an exactly solved model and beyond," *Annals of Physics*, vol. 321, no. 1, pp. 2–111, 2006.

[40] C. Nayak, S. Simon, A. Stern, M. Freedman, and S. Das Sarma, "Non-abelian anyons and topological quantum computation," *Reviews of Modern Physics*, vol. 80, no. 3, pp. 1083–1159, 2008.

[41] L. S. Georgiev, "Topological Quantum Computation with Non-Abelian Anyons in Fractional Quantum Hall States," *ArXiv e-prints: 1602.05035*, Feb. 2016.

[42] E. Dennis, A. Kitaev, A. Landahl, and J. Preskill, "Topological quantum memory," *Journal of Mathematical Physics*, vol. 43, no. 9, pp. 4452–4505, 2002.

[43] H. Bombin and M. Martin-Delgado, "Family of non-Abelian Kitaev models on a lattice: Topological condensation and confinement," *Physical Review B - Condensed Matter and Materials Physics*, vol. 78, no. 11, 2008.

[44] M. Levin and X.-G. Wen, "String-net condensation: A physical mechanism for topological phases," *Physical Review B - Condensed Matter and Materials Physics*, vol. 71, no. 4, 2005.

[45] D. Aharonov and I. Arad, "The bqp-hardness of approximating the Jones polynomial," *New J. Phys.*, vol. 13, p. 035019, 2011.

[46] P. Wocjan and J. Yard, "The jones polynomial: quantum algorithms and applications in quantum complexity theory," *Quantum Inf. Comp.*, vol. 8, p. 147, 2008.

[47] V. Jones, "Hecke algebra representations of braid groups and link polynomials," *Ann. Math.*, vol. 126, no. 2, pp. 335–388, 1987.

[48] R. Willett, L. Pfeiffer, and K. West, "Alternation and interchange of e/4 and e/2 period interference oscillations consistent with filling factor 5/2 non-abelian quasiparticles," *Physical Review B - Condensed Matter and Materials Physics*, vol. 82, no. 20, 2010.

[49] S. An, P. Jiang, H. Choi, W. Kang, S. Simon, L. Pfeiffer, K. West, and K. Baldwin, "Braiding of abelian and non-abelian anyons in the fractional quantum hall effect," 2011.

[50] R. Willett, C. Nayak, K. Shtengel, L. Pfeiffer, and K. West, "Magnetic-field-tuned aharonov-bohm oscillations and evidence for non-abelian anyons at $\nu = 5/2$," *Physical Review Letters*, vol. 111, no. 18, 2013.

[51] D. Banerjee, M. Dalmonte, M. Müller, E. Rico, P. Stebler, U.-J. Wiese, and P. Zoller, "Atomic quantum simulation of dynamical gauge fields coupled to fermionic matter: From string breaking to evolution after a quench," *Physical Review Letters*, vol. 109, no. 17, 2012.

[52] E. Zohar, J. Cirac, and B. Reznik, "Cold-atom quantum simulator for su(2) Yang-Mills lattice gauge theory," *Physical Review Letters*, vol. 110, no. 12, 2013.

[53] D. Banerjee, M. Bögli, M. Dalmonte, E. Rico, P. Stebler, U.-J. Wiese, and P. Zoller, "Atomic quantum simulation of u(n) and su(n) non-abelian lattice gauge theories," *Physical Review Letters*, vol. 110, no. 12, 2013.

[54] D. Marcos, P. Rabl, E. Rico, and P. Zoller, "Superconducting circuits for quantum simulation of dynamical gauge fields," *Physical Review Letters*, vol. 111, no. 11, 2013.

[55] E. Zohar, J. Cirac, and B. Reznik, "Quantum simulations of gauge theories with ultracold atoms: Local gauge invariance from angular-momentum conservation," *Physical Review A - Atomic, Molecular, and Optical Physics*, vol. 88, no. 2, 2013.

[56] E. Zohar, J. Cirac, and B. Reznik, "Quantum simulations of lattice gauge theories using ultracold atoms in optical lattices," *Reports on Progress in Physics*, vol. 79, no. 1, 2015.

[57] K. Wilson, "Confinement of quarks," *Physical Review D*, vol. 10, no. 8, pp. 2445–2459, 1974.

[58] J. Kogut and L. Susskind, "Hamiltonian formulation of Wilson's lattice gauge theories," *Physical Review D*, vol. 11, no. 2, pp. 395–408, 1975.

[59] J. Kogut, "An introduction to lattice gauge theory and spin systems," *Reviews of Modern Physics*, vol. 51, no. 4, pp. 659–713, 1979.

[60] J. Kogut, "The lattice gauge theory approach to quantum chromodynamics," *Reviews of Modern Physics*, vol. 55, no. 3, pp. 775–836, 1983.

[61] S. Chern and J. Simons, "Characteristic forms and geometric invariants," *Ann. Math.*, vol. 99, pp. 48–69, 1974.

[62] S. Deser, R. Jackiw, and S. Templeton, "Topologically massive gauge theories," *Annals of Physics*, vol. 140, no. 2, pp. 372–411, 1982.

[63] G. Dunne, R. Jackiw, and C. Trugenberger, "Chern-Simons theory in the schrödinger representation," *Annals of Physics*, vol. 194, no. 1, pp. 197–223, 1989.

[64] R. Jackiw and S.-Y. Pi, "Classical and quantal nonrelativistic Chern-Simons theory," *Physical Review D*, vol. 42, no. 10, pp. 3500–3513, 1990.

[65] G. Dunne *Aspects of Chern-Simons Theory, Les Houches Lectures*, 1999.

[66] A. Lerda, "Anyons: Quantum mechanics of particles with fractional statistics," *Lecture Notes in Physics*, vol. 14, p. m14, 1992.

[67] M. Berry, "Quantal phase factors accompanying adiabatic changes," *Proc. R. Soc. London, Ser. A*, vol. 392, pp. 45–57, 1984.

[68] B. Simon, "Holonomy, the quantum adiabatic theorem, and Berry's phase," *Physical Review Letters*, vol. 51, no. 24, pp. 2167–2170, 1983.

[69] M. Freedman, A. Kitaev, M. Larsen, and Z. Wang, "Topological quantum computation," *Bulletin of the American Mathematical Society*, vol. 40, no. 1, pp. 31–38, 2003.

[70] M. Freedman, C. Nayak, K. Shtengel, K. Walker, and Z. Wang, "A class of p, t-invariant topological phases of interacting electrons," *Annals of Physics*, vol. 310, no. 2, pp. 428–492, 2004.

[71] G. Brennen and J. Pachos, "Why should anyone care about computing with anyons?," *Proceedings of the Royal Society A: Mathematical, Physical and Engineering Sciences*, vol. 464, no. 2089, pp. 1–24, 2008.

[72] E. Witten, "Quantum field theory and the jones polynomial," *Communications in Mathematical Physics*, vol. 121, no. 3, pp. 351–399, 1989.

[73] M. Atiyah, "Topological quantum field theories," *Inst. Hautes Etudes Sci. Publ. Math.*, vol. 68, p. 175, 1989.

[74] J. Schonfeld, "A mass term for three-dimensional gauge fields," *Nuclear Physics, Section B*, vol. 185, no. 1, pp. 157–171, 1981.

[75] R. Jackiw and S. Templeton, "How super-renormalizable interactions cure their infrared divergences," *Physical Review D*, vol. 23, no. 10, pp. 2291–2304, 1981.

[76] S. Deser, R. Jackiw, and S. Templeton, "Three-dimensional massive gauge theories," *Physical Review Letters*, vol. 48, no. 15, pp. 975–978, 1982.

[77] E. Witten, "Topological quantum field theory," *Communications in Mathematical Physics*, vol. 117, no. 3, pp. 353–386, 1988.

[78] A. Coste and M. Lüscher, "Parity anomaly and fermion-boson transmutation in 3-dimensional lattice qed," *Nuclear Physics, Section B*, vol. 323, no. 3, pp. 631–659, 1989.

[79] M. Lüscher, "Bosonization in 2 + 1 dimensions," *Nuclear Physics, Section B*, vol. 326, no. 3, pp. 557–582, 1989.

[80] D. Eliezer and G. Semenoff, "Intersection forms and the geometry of lattice Chern-Simons theory," *Physics Letters B*, vol. 286, no. 1-2, pp. 118–124, 1992.

[81] D. Eliezer and G. Semenoff, "Anyonization of lattice Chern-Simons theory," *Annals of Physics*, vol. 217, no. 1, pp. 66–104, 1992.

[82] S. Zhang, T. Hansson, and S. Kivelson, "Effective-field-theory model for the fractional quantum Hall effect," *Physical Review Letters*, vol. 62, no. 1, pp. 82–85, 1989.

[83] J. Jain, "Composite-fermion approach for the fractional quantum hall effect," *Physical Review Letters*, vol. 63, no. 2, pp. 199–202, 1989.

[84] S. Zhang, "The Chern-Simons-Landau-Ginzburg theory of the fractional quantum hall effect," *Int. J. Mod. Phys. B*, vol. 6, pp. 25–58, 1992.

[85] E. Fradkin, "Jordan-Wigner transformation for quantum-spin systems in two dimensions and fractional statistics," *Physical Review Letters*, vol. 63, no. 3, pp. 322–325, 1989.

[86] E. Fradkin and F. Schaposnik, "Chern-Simons gauge theories, confinement, and the chiral spin liquid," *Physical Review Letters*, vol. 66, no. 3, pp. 276–279, 1991.

[87] A. Lopez, A. Rojo, and E. Fradkin, "Chern-Simons theory of the anisotropic quantum Heisenberg antiferromagnet on a square lattice," *Physical Review B*, vol. 49, no. 21, pp. 15139–15158, 1994.

[88] P. Fendley and E. Fradkin, "Realizing non-abelian statistics in time-reversal-invariant systems," *Physical Review B - Condensed Matter and Materials Physics*, vol. 72, no. 2, 2005.

[89] S.-P. Kou, M. Levin, and X.-G. Wen, "Mutual Chern-Simons theory for z_2 topological order," *Physical Review B - Condensed Matter and Materials Physics*, vol. 78, no. 15, 2008.

[90] G. Palumbo and J. Pachos, "Abelian Chern-Simons-Maxwell theory from a tight-binding model of spinless fermions," *Physical Review Letters*, vol. 110, no. 21, 2013.

[91] K. Kumar, K. Sun, and E. Fradkin, "Chern-Simons theory of magnetization plateaus of the spin- 1/2 quantum XXZ Heisenberg model on the kagome lattice," *Physical Review B - Condensed Matter and Materials Physics*, vol. 90, no. 17, 2014.

[92] R. Kantor and L. Susskind, "A lattice model of fractional statistics," *Nuclear Physics, Section B*, vol. 366, no. 3, pp. 533–568, 1991.

[93] D. Eliezer and G. Semenoff, "Anyonization and novel braid structure in dumb-bell Chern-Simons theory," *Physics Letters B*, vol. 266, no. 3-4, pp. 375–381, 1991.

[94] D. Adams, "A doubled discretization of abelian Chern-Simons theory," *Physical Review Letters*, vol. 78, no. 22, pp. 4155–4158, 1997.

[95] L. Susskind, "Lattice fermions," *Physical Review D*, vol. 16, no. 10, pp. 3031–3039, 1977.

[96] V. Müller, "Intermediate statistics in two space dimensions in a lattice-regularized hamiltonian quantum field theory," *Zeitschrift für Physik C Particles and Fields*, vol. 47, no. 2, pp. 301–310, 1990.

[97] F. Berruto, M. Diamantini, and P. Sodano, "On pure lattice Chern-Simons gauge theories," *Physics Letters, Section B: Nuclear, Elementary Particle and High-Energy Physics*, vol. 487, no. 3-4, pp. 366–370, 2000.

[98] B. Douçot, M. Feigel'man, L. Ioffe, and A. Ioselevich, "Protected qubits and Chern-Simons theories in Josephson junction arrays," *Physical Review B - Condensed Matter and Materials Physics*, vol. 71, no. 2, 2005.

[99] F. Bais and J. Romers, "Anyonic order parameters for discrete gauge theories on the lattice," *Annals of Physics*, vol. 324, no. 5, pp. 1168–1175, 2009.

[100] D. Freed and F. Quinn, "Chern-Simons theory with finite gauge group," *Communications in Mathematical Physics*, vol. 156, no. 3, pp. 435–472, 1993.

[101] F. Bais, P. Van Driel, and M. De Wild Propitius, "Quantum symmetries in discrete gauge theories," *Phys. Lett. B*, vol. 280, 1992.

[102] F. Alexander Bais, P. van Driel, and M. de Wild Propitius, "Anyons in discrete gauge theories with Chern-Simons terms," *Nuclear Physics, Section B*, vol. 393, no. 3, pp. 547–570, 1993.

[103] M. von Steinkirch, "Introduction to group theory for physicists," *http://www.astro.sunysb.edu/steinkirch/books/group.pdf*, 2011.

[104] *Mathematical Methods for Physics and Engineering*. Cambridge, 2006.

[105] "Groupprops, the group properties wiki `https://groupprops.subwiki.org/wiki/Main_Page`," 2017.

[106] W. Heisenberg, "Zur Theorie des Ferromagnetismus," *Zeitschrift für Physik*, vol. 49, no. 9, pp. 619–636, 1928.

[107] F. Haldane, "Continuum dynamics of the 1-d Heisenberg antiferromagnet: Identification with the o(3) nonlinear sigma model," *Physics Letters A*, vol. 93, no. 9, pp. 464 – 468, 1983.

[108] F. D. M. Haldane, "Nonlinear field theory of large-spin Heisenberg antiferromagnets: Semi-classically quantized solitons of the one-dimensional easy-axis Néel state," *Phys. Rev. Lett.*, vol. 50, pp. 1153–1156, Apr 1983.

[109] S. Chandrasekharan, F. J. Jiang, M. Pepe, and U. J. Wiese, "Rotor Spectra, Berry Phases, and Monopole Fields: From Antiferromagnets to QCD," *Phys. Rev.*, vol. D78, p. 077901, 2008.

[110] H. De Raedt and A. Lagendijk, "Monte Carlo calculation of the thermodynamic properties of a quantum model: A one-dimensional fermion lattice model," *Phys. Rev. Lett.*, vol. 46, pp. 77–80, Jan 1981.

[111] W. von der Linden, "A quantum Monte Carlo approach to many-body physics," *Physics Reports*, vol. 220, no. 2, pp. 53 – 162, 1992.

[112] S. A. Kivelson, D. S. Rokhsar, and J. P. Sethna, "Topology of the resonating valence-bond state: Solitons and high-T_c superconductivity," *Phys. Rev. B*, vol. 35, pp. 8865–8868, Jun 1987.

[113] D. S. Rokhsar and S. A. Kivelson, "Superconductivity and the quantum hard-core dimer gas," *Phys. Rev. Lett.*, vol. 61, pp. 2376–2379, Nov 1988.

[114] C. Sanderson and R. Curtin, "Armadillo: a template-based c++ library for linear algebra.," *Journal of Open Source Software*, vol. 1, 2016.

[115] N. Metropolis, A. W. Rosenbluth, M. N. Rosenbluth, A. H. Teller, and E. Teller, "Equation of state calculations by fast computing machines," *The Journal of Chemical Physics*, vol. 21, no. 6, pp. 1087–1092, 1953.

[116] W. K. Hastings, "Monte Carlo sampling methods using Markov chains and their applications," *Biometrika*, vol. 57, no. 1, pp. 97–109, 1970.

[117] H. F. Trotter, "On the product of semi-groups of operators," *Proc. Amer. Math. Soc. 10 (1959), 545-551*, 1959.

[118] M. Suzuki, "Generalized Trotter's formula and systematic approximants of exponential operators and inner derivations with applications to many-body problems," *Communications in Mathematical Physics*, vol. 51, pp. 183–190, Jun 1976.

[119] V. Banerjee, S. Dattagupta, and P. Sen, "Hysteresis in a quantum spin model," *Phys. Rev. E*, vol. 52, pp. 1436–1446, Aug 1995.

[120] H. Nielsen and M. Ninomiya, "Absence of neutrinos on a lattice," *Nuclear Physics B*, vol. 185, no. 1, pp. 20 – 40, 1981.

[121] H. Nielsen and M. Ninomiya, "A no-go theorem for regularizing chiral fermions," *Physics Letters B*, vol. 105, no. 2, pp. 219 – 223, 1981.

[122] S. Chandrasekharan and U.-J. Wiese, "An introduction to chiral symmetry on the lattice," *Progress in Particle and Nuclear Physics*, vol. 53, no. 2, pp. 373 – 418, 2004.

[123] M. Reed and B. Simon, "Methods of modern mathematical physics," *Fourier Analysis, Self-Adjointness*, vol. 2, 1975.

[124] J. Weidmann, "Spectral theory of ordinary differential operators," *Spectral Theory of Ordinary Differential Operators*, vol. 1258, 1987.

[125] M. Al-Hashimi and U.-J. Wiese, "Discrete accidental symmetry for a particle in a constant magnetic field on a torus," *Annals of Physics*, vol. 324, no. 2, pp. 343–360, 2009.

[126] J. Zak, "Magnetic translation group," *Physical Review*, vol. 134, no. 6A, pp. A1602–A1606, 1964.

[127] A. Wal, "The structure of magnetic translation group for a finite system," *Physica B: Condensed Matter*, vol. 404, no. 8-11, pp. 1040–1044, 2009.

[128] L. Landau, "Diamagnetismus der Metalle," *Zeitschrift für Physik*, vol. 64, no. 9-10, pp. 629–637, 1930.

[129] A. Stern, "Anyons and the quantum Hall effect-a pedagogical review," *Annals of Physics*, vol. 323, no. 1, pp. 204–249, 2008.

[130] G. 't Hooft, "A property of electric and magnetic flux in non-abelian gauge theories," *Nuclear Physics B*, vol. 153, pp. 141 – 160, 1979.

[131] G. Hooft, "Some twisted self-dual solutions for the Yang-Mills equations on a hypertorus," *Communications in Mathematical Physics*, vol. 81, no. 2, pp. 267–275, 1981.

[132] W. Fairbairn, T. Fulton, and W. Klink, "Finite and disconnected subgroups of su3 and their application to the elementary-particle spectrum," *Journal of Mathematical Physics*, vol. 5, no. 8, pp. 1038–1051, 1964.

[133] W. M. Fairbairn and T. Fulton, "Some comments on finite subgroups of su(3)," *Journal of Mathematical Physics*, vol. 23, no. 10, pp. 1747–1748, 1982.

[134] C. Luhn, S. Nasri, and P. Ramond, "Flavor group $\delta(3n2)$," *Journal of Mathematical Physics*, vol. 48, no. 7, 2007.

[135] P. Ludl, "Comments on the classification of the finite subgroups of su(3)," *Journal of Physics A: Mathematical and Theoretical*, vol. 44, no. 25, 2011.

[136] D. Mesterházy and S. Caspar *In preparation.*

[137] Y. Aharonov and D. Bohm, "Significance of electromagnetic potentials in the quantum theory," *Physical Review*, vol. 115, no. 3, pp. 485–491, 1959.

[138] B. P. Lanyon, C. Hempel, D. Nigg, M. Müller, R. Gerritsma, F. Zähringer, P. Schindler, J. T. Barreiro, M. Rambach, G. Kirchmair, M. Hennrich, P. Zoller, R. Blatt, and C. F. Roos, "Universal digital quantum simulation with trapped ions," *Science*, vol. 334, no. 6052, pp. 57–61, 2011.

[139] J. Barreiro, M. Müller, P. Schindler, D. Nigg, T. Monz, M. Chwalla, M. Hennrich, C. Roos, P. Zoller, and R. Blatt, "An open-system quantum simulator with trapped ions," *Nature*, vol. 470, no. 7335, pp. 486–491, 2011.

[140] R. Alicki, M. Fannes, and M. Horodecki, "A statistical mechanics view on Kitaev's proposal for quantum memories," *Journal of Physics A: Mathematical and Theoretical*, vol. 40, no. 24, pp. 6451–6467, 2007.

[141] C. Castelnovo and C. Chamon, "Entanglement and topological entropy of the toric code at finite temperature," *Physical Review B - Condensed Matter and Materials Physics*, vol. 76, no. 18, 2007.

[142] S. Chesi, B. Röthlisberger, and D. Loss, "Self-correcting quantum memory in a thermal environment," *Physical Review A - Atomic, Molecular, and Optical Physics*, vol. 82, no. 2, 2010.

[143] C. Brell, S. Burton, G. Dauphinais, S. Flammia, and D. Poulin, "Thermalization, error correction, and memory lifetime for Ising anyon systems," *Physical Review X*, vol. 4, no. 3, 2014.

[144] B. Brown, D. Loss, J. Pachos, C. Self, and J. Wootton *arXiv:1411.6643*, 2014.

[145] C. Freeman, C. Herdman, D. Gorman, and K. Whaley, "Relaxation dynamics of the toric code in contact with a thermal reservoir: Finite-size scaling in a low-temperature regime," *Physical Review B - Condensed Matter and Materials Physics*, vol. 90, no. 13, 2014.

Declaration of consent

on the basis of Article 28 para. 2 of the RSL05 phil.-nat.

Name/First Name: Olesen / Therkel Andreas Zøllner

Matriculation Number: 13-141-080

Study program: Physics

Bachelor ☐ Master ☐ Dissertation ☑

Title of the thesis: SU(2) Quantum Link Models and Doubled Lattice Chern-Simons Theories

Supervisor: Prof. Dr. Uwe-Jens Wiese

I declare herewith that this thesis is my own work and that I have not used any sources other than those stated. I have indicated the adoption of quotations as well as thoughts taken from other authors as such in the thesis. I am aware that the Senate pursuant to Article 36 para. 1 lit. r of the University Act of 5 September, 1996 is authorised to revoke the title awarded on the basis of this thesis. I allow herewith inspection in this thesis.

Bern / 29.08.2017

Place/Date

Signature

Curriculum Vitæ
Therkel A. Zøllner Olesen

Personal Data

Place and Date of Birth:	Silkeborg - Denmark | 4th of June 1987
Home Address:	2Bis rue du Jura 01630, Saint-Genis-Pouilly France
Current Work Address:	Albert Einstein Center for Fundamental Physics, Institute for Theoretical Physics – University of Bern Sidlerstrasse 5 CH-3012 Bern Switzerland
Office:	GS 237a
Office-Phone:	+41 31 631 54 60
email:	olesen@itp.unibe.ch

Education

2017 | PhD in Physics
Albert Einstein Center for Fundamental Physics, Institute for Theoretical Physics – University of Bern, under ERC Project†: "Atomic Gauge Simulators"
Thesis: *SU*(2) *Quantum Link Models and Doubled Lattice Chern-Simons Theories*
Project Title: "Classical and Atomic Quantum Simulation of Gauge Theories in Particle and Condensed Matter Physics"
Supervisor: Prof. Dr. Uwe-Jens Wiese | Detailed List of Courses Below
†ERC Grant Agreement 33920.

2013 | Master of Science in Physics (cand.scient.)
Niels Bohr Institute – University of Copenhagen
Thesis: "Twisted Mass Wilson-χPT-Fermions on the Lattice"
Supervisor: Associate Prof. Kim Splittorff & Prof. Poul Henrik Damgaard
GPA: 3.95 | Detailed List of Exams Below

2011 | Bachelor of Science in Physics (BSc)
Niels Bohr Institute – University of Copenhagen
Bachelor Project: "Search for Highly Ionizing particles with the ATLAS Detector"
Supervisor: Esben Bryndt Klinkby
GPA: 3.94 | Detailed List of Exams Below

Work Experience

2014 - 2017	PhD Student at the Albert Einstein Center for Fundamental Physics, Institute for Theoretical Physics – University of Bern, under ERC Project[‡]: "Atomic Gauge Simulators" *PhD student on the project; "Classical and Atomic Quantum Simulation of Gauge Theories in Particle and Condensed Matter Physics", in the group of Prof. Uwe-Jens Wiese.* [‡]ERC Grant Agreement 33920.
2014 - 2017	Teaching Assistant at Albert Einstein Center for Fundamental Physics, Institute for Theoretical Physics – University of Bern *Teaching assistant in the courses "Advanced Concepts of Theoretical Physics", "Quantum Field Theory I", "Quantum Field Theory II" and "Theoretical Exercises".*
2012	Summer Student at CERN *Worked in the ATLAS Collaboration, constructing a code for testing the alignment of the internal clocks with particle packages. Report titled: "Presentation of Work on the ATLAS CTP Clock Monitoring of Trigger Signal Phase Monitoring & Alignment of CTP Local Clock and BCID"*
2011 - 2012	Teaching Assistant at the University of Copenhagen *Teaching assistant in the courses "Introduction to Atomic Physics" and "Classical Mechanics 2". Substitute teaching assistant for "Quantum mechanics 1".*
2008-2012	"The Scientific Playroom" *Student run association, demonstrating physics experiments to the wider public.*

Attended Conferences & Workshops

2017	Nordic Winter School on Particle Physics and Cosmology *Gausdal, Norway*
2016	Quantum Matter – Centro de Ciencias de Benasque Pedro Pascual *Benasque, Spain*
2014	Complex Quantum Systems Summer School, (CoQuS) *Vienna, Austria*
2013	Nordic Winter School on Particle Physics and Cosmology *Gausdal, Norway*
2012	Standard Model @ LHC *Niels Bohr International Academy and Discovery Center, Denmark*

Publications

2016 | Doubled Lattice Chern-Simons-Yang-Mills Theories with Discrete Gauge Group
Authors: Stephan Caspar, David Mesterházy, Therkel Z. Olesen, Nadiia D. Vlasii, Uwe-Jens Wiese
Annals Phys. 374, (2016) 255–290
http://dx.doi.org/10.1016/j.aop.2016.08.017

2015 | From doubled Chern-Simons-Maxwell lattice gauge theory to extensions of the toric code
Authors: Therkel Z. Olesen, Nadiia D. Vlasii, Uwe-Jens Wiese
Annals Phys. 361 (2015) 303-329.
http://dx.doi.org/10.1016/j.aop.2015.06.020

Presentation of Work

2016 | "Quantum Matter" - Centro de Ciencias de Benasque Pedro Pascual, Spain
Poster Session: "Doubled Lattice Chern-Simons-Yang-Mills Theory with Discrete Gauge Group"

2017 | "Nordic Winter School on Particle Physics and Cosmology" - Gausdal, Norway
Talk: "$SU(2)$ Quantum Link Model (QLM)"

Computer Skills

Intermediate Knowledge	html	*HTML and PHP to setup smaller homepages.*
	Sun-Grid-Engine	*Clusters running the Sun Grid Engine during PhD studies.*
Proficient Knowledge	Linux	*Good knowledge of Linux, especially Arch, Red-Hat based and Ubuntu based distributions.*
	LaTeX	*Written long documents in LaTeX.*
	`C/C++`	*The majority of code have been written in* `C/C++`.
	Root	*Written larger programs in Root, especially during Bachelor studies and as a CERN Summer Student.*
	Python	*Learned and used Python during Bachelor Studies.*
	Mathematica	*Written larger programs in Mathematica during Master and PhD studies, especially for matrix manipulations*
	GNU Octave / MatLab	*Written larger programs in GNU Octave during PhD studies, especially for matrix manipulations.*
	GIT	*GIT as a backup and version control system during PhD studies.*
	Message Passing Interface (MPI)	*MPI to parallelise code during PhD studies.*

Languages

Danish	Mother tongue	
English	Fluent	*English as everyday language since 2013.*
Spanish	Basic Knowledge	*Self study since 2012.*
French	Basic Knowledge	*Two years of education in high school.*
German	Basic Knowledge	*Four years of education (7th-10th grade). Lived in Bern for two and a half year.*

PhD in Physics

Courses Attended

Course Title	Lecturer
Precision Electroweak Physics	Massimo Passera
Phase Transitions and critical Phenomena	Urs Wenger
Elementary Particle Physics	Jean-Pierre Derendinger
On the scale, Weyl and conformal behavior	Georg Bergner
Chiral Perturbation Theory	Lewis Tunstall
Supersymmetric gauge theories and their dualities	Susanne Reffert

---

Master of Science in Physics

Courses & Grades

Exam	Grade 7-point scale	Grade ECTS scale	ECTS credits
General relativity and cosmology	12	A	7.5
Applied Statistic: From data till results	12	A	7.5
Elementary Particle Physics	10	B	7.5
Experimental Nuclear- and Particle Physics	12	A	7.5
Quantum Field Theory 1	12	A	7.5
Particle Physics – At the energy frontier	12	A	7.5
Quantum Field Theory 2	12	A	7.5
CERN Summer School 2012	Passed	Passed	7.5
Master Thesis: "*Twisted Mass Wilson-χPT-Fermions on the Lattice*"	12	A	60
Total:	-	-	120
ECTS Averaged Grade:	11.9	-	-
GPA:	-	3.95	-

Bachelor of Science in Physics

Courses & Grades

Exam	Grade 7-point scale	Grade ECTS scale	ECTS credits
Introduction to Mathematics	12	A	7.5
Physics 1: Introduction, Mechanics and Relativitytheory	12	A	7.5
Linear Algebra	12	A	7.5
Physics 2 - Classical mechanics	12	A	7.5
Mathematics F	12	A	7.5
Physics 3 - Thermodynamics and project	12	A	7.5
Mathematics F2	12	A	7.5
Physics 4 - Electromagnetism	12	A	7.5
Physics 5 - Quantum mechanics I	12	A	7.5
Analytical mechanics and chaos	12	A	7.5
Physics 7 - Statistical Physics	12	A	7.5
Physics 6 - Electrodynamics and waves	12	A	7.5
Wave Optic	12	A	7.5
Physics 8 - Quantum Mechanics II	12	A	7.5
Theory of Science and Ethics for Physics	10	B	7.5
Introduction to Atomic Physics	Passed	Passed	7.5
Mathematical physics 2: Quantum Mechanics - mathematical aspects	10	B	7.5
Introduction to Nuclear and Particle Physics	12	A	7.5
Dynamical Systems and Chaos	12	A	7.5
Modelling and simulation (Scientific Computing)	12	A	7.5
Optical physics and lasers	12	A	7.5
Mathematical physics	12	A	7.5
Bachelor Project: "*Search for Highly Ionizing particles with the ATLAS Detector*"	12	A	15.0
Total:	-	-	180
ECTS Averaged Grade:	11.8	-	-
GPA:	-	3.94	-